Universidad de Valladolid

Escuela de Doctorado Universidad de Valladolid

PROGRAMA DE DOCTORADO EN QUÍMICA
Facultad de Ciencias

Departamento de Química Física y Química Inorgánica

TESIS DOCTORAL:

Microsolvation of biomolecular models by microwave spectroscopy: structure and cooperative effects.

Presentada por Pablo Pinacho Morante para optar al grado de
Doctor por la Universidad de Valladolid

Dirigida por:
Prof. Susana Blanco Rodríguez
Prof. Juan Carlos López Alonso.

La investigación llevada a cabo en esta Tesis Doctoral ha sido financiada por:

Ministerio de Economía y Competitividad

CTQ2013-40717-P

CTQ2016-75253-P

Junta de Castilla y León

Consejería de Educación

VA334U14

Universidad de Valladolid

Vicerrectorado de Investigación y Política Científica

Ayudas para estancias breves en el desarrollo de tesis doctorales

Movilidad Doctorandos UVa 2015

Movilidad Doctorandos UVa 2016

Universidad de Valladolid

"*You can't always get what you want,*
But if you try sometimes you might find
You get what you need"

The Rolling Stones

Aunque solo lo defiende una persona, el trabajo que se hace durante una tesis es un trabajo de equipo, y como en todos los equipos hay personas que lideran y guían. Quiero expresar mi más sincero agradecimiento a mis directores, la Prof. Susana Blanco Rodríguez y el Prof. Juan Carlos López Alonso por haber hecho una excelente labor de guía. Quiero agradecer a Juan Carlos por haberme enseñado tantísimas cosas (y las que me quedan por aprender de él). A Susana, además de por haberme enseñado tanto, quiero agradecerle especialmente por haber estado codo con codo a mi lado y por haber conseguido literalmente, que esta Tesis saliera adelante.

I have had the tremendous luck of doing short research stays in two of the best laboratories. I would like to thank PD Dr. Melanie Schnell for the stay in the Structure and Dynamics of Cold and Controlled Molecules group at the Max Planck Institute for the Structure and Dynamics of Matter in Hamburg. She is a great group leader and all the team mates I met there are awesome, thanks to all! I also would like to thank Prof. Dr. Hab. Zbigniew Kisiel for the stay in the Group of Vibrational and Rotational Spectroscopy group in the Institute of Physics of the Polish Academy of Sciences. He is one of the leading experts in the rotational spectroscopy field and I have learnt so many things from him!

Durante este periodo han pasado varios compañeros de TFG, TFM o doctorado por el departamento, quiero agradecer a todos, con mención propia a Alberto Macario, por tantos buenos momentos.

La lista de amigos a quien querría agradecer es demasiado extensa como para ponerlos a todos. ¡Gracias a todos! En especial a Pablo y Edu.

Por supuesto quiero agradecer a mi familia, especialmente a mis padres Soledad y Jose, que siempre me han apoyado en mis decisiones y ayudando a que continuara formándome. En casa también han estado siempre Balder y Clara, distrayéndome con sus juegos cuando lo necesitaba, y dándome muchísimo cariño. Son los mejores amigos que alguien podría tener.

Durante la última etapa de este doctorado he tenido la suerte de conocer a Teresa, gracias a ella, a su cariño y apoyo el finalizar la Tesis no ha sido tan duro.

CONTENTS

Chapter I

Introduction

The activity of biomolecules is function of their shapes, which are in turn determined by inter- and intramolecular interactions,[1,2] corresponding in most of the cases to hydrogen bonding (HB).[3-5] The presence of water in the biological environment is of special importance, not only as a solvent but as an active component. For example, the crystals of proteins can be considered as a highly concentrated solution with ≈ 20-50% of the total volume occupied by water.[6] The small size of water and its double donor/acceptor capabilities give water a particular flexibility to form hydrogen bonds, which have a central role in the solvation processes. These subtle non-covalent forces may control different kind of phenomena, such as conformational[7,8] or tautomeric equilibria,[9,10] charge stabilization,[11,12] or molecular recognition,[13,14] and may influence the structure, dynamics and function of biomolecules.[15,16]

It has been observed that water inserts between the carbonyl and amino functional groups in α–helices and is involved in the protein folding process.[17-20] On it, the protein minimizes the interaction with water of the hydrophobic chains located in the core, where the main interaction is the peptide hydrogen bond N–H···O=C. On the other hand, the polar side chains are located on the surface, exposed to interactions with water. It has been reported that water plays also a determinant function in the nucleation of protein folding as a mediator in the formation of the peptide hydrogen bond.

The effect of the interaction with water on different kind of molecules has been extensively studied in condensed phases by ^{1}H-NMR,[21-23] X-Ray spectroscopy,[24,25] or IR spectroscopy.[26-29] However, the understanding at a molecular level of the role of the subtle non-covalent interactions forces responsible for solvation requires isolating the molecules from the condensed phase environment to study them in the gas phase with a controlled hydration degree. This environment, in which a limited number of molecules of water interact with another molecule (the solute) in isolation is called microsolvation. Microsolvation is a consolidated field of research, as shown by the number of works[30-33] dedicated to bring light on it. Pioneering studies in the gas phase on molecules with biological interest were performed by electronic spectroscopy coupled with supersonic expansion.[34-37] In microwave spectroscopy, detailed works with molecules and clusters of different nature have set the basis for the research on hydrogen bond complexes,[38-42] opening the possibility to study many structural aspects of microsolvation.

Rotational spectroscopy coupled with supersonic expansion has proved to be an adequate experimental tool to characterize microsolvated complexes.[43] These microsolvated complexes can be easily generated in the supersonic expansion and further studied in an isolated environment[34,44-47] to determine their intrinsic properties. Complexes with different degrees of hydration can be formed in the supersonic expansion, furthermore, the number of water molecules in the complexes can be somehow controlled through the expansion conditions. The spacing between the rotational levels is intimately related to the mass distribution within the molecule or complex. Therefore the molecular structures obtained from rotational spectroscopy are characterized by its high accuracy. An important aspect of the microsolvation studies using rotationally resolved spectroscopy is the possibility to determine the rotational constants for a variety of isotopologues, allowing to derive accurate molecular structures by different approaches.[48,49] Coordinates, distances and angles for the water molecules can be directly obtained for conformers and clusters, so it is possible to obtain information about the evolution of distances and angles from the bare molecule to the first steps of solvation.

Apart from accurate structures, microwave spectroscopy techniques provide other relevant molecular properties. From their high-resolution it is possible to precisely determine the values for the nuclear quadrupole coupling constants determined by the presence in many biomolecules of certain nuclei as ^{14}N, which give rise to a hyperfine structure in the spectrum.[50,51] Those constants are related to the electric field gradient at the N nucleus and thus to the electronic environment. As a consequence, they can serve to reveal the subtle polarization changes occurring upon microsolvation. The information obtained from rotational spectra is not limited to static structural properties, in many cases, it is possible to obtain information about dynamical motions associated with tunneling effects. An example of this kind of dynamics that can be measured from the microwave spectra is the internal rotation for systems presenting an internal rotation top,[52,53] and to determine the barriers hindering the rotation. Internal rotation shows a high dependence on the structure around the rotating top,[54] and therefore, it is possible to correlate the values for the internal rotation barrier with structural changes occurring from isolation to microsolvation.

Microsolvation studies on small organic molecules by rotational spectroscopy,[8-10,55-69] provide a better knowledge about the solvent interactions in larger biomolecules,[70] showing the interplay existing between self-association and solvation. The majority of those studies have been done for monohydrated complexes, giving information about dynamics of water and characterizing the preferred sites of interaction. When increasing the number of water molecules, it is possible to obtain new information, such as the role of HB cooperativity in the solvation process,[4] the contribution to the stabilization of weak interactions apart from HB,[67,69] or the way in which solvation induces structural changes.[68]

In most cases, water self-association dominates the interactions since water molecules tend to link to other water molecules forming chains or cycles, as occurs in complexes where there is only one HB acceptor group.[66,67,69] However, in molecules with two donor/acceptor positions, as amides,[55-59] acids[60-63] or esters,[64,65] water molecules tend to close donor-acceptor-donor sequential cycles. The observation by microwave spectroscopy of organic molecules microsolvated by more than two molecules of water is complicated, and just a few examples have been reported.[61,62,67,69] This is noticeable since the research on pure water clusters[71-80] has significantly advanced with the development of microwave spectroscopy techniques in supersonic jets.[45,46]

The importance of HB cooperativity contributing to the stabilization of hydrated biomolecules has been widely described in the literature.[81-83] σ-bond cooperativity is associated with complexes forming chains or cycles such as the -OH group or any other group capable of acting simultaneously as hydrogen donor and acceptor.[3,4] When water molecules establish hydrogen bonds, they become polarized, enhancing their hydrogen donor and hydrogen acceptor capacity and further strengthening the interactions they involve in. σ-cooperativity has been described in detail elsewhere,[3,4] its main effects are the shortening of the HB distances and an increase in the HB stabilization energy. These effects are stronger as the number of cooperative molecules increase.

In amides as the peptide group, another kind of effect has been reported to occur when those participate in HB, which causes a polarization of the molecule.[3,4] This is represented by a major contribution of the partially charged resonant structures (see Scheme 1.1), further enhancing its donor/acceptor capabilities. The main effect of this polarization is the shortening of the C–N bond, due to a major double bond contribution, and the enlargement of the C=O bond, due to a major presence of the single bond resonant form. In addition, if the peptide bond has any substitution group, they can participate in the resonance interaction, extending the polarization effects over a wider range of groups in the molecule, as occurs in carbamates, which are ester-derivatives of amides (see Scheme 1.2).

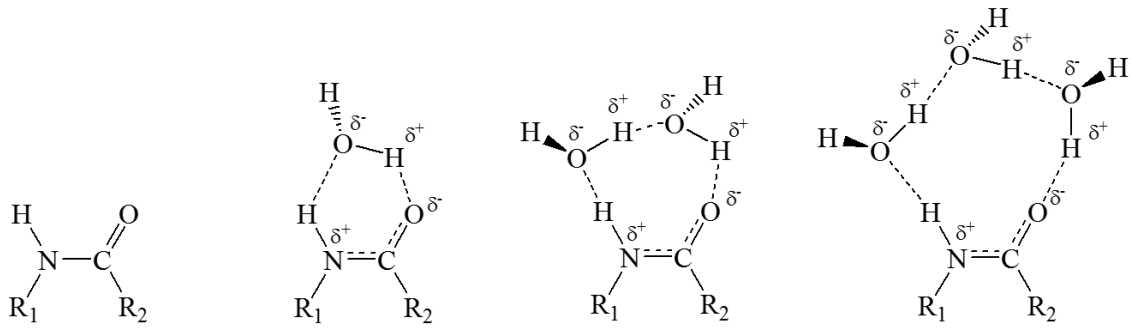

Scheme 1.1. Resonant contributing forms for peptide groups water complexes. Formamide: $R_{1,2}$ = H. Formanilide: R_1 = phenyl, R_2 = H. Methyl carbamate: R_1 = H, R_2 = O–CH_3. Ethyl carbamate: R_1 = H, R_2 = O–C_2H_5.

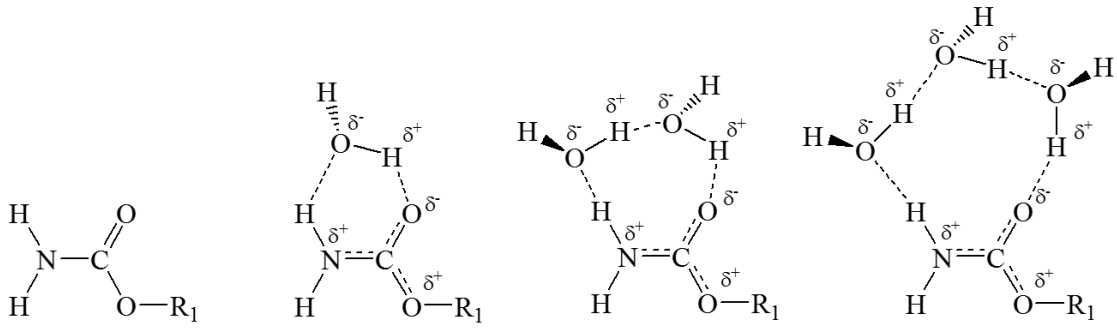

Scheme 1.2. Additional resonant contributing forms for carbamates water complexes. Methyl carbamate: R_1 = O–CH_3. Ethyl carbamate: R_1 = O–C_2H_5.

Thus, HB interactions are enhanced by resonance with the π–delocalized conjugated system, the so-called Resonance Assisted Hydrogen Bonding (RAHB), which in some works has been named π-cooperativity.[84-86] RAHB is a synergistic mechanism that causes the reinforcement of

both HB and π–delocalization, being the effects stronger as the number of cooperative HBs increases.[84,85] For the peptide linkage, π-cooperative bonding was first pointed out to occur in X-ray crystallographic studies of small amides.[86,87] RAHB cooperative effects have been also described for chains of amide molecules, stabilizing the secondary structure of proteins.[88] The polarization effects due to RAHB have been rarely observed in the gas phase.[56]

The changes in the C–N and C=O distances associated with π-cooperativity are usually in the limit of detection of usual methods due to vibrational effects, and therefore it is challenging to determine directly whether those changes occur or not. This missing experimental information can be supplied however by other properties directly determinable from the rotational spectra. One of such properties is the nuclear quadrupole coupling of ^{14}N present in amide groups. As has been mentioned above, it is possible to resolve the hyperfine structure and determine the associated nuclear quadrupole coupling constants, which are related to the electric field gradient and the electronic environment at the coupled nucleus.[51] These constants are very sensitive to the small changes associated with inductive cooperative effects. The electric field gradient has been in turn attributed to the unequal filling of the valence shell *p* orbitals in the coupling nucleus,[51] thus, it is possible to expect a possible correlation between the nuclear quadrupole coupling constant and the unbalanced 2*p* electronic charge obtained from Natural Bond Orbital analysis.[89] The inductive cooperative effects could be demonstrated by analyzing the tendencies in the values of the nuclear quadrupole coupling constants from isolation to the complexes with increasing hydration degrees, and consequently, quadrupole coupling constants could be used as a probe of the subtle effects due to π-cooperativity. A second probe of the RAHB effects could be the values of the internal rotation parameters of groups as methyl directly bonded to some of the amide group atoms.

Investigations by microwave spectroscopy of monohydrated and dihydrated complexes of different amides,[55-59] have led to remarkable pieces of information, as the preference of water to interact with the carbonyl group. This Thesis presents the microsolvation study of amides with different substitutes (see Figure 1.1) with the aim to model the local interactions between water and the peptide bond in different situations. Subsequent objectives in this work were i) to extend the previous studies to microsolvated complexes with additional water or solute molecules, ii) to characterize the structural changes due to HB cooperative effects, whereas those associated to σ-cooperativity are well known, the inductive polarization effects associated to π-cooperativity are less understood, iii) to determine the relation between the nuclear quadrupole coupling constants and the subtle effects caused by polarization, iv) to explore the HB interactions occurring between peptide groups, which has not received much attention in the gas phase.

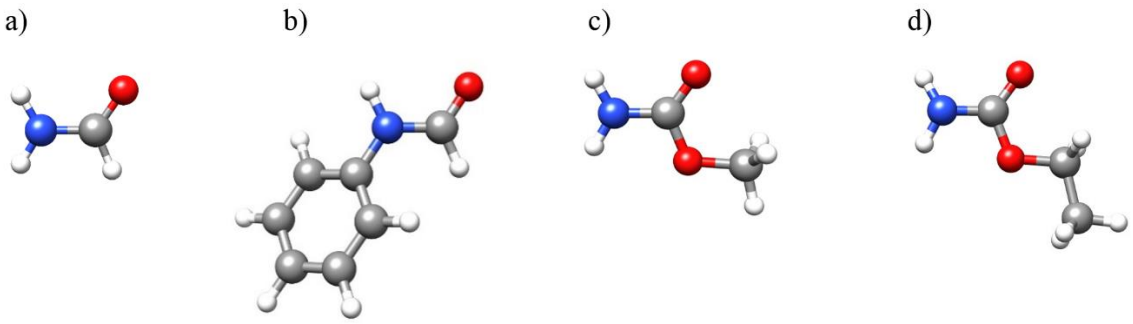

Figure 1.1. Amides for which microsolvated complexes have been studied in this work. a) Formamide. b) Formanilide. c) Methyl carbamate. d) Ethyl carbamate.

The experimental studies carried out are presented in the corresponding chapters within this Thesis, following a brief description of them will be given.

Formamide$_2$···(H$_2$O)[90]
Hydrogen-Bond Cooperativity in Formamide$_2$-Water: A Model for Water Mediated Interactions.
Susana Blanco, Pablo Pinacho, Juan Carlos López.
Angewandte Chemie International Edition, 2016, **55**, 9331–9335.

Formamide is the simplest amide, and thus it can be taken as a reference system. Its microsolvated complexes with one and two molecules of water have been already described in detail.[55,58] It presents diverse interaction sites, and its complexes with water can model the interaction with water of the *cis* and *trans* peptide linkage.

Our aim by studying this molecule was to extend the understanding of microsolvation to complexes increasing the number of molecules of formamide. We focused the search on a complex in which water acts as a bridge between two formamide molecules involving three hydrogen bonds (see Figure 1.2). The interest of searching for this complex lies in that it presents a unique hydrogen bond network that could serve to model the amide-water, amide-amide and amide-amide water-mediated interactions. The study of this complex could lead to a better understanding of the interplay between microsolvation and self-association.

We took special care in trying to determine very accurately the structure of the complex and the nuclear quadrupole coupling constants to test their possible use as a probe of the subtle inductive effects associated to π-cooperativity combining the results with the previous ones.[58]

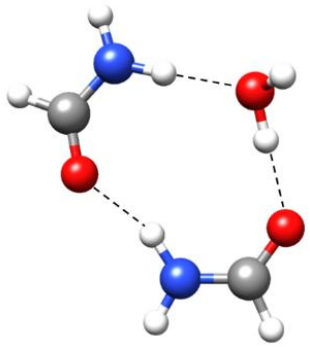

Figure 1.2. The formamide$_2$···(H$_2$O) complex.

Formamide···(H$_2$O)$_3$[91]
Structure and Dynamics in Formamide-(H$_2$O)$_3$: A Water Pentamer Analogue.
Susana Blanco, Pablo Pinacho, Juan Carlos López.
The Journal of Physical Chemistry Letters, **2017**, 8, 6060–6066.

After the detection of formamide$_2$···(H$_2$O), we searched for the most stable complex of formamide with three molecules of water since hitherto no complex of this type has been reported for amides. In this complex, water molecules are supposed to interact with the amide group closing a 10-membered sequential cycle (see Figure 1.3), and could be considered as a continuation of the monohydrated and dihydrated complexes of formamide showing similar

interactions with an extended network. Thus, the microsolvation of formamide···$(H_2O)_3$ could serve as a model of the interactions between water and the peptide bond in a *cis* arrangement.

In this context, we wanted to explore its planarity or not, and similarities between its structure and dynamics with those of pure water clusters $(H_2O)_n$ n = 2–5.[71-76] We wanted to continue the investigation of π-cooperative effects and the use of the nuclear quadrupole constants as a probe for the effects associated to polarization, in planar or not planar complexes.

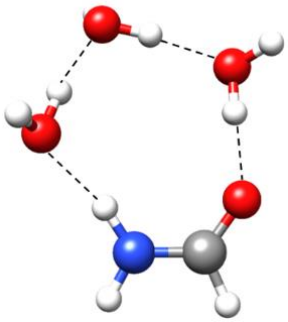

Figure 1.3. The most stable configuration for the formamide···$(H_2O)_3$ complex.

Formanilide···$(H_2O)_n$ n = 1,2
Manuscript in preparation.

The bonding between peptides occurs through amide linkages that can adopt *cis* or *trans* dispositions, regarding the relative arrangement of the amino and carbonyl groups, being the *trans*–peptide link much more represented in nature.

Formanilide, or N-phenylformamide (see Figure 1.4) exists in two conformations in the gas phase,[92] with the peptide group in *cis* or *trans* arrangement that model the peptide group arrangement in large systems. We proposed the investigation of its water complexes in the gas phase with microwave spectroscopy to model the local interactions of water with both forms of the peptide bond, and to find the main differences between them.

An interesting point we wanted to study was the possible alteration on the structures of formanilide forms as the number of water molecules increases. The *cis* arrangement is not planar, and its complexes are expected not to alter significantly the angle between the phenyl and the amide groups. Opposite, the *trans* arrangement is planar, and the sterical impediment of the phenyl ring blocks the possibility to form sequential cycles as in formamide.

We also wanted to continue the investigation of π-cooperativity in complexes of amides and the use of the nuclear quadrupole constants as a probe for the effects associated to polarization, in planar and not planar complexes.

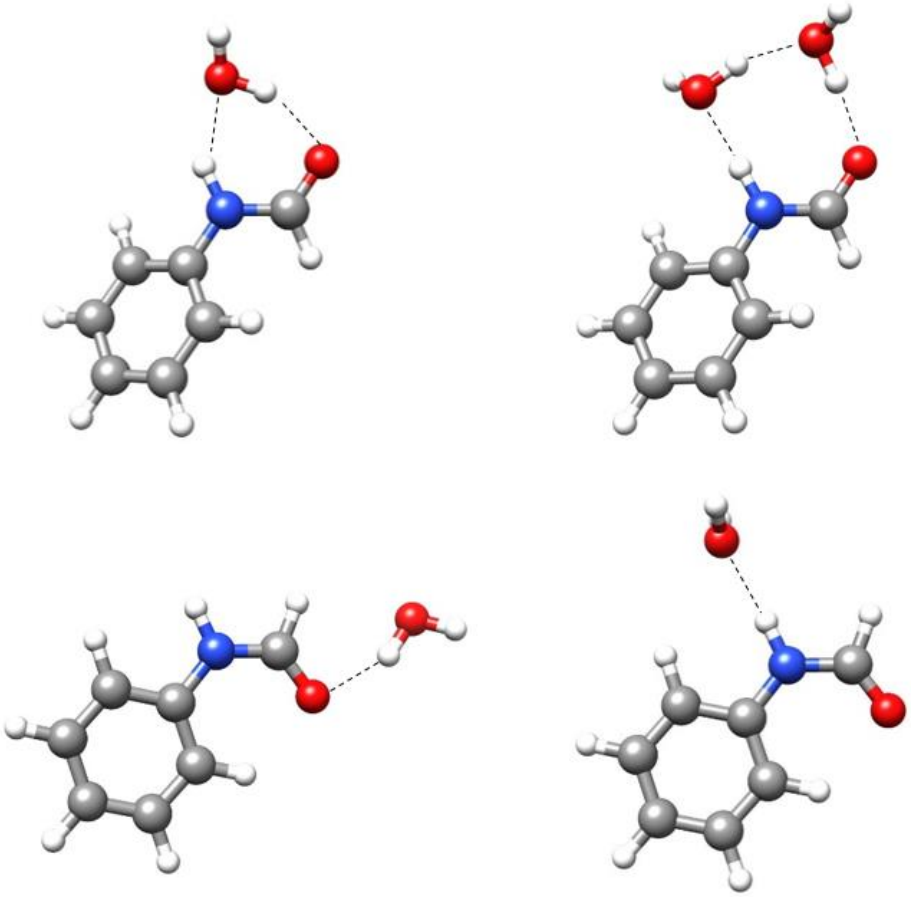

Figure 1.4. The most stable monohydrated and dihydrated complexes of formanilide for *cis* (up) and *trans* (down) conformations.

Methyl carbamate···$(H_2O)_n$ n = 1,2
Manuscript in preparation.

Methyl carbamate is an ester-derivative of an amide (see Figure 1.5). The aim for investigating its microsolvated complexes was to model the HB interactions with a substituted *cis*-peptide bond. The starting point for the search were complexes showing similar interactions as those in formamide and formanilide.

Methyl carbamate presents a heavy atom planar skeleton, and the water molecules in the complexes are expected to dispose in the plane of methyl carbamate. Therefore, these complexes could continue the investigation of quadrupole coupling as a probe of the π-cooperative effects started in previous studies.

Another main goal of this study was trying to find experimental evidence showing that the barrier to internal rotation can be a probe of RAHB effects. In this context, we searched for a correlation between nuclear quadrupole constants and internal rotation.

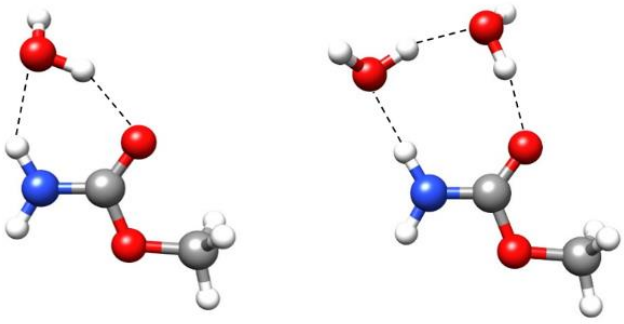

Figure 1.5. The complexes of methyl carbamate - water.

Ethyl carbamate···$(H_2O)_n$ n = 1,2,3
Manuscript in preparation.

Ethyl carbamate (see Figure 1.6) presents two conformations, planar and non-planar, that can be interconverted through a periodical potential function with a low barrier. This causes the observation of both conformers in a supersonic expansion to depend on the carrier gas used due to conformational relaxation in the supersonic jet.

The aim of investigating its microsolvation complexes was, apart from modelling the interactions of water with the carbamate group, to study the influence or not of water microsolvation in the corresponding conformational equilibrium.

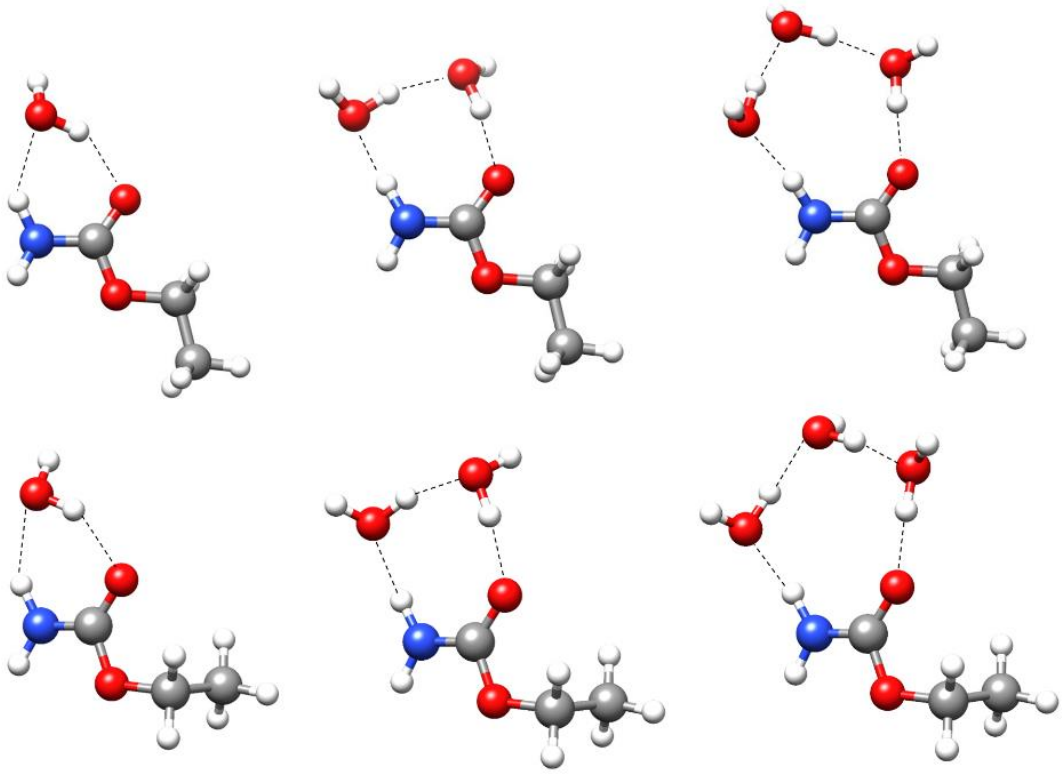

Figure 1.6. Complexes of ethyl carbamate I (up) and II (down) with up to three water molecules.

Ibuprofen···(H_2O)
Manuscript in preparation.

Ibuprofen is one of the most popular medicines, it presents a carboxylic acid group. We searched for the microsolvated complex with the aim of model the local interaction between water and acids in larger molecules.

The starting point of the investigation were the monohydrated complexes for the four ibuprofen monomer conformations previously studied in the gas phase.[93] The aim was to observe the complexes with the four rotamers, characterize them, and to analyze the possible influence of water on the conformational equilibrium. It is expected that water molecule closes a cycle with the carboxylic group, as depicted in Figure 1.7.

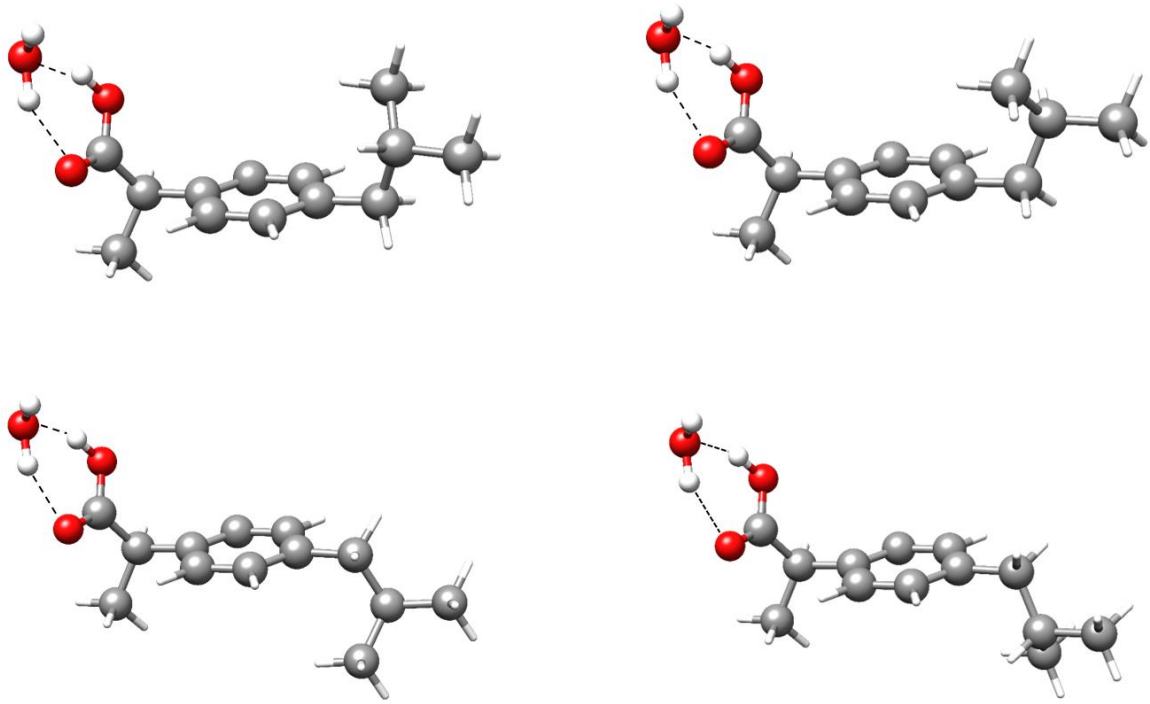

Figure 1.7. The predicted most stable complexes of water with the four rotamers observed for ibuprofen.

References

[1] Hofacker G.L. “Intra- and Intermolecular Interactions” in *Biophysics*, eds. Hoppe W., Lohmann W., Markl H., Ziegler H. Springer, Berlin, 1982.
[2] Baker, E. N., Hubbard, R. E. “Hydrogen bonding in globular proteins” *Prog. Biophys. Mol. Biol.*, **1984**, 44, 97–179.
[3] Saenger, W., Jeffrey, G. A. *Hydrogen Bonding in Biological Structures*, Springer-Verlag, Berlin, 1991.
[4] Jeffrey, G. A. *An Introduction to Hydrogen Bonding*, Oxford University Press, Oxford, 1997.
[5] McNaught, A. D., Wilkinson, A. *IUPAC, Compendium of Chemical Terminology (The "Gold Book")*, 2nd ed., Blackwell Scientific Publications, Oxford, 1997.
[6] Saenger, W. “Structure and Dynamics of Water Surrounding Biomolecules” *Ann. Rev. Biophys. Chem.*, **1987**, 16, 93–114.
[7] Schmitt, M., Böhm, M., Ratzer, C., Vu, C., Kalkman, I., Meerts, W. L. “Structural Selection by Microsolvation: Conformational Locking of Tryptamine” *J. Am. Chem. Soc.*, **2005**, 127, 10356–10364.
[8] Caminati, W., López, J. C., Blanco, S., Mata, S., Alonso, J. L. “How Water Links to *Cis* and *Trans* Peptidic Groups: The rotational Spectrum of N-Methylformamide-Water” *Phys. Chem. Chem. Phys.*, **2010**, 12, 10230–10234.
[9] Maris, A., Ottaviani P., Caminati, W. “Pure Rotational Spectrum of 2-Pyridone···Water and Quantum Chemical Calculations on the Tautomeric Equilibrium 2-Pyridone···Water/2-Hydroxypyridine···Water” *Chem. Phys. Lett.*, **2002**, 360, 155–160.
[10] Mata, S., Cortijo, V., Caminati, W., Alonso, J. L., Sanz, M. E., López, J. L., Blanco, S. “Tautomerism and Microsolvation in 2-Hydroxypyridine/2-Pyridone” *J. Phys. Chem. A*, **2010**, 114, 11393–11398.
[11] Wyttenbach, T., Paizs, B., Barran, P., Breci, L., Liu, D., Suhai, S., Wysocki, V. H., Bowers, M. T. “The Effect of the Initial Water of Hydration on the Energetics, Structures, and H/D Exchange Mechanism of a Family of Pentapeptides: An Experimental and Theoretical Study” *J. Am. Chem. Soc.*, **2003**, 125, 13768–13775.
[12] Xu, S. J., Nilles, M., Bowen, K. H., “Zwitterion Formation in Hydrated Amino Acid, Dipole Bound Anions: How Many Water Molecules Are Required?” *J. Chem. Phys.*, **2003**, 119, 10696–10701.
[13] Robinson, C. R., Sligar, S. G. “Molecular Recognition Mediated by Bound Water: A Mechanism for Star Activity of the Restriction Endonuclease *Eco*RI” *J. Mol. Biol.*, **1993**, 234, 302–306.
[14] Jayaram, B., Jain, T. A. “The Role of Water in Protein-DNA Recognition” *Annu. Rev. Biophys. Biomol. Struct.*, **2004**, 33, 343–361.
[15] Levy, Y., Onuchic, J. N. “Water Mediation in Protein Folding and Molecular Recognition” *Annu. Rev. Biophys. Biomol. Struct.*, **2006**, 35, 389–415.
[16] Biedermannová, L., Schneider, B. “Hydration of Proteins and Nucleic Acids: Advances in Experiment and Theory. A Review” *Biochimica et Biophysica Acta*, **2016**, 1860, 1821–1835.
[17] Groot, B. L., Grubmüller, H. “Water Permeation across Biological Membranes: Mechanism and Dynamics of Aquaporin-1 and GlpF” *Science*, **2001**, 294, 2353–2357.
[18] Ball, P. “Water as an Active Constituent in Cell Biology” *Chem. Rev.*, **2008**, 108, 74–108.
[19] Venkatachalam, C. M. “Stereochemical criteria for Polypeptides and Proteins. V. Conformation of a System of Three Linked Peptide Units” *Biopolymers*, **1968**, 6, 1425–1436.
[20] Chaplin, M. “Do We Underestimate the Importance of Water in Cell Biology?” *Nat. Rev. Mol. Cell Biol.*, **2006**, 7, 861–866.
[21] Modig, K., Liepinsh, E., Otting, G., Halle, B. “Dynamics of Protein and Peptide Hydration” *J. Am. Chem. Soc.*, **2004**, 126, 102–114.
[22] Nucci, N. V., Pometun, M. S., Wand, A. J. “Site-Resolved Measurement of Water-Protein Interactions by Solution NMR” *Nat. Struct. Mol. Biol.*, **2011**, 18, 245–249.
[23] Hilser, V. J. “Structural Biology: Finding the Wet Spots” *Nature*, **2011**, 469, 166–167.
[24] Egli, M., Portmann, S., Usman, N. “RNA Hydration: A Detailed Look” *Biochemistry*, **1996**, 35, 8489–8494.
[25] Schotte, F., Lim, M., Jackson, T. A., Smirnov, A. V., Soman, J., Olson, J. S., Phillips Jr, G. N., Wulff, M., Anfinrud, P. A. “Watching a Protein as it Functions with 150-ps Time-Resolved X-Ray Crystallography” *Science*, **2003**, 300, 1944–1947.
[26] Nibbering, E. T. J., Elsaesser, T. “Ultrafast Vibrational Dynamics of Hydrogen Bonds in the Condensed Phase” *Chem. Rev.*, **2004**, 104, 1887–1914.
[27] Bakker, H. J., Skinner, J. L. “Vibrational Spectroscopy as a Probe of Structure and Dynamics in Liquid Water” *Chem. Rev.*, **2010**, 110, 1498–1517.

[28] Tielrooij, K. J., García-Araez, N., Bonn, M., Bakker, H. J. "Cooperativity in Ion Hydration" *Science*, **2010**, 328, 1006–1009.
[29] Perera, A. S., Thomas, J., Poopari, M. R., Xu, Y. "The Clusters-in-a-Liquid Approach for Solvation: New Insights from the Conformer Specific Gas Phase Spectroscopy and Vibrational Optical Activity Spectroscopy" *Front. Chem.*, **2016**, 4, 1–17.
[30] *Chem. Rev.*, **2016**, 116, Issue 9 "Noncovalent interactions", 4911–5688.
[31] *Chem. Rev.*, **2016**, 116, Issue 13 "Water – The most anomalous liquid", 7459–7726.
[32] Bagchi, B. *Water in Biological and Chemical Processes: From structure and Dynamics to Function*, Cambridge University Press, Cambridge, 2013.
[33] Gerhards, M. "Spectroscopy of Neutral Peptides in the Gas Phase: Structure, reactivity, Microsolvation, Molecular Recognition*"* in *Principles of Mass Spectrometry Applied to Biomolecules*, eds. Laskin, J., Lifshitz, C., 2006.
[34] Levy, D. H. "Laser Spectroscopy of Cold Gas-Phase Molecules" *Annu. Rev. Phys. Chem.*, **1980**, 31, 197–225.
[35] Rizzo, T. R., Park, Y. D., Petenau, L., Levy, D. H. "Electronic Spectrum of the Amino Acid Tryptophan Cooled in a Supersonic Molecular Beam" *J. Chem. Phys.*, **1985**, 83, 4819–4820.
[36] Philips, L. A., Levy, D. H. "The Rotationally Resolved Electronic Spectrum of Indole in the Gas Phase" *J. Chem. Phys.*, **1986**, 85, 1327–1332.
[37] Philips, L. A., Levy, D. H. "Rotationally Resolved Electronic Spectroscopy of Tryptamine Conformers in a Supersonic Jet" *J. Chem. Phys.*, **1988**, 89, 85–90.
[38] Legon, A. C., Soper, P. D., Flygare, W. H. "The Rotational Spectrum, H, ^{19}F Nuclear Spin-Nuclear Spin Coupling, D Nuclear Quadrupole Coupling, and Molecular Geometry of a Weakly Bound Dimer of Carbon Monoxide and Hydrogen Fluoride" *J. Chem. Phys.*, **1981**, 74, 4944–4950.
[39] Legon, A. C., Aldrich, P. D., Flygare, W. H. "The Rotational Spectrum, Chlorine Nuclear Quadrupole Coupling Constants, and Molecular Geometry of a Hydrogen-Bonded Dimer of Cyclopropane and Hydrogen Chloride" *J. Am. Chem. Soc.*, **1982**, 104, 1486–1490.
[40] Legon, A. C., Millen, D. J. "Gas-Phase Spectroscopy and the Properties of Hydrogen-Bonded Dimers: HCN···HF as the Spectroscopic Prototype" *Chem. Rev.*, **1986**, 86, 635–657.
[41] Kisiel, Z., Fowler, P. W., Legon, A. C. "Investigation of the Rotational Spectrum of the Hydrogen-Bonded Dimer Formed between Methylenecyclopropane and HCl" *J. Chem. Phys.*, **1994**, 101, 4635–4643.
[42] Legon, A. C. "Prereactive Complexes of Dihalogens XY with Lewis Bases B in the Gas Phase: A Systematic Case for the Halogen Analogue B···XY of the Hydrogen Bond B···HX" *Angew. Chem. Int. Ed.*, **1999**, 38, 2686–2714.
[43] Becucci, M., Melandri, S. "High-Resolution Spectroscopic Studies of Complexes Formed by Medium-Size Organic Molecules" *Chem. Rev.*, **2016**, *116*, 5014–5037.
[44] Levy, D. H. "The Spectroscopy of Very Cold Gases" *Science*, **1981**, 214, 263–269.
[45] Miller, D. R. "Free Jet Sources" in *Atomic and Molecular Beam Methods* ed. Scoles, G. Oxford University press, Oxford, 1988, Volume 1, pp. 14–53.
[46] Montero, S., Maté, B., Tejeda, G., Fernández, J. M., Ramos, A. "Raman Studies of Free Jet Expansion" in *Atomic and Molecular Beams. The state of Art 2000* ed. Campargue, R. Springer-Verlag, Berlin, 2001, pp. 295–306.
[47] Maté, B., Graur, I. A., Elizarova, T., Chirokov, I., Tejeda, G., Fernández, J. M., Montero, S. "Experimental and Numerical Investigation of an Axisymmetric Supersonic Jet" *J. Fluid Mech.*, **2001**, 426, 177–197.
[48] Domenicano, A., Hargittai, I. *Accurate Molecular Structures: Their Determination and Importance* Oxford University Press, New York, 1992.
[49] Demaison, J. "Accurate Structures of Non-Rigid Molecules by Microwave Spectroscopy" in *Structures and Conformations of Non-Rigid Molecules* eds. Laane, J., Dakkouri, M., van der Veken, B., Oberhammer, H. Springer, Dordrecht, 1993, Volume 410, pp. 239–256.
[50] Braag, J. K. "The Interaction of Nuclear Electric Quadrupole Moments with Molecular Rotation in Asymmetric-Top Molecules. I" *Phys. Rev.*, **1948**, 74, 533–538.
[51] Gordy, W., Cook, R. L. *Microwave Molecular Spectra*, Wiley-Interscience, New York, 1984.
[52] Lin, C. C., Swalen, J. D. "Internal Rotation and Microwave Spectroscopy" *Rev. Mod. Phys.*, **1959**, 31, 841–892.
[53] Lister, D. G., Macdonald, J. N., Owen, N. L. "Internal Rotation and Inversion. An Introduction to Large Amplitude Motions in Molecules" Academic Press, London, 1978.

[54] Herschbach, D. R. "Calculation of Energy Levels for Internal Torsion and Over-All Rotation. III" *J. Chem. Phys.*, **1959**, 31, 91–108.
[55] Lovas, F. J., Suenram, R. D., Fraser, G. T., Gillies, C. W., Zozom, J. "The Microwave Spectrum of Formamide-Water and Formamide-Methanol Complexes" *J. Chem. Phys.*, **1988**, 88, 722–729.
[56] Held, A., Pratt, D. W. "Hydrogen Bonding in Water Complexes. Structures of 2-Pyridone-H_2O and 2-Pyrididone-$(H_2O)_2$ in Their S_0 and S_1 Electronic States" *J. Am. Chem. Soc.*, **1993**, 115, 9708–9717.
[57] Lavrich, R. J., Tubergen, M. J. "Conformation and Hydrogen Bonding in the Alaninamide-Water van der Waals Complex" *J. Am. Chem. Soc.*, **2000**, 122, 2938–2943.
[58] Blanco, S., López, J. C., Lesarri, A., Alonso, J. L. "Microsolvation of Formamide: A Rotational Study" *J. Am. Chem. Soc.*, **2006**, 128, 12111–12121.
[59] López, J. C., Sanchez, R., Blanco, S., Alonso, J. L. "Microsolvation of 2-Azetidinone: A Model for the Peptide Group-Water Interactions" *Phys. Chem. Chem. Phys.*, **2015**, 17, 2054–2066.
[60] Canagaratna, M., Phillips, J. A., Ott, M. E. Leopold, K. R. "The Nitric-Acid Complex: Microwave Spectrum, Structure and Tunneling" *J. Phys. Chem. A*, **1998**, 102, 1489–1497.
[61] Ouyang, B., Starkey, T. G., Howard, B. J. "High-Resolution Microwave Studies of Ring-Structured Complexes between Trifluoroacetic Acid and Water" *J. Phys. Chem. A*, **2007**, 111, 6165–6175.
[62] Ouyang, B., Howard, B. J. "Hydrates of *Trans*- and *Gauche*-Difluoroacetic Acids: A High-Resolution Microwave Spectroscopic Study" *J. Phys. Chem. A*, **2010**, 114, 4109–4117.
[63] Schnitzler, E. G., Jäger, W. "The Benzoic Acid-Water Complex: A Potential Atmospheric Nucleation Precursor Studied Using Microwave Spectroscopy and *Ab Initio* Calculations" *Phys. Chem. Chem. Phys.*, **2014**, 16, 2305–2314.
[64] Thomas, J., Sukhorukov, O., Jäger, W., Xu, Y. "Direct Spectroscopic Detection of the Orientation of Free OH Groups in Methyl Lactate-$(Water)_{1,2}$ Clusters: Hydration of a Chiral Hydroxy Ester" *Angew. Chem. Int. Ed.*, **2014**, 53, 1156–1159.
[65] Gall, J. T. A., Thomas, J., Xie, F., Wang, Z., Jäger, W., Xu, Y. "Rotational Spectroscopy of the Methyl-Glycidate-Water Complex: Conformation and Water and Methyl Rotor Tunneling Motions" *Phys. Chem. Chem. Phys.*, **2017**, 19, 29508–29515.
[66] Su, Z., Xu, Y. "Hydration of a Chiral Molecule: The Propylene Oxide···$(Water)_2$ Cluster in the Gas Phase" *Angew. Chem. Int. Ed.*, **2007**, *119*, 6275–6278.
[67] Pérez, C., Neill, J. L., Muckle, M. T., Zaleski, D. P., Peña, I., López, J. C., Alonso, J. L., Pate, B. H. "Water-Water and Water-Solute Interactions in Microsolvated Organic Complexes" *Angew. Chem. Int. Ed.*, **2014**, 54, 979–982.
[68] Pérez, C., López, J. C., Blanco, S., Schnell, M. "Water-Induced Structural Changes in Crown Ethers from Broadband Rotational Spectroscopy" *J. Phys. Chem. Lett.*, **2016**, *7*, 4053–4058.
[69] Pérez, C., Krin, A., Steber, A. L., López, J. C., Kisiel, Z., Schnell, M. "Wetting Camphor: Multi-Isotopic Substitution Identifies the Complementary Roles of Hydrogen Bonding and Dispersive Forces" *J. Phys. Chem. Lett.*, **2016**, *7*, 154–160.
[70] Bellissent-Funel, M.-C.; Hassanali, A.; Havenith, M.; Henchman, R.; Pohl, P.; Sterpone, F.; van der Spoel, D.; Xu, Y.; Garcia, A. E. "Water Determines the Structure and Dynamics of Proteins" *Chem. Rev.*, **2016**, 116, 7673–7697.
[71] Dyke, T. R.; Mack, K. M.; Muenter, J. S. "The Structure of Water Dimer from Molecular Beam Electric Resonance Spectroscopy" *J. Chem. Phys.*, **1977**, 66, 498–510.
[72] Keutsch, F. N.; Cruzan, J. D.; Saykally, R. J. "The Water Trimer" *Chem. Rev.*, **2003**, 103, 2533–2577.
[73] Cruzan, J. D.; Braly, L. B.; Liu, K.; Brown, M. G.; Loeser, J. G.; Saykally, R. J. "Quantifying Hydrogen Bond Cooperativity in Water: VRT Spectroscopy of the Water Tetramer" *Science*, **1996**, 271, 59–62.
[74] Liu, K.; Brown, M. G.; Cruzan, J. D.; Saykally, R. J. "Vibration-Rotation Tunneling Spectra of the Water Pentamer: Structure and Dynamics" *Science*, **1996**, 271, 62–64.
[75] Ramírez, F.; Hadad, C. Z.; Guerra, D.; David, J.; Restrepo, A. "Structural Studies of the Water Pentamer" *Chem. Phys. Lett.*, **2011**, 507, 229–233.
[76] Cole, W. T. S.; Fellers, R. S.; Viant, M. R.; Saykally, R. J. "Hydrogen Bond Breaking Dynamics in the Water Pentamer: Terahertz VRT Spectroscopy of a 20 μm Libration" *J. Chem. Phys.*, **2017**, 146, 14306.
[77] Pérez, C., Muckle, M. T., Zaleski, D. P., Seifert, N. A., Temelso, B., Shields, G. C., Kisiel, Z., Pate, B. H. "Structures of Cage, Prism, and Book Isomers of Water Hexamer from Broadband Rotational Spectroscopy" *Science*, **2012**, 336, 897–901.
[78] Richardson, J. O., Pérez, C., Lobsiger, S., Reid, A. A., Temelso, B., Shields, G. C., Kisiel, Z., Wales, D. J., Pate, B. H., Althorpe, S. C. "Concerted Hydrogen-Bond Breaking by Quantum Tunneling in the Water Hexamer Prism" *Science*, **2016**, 351, 1310–1313.

[79] Pérez, C., Lobsiger, S., Seifert, N. A., Zaleski, D. P., Temelso, B., Shields, G. C., Kisiel, Z., Pate, B. H. "Broadband Fourier Transform Rotational Spectroscopy for Structure Determination: The Water Heptamer" *Chem. Phys. Lett.*, **2013**, 571, 1–15.
[80] Pérez, C., Zaleski, D. P., Seifert, N. A., Temelso, B., Shields, G. C., Kisiel, Z., Pate, B. H. "Hydrogen Bond Cooperativity and the Three-Dimensional Structures of Water Nonamers and Decamers" *Angew. Chem. Int. Ed.*, **2014**, 53, 14368–14372.
[81] Del Bene, J. E. "Molecular Orbital Theory of the Hydrogen Bond. 18. Methyl Substituent Effects on Amide Hydrogen Bonding" *J. Am. Chem. Soc.*, **1978**, 100, 1387–1394
[82] Liang, W., Li, H., Hu, X., Han, S. "Proton Transfer of Formamide + *n*H2O (*n* = 0-3): Protective and Assistant Effect of the Water Molecule" *J. Phys. Chem. A*, **2004**, 108, 10219–10224.
[83] Venkataramanan, N. S. "Cooperativity of Intermolecular Hydrogen Bonds in Microsolvated DMSO and DMF Clusters: A DFT, AIM, and NCI Analysis" *J. Mol. Model*, **2016**, 22, 151–162.
[84] Gilli, G., Bellucci, F., Ferretti, V., Bertolasi, V. "Evidence for Resonance-Assisted Hydrogen Bonding from Crystal-Structure Correlations on the Enol Form of the *β*–Diketone Fragment" *J. Am. Chem. Soc.*, **1989**, 111, 1023–1028.
[85] Bertolasi, V., Gilli, P., Ferretti, V., Gilli, G. "Evidence for Resonance-Assisted Hydrogen Bonding. 2. Intercorrelation between Crystal Structure and Spectroscopic Parameters in Eight Intramolecularly Hydrogen Bonded 1,3.Diaryl-1,3-propanedione Enols" *J. Am. Chem. Soc.*, **1991**, 113, 4917–4925.
[86] Gilli, P., Bertolasi, V., Ferretti, V., Gilli, G. "Evidence for Intramolecular N-H···O Resonance Assisted Hydrogen Bonding in *β*-Enaminones and Related Heterodienes. A Combined Crystal-Structural, IR, and NMR Spectroscopic, and Quantum-Mechanical Investigation" *J. Am. Chem. Soc.*, **2000**, 122, 10405–10417.
[87] Ottersen, T. "On the structure of the Peptide Linkage. The Structures of Formamide and Acetamide at -165 Degrees C and an *Ab Initio* Study of Formamide, Acetamide and N-methylformamide" *Acta Chemica Scandinavica*., **1975**, 29a, 939–944.
[88] Kobko, N., Dannenberg, J. J. "Cooperativity in Amide Hydrogen Bonding Chains. Relation between Energy, Position, and H-Bond Chain in Peptide and Protein Folding Models" *J. Phys. Chem. A*, **2003**, 107, 10389–10395.
[89] Reed, A. E., Weinstock, R. B., Weinhold, F. "Natural Population Analysis" *J. Chem. Phys.*, **1985**, *83*, 735–746.
[90] Blanco, S., Pinacho, P., López, J. C. "Hydrogen-Bond Cooperativity in Formamide$_2$-Water: A Model for Water Mediated Interactions" *Angew. Chem. Int. Ed.*, 2016, **55**, 9331–9335.
[91] Blanco, S., Pinacho, P., López, J. C. "Structure and Dynamics in Formamide-$(H_2O)_3$: A Water Pentamer Analogue" *J Phys. Chem. Lett.*, **2017**, 8, 6060–6066.
[92] Blanco, S., López, J. C., Lesarri, A., Caminati, W., Alonso, J. L. "Conformational Equilibrium of Formanilide: Detection of the Pure Rotational Spectrum of the Tunnelling C*is* Conformer" *Mol. Phys.*, **2005**, 103, 1473-1479.
[93] Betz, T., Zinn S., Schnell, M. "The Shape of Ibuprofen in the Gas Phase" *Phys. Chem. Chem. Phys.*, **2015**, 17, 4538–4541.

Chapter II

Methodology

2.1 Introduction

Spectroscopy is defined by IUPAC as "the study of physical systems by the electromagnetic radiation with which they interact or that they produce".[1] It is an experimental discipline that studies the resonant or non-resonant interaction between the electromagnetic spectrum and the quantized states that matter presents at the microscopic scale. The application of Quantum Mechanics to analyze the spectrum obtained by spectroscopic techniques, allows us to obtain the energy for those quantized states, which are closely related to the molecular structures and the dynamics of the system.[2,3] This work is focused on rotational spectroscopy which uses microwave radiation lying in the centimeter-wave (1-30 GHz), in the millimeter-wave (30-300 GHz) and in the submillimeter-wave (>300 GHz) regions. The quantum-mechanical description of the mechanisms of molecular rotation can be found in the bibliography[4-8] and only a concise description focused on molecular rotation will be given here.

2.2 Rotational Spectroscopy

2.2.1 Rigid-Rotor Hamiltonian

The analysis of the microwave spectrum begins by obtaining the energies for the rotational levels. For a system at the microscopic scale, the quantized energy for the states can be calculated as the eigenvalues of the Hamiltonian operator in the Schrödinger equation:

$$\hat{H}\psi = E\psi$$

Considering the Born-Oppenheimer approximation, the nuclear Hamiltonian takes into account expressions for the kinetic and potential energies for the nuclei of the system and is a sum of the translation, vibrational and rotational motions. In a particular axis system with origin fixed at the center of mass, the rotational Hamiltonian can be approximately separated from the vibrational term. For a rotating system formed by *i* particles, each one with mass m_i and spatial coordinates x_i, y_i, z_i in a Cartesian axis system with origin fixed at the center of mass, the rotational kinetic energy is:

$$E_{\mathrm{rot}} = \frac{1}{2}\vec{\omega}^t I \vec{\omega} = \frac{1}{2}\left[I_{\mathrm{xx}}\omega_{\mathrm{xx}}^2 + I_{\mathrm{yy}}\omega_{\mathrm{yy}}^2 + I_{\mathrm{zz}}\omega_{\mathrm{zz}}^2 + 2I_{\mathrm{xy}}\omega_{\mathrm{x}}\omega_{\mathrm{y}} + 2I_{\mathrm{xz}}\omega_{\mathrm{x}}\omega_{\mathrm{z}} + 2I_{\mathrm{yz}}\omega_{\mathrm{y}}\omega_{\mathrm{z}}\right]$$

where $\omega_{\alpha\beta}$ (α,β = *x*, *y* or *z*) are the components of the angular velocity vector for the system in rotation, and $I_{\alpha\beta}$ (α,β = *x*, *y* or *z*) the components of the inertia tensor. The tensor of inertia can be written in matrix representation:

$$\begin{pmatrix} I_{\mathrm{xx}} & I_{\mathrm{xy}} & I_{\mathrm{xz}} \\ I_{\mathrm{yx}} & I_{\mathrm{yy}} & I_{\mathrm{yz}} \\ I_{\mathrm{zx}} & I_{\mathrm{zy}} & I_{\mathrm{zz}} \end{pmatrix}$$

The diagonal components are the moments of inertia and the non-diagonal elements are the products of inertia. The tensor of inertia depends on the masses of the particles and their spatial disposition:

$$I_{xx} = \sum_i m_i \left(y_i^2 + z_i^2\right) \qquad I_{yy} = \sum_i m_i \left(x_i^2 + z_i^2\right) \qquad I_{zz} = \sum_i m_i \left(x_i^2 + y_i^2\right)$$
$$I_{yx} = I_{xy} = \sum_i m_i \left(x_i y_i\right) \qquad I_{zx} = I_{xz} = \sum_i m_i \left(x_i z_i\right) \qquad I_{zy} = I_{yz} = \sum_i m_i \left(y_i z_i\right)$$

Any rotating system (molecule or cluster) has a characteristic inertia ellipsoid (Figure 2.1) defined by three semiaxes, each one proportional to the reciprocal of the square root of the correspondent moment of inertia.

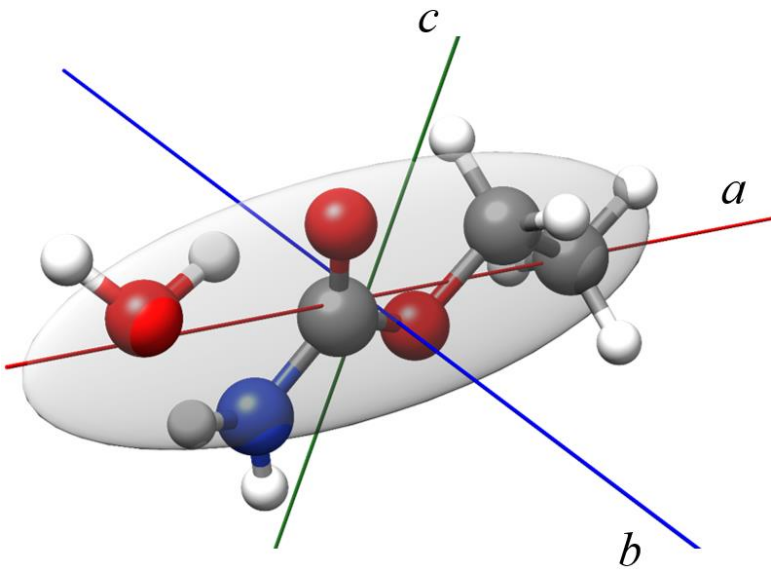

Figure 2.1. The inertial ellipsoid (transparent gray) for ethyl carbamate I – water-a complex (see Chapter VIII), an almost prolate top ($\kappa \approx -0.97$), with the *a*, *b* and *c* inertial axes.

To simplify the solution we can choose the axes in such a manner that the products of inertia become zero and the matrix results in a diagonal tensor. For each molecular system, there is a unique definition of the axes that fulfill this criterion, they are called the principal axes of inertia, labeled *a*, *b* and *c*, so that $I_a \leq I_b \leq I_c$. The values of the principal moments of inertia allow classifying the molecules as:

- Linear tops ($I_a = 0$, $I_b = I_c$).
- Spherical tops ($I_a = I_b = I_c$).
- Oblate symmetric tops ($I_a = I_b < I_c$).
- Prolate symmetric tops ($I_a < I_b = I_c$).
- Asymmetric tops ($I_a < I_b < I_c$).

In the principal axis system the rotational energy takes the form:

$$E_{\text{rot}} = \frac{1}{2}\left[I_a \omega_a^2 + I_b \omega_b^2 + I_c \omega_c^2\right]$$

This expression can be written in function of the angular momentum components ($\vec{J} = I\vec{\omega}$):

$$E_{\text{rot}} = \frac{1}{2}\left[\frac{J_a^2}{I_a} + \frac{J_b^2}{I_b} + \frac{J_c^2}{I_c}\right]$$

The quantum mechanical equivalent to $\vec{J}$ is the angular momentum operator $\hat{J}$. The operators of the angular momentum components in the molecule-fixed system are related to the overall angular momentum operator by $\hat{J}^2 = \hat{J}_x^2 + \hat{J}_y^2 + \hat{J}_z^2$. Therefore, the rigid-rotor Hamiltonian results:

$$\hat{H}_{\text{rig}}\psi = E_{\text{rot}}\psi$$

$$\hat{H}_{\text{rig}} = \frac{\hbar^2\hat{J}_a^2}{2I_a} + \frac{\hbar^2\hat{J}_b^2}{2I_b} + \frac{\hbar^2\hat{J}_c^2}{2I_c} = A\hat{J}_a^2 + B\hat{J}_b^2 + C\hat{J}_c^2$$

where $A = \hbar^2/2I_a$, $B = \hbar^2/2I_b$ and $C = \hbar^2/2I_c$ are the rotational constants.

The Hamiltonian commutes with $\hat{J}^2$. For symmetric tops, $\hat{J}_z$, the angular momentum operator component along the *z* axis in the principal axis system and $\hat{J}^2$ commute, that is, they have a common set of eigenfunctions because they are defined simultaneously. Furthermore, $\hat{J}_Z$, the angular momentum operator component along the *Z* axis in the laboratory system and $\hat{J}^2$ also commute because $\hat{J}^2$ is independent of the coordinate system chosen. This implies that there exist a common set of four eigenfunctions $\psi_{J,K,M}$ for the operators. Each operator has a correspondent eigenvalue (k_J, k_K and k_M) which are the solutions for the eigenvalue equation. Using bracket notation ($\psi_{J,K,M} \equiv \langle J, K, M|$):

$$\langle J, K, M|\hat{J}^2|J, K, M\rangle = k_J = \hbar^2 J(J+1)$$

$$\langle J, K, M|\hat{J}_z|J, K, M\rangle = k_K = K\hbar$$

$$\langle J, K, M|\hat{J}_Z|J, K, M\rangle = k_M = M\hbar$$

The eigenvalues of these equations are the quantized values of the energy for a wave function defined by the three quantum numbers *J*, *K*, and *M*. Quantum number *J* is related to the total rotational angular momentum of the system and takes 0 or any positive integer value. *K* and *M* are related to the projections of the angular momentum over the molecule-fixed axis z or over the laboratory-fixed axis Z respectively. Both *K* and *M* can take any integer value from –*J* to +*J*. All the levels with K ≠ 0 are doubly degenerated. It is possible to rearrange the Hamiltonian to be only a function of $\hat{J}^2$, $\hat{J}_z$, and $\hat{J}_Z$. From the quantum numbers simple expressions for the energy, and therefore for the frequencies can be obtained.

Asymmetric tops represent a different situation. Only *J* and *M* are good quantum numbers and it is not possible to solve directly the Schrödinger equation. To obtain the energy levels, the wave functions for an asymmetric top are described by a linear combination of the symmetric top functions and the problem is solved using a linear variational method. The energy levels for an asymmetric top obtained by this procedure can be correlated to the levels of the symmetric top limits as described in Diagram 2.1. The energy levels are not labeled with the *K* quantum number as in symmetric tops, but with two pseudo-quantum numbers, K_{-1} and K_{+1} which describe the values of *K* in the corresponding limits, prolate (K_{-1}) and oblate (K_{+1}).[6-9]

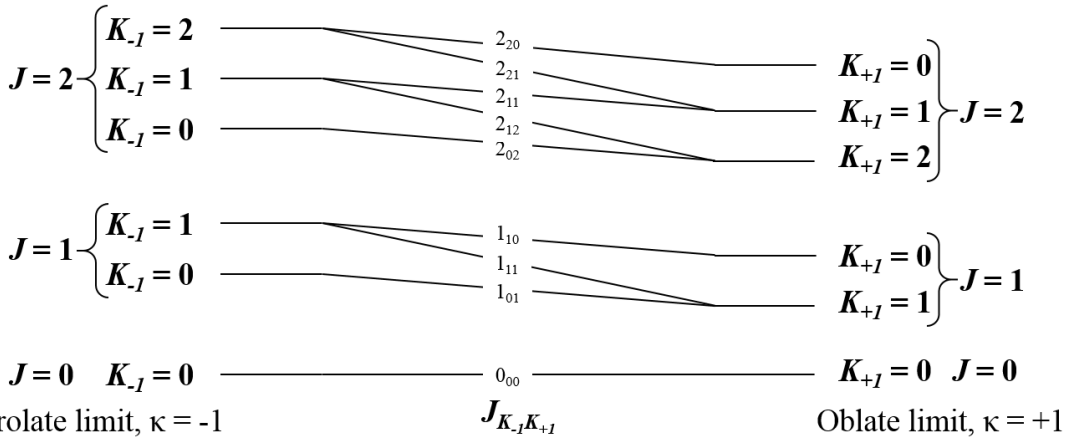

Diagram 2.1. Correlation diagram for the asymmetric top energy levels with those of the symmetric rotor in the prolate and oblate limits. Only the three lowest *J* levels are depicted.

Asymmetric tops present 2*J*+1 rotational levels for each value of *J*. Each rotational level is degenerated in 2*J*+1 levels for each value of *M*, but the quantization on *M* is only relevant in the presence of an external electric field. The degree of asymmetry of a molecular system can be evaluated by the value of the asymmetry parameter of Ray,[6,10] $\kappa = (2B\text{-}A\text{-}C)/(A\text{-}C)$ which can take values from -1 to +1. The limit situations correspond to the prolate ($B = C$, $\kappa = -1$) and the oblate ($A = B$, $\kappa = +1$) symmetric tops.

2.2.2 Distortable-Rotor Hamiltonian

The rigid-rotor model is an approximation in which molecules are treated as point nuclei held by rigid-bonds. However, the frequencies observed experimentally present shifts from those predicted by the rigid-rotor, being the differences larger with increasing *J*. This effect can be explained by the centrifugal distortion forces that elongate the bonds, changing the values of the moments of inertia. Therefore, chemical bonds are better represented as springs, with a finite restoring force, that can be distorted according to the rotation of the molecule. In order to obtain more accurate frequencies, it is needed to introduce correcting terms to the rotational Hamiltonian taking into account for the centrifugal distortion forces.[11-13] The Hamiltonian including up to sixth-order correction in the angular momentum operator terms centrifugal distortion constants is of the form:

$$\hat{H}_{\mathrm{rot}} = \hat{H}_{\mathrm{rig}} + \frac{\hbar^4}{4}\sum_{\alpha\beta\gamma\delta}\tau_{\alpha\beta\gamma\delta}\hat{J}_\alpha\hat{J}_\beta\hat{J}_\gamma\hat{J}_\delta + \hbar^6\sum_{\alpha\beta\gamma\delta\varepsilon\eta}\tau_{\alpha\beta\gamma\delta\varepsilon\eta}\hat{J}_\alpha\hat{J}_\beta\hat{J}_\gamma\hat{J}_\delta\hat{J}_\varepsilon\hat{J}_\eta$$

where α, β, γ, δ, ε and η in the summations can take any value of *a*, *b* or *c* coordinates in the principal axis system. It has been demonstrated thanks to symmetry and commutation properties that the number of those terms can be reduced to six terms for the fourth-order and 10 for the sixth-order corrections, being not possible to determine experimentally all those terms.[6,13] Watson demonstrated that only five linear combinations of the fourth-order and seven combinations of the sixth-order can be determined. Watson also proposed two possible combinations of terms giving rise to the reduced Hamiltonians usually used to analyze the centrifugal distortion, the S (symmetric) and the A (asymmetric) reductions.[5,14] Watson´s A reduced Hamiltonian in the I^r representation up to the sixth-order correction is of the form:

$$\hat{H}_{\mathrm{rot}} = \hat{H}_{\mathrm{rig}} + \hat{H}_{\mathrm{dis}}^{(4)} + \hat{H}_{\mathrm{dis}}^{(6)}$$

$$\hat{H}_{\mathrm{rig}}^{(\mathrm{A})} = A^{(\mathrm{A})}\hat{J}_a^2 + B^{(\mathrm{A})}\hat{J}_b^2 + C^{(\mathrm{A})}\hat{J}_c^2$$

$$\hat{H}_{\mathrm{dis}}^{(4)} = -\Delta_J\hat{J}^4 - \Delta_{JK}\hat{J}^2\hat{J}_a^2 - \Delta_K\hat{J}_a^4 - 2\delta_J\hat{J}^2(\hat{J}_b^2 - \hat{J}_c^2) - \delta_K[\hat{J}_a^2(\hat{J}_b^2 - \hat{J}_c^2) + (\hat{J}_b^2 - \hat{J}_c^2)\hat{J}_a^2]$$

$$\hat{H}_{\mathrm{dis}}^{(6)} = \Phi_J\hat{J}^6 + \Phi_{JK}\hat{J}^4\hat{J}_a^2 + \Phi_{KJ}\hat{J}^2\hat{J}_a^4 + \Phi_K\hat{J}_a^6 + 2\phi_J\hat{J}^4(\hat{J}_b^2 - \hat{J}_c^2) + \phi_{JK}\hat{J}^2[\hat{J}_a^2(\hat{J}_b^2 - \hat{J}_c^2) + (\hat{J}_b^2 - \hat{J}_c^2)\hat{J}_a^2] + \phi_K[\hat{J}_a^4(\hat{J}_b^2 - \hat{J}_c^2) + (\hat{J}_b^2 - \hat{J}_c^2)\hat{J}_a^4]$$

where Δ_J, Δ_{JK}, Δ_K, δ_J and δ_K are the quartic centrifugal distortion constants and Φ_J, Φ_{JK}, Φ_{KJ}, Φ_K, ϕ_J, ϕ_{JK} and ϕ_K are the sextic centrifugal distortion constants in the A reduction. However, if the system is very close to the symmetric top limits the A reduction may not be appropriate since δ_K, which depends on (*B*-*C*) in the denominator gets very large values.[6] In this situation the S reduction may result in a better description of the centrifugal forces. Watson´s S reduced Hamiltonian in the I^r representation up to the sixth-order energy terms is of the form:

$$\hat{H}_{\mathrm{rig}}^{(\mathrm{S})} = A^{(\mathrm{S})}\hat{J}_a^2 + B^{(\mathrm{S})}\hat{J}_b^2 + C^{(\mathrm{S})}\hat{J}_c^2$$

$$\hat{H}_{\mathrm{dis}}^{(4)} = -D_J\hat{J}^4 - D_{JK}\hat{J}^2\hat{J}_a^2 - D_K\hat{J}_a^4 + d_1\hat{J}^2(\hat{J}_+^2 + \hat{J}_-^2) + d_2(\hat{J}_+^4 + \hat{J}_-^4)$$

$$\hat{H}_{\mathrm{dis}}^{(6)} = +H_J\hat{J}^6 + H_{JK}\hat{J}^4\hat{J}_a^2 + H_{KJ}\hat{J}^2\hat{J}_a^4 + H_K\hat{J}_a^6 + h_1\hat{J}^4(\hat{J}_+^2 + \hat{J}_-^2) + h_2\hat{J}^2(\hat{J}_+^4 + \hat{J}_-^4) + h_3(\hat{J}_+^6 + \hat{J}_-^6)$$

being $\hat{J}_\pm = (\hat{J}_b \pm i\hat{J}_c)$ and where D_J, D_{JK}, D_K, d_1 and d_2 are now the quartic and H_J, H_{JK}, H_{KJ}, H_K, h_1, h_2 and h_3 the sextic centrifugal distortion constants.

From the analysis of the frequencies observed experimentally, it is possible to determine the values of the centrifugal distortion constants. Transitions between rotational levels with high values of *J* usually help to better determine the values of the fourth-order or sixth-order centrifugal distortion constants since the centrifugal distortion effects are larger with increasing *J*.

2.2.3 Nuclear quadrupole

The majority of the molecules studied in this work present a nitrogen atom. The most abundant isotope of nitrogen (≈ 99.6%), ^{14}N, has a nuclear spin angular momentum $I = 1$, that is, it presents a non-spherical distribution of the nuclear charge and a non-vanishing electric quadrupole moment, *eQ*. The nuclear quadrupole moment interacts with the electric field gradient created by the molecular charges at the nucleus, when the molecule or the cluster rotates in an external-field-free environment, and gives rise to the coupling between the nuclear spin angular momentum ($\vec{I}$) and the molecule rotational angular momentum ($\vec{J}$) to give a total angular momentum, $\vec{F}$, ($\vec{F} = \vec{J} + \vec{I}$). This angular momentum is quantized by the quantum number *F* that can take values $F = J + I, J + I - 1, \ldots, |J - I|$ (see Figure 2.2). The spectrum of molecular systems presenting quadrupole coupling shows a characteristic hyperfine structure pattern as a result of the splitting of each rotational transition into the several $F' \leftarrow F''$ allowed components.

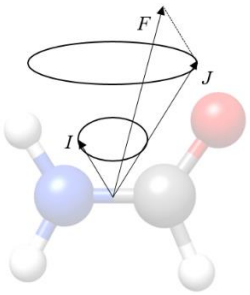

$$\vec{F} = \vec{J} + \vec{I}$$

$$F = J + I, J + I - 1, \ldots, |J - I|,$$

Figure 2.2. Schematic coupling of the nuclear spin angular momentum (*I*) with the molecular rotational angular momentum (*J*) in formamide.

The Hamiltonian for these systems needs a term to account for the nuclear quadrupole coupling from the Hamiltonian previously described:

$$\hat{H} = \hat{H}_{\mathrm{rot}} + \hat{H}_{\mathrm{q}}$$

$$\hat{H}_{\mathrm{q}} = \frac{eQq_j}{2J(2J-1)I(2I-1)}\left[\frac{3}{4}C(C+1) - J(J+1)I(I+1)\right]$$

$$C = F(F+1) - J(J+1) - I(I+1)$$

being eQ the nuclear quadrupole moment, and q_{j} represent the average field gradient in the direction of the axis on which $\vec{J}$ has maximum projection in the Cartesian axis system. The tensor q_{j} can be expressed in the principal axis system by a transformation that depends on the asymmetry of the molecule.[15] In the principal axis system its components are:

$$q_{\alpha\beta} = \frac{\partial^2 V}{\partial\alpha\partial\beta}$$

The $q_{\alpha\beta}$ (α,β = *a*, *b* or *c*) coefficients, are directly related to the nuclear quadrupole coupling constants $\chi_{\mathrm{ij}} = eQq_{\mathrm{ij}}$, which are the parameters that can be actually fitted from the analysis of the hyperfine structure observed in high-resolution rotational spectroscopy. The nuclear quadrupole coupling tensor in the principal axis system takes the form:

$$\chi = \begin{pmatrix} \chi_{\mathrm{aa}} & \chi_{\mathrm{ab}} & \chi_{\mathrm{ac}} \\ \chi_{\mathrm{ba}} & \chi_{\mathrm{bb}} & \chi_{\mathrm{bc}} \\ \chi_{\mathrm{ca}} & \chi_{\mathrm{cb}} & \chi_{\mathrm{cc}} \end{pmatrix}$$

For ^{14}N, usually only the diagonal elements of the quadrupole coupling tensor can be obtained from the experimental transitions available. The diagonal elements satisfy the rule: $\chi_{\mathrm{aa}} + \chi_{\mathrm{bb}} + \chi_{\mathrm{cc}} = 0$, implying that only two of them are linearly independent, and only two values can be resolved from the hyperfine structure of the spectrum. The value of those constants allows discriminating between conformers with similar rotational constants but with different electronic distribution around the quadrupolar nucleus.[16]

Molecules with two nuclei with quadrupole moment.

If there are two nuclei with quadrupole moment, the coupling scheme is more complex. Two coupling schemes are possible depending on the amplitude of the coupling of the nuclei.[15,17,18] The Bardeen-Townes scheme,[17] considers that the coupling of one of the nucleus is much larger

than the other, then, the nuclear spin angular momentum of the first nucleus, $\vec{I}_1$ couples with $\vec{J}$ resulting $\vec{F}_1$. The nuclear spin angular momentum of the second nucleus, $\vec{I}_2$ couples then with $\vec{F}_1$ to give $\vec{F}$ (see Figure 2.3a). The possible values F_1 and F can take are: $F_1 = J + I_1, J + I_1 - 1, \ldots, |J - I_1|$, and $F = F_1 + I_2, F_1 + I_2 - 1, \ldots, |F_1 - I_2|$.[17]

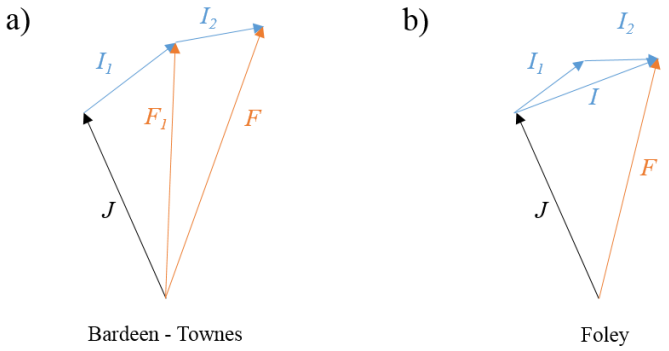

Figure 2.3. Coupling schemes for a system with two nuclei having quadrupole moment. a) Bardeen – Townes scheme,[17] considering the coupling of I_1 to be larger than that of I_2. b) Foley scheme,[18] considering both couplings of similar magnitude.

The Foley scheme[18] is adopted when the two nuclei have similar quadrupole moment coupling, as happens for systems with two ^{14}N atoms, the nuclear spin angular momentum of both nuclei, $\vec{I}_1$ and $\vec{I}_2$, couples first giving a total spin angular momentum, $\vec{I}$ (see Figure 2.3b). This couples then with $\vec{J}$ giving the total $\vec{F}$. The possible values for I and F are: $I = I_1 + I_2, I_1 + I_2 - 1, \ldots, |I_1 - I_2|$, and $F = J + I, J + I - 1, \ldots, |J - I|$.[18]

2.2.4 Selection rules

The Hamiltonian described so far implements distortable-rotor and nuclear quadrupole coupling corrections for an asymmetric top. It gives the energies for the rotational levels but it does not provide information whether a transition involving two levels is allowed or forbidden. A molecular system will be active in rotational spectroscopy if it has at least one non-zero component of the electric dipole moment. Asymmetric tops may have non-zero values for the three components of the dipole moment on each of the principal axes, thus, rotational transitions may be of *a*-, *b*- or *c*-type. A rotational transition $\left(J'_{K'_{-1},K'_{+1}} \leftarrow J''_{K''_{-1},K''_{+1}}\right)$ is permitted when the transition moment integral not vanishes.[6]

$$\left\langle J'_{K'_{-1},K'_{+1}} \middle| \mu_\alpha \middle| J''_{K''_{-1},K''_{+1}} \right\rangle \neq 0$$

This integral do not vanish when $J' = J''$ or $J' = J'' \pm 1$. Therefore, rotational transitions are only allowed for $\Delta J = 0, \pm 1$, giving rise to the P ($\Delta J = -1$), Q ($\Delta J = 0$) or R ($\Delta J = 1$) branches.

In the transition moment integral, μ_α (α = *a*, *b* or *c*) is the projection of the electric dipole moment on the principal axes. It is possible to evaluate by symmetry whether this integral vanishes or not. When the direct product of the irreducible symmetric representation of the integrands contains the totally symmetric representation for the point group of the inertia ellipsoid (D_2), the integral will not vanish.

$$\Gamma_{J'_{K'_{-1},K'_{+1}}} \otimes \Gamma_{\mu_\alpha} \otimes \Gamma_{J''_{K''_{-1},K''_{+1}}} \subseteq A$$

The electric dipole moment components, μ_α (α = *a*, *b* or *c*), will belong to the corresponding B_α (α = *a*, *b* or *c*) reducible representations for the D_2 point group (see Table 2.1). Therefore, we need only to evaluate the symmetry of the initial and the final levels to know if the direct product contains the totally symmetric representation. The symmetry classification of any level can be given in terms of the parity (even or odd) of the pseudo-quantum numbers, K_{-1} and K_{+1}. Table 2.1 gives the symmetry classification for an asymmetric top:

Table 2.1. Symmetry classification of the rotational levels for an asymmetric top for the D_2 point group indicated by the parity (e = even, o = odd) of K_{-1} and K_{+1}.

Γ	μ_α	Rotation	Parity $K_{-1}K_{+1}$.
A			*ee*
B_a	μ_a	R_a	*eo*
B_b	μ_b	R_b	*oo*
B_c	μ_c	R_c	*oe*

The selection rules in terms of the parity, or the allowed changes in K_{-1} and K_{+1} are collected in Table 2.2 and an example is depicted in Diagram 2.2.

Table 2.2. Selection rules for an asymmetric top in terms of the parity and the allowed changes in K_{-1} and K_{+1}.

Transition	Selection rule
P-branch	$\Delta J = -1$
Q-branch	$\Delta J = 0$
R-branch	$\Delta J = +1$

	Allowed changes		Allowed transitions
a-type	$\Delta K_{-1} = 0, \pm2, \ldots$	$\Delta K_{+1} = \pm1, \pm3, \ldots$	*ee* ↔ *eo; oe* ↔ *oo*
b-type	$\Delta K_{-1} = \pm1, \pm3, \ldots$	$\Delta K_{+1} = \pm1, \pm3, \ldots$	*ee* ↔ *oo; oe* ↔ *eo*
c-type	$\Delta K_{-1} = \pm1, \pm3, \ldots$	$\Delta K_{+1} = 0, \pm2, \ldots$	*ee* ↔ *oe; eo* ↔ *oo*

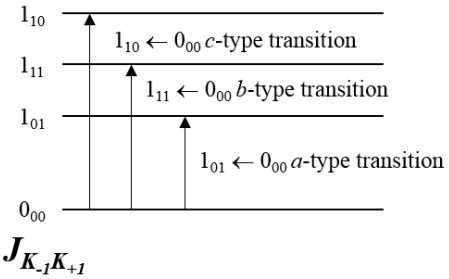

Diagram 2.2. *a*-, *b*- and *c*-type rotational transitions for an asymmetric rotor involving the 0_{00} level.

Besides this, there is an additional selection rule for the hyperfine transitions due to nuclear quadrupole coupling, which is $\Delta F = 0, \pm1$.

2.2.5 Large amplitude motions

It is possible, and a quite common situation for molecular systems, that vibrational motions lead the molecules in several equivalent configurations. All the equivalent configurations, having the same energy, correspond to minima in the potential energy surface (PES) along the vibrational coordinate (see Figure 2.4). The interconversion between them passes through at least one maximum that represents the value of the hindering barrier. The motions connecting the minima in the potential functions correspond to large amplitude motions.[4,6]

Large amplitude motions are vibrational motions with a low mechanical frequency. Furthermore, some vibrational transitions may lie in the radiofrequency, in the microwave or in the far-infrared regions. The vibrational spacing is not constant, in molecules with *n* equivalent minima in the potential energy function, the levels below the barrier or close to it, appear in groups of *n* levels. In the limit of an infinite barrier, the levels are degenerated. For barriers with finite values, this degeneration is broken and the levels appear to be split in *n* components according to the symmetry of the motion. The magnitude of the separation of the doublets is sensitive to the hindering barrier height and width, as those in Figure 2.4 for a double minimum potential function. Experimentally, this may be observed as a fine structure of the rotational spectrum. In a supersonic expansion (see Chapter III - Instrumentation), the rotational and vibrational temperatures are cooled down, and the molecules populate mainly the lowest energy states. Therefore, it is possible to observe the corresponding doublets in the spectrum.[6]

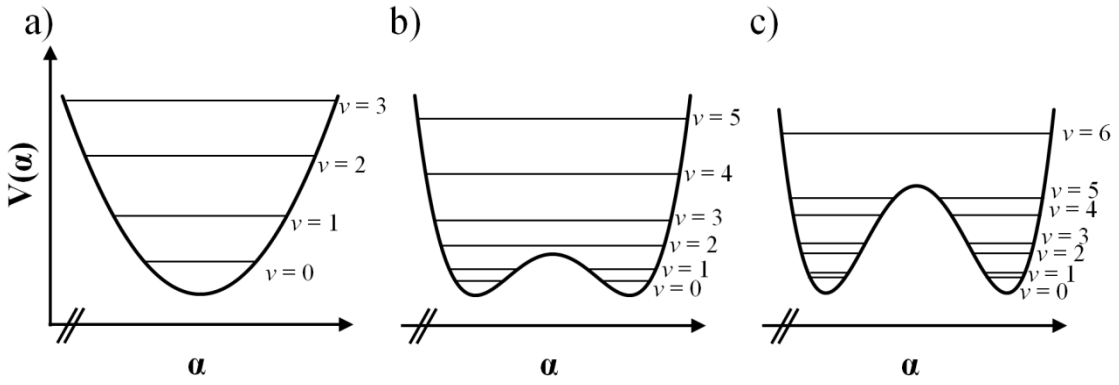

Figure 2.4. Schematic potential energy functions (cross sections of PES) showing the spacing between vibrational levels for a) a harmonic function with one minimum, b) a low hindering barrier, and c) a moderately high hindering barrier for the interconversion of two equivalent forms arising from a large amplitude motion.

There are large amplitude motions of different nature. Inversion, internal rotation, ring-puckering or pseudorotation among others can be identified as large amplitude motions. In this work, we have studied molecular systems presenting hindered internal rotation of a methyl group in the methylcarbamate$\cdots(H_2O)_n$ (n =1, 2 and 3) clusters, an almost-free internal rotation of a molecule of water in the *trans*-formanilide$\cdots(H_2O)$ Ic cluster and a complex motion resulting in the inversion of the structure for the formamide$\cdots(H_2O)_3$ complex. Hence a further description on these motions will be presented.

2.2.5.1 Internal rotation

Internal rotation is a vibration in which the motion connecting the *n* equivalent forms is the rotation of one part of the molecule (internal top) with respect to the rest of the molecule[19,20] (molecular frame). The coordinate that describes the motion is the internal rotation angle (α). This motion is hindered by a barrier. The potential function is symmetric and periodic in the angle α. If the barrier is low enough, the system may move from one minimum to another through tunneling effect. The levels below the barrier or close to it, are split into *n* components as discussed above.

We have studied the hindered internal rotation of a $–CH_3$ methyl group, which lead to a three-fold potential energy function with three equivalent minima and three equivalent maxima (see Figure 2.5). This potential function can be expressed in a cosine series:[6,19]

$$V(\alpha) = \frac{1}{2}V_3(1 - cos3\alpha) + \frac{1}{2}V_6(1 - cos6\alpha) + \ ...$$

where V_3 and V_6 are the three-fold and six-fold barriers. Usually only the first term (V_3) is considered and the other terms in the series are neglected in a first approximation to the problem.

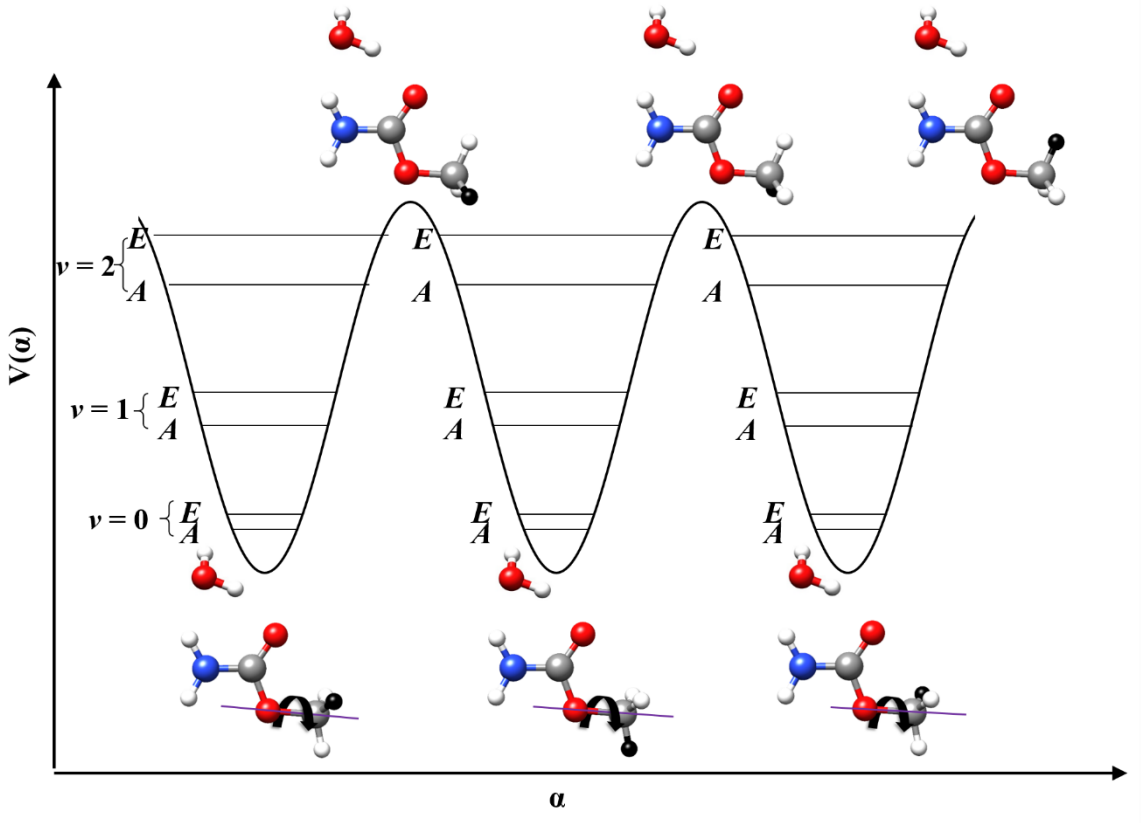

Figure 2.5. Schematic potential function energy for the internal rotation of the methyl group by an angle α along the internal axis (purple) for the methyl carbamate water-a complex (see Chapter VII). The potential function is depicted showing the corresponding minimum and maximum forms and the *A*-*E* splitting of each vibrational state.

If the three-fold potential barrier is low-enough, the levels are split into a non-degenerated *A* component and a doubly-degenerated *E* component (matching with the symmetry of the irreducible representations of the C_3 point group). As a result, each rotational transition appears split into two components of equal intensity (see Figure 2.6). The observed splitting in the spectrum depends on the barrier height principally, so their analysis allows determining the value of the barrier height and derive structural information about the orientation of the internal rotation axis.[6]

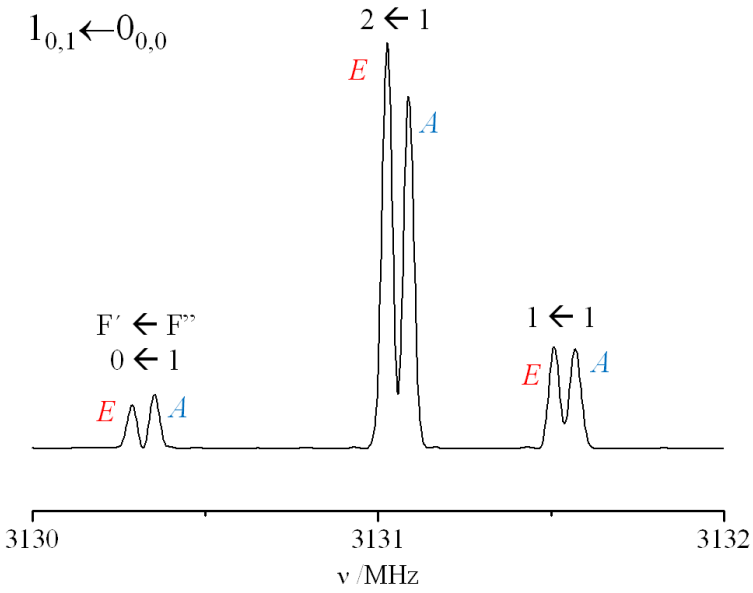

Figure 2.6. Excerpt of the chirped-pulse spectrum (see Chapter III - Instrumentation) for the $1_{0,1} \leftarrow 0_{0,0}$ rotational transition of the methyl carbamate water-a complex (see Chapter VII) showing the observed *A*-*E* doublets due to internal rotation and the quadrupole coupling components.

The Hamiltonian of a system with internal rotation yielding *n* equivalent forms is a combination of the reduced Hamiltonian for an asymmetric top and a term describing the internal rotation:

$$\hat{H} = \hat{H}_{\text{rot}} + \hat{H}_{\text{int}}$$

The internal rotation Hamiltonian term includes the *F* constant, which can be calculated from the moment of inertia of the internal top (I_α) and the direction cosines giving the orientation for the axes of the internal top with respect to the principal axis system (λ_x, $x = a, b, c$), and the potential function, $V(\alpha)$:[21-23]

$$\hat{H}_{\text{int}} = F\left(\hat{j}_{\text{int}} - \hat{J}\right)^2 + V(\alpha)$$

$$F = \frac{\hbar^2}{2rI_\alpha} \qquad\qquad r = 1 - \sum_x \frac{\lambda_x^2 I_\alpha}{I_x}$$

where $\hat{j}_{\text{int}}$ is the operator for the angular momentum of the internal rotation top and $\hat{J}$ is the total angular momentum operator. The $(\hat{j}_{\text{int}} - \hat{J})$ term, represents then the relative angular momentum of the rotating top in the molecular frame.

In a molecule with a methyl group internal rotation motion, an additional selection rule arises, transitions are only allowed between states of the same symmetry, $A \leftarrow A$ or $E \leftarrow E$.

We have also studied the almost-free internal rotation of a hydrogen-bonded water molecule along the N–H···OH_2 axis. The rotation leads to $n = 2$ equivalent minima in the periodic potential function, which has a two-fold barrier (see Figure 2.4b). In this case, the members of the observed doublets have been labeled as 0^+ and 0^-. The potential function is represented by a cosine series:[6,19]

$$V(\alpha) = \frac{1}{2}V_2[1 - \cos(2\alpha)]$$

where V_2 is the two-fold barrier. In general, allowed transitions for this situation are those occurring from $0^+ \leftarrow 0^+$ or $0^- \leftarrow 0^-$.

2.2.5.2 Coriolis interaction

In some cases, when there are two vibrational states very close in energy a shift in the frequencies of certain rotational transitions from those predicted using the semirigid rotor model may be observed. The shift appears as a result of an interaction between rotational levels from both vibrational states. Coriolis interaction occurs when the vibration generates an angular momentum that couples the rotational functions of the vibrational states close in energy. Coriolis coupling effects are observed when the direct product for the irreducible representation of the vibro-rotational levels involved and the irreducible representation of the vibrational angular momentum components P_α ($\alpha = a$, b or c) connecting both states, contains the totally symmetric representation: $\Gamma_{v_0} \otimes \Gamma_{v_1} \otimes \Gamma_{J_\alpha} \subseteq A$.[6]

The energy of the rotational levels in the two vibrational states can be described by a 2x2 block matrix Hamiltonian diagonal in J. The diagonal elements are the semirigid rotational Hamiltonians for the 0 and 1 vibrational states, and ΔE_{01} is the difference in energy between them. The non-diagonal elements ($\widehat{H}_{\mathrm{Cor}}^{0,1}$) take account of the Coriolis interaction:[24]

$$\widehat{H} = \begin{pmatrix} \langle 0|\widehat{H}_{\mathrm{rot}}|0\rangle & \langle 0|\widehat{H}_{\mathrm{Cor}}^{0,1}|1\rangle \\ \langle 1|\widehat{H}_{\mathrm{Cor}}^{0,1}|0\rangle & \langle 1|\widehat{H}_{\mathrm{rot}}|1\rangle + \Delta E_{01} \end{pmatrix}$$

In the principal inertial axis system: $\widehat{H}_{\mathrm{Cor}}^{0,1} = iG_\alpha \hat{J}_\alpha$

where G_α ($\alpha = a$, b or c) is the Coriolis coupling constant for a Coriolis interaction between two rotational levels connected by $\hat{J}_\mathrm{a}$.

2.2.6 Nuclear spin statistical weights

An alternation of the line intensities of the rotational transitions belonging to different vibrational substates is observed experimentally when the system presents equivalent nuclei that can be exchanged (see Figure 2.7). Any symmetry operation over the molecular system may leave the total wave function unchanged or changed only in sign, that is, the wave function is either symmetric or antisymmetric with respect to that symmetry operation. For the exchange of two equivalent nuclei, the total wave function is symmetric if the nuclei obey the Bose-Einstein

statistic (spin equal to zero or an integer), while for nuclei that obey the Fermi-Dirac statistic (spin equal to half odd integers) the total wave function is antisymmetric.[6]

We have studied the effect of the nuclear spin statistical weight in the formanilide···(H_2O) Ic complex (see Chapter VI), showing an almost-free internal rotation of the water molecule (see section 2.2.5.1 internal rotation), that exchanges the two hydrogen nuclei. Hydrogen atoms have a nuclear spin of ½ and obey the Fermi-Dirac statistic, therefore the total wave function $\psi_{tot} = \psi_e\psi_v\psi_r\psi_{ns}$ of the system, must be antisymmetric for the exchange of those hydrogen atoms. ψ_e, ψ_v, ψ_r, ψ_{ns} represent the corresponding electronic, vibrational, rotational and nuclear spin functions. Table 2.3 resumes the symmetry properties of the torsional, rotational and nuclear spin wave functions. The other wave functions are symmetric in this case.[6,25,26]

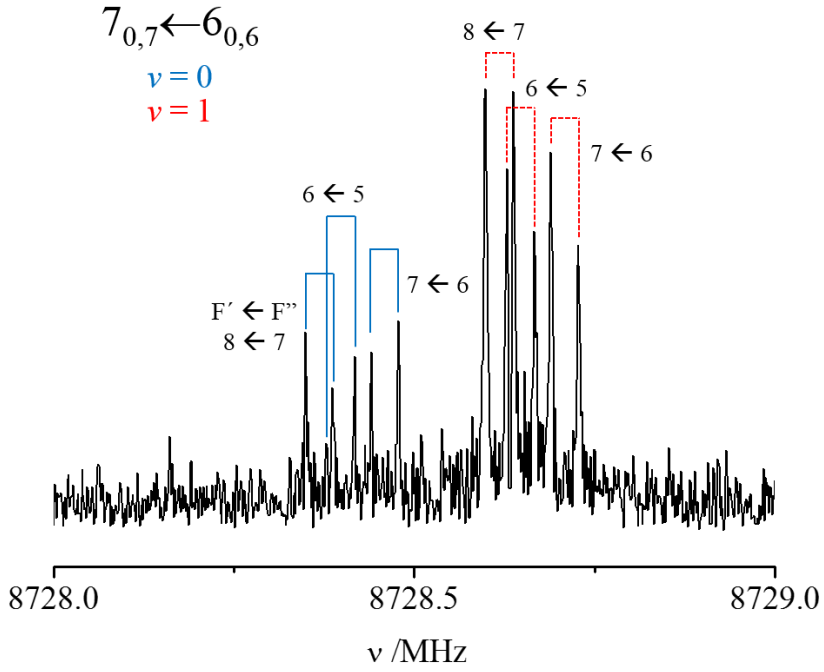

Figure 2.7. The $7_{0,7}$←$6_{0,6}$ rotational transition for the *trans*-formanilide···(H_2O) Ic complex (see Chapter VI) showing the intensity ratio between the v = 0 (blue solid lines) and v = 1 (red dashed lines) vibrational states. Each transition appears as a doublet due to the Doppler effect.

The number for the symmetric (g_I^{sym}) and antisymmetric (g_I^{asym}) nuclear spin wave functions depends on the nuclear spin (I) of the atom exchanged:[6]

$$g_I^{sym} = \frac{(2I+1)(I+1)}{(2I+1)^2} \qquad g_I^{asym} = \frac{(2I+1)I}{(2I+1)^2}$$

Experimentally is observed an intensity ratio between the two states, which can be calculated by the relation:

$$\frac{g_I^{sym}}{g_I^{asym}} = \frac{(I+1)}{I}$$

For two hydrogen atoms, with nuclear spin I = ½, the ratio between symmetric/antisymmetric nuclear spin wave functions is 3.

Table 2.3. Symmetry for the wave functions for the exchange of two equivalent hydrogen atoms in the formanilide···(H_2O) Ic complex. The symmetry of the rotational states is given in parentheses in terms of the parity (e = even, o = odd) of the K_{-1} and K_{+1} numbers. The symmetry of the nuclear spin functions is given to accomplish that the total wave function must be antisymmetric. The nuclear spin statistical weights explain the alternation of the line intensities observed experimentally.

Vibrational state	Rotational state	Nuclear spin	Nuclear spin statistical weight
0 (sym)	Symmetric (ee, oe)	Antisymmetric	1
	Antisymmetric (eo, oo)	Symmetric	3
1 (asym)	Symmetric (ee, oe)	Symmetric	3
	Antisymmetric (eo, oo)	Antisymmetric	1

2.2.7 Analysis of the spectra

The initial analysis of the microwave spectra, prediction of transition frequencies and assignment of experimental lines, has been done using the JB95 software.[27] Usually, the final fitting of the rotational parameters has been achieved by using Pickett´s SPCAT/SPIFT package.[28] This package allows fitting the spectrum using the rigid-rotor or the distortable-rotor reduced Hamiltonians. It is possible to implement the terms for fitting the nuclear quadrupole coupling constants for several nuclei and Coriolis coupling constants. The XIAM package[29] has been used in systems presenting internal rotation for the simultaneous fitting of the *A* and *E* transitions. XIAM allows fitting the internal rotation parameters for up to three internal tops together with the rotation constants, the centrifugal distortion constants, and nuclear quadrupole coupling constants. The AABS package[30,31] has been used for displaying the predicted transitions and measuring the experimental frequencies.

2.2.8 Molecular Structure

Microwave spectroscopy is considered as one of the most appropriate experimental technique to derive molecular structures. However, the determination of molecular structures with high accuracy from the experimental data is a challenging task. The rotational parameters derived from the microwave spectra are related with the molecular geometry (atom positions, bond lengths, and angles between atoms) through the inertial moments. However, molecules are not rigid due to vibrational motions, and therefore there is not a unique definition of molecular structure.[6,32,33]

2.2.8.1 Equilibrium Structure (r_e)

The equilibrium structure is that of a minimum in the potential energy surface (See Figure 2.8) and represents the distances between nuclei in a hypothetical vibrationless configuration. The equilibrium rotational constants are correlated to rotational constants in different vibrational states by:

$$A_e = A_v + \sum_i^{3N-6} \alpha_i (v_i + \frac{d_i}{2}) \quad B_e = B_v + \sum_i^{3N-6} \alpha_i (v_i + \frac{d_i}{2}) \quad C_e = C_v + \sum_i^{3N-6} \alpha_i (v_i + \frac{d_i}{2})$$

where α_i are rotation-vibration interaction constants and d_i accounts for vibrational degeneracy.

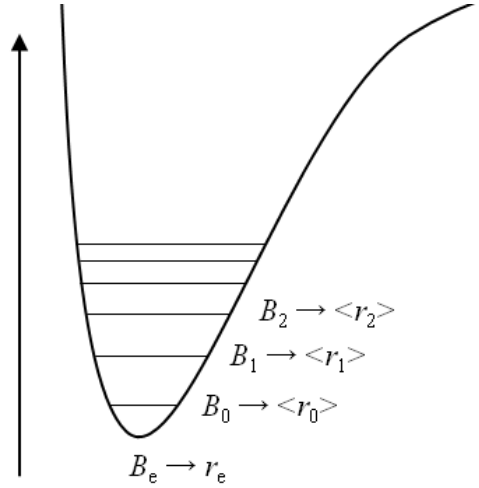

Figure 2.8. Potential energy function with vibrational states, rotational constants and the structures derived from them.

2.2.8.2 Effective Structure (r_0)

The effective structure is that which reproduces the experimentally obtained rotational constants, and therefore the inertial moments in a certain vibrational state, usually the ground state (v = 0).[34] The rotational constants in a particular vibrational state represent an average of the molecular motions. The effective structure parameters are obtained by a least-square fitting of the experimental rotational constants for the parent and all available isotopologue species.[35]

2.2.8.3 Substitution Structure (r_s)

The method for obtaining the substitution structure is based on the changes that the inertia moments undergo with isotopic substitution assuming that the internuclear distances are unchanging with the isotopic substitution. Kraitchman equations[36] provide the atomic coordinates (*a*, *b* or *c*) for the species substituted in the principal axis system of the parent molecule, allowing building the molecular structure atom by atom from the experimental parameters. r_s is considered to give an intermediate structure between those describe by r_0 and r_e. For an asymmetric top, the r_s coordinates can be calculated by the expressions:

$$|a| = \left[\frac{P_a}{\mu}\left(1 + \frac{P_b}{I_a - I_b}\right)\left(1 + \frac{P_c}{I_a - I_c}\right)\right]^{1/2}$$

$$|b| = \left[\frac{P_b}{\mu}\left(1 + \frac{P_c}{I_b - I_c}\right)\left(1 + \frac{P_a}{I_b - I_a}\right)\right]^{1/2}$$

$$|c| = \left[\frac{P_c}{\mu}\left(1 + \frac{P_a}{I_c - I_a}\right)\left(1 + \frac{P_b}{I_c - I_b}\right)\right]^{1/2}$$

being P_α (α = a, b or c) the planar moments of inertia. For example, $P_a = 1/2\,(\mathrm{I_b} + \mathrm{I_c} - \mathrm{I_a}) = \sum_i m_i a_i^2$. μ is the reduced mass for the isotopic substitution of a molecular system of mass M that undergoes a substitution of one atom with a mass increment of Δm: $\mu = M\Delta m/(M+\Delta m)$. To assign the uncertainty to the calculated coordinates, the Costain rule is followed:[37] $\delta\alpha = K/\alpha$. Where K is measured in squared Angstroms and can take different values depending on the substituted nuclei. For the substitution of nuclei other that hydrogen, a value of $K = 0.0015 Å^2$ is usually accepted.

Despite its simplicity, this method has several drawbacks. It neglects vibration-rotation interaction. It is not usual to obtain a complete structure since it needs full single-isotopic determination, except in systems with symmetry equivalent atoms. The r_s method gives absolute values for the coordinates so further information is needed to set the proper signs. In certain cases, when the coordinate values are too small, the Kraitchman method yields imaginary values.

2.3 Computational Methods

In general, prior to the recording of the microwave spectra a conformational search is performed by investigating the possible stable configuration for monomers or complexes having low energies. The diverse methods available to optimize the geometry[38] apply different approximations for solving the Schrödinger equation. From the calculated structure it is possible to extract information about the energy of the system and their spectroscopic parameters.

In a first stage, low-cost computational methods were employed to explore the potential energy surface of the system under study. Different conformations and arrangements for the molecules were considered to obtain the possible stable configurations. In this stage, DFT functionals,[39] usually B3LYP,[40] PBE0[41] or the Minnesota 06 suite of functionals[42] were used in combination with basis sets functions. Those methods require low computational resources, but usually they do not account well for long-range dispersive forces, such as hydrogen bonds.[43] In microsolvated systems those forces are important to determine the stability of the clusters and therefore, low-cost computational methods perform poor predictions for the geometry and energy of the clusters. Molecular structures can be somehow improved by implementing empirical data corrections, as that of Grimme *et al*.[44] Another way to obtain more precise geometries and energies is to investigate the structures with higher cost *ab initio* methods such as MP2[45] or CCSD[46] combined to high-level basis sets. Basis sets provide the starting functions for the calculations and are based on different representations of atomic orbitals which will be combined to yield the molecular orbitals. The selection of the basis set is crucial to achieve a satisfying description of molecular geometry. The implementation of polarization functions, which corrects the charge distribution around the nucleus, or diffuse functions, which improve the electronic density for long-range interactions, helps to achieve a more accurate description of the molecular geometries. Some of the most employed basis set were Pople´s 6-311++G(d,p)[47] or Dunning´s aug-cc-PVDZ[48] that implement polarization and diffuse functions.

After the conformational search, the microwave spectrum was simulated for the low-energy conformations on the basis of their rotational constants, quadrupole coupling constants and the electric dipole moment. The predicted spectra were then compared to the experimentally recorded to assign and identify the present species. In the cases when the molecular structures

were derived from the experimental parameters, comparison with the predicted structures allowed us to evaluate the quality of the calculations. When experimental molecular structures were not available, predicted and experimental rotational parameters are compared. Providing that there is an agreement between experimental and theoretical, the predicted structures were assumed to be close to the real ones.

Additionally, for some molecular systems, Natural Bond Orbital (NBO) calculations have been carried out using the natural population analysis method.[49,50] This method allows calculating atomic charges and orbital occupancies using a basis set of natural atomic orbitals. The orbital occupancies obtained for the non-bonding orbital in ^{14}N can be correlated to the quadrupole coupling constant perpendicular to the bond plane, allowing us to investigate the origin of the charge in the quadrupole coupling constants through hydrogen bonding.

References

[1] McNaught, A. D. Wilkinson, A. *IUPAC, Compendium of Chemical Terminology (The "Gold Book")*, 2nd ed., Blackwell Scientific Publications, Oxford, 1997.
[2] Pilar, F. L. *Elementary Quantum Chemistry* McGraw-Hill Publishing Company, Singapore, 1990.
[3] Levine, I. N. *Quantum Chemistry* Prentice-Hall, 2000.
[4] Townes, C. H., Schawlow, A. L. *Microwave Spectroscopy* McGraw-Hill Publishing Company, New York, 1955.
[5] Watson, J. K. G. in *Vibrational Spectra and Structure a Series of Advances, Vol 6* ed. Durig, J. R. Elsevier, New York, 1977, pp. 1–89.
[6] Gordy, W., Cook, R. L. *Microwave Molecular Spectra* Wiley-Interscience, New York, 1984.
[7] Kroto, H. W. *Molecular Rotation Spectra* Dover Publications Inc., New York, 1992.
[8] Steinfeld, J. I. *Molecules and Radiation* Dover Publications Inc., New York, 2005.
[9] King, G. W., Hainer, R. M., Cross, P. C. "The Asymmetric Rotor – I. Calculation and Symmetry Classification of Energy Levels" *J. Chem. Phys.*, **1943**, 11, 27–42.
[10] Ray, B. S. "Über die Eigenwerte des Asymmetrischen Kreisels" *Z. Physik.*, **1932**, 78, 74–91.
[11] Wilson Jr E. B., Howard, J. B. "The Vibration-Rotation Energy levels of Polyatomic Molecules – 1. Mathematical Theory of Semirigid Asymmetrical Top Molecules" *J. Chem. Phys.*, **1936**, 4, 260–268.
[12] Kivelson, D., Wilson, Jr E. B. "Approximate Treatment of the Effect of Centrifugal Distortion on the Rotational Energy Levels of Asymmetric-Rotor Molecules" *J. Chem. Phys.*, **1952**, 20, 1575–1579.
[13] Watson, J. K. G. "Centrifugal Corrections for Asymmetric-Top Molecules" *J. Chem. Phys.*, **1966**, 45, 1360–1361.
[14] Watson, J. K. G. "Determination of Centrifugal Distortion Coefficients of Asymmetric-Top Molecules" *J. Chem. Phys.*, **1967**, 46, 1935–1949.
[15] Braag, J. K. "The Interaction of Nuclear Electric Quadrupole Moments with Molecular Rotation in Asymmetric-Top Molecules. I" *Phys. Rev.*, **1948**, 74, 533–538.
[16] Blanco, S., Lesarri, A., López, J. C., Alonso, J. L. "The Gas-Phase Structure of Alanine" *J. Am. Chem. Soc.*, **2004**, 126, 11675–11683.
[17] Bardeen, J., Townes, C. H. "Calculation of Nuclear Quadrupole Effects in Molecules" *Phys. Rev.*, **1948**, 73, 97–105.
[18] Foley, H. M. "Note on the Nuclear Electric Quadrupole Spectrum of a Homonuclear Diatomic Molecular in a Magnetic Field" *Phys. Rev.*, **1947**, 71, 747–751.
[19] Lin, C. C., Swalen, J. D. "Internal Rotation and Microwave Spectroscopy" *Rev. Mod. Phys.*, **1959**, 31, 841–892.
[20] Lister, D. G., Macdonald, J. N., Owen, N. L. "Internal Rotation and Inversion. An Introduction to Large Amplitude Motions in Molecules" Academic Press, London, 1978.
[21] Herschbach, D. R. "Calculation of Energy Levels for Internal Torsion and Over-All Rotation. III" *J. Chem. Phys.*, **1959**, 31, 91–108.
[22] Woods, R. C. "A General Program for the Calculation of Internal Rotation Splittings in Microwave Spectroscopy" *J. Mol. Spectrosc.*, **1966**, 21, 4–24.
[23] Woods, R. C. "A General Program for the Calculation of Internal Rotation Splittings in Microwave Spectroscopy – Part II. The n-Top Problem" *J. Mol. Spectrosc.*, **1967**, 22, 49–59.
[24] Perevalov, V. I. Tyuterev, V. G. "Reduction of the Centrifugal Distortion Hamiltonian of Asymmetric Top Molecules in the Case of Accidental Resonances: Two Interacting States. Lower-Order Terms" *J. Mol. Spectrosc.*, **1982**, 96, 56–76
[25] Wilson Jr, E. B. "The Statistical Weights of the Rotational Levels of Polyatomic Molecules, Including Methane, Ammonia, Benzene, Cyclopropane and Ethylene" *J. Chem. Phys.*, **1935**, 3, 276–285.
[26] Trippel, S., Chang, Y. P., Stern, S., Mullins, T., Holmegaard, L., Küpper, J. "Spatial Separation of State- and Size-Selected Neutral Clusters" *Phys. Rev. A*, **2012**, 86, 033202.
[27] Plusquellic, D. JB95, *available at* http://www.nist.gov/pml/electromagnetics/grp05/jb95.cfm.
[28] Pickket, H. M. "The Fitting and Prediction of Vibrational-Rotation Spectra with Spin Interaction" *J. Mol. Spectrosc.*, **1991**, 148, 371–377.
[29] Hartwig, H. Dreizler, H. "The Microwave Spectrum of *Trans*-2,3-Dimethyloxirane in Torsional Excited States" *Z. Naturforsch*, **1996**, 51a, 923–932.
[30] Kisiel, Z., Pszczolkowski, L., Medvedev, I. R., Winnewisser, M., De Lucia, F. C., Herbst, E. "Rotational Spectrum of *trans-trans* Diethyl Ether in the Ground and Three Excited Vibrational States" *J. Mol. Spectrosc.*, **2005**, 233, 231–243.
[31] Kisiel, Z. PROSPE – Programs for ROtational SPEctroscopy, *available at*:

http://www.ifpan.edu.pl/~kisiel/prospe.htm
[32] Domenicano, A., Hargittai, I. *Accurate Molecular Structures: Their Determination and Importance* Oxford University Press, New York, 1992.
[33] Demaison, J. "Accurate Structures of Non-Rigid Molecules by Microwave Spectroscopy" in *Structures and Conformations of Non-Rigid Molecules* eds. Laane, J., Dakkouri, M., van der Veken, B., Oberhammer, H. Springer, Dordrecht, 1993, Volume 410, pp. 239–256.
[34] Rudolph, H. D. "Contribution to the Systematics of r_0-Derived Molecular Structure Determinations from Rotational Parameters" *Struct. Chem.*, **1991**, **2**, 581–588.
[35] Kisiel, Z. "Least-Squares Mass-Dependence Molecular Structures for Selected Weakly Bound Intermolecular Clusters" *J. Mol. Spectrosc.*, **2003**, 218, 58–67.
[36] Kraitchman, J. "Determination of Molecular Structure from Microwave Spectroscopic Data" *Am. J. Phys.*, **1953**, 21, 17–24.
[37] Costain, C. C. "Further Comments on the Accuracy of r_s Substitution Structures" *Trans. Am. Crystallogr. Assoc.*, **1966**, 2, 157–164.
[38] Gaussian 09, Revision D.01, Frisch M. J., Trucks G. W., Schlegel H. B., Scuseria G. E., Robb M. A., Cheeseman J. R., Scalmani G., Barone V., Petersson G. A., Nakatsuji H., Li X., Caricato M., Marenich A., Bloino J., Janesko B. G., Gomperts R., Mennucci B., Hratchian H. P., Ortiz J. V., Izmaylov A. F., Sonnenberg J. L., Williams-Young D., Ding F., Lipparini F., Egidi F., Goings J., Peng B., Petrone A., Henderson T., Ranasinghe D., Zakrzewski V. G., Gao J., Rega N., Zheng G., Liang W., Hada M., Ehara M., Toyota K., Fukuda R., Hasegawa J., Ishida M., Nakajima T., Honda Y., Kitao O., Nakai H., Vreven T., Throssell K., Montgomery, Jr. J. A., Peralta J. E., Ogliaro F., Bearpark M., Heyd J. J., Brothers E., Kudin K. N., Staroverov V. N., Keith T., Kobayashi R., Normand J., Raghavachari K., Rendell A., Burant J. C., Iyengar S. S., Tomasi J., Cossi M., Millam J. M., Klene M., Adamo C., Cammi R., Ochterski J. W., Martin R. L., Morokuma K., Farkas O., Foresman J. B., Fox D. J., *Gaussian, Inc., Wallingford CT*, 2016.
[39] a) Hohenberg, P., Kohn, W. "Inhomogeneous Electron Gas" *Phys. Rev.*, **1964**, 136, B864–B871; b) Kohn, W., Sham, L. J. "Self-Consistent Equations Including Exchange and Correlation Effects" *Phys. Rev.*, **1965**, 140, A1133–A1138.
[40] a) Lee, C., Yang, W., Parr, R. G. "Development of the Colle-Salvetti Correlation-Energy Formula into a Functional of the Electron Density" *Phys. Rev. B*, **1988**, 37, 785–789. b) Becke, A. D. "Density-Functional Thermochemistry. III. The Role of Exact Exchange" *J. Chem. Phys.*, **1993**, 98, 5648–5652. c) Vosko, S. H., Wilk, L., Nusair, M. "Accurate Spin-Dependent Electron Liquid Correlation Energies for Local Spin Density Calculations: a Critical Analysis" *Can. J. Phys.*, **1980**, 58, 1200–1211.
[41] a) Perdew, J. P., Burke, K., Ernzerhof, M. "Generalized Gradient Approximation Made Simple" *Phys. Rev. Lett.*, **1996**, 77, 3865–3868; b) Adamo, C., Barone, V. "Toward Reliable Density Functional Methods without Adjustable Parameters: the PBE0 Model" *J. Chem. Phys.*, **1999**, 110, 6158–6169.
[42] Zhao, Y., Truhlar, D.G. "The M06 Suite of Density Functionals for Main Group Thermochemistry, Thermochemical Kinetics, Noncovalent Interactions, Excited States, and Transition Elements: Two New Functionals and Systematic Testing of Four M06-Class Functionals and 12 Other Functionals" *Theor. Chem. Acc.*, **2008**, 120, 215–241.
[43] Pinacho, P., López, J. C., Blanco, S. "Prediction of the Rotational Spectra of Microsolvated Complexes with Low Cost DFT Methods" *J. Mol. Spectrosc.*, **2017**, 337, 145–152.
[44] Grimme, S., Antony, J., Ehrlich, Krieg, H. "A Consistent and Accurate *Ab Initio* Parametrization of Density Functional Dispersion Correction (DFT-D) for the 94 Elements H-Pu" *J. Chem. Phys.*, **2010**, 132, 154101.
[45] Møller, C., Plesset, M. S. "Note on an Approximation Treatment for Many-Electron Systems" *Phys. Rev.*, **1934**, 46, 618–622.
[46] Cizek, J. "On the Correlation Problem in Atomic and Molecular Systems. Calculation of Wavefunction Components in Ursell-Type Expansion Using Quantum-Field Theoretical Methods" *J. Chem. Phys.*, **1966**, 45, 4256–4266.
[47] Ditchfield, R., Hehre, W. J., Pople, J. A. "Self-Consistent Molecular-Orbital Methods. IX. An Extended Gaussian-Type Basis for Molecular-Orbital Studies of Organic Molecules" *J. Chem. Phys.*, **1971**, 54, 724–728.
[48] a) Dunning, T. H. "Gaussian Basis Sets for Use in Correlated Molecular Calculations. I. The Atoms Boron Through Neon and Hydrogen" *J. Chem. Phys.*, **1989**, 90, 1007–1023. b) Kendall, R. A., Dunning, T. H., Harrison, R. J. "Electron Affinities of the First-Row Atoms Revisited. Systematic Basis Sets and Wave Functions" *J. Chem. Phys.*, **1992**, 96, 6796–6806.
[49] Reed, A. E., Weinstock, R. B., Weinhold, F. "Natural Population Analysis" *J. Chem. Phys.*, **1985**, 83, 735–746.

[50] Reed, A. E., Curtiss, L. A., Weinhold, F. "Intermolecular Interactions from a Natural Bond Orbital, Donor-Acceptor Viewpoint" *Chem. Rev.*, **1988**, 88, 899–926.

Chapter III

Instrumentation

3.1 Introduction

Microwave spectroscopy exploits the information obtained from frequencies corresponding to rotational transitions of molecules and clusters, it allows deriving very precise structural parameters. In particular, the combination of supersonic jets[1-3] and Fourier transform microwave spectroscopy (FTMW)[4,5] is considered one of the most advanced experimental techniques to investigate the molecular structure in gas phase.[6,7] Molecular beam Fourier transform microwave spectroscopy (MB-FTMW), using a Fabry-Perot cavity, was first developed by Balle and Flygare[8] and further improved by Dreizler and co-workers.[9,10] MB-FTMW spectroscopy provides high-resolution spectra with very accurate frequency measurements of molecular systems in an isolated environment, allowing us to characterize their structure and the inter or intramolecular forces which drive conformational behavior. It also permits to resolve the fine structure due to tunneling motions, or the hyperfine structure as that arising from nuclear quadrupole coupling.

In the last decade, major advances have been done to improve microwave spectroscopy techniques. The major breakthrough has been the development of Chirped-pulse Fourier transform microwave spectroscopy (CP-FTMW),[11-13] which allows us to record a wide-band spectrum of several GHz in one event while keeping the accuracy and almost the high-resolution characteristic of FTMW spectroscopy. In addition, microwave three-wave mixing technique (M3WM) has been developed recently.[14-16] M3WM, based on the difference in the phase of the FID emission for the different enantiomers of a chiral molecule, is useful for the discrimination of enantiomers and the determination of the absolute configuration of a chiral sample.[17,18]

Four different spectrometers were used for recording the spectra presented in this work, all of them being described elsewhere: two Fabry-Perot cavity resonator FTMW spectrometers, one located at the University of Valladolid,[19,20] and one located at the Institute of Physics, Polish Academy of Science in Warsaw;[21] and two chirped-pulse FTMW spectrometers, one located at the University of Valladolid[11,12] and one located at the Max Planck Institute for the Structure and Dynamics of Matter in Hamburg [22]

3.2 Fourier transform microwave spectroscopy in supersonic jets

3.2.1 Supersonic jet

A supersonic jet[1,2] is generated by the isentropic expansion of a moderately high pressure ($P_0 \approx 1$ – 15 bar) gas mixture into a high vacuum chamber ($P_r \approx 10^{-4} – 10^{-7}$ mbar), through a small diameter nozzle (*ca*. 0.5 – 1.5 mm). For a given gas mixture, such supersonic expansion always occurs when the ratio P_0/P_r is higher than the critical value G ($G = [(\gamma + 1)/2]^{\gamma/(\gamma-1)}$,[3] being $\gamma = C_p/C_v$). The mixture is usually composed by the sample under analysis diluted (*ca*. 1-4%) in a carrier gas (He, Ne, Ar… or mixtures of them). The supersonic jet structure is depicted in Figure 3.1[3,23,24] where it is possible to distinguish their main parts: the zone of silence, the barrel shock and Mach disk.

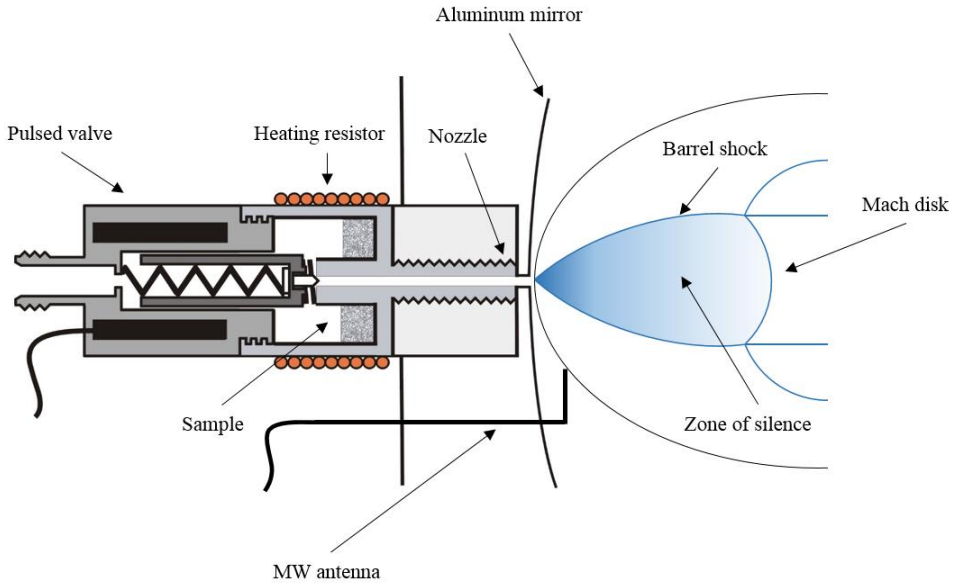

Figure 3.1. Schematic drawing of the heating valve[20] with the supersonic jet structure. The valve and the supersonic jet are not in the same scale. In our experiment the length of the valve is 5cm; the zone of silence is ≈ 20 m.

In the zone of silence, the velocity of the gas mixture exceeds the local speed of sound (v >> 1 M), providing a particular environment to study molecular systems in which it is possible to highlight three features:

1) Absence of collisions: As depicted in Figure 3.2, in the early stages of the expansion the collision rate is still moderately high but beyond a certain limit, the collision rate rapidly decreases, meaning that in the zone of silence the molecules are isolated.

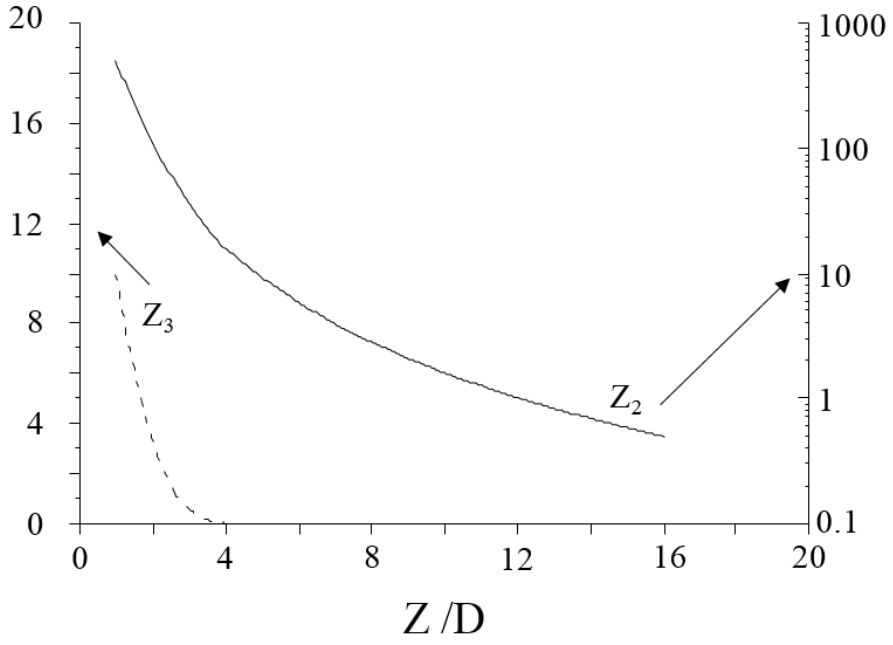

Figure 3.2. Two-body (Z_2) and three-body (Z_3) collision rate versus the distance from the exit in nozzle diameters units (D). Notice the different scale for two-body (right y-axis) and three-body (left y-axis) collisions. Taken from reference 22.

2) Two-body collisions cool down the vibration and rotational degrees of freedom of all molecular systems in the jet and convert the internal energy of the molecules in directional motion. As a consequence, all molecular systems reach the velocity of the carrier gas yielding a very low translational temperature. Sub-Doppler resolution can be achieved for two arrangements of the jet and the probing radiation: coaxial or perpendicular. Vibrational and rotational temperatures considerable decreases in the supersonic jet, in particular the rotational temperature goes to a few Kelvin.[3-24] Thus commonly, molecules populate the vibrational ground state and the low-energy rotational states simplifying the spectrum. Figure 3.3 illustrates the effect of cooling the rotational degrees of freedom by the comparison of the simulated spectra for the detected species in the supersonic jet of formanilide at 2 K and 298 K.

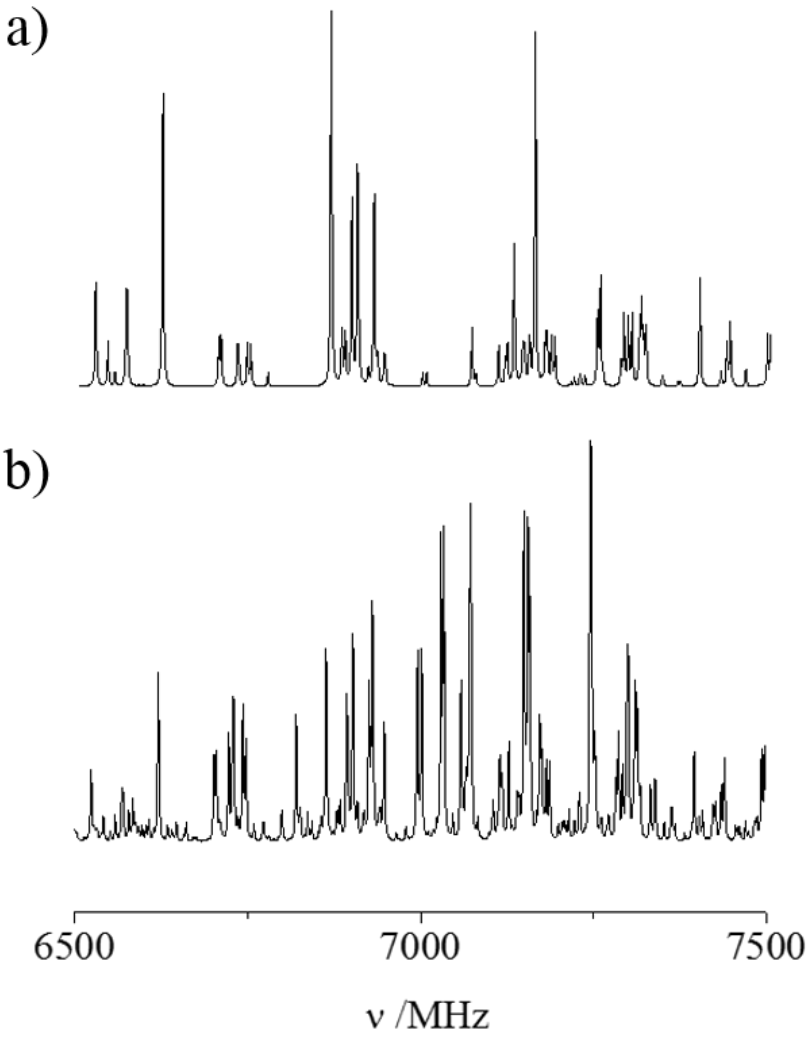

Figure 3.3. Excerpt of the simulated microwave spectra at the ground vibrational state for *cis* and *trans* formanilide, *cis*-formanilide···(H_2O) Ia, *cis*-formanilide···(H_2O)$_2$ IIa, *trans*-formanilide···(H_2O) Ib and *trans*-formanilide···(H_2O) Ic clusters at 2 K (a) and 298 K (b).

3) The three-body collisional rate is only important very close to the nozzle (See Figure 3.2). Three-body collisions are responsible for the generation of molecular clusters. The collision rate depends on the stagnation pressure and temperature, and the nozzle diameter. It decreases rapidly with the distance to the nozzle.[3] Weak molecular clusters only can be destroyed through additional two-body collisions, so once formed in the supersonic jet they progress in an isolated environment where they can be safely proved by spectroscopic methods.

3.2.2 MB-FTMW spectrometer

The MB-FTMW spectrometer at the University of Valladolid (Figure 3.4)[19,20] is based on a Fabry-Perot resonator cavity (11) formed by two aluminum mirrors (10) with a diameter of 54 cm and a radius of curvature of 90 cm disposed in a confocal arrangement. One of them is kept fixed while the other is mounted on a motorized slide rack (14) that allows us to move it in small steps (to regulate the distance between them) to tune the cavity to the polarization frequency. High vacuum is achieved by a diffusion pump (12) supported by a set formed by a roots blower and a rotary pump (13), and monitored by two vacuum meters (15, 16). The sample is supported in the valve (17) (see Figure 3.1) which is bounded by a heating resistor coil. This allows heating the valve to vaporize the sample and increase its concentration in the gas mixture.[20] This mixture of carrier gas and sample is then injected into the chamber (11) through the nozzle. The valve operates in pulsed mode to allow for the formation of the supersonic expansion and evacuation of the gas between pulses. Polarization radiation is fed into the cavity by an L-shaped antenna attached to the fixed mirror (see Figure 3.1), while in the opposite mirror there is another equal antenna for detecting the molecular emission radiation. Due to the coaxial disposition of the nozzle and the resonator, all the transitions in the spectrum present a Doppler splitting, being the molecular emission frequency the arithmetic mean of the two Doppler components. This spectrometer features a resolution power better than 5 kHz, with an accuracy in the frequency measurement better than 3 kHz.

Figure 3.4 also shows the electronic diagram of this MB-FTMW spectrometer. The microwave radiation of frequency ν-160 MHz, at ν the polarization frequency, is emitted by a synthesizer (1) and is directed either to the polarization or to the detection stages by a single pole double throw switch (2). In the polarization stage, the radiation is mixed with a 160 MHz frequency in a single sideband modulator (3). The 160 MHz radiation is provided by the multiplication (28) of a 10 MHz signal taken from the reference output of the microwave synthesizer (1, 27) which is in turn attenuated, filtered and amplified (29-33) prior to mixing (3). The resulting radiation of frequency ν, used to polarize the sample, is further leveled by a variable attenuator (4), an amplifier (5) and a programmable attenuator (8) prior to reach the cavity. A directional coupler allows extracting a minimum amount of radiation (-16dB) for power metering purposes (6-7). This allows a full control of the polarization power reaching the cavity to have uniform polarization level at all operational frequencies. This radiation is directed through a single pole double throw switch (9) to the resonator (11). Once the radiation-matter interaction has occurred, the signal due to the molecular emission of a frequency close to ν is collected by the antenna and amplified by a very-low-noise amplifier (18). During polarization, the switch 19 is driven to the position that protects the receiver, while during detection, switch 9 is programmed to avoid any signal from the polarization circuit to enter into the cavity. After being amplified, the molecular emission signal is mixed (20) with the radiation of frequency ν-160 MHz provided by the synthesizer (1) through the single pole double throw switch (2) which is attenuated (25) and amplified (26), to down-convert it to a signal centered at 160 MHz. This radiation is amplified, filtered and further down-converted (21-23) by mixing it with a 157.5 MHz radiation from the local radiofrequency synthesizer (24). The outcome signal centered at 2.5 MHz, which contains all the spectroscopic molecular information, is directed to a transient recorder (34-36) integrated into the computer. All the instruments are phase-locked to a 10 MHz signal provided by the microwave synthesizer (1) that grants the coherence of the signal and all repetitive events. The pulse sequencer (37) which is in turn computer programmed, controls all the switches and valve pulses (38) and provides the appropriate pulse sequence operation.

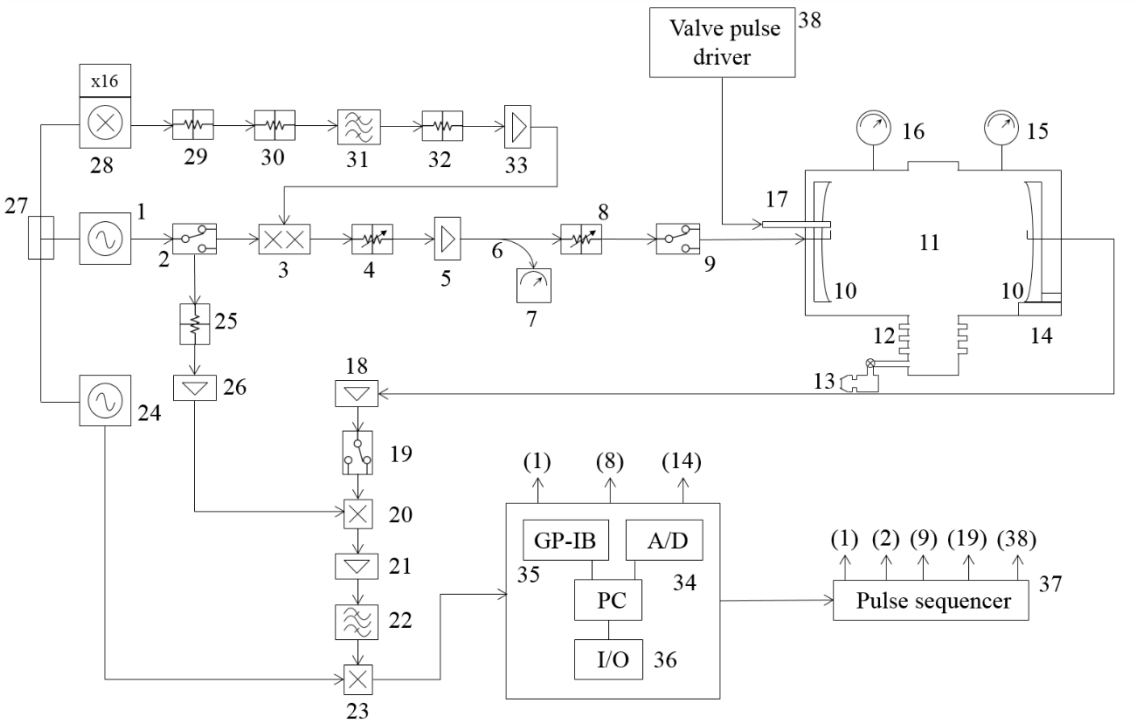

Figure 3.4. Electronic diagram of the FTMW spectrometer[19] (P = output power, IF = intermediate frequency, IL = insertion loss, G = gain, NF = noise figure, IS = isolation, IR = image rejection). (1) Microwave synthesizer, Hewlett-Packard 8672A, 2-18 GHz, P ≤ 10 dBm. (2) Microwave single pole double throw switch, Sierra Microwave Technologies (SMT) SFD0526-001S, 0.5-26 GHz, IL ~ 3 dB, IS > 50 dB. (3) Single sideband modulator, Miteq SM0226LC1-C, 2-26 GHz, IF = 150 MHz, IL = 10 dBm. (4) Microwave variable attenuator, Advanced Technical Materials P/N AV866J-20, 10-26.5 GHz, 0-20 dBm. (5) Microwave amplifier, JCA618-605, 6-18 GHz, G ~ 28 dB, NF ~ 4 dB, P = 20 dBm. (6) Directional coupler, Narda 4203-16, 2-18 GHz, 16 dBm. (7) Power meter, Anritsu ML4803A (power sensor, Anritsu M4701A, 0.01-18 GHz). (8) Programmable attenuator, Hewlett-Packard 11713A. (9) Microwave single pole double throw switch, SMT SFD0526-001S, 0.5-26 GHz, IL ~ 3 dB, IS > 50 dB. (10) Aluminum mirrors. (11) Fabry-Perot resonator. (12) Diffusion pump, Oerlikon Leybold Vacuum Dip 8000, 8000 l/s. (13) Set of roots blower, Oerlikon Leybold Vacuum WAU 501, 500 m^3/h and rotary pump, Oerlikon Leybold Vacuum Trivac D65B, 65 m^3/h. (14) Mirror stepping motor, Berger Lahr. (15) Vacuum meter, Thermovac TM20, gauge Oerlikon Leybold 162 02 B3. (16) Vacuum meter, Alcatel FA 111, gauge Alcatel Penning CF2P. (17) Pulse valve series 9, Parker Hannifin Corporation. (18) Microwave very-low-noise amplifier, Miteq JS4-08001800-16-8P, 8-18 GHz, G ~ 32 dB, NF ~ 1.6 dB, P = 8 dBm. (19) Microwave single pole double throw switch, SMT SFD0526-001S, 0.5-26 GHz, IL ~ 3 dB, IS > 50 dB. (20) Image rejection mixer, Miteq IR0618LC2C, 6-18 GHz, IR > 18 dB, IL ~ 10 dB. (21) Gain-control amplifier, Miteq VGC6-160/40, IF = 160 MHz, NF ~ 5 dB, G ~ 50 dB. (22) Bandpass filter, Reactel 3B4-160 2 S11, 160 MHz. (23) RF mixer, Mini-circuits 15542 ZAD-3, 0.025-200 MHz. (24) RF synthesizer, Hewlett-Packard 8656B, 0.1-990 MHz. (25) Coaxial fixed attenuator, Mini-circuits MCL BW S9W2+, 9 dB, 0-18 GHz. (26) Microwave amplifier, ALS 0618-20-08, 6-18 GHz, G ~ 20 dB, NF ~ 2.7 dB, P = 8.4 dBm. (27) Coaxial power splitter, Mini-circuits 15542 ZFSC 2-1, 20-500 MHz, IL ~ 3 dB, IS > 20 dB. (28) 10 MHz to 160 MHz cascade up converter. (29) Coaxial fixed attenuator, Mini-circuits MCL BW S8W2+, 8 dB, 0-18 GHz. (30) Coaxial fixed attenuator, Mini-circuits MCL BW S6W2+, 6 dB, 0-18 GHz. (31) Bandpass filter, TTE KC6-160M-20M, 160 MHz, BW ~ 20 MHz. (32) Coaxial fixed attenuator, 8 dB. (33) Wideband amplifier, Research Communication 9301, 0.1-500 MHz. (34) Integrated transient recorder, National Instruments. (35) GP-IB IEEE 488 interface. (36) I/O 8255 PC card, National Instruments. (37) TTL pulse sequencer. (38) Valve pulse driver, Parker Hannifin Corporation General Valve Division Iota One.

The sequence of operation in this MB-FTMW spectrometer describing the pulses and delays is represented in Figure 3.5:

1) First, the valve is opened from *ca*. 0.4 to 1 ms for generating the jet (Figure 3.5a). Molecules populate the low-energy rotational states in the jet.

2) After the gas pulse, there is a delay of about 0.4 to 0.8 ms and then a short microwave pulse at a discrete frequency (continuous wave) is emitted for about 2 μs. The microwave pulse induces a polarization of the sample, affecting the population of the rotational states involved, which oscillate at the Rabi frequency[25,26] (Figure 3.5b). The microwave power and pulse width should be set to meet the $\pi/2$ condition in order to have maximum free induction decay emission signal.

3) When the microwave pulse ceases, a small delay of *ca*. 0.1 μs is needed to dissipate the energy accumulated in the cavity. After the delay, the spontaneous molecular emission signal due to the relaxation to the initial equilibrium conditions is recorded for about 10 μs in the time domain. Then, the signal is converted into the frequency domain by applying a fast Fourier transform (Figure 3.5c).

Those steps can be repeated as soon as the vacuum in the chamber is recovered so the supersonic jet optimum conditions have been reached again; typical repetition rates of 2-10 Hz are used.

Recently, a multi-FID recorder has been implemented in the spectrometer in order to improve the signal and reduce the sample consumption. The multi-FID allows us to repeat multiple times the emission-detection cycle for each supersonic expansion pulse. Values of up to 4 repetitions per supersonic expansion have been used.

The MB-FTMW spectrometer at Warsaw is described elsewhere.[21] The main difference is that the sample injection is perpendicular to the microwave polarization signal, therefore the lines do not present Doppler splitting.

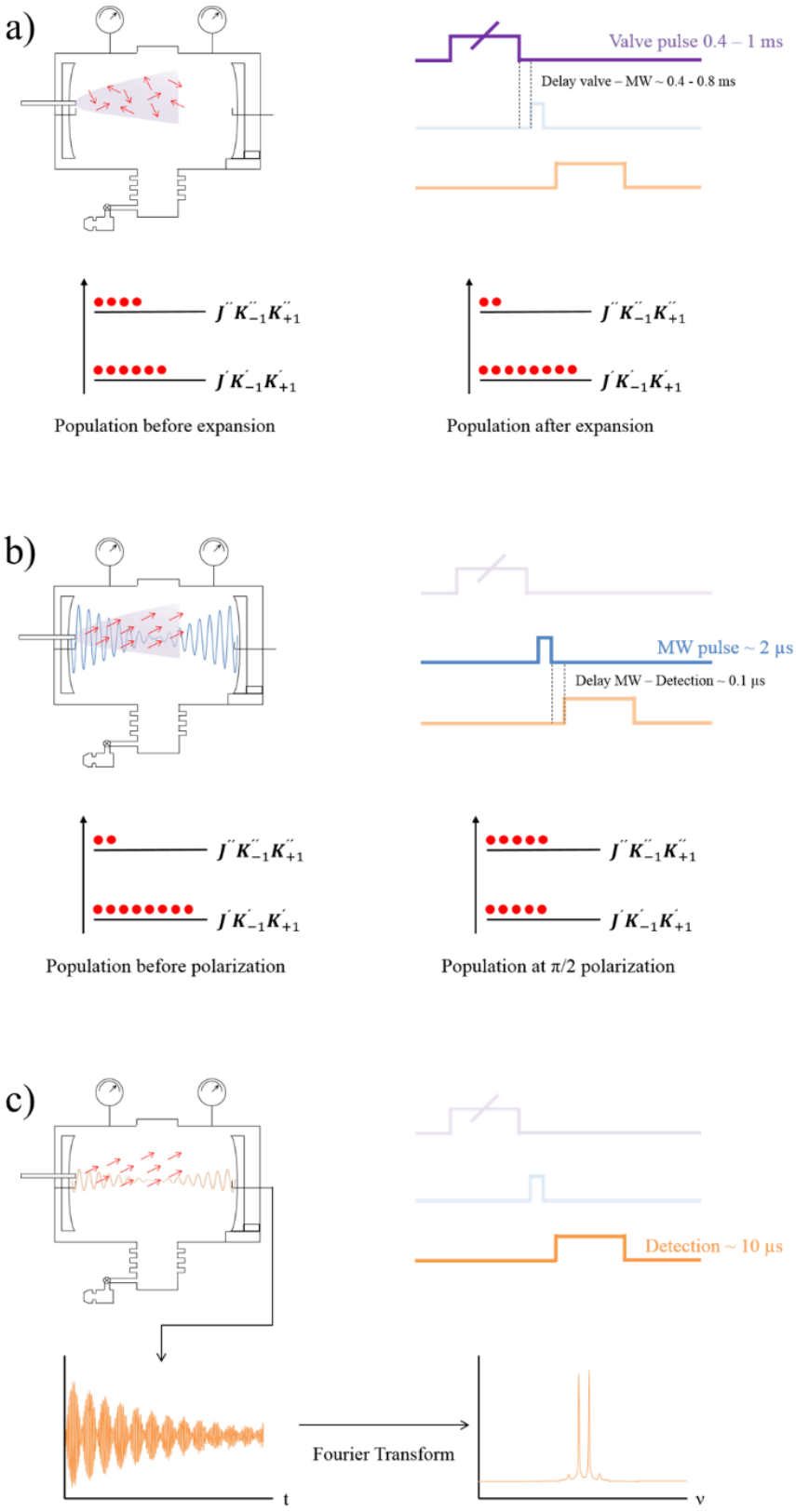

Figure 3.5. Scheme of the operation sequence in the MB-FTMW spectrometer at University of Valladolid. a) Valve pulse and supersonic expansion. b) Microwave pulse that causes macroscopic polarization. c) Molecular emission signal detection and Fourier transform. Red arrows represent the electric dipole moment orientation for each molecule. Red circles represent molecules populating each rotational state.

3.2.3 CP-FTMW spectrometer

In the CP-FTMW spectrometer (BrightSpec)[11,12] located at University of Valladolid (Figure 3.6), the supersonic expansion occurs in a high vacuum chamber (8) which holds two horn antennas (7), one to emit the polarization radiation and the other one to receive the molecular FID emission signal. The gas is evacuated by a diffusion pump (9) supported by a rotary vacuum pump (10). The vacuum in the chamber is measured in a vacuum meter (11). The sample injection system (12) is similar to that described for the MB-FTMW, and it also operates in pulsed mode regulated by a pulse driver (18), which is computer controlled (1). The chirp instrument has a perpendicular arrangement between the nozzle and the horn antennas, therefore the transitions do not present Doppler splitting. The resolution power in the CP-FTMW spectrometer is better than 10 kHz with accuracy in the measurement better than 15 kHz.

Figure 3.6 shows the electronic diagram of the CP-FTMW spectrometer. The chirped pulse, a linear frequency sweep in the range 2 to 8 GHz is generated by an Arbitrary Waveform Generator (AWG) (3), the pulse width of the chirp can be varied from 1 to 10 μs. This signal is attenuated (4) and pre-amplified (5) before to be power amplified by a solid-state amplifier (6) and broadcasted into the chamber (8) through the transmitter horn antenna (7). The weak FID molecular emission signal resulting from the radiation-matter interaction is detected by the receiver horn antenna (7). This signal goes through a power limiter pin diode (13), a switch (14) and is amplified by a low-noise amplifier (15). The power limiter and the switch are used to protect the receiver during polarization. This signal is recorded in the time domain by a digital oscilloscope (16) and converted into the frequency domain by a fast Fourier transform procedure. All instruments are phase-locked to a 10 MHz rubidium standard (2). The pulse sequences are set up in a computer (1), and controlled by a pulse generator (2), which communicates with the PC through a RS-232 port. The PC (1), the AWG (3) and the oscilloscope (16) are connected through an Ethernet Router (17). The limited power of the solid-state amplifier makes necessary to reduce the chirp bandwidth to less than 2 GHz.

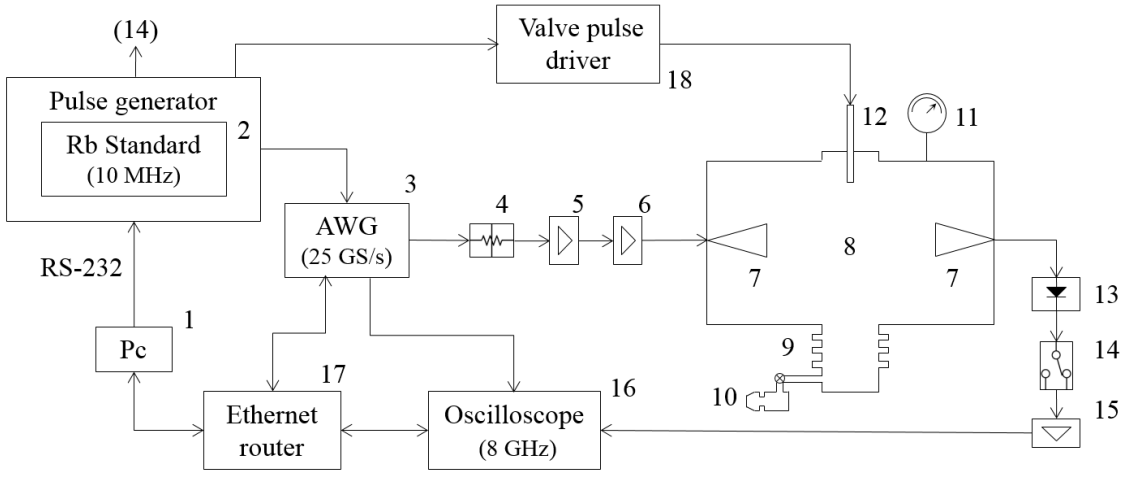

Figure 3.6. Electronic diagram of the CP-FTMW spectrometer[11,12] (P = output power, IL = insertion loss, G = gain, NF = noise figure, IS = isolation). (1) Control PC. (2) Pulse generator unit with 10 MHz rubidium frequency standard inside, Stanford Research Systems PRS10. (3) Arbitrary Waveform Generator, Tektronix AWG70002A, 25 GS/s. (4) Coaxial fixed attenuator, Mini-circuits BW-S20-2W263+, 20 dB, 0-26 GHz. (5) Ultra wide bandwidth pre-amplifier, Mini-circuits ZX60-14012L+, 0.3-14 GHz, G ~ 12 dB, NF ~ 5.5 dB, P = 11 dBm. (6) Solid-state amplifier, Microsemi AML056P4511, 0.5-6 GHz, G ~ 45 dB, NF ~ 6 dB, P = 40 dBm. (7) Transmitter and receiver horn antennas, Q-Par Angus

QWH-SL-2-18-N-HG-R, 2-18 GHz. (8) High vacuum chamber. (9) Diffusion pump, Agilent Technologies, VHS 10, 5300 l/s. (10) Rotary vacuum pump, Edwards Limited, E2M80, 96 m^3/h. (11) Vacuum meter, Kurt J. Lesker RS-485 com. (12) Pulse valve series 9, Parker Hannifin Corporation. (13) Pin diode power limiter, Aeroflex ACLM-4601C361K, 0.5-18 GHz, IL ~ 1.8 dB. (14) Pin diode solid state switch, Advanced Technical Materials Inc. S1517D, 0.5-18 GHz, IL ~ 2.5 dB, NF ~ 2.5 dB, IS ~ 80dB. (15) Microwave low-noise amplifier, Miteq AFS5-00100800-14-10P-5, 0.1-8 GHz, G ~ 42 dB, NF ~ 1.4 dB, P = 10 dBm. (16) Oscilloscope, Tektronix DPO70804C, 8 GHz, 25 GS/s. (17) Ethernet router, Linksys E1200. (18) Valve pulse driver, Parker Hannifin Corporation General Valve Division Iota One.

The sequence of operation of this CP-FTMW spectrometer is represented in Figure 3.7:

1) The supersonic jet is formed by opening the valve for about 800 to 900 μs (Figure 3.7a). As occurs in the MB-FTMW spectrometer, the molecules populate the lower energy rotational states.

2) After the gas pulse there is a delay of *ca*. 100 - 300 μs and then, a chirped pulse of *ca*. 1 - 10 μs covering a broadband of 2 GHz in frequency is emitted and polarizes the sample in this range (Figure 3.7b).

3) When the chirped pulse ceases, a small delay (*ca*. 1 μs) is needed to protect the receiver. Then, the FID molecular emission signal is recorded in the time domain for about 10 to 40 μs in the 2 GHz interval (Figure 3.7c). This molecular emission signal is then converted into the frequency domain by applying a fast Fourier transform. A multi-FID recorder, allows us to repeat the emission-detection (steps 2 and 3) up to 5 times for each supersonic expansion, and the accumulated spectra in the frequency domain can be seen in the control computer.

As occurs in the FTMW spectrometer, step 1 can be repeated as soon as the vacuum in the chamber has reached the pre-expansion value. Usually, molecular pulse repetition rates of 2-10 Hz are used.

The CP-FTMW spectrometer at the Max Planck Institute in Hamburg[22] follows the original design for the CP-FTMW technique.[11,12] The amplification step in this spectrometer is achieved with a high-power traveling wave tube (TWT), the FID molecular emission is recorded in a 100GS/s oscilloscope; that allows scanning a broadband range from 2 to 8 GHz in one pulse.

Detailed description of the experimental conditions and times for each molecular system is given in the experimental section of each chapter.

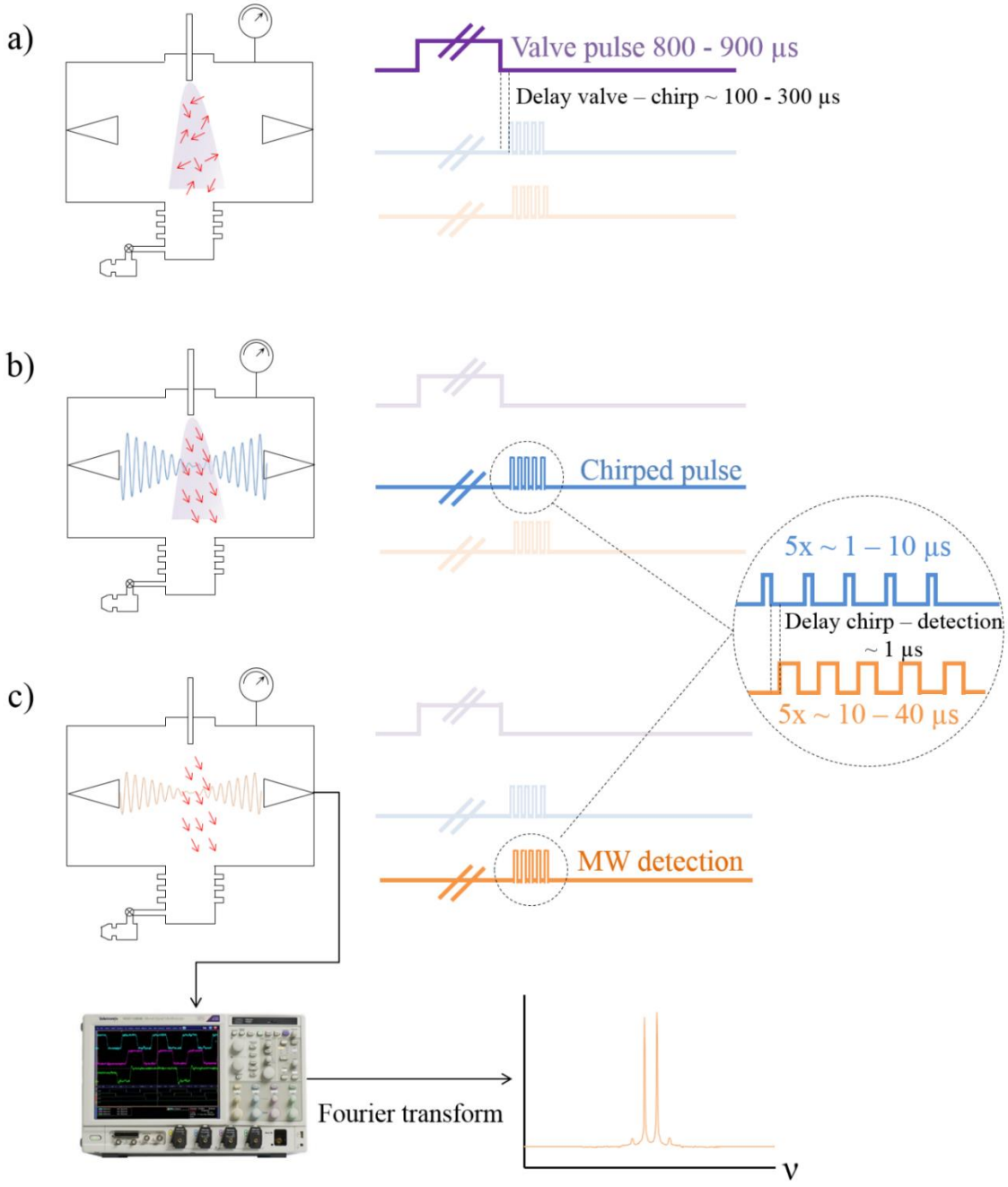

Figure 3.7. Scheme of the operation sequence in the CP-FTMW spectrometer at the University of Valladolid. a) Valve pulse and supersonic expansion. b) Chirped pulse that causes macroscopic polarization. c) FID detection at the oscilloscope and Fourier transform. The multi-FID of 5 frames is depicted.

References

[1] Levy, D. H. "Laser Spectroscopy of Cold Gas-Phase Molecules" *Annu. Rev. Phys. Chem.*, **1980**, 31, 197–225.
[2] Levy, D. H. "The Spectroscopy of Very Cold Gases" *Science*, **1981**, 214, 263–269.
[3] Miller, D. R. "Free Jet Sources" in *Atomic and Molecular Beam Methods* ed. Scoles, G. Oxford University press, Oxford, 1988, Volume 1, pp. 14–53.
[4] Dicke, R. H., Romer, R. H. "Pulse Techniques in Microwave Spectroscopy" *Rev. Sci. Instrum.*, **1955**, 26, 915–928.
[5] Ekkers, J., Flygare, W. H. "Pulsed Microwave Fourier Transform Spectrometer" *Rev. Sci. Instrum.*, **1976**, 47, 448–454.
[6] Domenicano, A., Hargittai, I. *Accurate Molecular Structures: Their Determination and Importance* Oxford University Press, New York, 1992.
[7] Demaison, J. "Accurate Structures of Non-Rigid Molecules by Microwave Spectroscopy" in *Structures and Conformations of Non-Rigid Molecules* eds. Laane, J., Dakkouri, M., van der Veken, B., Oberhammer, H. Springer, Dordrecht, 1993, Volume 410, pp. 239–256.
[8] Balle, T. J., Flygare, W. H. "Fabry-Perot Cavity Pulsed Fourier Transform Microwave Spectrometer with a Pulsed Nozzle Particle Source" *Rev. Sci. Instrum.*, **1981**, 52, 33–45.
[9] Andresen, U., Dreizler, H., Grabow, J. U., Stahl, W. "An Automatic Molecular Beam Microwave Fourier Transform Spectrometer" *Rev. Sci. Instrum.*, **1990**, 61, 3694–3699.
[10] Grabow, J. U., Stahl, W., Dreizler, H. "A Multioctave Coaxially Oriented Beam-Resonator Arrangement Fourier-Transform Microwave Spectrometer" *Rev. Sci. Instrum.*, **1996**, 67, 4072–4084.
[11] Brown, G. G., Dian, B. C., Douglass, K. O., Geyer, S. M., Pate, B. H. "The Rotational Spectrum of Epifluorohydrin Measured by Chirped-Pulse Fourier Transform Microwave Spectroscopy" *J. Mol. Spectrosc.*, **2006**, 238, 200–212.
[12] Brown, G. G., Dian, B. C., Douglass, K. O., Geyer, S. M., Shipman, S. T., Pate, B. H. "A Broadband Fourier Transform Microwave Spectrometer Based on Chirped Pulse Excitation" *Rev. Sci. Instrum.*, **2008**, 79, 053103.
[13] Park, G. B., Field, R. W. "Perspective: The First Ten Years of Broadband Chirped Pulse Fourier Transform Microwave Spectroscopy" *J. Chem. Phys.*, **2016**, 144, 200901.
[14] Patterson, D., Schnell, M., Doyle, J. M. "Enantiomer-Specific Detection of Chiral Molecules Via Microwave Spectroscopy" *Nature*, **2013**, 497, 475–477.
[15] Shubert, V. A., Schmitz, D., Patterson, D., Doyle, J. M., Schnell, M. "Identifying Enantiomers in Mixtures of Chiral Molecules with Broadband Microwave Spectroscopy" *Angew. Chem. Int. Ed.*, **2014**, 53, 1152–1155.
[16] Lobsiger, S., Pérez, C., Evangelisti, L., Lehmann, K. K., Pate, B. H. "Molecular Structure and Chirality Detection by Fourier Transform Microwave Spectroscopy" *J. Phys. Chem. Lett.*, **2015**, 6, 196–200.
[17] Shubert, V. A., Schmitz, D., Schnell, M. "Enantiomer-Sensitive Spectroscopy and Mixture Analysis of Chiral Molecules Containing Two Stereogenic Centers – Microwave Three-Wave Mixing of Menthone" *J. Mol. Spectrosc.*, **2014**, 300, 31–36.
[18] Shubert, V. A., Schmitz, D., Pérez, C., Medcraft, C., Krin, A., Domingos, S. R., Patterson, D. Schnell, M. "Chiral Analysis Using Broadband Rotational Spectroscopy" *J. Phys. Chem. Lett.*, **2016**, 7, 341–350.
[19] Alonso, J. L., Lorenzo, F. J., López, J. C., Lesarri, A., Mata, S., Dreizler, H. "Construction of a Molecular Beam Fourier Transform Microwave Spectrometer Used to Study the 2,5-Dihydrofuran-Argon Van Der Waals Complex" *Chem. Phys.*, **1997**, 218, 267–275.
[20] Blanco, S., López, J. C., Alonso, J. L., Ottaviani, P., Caminati, W. "Pure Rotational Spectrum and Model Calculations of Indole-Water" *J. Chem. Phys.*, **2003**, 119, 880–886.
[21] Kisiel, Z., Kosarzewski, J., Pszczółkowski, L. "Nuclear Quadrupole Coupling Tensor of CH_2Cl_2: Comparison of Quadrupolar and Structural Angles in Methylene Halides" *Acta Phys. Pol. A*, **1997**, 92, 507–516.
[22] Schmitz, D., Shubert, V. A., Betz, T., Schnell, M. "Multi-Resonance Effects within a Single Chirp in Broadband Rotational Spectroscopy: The Rapid Adiabatic Passage Regime for Benzonitrile" *J. Mol. Spectrosc.*, **2012**, 280, 77–84.
[23] Montero, S., Maté, B., Tejeda, G., Fernández, J. M., Ramos, A. "Raman Studies of Free Jet Expansion" in *Atomic and Molecular Beams. The state of Art 2000* ed. Campargue, R. Springer-Verlag, Berlin, 2001, pp. 295–306.
[24] Maté, B., Graur, I. A., Elizarova, T., Chirokov, I., Tejeda, G., Fernández, J. M., Montero, S. "Experimental and Numerical Investigation of an Axisymmetric Supersonic Jet" *J. Fluid Mech.*, **2001**, 426, 177–197.
[25] Steinfeld, J. I. *Molecules and Radiation* Dover Publications Inc., New York, 2005.

[26] Dyke, T. R., Tomasevich, G. R., Klemperer, W., Falconer, W. E. “Electric Resonance Spectroscopy of Hypersonic Molecular Beams” *J. Chem. Phys.*, **1972**, 57, 2277–2284.

Chapter IV

Hydrogen Bond Cooperativity in Formamide$_2$-Water, a Model for Water Mediated Interactions.

Direct transcription from: Blanco, S., Pinacho, P., López, J. C. *Angew. Chem. Int. Ed.*, **2016**, 128, 9477–9481.

Abstract

The rotational spectrum of formamide$_2$-H_2O formed in a supersonic jet has been characterized by Fourier transform microwave spectroscopy. This adduct provides a simple model of water mediated interaction involving the amide linkages, as occur in protein folding or amide association processes, showing the interplay between self-association and solvation. Mono-substituted ^{13}C, ^{15}N, ^{18}O and ^{2}H isotopologues have been observed to investigate the structure. The adduct forms an almost planar three body sequential cycle. The two formamide molecules link on one side through an N-H···O hydrogen bond and on the other side through a water-mediated interaction with the formation of C=O···H-O and O···H-N hydrogen bonds. The analysis of the quadrupole coupling effects due to the presence of two ^{14}N-nuclei reveals the subtle inductive forces associated to cooperative hydrogen bonding. These forces are involved in the changes detected in the C=O and C-N bond distances with respect to bare formamide.

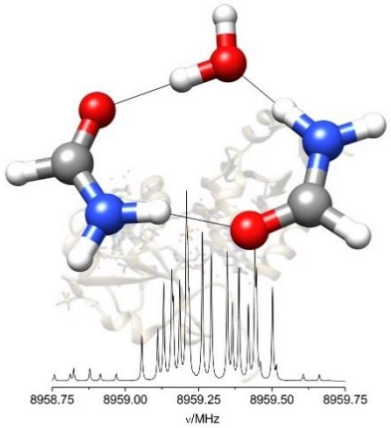

Hydrogen bonding (HB) is responsible for most of the inter- and intramolecular interactions that underpin protein folding, protein structure, biological activity and molecular recognition.[1,2] The HB interactions N-H···O=C involving the amide linkages dominate in the hydrophobic core of the proteins.[3] However, the mediation of water to form C=O···H-N contacts has been reported to occur in proteins with turn structures as far as the turns are located near the protein surface where they are exposed to interactions with water.[4] Water mediation has been also proposed to be important in the nucleation process of protein folding.[5] Another point of interest concerning HB in protein structures is the stabilization due to cooperative forces.[2,6,7] Cooperativity has contributions from entropy, due to the restrictions of internal motions, as well as from inductive polarization of the amide groups, not yet well established due to the short amount of experimental information on it.[8,9] The role of water to enhance, or not, HB cooperativity in those systems is still an open question.

Direct structural investigations of isolated clusters of molecules modeling amide-water, amide-amide and amide-amide water mediated interactions are important to better understand amide association processes showing the interplay between self-association and solvation. Under the isolated conditions of supersonic jets, clusters of molecules of different sizes can be formed in a controlled way. When jets are coupled to rotationally resolving techniques such as microwave spectroscopy accurate structural information can be obtained. Different examples of investigations on isolated hydrated amide clusters done in supersonic jets by microwave spectroscopy can be found in the literature.[9–16] These works, in particular the detailed investigation of the structures of formamide-$(H_2O)_n$ (n=1,2)[11] (see Figure 4.1), have led to the observation of the conformers build from the different docking sites of formamide and some of the structural signatures of the cooperative HB effects. In the present work we have undertaken the study of one of the simplest systems modeling amide-amide and amide-amide water-mediated interactions, the complex formed by two molecules of formamide and one water molecule (f_2w, see Figure 4.1). We have paid special attention to accurately determine its structure and the nuclear quadrupole coupling hyperfine constants of the two ^{14}N nuclei to search for the subtle signatures of cooperative effects, particularly those which cause the inductive polarization of the amide group.

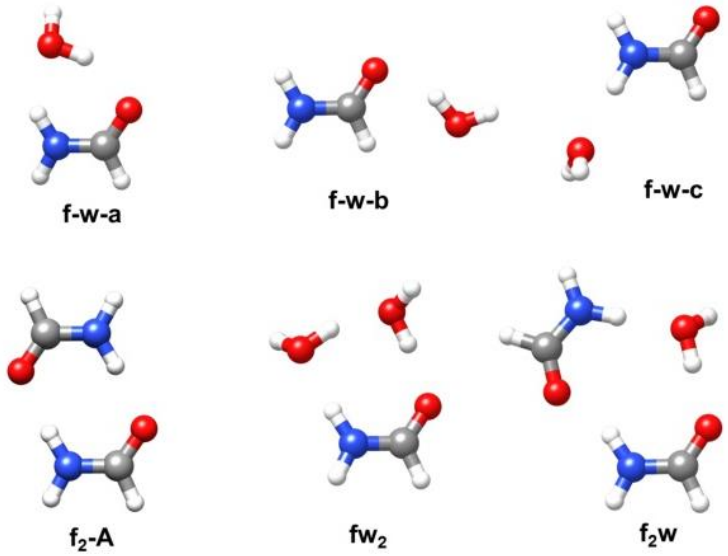

Figure 4.1. Adducts of formamide and water. The structures of formamide-H_2O (f-w-a, f-w-b, f-w-c),[11] formamide$_2$,[17] formamide-$(H_2O)_2$[11] and formamide$_2$-H_2O (this work) are shown.

We recorded the microwave spectrum of formamide-water complexes using the experimental setup described later. Once having dropped all signals with known frequencies,[11] several groups of unassigned lines appeared to show the complicated quadrupole coupling hyperfine structure (hfs) characteristic of species having two ^{14}N nuclei (see Figure 4.2).[18] This hfs results from the interaction of the nuclear quadrupole moment of the ^{14}N-nuclei (**I**=1), *eQ*, with the electric field gradient, *q*, at the site of the N nuclei. The corresponding spectroscopic constants, $\chi_{\alpha\beta}$ (α,β = *a*,*b*,*c*), are the elements of the nuclear quadrupole coupling tensor, set up in the inertial principal axis system representation, and are directly related to the electric field gradient at the nitrogen nuclei ($\chi_{\alpha\beta} = eQq_{\alpha\beta}$).

In order to identify these new lines we considered the spectroscopic constants predicted at the MP2/6-311++g(2d,p) level for the stable forms of formamide dimers[17] (f_2) and formamide$_2$-water (f_2w) adducts (see Supplementary Data Tables S4.1, S4.2 and Figures S4.1 and S4.2). The best match in both frequency and quadrupole coupling patterns corresponds to the predicted most stable f_2w conformer as can be seen in Figure 4.2. The most stable species of formamide dimer, f_2-A, (Figure 4.1), expected to be dominant by far in the gas phase, has an inversion center, and thus has no microwave spectrum. The assignment of the quadrupole coupling patterns for several R-branch μ_a-type transitions lead to the complete assignment of the μ_a- and μ_b-type R-branch spectra. The μ_c-type spectrum was not observed. The rotational parameters determined from the analysis of the spectrum are compared in Table 4.1 with the *ab initio* constants for the most stable form of f_2w complex.

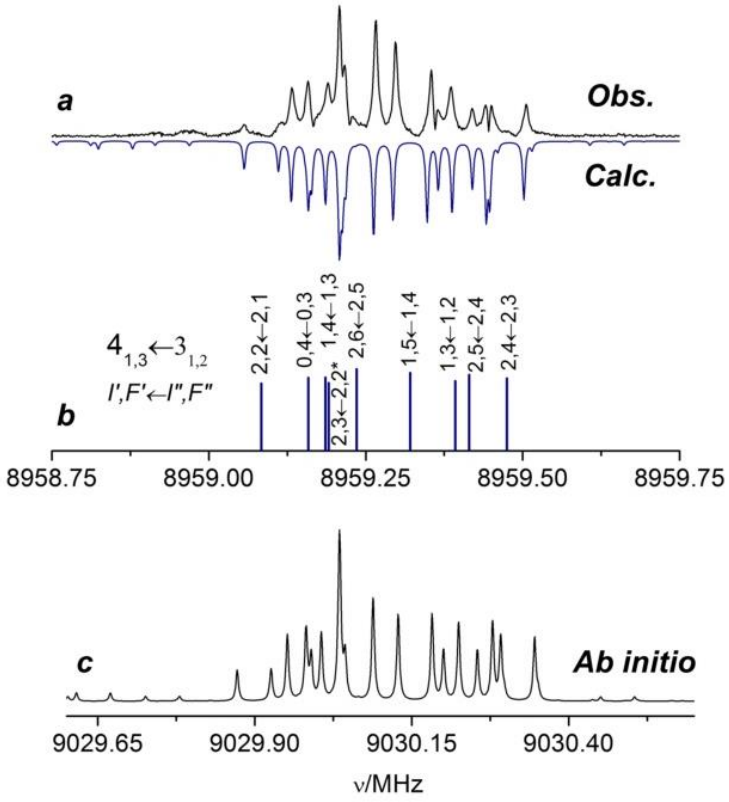

Figure 4.2. The transition observed around 8959.2 MHz shows the characteristic hyperfine structure of two ^{14}N nuclei, complicated by the Doppler doubling (54 kHz). (a) Comparison of the observed (upwards) and calculated (downwards) spectrum for the $4_{1,3}\leftarrow3_{1,2}$. (b) Assignment of the hyperfine components with the quantum numbers J, K_{-1}, K_{+1}, I, F (coupled basis set (I_1 I_2 I J F), $I_1 + I_2 = I$, $I + J = F$) (c) *Ab initio* prediction for conformer f_2w centered at 9029.2 MHz with a hyperfine structure comparable to that observed experimentally.

Table 4.1. Rotational parameters obtained from the analysis of the spectrum of the observed formamide$_2$-water adduct.

Fitted Parameters[a]	Exp. value[b]	*Ab initio* f2w
A/MHz	2769.21575(56)	2725
B/MHz	1232.34734(17)	1244
C/MHz	854.50629(10)	860
P_{cc} /uÅ^2	0.582754(80)	2.0317
$^{14}N_3$ χ_{aa}/MHz	1.0671(44)	1.09
$^{14}N_3$ χ_{bb}/MHz	1.9087(86)	2.05
$^{14}N_3\chi_{cc}$/MHz	-2.9757(86)	-3.14
$^{14}N_9$ χ_{aa}/MHz	1.2692(37)	1.20
$^{14}N_9$ χ_{bb}/MHz	1.7260(83)	1.80
$^{14}N_9$ χ_{cc}/MHz	-2.9952(83)	-3.00
N	206	
σ/kHz	1.5	

[a] *A*, *B* and *C* are the rotational constants. χ_{aa}, χ_{bb} and χ_{cc} are the quadrupole coupling constants for $^{14}N_3$ and $^{14}N_9$ nuclei (see Figure 4.3). N is the number of quadrupole hyperfine components fitted. σ is the rms deviations of the fit, the value 1.5 kHz is within the estimated accuracy of frequency measurements. $P_{cc} = (I_a + I_b - I_c)/2 = (\sum_i m_i c_i^2)/2$, is a planar moment of inertia (conversion factor 505679.1 MHz uÅ^2. [b] Standard error is given in parentheses in units of the last digit.

Well established structural determination methods beyond the simple conformation identification based on the comparison of the observed and *ab initio* rotational parameters use data from the spectra of the parent and isotopically substituted species. In order to exploit those methods, the spectra of the monosubstituted species $^{15}N_3$, $^{15}N_9$, $^{15}N_3$-$^{15}N_9$, $^{13}C_2$, $^{13}C_8$, $^{18}O_{14}$ and $^2H_{13}$ (see Figure 4.3 for labeling) were measured. The observation of the $^2H_{15}$ spectrum was not possible due to overlapping with other spectra. The complete sets of determined parameters, details of the analysis and observed frequencies are collected in the Supplementary Information, Tables S4.3-S4.12.

The nearly identical values of the B rotational constant (see Tables 4.1 and S4.4) for the parent and $^{18}O_{14}$ species indicates that the water oxygen atom lies along the *b* inertial axis. The planar moment of inertia, P_{cc}, which gives a measure of the mass extension out of the *ab* inertial plane, takes a nearly constant value (around 0.58 uÅ^2, see Tables 4.1 and S4.4) for all isotopologues. Therefore, a planar atom skeleton coincident with the *ab* inertial plane is concluded. Only the non-bonded water hydrogen atom, H_{15}, is out of this plane.

The Kraitchman, r_s, substitution method,[19] exploits changes in the moments of inertia upon mono-isotopic substitution to provide the absolute values of the atom coordinates of the substituted atoms in the principal inertial axis frame. This purely experimental approach allows to directly locating the different atoms of a molecule but it poses limitations for atoms located near the three principal axes. An alternative way to exploiting multi-isotopic information is to obtain the bond distances and angles from a least squares fit of all of the available rotational

parameters[20] to determine a total or partial effective ground state, r_0, structure. The r_0 principal inertial axis coordinates or those taken from *ab initio* computations can be used to assign the coordinate signs to the r_s coordinates allowing for the eventual unambiguous identification of a given cluster.

The results of the application of the r_s and r_0 methods are summarized in Figure 4.3 where they show a good consistency with the *ab initio* data. The r_s coordinates are collected in Table S4.13 of the supplementary information. The r_0 data and the details of the calculations are collected in Table S4.14 were they are compared to those of *ab initio* calculations. The experimental structure (see Figure 4.3) reflects that the two formamide subunits close a sequential cycle with water through three HBs, C=O···H–N, N–H···OH and O–H···O=C. This is possible thanks to the HB donor/acceptor double character of both water and formamide molecules. The HB lengths indicate that the dominant interaction is O-H···O=C as reported for related systems[11,12] and in agreement with the observed preference of water to interact with this group in globular proteins.[1]

The so called σ-bond cooperativity is associated to chains or cycles of hydrogen bonds between groups acting simultaneously as donor and acceptor.[2] Sequential cycles are characterized by a shortening of the hydrogen bond distances and an increment of hydrogen bond energy as the members of the cycle increase. The HB distances related to the O-H···O=C and N-H···O bonds of f_2w are shorter that those of related sequential cycles like formamide-$(H_2O)_n$ (n=1,2),[11] the water dimers[21] and trimers[22] or formamide dimer in liquid phase[23] (see Table S4.16). The f_2w bond lengths are only comparable to those of the three body adduct formamide-$(H_2O)_2$. Similar conclusions can be reached by considering the calculated dissociation energies (Table S4.16).
Resonance-assisted hydrogen bonding (RAHB)[8] or π-cooperative bonding was first pointed out to occur in the case of the peptide linkage[2,24] from studies of the crystal structures of small amides. The main effect of this cooperativity in the structure of formamide is the C=O bond enlargement and the C-N peptide bond length decrease due to the formation of open and closed dimers. This effect not yet reported in the gas phase from rotational spectroscopy has been observed in this work as illustrated in Scheme 4.1 where the r_0(C-N) and r_0(C=O) distances for formamide and f_2w (see Tables S4.14-S4.16) are shown.

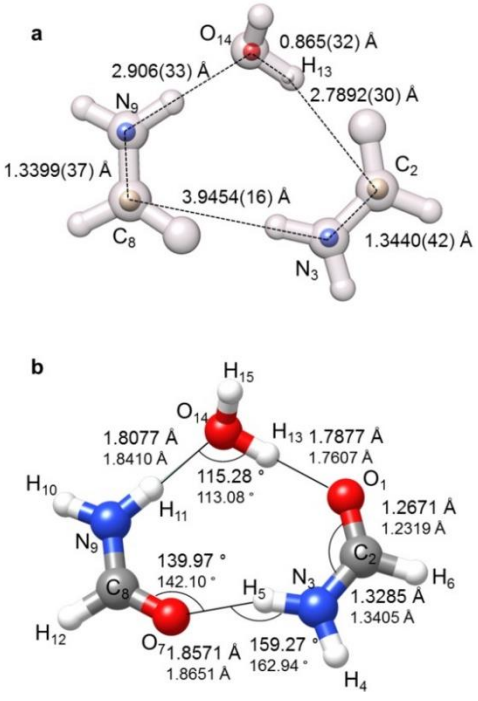

Figure 4.3. a) Comparison of the experimental r_s position of the isotopically substituted atoms of formamide$_2$-H_2O with the *ab initio* structure. The r_s interatomic distances are also given. b) The experimental r_0 bond lengths and angles of formamide$_2$-H_2O (upper values) compared to the *ab initio* MP2/6-311++G(2d,p) predictions.

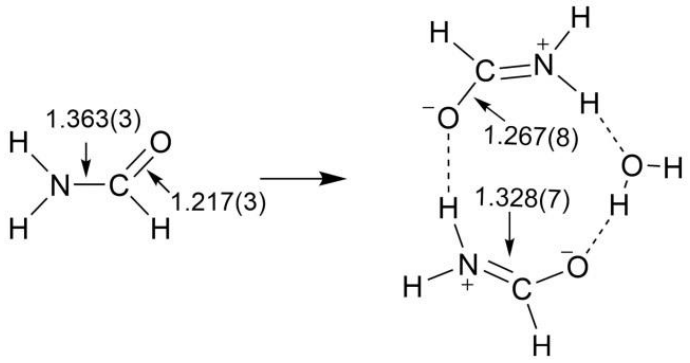

Scheme 4.1. Cooperative HB inductive effects in the formation of f_2w are evidenced by the C=O bond length enlargement and C-N bond length decrease.[2]

The ^{14}N quadruple coupling constants are expected to be very sensitive to the small changes in the electronic environment at these nuclei produced by inductive cooperative effects. A complete picture of the electric field gradient can only be obtained from the complete determination of the quadrupole coupling tensor. In the present case, only the diagonal elements have been determined, but we can still extract information from it. In bare formamide, the *c* inertial axis, perpendicular to the plane of the molecule, is parallel to one of the principal ^{14}N quadrupole coupling axis, say *z* ($\chi_{cc}=\chi_{zz}$). Given the planarity of the skeleton of f_2w, its *c* inertial axis is almost perpendicular to the formamide molecular planes so $\chi_{cc}\approx\chi_{zz}$. This planar arrangement is common to all complexes of water and formamide studied so far.[11] As shown in Table S4.17 there is a progressive decrease in the value of χ_{cc} going from formamide to its microsolvated complexes. The agreement between the experimental decrements and the *ab initio* values, based on a static picture, allow to discard intermolecular oscillations[25] as the main cause of this effect. This correlation in the values of χ_{cc} indicates that the electronic environment of the N atom of formamide is altered to some extent by the formation of one or successive HBs.

	f	f-w-a	fw_2	f_2wN_3	f_2wN_9	f-w-b
χ_{zz}/eQq_{210}	0.385	0.337	0.308	0.298	0.300	0.360
$-(U_p)_z$	0.382	0.330	0.299	0.299	0.301	0.364
η_D	0.042	0.224	0.348	0.346	0.384	0.038

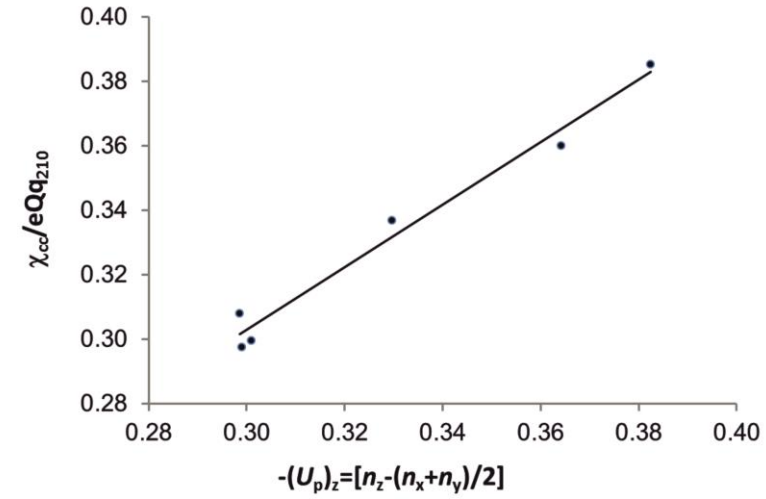

Figure 4.4. Plot of the values (see top table) of the quantity χ_{cc}/eQq_{210} vs. the unbalanced $2p_z$ electronic charge $(U_p)_z$ obtained from a NBO analysis of formamide, formamide-H_2O (f-w-a), formamide-$(H_2O)_2$ (fw_2) and formamide$_2$-H_2O (f_2w). The slope of the line is 0.96.

The electric field gradient giving rise to nuclear quadrupole coupling in molecules has often been attributed to the unequal filling of the p orbitals of the valence shell of the coupling atoms.[18] According to this, the ^{14}N χ_{zz} constants can be related to the unbalanced $2p_z$ electronic charge $(U_p)_z = \left[\left(n_x - n_y\right)/2 - n_z\right]$ by:

$$\chi_{zz}/eQq_{210} = -(U_p)_z \quad (1)$$

where n_α are the p_α orbital occupation numbers and q_{210} the electric field gradient associated to a 2p electron in an isolated atom (eQq_{210}≈-10 MHz for N). This definition of $(U_p)_z$ is such that its positive or negative values correspond respectively to electron deficit or excess along the *z* reference axis.[18] The values of χ_{zz}/eQq_{210} obtained from the experimental χ_{cc} values are plotted in Figure 4.4 *vs.* those calculated using the natural atomic orbital populations from a natural bond orbital (NBO) analysis.[26] Despite the approximations, they show and excellent agreement. According to the definition of $(U_p)_z$, the electron density excess along the *z* axis in formamide decreases progressively in the complexes as the size of the cycle increases. There is a small decrease even for f-w-b ($-(U_p)_z$=0.36), where the NH_2 is not involved in HB. This illustrates how the amide group is progressively polarized due to inductive effects, which increase with the number of cooperating hydrogen bonds.

The asymmetry parameter $\eta_D = \left|\left(\chi_{yy} - \chi_{xx}\right)/\chi_{zz}\right|$, which takes values between 0 and 1, measures the deviation of the charge distribution from axial symmetry (η_D = 0). The *ab initio* values of η_D (see Figure 4.4 and Table S4.17) show noticeable changes from formamide and f-w-b, which are predicted to have an almost symmetric distribution of charge(η_D = 0.04), to formamide-H_2O (η_D = 0.22) and for three body clusters (η_D = 0.35-0.38). The NBO analysis gives additional information about charge transfer in these clusters and allows us to give an interpretation of the steady enlargement of the C=O bond and decrease of C-N bond of formamide in the sequential cycle clusters based on the progressive increase of electron density on the carbonyl group π* antibonding orbital and the progressive decrease of the small electron density in the C-N bond σ* natural orbital, respectively.

In conclusion the adduct formamide$_2$-H_2O studied in this work illustrates the way in which water may act as mediator in amide association processes like those of protein folding. The structure of the complex reflects clearly the effects of hydrogen bonding σ and π-cooperativity.[2] The HB distances are shorter than in related sequential cycles. It adopts a cyclic planar structure for the heavy atom skeleton showing a directionality that may be important in the process of protein folding. The C-N and C=O distances of formamide subunits became shorter or larger, respectively, upon formation of the complex. One of the most interesting aspects of this research is the confirmation that the quadrupole coupling interaction can be taken as a probe for the inductive processes accompanying cooperativity which alter the electronic structure of the amide group upon polarization. Another remarkable result concerning cooperative effects, is the similarity observed in the structural and quadrupole coupling data in the three body adducts formamide$_2$-H_2O and formamide-$(H_2O)_2$. This suggests that the acid/base properties of formamide and water are not very different. In this way, if formamide-$(H_2O)_2$ is considered as a microsolvated formamide adduct, formamide$_2$-H_2O could also be seen as a microsolvated water adduct being formamide the solvent in this case. Finally this work shows that water is able to enhance cooperative HB effects which can be important when water mediates in the nucleation process of protein folding.

Experimental Section

Commercial samples of the parent and isotopic species of formamide and water were used. The molecular-beam Fourier transform microwave spectrometer (MB-FTMW), described elsewhere,[27] was operated in the frequency range 5-13 GHz. The supersonic jet was generated by expansion of a gas mixture He-Ne at backing pressures of about 12 bar through a small (0.9 mm diameter) pulsed heatable nozzle.[28] Formamide (b.p. 210ºC) was placed in a nozzle at about 50ºC and water in a reservoir inserted in the gas line just before the nozzle. Short (typ. 0.3 □s, 10-300 mW) microwave pulses were used for polarization purposes. Typically, a ca. 400 □s-length time domain spectrum was recorded in 40-100 ns intervals and converted to the frequency domain by a fast Fourier transformation. Due to the collinear arrangement of the jet and resonator axis each rotational transition splits in two Doppler components so the resonant frequencies are taken as the arithmetic mean of both components. Frequency accuracy is better than 3 kHz. *Ab initio* calculations (MP2/6-311++G(2d,p)) were done using the G09 package.[29] The counterpoise procedure[30] was used to calculate the dissociation energies. NBO analysis were also done using NBO 5.9.[31]

References

[1] Baker, E. N., Hubbard, R. E. "Hydrogen bonding in globular proteins" *Prog. Biophys. Mol. Biol.*, **1984**, 44, 97–179.
[2] Jeffrey, G. A. "*Introduction to Hydrogen Bonding"*, Oxford University Press, Oxford, 1997.
[3] Venkatachalam, C. M. "Stereochemical criteria for Polypeptides and Proteins. V. Conformation of a System of Three Linked Peptide Units" *Biopolymers*, **1968**, 6, 1425–1436.
[4] Kuntz, I. D. "Protein Folding" *J. Am. Chem. Soc.* **1972**, 94, 4009–4012.
[5] Busch, S., Bruce, C. D., Redfield, C., Lorenz, C. D., McLain, S. E. "Water Mediation is Essential to Nucleation of β-Turn Formation in Peptide Folding Motifs" *Angew. Chem. Int. Ed.* **2013**, 52, 13091–13095.
[6] Mahadevi, A. S., Sastry, G. N. "Cooperativity in Noncovalent Interactions" *Chem. Rev.* **2016**, 116, 2775–2825.
[7] Kawai, H., Katoono, R., Nishimura, K., Matsuda, S., Fujiwara, K., Tsuji, T., Suzuki, T. "Positive Homotropic Allosteric Binding of Benzenediols in a Hydrindacene-Based Exoditopic Receptor: Cooperativity in Amide Hydrogen Bonding" *J. Am. Chem. Soc.* **2004**, 126, 5034–5.
[8] Gilli, P., Bertolasi, V., Ferretti, V., Gilli, G. "Evidence for Intramolecular N-H···O Resonance Assisted Hydrogen Bonding in *β*-Enaminones and Related Heterodienes. A Combined Crystal-Structural, IR, and NMR Spectroscopic, and Quantum-Mechanical Investigation" *J. Am. Chem. Soc.*, **2000**, 122, 10405–10417.
[9] Held, A., Pratt, D. W. "Hydrogen Bonding in Water Complexes. Structures of 2-Pyridone-H_2O and 2-Pyrididone-(H2O)2 in Their S0 and S1 Electronic States" *J. Am. Chem. Soc.*, **1993**, 115, 9708–9717.
[10] Lovas, F. J., Suenram, R. D., Fraser, G. T., Gillies, C. W., Zozom, J. "The Microwave Spectrum of Formamide-Water and Formamide-Methanol Complexes" *J. Chem. Phys.*, **1988**, 88, 722–729.
[11] Blanco, S., López, J. C., Lesarri, A., Alonso, J. L. "Microsolvation of Formamide: A Rotational Study" *J. Am. Chem. Soc.*, **2006**, 128, 12111–12121.
[12] López, J. C., Sanchez, R., Blanco, S., Alonso, J. L. "Microsolvation of 2-Azetidinone: A Model for the Peptide Group-Water Interactions" *Phys. Chem. Chem. Phys.* **2015**, 17, 2054–2066.
[13] Caminati, W., López, J. C., Blanco, S., Mata, S., Alonso, J. L. "How Water Links to *Cis* and *Trans* Peptidic Groups: The Rotational Spectrum of N-Methylformamide-Water" *Phys. Chem. Chem. Phys.*, **2010**, 12, 10230–10234.
[14] Lavrich, R. J., Tubergen, M. J. "Conformation and Hydrogen Bonding in the Alaninamide-Water van der Waals Complex" *J. Am. Chem. Soc.* **2000**, 122, 2938–2943.
[15] Maris, A., Ottaviani P., Caminati, W. "Pure Rotational Spectrum of 2-Pyridone···Water and Quantum Chemical Calculations on the Tautomeric Equilibrium 2-Pyridone···Water/2-Hydroxypyridine···Water" *Chem. Phys. Lett.*, **2002**, 360, 155–160.
[16] Mata, S., Cortijo, V., Caminati, W., Alonso, J. L., Sanz, M. E., López, J. L., Blanco, S. "Tautomerism and Microsolvation in 2-Hydroxypyridine/2-Pyridone" *J. Phys. Chem. A*, **2010**, 114, 11393–11398.
[17] Colominas, C., Luque, F. J., Orozco, M. "Dimerization of Formamide in the Gas Phase and Solution. An *Ab Initio* MC-MST Study" *J. Phys. Chem. A* **1999**, 103, 6200–6208.
[18] Gordy, W., Cook, R. L. *Microwave Molecular Spectra* Wiley-Interscience, New York, 1984.
[19] Kraitchman, J. "Determination of Molecular Structure from Microwave Spectroscopic Data" *Am. J. Phys.*, **1953**, 21, 17–24.
[20] Kisiel, Z. "Least-Squares Mass-Dependence Molecular Structures for Selected Weakly Bound Intermolecular Clusters" *J. Mol. Spectrosc.*, **2003**, 218, 58–67.
[21] Dyke, T. R.; Mack, K. M.; Muenter, J. S. "The Structure of Water Dimer from Molecular Beam Electric Resonance Spectroscopy" *J. Chem. Phys.* **1977**, 66, 498–510.
[22] Keutsch, F. N.; Cruzan, J. D.; Saykally, R. J. "The Water Trimer" *Chem. Rev.* **2003**, 103, 2533–2577.
[23] Kálmán, E., Serke, I., Pálinkás, G., Zeidler, M. D., Wiesmann, F. J., Bertagnolli, H., Chieux, P. "The Molecular Structure and Hydrogen Bond Geometry in Liquid Formamide: Electron, Neutron, and X-Ray Diffraction Studies" *Zeitschrift für Naturforsch. A* **1983**, 38, DOI 10.1515/zna-1983-0221.
[24] Ottersen, T., Svanström, P., Tiddy, G. J. T., Heimbach, P., Skoglund, U., "On the structure of the Peptide Linkage. The Structures of Formamide and Acetamide at -165 Degrees C and an *Ab Initio* Study of Formamide, Acetamide and N-methylformamide" *Acta Chem. Scand.* **1975**, 29a, 939–944.
[25] Legon, A. C. "Non-Linear Hydrogen Bond and Rotational Spectroscopy: Measurement and Rationalisation of the Deviation from Linearity" *Faraday Discuss.* **1994**, *97*, 19-33.
[26] Reed, A. E., Weinstock, R. B., Weinhold, F. "Natural Population Analysis" *J. Chem. Phys.* **1985**, *83*, 735-746.

[27] Alonso, J. L., Lorenzo, F. J., López, J. C., Lesarri, A., Mata, S., Dreizler, H. "Construction of a Molecular Beam Fourier Transform Microwave Spectrometer Used to Study the 2,5-Dihydrofuran-Argon Van Der Waals Complex" *Chem. Phys.*, **1997**, 218, 267–275.
[28] Blanco, S., López, J. C., Alonso, J. L., Ottaviani, P., Caminati, W. "Pure Rotational Spectrum and Model Calculations of Indole-Water" *J. Chem. Phys.*, **2003**, 119, 880–886.
[29] *Gaussian09, Revis. E.01, M. J. Frisch et al., Gaussian Inc., Wallingford, CT* **2009**.
[30] Boys, S., Bernardi, F. "The Calculation of Small Molecular Interactions by the Differences of Spearate Total Energies. Some Procedures with Reduced Errors" *Mol. Phys.*, 1970, **19**, 553–566.
[31] E. D. Glendening, J. K. Badenhoop, A. E. Reed, J. E. Carpenter, J. A. Bohmann, C. M. Morales, F. Weinhold, *Theor. Chem. Institute, Univ. Wisconsin, Madison* **2001**.

Supplementary material for Chapter IV

Hydrogen Bond Cooperativity in Formamide$_2$-Water, a Model for Water Mediated Interactions.

Direct transcription from: Blanco, S., Pinacho, P., López, J. C. *Angew. Chem. Int. Ed.*, **2016**, 128, 9477–9481.

Abstract

The rotational spectrum of formamide$_2$-H_2O formed in a supersonic jet has been characterized by Fourier transform microwave spectroscopy. This adduct provides a simple model of water mediated interaction involving the amide linkages, as occur in protein folding or amide association processes, showing the interplay between self-association and solvation. Mono-substituted ^{13}C, ^{15}N, ^{18}O and ^{2}H isotopologues have been observed to investigate the structure. The adduct forms an almost planar three body sequential cycle. The two formamide molecules link on one side through an N-H···O hydrogen bond and on the other side through a water-mediated interaction with the formation of C=O···H-O and O···H-N hydrogen bonds. The analysis of the quadrupole coupling effects due to the presence of two ^{14}N-nuclei reveals the subtle inductive forces associated to cooperative hydrogen bonding. These forces are involved in the changes detected in the C=O and C-N bond distances with respect to bare formamide.

- Complete reference [29]

- Figures S4.1 and S4.2. Stable formamide$_2$ and formamide$_2$-water conformers.

- Tables S4.1 and S4.2. Results of *ab initio* computations on the stable formamide$_2$ and formamide$_2$-water conformers.

- Tables S4.3 and S4.4. Spectroscopic parameters determined for the parent and monosubstituted isotopologues of formamide$_2$-water adduct.

- Tables S4.5-S4.12. Observed transition frequencies.

- Tables S4.13-S4.16. Tables reporting the results of application of r_s and r_0 methods to formamide$_2$-water from the rotational parameters in tables S4.3 and S4.4.

- Table S4.17. Tables with the quadrupole coupling constants of different formamide and water adducts and comparison with the results of *ab initio* computations and NBO analysis.

Complete reference [29]

Gaussian 09, Revision E.01, M. J. Frisch, G. W. Trucks, H. B. Schlegel, G. E. Scuseria, M. A. Robb, J. R. Cheeseman, G. Scalmani, V. Barone, B. Mennucci, G. A. Petersson, H. Nakatsuji, M. Caricato, X. Li, H. P. Hratchian, A. F. Izmaylov, J. Bloino, G. Zheng, J. L. Sonnenberg, M. Hada, M. Ehara, K. Toyota, R. Fukuda, J. Hasegawa, M. Ishida, T. Nakajima, Y. Honda, O. Kitao, H. Nakai, T. Vreven, J. A. Montgomery, Jr., J. E. Peralta, F. Ogliaro, M. Bearpark, J. J. Heyd, E. Brothers, K. N. Kudin, V. N. Staroverov, R. Kobayashi, J. Normand, K. Raghavachari, A. Rendell, J. C. Burant, S. S. Iyengar, J. Tomasi, M. Cossi, N. Rega, J. M. Millam, M. Klene, J. E. Knox, J. B. Cross, V. Bakken, C. Adamo, J. Jaramillo, R. Gomperts, R. E. Stratmann, O. Yazyev, A. J. Austin, R. Cammi, C. Pomelli, J. W. Ochterski, R. L. Martin, K. Morokuma, V. G. Zakrzewski, G. A. Voth, P. Salvador, J. J. Dannenberg, S. Dapprich, A. D. Daniels, Ö. Farkas, J. B. Foresman, J. V. Ortiz, J. Cioslowski, and D. J. Fox, Gaussian, Inc., Wallingford CT, 2009.

Figure S4.1. Stable conformers predicted for formamide dimer following Colominas et al.[17]. The corresponding parameters are given in Table S4.1.

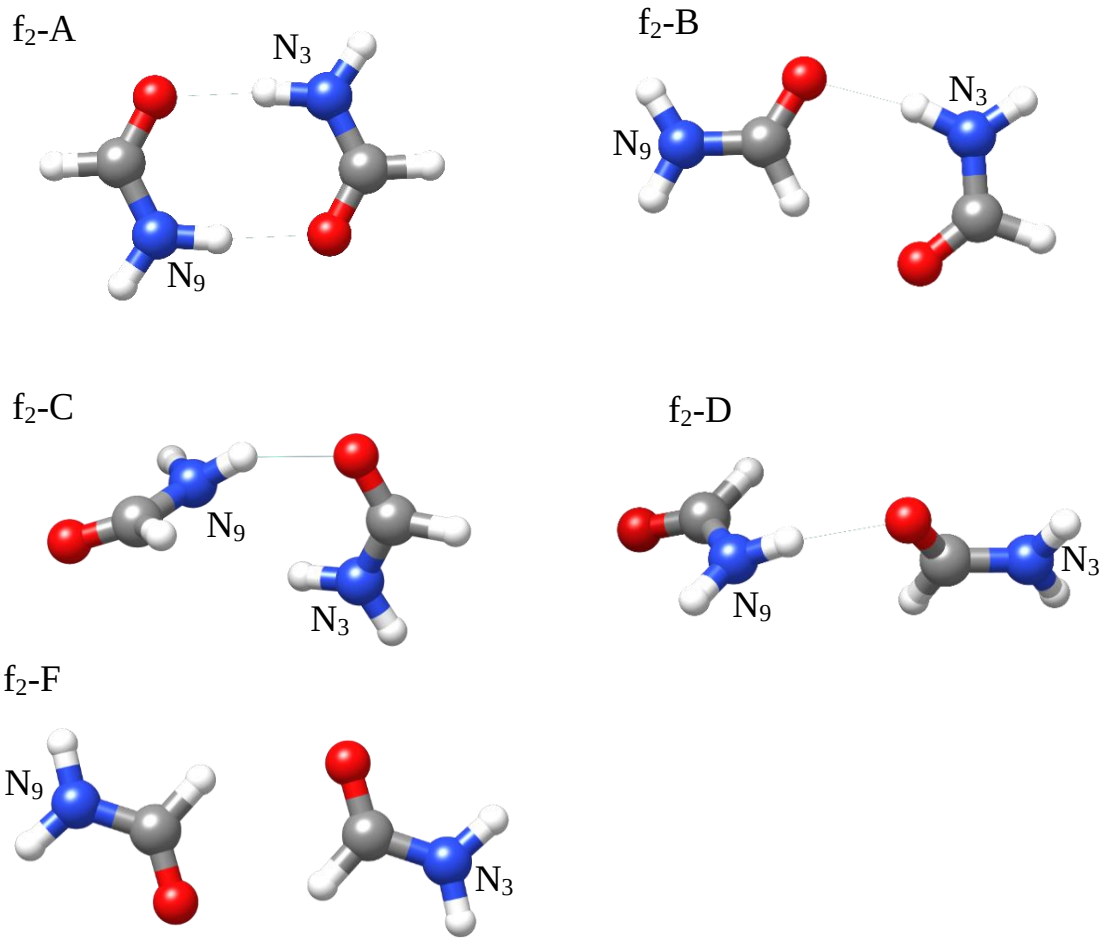

Figure S4.2. Stable conformers predicted for formamide$_2$-water heterotrimers. The corresponding parameters are given in S4.2.

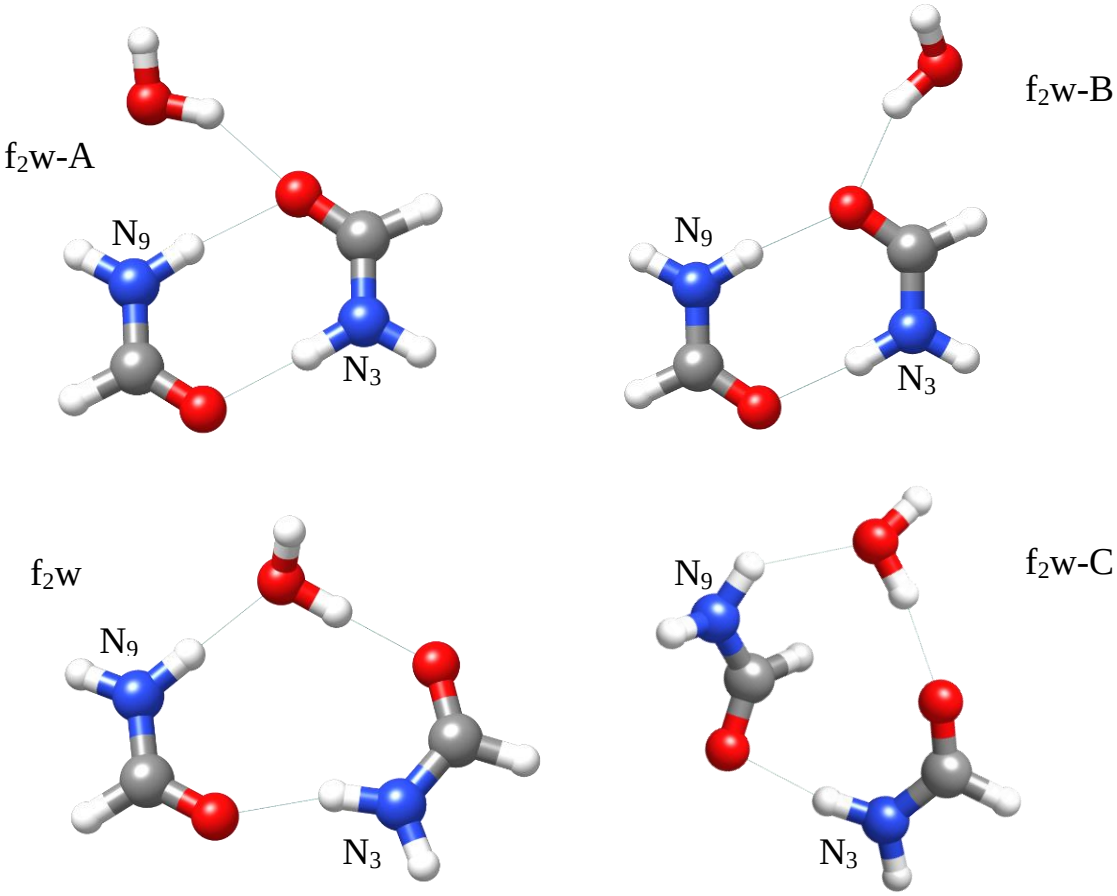

Table S4.1. Rotational parameters predicted from *ab initio* MP2/6-311++G(2d,p) calculations for the stable formamide dimers (f_2) conformers following ref [17].

Parameter[a]	**f_2-A**	**f_2-B**	**f_2-C**	**f_2-D**	**f_2-F**
A/MHz	5653	7041	7958	12110	9082
B/MHz	1995	1508	1288	964	1167
C/MHz	1474	1242	1185	924	1034
P_a /uÅ^2	253.3925	335.1315	377.6755	514.7334	433.0867
P_b /uÅ^2	89.4698	71.7760	48.8055	32.2136	55.6745
P_{cc}/uÅ^2	-0.0697	0.0006	14.7003	9.5187	-0.0283
μ_a/D	0.00	-1.70	-3.93	7.10	0.00
μ_b/D	0.00	0.40	-3.05	-1.10	0.00
μ_c/D	0.00	0.00	0.36	1.10	0.00
$^{14}N_3$ χ_{aa}/MHz	1.04	1.22	-1.57	0.86	1.61
$^{14}N_3$ χ_{bb}/MHz	2.18	2.19	1.06	-0.52	-3.60
$^{14}N_3\chi_{cc}$/MHz	-3.22	-3.42	0.52	-0.34	1.99
$^{14}N_3$ χ_{ab}/MHz	0.10	0.18	1.36	1.17	1.50
$^{14}N_3$ χ_{ac}/MHz	0.00	0.00	-2.41	-1.03	-0.03
$^{14}N_3\chi_{bc}$/MHz	0.00	0.00	0.93	2.58	0.00
$^{14}N_9$ χ_{aa}/MHz	1.04	1.97	-0.83	1.67	1.60
$^{14}N_9$ χ_{bb}/MHz	2.18	1.92	1.13	0.19	-3.59
$^{14}N_9$ χ_{cc}/MHz	-3.21	-3.89	-0.34	-1.86	1.99
$^{14}N_9$ χ_{ab}/MHz	0.10	0.03	-1.17	-0.84	1.51
$^{14}N_9$ χ_{ac}/MHz	0.00	0.00	2.49	-1.11	-0.03
$^{14}N_9$ χ_{bc}/MHz	0.00	0.00	0.60	-2.52	-0.01
E/h	-339.103830	-339.096787	-339.093730	-339.092444	-339.089576
ΔE/ kJmol^{-1}	0.0	18.5	27.0	30.0	37.0

[a] A, B and C are the rotational constants; χ_{aa}, χ_{bb}, χ_{cc}, χ_{ab}, χ_{ac} and χ_{bc} are the quadrupole coupling tensor elements for $^{14}N_3$ and $^{14}N_9$ nuclei. E is the calculated energy and ΔE the energy relative to conformer f2-A.

Table S4.2. Rotational parameters predicted from *ab initio* MP2/6-311++G(2d,p) calculations for the stable formamide$_2$-water (f_2w) conformers.

Parameter[a]	**f_2w-A**	**f_2w-B**	**f_2w**	**f_2w-C**
A/MHz	1994	3944	2725	2339
B/MHz	1688	938	1244	1589
C/MHz	915	759	860	962
P_a /uÅ^2	299.1361	538.2468	404.2216	313.6622
P_b /uÅ^2	253.1908	127.6018	183.4285	211.6799
P_{cc}/uÅ^2	0.2591	0.5369	2.0317	4.3864
μ_a/D	-0.5	1.7	-1.4	1.5
μ_b/D	1.6	-0.9	-0.9	0.9
μ_c/D	0.6	0.8	-0.7	0.1
$^{14}N_3$ χ_{aa}/MHz	1.97	1.07	1.09	1.34
$^{14}N_3$ χ_{bb}/MHz	1.07	1.93	2.05	1.87
$^{14}N_3\chi_{cc}$/MHz	-3.09	-3.00	-3.14	-3.21
$^{14}N_3$ χ_{ab}/MHz	0.43	0.37	0.24	0.46
$^{14}N_3$ χ_{ac}/MHz	-0.15	-0.01	-0.25	0.04
$^{14}N_3\chi_{bc}$/MHz	-0.15	-0.45	-0.32	0.33
$^{14}N_3$ χ_{xx}/MHz	2.15	2.10	2.14	2.15
$^{14}N_3$ χ_{yy}/MHz	0.90	0.94	1.04	1.09
$^{14}N_3\chi_{zz}$/MHz	-3.04	-3.04	-3.18	-3.24
$^{14}N_9$ χ_{aa}/MHz	1.89	1.19	1.20	0.04
$^{14}N_9$ χ_{bb}/MHz	1.20	2.06	1.80	0.72
$^{14}N_9$ χ_{cc}/MHz	-3.09	-3.25	-3.00	-0.75
$^{14}N_9$ χ_{ab}/MHz	0.28	0.32	-0.52	1.00
$^{14}N_9$ χ_{ac}/MHz	-0.06	-0.18	0.80	2.37
$^{14}N_9$ χ_{bc}/MHz	0.20	0.15	-0.31	1.29
$^{14}N_9$ χ_{xx}/MHz	1.99	2.17	2.12	2.05
$^{14}N_9$ χ_{yy}/MHz	1.11	1.09	0.842	1.36
$^{14}N_9$ χ_{zz}/MHz	-3.10	-3.26	-2.96	-3.41
E/h	-415.4062426	-415.4048891	-415.4082857	-415.4040319
ΔE/ cm^{-1}	448	745	0.0	933
ΔE/ kJmol^{-1}	5.4	8.9	0.0	11.2
D_e/kJmol^{-1}	85.1	83.3	89.8	78.6

[a] *A*, *B* and *C* are the rotational constants; χ_{aa}, χ_{bb}, χ_{cc}, χ_{ab}, χ_{ac} and χ_{bc} are the quadrupole coupling tensor elements set up in the principal inertial axis (a,b,c) system for $^{14}N_3$ and $^{14}N_9$ nuclei; χ_{xx}, χ_z, χ_{zz} are the corresponding elements for the tensor set up in the electric field gradient principal axis (x, y, z). E is the calculated energy and ΔE the energy relative to conformer f_2w. D_e is the dissociation energy calculated using BSSE corrections[30].

Table S4.3. Rotational parameters obtained from the analysis of the spectrum of the observed formamide$_2$-water adduct. The analysis of the spectrum [H. M. Pickett, *J. Mol. Spectrosc.* **1991**, *148*, 371–377] was done using a Hamiltonian including the semirigid rotor Hamiltonian of Watson [J. K. G. Watson, in *Vibrational Spectra and Structure Vol 6* (Ed.: J.R. Durig), Elsevier, New York, **1977**, pp. 1–89] (A-reduction, I^r representation) and a term to account for the quadrupole coupling contributions[18]. This term was set up in the coupled basis set (I_1 I_2 I J F), I_1 + I_2 = I, I + J = F [H. M. Foley, *Phys. Rev.* **1947**, *71*, 747–751]. The energy levels involved in each transition were labelled (see Figure 4.2). The rotational parameters determined from analysis of the spectrum are compared in Table 4.1 with the *ab initio* constants for the most stable form of f$_2$w complex.

Fitted parameters[a]	Exp. value[b]	*Ab initio* f$_2$w
A/MHz	2769.21575(56)	2725
B/MHz	1232.34734(17)	1244
C/MHz	854.506290(96)	860
Δ_J/kHz	0.3846(18)	0.41
Δ_{JK}/kHz	0.413(11)	0.33
Δ_K/kHz	6.71(11)	5.11
δ_J/kHz	0.13670(88)	0.12
δ_K/kHz	1.399(26)	1.24
$^{14}N_3$ 3/2(χ_{aa})/MHz	1.6006(66)	1.64
$^{14}N_3$ ¼(χ_{bb}-χ_{cc}) /MHz	1.2211(32)	1.30
$^{14}N_9$ 3/2(χ_{aa}) /MHz	1.9038(56)	1.81
$^{14}N_9$ ¼(χ_{bb}-χ_{cc}) /MHz	1.1803(33)	1.20
N	206	
σ/kHz	1.46	

Derived parameters		
P_a /uÅ^2	409.511936(80)	404.2216
P_b /uÅ^2	181.916244(80)	183.4285
P_c /uÅ^2	0.582753(80)	2.0317
$^{14}N_3$ χ_{aa}/MHz	1.0671(44)	1.09
$^{14}N_3$ χ_{bb}/MHz	1.9087(86)	2.05
$^{14}N_3\chi_{cc}$/MHz	-2.9757(86)	-3.14
$^{14}N_9$ χ_{aa}/MHz	1.2692(37)	1.20
$^{14}N_9$ χ_{bb}/MHz	1.7260(83)	1.80
$^{14}N_9$ χ_{cc}/MHz	-2.9952(83)	-3.00

[a] *A*, *B* and *C* are the rotational constants. Δ_J, Δ_{JK}, Δ_K, δ_J and δ_K are the quartic centrifugal distortion constants. χ_{aa}, χ_{bb} and χ_{cc} are the quadrupole coupling constants for $^{14}N_3$ and $^{14}N_9$ nuclei (see Figure 4.3). N is the number of quadrupole hyperfine components fitted. σ is the rms deviations of the fit. P_α (α= a, b or c) are the planar moments of inertia; these are derived from the moments of inertia I_α as for example $P_c=(I_a+I_b-I_c)/2$.[b] Standard errors are given in parentheses in units of the last digit.

Table S4.4. Rotational parameters obtained from the analysis of the spectrum of the observed isotopologues of the f_2w cluster

Fitted Parameters[a]	$^{18}O_{14}$	^{15}N-^{15}N	$^{15}N_3$	$^{15}N_9$	$^{13}C_2$	$^{13}C_8$	$^{2}H_{13}$
A/MHz	2633.7757(16)[b]	2733.6359(26)	2763.5246(13)	2739.0250(14)	2765.7480(38)	2761.7068(61)	2726.9915(83)
B/MHz	1232.365309(74)	1207.91087(20)	1214.74425(17)	1225.59897(23)	1214.56401(15)	1215.70040(24)	1230.83563(37)
C/MHz	841.158524(55)	839.36918(20)	845.48145(10)	848.38239(12)	845.596045(98)	845.76749(16)	849.73305(22)
$^{14}N_3$ 3/2(χ_{aa})/MHz	[1.6006] c	-	1.641(20)	-	[1.6006]	[1.6006]	[1.6006]
$^{14}N_3$ ¼(χ_{bb}-χ_{cc}) /MHz	[1.2225]	-	1.2245(46)	-	[1.2225]	[1.2225]	[1.2225]
$^{14}N_9$ 3/2(χ_{aa}) /MHz	[1.9038]	-	-	1.895(29)	[1.9038]	[1.9038]	[1.9038]
$^{14}N_9$ ¼(χ_{bb}-χ_{cc}) /MHz	[1.1803]	-	-	1.1764(49)	[1.1803]	[1.1803]	[1.1803]
N	70	27	34	38	44	47	22
σ/kHz	2.5	2.6	2.4	3.1	3.8	3.1	3.2
Derived Parameters							
P_a /uÅ^2	409.508989(90)	417.80533(16)	415.45191(10)	411.76973(12)	415.5157(19)	415.12704(30)	410.01201(40)
P_b /uÅ^2	191.304158(90)	184.28861(16)	182.28929(10)	183.92757(12)	182.14441(19)	182.41201(30	184.73842(40
P_c /uÅ^2	0.579721(90)	0.58572(16)	0.58554(10)	0.58301(12)	0.58341(19)	0.58320(30)	0.58636(40)
$^{14}N_3$ χ_{aa}/MHz	[1.0671]	-	1.094(13)	-	[1.0671]	[1.0671]	[1.0671]
$^{14}N_3$ χ_{bb}/MHz	[1.9087]	-	1.902(16)	-	[1.9087]	[1.9087]	[1.9087]
$^{14}N_3\chi_{cc}$/MHz	[-2.9757]	-	-2.996(16)	-	[-2.9757]	[-2.9757]	[-2.9757]
$^{14}N_9$ χ_{aa}/MHz	[1.2692]	-	-	1.263(19)	[1.2692]	[1.2692]	[1.2692]
$^{14}N_9$ χ_{bb}/MHz	[1.7260]	-	-	1.721(19)	[1.7260]	[1.7260]	[1.7260]
$^{14}N_9$ χ_{cc}/MHz	[-2.9952]	-	-	-2.984(19)	[-2.9952]	[-2.9952]	[-2.9952]

[a] *A*, *B* and *C* are the rotational constants. Δ_J, Δ_{JK}, Δ_K, δ_J and δ_K are the quartic centrifugal distortion constants. χ_{aa}, χ_{bb} and χ_{cc} are the quadrupole coupling constants for $^{14}N_3$ and $^{14}N_9$ nuclei. N is the number of quadrupole hyperfine components fitted. σ is the rms deviations of the fit. P_α (α= a, b or c) are the planar moments of inertia; these are derived from the moments of inertia I_α as for example $P_c=(I_a+I_b-I_c)/2$. [b] Standard errors are given in parentheses in units of the last digit. [c] Parameters in square brackets were kept fixed as those given for the parent species in the fit.

Table S4.5. Observed rotational transitions with resolved ^{14}N hyperfine structure and residuals (all the values in MHz) for the parent species of the cluster Formamide$_2$···H$_2$O in the ground vibrational state for transitions of the type $J'K'_{-1}K'_{+1}I'F' \leftarrow J''K''_{-1}K''_{+1}I''F''$.

J'	K'_{-1}	K'_{+1}	J''	K''_{-1}	K''_{+1}	I'	F'	I''	F''	Obs.	Obs. – Calc.
2	1	2	1	0	1	1	2	1	1	5332.2721	0.0031
						2	4	2	3	5332.4172	0.0004
						1	3	1	2	5332.8833	0.0001
						2	3	2	2	5333.1695	0.0008
						2	2	0	1	5333.6657	-0.0022
2	2	0	1	1	1	1	1	1	0	9600.0384	0.0043
						2	2	0	1	9600.0800	-0.0009
						2	3	2	2	9600.2477	0.0015
						2	3	2	3	9601.0629	-0.0020
						1	3	1	2	9601.1532	-0.0008
						2	4	2	3	9601.7800	-0.0001
						0	2	2	1	9603.1034	0.0010
2	2	1	1	1	0	2	1	2	1	9160.3770	0.0026
						0	2	2	1	9160.4648	-0.0011
						2	0	2	1	9160.6624	-0.0003
						1	1	1	1	9160.9924	-0.0009
						2	3	2	3	9161.3981	-0.0010
						1	2	1	1	9161.5732	-0.0042
						2	4	2	3	9161.9030	-0.0002
						1	3	1	2	9162.1034	-0.0010
						2	2	0	1	9162.4399	0.0026
						2	2	2	2	9162.5669	-0.0040
						2	3	2	2	9162.7392	-0.0033
						1	1	1	0	9163.2358	0.0035
3	0	3	2	0	2	1	3	1	2	6024.4645	0.0015
						2	5	2	4	6024.4804	0.0004
						0	3	0	2	6024.5116	-0.0022
						1	2	1	1	6024.6832	0.0025
						1	4	1	3	6024.7070	0.0002
						2	4	2	3	6024.7384	0.0007
						2	3	2	2	6024.9988	0.0010
3	1	2	2	1	1	0	3	0	2	6784.9451	0.0005
						1	3	1	2	6785.0365	-0.0003
						2	5	2	4	6785.1215	0.0007
						1	4	1	3	6785.1761	-0.0011
						2	3	2	2	6785.3159	-0.0003
						2	4	2	3	6785.3356	0.0012
3	1	3	2	1	2	2	5	2	4	5657.8918	0.0005
						1	3	1	2	5657.9237	-0.0028
						1	2	1	1	5657.9743	0.0027
						2	4	2	3	5658.0373	0.0014
						0	3	0	2	5658.0417	0.0010
						1	4	1	3	5658.1066	0.0009
						2	3	2	2	5658.3335	-0.0012

Table S4.5 (Continued).

J'	K'_{-1}	K'_{+1}	J''	K''_{-1}	K''_{+1}	I'	F'	I''	F''	Obs.	Obs. – Calc.
3	1	3	2	0	2	1	3	1	2	6878.1121	-0.0052
						0	3	0	2	6878.1329	0.0007
						2	5	2	4	6878.2254	-0.0001
						1	4	1	3	6878.7242	-0.0009
						1	2	1	1	6878.8229	-0.0001
						2	4	2	3	6878.9330	-0.0013
						2	3	2	2	6879.4344	0.0020
4	0	4	3	0	3	2	3	2	3	7809.4672	-0.0009
						1	4	1	3	7810.4912	-0.0040
						2	6	2	5	7810.5064	-0.0007
						0	4	0	3	7810.5189	0.0017
						2	2	2	1	7810.5189	-0.0031
						1	3	1	2	7810.7397	-0.0010
						1	5	1	4	7810.7489	0.0004
						2	5	2	4	7810.7705	-0.0007
						2	3	2	2	7810.7927	-0.0019
						2	4	2	3	7811.0288	-0.0006
						2	4	2	4	7811.5352	-0.0013
						2	5	2	5	7811.7432	-0.0011
4	1	3	3	1	2	2	2	2	1	8959.0865	0.0007
						0	4	0	3	8959.1603	-0.0009
						1	4	1	3	8959.1850	-0.0024
						2	3	2	2	8959.1999	0.0028
						2	6	2	5	8959.2372	-0.0003
						1	5	1	4	8959.3258	-0.0006
						1	3	1	2	8959.3911	-0.0003
						2	5	2	4	8959.4142	0.0003
						2	4	2	3	8959.4765	-0.0010
4	1	4	3	1	3	2	6	2	5	7485.3628	0.0007
						1	4	1	3	7485.3903	-0.0032
						0	4	0	3	7485.4373	-0.0007
						1	3	1	2	7485.4505	0.0012
						2	5	2	4	7485.4619	0.0024
						2	2	2	1	7485.5061	-0.0015
						1	5	1	4	7485.5218	0.0001
						2	4	2	3	7485.6566	-0.0008
						2	3	2	2	7485.6754	-0.0020
4	2	2	3	2	1	2	4	2	3	8835.2105	-0.0025
						2	3	2	2	8835.2105	0.0011
						1	5	1	4	8835.2628	0.0003
						2	2	2	1	8835.2628	-0.0009
						2	5	2	4	8835.2778	0.0007
						1	3	1	2	8835.2778	-0.0028
						0	4	0	3	8835.2879	-0.0011
						1	4	1	3	8835.3003	-0.0010
						2	6	2	5	8835.3157	0.0023

Table S4.5 (Continued).

J'	K'_{-1}	K'_{+1}	J''	K''_{-1}	K''_{+1}	I'	F'	I''	F''	Obs.	Obs. – Calc.
4	2	3	3	2	2	2	2	2	1	8298.9623	-0.0012
						0	4	2	3	8299.0133	-0.0002
						2	6	2	5	8299.0662	0.0001
						2	3	2	2	8299.1488	-0.0007
						1	5	1	4	8299.2242	0.0007
						1	3	1	2	8299.2775	-0.0010
						2	5	2	4	8299.3060	-0.0013
						2	4	0	3	8299.4532	-0.0007
4	0	4	3	1	3	2	5	2	4	6956.5761	0.0014
						2	4	2	3	6956.5965	0.0018
						1	3	1	2	6956.5967	-0.0018
						1	5	1	4	6956.7326	0.0023
						2	6	2	5	6956.7605	-0.0011
						1	4	1	3	6956.8429	0.0020
						0	4	0	3	6956.8994	0.0006
4	1	4	3	0	3	1	4	1	3	8339.0496	0.0019
						0	4	0	3	8339.0577	0.0013
						2	6	2	5	8339.1077	0.0001
						1	5	1	4	8339.5395	-0.0004
						2	5	2	4	8339.6564	0.0004
						2	4	2	3	8340.0938	0.0018
5	0	5	4	0	4	1	5	1	4	9510.6780	0.0010
						2	7	2	6	9510.6780	-0.0005
						0	5	0	4	9510.6919	0.0011
						2	3	2	2	9510.7048	0.0035
						1	4	1	3	9510.8757	-0.0033
						1	6	1	5	9510.8919	0.0007
						2	6	2	5	9510.8919	-0.0012
						2	4	2	3	9510.9269	-0.0009
						2	5	2	4	9511.1175	-0.0005
5	1	4	4	1	3	1	5	1	4	11040.8686	0.0003
						2	7	2	6	11040.9079	0.0003
						2	4	2	3	11040.9711	0.0006
						1	6	1	5	11041.0430	-0.0020
						1	4	1	3	11041.0752	0.0002
						2	6	2	5	11041.1010	-0.0011
						2	5	2	4	11041.2268	-0.0005
5	1	5	4	1	4	2	7	2	6	9277.8911	0.0004
						1	5	1	4	9277.9140	-0.0010
						0	5	0	4	9277.9364	-0.0011
						2	6	2	5	9277.9753	0.0013
						1	4	1	3	9277.9753	-0.0015
						2	3	2	2	9277.9850	0.0027
						1	6	1	5	9278.0230	0.0005
						2	4	2	3	9278.1108	-0.0005
						2	5	2	4	9278.1271	0.0007

Table S4.5 (Continued).

J'	K'_{-1}	K'_{+1}	J''	K''_{-1}	K''_{+1}	I'	F'	I''	F''	Obs.	Obs. – Calc.
5	2	3	4	2	2	2	5	2	4	11216.6389	-0.0003
						2	4	2	3	11216.6779	0.0015
						1	6	1	5	11216.7024	0.0013
						2	6	2	5	11216.7024	-0.0012
						1	4	1	3	11216.7024	-0.0028
						0	5	0	4	11216.7487	0.0006
						1	5	1	4	11216.7516	-0.0017
						2	7	2	6	11216.7612	0.0021
5	2	4	4	2	3	2	3	2	2	10297.6363	0.0011
						0	5	0	4	10297.6558	0.0015
						1	5	1	4	10297.6558	-0.0002
						2	7	2	6	10297.6730	-0.0006
						2	4	2	3	10297.7813	0.0020
						1	6	1	5	10297.8015	0.0002
						1	4	1	3	10297.8228	0.0005
						2	6	2	5	10297.8401	0.0014
						2	5	2	4	10297.9642	-0.0008
5	0	5	4	1	4	2	6	2	5	8982.0106	0.0023
						2	7	2	6	8982.0773	-0.0007
						1	6	1	5	8982.1019	0.0021
6	0	6	5	0	5	2	8	2	7	11182.7033	-0.0010
						1	6	1	5	11182.7121	0.0011
						0	6	0	5	11182.7222	0.0011
						2	4	2	3	11182.7342	-0.0029
						1	5	1	4	11182.8564	0.0024
						2	7	2	6	11182.8564	-0.0004
						1	7	1	6	11182.8694	-0.0014
						2	5	2	4	11182.9065	0.0002
						2	6	2	5	11183.0312	-0.0014
6	1	5	5	1	4	2	4	2	3	12995.4115	-0.0011
						1	6	0	5	12995.4560	0.0026
						0	6	1	5	12995.4560	-0.0020
						2	8	2	7	12995.4936	0.0008
						1	5	2	4	12995.6449	0.0005
						2	5	1	4	12995.6753	-0.0001
						2	7	1	6	12995.6909	0.0002
						1	7	2	6	12995.7085	-0.0007
						2	6	2	5	12995.9016	0.0006
6	1	6	5	1	5	2	8	2	7	11040.6463	0.0004
						1	6	1	5	11040.6674	0.0021
						0	6	0	5	11040.6788	0.0003
						2	4	2	3	11040.7103	-0.0001
						2	7	2	6	11040.7175	-0.0021
						1	7	1	6	11040.7583	-0.0001
						2	6	2	5	11040.8443	-0.0002

Table S4.5 (Continued).

J'	K'_{-1}	K'_{+1}	J''	K''_{-1}	K''_{+1}	I'	F'	I''	F''	Obs.	Obs. – Calc.
6	2	5	5	2	4	1	6	1	5	12249.0556	-0.0003
						0	6	0	5	12249.0556	-0.0010
						2	8	2	7	12249.0672	0.0011
						2	5	2	4	12249.1738	-0.0017
						1	7	1	6	12249.1839	-0.0003
						1	5	1	4	12249.1960	0.0015
						2	7	2	6	12249.2050	-0.0001
						2	6	2	5	12249.3232	-0.0004
7	0	7	6	0	6	2	9	2	8	12859.2212	-0.0002
						0	7	0	6	12859.2409	0.0014
						2	5	2	4	12859.2566	-0.0006
						2	8	2	7	12859.3253	-0.0004
						1	6	1	5	12859.3292	0.0001
						1	8	1	7	12859.3474	0.0002
						2	6	2	5	12859.3795	-0.0001
						2	7	2	6	12859.4600	0.0014
7	1	7	6	1	6	2	9	2	8	12781.3734	0.0008
						1	7	1	6	12781.3877	-0.0011
						0	7	0	6	12781.3965	-0.0009
						2	5	2	4	12781.4214	-0.0004
						2	8	2	7	12781.4345	-0.0020
						1	6	1	5	12781.4453	0.0009
						1	8	1	7	12781.4692	0.0003
						2	6	2	5	12781.5115	0.0013
						2	7	2	6	12781.5412	0.0002

Table S4.6. Observed rotational transitions with resolved ^{14}N hyperfine structure and residuals (all the values in MHz) for the $^{13}C_2$ isotopomer of the cluster (Formamide)$_2\cdots H_2O$ in the ground vibrational state for transitions of the type $J' K'_{-1} K'_{+1} I' F' \leftarrow J'' K''_{-1} K''_{+1} I'' F''$.

J'	K'_{-1}	K'_{+1}	J''	K''_{-1}	K''_{+1}	I'	F'	I''	F''	Obs.	Obs. – Calc.
3	0	3	2	0	2	2	5	2	4	5956.0174	-0.0006
						0	3	0	2	5956.0495	-0.0032
						1	4	1	3	5956.2405	-0.0004
						2	4	2	3	5956.2650	-0.0050
						2	3	2	2	5956.5274	0.0013
3	1	2	2	1	1	2	5	2	4	6694.0102	0.0009
						1	4	1	3	6694.0635	-0.0009
						2	4	2	3	6694.2211	0.0005
3	1	3	2	1	2	2	5	2	4	5592.8943	-0.0007
						1	3	1	2	5592.9327	0.0023
						1	2	1	1	5592.9793	0.0053
						2	4	2	3	5593.0412	0.0031
						1	4	1	3	5593.1109	0.0023
						2	3	2	2	5593.3334	-0.0028
4	0	4	3	0	3	1	4	1	3	7727.9013	-0.0016
						2	6	2	5	7727.9146	-0.0002
						0	4	0	3	7727.9263	0.0016
						2	2	2	1	7727.9263	-0.0031
						1	3	1	2	7728.1432	-0.0029
						1	5	1	4	7728.1540	0.0003
						2	5	2	4	7728.1767	0.0004
						2	4	2	3	7728.4343	0.0025
4	1	3	3	1	2	0	4	0	3	8842.6300	0.0014
						2	6	2	5	8842.7048	0.0006
						1	5	1	4	8842.7896	-0.0006
						1	3	1	2	8842.8533	-0.0013
						2	5	2	4	8842.8789	0.0023
						2	4	2	3	8842.9364	-0.0010
4	1	4	3	1	3	2	6	2	5	7401.3871	-0.0008
						1	4	1	3	7401.4181	-0.0013
						2	5	2	4	7401.4801	-0.0036
						1	5	1	4	7401.5480	0.0016
						2	4	2	3	7401.6805	-0.0001
5	0	5	4	0	4	1	5	1	4	9413.9621	0.0019
						2	7	2	6	9413.9621	-0.0001
						0	5	0	4	9413.9775	0.0038
						2	6	2	5	9414.1782	0.0004
						2	4	2	3	9414.2088	-0.0015
						2	5	2	4	9414.4043	0.0017
5	1	5	4	1	4	2	7	2	6	9176.1500	0.0012
						1	5	1	4	9176.1730	-0.0002
						2	6	2	5	9176.2312	0.0002
						1	4	1	3	9176.2312	-0.0027
						1	6	1	5	9176.2798	0.0001

Table S4.7. Observed rotational transitions with resolved ^{14}N hyperfine structure and residuals (all the values in MHz) for the $^{13}C_8$ isotopomer of the cluster (Formamide)$_2\cdots H_2O$ in the ground vibrational state for transitions of the type $J' K'_{-1} K'_{+1} I' F' \leftarrow J'' K''_{-1} K''_{+1} I'' F''$.

J'	K'_{-1}	K'_{+1}	J''	K''_{-1}	K''_{+1}	I'	F'	I''	F''	Obs.	Obs. – Calc.
3	0	3	2	0	2	2	5	2	4	5958.2641	-0.0002
						0	3	0	2	5958.2978	-0.0010
						1	2	1	1	5958.4707	0.0097
						1	4	1	3	5958.4846	-0.0033
						2	4	2	3	5958.5163	-0.0010
						2	3	2	2	5958.7709	-0.0032
3	1	2	2	1	1	0	3	0	2	6698.8710	0.0009
						2	5	2	4	6699.0439	-0.0019
						1	4	1	3	6699.0997	-0.0015
						2	4	2	3	6699.2544	-0.0031
3	1	3	2	1	2	2	5	2	4	5595.1159	0.0013
						1	3	1	2	5595.1458	-0.0043
						2	4	2	3	5595.2589	0.0008
						0	3	0	2	5595.2736	0.0092
						1	4	1	3	5595.3276	-0.0008
						2	3	2	2	5595.5508	-0.0054
4	0	4	3	0	3	1	4	1	3	7729.7035	-0.0021
						2	6	2	5	7729.7158	-0.0017
						0	4	0	3	7729.7278	0.0004
						2	2	2	1	7729.7337	0.0016
						1	5	1	4	7729.9603	0.0034
						2	5	2	4	7729.9781	-0.0014
						2	3	2	2	7729.9970	-0.0055
						2	4	2	3	7730.2339	-0.0016
4	1	3	3	1	2	1	4	1	3	8848.6396	0.0013
						2	6	2	5	8848.6885	0.0006
						1	5	1	4	8848.7732	-0.0012
						2	5	2	4	8848.8656	0.0047
						2	4	2	3	8848.9220	-0.0003
4	1	4	3	1	3	2	6	2	5	7403.9670	0.0018
						1	4	1	3	7403.9913	-0.0054
						0	4	0	3	7404.0433	0.0020
						2	5	2	4	7404.0667	0.0054
						2	2	2	1	7404.1141	0.0030
						1	5	1	4	7404.1230	-0.0010
						2	4	2	3	7404.2576	-0.0008
5	0	5	4	0	4	2	7	2	6	9415.4475	-0.0005
						0	5	0	4	9415.4626	0.0030
						2	6	2	5	9415.6643	0.0009
						2	4	2	3	9415.6962	-0.0001
						2	5	2	4	9415.8893	0.0011

Table S4.7 (Continued).

J'	K'_{-1}	K'_{+1}	J''	K''_{-1}	K''_{+1}	I'	F'	I''	F''	Obs.	Obs. – Calc.
5	1	5	4	1	4	2	7	2	6	9178.9256	0.0016
						2	6	2	5	9179.0058	-0.0006
						1	6	1	5	9179.0532	-0.0019
						1	5	1	4	9178.9480	-0.0004
						1	4	1	3	9179.0058	-0.0035
						0	5	0	4	9178.9690	-0.0019

Table S4.8. Observed rotational transitions with resolved ^{14}N hyperfine structure and residuals (all the values in MHz) for the $^{15}N_3$ isotopomer of the cluster $(Formamide)_2\cdots H_2O$ in the ground vibrational state for transitions of the type $J' K'_{-1} K'_{+1} F' \leftarrow J'' K''_{-1} K''_{+1} F''$.

J'	K'_{-1}	K'_{+1}	J''	K''_{-1}	K''_{+1}	F'	F''	Obs.	Obs. – Calc.
2	1	2	1	0	1	3	2	5284.0144	0.0007
						2	1	5284.5960	0.0020
3	1	3	2	0	2	4	3	6818.1922	-0.0005
						2	1	6818.1045	-0.0001
						3	2	6818.7730	-0.0024
4	0	4	3	0	3	5	4	7755.0569	0.0019
						3	2	7755.0683	0.0023
						4	3	7755.3011	-0.0026
4	1	3	3	1	2	3	2	8904.6883	-0.0009
						5	4	8904.7621	-0.0001
						4	3	8904.8974	-0.0004
4	1	4	3	1	3	5	4	7434.2509	-0.0004
						3	2	7434.3205	-0.0036
						4	3	7434.3820	-0.0002
4	2	2	3	2	1	3	2	8787.2910	-0.0022
						4	3	8787.2910	-0.0045
						5	4	8787.3172	-0.0047
4	2	3	3	2	2	3	2	8247.0640	-0.0020
						5	4	8247.1160	-0.0045
						4	3	8247.3277	-0.0046
4	0	4	3	1	3	5	4	6920.5792	0.0004
						3	2	6920.7174	0.0078
						4	3	6920.4847	-0.0001
4	1	4	3	0	3	5	4	8268.7263	-0.0012
						3	2	8268.6834	0.0030
						4	3	8269.1998	-0.0014
5	0	5	4	0	4	6	5	9441.5683	0.0015
						4	3	9441.5796	-0.0007
						5	4	9441.7770	0.0010
5	1	4	4	1	3	4	3	10970.6733	0.0017
						6	5	10970.7205	0.0002
						5	4	10970.8992	0.0124
5	1	5	4	1	4	6	5	9213.5290	0.0003
						4	3	9213.5730	-0.0019
						5	4	9213.6358	-0.0011
6	0	6	5	0	5	7	6	11101.2251	0.0014
						5	4	11101.2419	0.0006
						6	5	11101.3767	-0.0028

Table S4.9. Observed rotational transitions with resolved ^{14}N hyperfine structure and residuals (all the values in MHz) for the $^{15}N_9$ isotopomer of the cluster (Formamide)$_2\cdots H_2O$ in the ground vibrational state for transitions of the type $J' K'_{-1} K'_{+1} F' \leftarrow J'' K''_{-1} K''_{+1} F''$.

J'	K'_{-1}	K'_{+1}	J''	K''_{-1}	K''_{+1}	F'	F''	Obs.	Obs. – Calc.
2	1	2	1	0	1	3	2	5299.8040	0.0028
3	1	3	2	0	2	4	3	6830.5498	0.0003
						2	1	6830.4354	-0.0002
4	0	4	3	0	3	5	4	7727.0221	-0.0016
						3	2	7727.0262	-0.0023
						4	3	7727.2784	-0.0006
4	1	3	3	1	2	3	2	8843.0751	-0.0012
						5	4	8843.1540	-0.0003
						4	3	8843.2820	-0.0008
4	1	4	3	1	3	5	4	7400.8521	0.0001
						3	2	7400.9222	-0.0029
						4	3	7400.9784	0.0003
4	2	2	3	2	1	4	3	8708.2013	0.0040
						5	4	8708.2552	0.0009
4	2	3	3	2	2	3	2	8194.9212	0.0006
						5	4	8194.9672	-0.0022
						4	3	8195.1544	-0.0041
4	0	4	3	1	3	5	4	6852.1558	0.0015
						4	3	6852.0235	-0.0024
4	1	4	3	0	3	5	4	8275.7127	-0.0087
						3	2	8275.6642	0.0038
						4	3	8276.2323	0.0010
5	0	5	4	0	4	6	5	9412.5742	0.0005
						4	3	9412.5869	0.0040
						5	4	9412.7926	0.0005
5	1	4	4	1	3	4	3	10904.4119	0.0004
						6	5	10904.4624	-0.0014
						5	4	10904.6280	0.0015
5	1	5	4	1	4	6	5	9175.2980	0.0002
						4	3	9175.3456	0.0021
						5	4	9175.4038	-0.0008
6	0	6	5	0	5	7	6	11067.8606	0.0019
						5	4	11067.8753	0.0016
						6	5	11068.0226	-0.0004

Table S4.10. Observed rotational transitions and residuals (all the values in MHz) for the $^{15}N_3$-$^{15}N_9$ isotopomer of the cluster (Formamide)$_2$···H_2O in the ground vibrational state for transitions of the type $J' K'_{-1} K'_{+1} \leftarrow J'' K''_{-1} K''_{+1}$.

J'	K'_{-1}	K'_{+1}	J''	K''_{-1}	K''_{+1}	Obs.	Obs. – Calc.
3	0	3	2	0	2	5914.9689	-0.0018
3	1	2	2	1	1	6654.2140	-0.0023
3	1	3	2	1	2	5554.6403	-0.0030
3	2	1	2	2	0	6368.6137	-0.0051
3	2	2	2	2	1	6141.7937	0.0037
3	1	3	2	0	2	6770.8865	-0.0020
4	0	4	3	0	3	7671.7632	-0.0016
4	1	3	3	1	2	8788.4152	-0.0015
4	1	4	3	1	3	7349.7549	-0.0022
4	2	2	3	2	1	8659.5433	-0.0038
4	2	3	3	2	2	8142.7947	0.0010
4	3	1	3	3	0	8326.6415	0.0038
4	3	2	3	3	1	8291.2238	0.0033
5	0	5	4	0	4	9343.6948	-0.0011
5	1	4	4	1	3	10834.2148	0.0028
5	1	5	4	1	4	9111.0108	-0.0016
5	2	3	4	2	2	10993.7967	0.0015
5	2	4	4	2	3	10105.2798	0.0011
5	3	2	4	3	1	10503.4312	-0.0003
5	3	3	4	3	2	10384.1211	-0.0009
6	0	6	5	0	5	10986.5847	-0.0003
6	1	5	5	1	4	12758.1216	0.0053
6	1	6	5	1	5	10843.2193	-0.0007
6	2	4	5	2	3	13301.4496	0.0004
6	2	5	5	2	4	12022.3169	0.0024
6	3	3	5	3	2	12764.4527	-0.0046
6	3	4	5	3	3	12468.7488	-0.0002

Table S4.11. Observed rotational transitions with resolved ^{14}N hyperfine structure and residuals (all the values in MHz) for the $^{18}O_{14}$ isotopomer of the cluster (Formamide)$_2\cdots H_2O$ in the ground vibrational state for transitions of the type $J'K'_{-1}K'_{+1}I'F' \leftarrow J''K''_{-1}K''_{+1}I''F''$.

J'	K'_{-1}	K'_{+1}	J''	K''_{-1}	K''_{+1}	I'	F'	I''	F''	Obs.	Obs. – Calc.
4	0	4	3	0	3	1	4	1	3	7690.5782	-0.0026
						2	6	2	5	7690.5923	-0.0002
						0	4	0	3	7690.6060	0.0021
						2	2	2	1	7690.6060	-0.0039
						1	3	1	2	7690.8282	-0.0051
						1	5	1	4	7690.8425	0.0002
						2	5	2	4	7690.8630	-0.0017
						2	3	2	2	7690.8895	-0.0023
						2	4	2	3	7691.1316	-0.0007
4	1	3	3	1	2	0	4	0	3	8907.1344	0.0014
						1	4	1	3	8907.1564	-0.0033
						2	3	2	2	8907.1734	-0.0069
						2	6	2	5	8907.2116	-0.0007
						1	5	1	4	8907.3128	-0.0008
						1	3	1	2	8907.3816	0.0008
						2	5	2	4	8907.4056	0.0003
						2	4	2	3	8907.4810	0.0002
4	1	4	3	1	3	2	6	2	5	7390.7190	0.0010
						1	4	1	3	7390.7479	-0.0006
						0	4	0	3	7390.7940	0.0010
						1	3	1	2	7390.8074	-0.0029
						2	5	2	4	7390.8238	0.0026
						2	2	2	1	7390.8548	-0.0069
						1	5	1	4	7390.8827	0.0008
						2	4	2	3	7391.0236	0.0002
4	2	2	3	2	1	2	4	2	3	8840.6379	-0.0013
						1	5	1	4	8840.6931	0.0009
						2	5	2	4	8840.7001	-0.0088
						0	4	0	3	8840.7192	-0.0013
						1	4	1	3	8840.7327	-0.0016
						2	6	2	5	8840.7531	0.0056
4	2	3	3	2	2	0	4	2	3	8238.0976	0.0012
						1	4	1	3	8238.1144	0.0043
						2	6	2	5	8238.1504	0.0003
						2	3	2	2	8238.2391	0.0036
						1	5	1	4	8238.3137	0.0025
						2	5	2	4	8238.3931	-0.0034
						2	4	0	3	8238.5475	0.0010
5	0	5	4	0	4	1	5	1	4	9351.6851	0.0005
						2	7	2	6	9351.6851	0.0011
						0	5	0	4	9351.6999	0.0004
						1	4	1	3	9351.8788	-0.0010
						1	6	1	5	9351.8954	0.0004
						2	6	2	5	9351.8954	0.0026
						2	4	2	3	9351.9382	0.0012
						2	5	2	4	9352.1176	0.0006

Table S4.11 (Continued).

J'	K'_{-1}	K'_{+1}	J''	K''_{-1}	K''_{+1}	I'	F'	I''	F''	Obs.	Obs. – Calc.
5	1	4	4	1	3	2	3	2	2	10946.2254	0.0004
						1	5	1	4	10946.2921	0.0013
						2	7	2	6	10946.3324	-0.0007
						2	4	2	3	10946.4144	0.0014
						1	6	1	5	10946.4906	-0.0004
						1	4	1	3	10946.5189	0.0002
						2	6	2	5	10946.5497	0.0006
						2	5	2	4	10946.6936	-0.0009
5	1	5	4	1	4	2	7	2	6	9151.2679	0.0019
						1	5	1	4	9151.2889	-0.0011
						0	5	0	4	9151.3129	0.0004
						2	6	2	5	9151.3533	-0.0003
						1	4	1	3	9151.3566	0.0006
						2	3	2	2	9151.3566	-0.0004
						1	6	1	5	9151.4014	-0.0001
						2	4	2	3	9151.4909	0.0008
						2	5	2	4	9151.5078	-0.0019
6	1	6	5	1	5	2	8	2	7	10881.3337	-0.0028
						0	6	0	5	10881.3647	-0.0046
						2	4	2	3	10881.4053	0.0041
						2	7	2	6	10881.4130	0.0005
						1	7	1	6	10881.4530	0.0017
						2	5	2	4	10881.5089	-0.0006
						2	6	2	5	10881.5396	-0.0002

Table S4.12. Observed rotational transitions with resolved ^{14}N hyperfine structure and residuals (all the values in MHz) for the $^{2}H_{13}$ isotopomer of the cluster (Formamide)$_2\cdots H_2O$ in the ground vibrational state for transitions of the type $J'K'_{-1}K'_{+1}I'F' \leftarrow J''K''_{-1}K''_{+1}I''F''$.

J'	K'_{-1}	K'_{+1}	J''	K''_{-1}	K''_{+1}	I'	F'	I''	F''	Obs.	Obs. – Calc.
4	0	4	3	0	3	1	4	1	3	7767.8296	-0.0029
						2	6	2	5	7767.8411	-0.0034
						0	4	0	3	7767.8566	0.0018
						1	5	1	4	7768.0895	0.0010
						2	3	2	2	7768.1377	0.0024
4	1	3	3	1	2	2	6	2	5	8934.0939	0.0007
						1	5	1	4	8934.1842	-0.0012
						2	5	2	4	8934.2734	-0.0006
						2	4	2	3	8934.3423	0.0015
4	1	4	3	1	3	2	6	2	5	7449.8997	0.0005
						1	5	1	4	7450.0586	-0.0014
						2	4	2	3	7450.1913	-0.0060
						2	3	2	2	7450.2169	0.0015
5	0	5	4	0	4	2	7	2	6	9454.7736	-0.0008
						1	6	1	5	9454.9884	0.0015
						2	6	2	5	9454.9884	0.0008
						2	5	2	4	9455.2125	-0.0001
5	1	5	4	1	4	2	7	2	6	9231.3703	0.0053
						1	5	1	4	9231.3839	-0.0054
						0	5	0	4	9231.4155	0.0037
						2	6	2	5	9231.4445	-0.0051
						1	6	1	5	9231.5040	0.0061

Table S4.13. The so-called substitution, r_s, method, which uses Kraitchman equations,[19] exploits changes in the moments of inertia upon mono-isotopic substitution to provide the atom coordinates of the substituted atoms in the principal inertial axis frame. This purely experimental approach allows to directly locating the different atoms of a molecule but has several drawbacks: i) It is of application with only mono-isotopic substitution data, ii) it only delivers the magnitudes of the atomic r_s coordinates and iii) it poses limitations for atoms located near the three principal axes. This Table gives the r_s structure *a b* and *c* coordinates[19] of the isotopically substituted atoms of the f_2w cluster (errors quoted calculated according to the Costain rule [B. P. van Eijck, *J. Mol. Spectrosc.* **1982**, *91*, 348–362]) and their comparison with r_0 (2) (see Table S4.13), r_e (MP2/6-311++G(2d,p)) *ab initio* structure (ab) and planar skeleton *ab initio* structure (ab*) 25 cm^{-1} above equilibrium. Water oxygen atom lies practically along *b* inertial axis so the r_s method give imaginary values 0.038i and 0.040i for its *a* and *c* coordinates, respectively. The distances between the substituted atoms are given below. The distances in which the water oxygen atom is involved have been calculated by taking its *a* and *c* coordinates as zero. All coordinates and distances in Å.

Table S4.13

	atom	*a*	*b*	*c*
$\|r_s\|$	C_2	2.45627(61)	0.4853(31)	0.026(58)
r_0		2.4609(33)	-0.4923(46)	-0.00117(7)
ab*		2.4541	-0.4967	-0.0013
ab		2.4441	-0.5046	-0.0525
$\|r_s\|$	N_3	1.5051(10)	1.4339(10)	0.016(92)
r_0		1.5143(41)	-1.4243(32)	0.00986(4)
ab*		1.5076	-1.4459	0.0080
ab		1.4946	-1.4435	0.0669
$\|r_s\|$	C_8	2.37402(63)	0.7148(21)	0.021(71)
r_0		-2.3757(24)	-0.7074(48)	-0.00092(8)
ab*		-2.3813	-0.7109	-0.0017
ab		-2.3762	-0.7014	-0.0617
$\|r_s\|$	N_9	2.45004(61)	0.6225(24)	0.054(28)
r_0		-2.4525(19)	0.6188(28)	-0.0149(6)
ab*		-2.4365	0.6296	-0.0112
ab		-2.4159	0.6390	-0.1082
$\|r_s\|$	O_{14}	[0.0][a]	2.18424(69)	[0.0][a]
r_0		-0.0983(79)	2.1820(19)	0.0333 (13)
ab*		-0.0459	2.2117	0.0265
ab		-0.0357	2.2115	0.1002
$\|r_s\|$	H_{13}	0.7038(21)	1.6843(90)	0.061(25)
r_0		0.7452(50)	1.6726(41)	-0.0272 (11)
ab*		0.7733	1.6686	-0.0218
ab		0.7783	1.6723	-0.0124
		distance		distance
$\|r_s\|$	$r(C_2\text{-}N_3)$	1.3440(42)	$r(C_8\text{-}N_9)$	1.3399(37)
r_0		1.3285(69)		1.3285(69)
ab*		1.3405		1.3417
ab		1.3407		1.3418
$\|r_s\|$	$r(O_{14}\text{-}C_2)$	3.628(27)	$r(O_{14}\text{-}N_9)$	2.906(33)
r_0		3.7017(69)		2.8260(74)
ab*		3.6859		2.8667
ab		3.6811		2.8604
$\|r_s\|$	$r(H_{13}\text{-}O_{14})$	0.865(32)	$r(H_{13}\text{-}C_2)$	2.7892(30)
r_0		0.9854(95)		2.7625(70)
ab*		0.9829		2.7412
ab		0.9828		2.7415
$\|r_s\|$	$r(N_3\text{-}C_8)$	3.9454(17)		
r_0		3.9555(54)		
ab*		3.9577		
ab		3.9434		

[a] The Kraitchman equations give imaginary values for the coordinates in square brackets. These were fixed to zero to calculate the corresponding distances.

Table S4.14. Results of the fitting of the r_0 structure of f_2w adduct. We started from the usual assumption that the monomer structures are unchanged upon complexation. We used the r_0 structure of formamide calculated from previous data (see Table S4.14) and the r_0 structure of water.[a] Good fits of the rotational constants were obtained only by allowing the heavy atom parameters of formamide to float (fit $r_0(1)$). In a second step we correct the fixed formamide r_0 parameters by small amounts reflecting the changes upon complexation predicted from *ab initio* calculations ($r_0(2)$), see Tables S4.13 and S4.14). In both fits, $r_0(1)$ and $r_0(2)$, the formamide parameters fitted were constrained to keep the same values in both subunits. This is not unreasonable if we look at the *ab initio* results given in columns 3 and 4. The third column shows the *ab initio* MP2/6-311++G(2d,p) r_e equilibrium structure and the fourth column the *ab initio* results for a planar heavy atom structure. The differences in parameters for the *ab initio* structures for both formamide subunits are 0.07 %, 0.08 % and 0.3 % for the r(O-C), r(C-N) distances and ∠OCN angle respectively. This was considered in order to assume the same value of these parameters for both formamide subunits in the fit. The equilibrium structure predicted from *ab initio* calculations (see column 3) shows the formamide molecules with slight deviations from the co-planarity ($\angle H_{15}O_{14}O_1C_2 = 123.1^o$) resulting in a P_{cc} value of 2.03 uÅ^2. The predicted energy of this structure is only 25 cm^{-1} lower than the structure corresponding to the ground vibrational state with a planar heavy atom skeleton (P_{cc} =0.34 uÅ^2, $\angle H_{15}O_{14}O_1C_2 = 130.1$) and H_{15} lying out of this plane as the experimental data indicates. From the experimental value of P_{cc} the *c* coordinate of H_{15} atom is estimated to be 0.760 Å and by taking *r*(O-H) = 0.965 Å[a] the dihedral angle $\angle H_{15}O_{14}O_1C_2$ is estimated to be 128º.

[a] r_0 structure of water: M. D. Harmony, V. W. Laurie, R. L. Kuczkowski, R. H. Schwendeman, D. A. Ramsay, F. J. Lovas, W. J. Lafferty, A. G. Maki, *J. Phys. Chem. Ref. Data* **1979**, *8*, 619.

Table S4.14

	r_0		MP2/6-311++G(2d,p)	
Parameter [a]	(1)	(2)	r_e	Planar skeleton
$r(O_1\text{-}C_2)$/Å	1.2618(58)	1.2671(84)	1.2319	1.2319
$r(C_2\text{-}N_3)$/Å	1.3315(48)	1.3285(69)	1.3407	1.3405
$r(N_3\text{-}H_4)$/Å	[0.9917]	[0.9928]	1.0072	1.0072
$r(N_3\text{-}H_5)$/Å	[1.0015]	[1.0155]	1.0229	1.0229
r(C2-H6)/Å	[1.1018]	[1.0994]	1.1011	1.1011
$\angle O_1C_2N_3$/°	126.65(26)	126.51(37)	125.86	125.84
$\angle H_4N_3C_2$/°	[120.61]	[118.59]	118.99	119.06
$\angle H_5N_3C_2$/°	[118.08]	[121.54]	122.69	122.63
$\angle H_6C_2N_3$/°	[114.8]	[115.91]	113.65	113.67
$r(O_7\text{-}C_8)$/Å	1.2618(58)	1.2671(84)	1.2310	1.2308
$r(C_8\text{-}N_9)$/Å	1.3315(48)	1.3285(69)	1.3418	1.3417
$r(N_9\text{-}H_{10})$/Å	[0.9917]	[0.9926]	1.0071	1.0070
$r(N_9\text{-}H_{11})$/Å	[1.0015]	[1.0183]	1.0259	1.0257
$r(C_8\text{-}H_{12})$/Å	[1.1018]	[1.1001]	1.1018	1.1018
$\angle O_7\text{-}C_8\text{-}N_9$/°	126.65(26)	126.51(37)	125.45	125.48
$\angle H_{10}\text{-}N_9\text{-}C_8$/°	[120.61]	[118.49]	118.99	118.96
$\angle H_{11}\text{-}N_9\text{-}C_8$/°	[118.08]	[120.26]	121.29	121.35
$\angle H_{12}\text{-}C_8\text{-}N_9$/°	[114.8]	[115.99]	113.77	113.75
$\angle C_2N_3H_5O_7$/°	[180]	[180]	172.27	180.0
$\angle N_3H_5O_7C_8$/°	[180]	[180]	-162.97	180.0
$\angle H_5O_7C_8N_9$/°	[0]	[0]	-14.85	0.0
$r(O_{14}\text{-}H_{13})$/Å	[0.965]	[0.9854]	0.983	0.983
$r(O_{14}\text{-}H_{15})$/Å	[0.965]	[0.9654]	0.963	0.963
$\angle H_{13}\text{-}O_{14}\text{-}H_{15}$/°	[104.8]	[105.15]	104.84	104.95
$\angle O_7C_8N_9O_{14}$/°	[0]	[0]	2.731	0.0
$\angle O_{14}O_1C_2N_3$/°	[0]	[0]	5.126	0.0
$r(O_7\text{-}H_5)$/Å	1.8979(39)	1.8571(58)	1.8687	1.8651
$r(O_7\text{-}N_3)$/Å	2.8301(51)	2.8260(74)	2.8587	2.8288
$\angle O_7H_5N_3$/°	154.46(32)	159.27(48)	162.42	162.94
$\angle C_8O_7H_5$/°	138.39(37)	139.97(54)	140.31	142.10
$r(H_{11}\text{-}O_{14})$/Å	1.8297(54)	1.8077(78)	1.8349	1.8410
$\angle N_9H_{11}O_{14}$/°	176.73(32)	179.98(38)	177.73	179.67
$\angle H_{11}O_{14}H_{13}$/°	113.82(26)	115.28(37)	112.38	113.08
$r(O_1\text{-}H_{13})$/Å	1.8059(62)	1.7877(89)	1.7641	1.7607
$\angle H_{13}O_1C_2$/°	128.59(47)	128.66(68)	131.61	131.89
$\angle O_{14}H_{13}O_1$/°	179.06(40)	179.49(56)	176.95	179.10
$\angle H_{15}O_{14}O_1C_2$/°	123.15(30)	123.04(44)	123.15	130.13

[a] Values in square brackets were kept fixed in the fit.

Table S4.15. The r_0 and the r_e MP2/6-311++G(2d,p) structures of formamide. The r_0 formamide structure has been recalculated from the data on (E. Hirota R. Sugisaki, C. J. Nielsen, G. O. Sørensen, *J. Mol. Spectrosc.*, **1974**, *49*, 251) and reference [11]. There is a good agreement between r_0 and theoretical parameters.

	$r_0(1)$	*Ab initio* r_e
$r(O_1\text{-}C_2)$/Å	1.2165(33)	1.2179
$r(C_2\text{-}N_3)$/Å	1.3630(32)	1.3608
$r(N_3\text{-}H_4)$/Å	0.9917(31)	1.0061
$r(N_3\text{-}H_5)$/Å	1.0015(26)	1.0088
$r(C_2H_6)$/Å	1.1018(25)	1.1034
$\angle O_1C_2N_3$/°	124.256(71)	124.7900
$\angle H_4N_3C_2$/°	120.61(32)	121.0800
$\angle H_5N_3C_2$/°	118.08(16)	119.1600
$\angle H_6C_2N_3$/°	114.8(18)	112.5700
$\angle H_4N_3C_2O_1$/°	[0]	0.08
$\angle H_5N_3C_2O_1$/°	[180]	179.90
$\angle H_6C_2N_3H_5$/°	[0]	-0.11

Table S4.16. (a)-(b) Comparison of the r_0 bond length parameters (Å) of formamide$_2$-H_2O with related systems as formamide, formamide-$(H_2O)_n$ with n=1 (f-w-a) and 2 (fw2), formamide$_2$ (f_2) and water dimer/trimer. Some available r_s values are also compared. (c) Comparison of r(C-N) and r (O-C) of formamide for the different complexes. Experimental r_0 and *ab initio* r_e values are included. (d) The *ab initio* BSSE corrected dissociation energies show that formamide$_2$-water has the higher dissociation energies, followed by the other three body adduct formamide-water$_2$. Formamide dimer has also a higher energy compared to formamide-water complex.

(a)	f_2w[a]	f-w-a[b]	fw_2[b]	w_2[c]/w_3[d]
$r_0(O_1\text{-}O_{14})$	2.7730(91)	2.8231(35)	2.7755(30)	2.98/2.85
$r_0(O_1\text{-}H_{13})$	1.7877(89)	1.9304(98)	1.7969(83)	
$r_s(O_{14}\text{-}N_9)$	2.906(33)	2.8910(17)	2.9095(12)	
$r_0(O_{14}\text{-}N_9)$	2.8260(74)	2.8935(32)	2.9342(55)	
$r_0(H_{11}\text{-}O_{14})$	1.8077(78)	2.0607(45)	1.9363(60)	

(b)	f_2w	f_2 [e]
$r_0(O_7\text{-}N_3)$	2.8260(74)	2.90-2.92
$r_0(O_7\text{-}H_5)$	1.8571(58)	1.90-1.93

(c)	f_2w	formamide[f]	f-w-a[b]	fw_2[b]	f_2
$r_0(C_2\text{-}N_3)$	1.3285(69)	1.363(3)			
$r_e(C_2\text{-}N_3)$	1.3407	1.361	1.350	1.343	1.344
$r_e(C_8\text{-}N_9)$	1.3418				
$r_0(O_1\text{-}C_2)$	1.2671(84)	1.217(3)			
$r_e(O_1\text{-}C_2)$	1.2319	1.218	1.229	1.231	1232
$r_e(O_7\text{-}C_8)$	1.2310				

(d)	f_2w	f-w-a[a]	f_2	fw_2[b]
E_D[g]/kJ/mol	85.1	37.4	57.4	74.51

[a] This work; [b] ref. [11]; [c] ref. [21];[d] ref. [22]; [e] Liquid formamide, electron, neutron and X-ray diffraction data [23]; [f] This work (Table S4.14) and ref. [11];[g] Counterpoise corrected dissociation energy [30].

Table S4.17. Experimental and *ab initio* MP2/6-311++G(2d,p) quadrupole coupling constants (χ_{aa}, χ_{bb}, χ_{cc}) of different formamide-water complexes (see Figure 4.1 of the paper) together with the values of the unbalanced $2p_z$ electronic charge ($(U_p)_z$) calculated from the equation: $\chi_{cc}/eQq_{n10} = -(U_p)_z$. These values are compared to those ($-(U_p)_z = [n_z - (n_x - n_y)/2]$) calculated from the natural atomic orbital populations n_x, n_y, n_z of the 2p orbitals of N atom derived from a Natural Bond Orbital (NBO) analysis. The *ab initio* quadrupole coupling constants list include the non-diagonal elements of the quadrupole coupling tensor set up in the principal inertial axis system (χ_{ab}, χ_{ac}, χ_{bc}) and the constants in the principal quadrupole coupling axis (χ_{xx}, χ_{yy}, χ_{zz}). The *ab initio* χ_{cc} and χ_{zz} values are nearly equal and this justifies the assumption that the *c* principal inertial axis, perpendicular to the molecular skeleton plane, is coincident with the z axis. The $-(U_p)_z$ values calculated from the *ab initio* χ_{zz} constants differ from those obtained from the experimental χ_{cc} value by an almost constant factor, as the experimental χ_{cc} and theoretical χ_{zz} values do, but reproduce the same trends. The values of the *ab initio* η_D asymmetry parameter that measures the deviation of the charge distribution from axial symmetry reflect also the polarization of the amide group by hydrogen bonding and clearly show the effects of cooperative hydrogen bonding.

Parameter[a]	f	f-w-b	f-w-a	fw_2	f_2w N_3	f_2w N_9
Experimental						
χ_{aa}/MHz	1.961(3)	1.863(2)	1.332(4)	1.074(3)	1.0671(44)	1.2692(37)
χ_{bb}/MHz	1.893(5)	1.739(4)	2.037(2)	2.006(5)	1.9087(86)	1.7260(83)
χ_{cc}/MHz	-3.854(5)	-3.602(4)	-3.37(1)	-3.080(5)	-2.9757(86)	-2.9952(83)
χ_{cc}/eQq_{210}	0.385	0.360	0.337	0.308	0.298	0.300
Ab initio						
$-(U_p)_z$(NBO)	0.382	0.364	0.330	0.299	0.299	0.301
χ_{aa}/MHz	2.12	2.02	1.36	1.05	1.10	1.37
χ_{bb}/MHz	1.96	1.91	2.16	2.15	2.08	1.81
χ_{cc}/MHz	-4.08	-3.93	-3.52	-3.20	-3.18	-3.17
χ_{ab}/MHz	0.01	0.05	0.01	-0.10	0.25	-0.57
χ_{ac}/MHz	-0.01	0.11	-0.24	0.26	-0.01	0.10
χ_{bc}/MHz	0.00	-0.03	-0.07	-0.28	0.02	-0.06
χ_{xx}/MHz	2.12	2.04	2.16	2.17	1.04	0.98
χ_{yy}/MHz	1.96	1.89	1.37	1.05	2.14	2.20
χ_{zz}/MHz	-4.08	-3.93	-3.53	-3.22	-3.18	-3.17
η_D	0.04	0.04	0.22	0.35	0.35	0.38
χ_{zz}/eQq_{210}	0.408	0.393	0.352	0.322	0.318	0.317

[a] q_{210} is the electric field gradient associated to a 2p electron in an isolated atom. A value of eQq_{210} = -10 MHz has been used [18]. η_D is the asymmetry parameter that measures the deviation of the charge distribution from axial symmetry, $\eta_D = |(\chi_{yy} - \chi_{xx})/\chi_{zz}|, 0 \leq \eta_D \leq 1$. See Figure 4.3 of the paper for labeling.

Chapter V

Structure and Dynamics in Formamide-$(H_2O)_3$: a Water-Pentamer Analogue

Direct transcription from: Blanco, S., Pinacho, P., López, J. C. *J Phys. Chem. Lett.*, **2017**, 8, 6060–6066.

Abstract

Water self-association dominates the formation of microsolvated molecular clusters which may give rise to complex structures resembling those of pure water clusters. We present a rotational study of the complex formamide-$(H_2O)_3$ formed in a supersonic jet and several monosubstituted isotopologues. Formamide and water molecules form a four-body sequential cycle through N-H···O, O-H···O and O-H···O=C hydrogen bonds, resulting in a chiral structure with a non-planar skeleton that can be overlapped to that of water pentamer. The analysis of the ^{14}N-nucleus quadrupole coupling effects shows the depletion of the electron density of the N atom lone pair with respect to the bare formamide that affects to the amide group C-N and C=O distances. The study of the observed tunneling doublets shows that formamide-$(H_2O)_3$ follows a path to invert its structure driven by the flipping of water subunits and passing through successive non-planar configurations, a motion reminiscent of the pseudorotation of water pentamer.

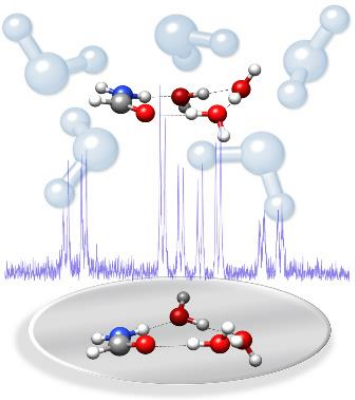

The investigation of the initial steps of the solvation process through the study of microsolvated molecular systems has been an important subject for Chemistry.[1-3] The corresponding molecular clusters can be isolated in the cold environment of supersonic jets and spectroscopically probed. Rotationally resolved spectroscopy techniques are ideal for this purpose since they have an inherent high resolution and are exceptional tools to determine the structure.[4-6] Rotational studies of microsolvated model organic molecules[7-17] have provided a better understanding on the solvent interactions in large biomolecules,[18] the role of hydrogen bond (HB) cooperativity[19] and on the way in which solvation induces structural changes in the solute molecule.[9,12,17,20] This research has also led to a better understanding of the association processes, showing the interplay between self-association and solvation. In fact, with few exceptions,[20] one of the most important observations in complexes with several H_2O molecules is that water prefers to link to other water molecules, forming chains or cycles as occurs in clusters with only one HB acceptor site.[10,13,14] In molecules with double HB donor/acceptor character, water molecules close sequential cycles[19] as observed in amides[7-9] acids,[15,16] or esters.[11] However, with the exception of some organic acids,[15,16] there is no information on clusters with more than two water molecules on the last kind of systems.

The complexes of formamide, the smallest system having an amide group, with water (formamide-$(H_2O)_n$, n=1,2)[7,8] see Figure 5.1) have been used as a benchmark to model the local interactions of water in proteins. Their structures could suggest that formamide-$(H_2O)_n$ clusters would resemble $(H_2O)_{n+2}$ clusters so that formamide might fit into the structure of larger water clusters.[4-6,21,22] This hypothesis can be confirmed from the structures of the microsolvated clusters of formamide with n>2.

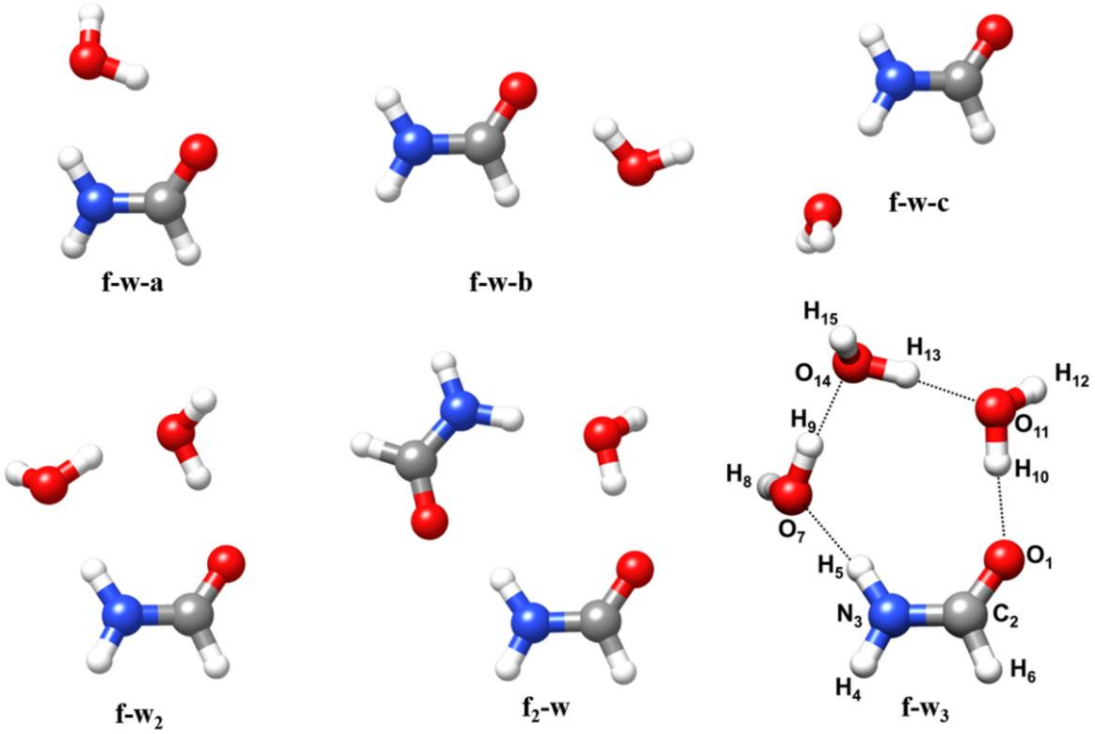

Figure 5.1. Observed formamide$_m$-$(H_2O)_n$ (m=1,2; n=1-3) clusters and atom labeling for formamide-$(H_2O)_3$ (f-w$_3$).

In this context, we present the rotational study of the cluster formamide-$(H_2O)_3$ (f-w_3). One of the main objectives was to compare its structure and dynamics with those of the structure of water pentamer. A second purpose was the observation of the structural signatures of cooperative HB, especially the characterization of inductive polarization effects related to resonance-assisted hydrogen bonding (RAHB)[19] scarcely observed in the gas phase[9,17] through the ^{14}N nuclear quadrupole coupling constants which have been shown[17] to be an experimental probe alternative to the elusive detection of small C-N or C=O structural changes.

A theoretical investigation[23] on the possible forms of f-w_3 (see Supporting Information) predict the lowest energy forms as those in which f-w_3 adopts a cyclic arrangement, being f-w_3-c1 (Figure 5.1) the global minimum. The spectrum of a species identifiable as one of the cyclic forms was observed to show the hyperfine structure characteristic of species having one ^{14}N nucleus plus an additional splitting attributable to a tunneling motion (Figure 5.2). It was analyzed[24] using a two-state Hamiltonian including semirigid rotor,[25] quadrupole coupling[26] and Coriolis coupling terms.[27] A summary of the results is given in Table 5.1. The spectra of the $^{15}NH_2$-CHO$\cdots$$(H_2O)_3$, NH_2-^{13}CHO$\cdots$$(H_2O)_3$, the three NH_2-CHO$\cdots$$(H_2{}^{18}O\cdots(H_2O)_2)$ isotopologues and the monodeuterated species of the atoms involved in the HB were also recorded. The details of the analysis, the complete results and the frequency tables are given in the Supporting Information.

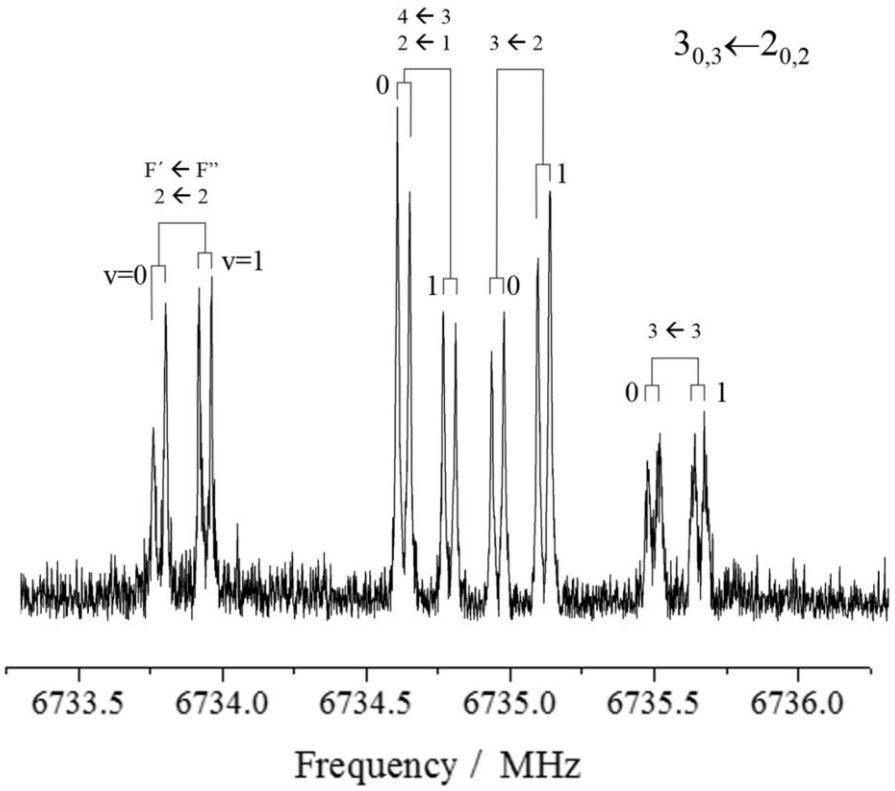

Figure 5.2. The $3_{0,3} \leftarrow 2_{0,2}$ rotational transition of the formamide-$(H_2O)_3$ (f-w_3) complex showing the quadrupole hyperfine components labeled with the F quantum number (F'←F"). The additional splitting into two levels labeled v=0 and v=1 is due to a tunneling vibration. Each line is further split due to Doppler effect.

Table 5.1. Rotational parameters obtained from the analysis of the spectrum of the observed formamide-$(H_2O)_3$ (f-w_3) cluster and calculated at the MP2/6-311++G(2d,p) level for the global minimum.

Parameters[a]	Exp. Value		f-w_3
	v=0	v=1	
A/MHz	2552.02481(25)[b]	2552.02697(24)	2513
B/MHz	1458.29390(17)	1458.30123(17)	1497
C/MHz	952.624138(92)	52.656823(92)	957
P_{cc} /uÅ^2	7.03654(6)	7.04468(6)	5.4
χ_{aa}/MHz	0.8679(10)		0.86
χ_{bb}/MHz	1.9524(14)		2.02
χ_{cc}/MHz	-2.8204(14)		-2.88
ΔE_{01}/MHz	370.4(47)		
<0|iG_a|1>	1.1275(92)		
n	319		
σ/kHz	2.6		

[a] *A*, *B* and *C* are the rotational constants. $P_{cc} = (I_a + I_b - I_c)/2 = (\sum_i m_i c_i^2)/2))$ is the planar moment of inertia derived from the inertial moments I_α (α = *a*, *b* or *c*). χ_{aa}, χ_{bb} and χ_{cc} are the quadrupole coupling constants for ^{14}N. ΔE_{01} is the energy difference between the vibrational states labeled v=0 and v=1. <0|iG_a|1> is the Coriolis coupling term connecting both vibrational states. *n* is the number of hyperfine quadrupole coupling components fitted. σ is the rms deviations of the fit. [b] Standard errors are given in parentheses in units of the last digit.

A first insight on the structure can be obtained from the analysis of the determined planar moment of inertia P_{cc} (7.03654(6) uÅ^2) which measures the mass extension out of the *ab* inertial plane. It can be compared with the values for related species like formamide (-0.0036 uÅ^2),[28] the planar skeleton complexes formamide$_m$-$(H_2O)_n$ (m,n=1,2)[7,8,17] (0.054-0.6541 uÅ^2), or the value of *ca.* 1.4 uÅ^2 estimated for a planar skeleton of f-w_3 with three out-of-plane water hydrogen atoms. This allows us to conclude that the skeleton of the f-w_3 complex is not planar. The changes in the planar moments upon isotopic substitution indicate that all heavy substituted atoms are out of the *ab* inertial plane.

We have determined the r_s[29] and r_0[30] structures from the rotational constants of the parent species and isotopologues. The results, given in supplementary information, are summarized in Figure 5.3. The r_s method, a purely experimental approach, gives the absolute coordinates of each substituted atom in the principal axis system of the parent species (the signs can be taken from the r_0 or r_e structure). It allows to directly locate the different subunits of a complex although it poses limitations for atoms located near the principal axes. The r_0 method provides a total or partial determination of the effective ground state structural parameters from a least squares fit of all of the available rotational parameters.

The comparison of the r_s, r_0 and r_e structures indicates that the observed form corresponds to conformer f-w$_3$-c1 (Figure 5.3). The experimental structure reflects that formamide and water subunits close a sequential cycle through four HBs, C=O···H-O, O-H···O, O-H···O and O-H···N thanks to the HB donor/acceptor double character of both molecules. The HB lengths indicate that the dominant interactions are O-H···O. The shorter distance of the O-H···O=C compared to that of O-H···N indicates that the interaction of water with the carbonyl group is stronger than with the amino group. The effects of σ-bond cooperativity[19] can be clearly seen from the comparison of the observed structure of f-w$_3$ with those of previously observed complexes of formamide and water[7,8] (see Figure 5.1, Tables 5.2 and S5.20). This confirms that the H···O, O···O and N···O distances associated to HBs decrease as the number of water molecules increase, as a characteristic of sequential cycles.

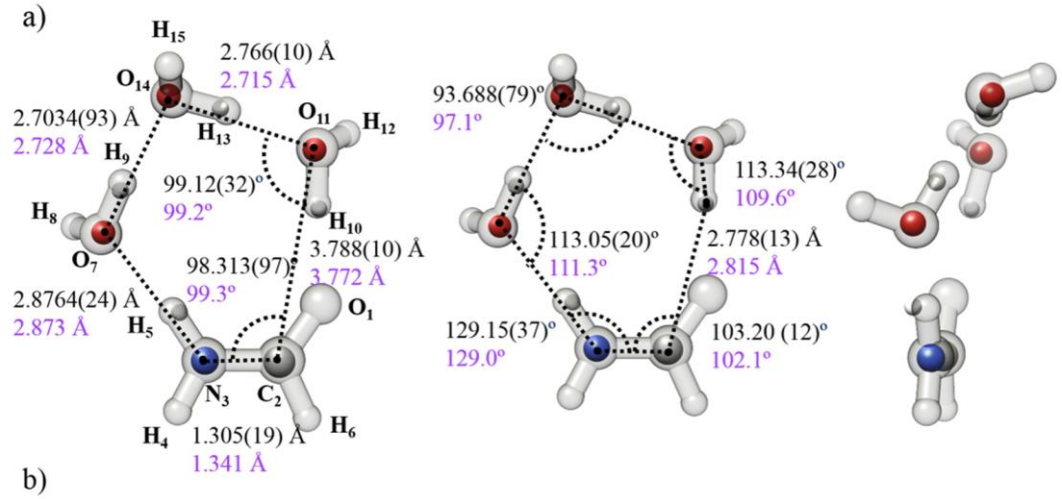

	r_s	r_0	r_e
∠$H_{10}O_1C_2N_3$		24.525(54)°	21.1°
∠$C_2N_3O_7O_{14}$	-25.9(10)°	-27.91(25)°	-23.6°
∠$N_3O_7O_{14}O_{11}$	25.38(36)°	23.347(96)°	18.9°

	r_s	r_0	r_e
∠$O_7O_{14}O_{11}C_2$	-18.93(31)°	-16.313(74)°	-13.1°
∠$C_2O_{11}O_7O_{14}$	-158.6(36)°	-157.36(49)°	-164.9°
∠$C_2N_3O_7O_{11}$	-7.80(90)°	-7.66(84)°	-10.5°

Figure 5.3. a) Comparison of the experimental r_s position of the isotopically substituted atoms of formamide-$(H_2O)_3$ (f-w$_3$) with the *ab initio* MP2/6-311++G(2d,p) structure. The r_s interatomic distances and angles are also given. b) The experimental r_0 bond lengths and angles of f-w$_3$ compared to the *ab initio* predictions.

Table 5.2. (a) Geometrical parameters (distances in Å, angles in degree) of formamide-(H_2O) (f-w-a), formamide-$(H_2O)_2$ (f-w_2) and formamide-$(H_2O)_3$ (f-w_3) clusters. (b) Geometrical parameter of w_n (n=2-5) clusters.

(a)	f-w-a[b]	f-w_2[b]	f-w_3[a]
$r_0(O_1\text{-}O_{11})$	2.8231(35)	2.7755(30)	2.7621(60)
$r_0(O_1\text{-}H_{10})$	1.9304(98)	1.7969(83)	1.7777(64)
$r_0(O_{11}\text{-}O_{14})$		2.755(3)	2.7167(55)
$r_0(H_{13}\text{-}O_{11})$		1.829(4)	1.7380(49)
$r_s(O_{14}\text{-}O_7)$			2.7606(53)
$r_0(H_9\text{-}O_{14})$			1.7810(52)
$r_0(O_7\text{-}N_3)$	2.8910(17)	2.9095(12)	2.8821(49)
$r_0(H_5\text{-}O_7)$	2.0607(45)	1.9363(60)	1.8748(44)
$\angle(O_1\text{-}O_{11}\text{-}O_{14})$			112.76(20)
$\angle(O_7\text{-}O_{14}\text{-}O_{11})$		86.30(15)	93.67(12)
$\angle(N_3\text{-}O_7\text{-}O_{14})$		84.04(13)	112.01(18)

(b)	w_2[c]	w_3[d]	w_4[e]	w_5[f]
r(O-O)	2.976	2.85	2.78	2.76
$\angle$(O-O-O)		60.	90.	107.9

[a] This work. [b] Ref. 8. [c] Ref. 31. [d] Ref. 32. [e] Ref. 33. [f] Refs. 21 and 22.

The comparison of the average O···O distances and O···O···O or N···O···O angles of f-w_3 with those of water clusters $(H_2O)_n$ with n=2-5 (see Table 5.2)[21,22,31–33] indicate that these are close to those of water pentamer.[21,22] In fact, the observed structure of the f-w_3 is so close to that of the more stable predicted form of w_5[34] that even the orientation of the non-bonded hydrogen atoms of the -w_3 fragment are practically the same. Both complexes are in fact superimposable (Figure 5.4). The geometry of w_5 is usually associated to that of a five membered-ring so it is reported to have a bent-ring configuration with a bending angle β of 164.5°.[22] A similar configuration can be devised for f-w_3 so for the r_0 structure a bending angle of 157.3(5)° and a small twisting angle τ of -8.0(6)° are estimated. The similarities extend to other couples (Figure 5.4) like f/w_2, f-w-a/w_3 and f-w_2/w_4 which can be approximately superimposed. The origin of this behavior lies in the similar geometrical arrangement of the C=O and N-H groups in formamide with the groups having the same HB donor/acceptor roles in the water dimer. In this way, formamide could be able to substitute the position of a water dimer fragment in water clusters so the structure of f-w_n complexes might turn out to be similar to $(w)_{n+2}$ clusters.

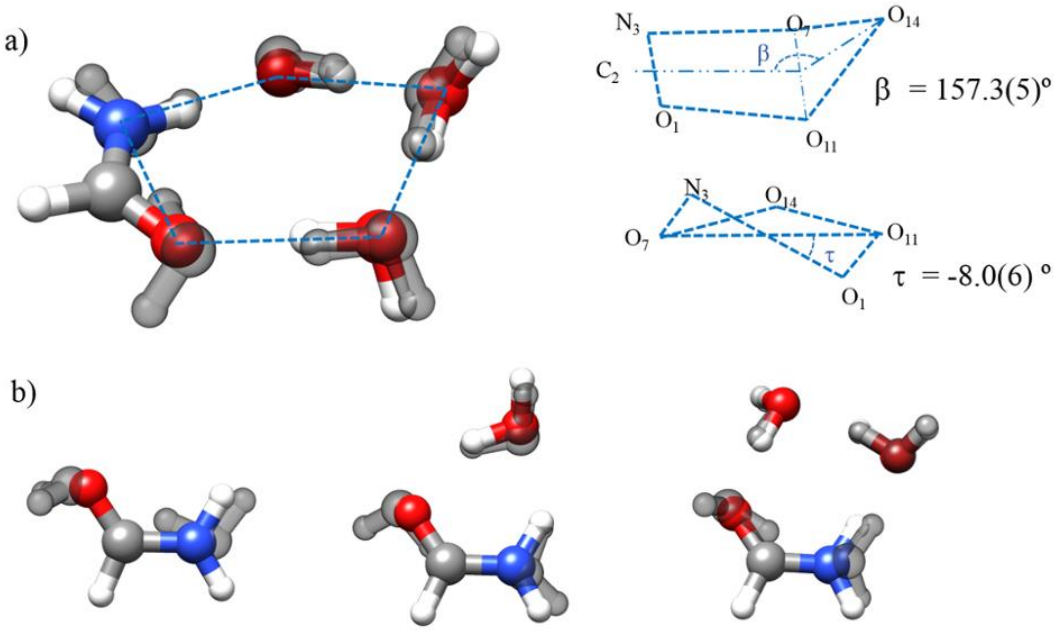

Figure 5.4. a) A comparison of the structure of formamide-$(H_2O)_3$ (f-w_3) found in this work with that of the global minimum of $(H_2O)_5$ (w_5) (superimposed in grey) and definition of the β and τ dihedral angles describing the conformation of a five-membered ring. b) The geometry similarities between formamide (f) and $(H_2O)_2$ (w_2), formamide-(H_2O)-a (f-w-a) and $(H_2O)_3$ (w_3) or formamide-$(H_2O)_2$ (f-w_2) and $(H_2O)_4$ (w_4) are shown (water clusters superimposed in grey).

Resonance-assisted hydrogen bonding (RAHB), often called π-cooperative bonding,[19] was first pointed out to occur in the case of the peptide linkage.[35,36] Its main effect is the simultaneous peptide C=O bond enlarging and C-N bond shortening when amide dimers are formed. This effect has been experimentally observed in the gas phase for f_2-w[17] and from the structure determined in this work, it seems to take place also for f-w_3 (see Scheme 5.1). However, it was not observable for other formamide-water complexes[7,8] and the structure comparison along the series should be based on theoretical predictions as shown in Figure S5.5. Nevertheless, this missed experimental information could be supplied by the analysis of the ^{14}N quadrupole coupling effects. These arise from the interaction of the electric quadrupole moment, eQ, of the ^{14}N nucleus with the electric field gradient q at the nitrogen nucleus site.[26] The associated spectroscopic constants ${}_{\beta\alpha}\chi=eQq_{\beta\alpha}$ (β, $\alpha=a,b,c$, the principal inertial axes) are very sensitive to changes in the electronic environment at this nucleus.

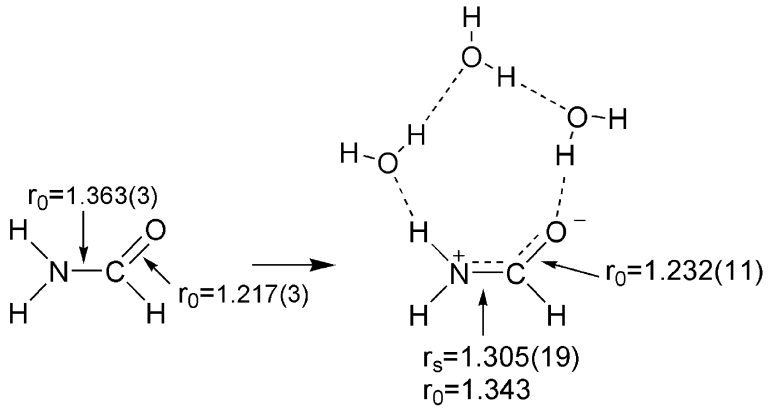

Scheme 5.1. RAHB inductive effects in the formation of formamide-$(H_2O)_3$ (f-w_3) are evidenced by the C=O bond length enlargement and C-N bond length decrease.

We have shown for formamide$_2$-water[17] that the quadrupole coupling constant χ_{cc} reflects the changes due to RAHB inductive effects (Figure S5.5). In bare formamide, the *c* inertial axis, perpendicular to the plane of the molecule, is parallel to one of the principal ^{14}N quadrupole coupling axis, say *z* ($\chi_{cc} \equiv \chi_{zz}$). Given the skeleton planarity of the formamide-water complexes studied so far[7,8,17] it can be reasonably assumed that $\chi_{cc} \approx \chi_{zz}$. In f-$w_3$ the angle between the *c* inertial and the *z* quadrupole axes is of only 13° thus the χ_{zz} constant can be confidently estimated form the *ab initio* results. The ^{14}N χ_{zz} constant can be related to the unbalanced $2p_z$ electronic charge $(U_p)_z = \left[(n_x - n_y)/2 - n_z\right]$ by:[26]

$$\chi_{zz}/eQq_{210} = -(U_p)_z \quad (1)$$

where n_α are the p_α orbital occupation numbers and q_{210} is the electric field gradient associated to a 2*p* electron in an isolated atom ($eQq_{210} \approx$-10 MHz for N). In Figure 5.5, the experimental values of χ_{zz}/eQq_{210} for the different formamide-water clusters are plotted *vs.* $-(U_p)_z$ calculated from a natural bond orbital (NBO) analysis (see Figure S5.6).[37] Despite the approximations, they show and excellent correlation. According to the definition of $(U_p)_z$, the electron density excess along the *z* axis in formamide progressively decreases. This electron density can be associated to the population of the N-atom lone pair which is calculated to deplete correspondingly (Figure S5.7).

The calculated values of η_D (see Table S5.21) show noticeable changes from formamide and f-w-b, which are predicted to have an almost symmetric distribution of charge (η_D = 0.04), to formamide-H_2O-a (η_D = 0.22) and the three- (f_2-w and f-w_2) and four-body (f-w_3) clusters (η_D = 0.35-0.38 range). All the magnitudes considered through this discussion, the constant χ_{cc}, the bond lengths C-N and C=O or the η_D parameter seem to have similar values for the complexes of three and four bodies. This indicates that while adding a water molecule to the f-w-a complex to form f-w_2 notably alters χ_{cc}, C-N and C=O, or η_D, adding a new water molecule to form f-w_3 practically does not increase polarization effects so much. Probably this is a good reason to wonder to what extension the concept of RAHB could be related to cooperativity.[38]

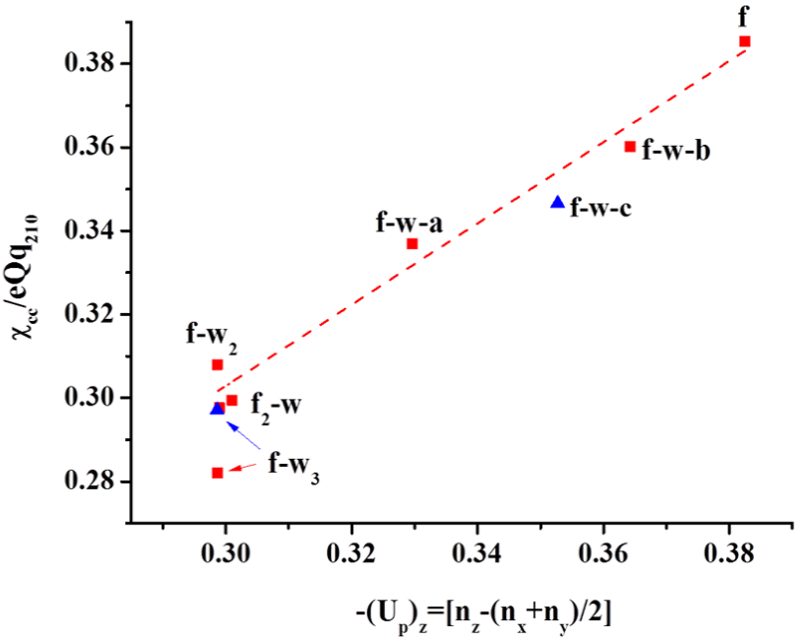

Figure 5.5. Plot showing the correlation between the experimental values (■) of the quantity χ_{cc}/eQq_{210} and the unbalanced $2p_z$ NBO electronic charge -(Up)$_z$ (slope 0.97) for formamide (f), the formamide-H_2O forms (f-w-a and f-w-b), formamide-$(H_2O)_2$ (f-w$_2$), formamide$_2$-H_2O (f$_2$-w) and formamide-$(H_2O)_3$ (f-w$_3$) (see Figure 5.1). The points with triangle symbol (▲) correspond to scaled χ_{zz} *ab initio* values (see Table S5.21 and Figure S5.6) for formamide-H_2O form c (f-w-c) and f-w$_3$.

The doublets observed in the spectra indicate that the "puckered" configuration of f-w$_3$ has a two-fold degeneracy. If we consider the inversion through the planar C_s configuration of the adduct it is easy to see that both degenerate forms constitute a pair of mirror images that cannot be superimposed, being thus enantiomeric forms. Although f-w$_3$ does not have any chiral center, it shows transient chirality and the tunneling splitting of about 370 MHz (0.0090(4) cm^{-1}) observed in the spectrum of f-w$_3$ arise by a vibrational motion connecting the two equivalent enantiomeric structures.

The analysis of the potential energy surface (PES) of f-w$_3$ to determine the nature of the observed splittings is not easy due to its multidimensional nature. The complete inversion of the structure requires motions associated to the reorientation of water molecules concerted to the "ring-puckering" motions of the heavy atom skeleton. The water motions include the rotation around the HB axes (flipping) or the more energetic bifurcation mechanism.[32] We have not observed spin statistic effects. The spectra of all detected isotopologues, including those of the deuterium atoms, show similar tunneling splittings. This observation suggests that there is not an observable exchange of equivalent hydrogen atoms ruling out a bifurcation mechanism. The inversion of the structure passing through the planar configuration by simultaneous torsion of all three water molecules require a rather high barrier, calculated in the range 700 cm^{-1} to 950 cm^{-1} (see Figure S5.8). Simple

estimations with one-dimensional double minimum potential functions predict the observed inversion splittings corresponding to barriers close to 300 cm^{-1}. For this reason, other possible paths should be considered.

Alternative paths have been investigated such as those driving conformational change by the flipping motion of one water molecule at a time (see Figure 5.6). This path passes by the different energy minima calculated for cyclic forms of f-w_3. They have been labeled as f-w_3-udu (mirror image -dud), f-w_3-diu (-uid) and f-w_3-dui (-udi) from the orientation up (u), down (d) or in the plane (i) of the non-bonded hydrogen atoms of the three water molecules $w_{(1)}$, $w_{(2)}$ and $w_{(3)}$, respectively. It can be seen that flipping of $w_{(1)}$, drives the change from the global minimum f-w_3-udu to f-w_3-diu. Then $w_{(2)}$ rotation brings the system from f-w_3-diu to f-w_3-dui and finally $w_{(3)}$ flipping brings the cluster to f-w_3-dud inverting the puckered form of the skeleton and completing the inversion of the structure from the starting point f-w_3-udu to its enantiomeric form f-w_3-dud. Each motion drives a change in the conformation of the cluster through a reasonably small potential energy barrier, as also occurs in other water complexes.[39] The non-observation of f-w_3-diu and f-w_3-dui conformers confirms the low barrier since collisional relaxation might take place in the supersonic jet.[40] From this description at the origin of the observed vibrational doubling of the rotational spectrum it is easy to devise a periodic potential energy function inverting the structure without passing by the planar form. This periodic potential function would be similar to pseudorotation reported in five-membered rings[41] and suggested for w_5[21] and would be at the origin of the observed vibrational doubling of the rotational spectra of f-w_3.

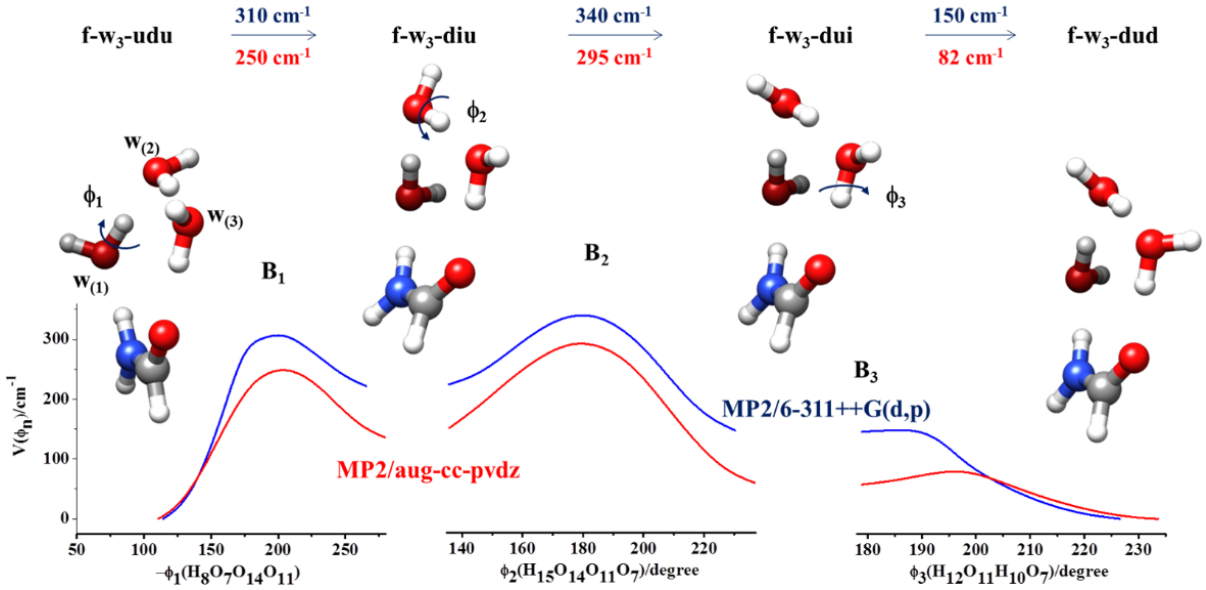

Figure 5.6. A possible path for inversion of the configuration of formamide-$(H_2O)_3$ (f-w_3) calculated in three steps by scanning successively the flipping angles ϕ_1, ϕ_2 and ϕ_3. Through this path, as in pseudorotation, the f-w_3 cluster transforms from the f-w_3-udu form to the f-w_3-dud enantiomeric equivalent forms passing through small barriers by the different stable conformers. Calculations have been done at MP2(FC)/6-311++G(d,p), MP2(FC)/6-311++G(2d,p) and MP2(FC)/Aug-cc-pVDZ levels. MP2(FC)/6-311++G(2d,p) give barriers intermediate between those shown in the figure.

In summary, the analysis of the spectrum of the complex of formamide with three water molecules has revealed interesting structural and dynamical features. The donor/acceptor hydrogen bonding properties of water and formamide lead to a structure in which the water molecules close a sequential cycle with formamide. In contrast with previously observed formamide-water clusters[7,8,17] the heavy atom skeleton is not planar and adopts a chiral structure. One of the most interesting features of this structure is that it can be superimposed to the structure of the water pentamer. As a conclusion of this work, we show that all the formamide-$(H_2O)_n$ clusters studied so far have structural similarities to $(H_2O)_{n+2}$ clusters. This is an interesting feature giving the total miscibility of formamide and water, which is observed even at the onset of microsolvation. The quadrupole coupling constants prove the progressive depletion of the electronic density of the N-atom lone pair along a series of formamide-water complexes and that these constants are linearly correlated to the changes of the C-N and C=O distances associated to RAHB. These effects are noticeable in passing from the monomer to complexes with n=1 and 2, but are not so important in passing from n=2 to 3 water molecules. This led us to wonder to which extension RAHB ought to be considered within the context of cooperativity.[38] The small tunneling splitting results from the interconversion between the enantiomeric observed structures giving rise to transient chirality. The exploration of the potential energy surface suggests a mechanism driven by non-simultaneous flipping motions of the water molecules. This dynamics can be taken as reminiscent of the complex vibrational motions of water pentamer, which are related to the pseudorotation of a five-membered ring, reinforcing the structural similarity between these systems. In addition, these results led one to wonder if similar effects could take place in larger systems as proteins where water motions can couple to protein motions which are very important to define their functions.
Further research on higher order complexes of formamide and water would be done to confirm these results.

Experimental Methods

The microwave spectra (5-13 GHz) were recorded using a molecular-beam Fourier transform microwave spectrometer (MB-FTMW), described elsewhere.[42] The commercial samples of formamide were heated at about 50ºC, water was placed in a reservoir inserted in the gas line, and a He-Ne gas mixture was used as the carrier gas (backing pressure *ca.* 12 bar) dragging the molecules to form the complexes in the jet expansion. A detailed description of the experiment is included in the Supporting Information.

References

[1] Desfrançois, C., Carles, S., Schermann, J. P. "Weakly Bound Clusters of Biological Interest" *Chem. Rev.* **2000**, 100, 3943–3962.

[2] Dopfer, O., Fujii, M. "Probing Solvation Dynamics around Aromatic and Biological Molecules at the Single-Molecular Level" *Chem. Rev.* **2016**, 116, 5432–5463.

[3] Becucci, M., Melandri, S. "High-Resolution Spectroscopic Studies of Complexes Formed by Medium-Size Organic Molecules" *Chem. Rev.* **2016**, 116, 5014–5037.

[4] Pérez, C., Muckle, M. T., Zaleski, D. P., Seifert, N. A., Temelso, B., Shields, G. C., Kisiel, Z., Pate, B. H. "Structures of Cage, Prism, and Book Isomers of Water Hexamer from Broadband Rotational Spectroscopy" *Science* **2012**, 336, 897–901.

[5] Pérez, C., Zaleski, D. P., Seifert, N. A., Temelso, B., Shields, G. C., Kisiel, Z., Pate, B. H. "Hydrogen Bond Cooperativity and the Three-Dimensional Structures of Water Nonamers and Decamers" *Angew. Chem. Int. Ed.* **2014**, 53, 14368–14372.

[6] Richardson, J. O., Pérez, C., Lobsiger, S., Reid, A. A., Temelso, B., Shields, G. C., Kisiel, Z., Wales, D. J., Pate, B. H., Althorpe, S. C. "Concerted Hydrogen-Bond Breaking by Quantum Tunneling in the Water Hexamer Prism" *Science* **2016**, 351, 1310–1313.

[7] Lovas, F. J., Suenram, R. D., Fraser, G. T., Gillies, C. W., Zozom, J. "The Microwave Spectrum of Formamide-Water and Formamide-Methanol Complexes" *J. Chem. Phys.* **1988**, 88, 722–729.

[8] Blanco, S., López, J. C., Lesarri, A., Alonso, J. L. "Microsolvation of Formamide: A Rotational Study" *J. Am. Chem. Soc.* **2006**, 128, 12111–12121.

[9] Held, A., Pratt, D. W. "Hydrogen Bonding in Water Complexes. Structures of 2-Pyridone-H_2O and 2-Pyridone-$(H_2O)_2$ in Their S_0 and S_1 Electronic States" *J. Am. Chem. Soc.* **1993**, 115, 9708–9717.

[10] Su, Z., Xu, Y. "Hydration of a Chiral Molecule: The Propylene Oxide···$(Water)_2$ Cluster in the Gas Phase" *Angew. Chem. Int. Ed.* **2007**, 119, 6275–6278.

[11] Thomas, J., Sukhorukov, O., Jäger, W., Xu, Y. "Direct Spectroscopic Detection of the Orientation of Free OH Groups in Methyl Lactate–$(Water)_{1,2}$ Clusters: Hydration of a Chiral Hydroxy" *Angew. Chem. Int. Ed.* **2014**, 53, 1156–1159.

[12] Pérez, C., López, J. C., Blanco, S., Schnell, M. "Water-Induced Structural Changes in Crown Ethers from Broadband Rotational Spectroscopy" *J. Phys. Chem. Lett.* **2016**, 7, 4053–4058.

[13] Pérez, C., Neill, J. L., Muckle, M. T., Zaleski, D. P., Peña, I., López, J. C., Alonso, J. L., Pate, B. H. "Water-Water and Water-Solute Interactions in Microsolvated Organic Complexes" *Angew. Chem. Int. Ed.* **2015**, 54, 979–982.

[14] Pérez, C., Krin, A., Steber, A. L., López, J. C., Kisiel, Z., Schnell, M. "Wetting Camphor: Multi-Isotopic Substitution Identifies the Complementary Roles of Hydrogen Bonding and Dispersive Forces" *J. Phys. Chem. Lett.* **2016**, 7, 154–160.

[15] Ouyang, B., Starkey, T. G., Howard, B. J. "High-Resolution Microwave Studies of Ring-Structured Complexes between Trifluoroacetic Acid and Water" *J. Phys. Chem. A* **2007**, 111, 6165–6175.

[16] Ouyang, B., Howard, B. J. "Hydrates of *Trans*- and *Gauche*-Difluoroacetic Acids: A High-Resolution Microwave Spectroscopic Study" *J. Phys. Chem. A* **2010**, 114, 4109–4117.

[17] Blanco, S., Pinacho, P., López, J. C. "Hydrogen-Bond Cooperativity in $Formamide_2$-Water: A Model for Water-Mediated Interactions" *Angew. Chem. Int. Ed.* **2016**, 128, 9477–9481.

[18] Bellissent-Funel, M.-C., Hassanali, A., Havenith, M., Henchman, R., Pohl, P., Sterpone, F., van der Spoel, D., Xu, Y., Garcia, A. E. "Water Determines the Structure and Dynamics of Proteins" *Chem. Rev.* **2016**, 116, 7673–7697.

[19] Jeffrey, G. A. *An Introduction to Hydrogen Bonding*, Topics in Physical Chemistry, Oxford University Press, Oxford University Press, 1997.

[20] Shubert, V. A., Müller, C. W., Zwier, T. S. "Water's Role in Reshaping a Macrocycle's Binding Pocket: Infrared and Ultraviolet Spectroscopy of Benzo-15-Crown-5-$(H_2O)(n)$ and 4-aminobenzo-15-Crown-5-$(H_2O)(n)$, n = 1, 2" *J. Phys. Chem. A* **2009**, 113, 8067−8079.

[21] Liu, K., Brown, M. G., Cruzan, J. D., Saykally, R. J. "Vibration-Rotation Tunneling Spectra of the Water Pentamer: Structure and Dynamics" *Science* **1996**, 271, 62–64.

[22] Cole, W. T. S., Fellers, R. S., Viant, M. R., Saykally, R. J. "Hydrogen Bond Breaking Dynamics in the Water Pentamer: Terahertz VRT Spectroscopy of a 20 μM Libration" *J. Chem. Phys.* **2017**, 146, 14306.
[23] Gaussian 09, Revision D.01, Frisch M. J., Trucks G. W., Schlegel H. B., Scuseria G. E., Robb M. A., Cheeseman J. R., Scalmani G., Barone V., Petersson G. A., Nakatsuji H., Li X., Caricato M., Marenich A., Bloino J., Janesko B. G., Gomperts R., Mennucci B., Hratchian H. P., Ortiz J. V., Izmaylov A. F., Sonnenberg J. L., Williams-Young D., Ding F., Lipparini F., Egidi F., Goings J., Peng B., Petrone A., Henderson T., Ranasinghe D., Zakrzewski V. G., Gao J., Rega N., Zheng G., Liang W., Hada M., Ehara M., Toyota K., Fukuda R., Hasegawa J., Ishida M., Nakajima T., Honda Y., Kitao O., Nakai H., Vreven T., Throssell K., Montgomery, Jr. J. A., Peralta J. E., Ogliaro F., Bearpark M., Heyd J. J., Brothers E., Kudin K. N., Staroverov V. N., Keith T., Kobayashi R., Normand J., Raghavachari K., Rendell A., Burant J. C., Iyengar S. S., Tomasi J., Cossi M., Millam J. M., Klene M., Adamo C., Cammi R., Ochterski J. W., Martin R. L., Morokuma K., Farkas O., Foresman J. B., Fox D. J., *Gaussian, Inc., Wallingford CT*, 2016.
[24] Pickett, H. M. "The Fitting and Prediction of Vibration-Rotation Spectra with Spin Interactions" *J. Mol. Spectrosc.* **1991**, 148, 371–377.
[25] Watson, J. K. G. "Aspects of Quartic and Sextic Centrifugal Effects on Rotational Energy Levels" in *Vibrational Spectra and Structure a Series of Advances, Vol 6*, Durig, J. R., Ed., Elsevier: New York, 1977, pp 1–89.
[26] Gordy, W., Cook, R. L. *Microwave Molecular Spectra*, Wiley-Interscience: New York, 1984.
[27] Papoušek D., Aliev, M. R., in *Molecular Vibrational and Rotational Spectra*, Vol. 17: Studies in Physical and Theoretical Chemistry. Elsevier Scientific Publishing Company, Amsterdam, Oxford, New York, 1982.
[28] Hirota, E., Sugisaki, R., Nielsen, C. J., Sørensen, G. O. "Molecular Structure and Internal Motion of Formamide from Microwave Spectrum" *J. Mol. Spectrosc.* **1974**, 49, 251–267.
[29] Kraitchman, J. "Determination of Molecular Structure from Microwave Spectroscopic Data" *Am. J. Phys.* **1953**, 21, 17–24.
[30] Kisiel, Z. "Least-Squares Mass-Dependence Molecular Structures for Selected Weakly Bound Intermolecular Clusters" *J. Mol. Spectrosc.* **2003**, 218, 58–67.
[31] Dyke, T. R., Mack, K. M., Muenter, J. S. "The Structure of Water Dimer from Molecular Beam Electric Resonance Spectroscopy" *J. Chem. Phys.* **1977**, 66, 498-510.
[32] Keutsch, F. N., Cruzan, J. D., Saykally, R. J. "The Water Trimer" *Chem. Rev.* **2003**, 103, 2533–2577.
[33] Cruzan, J. D., Braly, L. B., Liu, K., Brown, M. G., Loeser, J. G., Saykally, R. J. "Quantifying Hydrogen Bond Cooperativity in Water: VRT Spectroscopy of the Water Tetramer" *Science* **1996**, 271, 59–62.
[34] Ramírez, F., Hadad, C. Z., Guerra, D., David, J., Restrepo, A. "Structural Studies of the Water Pentamer" *Chem. Phys. Lett.* **2011**, 507, 229–233.
[35] Gilli, P., Bertolasi, V., Ferretti, V., Gilli, G. "Evidence for Intramolecular N−H···O Resonance-Assisted Hydrogen Bonding in β-Enaminones and Related Heterodienes. A Combined Crystal-Structural, IR and NMR Spectroscopic, and Quantum-Mechanical Investigation" *J. Am. Chem. Soc.* **2000**, 122, 10405–10417.
[36] Ottersen, T. "On the Structure of the Peptide Linkage. The Structures of Formamide and Acetamide at -165 Degrees C and an Ab Initio Study of Formamide, Acetamide, and N-Methylformamide" *Acta Chemica Scandinavica*. **1975**, 29a, 939–944.
[37] Reed, A. E., Weinstock, R. B., Weinhold, F. "Natural Population Analysis" *J. Chem. Phys.* **1985**, 83, 735-746.
[38] Mahadevi, A. S., Sastry, G. N. "Cooperativity in Noncovalent Interactions" *Chem. Rev.* **2016**, 116, 2775–2825.
[39] Gall, J. T. A., Thomas, J., Xie, F., Wang, Z., Jäger, W., Xu, Y. "Rotational Spectroscopy of the Methyl Glycidate-Water Complex: Conformation and Water and Methyl Rotor Tunneling Motions" *Phys. Chem. Chem. Phys*. **2017**, 19, 29508-29515.
[40] Ruoff, R. S., Klots, T. D., Emilson, T., Gutowsky, H. S., "Relaxation of Conformers and Isomers in Seeded Supersonic Jets of Inert Gases" *J. Chem. Phys*. **1990**, 93, 3142-3150.
[41] Kilpatrick, J. E., Pitzer, K. S., Spitzer, R. "The Thermodynamics and Molecular Structure of Cyclopentane" *J. Am. Chem. Soc.* **1947**, 69, 2483–2488.
[42] Alonso, J. L., Lorenzo, F. J., López, J. C., Lesarri, A., Mata, S., Dreizler, H. "Construction of a Molecular Beam Fourier Transform Microwave Spectrometer Used to Study the 2,5-Dihydrofuran-Argon van Der Waals Complex" *Chem. Phys.* **1997**, 218, 267–275.

Supplementary material for Chapter V

Structure and Dynamics in Formamide-$(H_2O)_3$: a Water-Pentamer Analogue

Direct transcription from: Blanco, S., Pinacho, P., López, J. C. *J Phys. Chem. Lett.*, **2017**, 8, 6060–6066.

Abstract

Water self-association dominates the formation of microsolvated molecular clusters which may give rise to complex structures resembling those of pure water clusters. We present a rotational study of the complex formamide-$(H_2O)_3$ formed in a supersonic jet and several monosubstituted isotopologues. Formamide and water molecules form a four-body sequential cycle through N-H···O, O-H···O and O-H···O=C hydrogen bonds, resulting in a chiral structure with a non-planar skeleton that can be overlapped to that of water pentamer. The analysis of the ^{14}N-nucleus quadrupole coupling effects shows the depletion of the electron density of the N atom lone pair with respect to the bare formamide that affects to the amide group C-N and C=O distances. The study of the observed tunneling doublets shows that formamide-$(H_2O)_3$ follows a path to invert its structure driven by the flipping of water subunits and passing through successive non-planar configurations, a motion reminiscent of the pseudorotation of water pentamer.

- **Annex 5.1.-** Experimental conditions.

- **Annex 5.2.-** Structural predictions and analysis of the spectrum.

- **Table S5.1.** Rotational parameters predicted from *ab initio* MP2/6-311++G(d,p) calculations for several stable formamide-$(H_2O)_3$ (f-w$_3$) conformers.

- **Table S5.2**. Rotational parameters predicted from *ab initio* MP2/6-311++G(2d,p) calculations for the stable cyclic formamide-$(H_2O)_3$ (f-w$_3$) conformers.

- **Table S5.3.** Rotational parameters obtained from the analysis of the spectrum of parent formamide-$(H_2O)_3$ (f-w$_3$) complex and those calculated at the MP2/6-311++G(2d,p) level for the global minimum.

- **Table S5.4.** Rotational parameters obtained from the analysis of the spectra of the observed $^{15}N_3$ and $^{13}C_2$ isotopologues of formamide-$(H_2O)_3$ (f-w$_3$) complex.

- **Table S5.5**. Rotational parameters obtained from the analysis of the spectra of the observed ^{18}O isotopologues of the formamide-$(H_2O)_3$ (f-w$_3$) complex.

- **Table S5.6.** Rotational parameters obtained from the analysis of the spectra of the observed ^{2}H isotopologues of the formamide-$(H_2O)_3$ (f-w$_3$) complex.

- **Table S5.7.** Observed rotational transitions with resolved ^{14}N hyperfine structure and residuals for the parent species of the complex formamide-$(H_2O)_3$ (f-w$_3$).

- **Table S5.8.** Observed rotational transitions with resolved ^{14}N hyperfine structure and residuals for the $^{13}C_2$ isotopologue of the complex formamide-$(H_2O)_3$ (f-w$_3$).

- **Table S5.9.** Observed rotational transitions and residuals for the $^{15}N_3$ isotopologue of the complex formamide-$(H_2O)_3$ (f-w$_3$).

- **Table S5.10.** Observed rotational transitions with resolved ^{14}N hyperfine structure and residuals for the $^{18}O_7$ isotopologue of the complex formamide-$(H_2O)_3$ (f-w$_3$).

- **Table S5.11.** Observed rotational transitions with resolved ^{14}N hyperfine structure and residuals for the $^{18}O_{11}$ isotopologue of the complex formamide-$(H_2O)_3$ (f-w$_3$).

- **Table S5.12**. Observed rotational transitions with resolved ^{14}N hyperfine structure and residuals for the $^{18}O_{14}$ isotopologue of the complex formamide-$(H_2O)_3$ (f-w$_3$).

- **Table S5.13.** Observed rotational transitions with resolved ^{14}N hyperfine structure and residuals for the $^{2}H_5$ isotopologue of the complex formamide-$(H_2O)_3$ (f-w$_3$).

- **Table S5.14.** Observed rotational transitions with resolved ^{14}N hyperfine structure and residuals for the $^{2}H_9$ isotopologue of the complex formamide-$(H_2O)_3$ (f-w$_3$).

- **Table S5.15.** Observed rotational transitions with resolved ^{14}N hyperfine structure and residuals for the $^{2}H_{10}$ isotopologue of the complex formamide-$(H_2O)_3$ (f-w$_3$).

- **Table S5.16.** Observed rotational transitions with resolved ^{14}N hyperfine structure and residuals for the $^{2}H_{13}$ isotopologue of the complex formamide-$(H_2O)_3$ (f-w$_3$).

- **Table S5.17.** r_s coordinates of the isotopically substituted atoms of the complex formamide-$(H_2O)_3$ (f-w$_3$) compared to r_0 and r_e (MP2/6-311++G(2d,p)) *ab initio* (*ab*) coordinates for the three most stable conformers.

- **Table S5.18.** r_0 structure of the complex formamide-$(H_2O)_3$ (f-w_3) derived from the fit of the observed rotational constants.
- **Table S5.19.** r_s distances and angles derived from the coordinates of Table S5.17 compared to *ab initio* parameters for the global minimum of the complex formamide-$(H_2O)_3$ (f-w_3-c1) and the r_0 parameters.
- **Table S5.20.** Comparison of geometrical parameters of formamide-$(H_2O)_3$ (f-w_3) with those of related systems.
- **Table S5.21.** Experimental and *ab initio* quadrupole coupling constants of formamide and different formamide-water complexes together with the values of the unbalanced $2p_z$ electronic charge.
- **Figure S5.1.** Calculated cyclic conformers for the complex formamide-$(H_2O)_3$ (f-w_3).
- **Figure S5.2.** Calculated conformers for the complex formamide-$(H_2O)_3$ (f-w_3), with water molecules forming a trimer.
- **Figure S5.3**. Other calculated conformers for the complex formamide-$(H_2O)_3$ (f-w_3).
- **Figure S5.4**. Comparison of the r_s structure and the *ab initio* structures for the lowest energy conformers of the complex formamide-$(H_2O)_3$ (f-w_3).
- **Figure S5.5.** Predicted variation of the distances C-N and C=O and the experimental values of χ_{cc} for formamide for the different experimentally observed adducts of formamide and water.
- **Figure S5.6.** Plot of the values of the quantity χ_{cc}/eQq_{210} (experimental) *vs*. the unbalanced $2p_z$ electronic charge obtained from a NBO analysis of formamide and the different experimentally observed adducts of formamide and water.
- **Figure S5.7.** Plot of the values of the quantity χ_{cc}/eQq_{210} (experimental) *vs*. the lone pair occupancy of the N atom of formamide and the different experimentally observed adducts of formamide and water.
- **Figure S5.8.** MP2-calculated potential energy function for the pure inversion of the conformation of the complex formamide-$(H_2O)_3$ (f-w_3).

Annex 5.1.- Experimental conditions.

Commercial samples of the parent and isotopic species of formamide and water were used. The molecular-beam Fourier transform microwave spectrometer (MB-FTMW), described in the bibliography (Alonso, J. L., Lorenzo, F. J., López, J. C., Lesarri, A., Mata, S., Dreizler, H. *Chem. Phys.* **1997**, *218*, 267–275), was operated in the frequency range 5-13 GHz. The supersonic jet was generated by expansion of a He-Ne gas mixture at backing pressures of about 12 bar through a small (0.9 mm diameter) pulsed heatable nozzle (Blanco, S., López, J. C., Alonso, J. L., Ottaviani, P., Caminati, W. *J. Chem. Phys.* **2003**, *119*, 880-886). Formamide (b.p. 210°C) was placed in a nozzle at about 50°C and water in a reservoir inserted in the gas line just before the nozzle. Short microwave pulses (typ. 0.3 μs, 10-300 mW) were used for polarization purposes. Typically, a *ca*. 400 μs-length time domain spectrum was recorded in 40-100 ns intervals and converted to the frequency domain by a fast Fourier transformation. Due to the collinear arrangement of the jet and resonator axis each rotational transition splits in two Doppler components so the resonant frequencies are taken as the arithmetic mean of both components. Frequency accuracy is better than 3 kHz.

Annex 5.2.- Structural predictions and analysis of the spectrum

Prior to analyze the microwave spectrum, *ab initio* calculations (Gaussian 09, Revision D.01, Frisch M. J. *et al*, *Gaussian, Inc., Wallingford CT*, 2016) using MP2/6-311++G(d,p) were done on the possible forms that the adduct f-w_3 may adopt. The results are collected in Table S5.1 and Figures S5.1-S5.3 (supporting information). We considered the cyclic arrangement (Figure S5.1), which gives rise to three different forms, labeled f-w_3-c1, f-w_3-c2, f-w_3-c3 in order of energy, the arrangements in which water molecules form a trimer interacting with formamide (Figure S5.2), and other possible conformers formed from observed f-w or f-w_2 adducts (Figure S5.3). The lowest energy forms are those in which f-w_3 adopts a cyclic arrangement, being f-w_3-c1 (see Figure S5.1) the global minimum. The spectroscopic parameters of those cyclic forms, given in Table S5.2, were then predicted using MP2/6-311++G(2d,p).

The microwave spectra of formamide-water complexes were recorded in the 5-13 GHz frequency range. Once dropped all known frequencies belonging to f-w, f-w_2 (Blanco, S.; López, J. C.; Lesarri, A.; Alonso, J. L. *J. Am. Chem. Soc.* **2006**, *128*, 12111–12121) and f_2-w (Blanco, S.; Pinacho, P.; López, J. C. *Angew. Chemie* **2016**, *128*, 9477–9481) species (see Figure 5.1), several groups of unassigned lines remain in the spectrum with appreciable intensity. These show the quadrupole coupling (hfs) characteristic of species having one ^{14}N nuclei and a doubling attributable to a tunneling motion (see Figure 5.2).

In order to have a first identification of the species giving rise to these lines we considered the predictions for formamide-$(H_2O)_3$ forms and found an acceptable match in frequency and hfs patterns for the calculated cyclic forms of f-w_3 complex (see Figure S5.1). In the initial assignment of the spectra the tunneling states, labeled v=0 and v=1 were considered separately. The semirigid rotor Hamiltonian (Watson, J. K. G. In *Vibrational Spectra and Structure a Series of Advances, Vol 6*; Durig, J. R., Ed.; Elsevier: New York, 1977; pp 1–89), H_R, supplemented by a term, H_Q, describing the quadrupole coupling interaction (Gordy, W., Cook, R. L. *Microwave Molecular Spectra*; Wiley-Interscience: New York, 1984, Vol. 11) was used for the analysis (Pickett, H. M. *J. Mol. Spectrosc.* **1991**, *148*, 371–377). This term was set up in the basis set (I J F), I + J = F. The energy levels involved in each transition were labeled with the quantum numbers J, K_{-1}, K_{+1}, F. This model fails for the high K_{-1} doublets indicating the existence of an *a*-type Coriolis coupling interaction. To take into account this interaction a two-state Hamiltonian,

$$H=\begin{pmatrix} \langle 0|H_R+H_Q|0\rangle & \langle 0|iG_a|1\rangle \\ \langle 1|iG_a|0\rangle & \langle 1|H_R+H_Q|1\rangle+\Delta E_{01} \end{pmatrix} \quad (1)$$

was used, where <0|i*G*a|1> is the coupling interaction term, connecting both states and ΔE_{01} the energy difference between them. The complete results are given in Table S5.3.

To investigate the structure of the complex we recorded the spectra of $^{15}NH_2$-CHO$\cdots(H_2O)_3$, NH_2-^{13}CHO$\cdots(H_2O)_3$ and the three possible NH_2-CHO$\cdots(H_2{}^{18}O\cdots(H_2O)_2)$ isotopologues. Measurements of monosubstituted deuterated species were possible only for the atoms involved in hydrogen bonds. The $^{15}NH_2$-CHO$\cdots$ $(H_2O)_3$ isotopologue shows no hfs structure so the H_Q terms were dropped from the Hamiltonian. In this case all the parameters were fitted from the spectrum and the values of the ΔE_{01} and i*G*a were determined to be the same as those determined for the parent species within the errors quoted. For the rest of the isotopologues the same Hamiltonian as for the parent was used and the fits were optimal by keeping all the parameters fixed to the parent species values except the rotational constants. The complete results are shown in Tables S5.3-S5.6 and the observed frequencies are given in Tables S5.7-S5.16 of the supplementary material.

Table S5.1. Rotational parameters predicted from *ab initio* MP2/6-311++G(d,p) calculations for several stable formamide-$(H_2O)_3$ (f-w$_3$) conformers.

	f-w$_3$-c1	**f-w$_3$-c2**	**f-w$_3$-c3**	**f-w$_3$-c4**	**f-w$_3$-c5**	**f-w$_3$-c6**
	f-w$_3$-dud	**f-w$_3$-dui**	**f-w$_3$-diu**			
A[a]/MHz	2503	2590	2520	2066	2802	2520
B/MHz	1498	1472	1497	1975	1440	1497
C/MHz	963	978	979	1021	1305	979
P_{aa}/uÅ^2	329.8	331.8	326.7	253.1	278.9	438.3
P_{bb}/uÅ^2	194.4	185.0	189.7	241.7	108.3	142.5
P_{cc}/uÅ^2	7.4	11.6	10.9	2.8	72.0	2.4
χ_{aa}/MHz	0.83	0.70	0.52	1.46	-0.10	1.26
χ_{bb}/MHz	1.97	2.16	1.95	0.73	2.07	1.67
χ_{cc}/MHz	-2.79	-2.86	-2.47	-2.18	-1.97	-2.94
μ_a/D	1.0	-1.7	0.5	1.1	-0.8	-1.8
μ_b/D	1.2	-0.6	-0.7	-1.3	-4.3	1.2
μ_c/D	0.0	0.1	0.3	-1.2	0.8	0.7
E/h	-398.38119	-398.38053	-398.38018	-398.37767	-398.37588	-398.37578
ΔE/cm^{-1}	0	147	222	774	1167	1188

	f-w$_3$-c7	**f-w$_3$-c8**	**f-w$_3$-c9**	**f-w$_3$-c10**	**f-w$_3$-c11**	**f-w$_3$-c12**
A[a]/MHz	2952	3213	4255	3826	3146	3188
B/MHz	1354	1045	838	1089	1096	1042
C/MHz	1199	797	794	853	1021	1011
P_{aa}/uÅ^2	311.7	479.9	560.3	462.3	397.9	413.1
P_{bb}/uÅ^2	109.7	153.8	75.8	130.2	97.2	86.7
P_{cc}/uÅ^2	61.5	3.5	43.0	1.9	63.4	71.8
χ_{aa}/MHz	0.21	1.24	1.31	1.47	1.69	1.59
χ_{bb}/MHz	2.16	1.75	-2.36	1.89	1.94	0.74
χ_{cc}/MHz	-2.37	-2.99	1.04	-3.36	-3.63	-2.33
μ_a/D	-0.8	1.24	-1.2	-1.1	-2.7	-4.5
μ_b/D	4.5	1.75	-1.7	0.6	-4.1	2.0
μ_c/D	1.7	-2.99	2.1	0.4	0.8	0.6
E/h	-398.37565	-398.37493	-398.37382	-398.37327	-398.37056	-398.36967
ΔE/cm^{-1}	1216	1376	1618	1740	2335	2528

[a] A, B and C are the rotational constants. $P_{\alpha\alpha}$ (α= a, b or c) are the planar moments of inertia; these are derived from the moments of inertia I_α as for example $P_{cc} = (I_a + I_b - I_c)/2 = (\sum_i m_i c_i^2)/2)$. χ_{aa}, χ_{bb} and χ_{cc} are the quadrupole coupling constants for ^{14}N. μ_a, μ_b, μ_c are the electric dipole moment components along the principal inertial axes. E is the conformer energy; ΔE is the energy relative to the most stable conformer.

Table S5.2. Rotational parameters predicted from *ab initio* MP2/6-311++G(2d,p) calculations for the stable cyclic formamide-$(H_2O)_3$ (f-w$_3$) conformers.

	f-w$_3$-c1	**f-w$_3$-c2**	**f-w$_3$-c3**
	f-w$_3$-dud[b]	**f-w$_3$-dui**	**f-w$_3$-diu**
A[a]/MHz	2513	2591	2534
B/MHz	1497	1482	1509
C/MHz	957	989	991
P_{aa}/uÅ^2	332.3	328.4	322.6
P_{bb}/uÅ^2	195.7	182.5	187.2
P_{cc}/uÅ^2	5.4	12.6	12.3
Δ_J/kHz	0.89	1.17	1.30
Δ_{JK}/kHz	-0.91	-1.84	-1.71
Δ_K/kHz	7.06	9.30	8.12
δ_J/kHz	0.31	0.27	0.24
δ_K/kHz	1.51	1.67	1.69
χ_{aa}/MHz	0.86	0.81	0.67
χ_{bb}/MHz	2.02	2.13	2.01
χ_{cc}/MHz	-2.88	-2.93	-2.68
μ_a/D	1.0	-1.7	0.5
μ_b/D	1.2	-0.6	-0.7
μ_c/D	0.0	0.1	0.3
E/h	-398.46112	-398.38053	-398.38018
ΔE/cm^{-1}	0.0	147	222
ΔE/kJmol^{-1}	0.0	1.8	2.7
D_e/kJmol^{-1}	115.2	114.2	112.7

[a] A, B and C are the rotational constants. $P_{\alpha\alpha}$ (α= a, b or c) are the planar moments of inertia; these are derived from the moments of inertia I_α as for example $P_{cc} = (I_a + I_b - I_c)/2 = (\sum_i m_i c_i^2)/2))$. Δ_J, Δ_{JK}, Δ_K, δ_J and δ_K are the quartic centrifugal distortion constant. χ_{aa}, χ_{bb} and χ_{cc} are the quadrupole coupling constants for ^{14}N. μ_a, μ_b, μ_c are the electric dipole moment components along the principal inertial axes. E is the conformer energy; ΔE is the energy relative to the most stable conformer; D_e is the dissociation energy calculated using BSSE corrections (Boys, S. F.; Bernardi, F. *Mol. Phys*. **1970**, *19*, 553-566; Xantheas, S. S. *J. Chem. Phys*. **1996**, *104*, 8821-8824). [b] See text for notation.

Table S5.3. Rotational parameters obtained from the analysis of the spectrum of parent formamide-$(H_2O)_3$ (f-w_3) complex and those calculated at the MP2/6-311++G(2d,p) level for the global minimum.

Fitted Parameters	**Exp. Value**		***Ab initio* f-w_3-c1**
	$v = 0$	$v = 1$	
A[a]/MHz	2552.02481(25)[b]	2552.02697(24)	2513
B/MHz	1458.29390(17)	1458.30123(17)	1497
C/MHz	952.624138(92)	952.656823(92)	957
Δ_J/kHz	1.1750(32)		0.89
Δ_{JK}/kHz	-2.192(13)		-0.91
Δ_K/kHz	11.946(20)		7.06
δ_J/kHz	0.3794(14)		0.31
δ_K/kHz	1. 899(21)		1.51
ΔE_{01}/MHz	370.4(47)		
$\langle 0\|iG_a\|1\rangle$	1.1275(92)		
3/2(χ_{aa})/MHz	1.3020(16)		1.28
1/4(χ_{bb}-χ_{cc})/MHz	1.19320(45)		1.22
n	319		
σ/kHz	2.6		

Derived Parameters	**Exp. Value**		***Ab initio* f-w_3-c1**
	$v = 0$	$v = 1$	
P_{aa}/uÅ^2	339.51850(6)	339.50859(6)	332.3
P_{bb}/uÅ^2	190.99410(6)	190.98580(6)	195.7
P_{cc}/uÅ^2	7.03654(6)	7.04468(6)	5.4
χ_{aa}/MHz	0.8679(10)		0.86
χ_{bb}/MHz	1.9524(14)		2.02
χ_{cc}/MHz	-2.8204(14)		-2.88

[a] A, B and C are the rotational constants. Δ_J, Δ_{JK}, Δ_K, δ_J and δ_K are the quartic centrifugal distortion constants. ΔE_{01} is the energy difference between vibrational states labeled v=0 and v=1. $\langle 0|iG_a|1\rangle$ is the Coriolis coupling term connecting both vibrational states. χ_{aa}, χ_{bb} and χ_{cc} are the quadrupole coupling constants for ^{14}N. n is the number of hyperfine quadrupole coupling components fitted. σ is the rms deviations of the fit. $P_{\alpha\alpha}$ (α= a, b or c) are the planar moments of inertia; these are derived from the moments of inertia I_α as for example $P_{cc} = (I_a + I_b - I_c)/2 = (\sum_i m_i c_i^2)/2))$. [b] Standard errors are given in parentheses in units of the last digit.

Table S5.4. Rotational parameters obtained from the analysis of the spectra of the observed $^{15}N_3$ and $^{13}C_2$ isotopologues of formamide-$(H_2O)_3$ (f-w_3) complex.

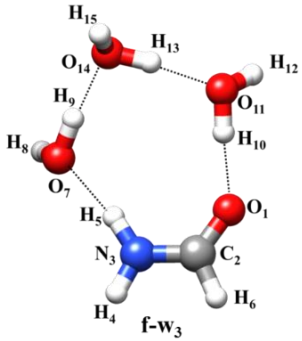

Fitted Parameters	**$^{15}N_3$**		**$^{13}C_2$**	
	$v = 0$	$v = 1$	$v = 0$	$v = 1$
A[a]/MHz	2535.70857(88)[b]	2535.70922(90)	2551.72492(35)	2551.72688(35)
B/MHz	1445.06037(74)	1445.06750(73)	1437.07086(18)	1437.07761(18)
C/MHz	944.78684(44)	944.81901(44)	943.544235(85)	943.576290(84)
Δ_J/kHz	1.155(17)		[1.1774][c]	
Δ_{JK}/kHz	-2.043(81)		[-2.200]	
Δ_K/kHz	11.33(10)		[11.964]	
δ_J/kHz	0.3678(72)		[0.3801]	
δ_K/kHz	1.91(12)		[1.912]	
ΔE_{01}/MHz	338.5(61)		[370.4]	
$<0\|iG_a\|1>$	1.121(29)		[1.1275]	
n	54		89	
σ/kHz	3.1		2.6	

Derived Parameters	**$^{15}N_3$**		**$^{13}C_2$**	
	$v = 0$	$v = 1$	$v = 0$	$v = 1$
P_{aa}/uÅ^2	342.66859(25)	342.65865(25)	344.618479(60)	344.608631(60)
P_{bb}/uÅ^2	192.24476(25)	192.23650(25)	190.999335(60)	190.990986(60)
P_{cc}/uÅ^2	7.06012(25)	7.06834(25)	7.054576(60)	7.062772(60)

[a] A, B and C are the rotational constants. Δ_J, Δ_{JK}, Δ_K, δ_J and δ_K are the quartic centrifugal distortion constants. Quadrupole coupling constants parameters for ^{13}C atom were kept fixed to the parent species values (see Table S5.3). ΔE_{01} is the energy difference between vibrational states labeled v=0 and v=1. $<0|iG_a|1>$ is the Coriolis coupling term connecting both vibrational states. n is the number of hyperfine quadrupole coupling components fitted. σ is the rms deviations of the fit. $P_{\alpha\alpha}$ (α= a, b or c) are the planar moments of inertia; these are derived from the moments of inertia I_α as for example $P_{cc} = (I_a + I_b - I_c)/2 = (\sum_i m_i c_i^2)/2)$. [b] Standard errors are given in parentheses in units of the last digit. [c] Parameters in square brackets were kept fixed to the parent species values (see Table S5.3).

Table S5.5. Rotational parameters obtained from the analysis of the spectra of the observed ^{18}O isotopologues of the formamide-$(H_2O)_3$ (f-w_3) complex. In the fit of the spectra all the quartic centrifugal distortion constants, quadrupole coupling constants and vibration-rotation interactions parameters were kept fixed to the parent species values (see Table S5.3).

Fitted parameters	**$^{18}O_7$**		**$^{18}O_{11}$**		**$^{18}O_{14}$**	
	$v = 0$	$v = 1$	$v = 0$	$v = 1$	$v = 0$	$v = 1$
A[a]/MHz	2452.28304(44)[b]	2452.28506(44)	2457.77599(46)	2457.77958(46)	2549.72788(52)	2549.72882(52)
B/MHz	1450.20353(32)	1450.20951(32)	1449.43857(35)	1449.44507(35)	1397.12719(39)	1397.13501(39)
C/MHz	935.55461(17)	935.58488(17)	935.64433(18)	935.67588(18)	926.35838(21)	926.38827(21)
n	54		54		50	
σ/kHz	2.9		3.1		3.5	

Derived parameters	**$^{18}O_7$**		**$^{18}O_{11}$**		**$^{18}O_{14}$**	
	$v = 0$	$v = 1$	$v = 0$	$v = 1$	$v = 0$	$v = 1$
P_{aa}/uÅ^2	341.29762(11)	341.28824(11)	341.59397(11)	341.58423(11)	354.53647(13)	354.52669(13)
P_{bb}/uÅ^2	198.89437(11)	198.88626(11)	198.54621(11)	198.53774(11)	191.01816(13)	191.01034(13)
P_{cc}/uÅ^2	7.19078(11)	7.19872(11)	7.07834(11)	7.08652(11)	7.19087(13)	7.19863(13)

[a] A, B and C are the rotational constants. n is the number of hyperfine quadrupole coupling components fitted. σ is the rms deviations of the fit. $P_{\alpha\alpha}$ (α= a, b or c) are the planar moments of inertia; these are derived from the moments of inertia I_α as for example $P_{cc} = (I_a + I_b - I_c)/2 = (\sum_i m_i c_i^2)/2))$. [b] Standard errors are given in parentheses in units of the last digit.

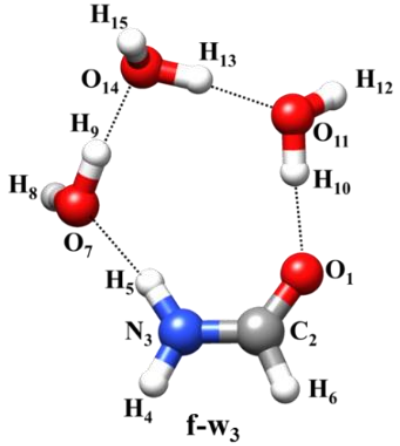

Table S5.6. Rotational parameters obtained from the analysis of the spectra of the observed ^{2}H isotologues of formamide-$(H_2O)_3$ (f-w_3) complex. In the fit of the spectra the quadrupole coupling constants and vibration-rotation interactions parameters were kept fixed to the parent species values (see Table S5.3).

Fitted Parameters	**^{2}H$_5$**		**^{2}H$_9$**		**^{2}H$_{10}$**		**^{2}H$_{13}$**	
	$v = 0$	$v = 1$	$v = 0$	$v = 1$	$v = 0$	$v = 1$	$v = 0$	$v = 1$
A[a]/MHz	2531.2598(51)[b]	2531.2687(48)	2524.6477(50)	2524.6489(50)	2516.7683(77)	2516.7605(77)	2546.6221(41)	2546.6280(41)
B/MHz	1454.86945(28)	1454.87654(28)	1448.61269(28)	1448.61903(28)	1458.42476(44)	1458.43169(44)	1437.25661(23)	1437.26544(23)
C/MHz	948.46974(26)	948.50031(26)	944.73158(27)	944.76137(27)	947.76587(40)	947.79857(40)	942.86967(21)	942.89910(21)
Δ_J/kHz	1.1607(54)		1.1673(54)		1.1667(84)		1.1598(43)	
Δ_{JK}/kHz	[-2.200][c]		[-2.200]		[-2.200]		[-2.200]	
Δ_K/kHz	[11.964]		[11.964]		[11.964]		[11.964]	
δ_J/kHz	[0.3801]		[0.3801]		[0.3801]		[0.3801]	
δ_K/kHz	[1.912]		[1.912]		[1.912]		[1.912]	
n	41		42		40		40	
σ/kHz	2.1		2.2		3.3		1.7	

Derived Parameters	**^{2}H$_5$**		**^{2}H$_9$**		**^{2}H$_{10}$**		**^{2}H$_{13}$**	
	$v = 0$	$v = 1$	$v = 0$	$v = 1$	$v = 0$	$v = 1$	$v = 0$	$v = 1$
P_{aa}/uÅ^2	340.27594(31)	340.26686(30)	341.81884(30)	341.80969(30)	339.47552(66)	339.46519(66)	344.58886(35)	344.57965(35)
P_{bb}/uÅ^2	192.56035(31)	192.55226(30)	193.12581(30)	193.11809(30)	193.75639(66)	193.74832(66)	191.41205(35)	191.40453(35)
P_{cc}/uÅ^2	7.09482(31)	7.10220(30)	7.05226(30)	7.05988(30)	7.04835(66)	7.05704(66)	7.03868(35)	7.04573(35)

[a] A, B and C are the rotational constants. Δ_J, Δ_{JK}, Δ_K, δ_J and δ_K are the quartic centrifugal distortion constants. n is the number of hyperfine quadrupole coupling components fitted. σ is the rms deviations of the fit. $P_{\alpha\alpha}$ (α= a, b or c) are the planar moments of inertia; these are derived from the moments of inertia I_α as for example $P_{cc} = (I_a + I_b - I_c)/2 = (\sum_i m_i c_i^2)/2)$. [b] Standard errors are given in parentheses in units of the last digit. [c] Parameters in square brackets were kept fixed to the parent species values.

Table S5.7. Observed rotational transitions with resolved ^{14}N hyperfine structure and residuals (all the values in MHz) for the parent species of the complex formamide-$(H_2O)_3$ (f-w3) in the v = 0 and v = 1 vibrational states for transitions of the type $J'K'_{-1}K'_{+1}v'F' \leftarrow J''K''_{-1}K''_{+1}v''F''$.

J'	K'_{-1}	K'_{+1}	J''	K''_{-1}	K''_{+1}	v'	v''	F'	F''	Obs.	Obs. - Calc
2	1	1	1	1	0	*0*	*0*	1	0	5326.5252	-0.0020
								2	2	5326.8228	0.0029
								3	2	5327.4515	0.0040
								2	1	5327.6624	-0.0034
								1	1	5328.6363	-0.0059
2	1	1	1	1	0	*1*	*1*	1	0	5326.5890	-0.0002
								2	2	5326.8866	0.0045
								3	2	5327.5124	0.0027
								2	1	5327.7202	-0.0079
								1	1	5328.6966	-0.0079
2	1	2	1	0	1	*0*	*0*	1	1	5408.9648	0.0014
								1	0	5409.6112	-0.0028
								3	2	5409.7283	0.0011
								2	1	5410.3764	0.0030
								2	2	5410.6270	-0.0066
2	1	2	1	0	1	*1*	*1*	1	1	5409.0641	0.0010
								3	2	5409.8283	0.0013
								2	1	5410.4759	0.0027
								2	2	5410.7282	-0.0052
2	2	1	1	1	0	*0*	*0*	1	0	8607.3229	-0.0004
								2	2	8608.1578	-0.0004
								3	2	8608.4355	-0.0016
								2	1	8609.0026	-0.0015
								1	1	8609.4407	0.0023
2	2	1	1	1	0	*1*	*1*	1	0	8607.4058	0.0043
								2	2	8608.2408	0.0043
								3	2	8608.5151	-0.0003
								2	1	8609.0822	-0.0003
								1	1	8609.5182	0.0015
2	2	0	1	1	1	*0*	*0*	2	1	9252.0991	0.0014
								2	2	9252.6844	0.0010
								1	1	9252.9361	-0.0003
								3	2	9253.2237	0.0012
								1	0	9254.4020	0.0013
2	2	0	1	1	1	*1*	*1*	2	1	9252.1380	-0.0008
								2	2	9252.7252	0.0008
								1	1	9252.9764	-0.0012
								3	2	9253.2638	0.0003
								1	0	9254.4458	0.0041
3	0	3	2	0	2	*0*	*0*	2	2	6733.7804	-0.0002
								4	3	6734.6243	0.0016
								2	1	6734.6243	0.0049
								3	2	6734.9489	-0.0001

Table S5.7. (Continued).

J'	K'_{-1}	K'_{+1}	J''	K''_{-1}	K''_{+1}	v'	v''	F'	F''	Obs.	Obs. - Calc
								3	3	6735.4891	0.0009
3	0	3	2	0	2	*1*	*1*	2	2	6733.9378	-0.0019
								4	3	6734.7835	0.0017
								2	1	6734.7835	0.0050
								3	2	6735.1086	0.0004
								3	3	6735.6497	0.0023
3	1	3	2	1	2	*0*	*0*	2	2	6395.3086	-0.0008
								4	3	6396.5973	0.0017
								2	1	6396.7205	0.0009
								3	2	6396.7759	0.0021
								3	3	6397.6795	-0.0007
3	1	3	2	1	2	*1*	*1*	2	2	6395.4718	-0.0024
								4	3	6396.7607	0.0003
								2	1	6396.8866	0.0022
								3	2	6396.9380	-0.0004
								3	3	6397.8440	-0.0010
3	2	2	2	2	1	*0*	*0*	2	1	7232.4654	-0.0026
								3	3	7232.6294	0.0063
								4	3	7232.6294	0.0063
								3	2	7232.8999	-0.0021
								2	2	7232.8999	-0.0022
3	2	2	2	2	1	*1*	*1*	2	1	7232.5486	0.0043
								3	3	7232.7006	0.0013
								4	3	7232.7006	0.0013
								3	2	7232.9752	-0.0030
								2	2	7232.9752	-0.0032
3	2	1	2	2	0	*0*	*0*	2	1	7730.5446	-0.0082
								3	2	7730.6174	0.0037
								4	3	7730.6450	-0.0057
								2	2	7731.3975	0.0058
3	2	1	2	2	0	*1*	*1*	3	3	7730.1127	0.0010
								2	1	7730.5995	0.0095
								4	3	7730.6878	0.0000
								2	2	7731.4216	-0.0071
3	1	2	2	1	1	*0*	*0*	3	3	7888.1477	-0.0010
								2	1	7888.4330	-0.0012
								4	3	7888.6184	-0.0001
								3	2	7888.7775	0.0012
								2	2	7889.4093	-0.0013
3	1	2	2	1	1	*1*	*1*	3	3	7888.2400	-0.0005
								2	1	7888.5251	-0.0010
								4	3	7888.7091	-0.0012
								3	2	7888.8672	-0.0008
								2	2	7889.5000	-0.0025
3	0	3	2	1	2	*0*	*0*	2	2	6006.5750	-0.0026

Table S5.7. (Continued).

J'	K'_{-1}	K'_{+1}	J''	K''_{-1}	K''_{+1}	v'	v''	F'	F''	Obs.	Obs. - Calc
								3	2	6007.7489	0.0028
								4	3	6007.7861	-0.0009
								2	1	6007.9804	-0.0073
								3	3	6008.6511	-0.0015
3	0	3	2	1	2	*1*	*1*	2	2	6006.7296	0.0006
								3	2	6007.9011	0.0037
								4	3	6007.9389	0.0006
								2	1	6008.1392	0.0002
								3	3	6008.8003	-0.0035
3	1	3	2	0	2	*0*	*0*	2	2	7122.5110	-0.0014
								2	1	7123.3531	0.0019
								4	3	7123.4322	0.0010
								3	2	7123.9798	0.0031
								3	3	7124.5134	-0.0024
3	1	3	2	0	2	*1*	*1*	2	2	7122.6843	-0.0008
								2	1	7123.5231	-0.0007
								4	3	7123.6039	0.0000
								3	2	7124.1507	0.0013
								3	3	7124.6948	0.0063
3	2	2	2	1	1	*0*	*0*	2	1	10513.2617	-0.0024
								3	3	10513.6146	0.0017
								4	3	10513.6146	0.0017
								3	2	10514.2391	-0.0012
								2	2	10514.2391	-0.0014
3	2	2	2	1	1	*1*	*1*	2	1	10513.3530	-0.0033
								3	3	10513.7065	0.0014
								4	3	10513.7065	0.0014
								3	2	10514.3305	-0.0020
								2	2	10514.3305	-0.0022
3	2	1	2	1	2	*0*	*0*	3	2	12666.3022	0.0006
								4	3	12667.7839	-0.0003
								2	1	12668.4950	0.0053
3	2	1	2	1	2	*1*	*1*	3	2	12666.3352	-0.0010
								4	3	12667.8159	-0.0030
								2	1	12668.5272	0.0028
3	3	1	2	2	0	*0*	*0*	2	1	13903.3961	0.0059
								4	3	13903.5434	0.0055
								3	2	13903.6388	-0.0043
3	3	1	2	2	0	*1*	*1*	2	1	13903.4590	0.0024
								4	3	13903.6069	0.0025
								3	2	13903.7039	-0.0056
3	3	0	2	2	1	*0*	*0*	3	2	14067.1533	-0.0033
								4	3	14067.3444	-0.0034
								2	1	14067.3572	-0.0001
3	3	0	2	2	1	*1*	*1*	3	2	14067.2080	-0.0001

Table S5.7. (Continued).

J'	K'_{-1}	K'_{+1}	J''	K''_{-1}	K''_{+1}	v'	v''	F'	F''	Obs.	Obs. - Calc
								4	3	14067.3973	-0.0020
								2	1	14067.4154	0.0065
3	2	2	3	1	3	*0*	*0*	3	3	5633.2337	-0.0007
								4	3	5633.2337	-0.0007
								3	2	5634.7000	0.0012
								2	2	5634.7000	0.0011
3	2	2	3	1	3	*1*	*1*	3	3	5633.0852	-0.0006
								4	3	5633.0852	-0.0007
								3	2	5634.5499	-0.0002
								2	2	5634.5499	-0.0004
3	2	2	3	0	3	*0*	*0*	3	3	6022.2591	-0.0029
								2	2	6023.4318	0.0011
3	2	2	3	0	3	*1*	*1*	3	3	6022.1282	0.0011
								4	4	6022.9865	-0.0061
								2	2	6023.2994	0.0037
3	3	1	3	2	2	*0*	*0*	3	3	6809.3581	0.0005
								4	4	6809.7930	0.0015
								2	2	6809.9422	-0.0010
								2	2	6809.9184	-0.0032
4	0	4	3	0	3	*0*	*0*	3	3	8626.3164	-0.0003
								5	4	8627.4715	-0.0012
								3	2	8627.4880	0.0028
								4	3	8627.7375	0.0004
								4	4	8628.6048	0.0021
4	0	4	3	0	3	*1*	*1*	3	3	8626.5457	-0.0016
								5	4	8627.7046	0.0012
								3	2	8627.7179	0.0021
								4	3	8627.9663	-0.0014
								4	4	8628.8318	-0.0014
4	1	4	3	1	3	*0*	*0*	3	3	8412.0997	-0.0013
								5	4	8413.5003	-0.0007
								3	2	8413.5648	-0.0004
								4	3	8413.6435	0.0004
								4	4	8414.7305	0.0027
4	1	4	3	1	3	*1*	*1*	3	3	8412.3271	-0.0017
								5	4	8413.7283	-0.0005
								3	2	8413.7929	-0.0001
								4	3	8413.8709	0.0000
								4	4	8414.9522	-0.0033
4	2	3	3	2	2	*0*	*0*	3	2	9533.3492	-0.0069
								3	3	9533.3492	-0.0070
								5	4	9533.4057	0.0019
								4	3	9533.5876	-0.0012
								4	4	9533.5876	-0.0012
4	2	3	3	2	2	*1*	*1*	3	2	9533.5374	0.0001

Table S5.7. (Continued).

J'	K'_{-1}	K'_{+1}	J''	K''_{-1}	K''_{+1}	v'	v''	F'	F''	Obs.	Obs. - Calc
								3	3	9533.5374	0.0000
								5	4	9533.5876	0.0027
								4	3	9533.7697	-0.0003
								4	4	9533.7697	-0.0002
4	3	2	3	3	1	*0*	*0*	3	2	9862.0202	-0.0006
								5	4	9862.1126	0.0080
								4	3	9862.2705	-0.0027
4	3	2	3	3	1	*1*	*1*	3	2	9862.1741	-0.0020
								4	3	9862.4309	0.0024
4	3	1	3	3	0	*0*	*0*	5	4	10003.5039	0.0019
								4	3	10003.5625	-0.0003
4	3	1	3	3	0	*1*	*1*	5	4	10003.6429	0.0025
								4	3	10003.7005	-0.0008
4	2	2	3	2	1	*0*	*0*	4	3	10545.5241	0.0011
								3	2	10545.5623	0.0070
								5	4	10545.5922	0.0009
4	2	2	3	2	1	*1*	*1*	4	3	10545.6348	0.0006
								3	2	10545.6617	-0.0047
								5	4	10545.7043	0.0018
4	1	3	3	1	2	*0*	*0*	3	2	10294.4652	-0.0013
								5	4	10294.5649	-0.0001
								4	3	10294.7786	0.0000
								3	3	10295.1005	-0.0004
4	1	3	3	1	2	*1*	*1*	3	2	10294.6088	-0.0009
								5	4	10294.7073	-0.0010
								4	3	10294.9192	-0.0026
								3	3	10295.2423	-0.0019
4	0	4	3	1	3	*0*	*0*	3	3	8237.2879	-0.0012
								5	4	8238.6663	0.0020
								4	3	8238.7086	-0.0008
								3	2	8238.7509	-0.0024
								4	4	8239.7877	-0.0064
4	0	4	3	1	3	*1*	*1*	3	3	8237.5048	-0.0013
								5	4	8238.8836	0.0022
								4	3	8238.9247	-0.0018
								3	2	8238.9678	-0.0026
								4	4	8240.0081	-0.0030
4	1	4	3	0	3	*0*	*0*	3	3	8801.1306	0.0019
								3	2	8802.2953	-0.0017
								5	4	8802.3105	0.0008
								4	3	8802.6709	0.0002
								4	4	8803.5395	0.0032
4	1	4	3	0	3	*1*	*1*	3	3	8801.3689	-0.0011
								3	2	8802.5362	-0.0022
								5	4	8802.5507	-0.0002

Table S5.7. (Continued).

J'	K'_{-1}	K'_{+1}	J''	K''_{-1}	K''_{+1}	v'	v''	F'	F''	Obs.	Obs. - Calc
								4	3	8802.9115	-0.0005
								4	4	8803.7801	0.0025
4	2	3	3	2	1	*0*	*0*	3	2	12158.1853	-0.0006
								5	4	12158.3976	-0.0004
								4	3	12159.0545	0.0015
4	2	3	3	2	1	*1*	*1*	3	2	12158.3643	-0.0032
								5	4	12158.5791	-0.0004
								4	3	12159.2339	-0.0006
4	2	3	4	1	4	*0*	*0*	4	4	6753.1783	-0.0019
								5	5	6754.2214	-0.0004
								3	3	6754.4919	0.0021
4	2	3	4	1	4	*1*	*1*	4	4	6752.9815	-0.0035
								5	5	6754.0266	0.0000
								3	3	6754.2941	-0.0003
5	1	5	4	1	4	*0*	*0*	6	5	10379.4933	0.0001
								4	3	10379.5348	0.0000
								5	4	10379.6136	0.0024
5	1	5	4	1	4	*1*	*1*	6	5	10379.7869	0.0003
								4	3	10379.8333	0.0052
								5	4	10379.9053	0.0007
5	0	5	4	0	4	*0*	*0*	6	5	10484.1504	0.0020
								4	3	10484.1712	-0.0012
								5	4	10484.3277	0.0007
5	0	5	4	0	4	*1*	*1*	6	5	10484.4467	0.0003
								4	3	10484.4696	-0.0007
								5	4	10484.6246	-0.0002
5	2	4	4	2	3	*0*	*0*	4	3	11747.6374	0.0018
								6	5	11747.6589	-0.0001
								5	4	11747.8223	0.0000
5	2	4	4	2	3	*1*	*1*	4	3	11747.8620	-0.0005
								6	5	11747.8869	0.0009
								5	4	11748.0487	-0.0005
5	2	3	4	2	2	*0*	*0*	4	3	13288.9836	-0.0029
								6	5	13289.0189	-0.0042
								5	4	13289.0360	0.0023
5	2	3	4	2	2	*1*	*1*	4	3	13289.1184	-0.0018
								6	5	13289.1531	-0.0037
								5	4	13289.1673	0.0000
5	1	4	4	1	3	*0*	*0*	4	3	12470.0535	-0.0012
								6	5	12470.1251	-0.0002
								5	4	12470.4045	0.0001
5	1	4	4	1	3	*1*	*1*	4	3	12470.2682	-0.0010
								6	5	12470.3390	-0.0008
								5	4	12470.6188	0.0000
5	0	5	4	1	4	*0*	*0*	4	4	10307.8189	0.0004

Table S5.7. (Continued).

J'	K'_{-1}	K'_{+1}	J''	K''_{-1}	K''_{+1}	v'	v''	F'	F''	Obs.	Obs. - Calc
								6	5	10309.3124	0.0008
								4	3	10309.3601	-0.0003
								5	4	10309.3931	-0.0002
5	0	5	4	1	4	*1*	*1*	4	4	10308.1066	0.0009
								6	5	10309.5981	-0.0006
								4	3	10309.6480	0.0003
								5	4	10309.6801	-0.0004
5	1	5	4	0	4	*0*	*0*	6	5	10554.3299	-0.0001
								4	3	10554.3447	-0.0019
								5	4	10554.5432	-0.0015
5	1	5	4	0	4	*1*	*1*	6	5	10554.6331	-0.0010
								4	3	10554.6501	-0.0006
								5	4	10554.8484	-0.0004
5	1	4	4	2	3	*0*	*0*	5	4	10606.1333	0.0032
								6	5	10606.2950	0.0026
								4	3	10606.3360	0.0006
5	1	4	4	2	3	*1*	*1*	5	4	10606.3094	0.0031
								6	5	10606.4743	0.0057
								4	3	10606.5132	0.0017
5	2	3	4	1	3	*0*	*0*	4	3	13611.3546	-0.0004
								6	5	13611.4917	-0.0002
								5	4	13612.0984	0.0017
5	2	3	4	1	3	*1*	*1*	4	3	13611.6224	0.0021
								6	5	13611.7571	-0.0001
								5	4	13612.3639	0.0019
6	1	6	5	1	5	*0*	*0*	7	6	12313.2731	0.0003
								5	4	12313.3040	0.0006
								6	5	12313.3686	-0.0004
6	1	6	5	1	5	*1*	*1*	7	6	12313.6327	0.0003
								5	4	12313.6634	0.0004
								6	5	12313.7285	-0.0002
6	0	6	5	0	5	*0*	*0*	7	6	12357.2178	0.0000
								5	4	12357.2419	-0.0012
								6	5	12357.3373	-0.0005
6	0	6	5	0	5	*1*	*1*	7	6	12357.5811	0.0005
								5	4	12357.6060	0.0000
								6	5	12357.7002	-0.0005
6	1	5	5	1	4	*0*	*0*	5	4	14412.1752	-0.0017
								7	6	14412.2250	-0.0005
								6	5	14412.5207	0.0021
6	1	5	5	1	4	*1*	*1*	5	4	14412.4704	-0.0025
								7	6	14412.5225	0.0008
								6	5	14412.8144	-0.0002
6	1	6	5	0	5	*0*	*0*	7	6	12383.4548	0.0004
								5	4	12383.4756	-0.0020

Table S5.7. (Continued).

J'	K'_{-1}	K'_{+1}	J''	K''_{-1}	K''_{+1}	v'	v''	F'	F''	Obs.	Obs. - Calc
								6	5	12383.5874	0.0005
6	1	6	5	0	5	*1*	*1*	7	6	12383.8213	0.0011
								5	4	12383.8416	-0.0018
								6	5	12383.9525	-0.0001

Table S5.8. Observed rotational transitions with resolved ^{14}N hyperfine structure and residuals (all the values in MHz) for the $^{13}C_2$ isotologue of the complex formamide-$(H_2O)_3$ (f-w_3) in the v = 0 and v = 1 vibrational states for transitions of the type $\boldsymbol{J'K'_{-1}K'_{+1}v'F' \leftarrow J''K''_{-1}K''_{+1}v''F''}$.

J'	K'_{-1}	K'_{+1}	J''	K''_{-1}	K''_{+1}	v'	v''	F'	F''	Obs.	Obs. - Calc
2	2	1	1	1	0	*0*	*0*	1	0	8597.3400	-0.0026
								3	2	8598.4555	-0.0010
								2	1	8599.0225	-0.0009
2	2	1	1	1	0	*1*	*1*	1	0	8597.4227	0.0027
								3	2	8598.5339	0.0000
								2	1	8599.1000	-0.0010
2	2	0	1	1	1	*0*	*0*	2	1	9222.1681	-0.0020
								3	2	9223.2911	0.0039
								1	0	9224.4611	0.0000
2	2	0	1	1	1	*1*	*1*	2	1	9222.2057	-0.0051
								3	2	9223.3245	-0.0032
								1	0	9224.5072	0.0056
3	1	3	2	1	2	*0*	*0*	4	3	6328.0428	-0.0023
								3	2	6328.2243	0.0028
3	1	3	2	1	2	*1*	*1*	4	3	6328.2035	-0.0026
								2	1	6328.3268	-0.0039
								3	2	6328.3820	-0.0003
3	0	3	2	0	2	*0*	*0*	4	3	6668.7781	-0.0015
								2	1	6668.7781	0.0016
								3	2	6669.0996	-0.0017
3	0	3	2	0	2	*1*	*1*	4	3	6668.9336	-0.0009
								2	1	6668.9336	0.0022
								3	2	6669.2561	0.0000
3	2	2	2	2	1	*0*	*0*	2	1	7141.5534	-0.0057
								4	3	7141.7196	0.0053
								3	2	7141.9907	-0.0025
3	2	2	2	2	1	*1*	*1*	2	1	7141.6230	-0.0068
								4	3	7141.7887	0.0037
								3	2	7142.0609	-0.0030
3	2	1	2	2	0	*0*	*0*	2	1	7614.5782	-0.0016
								3	2	7614.6465	0.0008
								4	3	7614.6799	0.0020
3	2	1	2	2	0	*1*	*1*	2	1	7614.6023	-0.0098
								3	2	7614.6799	0.0020
								4	3	7614.7121	0.0019
3	1	2	2	1	1	*0*	*0*	2	1	7785.7031	-0.0002
								4	3	7785.8865	0.0003
								3	2	7786.0405	0.0009
3	1	2	2	1	1	*0*	*0*	2	1	7785.7893	-0.0020
								4	3	7785.9763	0.0021
								3	2	7786.1301	0.0025
3	0	3	2	1	2	*0*	*0*	3	2	5916.6352	-0.0023
								4	3	5916.6906	-0.0004

Table S5.8. (Continued).

J'	K'_{-1}	K'_{+1}	J''	K''_{-1}	K''_{+1}	v'	v''	F'	F''	Obs.	Obs. - Calc
								2	1	5916.8927	-0.0034
3	0	3	2	1	2	*1*	*1*	3	2	5916.7806	-0.0033
								4	3	5916.8404	0.0030
								2	1	5917.0424	0.0000
3	1	3	2	0	2	*0*	*0*	2	1	7080.0486	-0.0015
								4	3	7080.1344	0.0006
								3	2	7080.6841	-0.0010
3	1	3	2	0	2	*1*	*1*	2	1	7080.2166	-0.0029
								4	3	7080.3023	-0.0009
								3	2	7080.8550	0.0003
4	1	4	3	1	3	*0*	*0*	5	4	8327.3774	-0.0013
								3	2	8327.4410	-0.0021
								4	3	8327.5180	-0.0010
4	1	4	3	1	3	*1*	*1*	5	4	8327.6004	-0.0009
								3	2	8327.6666	0.0008
								4	3	8327.7416	0.0000
4	0	4	3	0	3	*0*	*0*	5	4	8549.0654	-0.0004
								3	2	8549.0813	0.0045
								4	3	8549.3360	0.0045
4	0	4	3	0	3	*1*	*1*	5	4	8549.2908	-0.0003
								3	2	8549.3038	0.0017
								4	3	8549.5574	0.0006
4	1	3	3	1	2	*0*	*0*	3	2	10171.9973	0.0015
								5	4	10172.0939	0.0012
								4	3	10172.2999	0.0015
4	1	3	3	1	2	*1*	*1*	3	2	10172.1362	0.0031
								5	4	10172.2338	0.0038
								4	3	10172.4395	0.0038
4	0	4	3	1	3	*0*	*0*	5	4	8137.7110	-0.0007
								4	3	8137.7456	-0.0019
								3	2	8137.8009	-0.0021
4	0	4	3	1	3	*1*	*1*	5	4	8137.9231	0.0006
								4	3	8137.9577	-0.0005
								3	2	8138.0098	-0.0040
4	1	4	3	0	3	*0*	*0*	3	2	8738.7167	-0.0001
								5	4	8738.7337	0.0008
								4	3	8739.1028	-0.0001
4	1	4	3	0	3	*1*	*1*	3	2	8738.9516	-0.0024
								5	4	8738.9695	-0.0005
								4	3	8739.3393	-0.0008
5	1	5	4	1	4	*0*	*0*	6	5	10276.8581	-0.0004
								4	3	10276.9009	0.0009
								5	4	10276.9762	0.0006
5	1	5	4	1	4	*1*	*1*	6	5	10277.1465	0.0011
								4	3	10277.1878	0.0009

Table S5.8. (Continued).

J'	K'_{-1}	K'_{+1}	J''	K''_{-1}	K''_{+1}	v'	v''	F'	F''	Obs.	Obs. - Calc
								5	4	10277.2641	0.0016
5	0	5	4	0	4	*0*	*0*	6	5	10388.4527	0.0009
								4	3	10388.4756	0.0010
								5	4	10388.6338	0.0006
5	0	5	4	0	4	*1*	*1*	6	5	10388.7448	0.0013
								4	3	10388.7672	0.0009
								5	4	10388.9268	0.0019

Table S5.9. Observed rotational transitions and residuals (all the values in MHz) for the $^{15}N_3$ isotologue of the complex formamide-$(H_2O)_3$ (f-w_3) in the v = 0 and v = 1 vibrational states for transitions of the type $J'K'_{-1}K'_{+1}v' \leftarrow J''K''_{-1}K''_{+1}v''$.

J'	K'_{-1}	K'_{+1}	J''	K''_{-1}	K''_{+1}	v'	v''	Obs.	Obs. - Calc
2	1	1	1	1	0	*0*	*0*	5279.9134	0.0003
						1	*1*	5279.9734	0.0009
2	1	2	1	0	1	*0*	*0*	5370.0581	0.0010
						1	*1*	5370.1545	0.0006
2	2	1	1	1	0	*0*	*0*	8551.7382	0.0004
						1	*1*	8551.8141	0.0013
2	2	0	1	1	1	*0*	*0*	9188.5188	0.0111
						1	*1*	9188.5478	0.0017
3	1	3	2	1	2	*0*	*0*	6342.7983	-0.0022
						1	*1*	6342.9595	-0.0029
3	0	3	2	0	2	*0*	*0*	6679.2539	-0.0004
						1	*1*	6679.4099	-0.0004
3	2	2	2	2	1	*0*	*0*	7169.4745	0.0028
						1	*1*	7169.5469	0.0030
3	2	1	2	2	0	*0*	*0*	7659.6817	0.0131
						1	*1*	7659.7031	0.0004
3	1	2	2	1	1	*0*	*0*	7819.1679	-0.0008
						1	*1*	7819.2604	0.0018
3	0	3	2	1	2	*0*	*0*	5952.3418	-0.0012
						1	*1*	5952.4908	-0.0015
3	1	3	2	0	2	*0*	*0*	7069.7123	0.0005
						1	*1*	7069.8798	-0.0006
3	2	1	2	1	2	*0*	*0*	12568.7533	-0.0105
						1	*1*	12568.7207	-0.0061
3	3	0	2	2	1	*0*	*0*	13973.3694	-0.0008
						1	*1*	13973.4171	0.0012
4	1	4	3	1	3	*0*	*0*	8343.4314	-0.0008
						1	*1*	8343.6549	-0.0011
4	0	4	3	0	3	*0*	*0*	8557.4997	-0.0004
						1	*1*	8557.7256	-0.0007
4	2	3	3	2	2	*0*	*0*	9451.0322	-0.0007
						1	*1*	9451.2088	-0.0005
4	2	2	3	2	1	*0*	*0*	10449.0331	-0.0002
						1	*1*	10449.1432	0.0019
4	3	2	3	3	1	*0*	*0*	9774.4889	-0.0006
						1	*1*	9774.6451	-0.0012
4	3	1	3	3	0	*0*	*0*	9912.6710	-0.0010
						1	*1*	9912.8137	0.0010
4	1	3	3	1	2	*0*	*0*	10206.0882	-0.0015
						1	*1*	10206.2308	0.0011
4	0	4	3	1	3	*0*	*0*	8167.0421	-0.0006
						1	*1*	8167.2555	-0.0008
4	1	4	3	0	3	*0*	*0*	8733.8894	-0.0002

Table S5.9. (Continued).

J'	K'_{-1}	K'_{+1}	J''	K''_{-1}	K''_{+1}	v'	v''	Obs.	Obs. - Calc
						1	*1*	8734.1256	-0.0005
5	1	5	4	1	4	*0*	*0*	10293.6611	-0.0008
						1	*1*	10293.9474	-0.0028
5	0	5	4	0	4	*0*	*0*	10398.9200	0.0002
						1	*1*	10399.2117	-0.0005
5	1	4	4	1	3	*0*	*0*	12366.4736	0.0000
						1	*1*	12366.6840	0.0010
6	1	6	5	1	5	*0*	*0*	12211.8549	-0.0009
						1	*1*	12212.2110	0.0016
6	0	6	5	0	5	*0*	*0*	12256.2763	0.0011
						1	*1*	12256.6336	0.0019

Table S5.10. Observed rotational transitions with resolved ^{14}N hyperfine structure and residuals (all the values in MHz) for the $^{18}O_7$ isotologue of the complex formamide-$(H_2O)_3$ (f-w_3) in the v = 0 and v = 1 vibrational states for transitions of the type $\boldsymbol{J'K'_{-1}K'_{+1}v'F'} \leftarrow \boldsymbol{J''K''_{-1}K''_{+1}v''F''}$.

J'	K'_{-1}	K'_{+1}	J''	K''_{-1}	K''_{+1}	v'	v''	F'	F''	Obs.	Obs. - Calc
2	2	1	1	1	0	*0*	*0*	1	0	8291.0346	0.0052
								3	2	8292.1412	-0.0020
								2	1	8292.7076	-0.0026
2	2	1	1	1	0	*1*	*1*	1	0	8291.1109	0.0057
								3	2	8292.2213	0.0021
								2	1	8292.7825	-0.0036
2	2	0	1	1	1	*0*	*0*	2	1	8959.0060	0.0010
								3	2	8960.1477	-0.0012
								1	0	8961.3377	-0.0002
2	2	0	1	1	1	*1*	*1*	2	1	8959.0415	-0.0028
								3	2	8960.1874	-0.0009
								1	0	8961.3782	0.0010
3	1	3	2	1	2	*0*	*0*	4	3	6300.3200	0.0012
								2	1	6300.4402	-0.0008
								3	2	6300.4995	-0.0020
3	1	3	2	1	2	*1*	*1*	4	3	6300.4677	-0.0030
								2	1	6300.5988	0.0057
								3	2	6300.6512	-0.0023
3	0	3	2	0	2	*0*	*0*	4	3	6616.9327	-0.0011
								2	1	6616.9327	0.0018
								3	2	6617.2701	-0.0006
3	0	3	2	0	2	*1*	*1*	4	3	6617.0811	-0.0007
								2	1	6617.0811	0.0022
								3	2	6617.4177	-0.0010
3	2	2	2	2	1	*0*	*0*	2	1	7156.9858	-0.0025
								4	3	7157.1485	0.0051
								3	2	7157.4204	-0.0020
3	2	2	2	2	1	*1*	*1*	2	1	7157.0597	0.0045
								4	3	7157.2209	0.0106
								3	2	7157.4962	0.0069
3	1	2	2	1	1	*0*	*0*	2	1	7814.0092	0.0012
								4	3	7814.1952	-0.0009
								3	2	7814.3638	-0.0010
3	1	2	2	1	1	*1*	*1*	2	1	7814.0870	-0.0036
								4	3	7814.2764	-0.0023
								3	2	7814.4452	-0.0022
4	1	4	3	1	3	*0*	*0*	5	4	8276.7909	0.0014
								3	2	8276.8529	-0.0002
								4	3	8276.9370	0.0016
4	1	4	3	1	3	*1*	*1*	5	4	8277.0004	0.0001
								3	2	8277.0627	-0.0011
								4	3	8277.1453	-0.0007
4	0	4	3	0	3	*0*	*0*	5	4	8463.8363	-0.0001

Table S5.10. (Continued).

J'	K'_{-1}	K'_{+1}	J''	K''_{-1}	K''_{+1}	v'	v''	F'	F''	Obs.	Obs. - Calc
								3	2	8463.8524	-0.0002
								4	3	8464.0954	-0.0013
4	0	4	3	0	3	*1*	*1*	5	4	8464.0504	0.0000
								3	2	8464.0646	-0.0019
								4	3	8464.3092	-0.0014
4	1	3	3	1	2	*0*	*0*	3	2	10166.7229	0.0004
								5	4	10166.8238	-0.0013
								4	3	10167.0600	0.0014
4	1	3	3	1	2	*1*	*1*	3	2	10166.8509	-0.0037
								5	4	10166.9569	-0.0003
								4	3	10167.1886	-0.0021

Table S5.11. Observed rotational transitions with resolved ^{14}N hyperfine structure and residuals (all the values in MHz) for the $^{18}O_{11}$ isotologue of the complex formamide-$(H_2O)_3$ (f-w$_3$) in the v = 0 and v = 1 vibrational states for transitions of the type $J'K'_{-1}K'_{+1}v'F' \leftarrow J''K''_{-1}K''_{+1}v''F''$.

J'	K'_{-1}	K'_{+1}	J''	K''_{-1}	K''_{+1}	v'	v''	F'	F''	Obs.	Obs. - Calc
2	2	1	1	1	0	*0*	*0*	1	0	8307.5946	-0.0032
								3	2	8308.7100	-0.0017
								2	1	8309.2802	0.0014
2	2	1	1	1	0	*1*	*1*	1	0	8307.6807	0.0011
								3	2	8308.7913	-0.0022
								2	1	8309.3579	-0.0026
2	2	0	1	1	1	*0*	*0*	2	1	8973.5589	-0.0044
								3	2	8974.7093	0.0034
								1	0	8975.8963	0.0022
2	2	0	1	1	1	*1*	*1*	2	1	8973.6026	-0.0049
								3	2	8974.7532	0.0032
								1	0	8975.9429	0.0048
3	1	3	2	1	2	*0*	*0*	4	3	6300.1675	-0.0022
								2	1	6300.2899	-0.0023
								3	2	6300.3483	-0.0039
3	1	3	2	1	2	*1*	*1*	4	3	6300.3301	0.0015
								2	1	6300.4519	0.0009
								3	2	6300.5147	0.0036
3	0	3	2	0	2	*0*	*0*	4	3	6618.3072	0.0000
								2	1	6618.3072	0.0030
								3	2	6618.6435	0.0000
3	0	3	2	0	2	*1*	*1*	4	3	6618.4612	-0.0008
								2	1	6618.4612	0.0021
								3	2	6618.7972	-0.0010
3	2	2	2	2	1	*0*	*0*	2	1	7154.9615	-0.0011
								4	3	7155.1157	-0.0019
								3	2	7155.3892	-0.0074
3	2	2	2	2	1	*1*	*1*	2	1	7155.0264	-0.0082
								4	3	7155.1868	-0.0029
								3	2	7155.4707	0.0019
3	1	2	2	1	1	*0*	*0*	2	1	7811.7153	-0.0013
								4	3	7811.9045	0.0000
								3	2	7812.0709	-0.0014
3	1	2	2	1	1	*1*	*1*	2	1	7811.8016	-0.0021
								4	3	7811.9903	-0.0013
								3	2	7812.1585	-0.0009
4	1	4	3	1	3	*0*	*0*	5	4	8277.2635	-0.0001
								3	2	8277.3255	-0.0018
								4	3	8277.4073	-0.0019
4	1	4	3	1	3	*1*	*1*	5	4	8277.4821	-0.0015
								3	2	8277.5501	0.0027
								4	3	8277.6278	-0.0014
4	0	4	3	0	3	*0*	*0*	5	4	8466.2074	0.0001

Table S5.11. (Continued).

J'	K'_{-1}	K'_{+1}	J''	K''_{-1}	K''_{+1}	v'	v''	F'	F''	Obs.	Obs. - Calc
								3	2	8466.2321	0.0089
								4	3	8466.4676	-0.0003
4	0	4	3	0	3	*1*	*1*	5	4	8466.4319	0.0010
								3	2	8466.4445	-0.0022
								4	3	8466.6907	-0.0008
4	1	3	3	1	2	*0*	*0*	3	2	10165.9965	0.0049
								5	4	10166.0965	0.0025
								4	3	10166.3299	0.0040
4	1	3	3	1	2	*1*	*1*	3	2	10166.1345	0.0037
								5	4	10166.2357	0.0026
								4	3	10166.4672	0.0022

Table S5.12. Observed rotational transitions with resolved ^{14}N hyperfine structure and residuals (all the values in MHz) for the $^{18}O_{14}$ isotologue of the complex formamide-$(H_2O)_3$ (f-w$_3$) in the v = 0 and v = 1 vibrational states for transitions of the type $J'K'_{-1}K'_{+1}v'F' \leftarrow J''K''_{-1}K''_{+1}v''F''$.

J'	K'_{-1}	K'_{+1}	J''	K''_{-1}	K''_{+1}	v'	v''	F'	F''	Obs.	Obs. - Calc
2	2	1	1	1	0	*0*	*0*	1	0	8574.1677	0.0045
								3	2	8575.2790	0.0021
								2	1	8575.8431	-0.0006
2	2	1	1	1	0	*1*	*1*	1	0	8574.2455	0.0088
								3	2	8575.3472	-0.0034
								2	1	8575.9153	-0.0023
2	2	0	1	1	1	*0*	*0*	2	1	9162.4981	0.0014
								3	2	9163.5933	-0.0062
								1	0	9164.7638	-0.0017
2	2	0	1	1	1	*1*	*1*	2	1	9162.5378	-0.0014
								3	2	9163.6328	-0.0090
								1	0	9164.8143	0.0066
3	1	3	2	1	2	*0*	*0*	4	3	6198.1305	-0.0025
								2	1	6198.2644	0.0055
								3	2	6198.3027	-0.0030
3	1	3	2	1	2	*1*	*1*	4	3	6198.2834	-0.0013
								2	1	6198.4098	-0.0008
								3	2	6198.4549	-0.0026
3	0	3	2	0	2	*0*	*0*	4	3	6542.3385	-0.0026
								2	1	6542.3385	0.0000
								3	2	6542.6502	-0.0030
3	0	3	2	0	2	*1*	*1*	4	3	6542.4843	-0.0017
								2	1	6542.4843	0.0010
								3	2	6542.7960	-0.0021
3	2	2	2	2	1	*0*	*0*	3	2	6970.6044	-0.0002
3	2	2	2	2	1	*1*	*1*	3	2	6970.6716	0.0053
3	1	2	2	1	1	*0*	*0*	2	1	7591.2477	-0.0026
								4	3	7591.4296	-0.0008
								3	2	7591.5726	-0.0037
3	1	2	2	1	1	*1*	*1*	2	1	7591.3356	-0.0024
								4	3	7591.5145	-0.0036
								3	2	7591.6574	-0.0066
4	1	4	3	1	3	*0*	*0*	5	4	8163.7203	-0.0003
								3	2	8163.7858	0.0001
								4	3	8163.8570	-0.0009
4	1	4	3	1	3	*1*	*1*	5	4	8163.9283	-0.0012
								3	2	8163.9946	0.0001
								4	3	8164.0654	-0.0013
4	0	4	3	0	3	*0*	*0*	5	4	8399.0577	0.0002
								3	2	8399.0668	0.0010
								4	3	8399.3231	-0.0014
4	0	4	3	0	3	*1*	*1*	5	4	8399.2667	-0.0009
								3	2	8399.2784	0.0024

Table S5.12. (Continued).

J'	K'_{-1}	K'_{+1}	J''	K''_{-1}	K''_{+1}	v'	v''	F'	F''	Obs.	Obs. - Calc
								4	3	8399.5354	0.0006
4	1	3	3	1	2	*0*	*0*	3	2	9937.8104	0.0033
								5	4	9937.9024	0.0016
								4	3	9938.0980	0.0054
4	1	3	3	1	2	*1*	*1*	3	2	9937.9429	0.0032
								5	4	9938.0369	0.0035
								4	3	9938.2299	0.0047

Table S5.13. Observed rotational transitions with resolved ^{14}N hyperfine structure and residuals (all the values in MHz) for the $^{2}H_5$ isotologue of the complex formamide-$(H_2O)_3$ (f-w_3) in the v = 0 and v = 1 vibrational states for transitions of the type $J'K'_{-1}K'_{+1}v'F' \leftarrow J''K''_{-1}K''_{+1}v''F''$.

J'	K'_{-1}	K'_{+1}	J''	K''_{-1}	K''_{+1}	v'	v''	F'	F''	Obs.	Obs. - Calc
3	1	3	2	1	2	*0*	*0*	4	3	6371.6972	-0.0019
								2	1	6371.8244	0.0015
								3	2	6371.8772	-0.0008
3	1	3	2	1	2	*1*	*1*	4	3	6371.8531	-0.0008
								2	1	6371.9766	-0.0010
								3	2	6372.0314	-0.0014
3	0	3	2	0	2	*0*	*0*	2	1	6705.7364	0.0025
								4	3	6705.7364	-0.0007
								3	2	6706.0633	-0.0021
3	0	3	2	0	2	*1*	*1*	2	1	6705.8918	0.0066
								4	3	6705.8918	0.0033
								3	2	6706.2193	0.0025
3	1	2	2	1	1	*0*	*0*	2	1	7864.9780	-0.0017
								4	3	7865.1630	-0.0016
								3	2	7865.3260	0.0019
3	1	2	2	1	1	*1*	*1*	2	1	7865.0698	0.0025
								4	3	7865.2497	-0.0024
								3	2	7865.4100	-0.0016
4	1	4	3	1	3	*0*	*0*	5	4	8379.1070	-0.0001
								3	2	8379.1688	-0.0024
								4	3	8379.2546	0.0048
4	1	4	3	1	3	*1*	*1*	5	4	8379.3214	0.0000
								3	2	8379.3864	0.0009
								4	3	8379.4665	0.0024
4	0	4	3	0	3	*0*	*0*	5	4	8588.1972	0.0021
								4	3	8588.4573	-0.0014
4	0	4	3	0	3	*1*	*1*	5	4	8588.4134	-0.0003
								3	2	8588.4232	-0.0035
								4	3	8588.6744	-0.0030
4	1	3	3	1	2	*0*	*0*	3	2	10259.0029	-0.0006
								5	4	10259.1024	-0.0003
								4	3	10259.3218	0.0023
4	1	3	3	1	2	*1*	*1*	3	2	10259.1456	0.0044
								5	4	10259.2389	-0.0014
								4	3	10259.4547	-0.0024
5	0	5	4	0	4	*0*	*0*	6	5	10436.6971	0.0000
								4	3	10436.7219	0.0003
								5	4	10436.8727	-0.0017
5	0	5	4	0	4	*1*	*1*	6	5	10436.9784	-0.0001
								4	3	10437.0019	-0.0011
								5	4	10437.1579	0.0020

Table S5.14. Observed rotational transitions with resolved ^{14}N hyperfine structure and residuals (all the values in MHz) for the $^{2}H_9$ isotologue of the complex formamide-$(H_2O)_3$ (f-w$_3$) in v = 0 and v = 1 vibrational states for transitions of the type $J'K'_{-1}K'_{+1}v'F' \leftarrow J''K''_{-1}K''_{+1}v''F''$.

J'	K'_{-1}	K'_{+1}	J''	K''_{-1}	K''_{+1}	v'	v''	F'	F''	Obs.	Obs. - Calc
3	1	3	2	1	2	*0*	*0*	4	3	6346.1361	-0.0007
								2	1	6346.2604	-0.0002
								3	2	6346.3198	0.0041
3	1	3	2	1	2	*1*	*1*	4	3	6346.2852	-0.0014
								2	1	6346.4122	0.0017
								3	2	6346.4636	-0.0018
3	0	3	2	0	2	*0*	*0*	2	1	6679.7035	0.0031
								4	3	6679.7035	-0.0002
								3	2	6680.0299	-0.0016
3	0	3	2	0	2	*1*	*1*	2	1	6679.8479	-0.0003
								4	3	6679.8479	0.0029
								3	2	6680.1727	-0.0033
3	1	2	2	1	1	*0*	*0*	2	1	7832.1792	-0.0012
								4	3	7832.3647	-0.0004
								3	2	7832.5236	-0.0005
3	1	2	2	1	1	*1*	*1*	2	1	7832.2674	0.0046
								4	3	7832.4470	-0.0005
								3	2	7832.6047	-0.0017
4	1	4	3	1	3	*0*	*0*	5	4	8345.8778	0.0004
								3	2	8345.9398	-0.0017
								4	3	8346.0197	-0.0001
4	1	4	3	1	3	*1*	*1*	5	4	8346.0862	0.0016
								3	2	8346.1466	-0.0021
								4	3	8346.2276	0.0005
4	0	4	3	0	3	*0*	*0*	5	4	8555.3001	0.0011
								3	2	8555.3078	-0.0040
								4	3	8555.5653	0.0024
4	0	4	3	0	3	*1*	*1*	5	4	8555.5083	-0.0003
								3	2	8555.5246	0.0031
								4	3	8555.7723	-0.0002
4	1	3	3	1	2	*0*	*0*	3	2	10217.4382	0.0016
								5	4	10217.5355	-0.0001
								4	3	10217.7518	0.0002
4	1	3	3	1	2	*1*	*1*	3	2	10217.5642	-0.0015
								5	4	10217.6647	0.0000
								4	3	10217.8805	-0.0001
5	0	5	4	0	4	*0*	*0*	6	5	10396.5097	0.0039
								4	3	10396.5232	-0.0068
								5	4	10396.6859	0.0025
5	0	5	4	0	4	*1*	*1*	6	5	10396.7779	0.0011
								4	3	10396.7996	-0.0015
								5	4	10396.9549	0.0004

Table S5.15. Observed rotational transitions with resolved ^{14}N hyperfine structure and residuals (all the values in MHz) for the $^{2}H_{10}$ isotologue of the complex formamide-$(H_2O)_3$ (f-w_3) in the v = 0 and v = 1 vibrational states for transitions of the type $J'K'_{-1}K'_{+1}v'F' \leftarrow J''K''_{-1}K''_{+1}v''F''$.

J'	K'_{-1}	K'_{+1}	J''	K''_{-1}	K''_{+1}	v'	v''	F'	F''	Obs.	Obs. - Calc
3	1	3	2	1	2	*0*	*0*	4	3	6371.7923	-0.0020
								2	1	6371.9158	-0.0018
								3	2	6371.9727	-0.0016
3	1	3	2	1	2	*1*	*1*	4	3	6371.9644	0.0060
								2	1	6372.0923	0.0106
								3	2	6372.1340	-0.0043
3	0	3	2	0	2	*0*	*0*	2	1	6702.0961	0.0070
								4	3	6702.0961	0.0038
								3	2	6702.4187	-0.0045
3	0	3	2	0	2	*1*	*1*	2	1	6702.2522	0.0067
								4	3	6702.2522	0.0034
								3	2	6702.5739	-0.0057
3	1	2	2	1	1	*0*	*0*	2	1	7876.5645	0.0015
								4	3	7876.7475	-0.0013
								3	2	7876.9138	0.0029
3	1	2	2	1	1	*1*	*1*	2	1	7876.6509	-0.0017
								4	3	7876.8387	0.0002
								3	2	7876.9976	-0.0028
4	1	4	3	1	3	*0*	*0*	5	4	8376.7465	0.0011
								3	2	8376.8113	0.0019
								4	3	8376.8881	-0.0008
4	1	4	3	1	3	*1*	*1*	5	4	8376.9692	-0.0026
								3	2	8377.0334	-0.0024
								4	3	8377.1117	-0.0037
4	0	4	3	0	3	*0*	*0*	5	4	8580.1207	-0.0001
								4	3	8580.3824	-0.0013
4	0	4	3	0	3	*1*	*1*	5	4	8580.3489	0.0012
								4	3	8580.6087	-0.0018
4	1	3	3	1	2	*0*	*0*	3	2	10266.7712	-0.0040
								5	4	10266.8764	0.0009
								4	3	10267.0976	0.0006
4	1	3	3	1	2	*1*	*1*	3	2	10266.9140	-0.0006
								5	4	10267.0165	0.0016
								4	3	10267.2386	0.0022
5	0	5	4	0	4	*0*	*0*	6	5	10427.1809	0.0025
								4	3	10427.2024	-0.0011
								5	4	10427.3548	0.0007
5	0	5	4	0	4	*1*	*1*	6	5	10427.4744	0.0019
								4	3	10427.4936	-0.0040
								5	4	10427.6507	0.0025

Table S5.16. Observed rotational transitions with resolved ^{14}N hyperfine structure and residuals (all the values in MHz) for the $^{2}H_{13}$ isotologue of the complex formamide-$(H_2O)_3$ (f-w_3) in the v = 0 and v = 1 vibrational states for transitions of the type $J'K'_{-1}K'_{+1}v'F' \leftarrow J''K''_{-1}K''_{+1}v''F''$.

J'	K'_{-1}	K'_{+1}	J''	K''_{-1}	K''_{+1}	v'	v''	F'	F''	Obs.	Obs. - Calc
3	1	3	2	1	2	*0*	*0*	4	3	6324.8214	0.0002
								2	1	6324.9472	0.0014
								3	2	6324.9956	-0.0021
3	1	3	2	1	2	*1*	*1*	4	3	6324.9721	-0.0002
								2	1	6325.1037	0.0068
								3	2	6325.1453	-0.0035
3	0	3	2	0	2	*0*	*0*	2	1	6664.5221	0.0035
								4	3	6664.5221	0.0003
								3	2	6664.8441	-0.0001
3	0	3	2	0	2	*1*	*1*	2	1	6664.6670	0.0020
								4	3	6664.6670	-0.0012
								3	2	6664.9895	-0.0011
3	1	2	2	1	1	*0*	*0*	4	3	7784.9631	0.0011
								3	2	7785.1129	-0.0031
3	1	2	2	1	1	*1*	*1*	4	3	7785.0523	-0.0014
								3	2	7785.2066	-0.0012
4	1	4	3	1	3	*0*	*0*	5	4	8322.5112	-0.0005
								3	2	8322.5783	0.0021
								4	3	8322.6521	-0.0001
4	1	4	3	1	3	*1*	*1*	5	4	8322.7194	-0.0003
								3	2	8322.7843	0.0001
								4	3	8322.8591	-0.0012
4	0	4	3	0	3	*0*	*0*	5	4	8542.6244	-0.0006
								3	2	8542.6357	-0.0004
								4	3	8542.8898	-0.0006
4	0	4	3	0	3	*1*	*1*	5	4	8542.8348	-0.0008
								3	2	8542.8472	0.0004
								4	3	8543.1005	-0.0004
4	1	3	3	1	2	*0*	*0*	3	2	10169.0459	-0.0001
								5	4	10169.1445	0.0012
								4	3	10169.3505	0.0003
4	1	3	3	1	2	*1*	*1*	3	2	10169.1869	0.0018
								5	4	10169.2848	0.0026
								4	3	10169.4869	-0.0021
5	0	5	4	0	4	*0*	*0*	6	5	10380.6080	-0.0004
								4	3	10380.6315	0.0001
								5	4	10380.7891	-0.0002
5	0	5	4	0	4	*1*	*1*	6	5	10380.8798	0.0002
								4	3	10380.9024	-0.0001
								5	4	10381.0607	0.0001

Table S5.17. r_s coordinates (in Å) of the isotopically substituted atoms of the complex formamide-$(H_2O)_3$ (f-w_3) (errors quoted calculated according to the Costain rule [Costain C. C. *Trans. Am. Crystallogr. Assoc.* **1966**, *2*, 157-164]) compared with r_0 (see Table S5.18) and r_e (MP2/6-311++G(2d,p)) *ab initio* (*ab*) coordinates for the three most stable conformers (f-w_3-c1, f-w_3-c2 and f-w_3-c3: See Figure S5.1). The r_s method gives an imaginary value for the *a* coordinate of H_{10} hydrogen atom (see Figure 5.3).

		a	*b*	*c*
$\|r_s\|$	C_2	2.26488(66)	0.073(20)	0.136(11)
ab-f-w_3-c1		2.250	-0.115	-0.107
ab-f-w_3-c2		2.244	-0.091	-0.045
ab-f-w_3-c3		2.219	-0.130	-0.191
r_0		2.2676(28)	-0.1069(38)	-0.1446(23)
$\|r_s\|$	N_3	1.77808(84)	1.1369(13)	0.1559(96)
ab-f-w_3-c1		1.768	1.135	-0.179
ab-f-w_3-c2		1.749	1.152	-0.098
ab-f-w_3-c3		1.753	1.126	-0.225
r_0		1.7808(36)	1.1447(35)	-0.161(12)
$\|r_s\|$	O_7	0.9250(16)	2.01483(74)	0.2867(52)
ab-f-w_3-c1		-0.921	2.060	0.226
ab-f-w_3-c2		-0.961	1.970	0.361
ab-f-w_3-c3		-0.898	2.008	0.416
r_0		-0.9273(23)	2.0171(16)	0.299(10)
$\|r_s\|$	O_{14}	2.76176(54)	0.116(13)	0.2863(52)
ab-f-w_3-c1		-2.732	0.063	-0.194
ab-f-w_3-c2		-2.707	0.028	-0.460
ab-f-w_3-c3		-2.638	0.100	-0.509
r_0		-2.7649(10)	0.0445(58)	-0.2944(80)
$\|r_s\|$	O_{11}	1.0005(15)	1.97248(76)	0.149(10)
ab-f-w_3-c1		-1.003	-2.016	0.056
ab-f-w_3-c2		-0.990	-1.893	0.393
ab-f-w_3-c3		-1.043	-1.953	0.300
r_0		-1.0035(23)	-1.9747(17)	0.154(15)
$\|r_s\|$	H_5	0.8670(17)	1.2534(12)	0.2432(62)
ab-f-w_3-c1		0.783	1.361	-0.007
ab-f-w_3-c2		0.760	1.341	0.102
ab-f-w_3-c3		0.784	1.359	0.019
r_0		0.7995(43)	1.3394(55)	0.0273(73)
$\|r_s\|$	H_9	1.5180(10)	1.4734(10)	0.127(12)
ab-f-w_3-c1		-1.625	1.396	0.042
ab-f-w_3-c2		-1.639	1.339	0.031
ab-f-w_3-c3		-1.601	1.407	0.080
r_0		1.6272(28)	1.3710(14)	0.0487(66)
$\|r_s\|$	H_{10}	0.2055(73)i	1.66426(90)	0.110(14)
ab-f-w_3-c1		-0.083	-1.676	0.095
ab-f-w_3-c2		-0.061	-1.604	0.259
ab-f-w_3-c3		-0.122	-1.613	0.297
r_0		-0.0735(20)	-1.6508(24)	0.1353(30)
$\|r_s\|$	H_{13}	2.25198(67)	0.6585(23)	0.047(32)
ab-f-w_3-c1		-2.175	-0.744	-0.099
ab-f-w_3-c2		-2.183	-0.766	-0.214
ab-f-w_3-c3		-2.148	0.713	-0.252
r_0		-2.1965(17)	-0.7407(44)	-0.1190(23)

Table S5.18. r_0 structure of the complex formamide-$(H_2O)_3$ (f-w_3) derived from the fit of the observed rotational constants. In the fit of the r_0 structure (Kisiel, Z. *J. Mol. Spectrosc.* **2003**, *218*, 58–67) the starting values of the geometrical parameters for the monomers of formamide and water were calculated by correcting their experimental r_0 structures (r_0 structure of formamide: see Table S4.15 in Supplementary Material of the reference (Blanco, S., Pinacho, P., López, J. C. *Angew. Chemie* **2016**, *128*, 9477–9481); r_0 structure of water: M. D. Harmony; V. W. Laurie; R. L. Kuczkowski; R. H. Schwendeman; D. A. Ramsay; F. J. Lovas; W. J. Lafferty; A. G. Maki; *J. Phys. Chem. Ref. Data* **1979**, *8*, 619-721) with the small changes predicted to occur upon complexation from *ab initio* computations. The rest of geometrical parameters determining the relative positions of the different subunits were taken from the *ab initio* (MP2/6-311++G(2d,p)) predictions for the global minimum (f-w_3-c1). We explored the combinations of parameters that could be fitted and fix the rest of parameters. The rotational constants of the deuterated isotologues were not initially used, but their rotational constants were reasonably reproduced from the final fit. The results, summarized in Figure 5.3, are also compared to *ab initio* and r_s results in Tables S5.17 and S5.19.

Parameter	r_0	MP2/6-311++G(2d,p)
$r(O_1\text{-}C_2)$/Å	1.232(11)	1.231
$r(O_7\text{-}H_5)$/Å	1.8748(44)	1.857
$r(H_{10}\text{-}O_1)$/Å	1.7777(64)	1.768
$r(H_{13}\text{-}O_{11})$/Å	1.7380(49)	1.736
$\angle O_1C_2N_3$/°	126.14(38)	126.0
$\angle O_7H_5N_3$/°	168.68(42)	170.3
$\angle H_{10}O_1C_2$/°	138.17(54)	138.9
$\angle H_{13}O_{11}H_{10}$/°	114.30(21)	112.5
$\angle H_{10}O_1C_2N_3$	17.2(21)	21.1
$\angle H_8O_7H_9O_{14}$	-133.7(90)	-98.0
$\angle O_{11}H_{10}O_1C_2$	155.0(29)	143.7
Fixed Parameters	r_0	MP2/6-311++G(2d,p)
$r(C_2\text{-}N_3)$/Å	[1.343]	1.341
$r(N_3\text{-}H_4)$/Å	[0.993]	1.007
$r(N_3\text{-}H_5)$/Å	[1.018]	1.025
$r(C_2\text{-}H_6)$/Å	[1.100]	1.101
$\angle H_4N_3C_2$/°	[118.1]	118.6
$\angle H_5N_3C_2$/°	[121.7]	122.7
$\angle H_6C_2N_3$/°	[115.8]	113.6
$r(O_7\text{-}H_8)$/Å	[0.965]	0.963
$r(O_7\text{-}H_9)$/Å	[0.985]	0.984
$\angle H_9O_7H_8$/°	[105.6]	104.9
$r(O_{11}\text{-}H_{10})$/Å	[0.985]	0.985
$r(O_{11}\text{-}H_{12})$/Å	[0.965]	0.963
$\angle H_{10}O_{11}H_{12}$/°	[105.6]	105.3
$r(O_{14}\text{-}H_{13})$/Å	[0.985]	0.981
$r(O_{14}\text{-}H_{15})$/Å	[0.965]	0.963
$\angle H_{13}O_{14}H_{15}$/°	[105.6]	105.6
$\angle H_9O_7H_{14}$/°	[4.8]	4.8
$\angle O_{11}H_{10}O_1$/°	[177.7]	177.7
$\angle O_{14}H_{13}O_{11}$/°	[171.9]	171.9
$\angle H_9O_7O_{14}H_{13}$/°	[163.0]	163.0
$\angle H_{12}O_{11}H_{10}O_1$	[65.9]	65.9
$\angle H_{13}O_{11}H_{10}O_1$	[-159.2]	-159.2
$\angle O_{14}H_{13}O_{11}H_{10}$	[3.8]	3.5
$\angle H_{15}O_{14}H_{13}O_{11}$	[115.8]	115.8

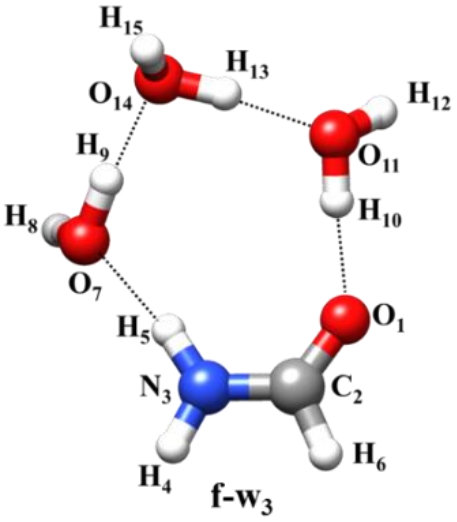

Derived parameters	r_0	MP2/6-311++G(2d,p)
$r(H_9\text{-}O_{14})$/Å	1.7810(52)	1.749
$r(O_7\text{-}N_3)$/Å	2.8821(49)	2.873
$r(O_7\text{-}O_{14})$/Å	2.7621(60)	2.728
$r(O_{14}\text{-}O_{11})$/Å	2.7606(53)	2.715
$r(O_1\text{-}O_{11})$/Å	2.7167(55)	2.749
$\angle O_7H_9O_{14}$/°	172.55(47)	172.5
$\angle H_9O_7H_5$/°	112.36(37)	112.2
$\angle H_9O_{14}H_{13}$/°	101.00(27)	104.7
$\angle C_2N_3O_7$/°	128.18(57)	129.0
$\angle N_3O_7O_{14}$/°	112.01(18)	111.3
$\angle O_7O_{14}O_{11}$/°	93.67(12)	97.1
$\angle O_{14}O_{11}O_1$/°	112.76(21)	111.0
$\angle O_{11}O_1C_2$/°	138.92(50)	139.6

Table S5.19. r_s distances (Å) and angles (degree) derived from the coordinates of Table S5.17 compared to *ab initio* (MP2/6-311++G(2d,p)) parameters for the global minimum of the complex formamide-$(H_2O)_3$ (f-w$_3$-c1) and the r_0 parameters (Table S5.18). The parameters in which the H_{10} atom is involved have been calculated by taking its r_s *a* coordinate as zero. Parameters in square brackets were kept fixed in the r_0 fit.

$\|r_s\|$	$r(C_2\text{-}N_3)$	1.305(19)	$\angle H_9O_{14}H_{13}$	99.93(58)
ab-f-w$_3$-c1		1.341		104.7
r_0		[1.343(5)]		101.00(27)
$\|r_s\|$	$r(N_3\text{-}O_7)$	2.8764(24)	$\angle O_{14}H_{13}O_{11}$	166.9(19)
ab-f-w$_3$-c1		2.873		171.9
r_0		2.8821(49)		[171.90(36)]
$\|r_s\|$	$r(O_7\text{-}O_{14})$	2.7034(93)	$\angle H_{13}O_{11}H_{10}$	116.03(23)
ab-f-w$_3$-c1		2.728		112.5
r_0		2.7621(60)		114.30(21)
$\|r_s\|$	$r(O_{14}\text{-}O_{11})$	2.766(10)	$\angle O_7O_{14}O_{11}$	93.688(79)
ab-f-w$_3$-c1		2.715		97.1
r_0		2.7606(53)		93.67(12)
$\|r_s\|$	$r(O_{11}\text{-}H_{10})$	1.0476(71)	$\angle O_{14}O_{11}H_{10}$	113.34(28)
ab-f-w$_3$-c1		0.981		109.6
r_0		[0.985(3)]		111.38(27)
$\|r_s\|$	$r(C_2\text{-}O_{11})$	3.788(10)	$\angle O_{14}O_{11}C_2$	99.12(31)
ab-f-w$_3$-c1		3.772		99.2
r_0		3.7787(39)		100.42(13)
$\|r_s\|$	$r(C_2\text{-}H_{10})$	2.779(13)	$\angle O_{11}C_2N_3$	98.313(97)
ab-f-w$_3$-c1		2.815		99.3
r_0		2.8183(38)		98.50(21)
$\|r_s\|$	$r(O_7\text{-}H_9)$	0.8115(30)	$\angle N_3C_2H_{10}$	103.20(12)
ab-f-w$_3$-c1		0.984		102.1
r_0		[0.985(42)]		102.16(22)
$\|r_s\|$	$r(H_9\text{-}O_{14})$	1.8936(98)	$\angle C_2N_3O_7O_{14}$	-25.9(10)
ab-f-w$_3$-c1		1.750		-23.6
r_0		1.7810(52)		-25.8(10)
$\|r_s\|$	$r(O_{14}\text{-}H_{13})$	0.957(13)	$\angle N_3O_7O_{14}O_{11}$	25.38(36)
ab-f-w$_3$-c1		0.984		19.9
r_0		[0.985(61)]		25.98(55)
$\|r_s\|$	$r(H_{13}\text{-}O_{11})$	1.8253(41)	$\angle O_7O_{14}O_{11}H_{10}$	-19.08(11)
ab-f-w$_3$-c1		1.736		-9.1
r_0		1.7380(49)		-18.2(11)
$\|r_s\|$	$r(N_3\text{-}H_5)$	0.9231(22)	$\angle O_7O_{14}O_{11}C_2$	-18.93(31)
ab-f-w$_3$-c1		1.025		-13.0
r_0		[1.018]		-19.71(42)
$\|r_s\|$	$\angle H_5N_3C_2$	119.32(37)	$\angle O_{14}O_{11}H_{10}C_2$	0.6(4.1)
ab-f-w$_3$-c1		122.8		-20.5
r_0		[121.7]		-7.6(39)
$\|r_s\|$	$\angle C_2N_3O_7$	129.15(37)	$\angle O_{14}O_{11}C_2N_3$	9.65(74)
ab-f-w$_3$-c1		129.0		3.0
r_0		128.18(57)		10.52(69)
$\|r_s\|$	$\angle N_3O_7O_{14}$	113.05(20)	$\angle O_{11}C_2N_3O_7$	7.94(92)
ab-f-w$_3$-c1		111.3		11.1
r_0		112.01(18)		7.84(87)
$\|r_s\|$	$\angle N_3O_7H_9$	116.18(29)	$\angle C_2O_{11}O_7O_{14}$	-158.06(36)
ab-f-w$_3$-c1		115.2		-164.9
r_0		115.37(34)		-157.36(49)
$\|r_s\|$	$\angle O_7H_9O_{14}$	175.53(45)	$\angle C_2N_3O_7O_{11}$	-7.80(90)
ab-f-w$_3$-c1		172.5		-10.5
r_0		172.55(47)		-7.66(84)

Table S5.20. (a)-(b) Comparison of geometrical parameters (distances in Å, angles in degree) of formamide-$(H_2O)_3$ (f-w_3) with those of related systems as formamide (f), formamide-$(H_2O)_n$ with n=1 (f-w-a) and n=2 (f-w_2), water dimer (w_2), water trimer (w_3), water tetramer (w_4) and water pentamer (w_5). (b) Comparison of *r*(C-N) and *r*(O=C) of formamide for the different complexes, including formamide$_2$-H_2O (f_2-w). Experimental r_0 and *ab initio* r_e values are included. (c) The *ab initio* BSSE corrected dissociation energies show that f-w_3 has the higher dissociation energies, followed by the three-body adducts f_2-w and f-w_2. Formamide dimer (f_2) has also a higher energy compared to formamide-water complex.

(a)	f-w_3[a]	f-w-a[b]	f-w_2[b]	w_2[c]	w_3[d]	w_4[e]	w_5[f]
$r_0(O_1\text{-}O_{11})$	2.7167(55)	2.8231(35)	2.7755(30)				
$r_0(O_1\text{-}H_{10})$	1.7777(64)	1.9304(98)	1.7969(83)				
$r_0(O_{11}\text{-}O_{14})$	2.7606(53)		2.755(3)				
$r_0(H_{13}\text{-}O_{11})$	1.7380(49)		1.829(4)				
$r_0(O_{14}\text{-}O_7)$	2.7621(60)						
$r_0(H_9\text{-}O_{14})$	1.7810(52)						
$r_0(O_7\text{-}N_3)$	2.8821(49)	2.8910(17)	2.9095(12)				
$r_0(H_5\text{-}O_7)$	1.8748(44)	2.0607(45)	1.9363(60)				
r(O-O)				2.976	2.85	2.78	2.76
$\angle(O_1\text{-}O_{11}\text{-}O_{14})$	112.76(20)						
$\angle(O_7\text{-}O_{14}\text{-}O_{11})$	93.67(12)		86.30(15)				
$\angle(N_3\text{-}O_7\text{-}O_{14})$	112.01(18)		84.04(13)				
∠(O-O-O)					60.	90.	107.9

(b)	f-w_3	f[g]	f-w-a[b]	f-w_2[b]	f_2-w[h]
$r_0(C_2\text{-}N_3)$	[1.343(5)]	1.363(3)			1.3285(69)
$r_e(C_2\text{-}N_3)$	1.341	1.361	1.350	1.343	1.341/1.342
$r_s(C_2\text{-}N_3)$	1.305(19)				1.344(4)/1.340(4)
$r_0(O_1\text{-}C_2)$	1.232(11)	1.217(3)			1.2671(84)
$r_e(O_1\text{-}C_2)$	1.231	1.218	1.229	1.231	1.232/1.231

(c)	f-w_3	f-w-a[a]	f-w_2[b]	f_2-w	f_2
E_D[i]/kJ/mol	115.2	37.4	74.51	85.1	57.4

[a] This work. [b] Blanco, S., López, J. C., Lesarri, A., Alonso, J. L. *J. Am. Chem. Soc*. **2006**, *128*, 12111–12121. [c] Dyke, T. R., Mack, K. M., Muenter, J. S. *J. Chem. Phys.* **1977**, *66*, 498-510. [d] Keutsch, F. N., Cruzan, J. D., Saykally, R. J. *Chem. Rev.* **2003**, *103*, 2533–2577. [e] Cruzan, J. D., Braly, L. B., Liu, K., Brown, M. G., Loeser, J. G., Saykally, R. J. *Science* **1996**, *271*, 59–62. [f] References: Liu, K., Brown, M. G., Cruzan, J. D., Saykally, R. J. *Science* **1996**, *271*, 62–64; and Cole, W. T. S., Fellers, R. S., Viant, M. R., Saykally, R. J. *J. Chem. Phys.* **2017**, *146*, 14306. [g] References: Blanco, S., Pinacho, P., López, J. C. *Angew. Chemie* **2016**, *128*, 9477–9481; and Hirota, E., Sugisaki, R., Nielsen, C. J., Sørensen, G. O. *J. Mol. Spectrosc*. **1974**, *49*, 251–267. [h] Blanco, S., Pinacho, P., López, J. C. *Angew. Chemie* **2016**, *128*, 9477–9481. [i] MP2/6-311++G(2d,p) counterpoise corrected dissociation energy (Boys, S. F.; Bernardi, F. *Mol. Phys*. **1970**, *19*, 553-566; Xantheas, S. S. *J. Chem. Phys*. **1996**, *104*, 8821-8824).

Table S5.21. Experimental and *ab initio* MP2/6-311++G(2d,p) quadrupole coupling constants (χ_{aa}, χ_{bb}, χ_{cc}) of formamide (f) and different formamide-water complexes (see Figure 5.1 of the paper) together with the values of the unbalanced $2p_z$ electronic charge ($(U_p)_z$) calculated from the equation: $\chi_{cc}/eQq_{n10} = -(U_p)_z$ (q_{210} is the electric field gradient associated to a $2p$ electron in an isolated atom). A value of eQq_{210} = -10 MHz has been used (Gordy, W., Cook, R. L. *Microwave Molecular Spectra*, Wiley-Interscience: New York, 1984, Vol. 11). These values are compared to those ($-(U_p)_z = [n_z - (n_x - n_y)/2]$) calculated from the natural atomic orbital populations n_x, n_y, n_z of the $2p$ orbitals of N atom derived from a Natural Bond Orbital (NBO) analysis (Reed, A. E., Weinstock, R. B., Weinhold, F. *J. Chem. Phys.* **1985**, *83*, 735-746). The *ab initio* constants list include the non-diagonal elements of the quadrupole coupling tensor set up in the principal inertial axis system (χ_{ab}, χ_{ac}, χ_{bc}) and the constants in the principal quadrupole coupling axis (χ_{xx}, χ_{yy}, χ_{zz}). Except for formamide-$(H_2O)_3$ (f-w_3) the *ab initio* χ_{cc} and χ_{zz} values are nearly equal and this justifies the assumption that the *c* principal inertial axis, perpendicular to the molecular skeleton plane, is coincident with the z axis. The $-(U_p)_z$ values calculated from the *ab initio* χ_{zz} constants differ from those obtained from the experimental χ_{cc} value by an almost constant factor, as the experimental χ_{cc} and theoretical χ_{zz} values do, but reproduce the same trends. To account for this factor and in order to estimate the value of χ_{zz} for f-w_3, the *ab initio* constants have been scaled (χ^{s}_{xx}, χ^{s}_{yy}, χ^{s}_{zz}) using the theoretical and experimental values of formamide. The values of the *ab initio* η_D asymmetry parameter ($\eta_D = |(\chi_{yy} - \chi_{xx})/\chi_{zz}|, 0 \leq \eta_D \leq 1$) that measures the deviation of the charge distribution from axial symmetry reflect also the polarization of the amide group by hydrogen bonding and clearly show the effects of cooperative hydrogen bonding.

Table S5.21. Continued.

	Parameter	f[a]	f-w-b	f-w-c	f-w-a	f-w_2	f_2-w N_3	f_2-w N_9	f-w_3
Experiment	χ_{aa}/MHz	1.961(3)	1.863(2)	-	1.332(4)	1.074(3)	1.0671(44)	1.2692(37)	0.8679(10)
	χ_{bb}/MHz	1.893(5)	1.739(4)	-	2.037(2)	2.006(5)	1.9087(86)	1.7260(83)	1.9524(14)
	χ_{cc}/MHz	-3.854(5)	-3.602(4)	-	-3.37(1)	-3.080(5)	-2.9757(86)	-2.9952(83)	-2.8204(14)
	χ_{cc}/eQq_{210}	0.385	0.360	-	0.337	0.308	0.298	0.300	0.282
Ab initio	$-(U_p)_z$(NBO)	0.382	0.364	0.353	0.330	0.299	0.299	0.301	0.299
	χ_{aa}/MHz	2.12	2.02	1.56	1.36	1.05	1.10	1.37	0.86
	χ_{bb}/MHz	1.96	1.91	2.10	2.16	2.15	2.08	1.81	2.02
	χ_{cc}/MHz	-4.08	-3.93	-3.67	-3.52	-3.20	-3.18	-3.17	-2.88
	χ_{ab}/MHz	0.01	0.05	-0.16	0.01	-0.10	0.25	-0.57	0.10
	χ_{ac}/MHz	-0.01	0.11	0.00	-0.24	0.26	-0.01	0.10	-0.84
	χ_{bc}/MHz	0.00	-0.03	0.00	-0.07	-0.28	0.02	-0.06	-0.70
	χ_{xx}/MHz	2.12	2.04	2.15	2.16	2.17	1.04	0.98	0.99
	χ_{yy}/MHz	1.96	1.89	1.52	1.37	1.05	2.14	2.20	2.16
	χ_{zz}/MHz	-4.08	-3.93	-3.67	-3.53	-3.22	-3.18	-3.17	-3.15
	η_D	0.04	0.04	0.17	0.22	0.35	0.35	0.38	0.37
	χ_{zz}/eQq_{210}	0.408	0.393	0.367	0.352	0.322	0.318	0.317	0.315
scaled	χ^s_{xx}/MHz	2.00	1.93	2.03	2.04	2.05	2.02	2.07	2.04
	χ^s_{yy}/MHz	1.84	1.79	1.44	1.29	0.99	0.98	0.91	0.93
	χ^s_{zz}/MHz	-3.85	-3.71	-3.47	-3.33	-3.04	-3.00	-2.98	-2.97
	η^s_D	0.04	0.04	0.17	0.22	0.35	0.35	0.39	0.37
	χ^s_{zz}/eQq_{210}	0.385	0.371	0.347	0.333	0.304	0.300	0.298	0.297

[a] f: formamide; f-w-a, f-w-b, f-w-c: formamide-H_2O; (f-w_2): formamide-$(H_2O)_2$; f_2-w: $formamide_2$-H_2O; f-w_3: formamide-$(H_2O)_3$.

Figure S5.1. Calculated cyclic conformers for the complex formamide-$(H_2O)_3$ (f-w_3). See text for notation.

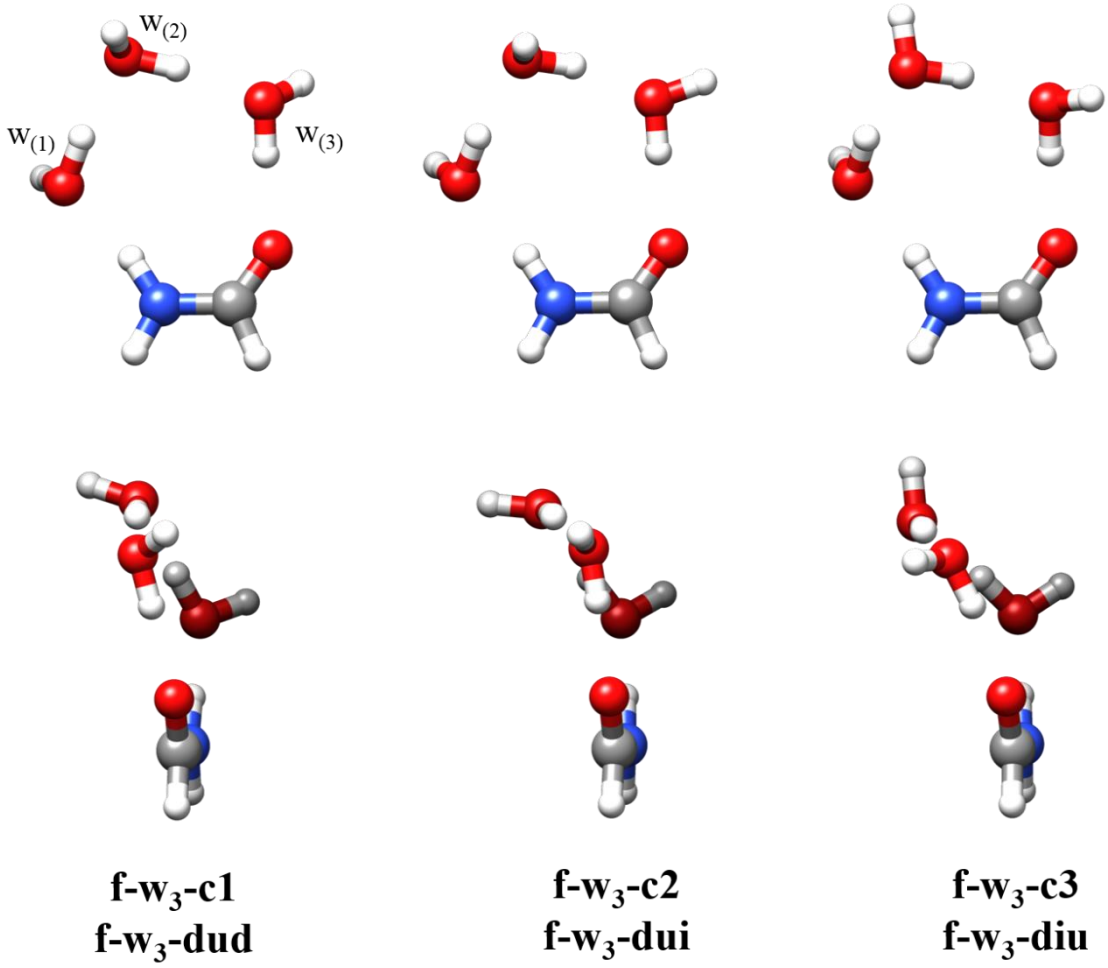

Figure S5.2. Calculated conformers for the complex formamide-$(H_2O)_3$ (f-w_3), with water molecules forming a trimer.

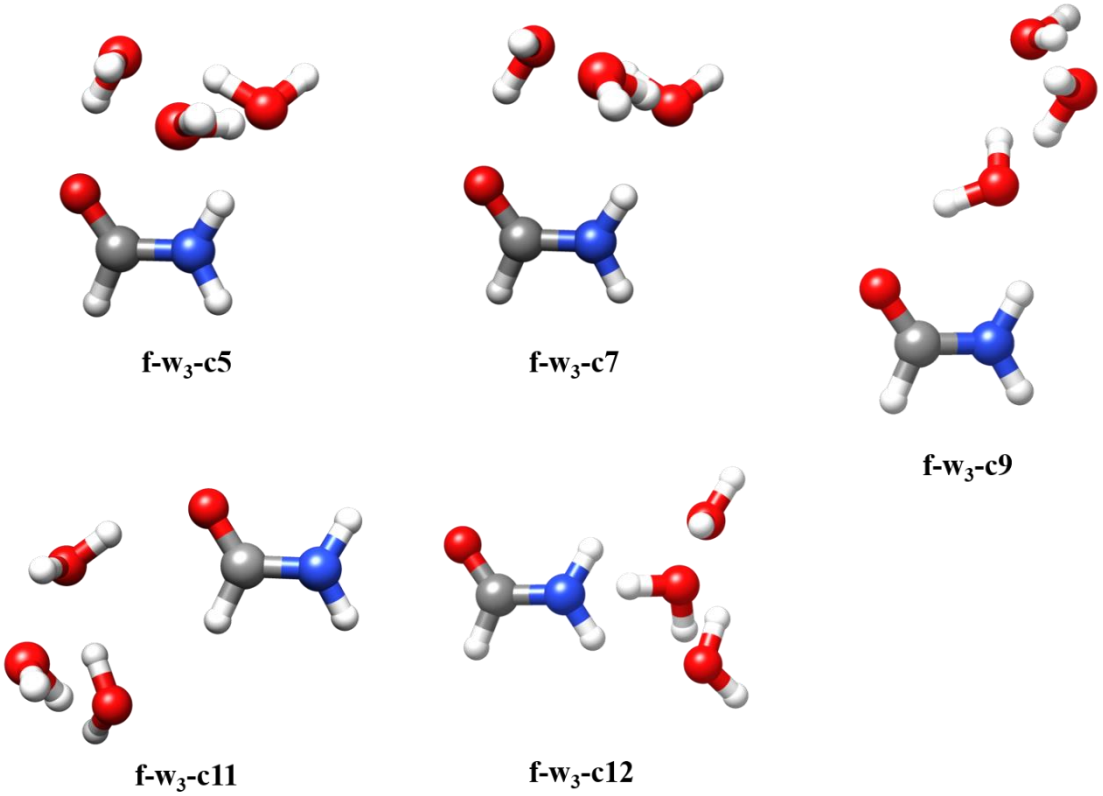

Figure S5.3. Other calculated conformers for the complex formamide-$(H_2O)_3$ (f-w_3).

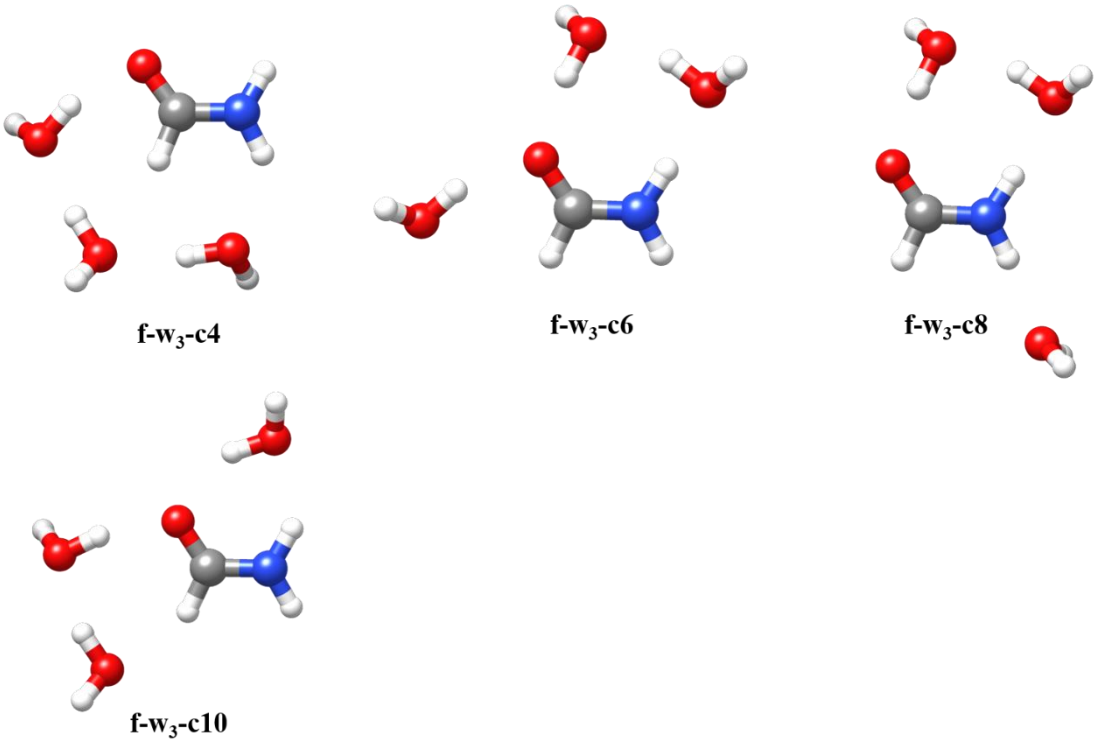

Figure S5.4. a) Comparison of the r_s structure and the *ab initio* structures for the lowest energy conformers of the complex formamide-$(H_2O)_3$ (f-w_3). b) 3D model of the r_0 structure.

a)

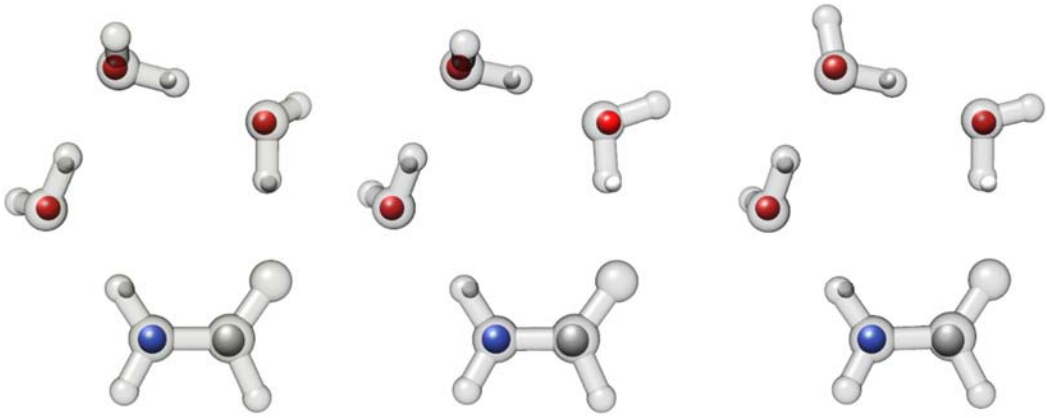

b)

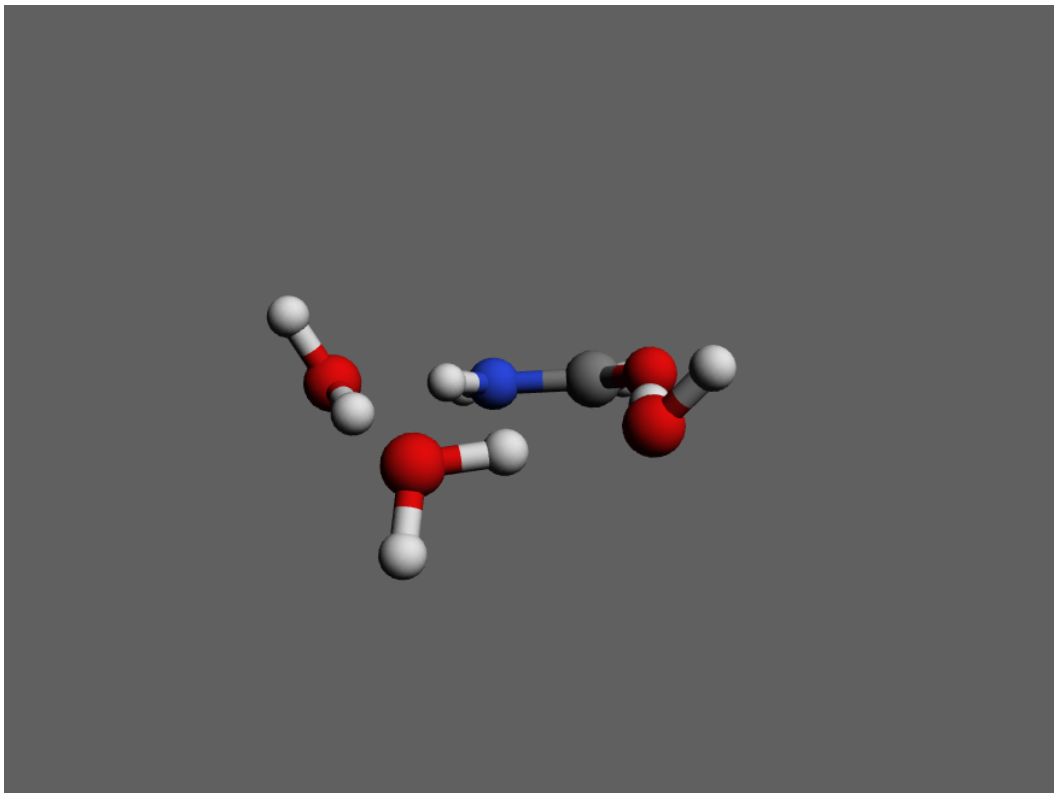

Figure S5.5. a) Predicted MP2/6-311++G(2d,p) variation of the distances C-N and C=O and the experimental values of χ_{cc} for the different observed adducts of formamide and water. For formamide-H_2O-c (f-w-c, value of χ_{cc} not available) and formamide-$(H_2O)_3$ (f-w_3) the scaled *ab initio* χ_{zz} values (see Table S5.21) are given (marked with *). The progressive variation of these parameters associated to resonance-assisted hydrogen bond (RAHB) cooperativity is apparent for the series formamide (f) – formamide-H_2O-a (f-w-a) – formamide-$(H_2O)_2$ (f-w_2). The distances in formamide-$(H_2O)_3$ (f-w_3) and formamide$_2$-H_2O (f_2-w) are close to those of formamide-$(H_2O)_2$ (f-w_2) indicating that the distances do not change beyond three body clusters. It is also interesting to see how the values corresponding to the formamide-H_2O-b (f-w-b) and formamide-H_2O-c (f-w-c) with different hydrogen bonding lie between those of formamide and formamide-H_2O-a (f-w-a). b) Almost linear correlation between the predicted MP2/6-311++G(2d,p) C-N/C=O distances with χ_{cc} for the different clusters.

a)

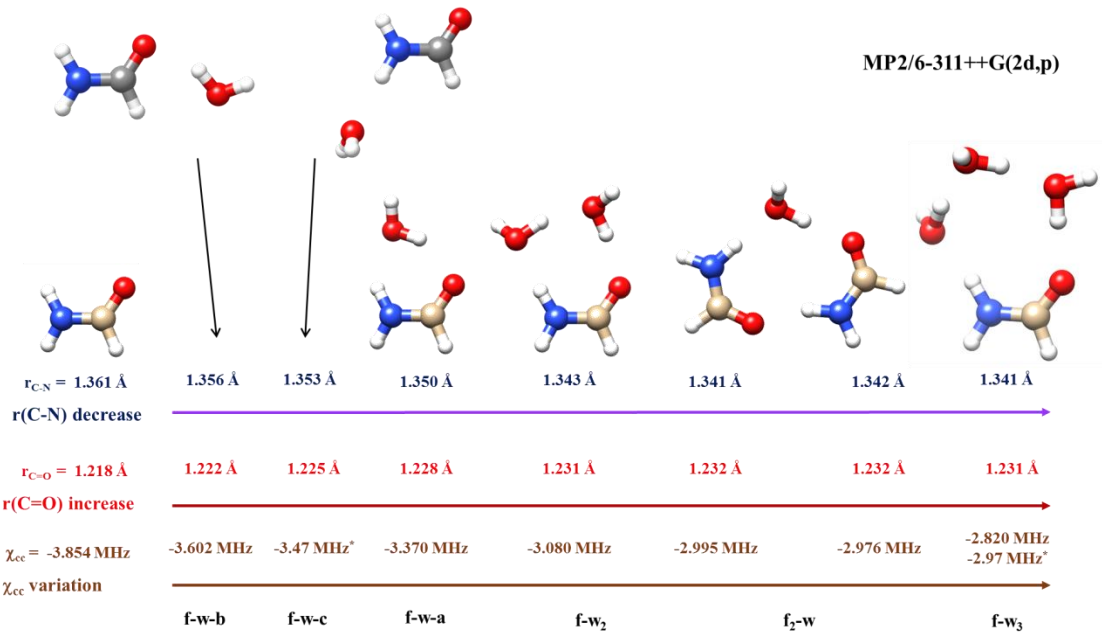

b)

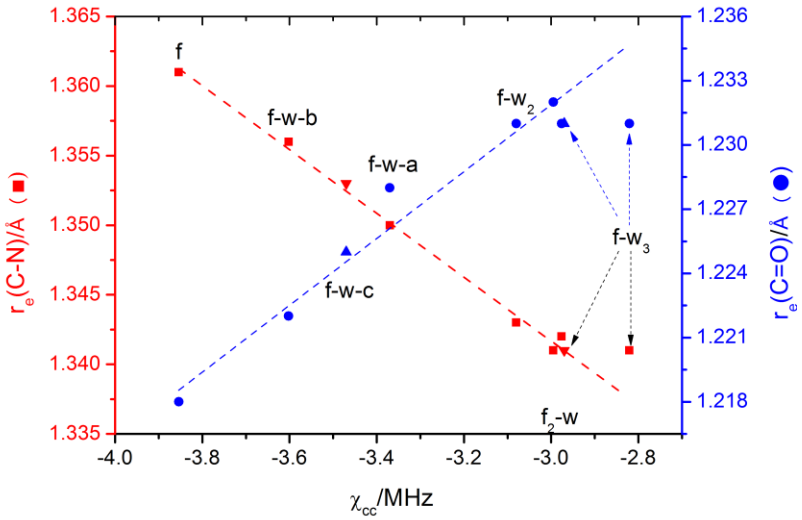

Figure S5.6. (a) Plot of the values (see top table) of the quantity χ_{cc}/eQq_{210} (experimental) *vs*. the unbalanced $2p_z$ electronic charge $(U_p)_z$ obtained from a MP2/6-311++G(2d,p) NBO analysis of formamide (f), formamide-H_2O forms (f-w-a, f-w-b, f-w-c), formamide-$(H_2O)_2$ (f-w_2), formamide$_2$-H_2O (f_2-w) and formamide-$(H_2O)_3$ (f-w_3). q_{210} is the electric field gradient associated to a $2p$ electron in an isolated atom; a value of eQq_{210} = -10 MHz has been used for ^{14}N (Gordy, W., Cook, R. L. *Microwave Molecular Spectra*, Wiley-Interscience: New York, 1984, Vol. 11). The slope is 1.08. (b) The same representation using the MP2/6-311++G(d,p) *ab initio* χ_{zz} values scaled with the factor needed to reproduce the experimental formamide values. The slope is 1.02.

	NBO $-(U_p)_z$	Exp. χ_{cc}/MHz	Exp. χ_{cc}/eQq_{210}	*Ab initio* χ_{zz}/eQq_{210}	Scaled *ab* χ_{zz}/eQq_{210}
formamide	0.382	-3.854	0.385	0.408	0.385
f-w-b	0.364	-3.602	0.360	0.393	0.371
f-w-c	0.353	-	-	0.367	0.347
f-w-a	0.330	-3.370	0.337	0.352	0.333
f-w_2	0.299	-3.080	0.308	0.322	0.304
f_2-w N_3	0.299	-2.976	0.298	0.319	0.301
f_2-w N_9	0.301	-2.995	0.300	0.317	0.299
f-w_3	0.299	-2.820	0.282	0.315	0.297

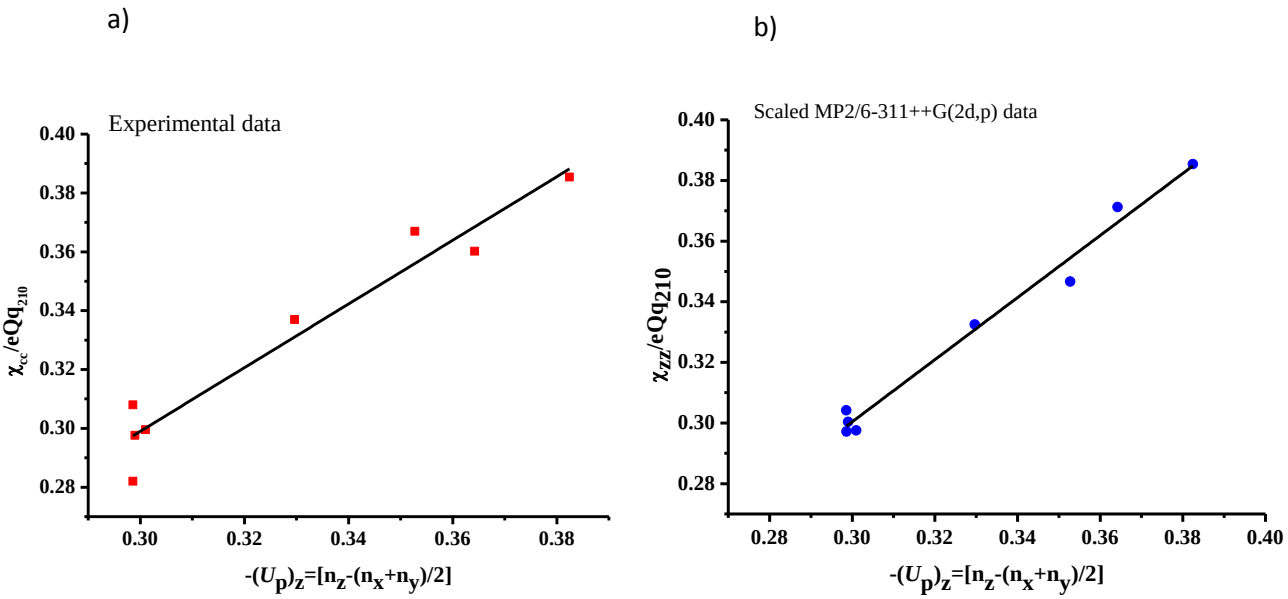

Figure S5.7. Plot of the values (see top table) of the quantity χ_{cc}/eQq_{210} (experimental) *vs*. the lone pair occupancy of the N atom of formamide (f), formamide-H_2O forms (f-w-a, f-w-b, f-w-c), formamide-$(H_2O)_2$ (f-w_2), formamide$_2$-H_2O (f_2-w) and formamide-$(H_2O)_3$ (f-w_3). q_{210} is the electric field gradient associated to a 2*p* electron in an isolated atom; a value of eQq_{210} = -10 MHz has been used for ^{14}N (Gordy, W., Cook, R. L. *Microwave Molecular Spectra*, Wiley-Interscience: New York, 1984, Vol. 11). For f-w_3 and f-w-c values see Table S5.21.

	N lone pair occupancy	Exp. χ_{cc}/MHz	Exp. χ_{cc}/eQq_{210}	*Ab initio* χ_{zz}/eQq_{210}	Scaled *ab* χ_{zz}/eQq_{210}
formamide	1.730	-3.854	0.385	0.408	0.385
f-w-b	1.715	-3.602	0.360	0.393	0.371
f-w-c	1.713	-	-	0.367	0.347
f-w-a	1.693	-3.370	0.337	0.352	0.333
f-w_2	1.681	-3.080	0.308	0.322	0.304
f_2-w N_3	1.667	-2.976	0.298	0.319	0.301
f_2-w N_9	1.670	-2.995	0.300	0.317	0.299
f-w_3	1.668	-2.820	0.282	0.315	0.297

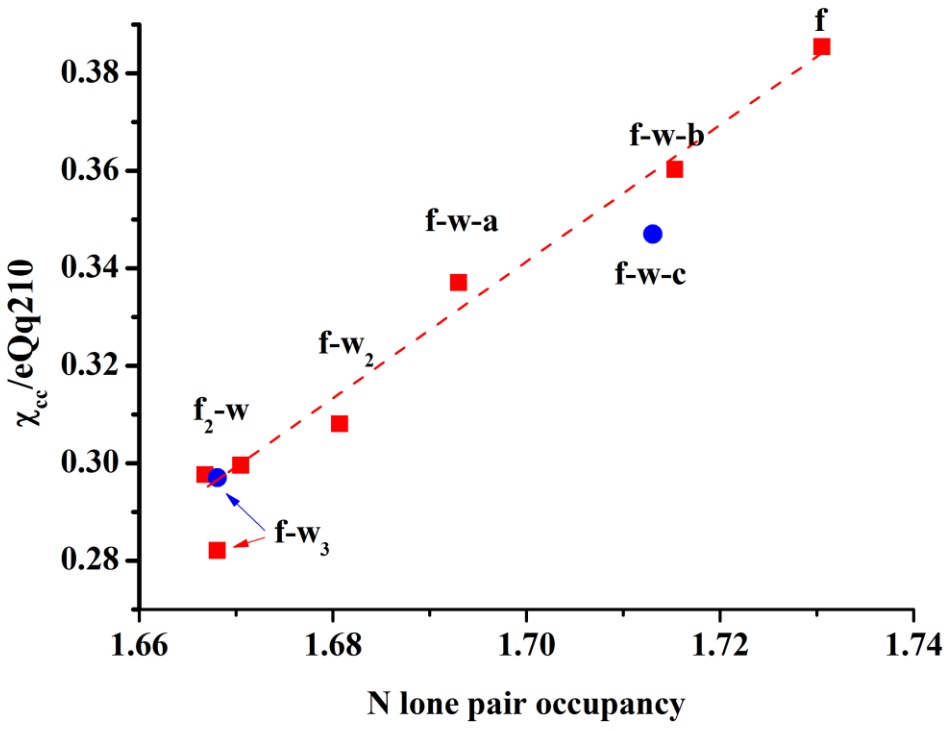

Figure S5.8. MP2-calculated potential energy function for the pure inversion of the conformation of the complex formamide-$(H_2O)_3$ (f-w_3). This path involves the simultaneous flipping rotation (ϕ_1, ϕ_2 and ϕ_3) of the three water subunits. The ring puckering β coordinate has been taken as inversion coordinate. The barrier at the planar configuration is sensible to the basis set used and takes the values: 730 cm^{-1} for aug-cc-pvdz, 823 cm^{-1} for 6-311++G(2d,p) and 935 cm^{-1} for 6-311++G(d,p). In all cases the energy levels under the barrier form the typical tunneling inversion pairs, being the lowest pair nearly degenerate for those barriers. The experimental tunneling splitting of *ca*. 370 MHz is reproduced for barriers near 300 cm^{-1}.

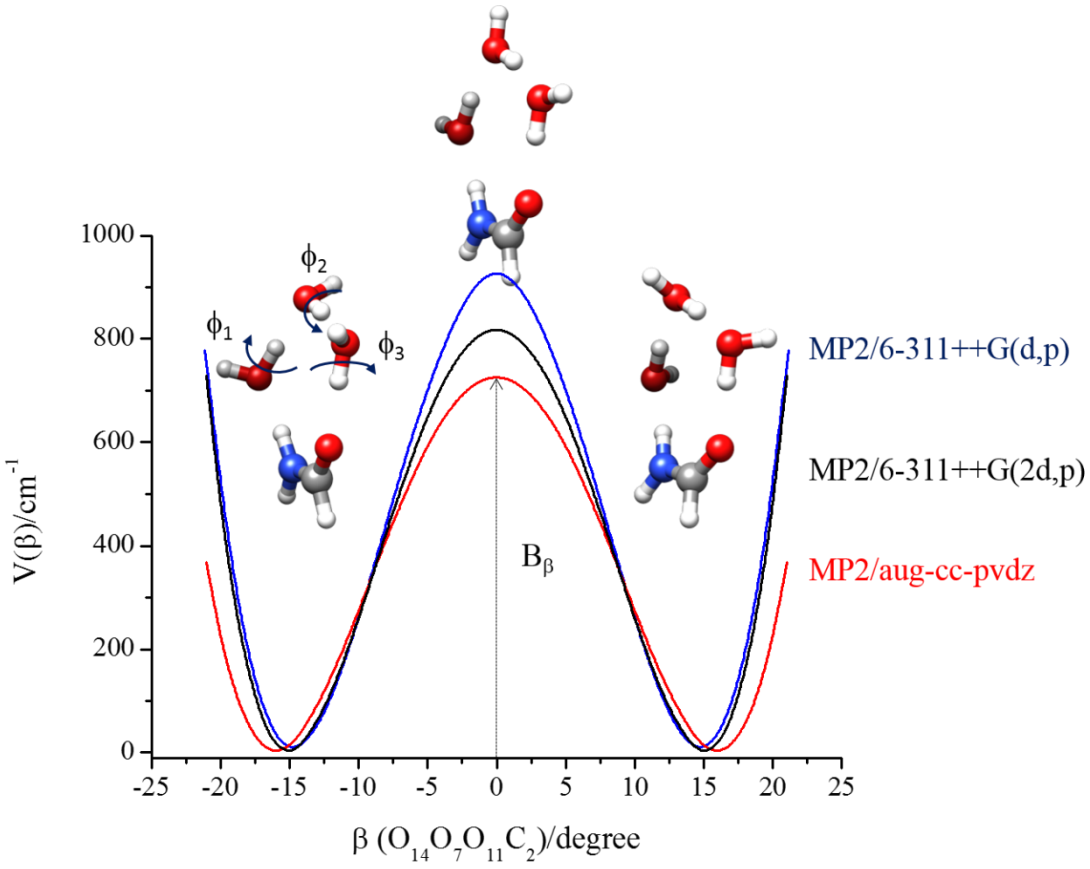

Chapter VI

Microsolvation of Formanilide Conformers: A Model For Peptide Solvation.

Manuscript in preparation.

Abstract

Microsolvated complexes of formanilide with different degrees of hydration have been generated in a supersonic expansion and characterized by Fourier transform microwave spectroscopy. Three 1:1 microsolvated complexes have been observed for both *cis* and *trans* configurations of formanilide in agreement with previous studies. The lowest energy 1:2 microsolvated complex of *cis*-formanilide has been detected. In both mono and dihydrated *cis*-formanilide complexes, water closes sequential cycles of 6 and 8 members respectively, trough simultaneous hydrogen bonds with the amino and the carbonyl groups. Furthermore *cis*-formanilide has almost the same non planar configuration observed in the monomer. In the higher energy monohydrated complexes detected with *trans*-formanilide, a planar skeleton is determined with water interacting solely with either the amino or the carbonyl group. For all species the spectra of parent and several water isotopologues have been observed, allowing us to precisely locate the position of water.

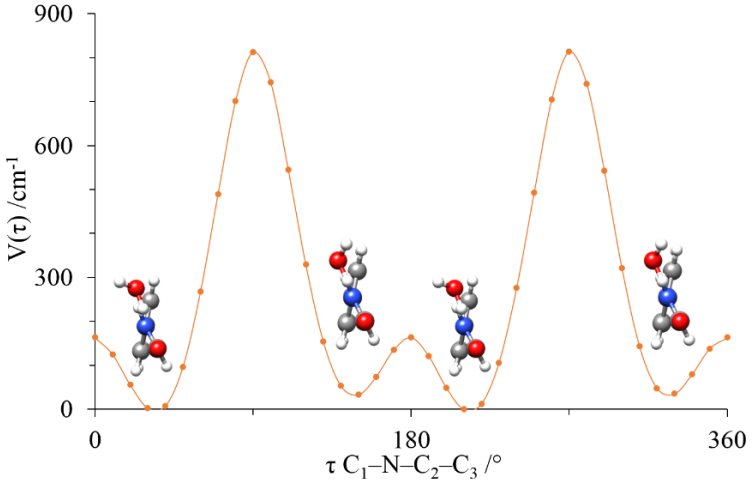

6.1 Introduction

The activity of biomolecules is closely related to their shapes. In solution, those are determined by the forces driven by the water. The interactions established by the solute molecules with water are mainly hydrogen bonds.[1-3] Water molecules can drive changes in conformational[4,5] or tautomeric[6,7] equilibria, and drive the folding of proteins to their final active conformations.[8,9] Studying the interactions between water and biomolecules in condensed phases is a difficult task, but it is possible to characterize the forces established in the initial steps of the solvation process through the characterization of the microsolvated complexes of model molecules in the gas phase. The microsolvation environment, in which a limited number of molecules of water interact with another molecule, is an important field of research.[10,11] Microsolvated complexes with different degrees of hydration can be easily formed in a supersonic jet and their structures characterized in isolation by high-resolution techniques, such as microwave spectroscopy. Fourier transform microwave spectroscopy coupled to the supersonic expansion has proved to be an excellent tool to determine the molecular structure of complexes with water in the gas phase and the interactions involved in the clustering.[12-14]

The microsolvation complexes of molecules bearing the amide group,[15-18] the same moiety occurring in the peptide bond that forms proteins are of special interest. Those complexes can serve as a model to investigate how water establishes hydrogen bonds with the peptide linkage, to identify the preferred sites for interactions and to recognize the subtle effects of water interaction and cooperativity on the peptide group. Formanilide (IUPAC name N-phenylformamide, C_7H_7NO, see Scheme 6.1) is a small biological molecule similar to formamide with a phenyl ring substitute on the amino group. Formanilide presents the amide moiety and shows a *cis-trans* conformational equilibrium, resembling the *cis* and *trans* peptide bonds. In this context, the microsolvation of formanilide in a supersonic expansion can serve as a model for the solvation of the peptide linkage to analyze the main differences in the interaction with water of the *cis* and *trans* peptide group.

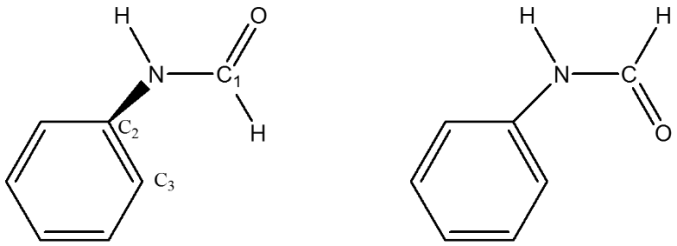

Scheme 6.1. Formanilide or N-Phenylformamide in the *cis* (left) and *trans* (right) configurations. The angle between the amide and the phenyl ring in the *cis* configuration defined as the dihedral angle C_1–N–C_2–C_3 was found experimentally to be of about 34.7 degrees.[23] The *trans* configuration is planar.

The microsolvation of formanilide in a supersonic jet environment was first studied by Dickinson *et al*.[19] using laser-induced fluorescence excitation spectroscopy together with mass-selected, resonant two-photon ionization spectroscopy (R2PI) and rotational band contour analysis. They reported experimental parameters attributed to two 1:1 and two 1:2 complexes between *trans*-formanilide and water establishing interactions with the amino and the carbonyl sites of formanilide.[19] This work was later extended by Fedorov *et al*.[20] using the R2PI technique to analyze clusters of formanilide with water and ammonia. In addition to the previously found complexes, another 1:2 complex and even a 1:4 formanilide – water complex

were reported, all of them with the *trans* conformer, based on the assumption that the *cis* conformer of formanilide is less abundant in the supersonic jet according to previous studies.[21] However, the formanilide monomer was studied by high-resolution rotational spectroscopy[22,23] showing that both forms of formanilide are present in a supersonic expansion with similar populations. In the present work, we report for the first time microsolvation complexes of both *cis* and *trans* formanilide forms with one and two molecules of water observed in a molecular beam Fourier transform microwave spectrometer.

6.2 Experimental and theoretical methods

Commercial samples of formanilide (m.p. 48ºC), $H_2{}^{18}O$ and ^2H_2O were used. The rotational spectra of the formanilide-water complexes were investigated in the frequency range 2-13 GHz using a chirped-pulse Fourier transform microwave spectrometer (CP-FTMW), which follows Pate's design[24,25] and a molecular-beam Fourier transform microwave spectrometer (MB-FTMW).[26] The rotational spectra of the ^{18}O-water isotopologues were recorded in the MB-FTMW spectrometer. The spectra of the deuterated species were recorded in the CP-FTMW instrument.

In the CP-FTMW instrument, operated between 2 and 8 GHz, the spectra were recorded in steps of 2 GHz. The carrier gas was Ar at backing pressures of about 3 bar expanding in the vacuum chamber through a 1.0 mm nozzle in pulses of 900 µs. The sample was polarized by 2 GHz range chirp pulses of 4 µs created by an arbitrary waveform generator and amplified to 20 W. The polarization signal was radiated from a horn antenna in a direction perpendicular to that of the expanding gas. A molecular transient emission spanning 40 µs is then detected through a second horn, recorded with a digital oscilloscope and Fourier-transformed to the frequency domain. The accuracy of frequency measurements is better than 10 kHz.

In the MB-FTMW instrument, operated in the frequency range 5-13 GHz, He-Ne mixtures were used at stagnation pressures ranging up to 4 bar expanding in pulses of about 800 µs through a 0.8 mm nozzle. Short (typ. 0.3 µs, 10-300 mW) microwave pulses were used for polarization purposes. Typically, a *ca*. 400 µs-length time domain spectrum was recorded in 40-100 ns intervals and converted to the frequency domain by a fast Fourier transformation. Due to the collinear arrangement of the jet and resonator axis each rotational transition splits in two Doppler components so the resonant frequencies are taken as the arithmetic mean of both components. Frequency accuracy is better than 3 kHz.

Prior to the recording of the spectrum, *ab initio* calculations[27] were performed to predict the rotational constants, the centrifugal distortion constants, quadrupole coupling constants and dipole moments of the conformers of the complexes between formanilide and water (see Figures 6.1 and 6.2) previously described.[19] Calculations were done at the B3LYP-D3/6-311++G(d,p), MP2/6-311++G(d,p), MP2/6-311++G(2d,p) and MP2/aug-cc-pvdz level of theory. Calculation of vibrational frequencies was done considering only harmonic contributions. The rotational parameters calculated together with the predicted energies are collected in Tables S6.1-S6.4 in supplementary material for the B3LYP-D3/6-311++G(d,p) and the MP2/6-311++G(2d,p) theory.

6.3 Results

The investigations done by Dickinson *et al*[19] on the electronic spectra of the formanilide-water complexes included a conformational search of the different complexes. In the following lines we describe their main features using the results of our own calculations. We include here a description not included in the previous work concerning the different configurations of the *cis*-formanilide complexes arising from the non-planarity of this species

1:1 formanilide – water complexes

For the 1:1 complexes between formanilide and water the *ab initio* calculations predict two stable conformers for the *cis* and three for the *trans* configurations of formanilide (see Figure 6.1 and Tables S6.1-S6.2). The interactions established are basically the same that occur in related systems such as formamide-water complexes[16] and for this reason we use the same notation used to label them. As a difference, in formanilide, the steric impediment of the phenyl ring in the amine group blocks some positions for the water molecule.[16] In addition while *trans*-formanilide, as formamide, is planar, in *cis*-formanilide the phenyl and formamide groups are not co-planar. The torsion around the C-N phenyl-formamide bond is governed by a potential function with a maximum at the planar configuration. The equilibrium dihedral angle was reported to be 34.7º and the barrier to planarity of 152 cm^{-1}.[23] This gives rise to two possible non-equivalent forms for each *cis*-formanilide water complex.

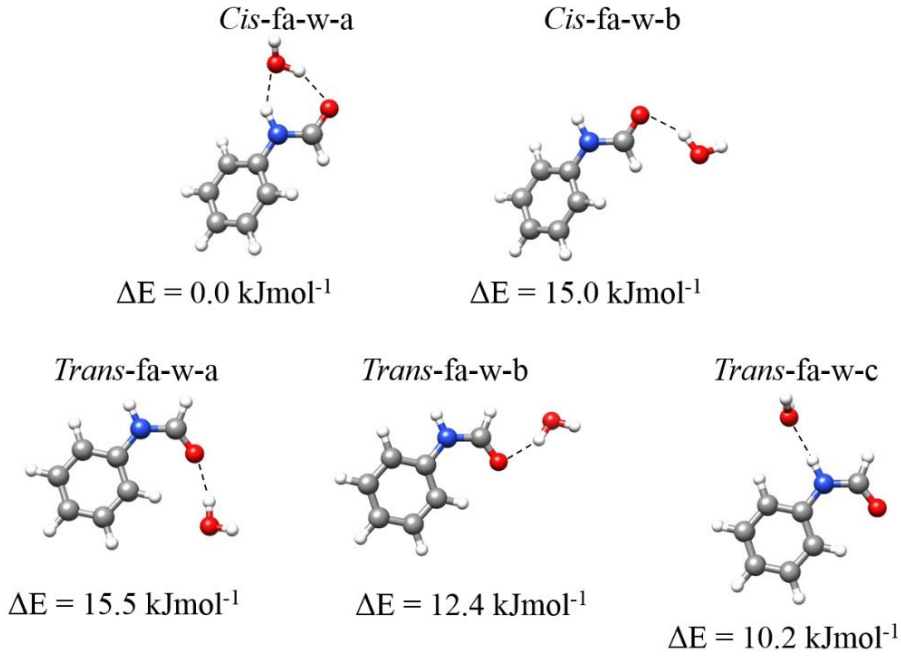

Figure 6.1. Monohydrated microsolvation complexes for the *cis* and *trans* configurations of formanilide with labeling and stabilization energy (MP2/6-311++G(2d,p)) related to the most stable complex (*cis*-fa-w-a). Black dashed lines indicate the interactions established through hydrogen bonds.

The most stable complexes *cis*-formanilide···(H_2O) Ia (*cis*-fa-w-a) and *cis*-formanilide···(H_2O) Ia' (*cis*-fa-w-a') are formed with *cis*-formanilide, each one with the two equivalent forms (see Figure S6.3). Both amide group and water act simultaneously as hydrogen donors and acceptors closing a sequential cycle through O···H–N and O–H···O=C hydrogen bonds. The difference between the w-a and w-a' forms lies in the orientation of the non-bonded hydrogen of water that

lies out of the formamide subunit plane. *Cis*-formanilide can form another complex (*cis*-formanilide···(H_2O) Ib, *cis*-fa-w-b) with the molecule of water establishing a O–H···O=C hydrogen bond and a weak interaction with the hydrogen atom in the carbonyl group, similar to the w-b complex found for formamide. In formamide, a third complex is possible by the interaction of the water molecule solely with the amino group. However, in *cis*-formanilide this position is not possible due to the presence of the phenyl ring.

For the *trans* conformation of formanilide, three complexes with one molecule of can be formed (see Figure 6.1). In the *trans*-formanilide···(H_2O) Ia complex (*trans*-fa-w-a), the molecule of water establishes a O–H···O=C hydrogen bond with the carbonyl group and a weak interaction with the closest hydrogen in the phenyl ring. The *trans*-formanilide···(H_2O) Ib complex (*trans*-fa-w-b) is identical to that in the *cis* form and is not affected by the presence of the phenyl. In the *trans*-formanilide···(H_2O) Ic complex (*trans*-fa-w-c) there is a O···H–N hydrogen bond to the amino group supported with and additional weak interaction to one hydrogen from the phenyl ring that increases the stability of this complex.

Complexes *cis*-fa-w-a and *cis*-fa-w-a' have low predicted energies compared to *trans*-fa-w-b and *trans*-fa-w-c, *trans*-fa-w-a or *cis*-fa-w-b (see Figure 6.1 and Tables S6.1-S6.2). However only the spectra of *cis*-fa-w-a, *trans*-fa-w-b and *trans*-fa-w-c have been detected.

1:2 formanilide – water complexes

The 1:2 complexes considered are formed by adding a water molecule to the 1:1 predicted complexes, resulting in four stable structures (see Figure 6.2). In these complexes, the two molecules of water are disposed forming a chain through a O···H–O hydrogen bond.

In *cis*-formanilide···$(H_2O)_2$ IIa (*cis*-fa-w_2), the two water molecules close an 8-membered sequential cycle through O···H–N, O–H···O=C and O···H–O hydrogen bonds. In the *cis*-formanilide···$(H_2O)_2$ IIb (*cis*-fa-w_2-b) complex one of the molecules of water interacts through a O–H···O=C hydrogen bond to the carbonyl group and a O···H–O to the second molecule of water, which in turns establishes two weak interactions with hydrogen atoms in the carbonyl and phenyl groups. As for the 1:1 conformers the non-planar structure of *cis*-formanilide subunit gives rise to two conformers in each case depending on the orientation on the non-bonding water hydrogen atoms. For the most stable forms these two conformers have been labelled *cis*-fa-w_2 and *cis*-fa-w_2' (see Figure S6.4). Each one of these conformers have two equivalent forms.

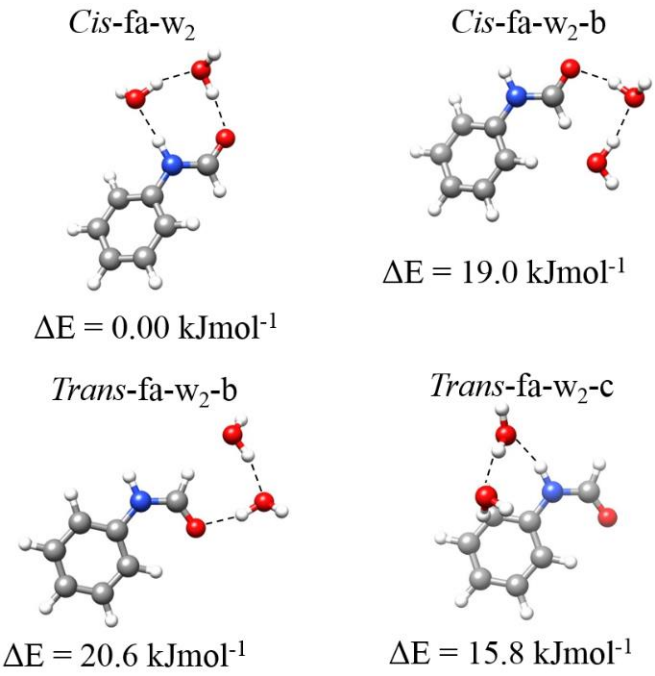

Figure 6.2. Dihydrated microsolvation complexes for the *cis* and *trans* configurations of formanilide with labeling and stabilization energy (MP2/6-311++G(2d,p)) related to the most stable complex (*cis*-fa-w$_2$). Black dashed lines indicate the interactions established through hydrogen bonds.

The *trans*-formanilide···(H$_2$O)$_2$ IIb (*trans*-fa-w-b) complex is similar to the equivalent *cis*-fa-w$_2$-b without the additional stabilizing interaction between the water molecule and the hydrogen in the phenyl ring, explaining why this complex is predicted to be less stable (see Figure 6.2 and Tables S6.3-S6.4). In *trans*-formanilide···(H$_2$O)$_2$ IIc (*trans*-fa-w-c), there is a highly distorted hydrogen bond between one of the molecules of water and the amino group, while the second molecule of water establishes a perpendicular π-interaction with the delocalized electron density in the phenyl ring.

Contrary to the experimental results reported previously using R2PI spectroscopy,[19,20] in this work only the *cis*-fa-w$_2$ complex, which is predicted to be the lowest in energy (see Tables S6.3-S6.4), has been observed experimentally. Despite an extensive search, no complex between two molecules of water and *trans*-formanilide has been detected so far.

Microwave spectra

The rotational spectrum was first recorded using the CP-FTMW spectrometer. The spectra of *trans*- and *cis*-formanilide were first measured and removed prior to the search of the rotational transitions of formanilide-water complexes. Most of 1:1 and 1:2 complexes were predicted to be prolate asymmetric tops with the electric dipole moment mainly oriented along the *a* axis. We searched for the pattern characteristic of the R-branch *a*-type lines which appear as groups regularly spaced in frequency by *B*+*C*. Focusing the exploration of the spectrum on that patterns lead to the assignment of the species *cis*-fa-w-a, *cis*-fa-w$_2$ and *trans*-fa-w-b. While the *cis*-formanilide complexes do not show *b*- or *c*-type spectra, *trans*-fa-w-b show a weak *b*-type spectrum. It was observed that many other lines consist of doublets of moderate intensity that finally were identified as belonging to the species *trans*-fa-w-c. All the spectra show a hyperfine

structure (hfs) due to the presence of a ^{14}N nucleus in the formanilide subunit. Once we had preliminary sets of rotational parameters we proceeded to measure the spectrum with the MB-FTMW spectrometer which has superior resolution and allows us to completely resolve the quadrupole coupling hfs and any additional splitting. The spectra were analyzed employing Pickett´s SPFIT[28] program using a Hamiltonian with semirigid rotor (A-reduction, I^r representation) and quadrupole coupling terms.[29] In the cases were vibrational doublets have been detected, we have not observed the effects of Coriolis perturbations. Nevertheless, a two state Hamiltonian was used with common sets of centrifugal distortion and quadrupole coupling constants.

Cis-formanilide···(H_2O) Ia

The *cis*-fa-w-a spectrum shows, in addition to the ^{14}N hfs, small splittings of *ca*. 2.5 kHz attributable to rotational transitions in two vibrational levels very close in energy (see Figure 6.3). This splitting, only observable in the MB-FTMW spectrum, do not show statistical weight spin effects so it can not be correlated to a motion of water exchanging the hydrogen atoms. The doubling in the spectrum implies the existence of two equivalent forms. Both the flipping of water or the torsion of the formamide fragment around the N-C_2 bond exchange the *cis*-fa-w-a and *cis*-fa-w-a' conformers by different paths. Thus, only a combination of both motions would give rise to the observed doublets as discussed below. The vibrational sub-levels were labeled as $v = 0$ and $v = 1$ for the lowest and highest frequency components respectively.

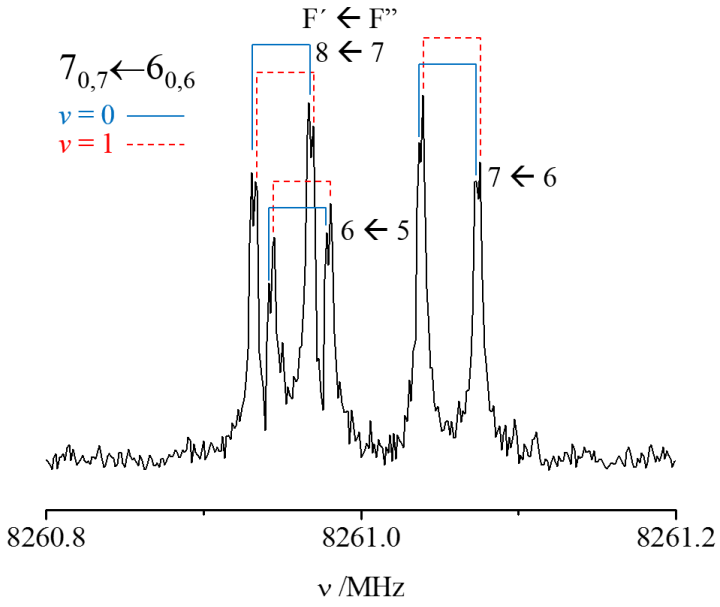

Figure 6.3. The $7_{0,7}$←$6_{0,6}$ rotational transition for the *cis*-fa-w-a complex with the hyperfine structure arising from the quadrupole coupling interaction (F´←F´´ transitions). The small splittings of *ca*. 2.5 kHz correspond to the rotational transitions in the $v = 0$ (blue solid lines) and $v = 1$ (red dashed lines) torsional states due to tunneling between two equivalent non-planar configurations. Each transition appears as a doublet because of the Doppler effect.

Only R-branch *a*-type transitions up to $J = 10$ were measured, despite the μ_c dipole moment component could be not negligible according to the *ab initio* prediction (see Tables S6.1-S6.2). However, μ_c changes its sign when the *cis*-formanilide inverts its configuration through the torsional motion so it is antisymmetric. Thus *c*–type lines are only allowed to connect rotational

levels of different vibrational state and would occur as doublets measuring two times the vibrational energy spacing. No such doublets have been observed. For this species the spectra of the water ^{18}O and ^{2}H isotopologues were also measured. For the later the spectrum was collected in the CP-FTMW and no tunneling splittings were observed.

From the analysis of the spectrum, the rotational constant *B* for each torsional state could be determined separately, while *A* and *C* were determined for both states simultaneously (see Table 6.1). Just three of the five quartic centrifugal distortion constants could be determined, the other were fixed to zero. In the fit of the monosubstituted isotopologue spectra (see Table S6.5), all the parameters, except the rotational constants were fixed to the values determined for the parent species. For the $^{18}O_w$ isotopologue observed in the MB-FTMW spectrometer, the rotational constants could be determined as for the parent species. For the deuterated species, observed only in the CP-FTMW spectrometer which has no enough resolution to solve the small tunneling doublets, just one set of rotational constants were determined (see Table S6.5). The frequencies for the measured transitions for the parent and the observed isotopologues of the *cis*-fa-w-a complex are collected in Tables S6.14-S6.18 in supplementary material.

Table 6.1. Rotational parameters obtained from the analysis of the spectrum of the observed *cis*-fa-w-a complex, compared with *ab initio* (MP2/6-311++G(2d,p)).

Parameters[a]	experimental		*ab initio*
	$v = 0$	$v = 1$	
A /MHz	2831.4048(56)[b]		2840.71
B /MHz	662.38699(14)	662.38850(14)	664.06
C /MHz	549.51811(11)		554.39
Δ_J /kHz	0.04469(47)		0.038
Δ_{JK} /kHz	[0.]		0.015
Δ_K /kHz	[0.]		1.779
δ_J /kHz	0.01078(36)		0.009
δ_K /kHz	0.480(27)		0.430
^{14}N 3/2(χ_{aa}) /MHz	3.2149(93)		3.36
^{14}N ¼(χ_{bb}-χ_{cc}) /MHz	0.9885(67)		0.89
N	246/41/41		
σ /kHz	2.5/2.9/2.0		
Derived Parameters			
P_a /uÅ^2	752.07627(21)		747.36
P_b /uÅ^2	167.60044(21)		164.23
P_c /uÅ^2	10.89011(21)		13.68

[a] *A*, *B* and *C* are the rotational constants. Δ_J, Δ_{JK}, Δ_K, δ_J and δ_K are the quartic centrifugal distortion constants, χ_{aa}, χ_{bb} and χ_{cc} are the quadrupole coupling tensor diagonal elements for ^{14}N atom. *N* is the number of quadrupole hyperfine components/rotational transitions fitted. σ is the rms deviations of the fit. P_α (α= *a*, *b* or *c*) are the planar moments of inertia, these are derived from the moments of inertia I_α as for example $P_c = (I_a+I_b-I_c)/2$. [b] Standard errors are given in parentheses in units of the last digit.

Trans-formanilide···(H_2O) Ib

For the *trans*-fa-w-b complex only R-branch *a*-type transitions up to J = 11 were observed. From their analysis, the rotational constants, the quadrupole coupling constants and all the quartic centrifugal distortion constants, except δ_K, could be determined (see Table 6.2). All the parameters except the rotational constants were fixed to the value of the parent species in the analysis of the spectra of the isotopologues $^{18}O_w$ and $^{2}H_{w1}$ (see Figure S6.1 for atom labeling). The spectrum of the $^{2}H_{w2}$ isotopologues was not observed. The rotational parameters for all the detected species are collected in Table S6.6. The experimental frequencies are collected in Tables S6.19-S6.21 in supplementary material.

Table 6.2. Rotational parameters obtained from the analysis of the spectrum of the observed *trans*-fa-w-b complex, compared with *ab initio* (MP2/6-311++G(2d,p)).

Fitted Parameters[a]	experimental	*ab initio*
A /MHz	4094.8678(75)[b]	4125.16
B /MHz	539.02116(10)	542.43
C /MHz	476.89366(10)	479.62
Δ_J /kHz	0.02959(23)	0.026
Δ_{JK} /kHz	0.4586(77)	0.315
Δ_K /kHz	4.44(74)	1.751
δ_J /kHz	0.00323(27)	0.003
δ_K /kHz	[0.]	0.228
^{14}N 3/2(χ_{aa}) /MHz	2.802(16)	2.85
^{14}N ¼(χ_{bb}-χ_{cc}) /MHz	1.3153(44)	1.33
N	111/3.8	
σ /kHz	2.5	
Derived Parameters		
P_a /uÅ^2	936.94997(36)	931.44
P_b /uÅ^2	122.78105(36)	122.25
P_c /uÅ^2	0.63661(36)	0.26

[a] A, B and C are the rotational constants. Δ_J, Δ_{JK}, Δ_K, δ_J and δ_K are the quartic centrifugal distortion constants. χ_{aa}, χ_{bb} and χ_{cc} are the quadrupole coupling tensor diagonal elements for ^{14}N atom. N is the number of quadrupole hyperfine components/rotational transitions fitted. σ is the rms deviations of the fit. P_α (α= *a*, *b* or *c*) are the planar moments of inertia, these are derived from the moments of inertia I_α as for example $P_c = (I_a+I_b-I_c)/2$. [b] Standard errors are given in parentheses in units of the last digit.

Trans-formanilide···(H_2O) Ic

In the analysis of the *trans*-fa-w-c spectrum splittings of *ca*. 250 kHz were detected in the rotational transitions (see Figure 6.4) together with the hfs from the ^{14}N quadrupole coupling. The components of the splittings presented an intensity ratio of approximately 3:1. This corresponds to the nuclear spin statistical weight effect of a motion exchanging a pair of

hydrogen atoms. The doublets were attributed to the internal rotation the water molecule around the hydrogen bond axis which exchanges the two hydrogen atoms from water. As a consequence of this motion each rotational transitions appears split into two torsional states, which could be assigned as $v = 0$ and $v = 1$ by taking into account the 3:1 intensities.

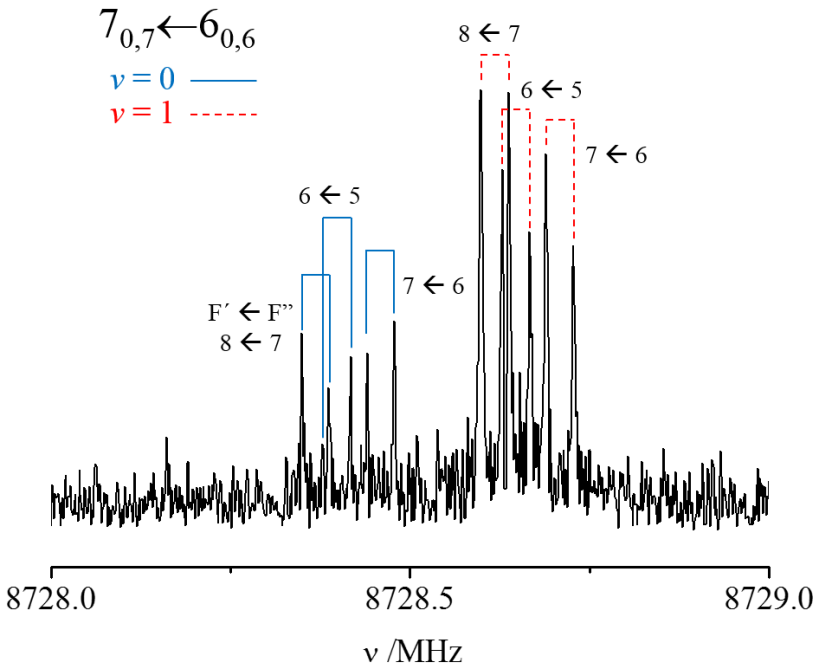

Figure 6.4. The $7_{0,7} \leftarrow 6_{0,6}$ rotational transition for the *trans*-fa-w-c complex with the hfs arising from the quadrupole coupling interaction (F´←F´´ transitions). The splitting of *ca*. 250 kHz correspond to the rotational transitions in the $v = 0$ (blue solid lines) and $v = 1$ (red dashed lines) torsional states due to the almost-free internal rotation of the water molecule. Each transition appears as a doublet because the Doppler effect.

For this complex several R-branch *a*- and *b*-type transitions up to $J = 8$ were measured, being *b*-type transitions more intense in good agreement with the predicted dipole moment components (see Tables S6.1-S6.2). The rotational constants for each torsional state could be determined separately as shown in Table 6.3. The quartic centrifugal distortion constants and the quadrupole coupling tensor diagonal elements were constrained to have the same value for both states. The spectrum of the formanilide···$H_2{}^{18}O$ isotopologue was measured for this complex, showing doublets of the same magnitude as those observed for the parent molecule. The rotational constants for both torsional states were determined from a fit in which the quartic centrifugal distortion constants and the nuclear quadrupole coupling constants were fixed to the parent species values (see Table S6.7). The frequencies for the measured transitions for the parent and the $^{18}O_w$ isotopologue for the *trans*-fa-w-c complex are collected in Tables S6.22-S6.23 respectively.

Table 6.3. Rotational parameters obtained from the analysis of the spectrum of the observed *trans*-fa-w-c complex, compared with *ab initio* (MP2/6-311++G(2d,p)).

Parameters[a]	experimental		*ab initio*
	$v = 0$	$v = 1$	
A /MHz	1608.09000(26)[b]	1607.55924(26)	1561.92
B /MHz	907.81842(11)	907.76796(11)	942.17
C /MHz	581.604742(46)	581.640188(46)	589.30
Δ_J /kHz	0.4732(12)		0.318
Δ_{JK} /kHz	5.711(18)		3.035
Δ_K /kHz	-2.6208(51)		-1.521
δ_J /kHz	0.21434(63)		0.143
δ_K /kHz	0.1124(65)		0.068
^{14}N 3/2(χ_{aa}) /MHz	3.0600(42)		3.244
^{14}N ¼(χ_{bb}-χ_{cc}) /MHz	1.16089(85)		1.187
N	274/46		
σ/kHz	1.3/1.3/1.3		
Derived Parameters			
P_a /uÅ^2	555.68112(11)	555.61823(11)	535.22
P_b /uÅ^2	313.25781(11)	313.26775(11)	322.38
P_c /uÅ^2	1.01502(11)	1.10885(11)	1.18

[a] A, B and C are the rotational constants. Δ_J, Δ_{JK}, Δ_K, δ_J and δ_K are the quartic centrifugal distortion constants. χ_{aa}, χ_{bb} and χ_{cc} are the quadrupole coupling tensor diagonal elements for ^{14}N atom. N is the number of quadrupole hyperfine components/rotational transitions fitted. σ is the rms deviations of the fit. P_α (α= a, b or c) are the planar moments of inertia, these are derived from the moments of inertia I_α as for example $P_c = (I_a+I_b-I_c)/2$. [b] Standard errors are given in parentheses in units of the last digit.

Cis-formanilide···$(H_2O)_2$ IIa

The spectrum of the *cis*-fa-w_2 complex did not show any tunneling splitting, but it presents the hfs due to the ^{14}N. R-branch *a*-type transitions up to J = 13 were observed for this complex. No *b*- or *c*-type transitions were observed in agreement with the low predicted values for the μ_b and μ_c dipole moment components (see Tables S6.3-S6.4). The rotational constants, the diagonal elements of the quadrupole coupling tensor and four quartic centrifugal distortion constants were determined as shown in Table 6.4. Δ_K quartic constant could not be determined due to the nature of the set of rotational transitions measured. The spectra of the species formed by single substitution of ^{18}O atom in the water molecules were detected. Their rotational constants were obtained by keeping the rest of the rotational parameters fixed to the values of the parent species. All the rotational parameters for the parent and the isotopologues are collected in Table S6.8. The frequencies for the measured transitions for the parent and the observed isotopologues are collected in Tables S6.24-S6.26 in the supplementary material.

Table 6.4. Rotational parameters obtained from the analysis of the spectrum of the observed *cis*-fa-w_2 complex, compared with *ab initio* (MP2/6-311++G(2d,p)).

Fitted Parameters[a]	experimental	*ab initio*
A /MHz	1992.9001(14)[b]	2007.09
B /MHz	494.434394(34)	496.02
C /MHz	405.007349(26)	408.56
Δ_J /kHz	0.058560(87)	0.051
Δ_{JK} /kHz	-0.4858(11)	-0.372
Δ_K /kHz	[0.]	2.175
δ_J /kHz	0.016610(57)	0.015
δ_K /kHz	0.1667(46)	0.221
^{14}N 3/2(χ_{aa}) /MHz	3.0130(72)	3.10
^{14}N ¼(χ_{bb}-χ_{cc}) /MHz	0.9797(23)	0.91
N	156/52	
σ /kHz	0.8	
Derived Parameters		
P_a /uÅ^2	1008.18632(21)	1002.02
P_b /uÅ^2	239.64043(21)	234.94
P_c /uÅ^2	13.94930(21)	16.85

[a] A, B and C are the rotational constants. Δ_J, Δ_{JK}, Δ_K, δ_J and δ_K are the quartic centrifugal distortion constants. χ_{aa}, χ_{bb} and χ_{cc} are the quadrupole coupling tensor diagonal elements for ^{14}N atom. N is the number of quadrupole hyperfine components fitted. σ is the rms deviations of the fit. P_α (α= a, b or c) are the planar moments of inertia, these are derived from the moments of inertia I_α as for example $P_c = (I_a+I_b-I_c)/2$. [b] Standard errors are given in parentheses in units of the last digit.

6.4 Structure

Cis-formanilide···(H_2O) Ia

The good agreement between the rotational parameters obtained experimentally and the predicted values (see Table 6.1) suggests that the structure of the *cis*-fa-w-a complex is reasonably well described by the calculations at both B3LYP-D3/6-311++G(d,p) and MP2/6-311++G(2d,p). The molecule of water interacts simultaneously with the amino and the carbonyl groups trough $O_w\cdots H_1$–N and O_w–$H_{w1}\cdots O_1$=C_1 hydrogen bonds closing a 6 members cycle (see Figure S6.1 for atom labeling). The inclusion of the water molecule in the structure seems not to alter significantly the angle between the amide and the phenyl ring planes in *cis*-formanilide in going from the monomer to the complex. This angle, defined as the dihedral angle $\angle C_1$–N–C_2–C_3, was reported to be 34.7 degrees for the monomer.[23] The B3LYP-D3/6-311++G(d,p) reproduces this value and predicts an angle of 34.1 for conformer *cis*-fa-w-a and 30.1 for conformer *cis*-fa-w-a'. In contrast the other methods tested predict values for this angle of around 40º.

The planar moment of inertia P_c, which gives the mass extension out of the *ab* inertial plane increases largely in passing from the *cis* monomer (3.900 uÅ^2) to the Ia complex (10.890 uÅ^2, see Table S6.9) indicating the non-planar structure of the monomer. The slight changes induced in P_c by the isotopic substitution of the atoms in the water molecule (see Table S6.5) indicate that these atoms are not far from the *ab* inertial plane. The predicted small value of the dihedral angle $\angle N–C_1–O_1–O_w$, indicates that the water oxygen atom lies nearly in the same plane as the heavy atoms of the amide group. The B3LYP-D3/6-311++G(d,p) level predict a value of P_c of 10.94 uÅ^2 and 11.85 uÅ^2 for conformers *cis*-fa-w-a and *cis*-fa-w-a' respectively, indicating that the observed form is *cis*-fa-w-a. The experimental value of P_c is reproduced at the MP2/6-311++G(2d,p) level by doing a partial optimization of the structure by fixing the $\angle C_1–N–C_2–C_3$ dihedral angle to 33.6º. This structure results in a good approach to the experimental rotational constants as shown in Table S6.5.

From the rotational constants obtained upon isotopic substitution, the coordinates of the water molecule in the complex can be derived and compared to the *ab initio* values (see Table S6.10). The substitution structure, r_s, gives the atomic coordinates for monosubstituted species in the molecular frame by solving the Kraitchman equations, based on the changes of the principal moments of inertia due to the substitution.[30] The sign of the coordinates are assigned from the *ab initio* structure and the uncertainty is calculated according to the Costain rule.[31] The r_s $O_w–H_{w1}$ and $O_w–H_{w2}$ distances derived differ from the expected values due to the poor determination of the *A* rotational constant for both deuterated species from the CP-FTMW spectra.

Alternatively a partial effective structure, r_0,[32] of the hydrogen bond parameters and the dihedral angle $\angle C_1–N–C_2–C_3$ was also determined from a least-squares fit of the rotational constants[33] for all the detected species by fixing the rest of molecular parameters to the *ab initio* MP2/6-311++G(2d,p) calculated values for the structure with $\angle C_1–N–C_2–C_3$ fixed to 33.6º. The r_0 structure obtained for the *cis*-fa-w-a complex is summarized in Figure 6.5 (see Table S6.10).

Trans-formanilide···(H_2O) Ib

This complex is expected to have a planar skeleton inheriting the planar structure of the *trans*-formamide monomer, the *ab initio* calculations confirm this result (see Table 6.2). The rotational constants, the quartic centrifugal distortion constants and the quadrupole coupling constants are reasonably well predicted at both B3LYP-D3/6-311++G(d,p) and MP2/6-311++G(2d,p). The experimental value for the P_c planar moment of inertia (0.636 uÅ^2) is higher than the predicted values (0.05 uÅ^2 and 0.3 uÅ^2, respectively). According to the experimental value the complex is practically planar with only the H_{w2} being out of the molecular plane (see Figure S6.1 for labeling) and contributing to the non-zero value of P_c. This is confirmed by the nearly unchanging value for P_c observed upon the isotopic substitution of both O_w and H_{w1} (see Table S6.6).

The r_s and r_0 coordinates for O_w and H_{w1} atoms in the *trans*-fa-w-b complex were obtained from the isotopic substitution. The values are collected and compared with the *ab initio* values in the Table S6.11 and Figure 6.5. Both atoms lie close to the *a* inertial axis, having *b* and *c* coordinates close to zero with a large uncertainty associated to the derived value. From the r_s and r_0 coordinates the $O_w–H_{w1}$ distance can be calculated. The values of both structures are in good agreement with the r_e theoretical structure and is a reasonable value for a O–H bond involved in a hydrogen bond.

Trans-formanilide···(H_2O) Ic

The equilibrium conformation of the *trans*-fa-w-c complex seems to have C_s symmetry. *Trans*-formanilide subunit is planar, water oxygen atom lies in the symmetry plane and the water hydrogen atoms are out of the plane in symmetrical positions. The only stabilizing interaction is an $O_w\cdots H_1$–N hydrogen bond in which the molecule of water acts as hydrogen acceptor (see Figure S6.1 for atom labeling). The *ab initio* predictions locate the water oxygen atom in a position in which it can establish a weak interaction with the closest hydrogen atom from the phenyl ring. The agreement between calculated and experimental rotational parameters for this complex is worse than for the monomers and the other complexes. This may be attributed to the fact that *ab initio* optimizations of the structure lead to a static picture of the complex which do not reflect the fact that water molecule in this complex is rotating with a low hindering barrier. The experimental values are expected values for the ground state which may have important torsional contributions.

The experimental P_c value (1.015 uÅ^2) suggests that the complex is, as predicted (1.18 uÅ^2), practically planar with only the two hydrogen atoms of the water out of the plane defined by the heavy atoms. This idea is reinforced by the P_c value for the $^{18}O_w$ isotopologue (0.994 uÅ^2, see Table S6.7), slightly smaller than the parent value indicating that oxygen atom may be affected by some vibrational in-plane contribution.

From the rotational constants of the $^{18}O_w$ isotopologue, the r_s and r_0 coordinates for the oxygen atom in the water molecule were obtained (see Table S6.12). The r_s confirms that this oxygen lies in the *ab* inertial plane (see Figure S6.1), having a 0 value for the *c* coordinate. A reasonable fit of the experimental rotational constants is obtained by fitting the $r(H_1\cdots O_w)$ distance and the $\angle$N-$H_1\cdots O_w$ angle. The results are shown in Table S6.12 and summarized in Figure 6.5.

Cis-formanilide···(H_2O)$_2$ IIa

The relatively good agreement between experimental and theoretical rotational parameters at the same levels as for the *cis*-fa-w-a complex, indicate that the structure of the *cis*-fa-w_2 complex is similar to the optimized geometry and its structure is equivalent to that of the f-w_2 complex of formamide.[16] The two molecules of water act as a bridge closing a sequential cycle with the amino and carbonyl groups in formanilide. The three molecules in the complex act simultaneously as hydrogen donor and hydrogen acceptor forming three hydrogen bonds, $O_{w2}\cdots H_1$–N, $C_1{=}O_1\cdots H_{w1}$–O_{w1}, and O_{w2}–$H_{w3}\cdots O_{w1}$ (see Figure S6.2 for atom labeling). *Ab initio* calculation confirms that the two oxygen atoms from the water molecules lie nearly in the plane of the amide group heavy atoms plane as indicated by the values of the dihedral angles N–C_1–O_1–O_{w1} and N–C_1–O_1–O_{w2} close to zero. The dihedral angle $\angle C_1$–N–C_2–C_3 is predicted at the B3LYP-D3/6-311++G(d,p) to have values of 34.1º and 32.0º for the *cis*-fa-w_2 and *cis*-fa-w_2' conformers with different orientations of the non-bonded oxygen atoms.

The experimental P_c moment of inertia of the *cis*-fa-w_2 complex is higher (13.949 uÅ^2) than that of the cis-fa-w-a complex (10.889 uÅ^2) (see Table S6.8) due to the addition of the second molecule of water in almost the plane of the amide group. The P_c values obtained by the isotopic substitution of the oxygen atom in both molecules of water reinforce this idea (see Table S6.8). The predicted values for P_c at the B3LYP-D3/6-311++G(d,p) level are of 13.37 and 15.66 for the *cis*-fa-w_2 and *cis*-fa-w_2' forms. The MP2/6-311++G(2d,p) level reproduces the experimental P_c value for a dihedral angle $\angle C_1$–N–C_2–C_3 of 33.3º (see Table S6.8).

The r_s coordinates for the two oxygen atoms in both water molecules in *cis*-fa-w_2 are collected and compared with the *ab initio* and r_0 values in Table S6.13. The oxygen atoms lie almost in the *ab* inertial plane, therefore, their *c* coordinates are close to zero. From the r_s coordinates, the distance between the two atoms of oxygen can be derived. This distance is in good agreement with the *ab initio* value and is in the same order as similar microsolvated complexes involving a hydrogen bond between two molecules of water.[16,34] A partial r_0 structure has been investigated by fitting some of the hydrogen bond parameters and the dihedral angle $\angle C_1–N–C_2–C_3$ to the experimental rotational constants. The rest of molecular parameters were fixed to the MP2-6-311++G(2d,p) parameters obtained from the optimization with fixed dihedral angle $\angle C_1–N–C_2–C_3$ at 33.3º. The results are given in Table S6.13 and summarized in Figure 6.5.

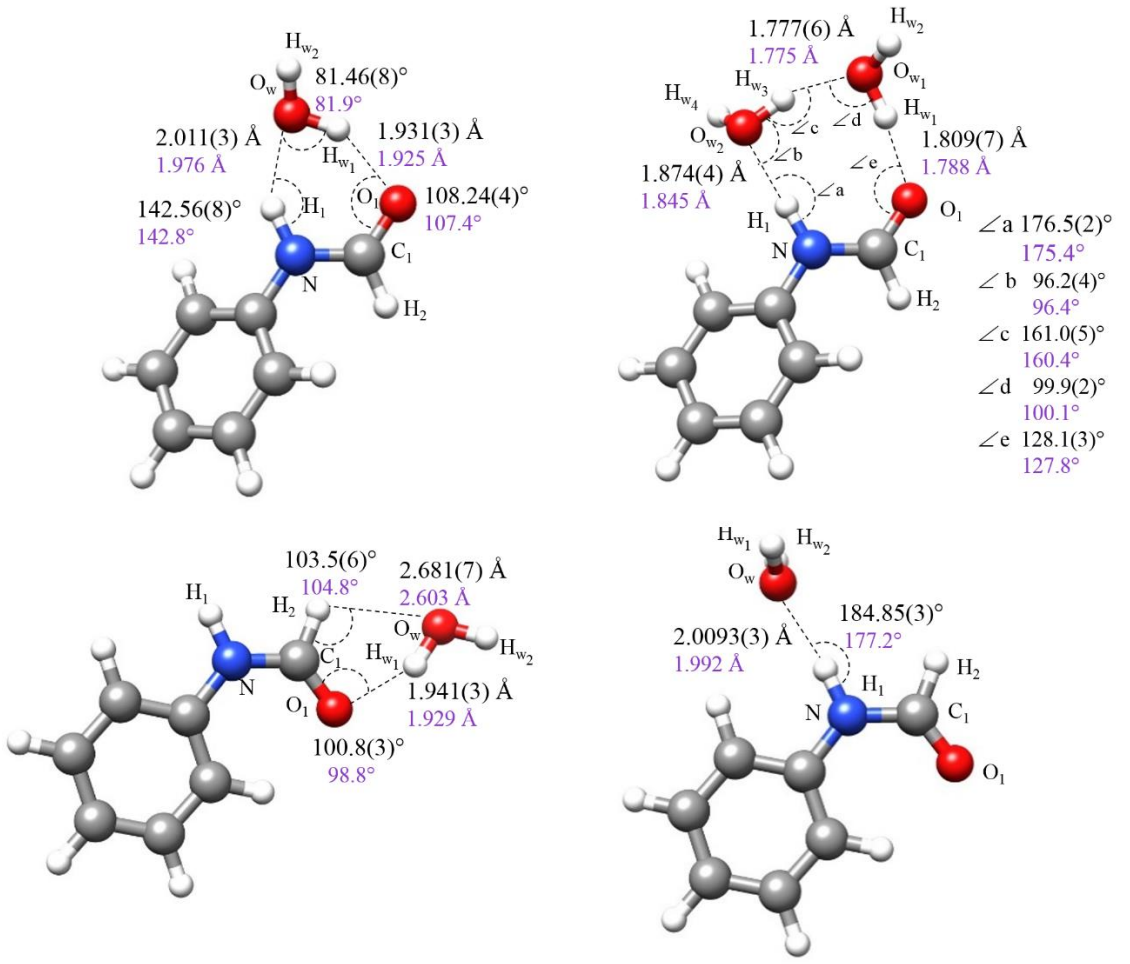

Figure 6.5. Experimental r_0 hydrogen bond lengths and angles for the observed microsolvates of formanilide compared to the ab initio predictions.

Table 6.5. Values of the $C_1–N–C_2–C_3$ dihedral angle (see Figures S6.1-S6.2 for atom labeling) determined from r_0 structure when passing from isolated formanilide to the complexes with one molecule and two molecules of water.

	Cis monomer.[23]	*Cis*-fa-w-a	*Cis*-fa-w_2
τ $C_1–N–C_2–C_3$ /°	34.7	33.5(1)	32.73(9)

6.5 Internal Dynamics

In all the observed complexes, the formanilide subunit keeps the same planar (*trans*) or non-planar (*cis*) forms observed for the monomer.[23] Both detected *cis*-formanilide complexes inherit the non-planar configuration of the formanilide subunit observed in bare *cis*-formanilide. As shown in Table 6.5 the experimental value of the dihedral angle ∠C_1–N–C_2–C_3 between the phenyl and formamide planes seem to steadily decrease from the monomer to the 1:1 and 1:2 hydrates in steps of *ca.* 1º. This behavior is in good agreement with theoretical calculations at different levels which predict very small changes values for the equilibrium dihedral angle for the *cis* monomer and its complexes.

In the same context, the tunneling splittings observed for the *cis*-formanilide (*cis*-fa) monomer in the microwave spectrum reveal the existence of two non-planar equivalent conformers with a barrier of 152 cm^{-1} at the planar *cis*-fa form, estimated from a flexible one-dimensional model of the ∠C_1–N–C_2–C_3 torsion.[23] For the 1:1 complex, closely spaced doublets in the limit of the MB-FTMW resolution were observed, while for the 1:2 complex no doublets were observed. These small doublets are also related to the existence of two equivalent non-planar conformers of *cis*-fa-w-a (see Figure S6.3). However the mechanism of interconversion cannot be treated with a one-dimensional model of the ∠C_1–N–C_2–C_3 torsion as shown in Figure 6.6 where the predicted (B3LYP-D3/6-311++G(d,p)) potential energy function for the monomer and the complex are compared. Theoretical calculations predict only small changes on the barriers to ∠C_1–N–C_2–C_3 torsion at 0º and 90º but the minima around the planar *cis*-formanilide form are not equivalent. Another motion, the flipping motion of water interconvert the *cis*-fa-w-a and *cis*-fa-w-a' forms which are in turn non-equivalent. In fact the interconversion between the equivalent w-a forms of the complexes would involve a concerted motion of the torsion and the flipping motion of water which may result in higher barriers. The decrease in the torsional splitting observed for *cis*-fa-w-a with respect to *cis*-fa can then be attributed to the barrier increment to 163 cm^{-1} together with the increased reduced mass due to the presence of water in the rotating group.

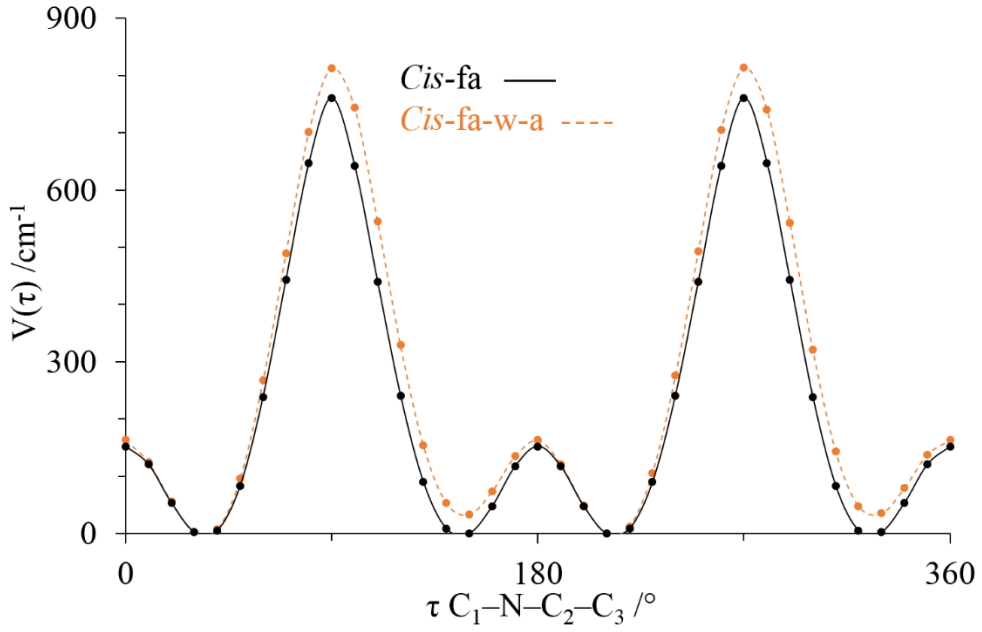

Figure 6.6. Periodic potential function for the C_1–N–C_2–C_3 torsion of *cis*-fa monomer and *cis*-fa-w-a complex calculated at the B3LYP-D3/6-311++G(d,p) level of theory.

The observation of doublets in the spectrum of *trans*-fa-w-c form should be also discussed. The fact that the observed doublets show statistical weight spin effects due to the exchange of two hydrogen atoms reveals that the associated tunneling motion is related to the internal rotation of the H_2O molecule around its local C_2 axis. *Ab initio* calculations (B3LYP-D3/6-311++G(d,p)) along the water rotation angle reveal a twofold periodical potential energy function with a barrier of 311 cm^{-1} at the planar configuration were H···H repulsive interactions may take place (see Figure 6.7). The same dynamics were observed for the related complex formamide-w-c[16] with an identical environment and a barrier of 117 cm^{-1} to planarity and in indole···H_2O[35] with a barrier of 182 cm^{-1}.

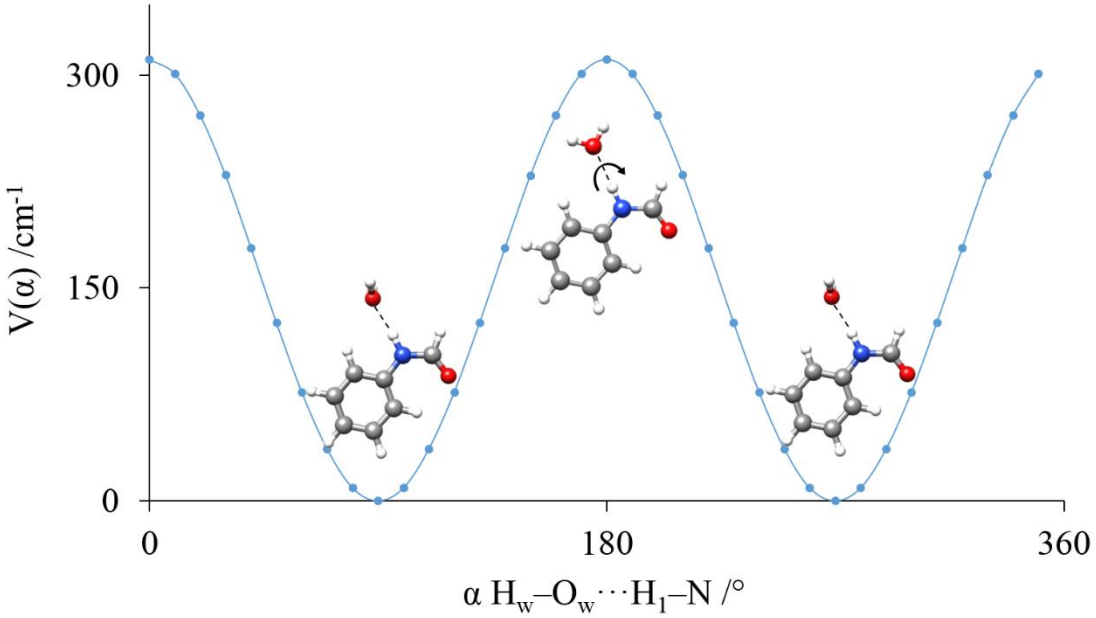

Figure 6.7. Periodic potential function for the internal rotation of water molecule in the *trans*-fa-w-c complex calculated at the B3LYP-D3/6-311++G(d,p) level of theory.

6.6 Discussion

The way in which water interacts with the amide group is very different for the *cis* and *trans* forms of formanilide. In the *cis* configuration the hydrogen bond donor (N-H) and hydrogen bond acceptor (C=O) sites may interact simultaneously with one or several water molecules forming sequential cycles as those observed for *cis*-fa-w-a and *cis*-fa-w_2. However for the *trans* form, which models the *trans*-peptide arrangement, the donor (N-H) an acceptor (C=O) sites are pointing in opposite sides of the amide chain so water cannot interact with both simultaneously as occur for the *cis* form. In this way we have observed two different complexes. The *trans*-fa-w-b complex is formed through an O-H···O=C hydrogen bond with water further stabilized by a weak C-H···O contact. The second complex, *trans*-fa-w-c, is formed by a N-H···O hydrogen bond but water do not establishes any other contact and thus is able to rotate around the hydrogen bond axis exchanging the hydrogen atoms as the statistical spin weight effects observed on its microwave spectrum splittings show. These are important results concerning the way in which water may interact with *cis* or *trans* peptide groups. In the *cis* form water satisfies its proton donor/acceptor potential and forms sequential cycles reinforced by cooperativity. In the *trans* form which dominates largely in proteins and peptides, water establishes either N-

H···O or O-H···O=C bonds but cannot completely satisfy the multiple donor/acceptor capacity since it is in an hydrophobic environment.

The r_0 structures observed are comparable to those of similar microsolvated complexes modelling the peptide group like formamide,[16] *trans*-N-methyl formamide,[5] 2-pyridone[7] or azetidinone.[36] As shown in Tables S6.10-6.13 they compare very well with the microsolvated complexes of the reference molecule formamide, which as formanilide, covers all possible interactions observable between water and the *cis* or *trans* forms of peptide group. In all cases, the formamide group and the interacting water atoms are nearly coplanar as found in other systems. The hydrogen bond distances, which are related to the strength of the interactions, reveal interesting details. In the *cis*-formanilide complexes, particularly in the *cis*-fa-w-a complex, where there is a competition between the C=O··H-O and N-H···O interactions, the distances show that the dominant interaction is the C=O··H-O one. The same can be said if we compare the corresponding distances between the *trans*-formanilide complexes. This is in good agreement with the preference of water to interact with the carbonyl group observed in globular proteins.[3]

The signatures of σ-bond cooperativity[2] can be seen in the shorter hydrogen bond distances observed in the *cis*-fa-w_2 with respect to *cis*-fa-w-a. These distances have been observed to decrease as the number of water molecules, as an important characteristic of sequential cycles. A second signature of this kind of cooperativity can be obtained by analyzing the dissociation energies per hydrogen bond of the *cis*-formanilide complexes. If we consider the dissociation energies per bond,[37] 33.2 kJ/mol for *cis*-fa-w_2 and 23.2 kJ/mol for *cis*-fa-w-a, indicating the reinforcement of the hydrogen bond interactions when increasing the number of cooperative interactions. These dissociation energies (see Table 6.6) indicate, on the other hand, that the *cis*-formanilide complexes, formed by sequential cycles reinforced by cooperativity, are more stable than the *trans*-formanilide complexes.

Table 6.6. Dissociation energies for the observed complexes of formanilide.

D_E /kJmol^{-1}	B3LYP-D3 6-311++G(d,p)	MP2 6-311++G(2d,p)
cis-fa-w-a	46.4	35.3
cis-fa-w_2	99.6	75.9
trans-fa-w-b	30.3	23.0
trans-fa-w-c	28.8	24.0

Resonance assisted hydrogen bonding or π-cooperativity polarizes the amide group π-electron distribution and causes the C=O bond enlargement and C-N bond shortening. This effect, first pointed out to occur in chains of small amides[38] has been detected only in few cases in gas phase complexes. We have recently shown for the series of formamide-water complexes[17,34] that the ^{14}N quadrupole coupling constants can be taken as a probe for this effect since it gives information about the electronic environment around the N atom. In particular the planarity of formamide-water complexes has allowed finding that the steady variation of the χ_{cc} constant when increasing the number of interacting water molecules can be taken as a signature of π-cooperativity effects. The variation of the χ_{cc} constant show linear correlation with the C=O and C-N distances as well as with the unbalanced correlation between $2p_z$ electronic charge obtained from NBO calculations.[39] This suggests that the electron density associated with the population of the N atom lone pair depletes along the series of complexes when increasing the number of

interacting molecules. The predicted changes (MP2/6-311++G(2d,p)) in the C_1=O_1 and C_1-N distances for the complexes of formanilide are given in Table 6.7. The non-planarity of *cis*-formanilide does not allow us to take the experimental values of χ_{cc} as equal to χ_{zz} the principal quadrupole coupling axis constants. However we have considered the *ab initio* quadrupole coupling tensor which reasonably reproduces the experimental data for the *cis*-formanilide complexes. The diagonalized χ_{zz} values for the monomer and the 1:1 and 1:2 hydrated complexes show practically the same trends as observed for formamide-water complexes as can be seen in Table 6.7. In the case of the *trans*-formanilide complexes the planarity of the formanilide subunit allows us to assume χ_{cc}=χ_{zz}. The changes in this constant from the monomer to the complexes also compares very well with those observed for the corresponding complexes for the reference molecule formamide. This allows us to conclude that resonance assisted hydrogen bond inductive effects occurs also in the formanilide microsolvates to the same extent that in formamide microsolvates. One may wonder also if these effects have some influence in the potential energy function of the $\angle C_1$–N–C_2–C_3 torsion of *cis*-formanilide and on the small changes in the corresponding equilibrium angles (see Table 6.5).

Table 6.7. Experimental and *ab initio* (MP2/6-311++G(2d,p)) quadrupole coupling constants for *cis* and *trans*-formanilide and their complexes, together with the values of the unbalanced $2p_z$ electronic charge ($(U_p)_z$) obtained by a Natural Bond Orbital Analysis and the distances C_1=O_1 and C_1-N.

Exp.	*Cis*-fa	*Cis*-fa-w-a	*Cis*-fa-w_2	*Trans*-fa	*Trans*-fa-w-b	*Trans*-fa-w-c
χ_{aa} /MHz	2.173(53)	2.1433(61)	2.0087(48)	1.9267(40)	1.868(11)	2.0400(28)
χ_{bb} /MHz	0.593(87)	0.905(16)	0.9551(70)	1.7447(60)	1.697(14)	1.3018(31)
χ_{cc} /MHz	-2.767(87)	-3.049(16)	-2.9637(70)	-3.6713(60)	-3.565(14)	-3.3418(31)
χ_{cc}/eQq_{210}	0.2767	0.3049	0.29637	0.36713	0.3565	0.33418
ab initio						
χ_{aa} /MHz	2.26	2.21	2.07	1.81	1.90	2.07
χ_{bb} /MHz	0.48	0.78	0.83	1.76	1.71	1.24
χ_{cc} /MHz	-2.74	-2.99	-2.90	-3.57	-3.60	-3.31
χ_{xx} /MHz	2.31	2.31	2.31	2.14	2.09	2.18
χ_{yy} /MHz	1.10	1.10	0.81	1.60	1.52	1.13
χ_{zz} /MHz	-4.00	-3.41	-3.12	-3.74	-3.61	-3.31
χ_{zz}/eQq_{210}	0.400	0.341	0.312	0.374	0.361	0.331
$-(U_p)_z$ NBO	0.219	0.238	0.236	0.319	0.306	0.286
C_1=O_1	1.219	1.230	1.233	1.230	1.227	1.222
C_1-N	1.370	1.357	1.350	1.376	1.361	1.365

6.7 Conclusions

From the analysis of the spectrum of microsolvated formanilide, three complexes with one molecule of water and one complex with two molecules of water were characterized. In the most stable monohydrated complex, water and *cis*-formanilide form a 6-membered cycle through $O_w\cdots H–N$ and $O_w–H_w\cdots O=C$ hydrogen bonds. Water molecule interacts simultaneously with the amino and carbonyl groups. In the higher energy complexes between *trans*-formanilide with one molecule of water, one stabilizing hydrogen bond is formed with either the amino or the carbonyl group. The calculated as the most stable complex with two molecules of water is formed with *cis*-formanilide, and although it was predicted before, this is the first experimental report of such complex. *Cis*-fa-w_2 is stabilized by three $O_w\cdots H–N$, $C=O\cdots H_w–O_w$, and $O_w–H_w\cdots O_w$ hydrogen bonds closing an 8 members cycle. The observation of species occurring upon monoisotopic substitution of the oxygen or the hydrogen atoms from water, allowed determining accurately its position in the molecular frame. The inclusion of one or two molecules of water seems not to alter essentially the structure of *cis* or *trans* formanilide as reflected by the almost constant value of the $C_1–N–C_2–C_3$ dihedral angle from isolation to microsolvation in the observed complexes. This work illustrates the preferred interactions sites of water with formanilide and the stabilization interactions established for the different complexes formed. Thus, it complements previous studies about microsolvation of formanilide[19,20] and the amide moiety in general,[15-18] and provides further models to understand the solvation of the peptide bond.

References

[1] Saenger, W., Jeffrey, G. A. *Hydrogen Bonding in Biological Structures*, Springer-Verlag, Berlin 1991.
[2] Jeffrey, G. A. *An Introduction to Hydrogen Bonding*, Oxford University Press, Oxford, 1997.
[3] Baker, E. N., Hubbard, R. E. "Hydrogen bonding in globular proteins" *Prog. Biophys. Mol. Biol.*, **1984**, 44, 97–179.
[4] Schmitt, M., Böhm, M., Ratzer, C., Vu, C., Kalkman, I., Meerts, W. L. "Structural Selection by Microsolvation: Conformational Locking of Tryptamine" *J. Am. Chem. Soc.*, **2005**, 127, 10356–10364.
[5] Caminati, W., López, J. C., Blanco, S., Mata, S., Alonso, J. L. "How Water Links to *Cis* and *Trans* Peptidic Groups: The Rotational Spectrum of N-Methylformamide-Water" *Phys. Chem. Chem. Phys.*, **2010**, 12, 10230–10234.
[6] Maris, A., Ottaviani P., Caminati, W. "Pure Rotational Spectrum of 2-Pyridone···Water and Quantum Chemical Calculations on the Tautomeric Equilibrium 2-Pyridone···Water/2-Hydroxypyridine···Water" *Chem. Phys. Lett.*, **2002**, 360, 155–160.
[7] Mata, S., Cortijo, V., Caminati, W., Alonso, J. L., Sanz, M. E., López, J. L., Blanco, S. "Tautomerism and Microsolvation in 2-Hydroxypyridine/2-Pyridone" *J. Phys. Chem. A*, **2010**, 114, 11393–11398.
[8] Levy, Y., Onuchic, J. N. "Water Mediation in Protein Folding and Molecular Recognition" *Annu. Rev. Biophys. Biomol. Struct.*, **2006**, 35, 389–415.
[9] Ball, P. "Water as an Active Constituent in Cell Biology" *Chem. Rev.*, **2008**, 108, 74–108.
[10] Dopfer, O., Fujii, M. "Probing Solvation Dynamics around Aromatic and Biological Molecules at the Single-Molecular Level" *Chem. Rev.*, **2016**, 116, 5432–5463.
[11] Becucci, M., Melandri, S. "High-Resolution Spectroscopic Studies of Complexes Formed by Medium-Size Organic Molecules" *Chem. Rev.*, **2016**, 116, 5014–5037.
[12] Pérez, C., Muckle, M. T., Zaleski, D. P., Seifert, N. A., Temelso, B., Shields, G. C., Kisiel, Z., Pate, B. H. "Structures of Cage, Prism, and Book Isomers of Water Hexamer from Broadband Rotational Spectroscopy" *Science*, **2012**, 336, 897–901.
[13] Pérez, C., López, J. C., Blanco, S., Schnell, M. "Water-Induced Structural Changes in Crown Ethers from Broadband Rotational Spectroscopy" *J. Phys. Chem. Lett.*, **2016**, 7, 4053–4058.
[14] Pérez, C., Krin, A., Steber, A. L., López, J. C., Kisiel, Z., Schnell, M. "Wetting Camphor: Multi-Isotopic Substitution Identifies the Complementary Roles of Hydrogen Bonding and Dispersive Forces" *J. Phys. Chem. Lett.*, **2016**, 7, 154–160.
[15] Lovas, F. J., Suenram, R. D., Fraser, G. T., Gillies, C. W., Zozom, J. "The Microwave Spectrum of Formamide-Water and Formamide-Methanol Complexes" *J. Chem. Phys.*, **1988**, 88, 722–729.
[16] Blanco, S., López, J. C., Lesarri, A., Alonso, J. L. "Microsolvation of Formamide: A Rotational Study" *J. Am. Chem. Soc.*, **2006**, 128, 12111–12121.
[17] Blanco, S., Pinacho, P., López, J. C. "Hydrogen-Bond Cooperativity in Formamide$_2$-Water: A Model for Water Mediated Interactions" *Angew. Chem. Int. Ed.*, **2016**, 128, 9477–9481. Chapter IV within this Thesis.
[18] Held, A., Pratt, D. W. "Hydrogen Bonding in Water Complexes. Structures of 2-Pyridone-H_2O and 2-Pyridone-$(H_2O)_2$ in Their S_0 and S_1 Electronic States" *J. Am. Chem. Soc.*, **1993**, 115, 9708–9717.
[19] Dickinson, J. A., Hockridge, M. R., Robertson, E. G., Simons, J. P. "Molecular and Supramolecular Structures of N-Phenyl Formamide and its Hydrated Clusters" *J. Phys. Chem. A*, **1999**, 103, 6938-6949.
[20] Fedorov, A. V., Cable, J. R. "Spectroscopy of Hydrogen-Bonded Formanilide Clusters in a Supersonic Jet: Solvation of a Model *Trans* Amide" *J. Phys. Chem. A*, **2000**, 104, 4943-4952.
[21] Manea, V. P., Wilson, K. J., Cable, J. R. "Conformations and Relative Stabilities of the *Cis* and *Trans* Isomers in a Series of isolated N-Phenylamides" *J. Am. Chem. Soc.*, **1997**, 119, 2033-2039.
[22] Ottaviani, P., Melandri, S., Maris, A., Favero, P. G., Caminati, W. "Free-jet Rotational Spectrum and *Ab Initio* Calculations of Formanilide" *J. Mol. Spectrosc.*, **2001**, 205, 173-176.
[23] Blanco, S., López, J. C., Lesarri, A., Caminati, W., Alonso, J. L. "Conformational Equilibrium of Formanilide: Detection of the Pure Rotational Spectrum of the Tunnelling *Cis* Conformer" *Mol. Phys.*, **2005**, 103, 1473-1479.
[24] Brown, G. G., Dian, B. C., Douglass, K. O., Geyer, S. M., Pate, B. H. "The Rotational Spectrum of Epifluorohydrin Measured by Chirped-Pulse Fourier Transform Microwave Spectroscopy" *J. Mol. Spectrosc.*, **2006**, 238, 200–212.
[25] Brown, G. G., Dian, B. C., Douglass, K. O., Geyer, S. M., Shipman, S. T., Pate, B. H. "A Broadband Fourier Transform Microwave Spectrometer Based on Chirped Pulse Excitation" *Rev. Sci. Instrum.*, **2008**, 79, 053103.

[26] Alonso, J. L., Lorenzo, F. J., López, J. C., Lesarri, A., Mata, S., Dreizler, H. "Construction of a Molecular Beam Fourier Transform Microwave Spectrometer Used to Study the 2,5-Dihydrofuran-Argon Van Der Waals Complex" *Chem. Phys.*, **1997**, 218, 267–275.
[27] Gaussian 09, Revision D.01, Frisch M. J., Trucks G. W., Schlegel H. B., Scuseria G. E., Robb M. A., Cheeseman J. R., Scalmani G., Barone V., Petersson G. A., Nakatsuji H., Li X., Caricato M., Marenich A., Bloino J., Janesko B. G., Gomperts R., Mennucci B., Hratchian H. P., Ortiz J. V., Izmaylov A. F., Sonnenberg J. L., Williams-Young D., Ding F., Lipparini F., Egidi F., Goings J., Peng B., Petrone A., Henderson T., Ranasinghe D., Zakrzewski V. G., Gao J., Rega N., Zheng G., Liang W., Hada M., Ehara M., Toyota K., Fukuda R., Hasegawa J., Ishida M., Nakajima T., Honda Y., Kitao O., Nakai H., Vreven T., Throssell K., Montgomery, Jr. J. A., Peralta J. E., Ogliaro F., Bearpark M., Heyd J. J., Brothers E., Kudin K. N., Staroverov V. N., Keith T., Kobayashi R., Normand J., Raghavachari K., Rendell A., Burant J. C., Iyengar S. S., Tomasi J., Cossi M., Millam J. M., Klene M., Adamo C., Cammi R., Ochterski J. W., Martin R. L., Morokuma K., Farkas O., Foresman J. B., Fox D. J., *Gaussian, Inc., Wallingford CT*, 2016.
[28] Pickett, H. M. "The Fitting and Prediction of Vibrational-Rotation Spectra with Spin Interaction" *J. Mol. Spectrosc.*, **1991**, 148, 371–377.
[29] Gordy, W., Cook, R. L. *Microwave Molecular Spectra* Wiley-Interscience, New York, 1984.
[30] Kraitchman, J. "Determination of Molecular Structure from Microwave Spectroscopic Data" *Am. J. Phys.*, **1953**, 21, 17–24.
[31] Costain, C. C. "Further Comments on the Accuracy of r_s Substitution Structures" *Trans. Am. Crystallogr. Assoc.*, **1966**, 2, 157–164.
[32] Rudolph, H. D. "Contribution to the Systematics of r_0-Derived Molecular Structure Determinations from Rotational Parameters" *Struct. Chem.*, **1991**, **2**, 581–588.
[33] Kisiel, Z. "Least-Squares Mass-Dependence Molecular Structures for Selected Weakly Bound Intermolecular Clusters" *J. Mol. Spectrosc.*, **2003**, 218, 58–67.
[34] Blanco, S., Pinacho, P., López, J. C. "Structure and Dynamics in Formamide-$(H_2O)_3$: A Water Pentamer Analogue" *J. Phys. Chem. Lett.*, **2017**, 8, 6060–6066. Chapter V within this Thesis.
[35] Blanco, S., López, J. C., Alonso, J. L., Ottaviani, P., Caminati, W., "Pure Rotational Spectrum and Model Calculations of Indole-Water" *J. Chem. Phys.*, **2003**, 119, 880–886.
[36] López, J. C., Sanchez, R., Blanco, S., Alonso, J. L. "Microsolvation of 2-Azetidinone: A Model for the Peptide Group-Water Interactions" *Phys. Chem. Chem. Phys.*, **2015**, 17, 2054–2066.
[37] a) Boys, S., Bernardi, F. "The Calculation of Small Molecular Interactions by the Differences of Spearate Total Energies. Some Procedures with Reduced Errors" *Mol. Phys.*, **1970**, *19*, 553–566. b) Xantheas, S. S. "On the Importance of the Fragment Relaxation Energy Terms in the Estimation of the Basis Set Superposition Error Correction to the Intermolecular Interaction Energy" *J. Chem. Phys.*, **1996**, *21*, 8821–8824.
[38] Ottersen, T. "On the Structure of the Peptide Linkage. The Structures of Formamide and Acetamide at -165 Degrees C and an *Ab Initio* Study of Formamide, Acetamide and N-methylformamide" *Acta Chemica Scandinavica*., **1975**, *29a*, 939–944.
[39] Reed, A. E., Weinstock, R. B., Weinhold, F. "Natural Population Analysis" *J. Chem. Phys.*, **1985**, *83*, 735-746.

Supplementary material for Chapter VI

Microsolvation of Formanilide Conformers: A Model For Peptide Solvation.

Manuscript in preparation.

Abstract

Microsolvated complexes of formanilide with different degrees of hydration have been generated in a supersonic expansion and characterized by Fourier transform microwave spectroscopy. Three 1:1 microsolvated complexes have been observed for both *cis* and *trans* configurations of formanilide in agreement with previous studies. The lowest energy 1:2 microsolvated complex of *cis*-formanilide has been detected. In both mono and dihydrated *cis*-formanilide complexes, water closes sequential cycles of 6 and 8 members respectively, trough simultaneous hydrogen bonds with the amino and the carbonyl groups. Furthermore *cis*-formanilide has almost the same non planar configuration observed in the monomer. In the higher energy monohydrated complexes detected with *trans*-formanilide, a planar skeleton is determined with water interacting solely with either the amino or the carbonyl group. For all species the spectra of parent and several water isotopologues have been observed, allowing us to precisely locate the position of water.

- **Figure S6.1.** Observed *cis* and *trans* formanilide complexes with one molecule of water.

- **Figure S6.2.** Observed *cis* and *trans* formanilide complexes with two molecules of water.

- **Figure S6.3.** Predicted *cis*-fa-w-a and *cis*-fa-w-a' complexes.

- **Figure S6.4.** Predicted *cis*-fa-w2 and *cis*-fa-w2' complexes.

- **Table S6.1.** *Ab initio* rotational parameters (B3LYP-D3/6-311++G(d,p)) for *cis* and *trans* formanilide complexes with one molecule of water.

- **Table S6.2.** *Ab initio* rotational parameters (MP2/6-311++G(2d,p)) for *cis* and *trans* formanilide complexes with one molecule of water.

- **Table S6.3.** *Ab initio* rotational parameters (B3LYP-D3/6-311++G(d,p)) for *cis* and *trans* formanilide complexes with two molecules of water.

- **Table S6.4.** *Ab initio* rotational parameters (MP2/6-311++G(2d,p)) for *cis* and *trans* formanilide complexes with two molecules of water.

- **Table S6.5.** Observed rotational parameters for the *cis*-fa-w-a complex for the parent and the observed isotopologues.

- **Table S6.6.** Observed rotational parameters for the *trans*-fa-w-b complex for the parent and the observed isotopologues.

- **Table S6.7.** Observed rotational parameters for the *trans*-fa-w-c complex for the parent and the observed isotopologue.

- **Table S6.8.** Observed rotational parameters for the *cis*-fa-w_2 complex for the parent and the $^{18}O_w$ isotopologues.

- **Table S6.9.** Comparison of the planar moments of inertia of *cis* and *trans* formanilide and their complexes.

- **Table S6.10.** r_0 , r_s and r_e structures for the *cis*-fa-w-a complex.

- **Table S6.11.** r_0 , r_s and r_e structures for the *trans*-fa-w-b complex.

- **Table S6.12.** r_0 , r_s and r_e structures for the *trans*-fa-w-c complex.

- **Table S6.13.** r_0 , r_s and r_e structures for the *cis*-fa-w_2 complex.

- **Table S6.14-S6.18.** Observed transition frequencies for the *cis*-fa-w-a complex for the parent and the observed isotopologues.

- **Table S6.19-S6.21.** Observed transition frequencies for the *trans*-fa-w-b complex for the parent and the observed isotopologues.

- **Table S6.22-S6.23.** Observed transition frequencies for the *trans*-fa-w-b complex for the parent and the observed isotopologue.

- **Table S6.24-S6.26.** Observed transition frequencies for the *trans*-fa-w-b complex for the parent and the observed isotopologues.

Figure S6.1. Observed *cis* and *trans* formanilide complexes with one molecule of water showing atom labeling and the inertial axes *a* (red), *b* (blue) and *c* (green).

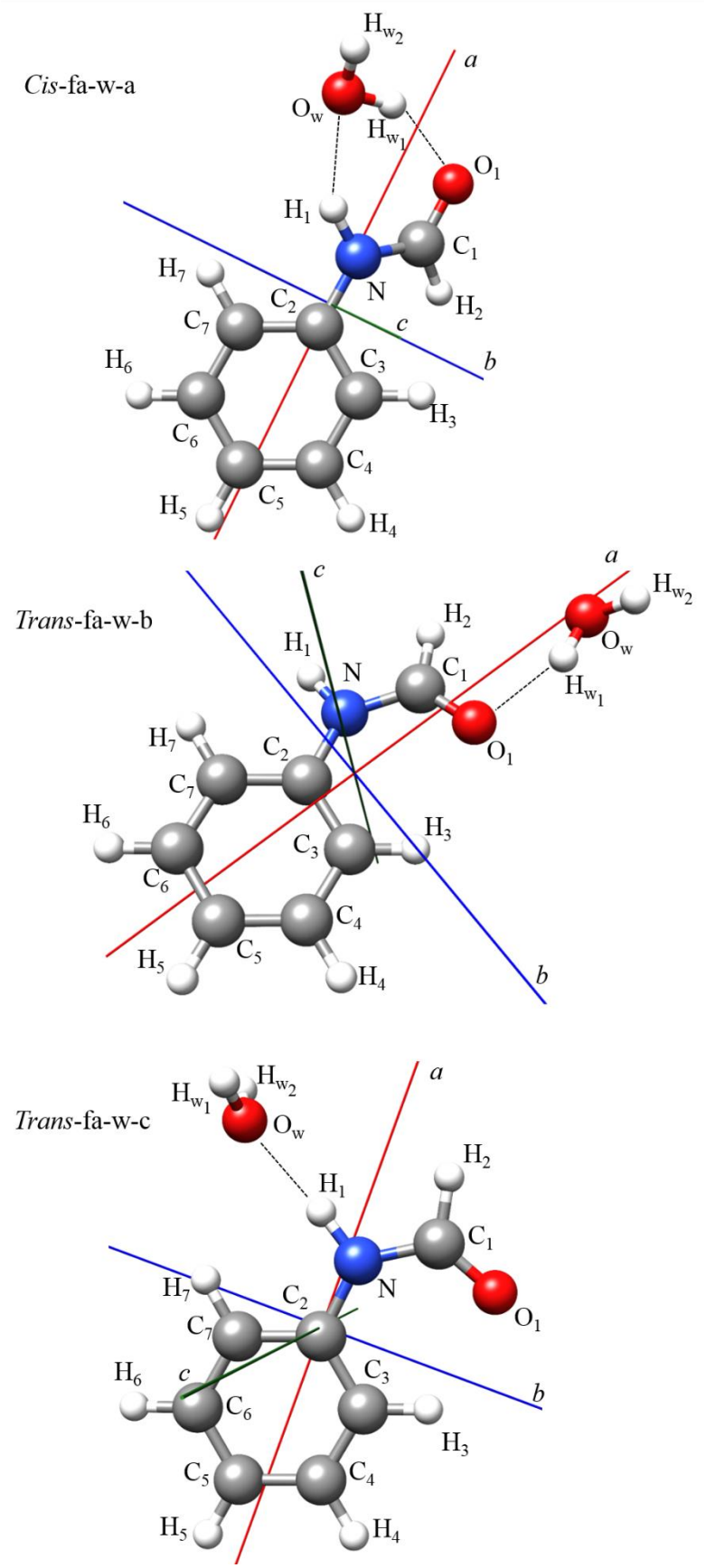

Figure S6.2. Observed *cis*-formanilide complex with two molecules of water showing atom labeling and the inertial axes *a* (red), *b* (blue) and *c* (green).

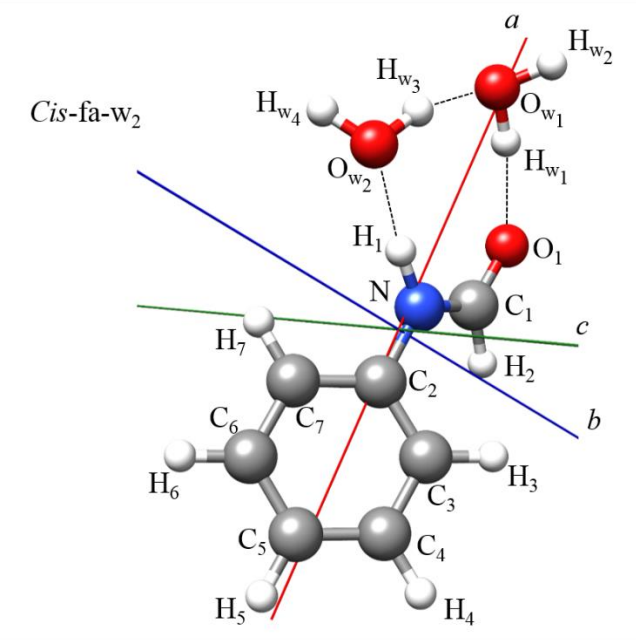

Figure S6.3. Predicted *cis*-fa-w-a and *cis*-fa-w-a' complexes showing the different equivalent forms.

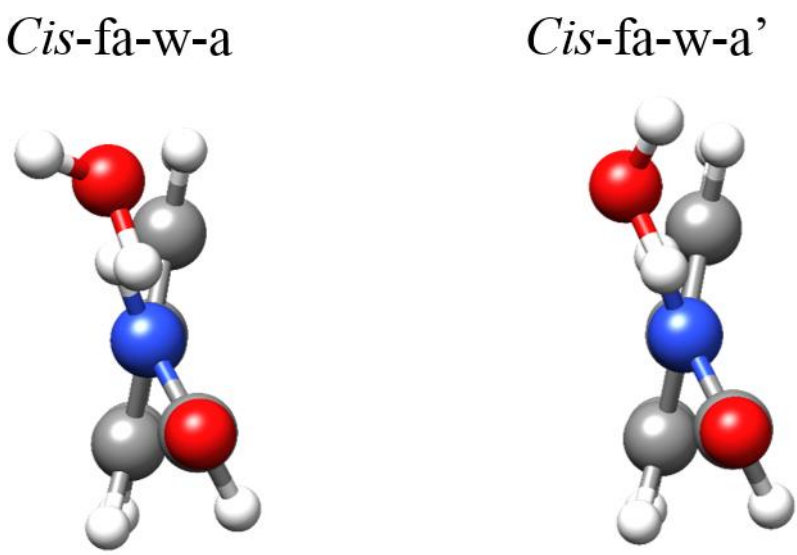

Figure S6.4. Predicted *cis*-fa-w2 and *cis*-fa-w2' complexes showing the different equivalent forms.

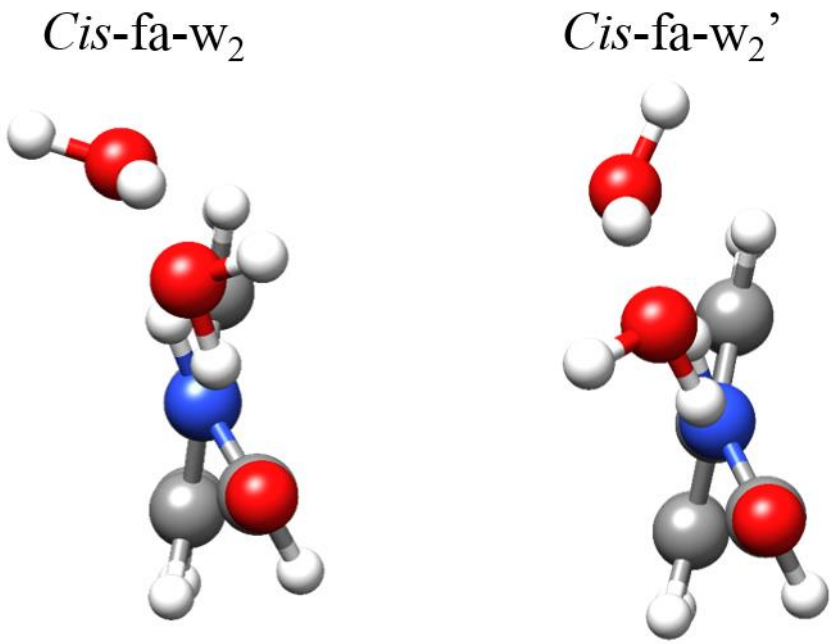

Table S6.1. *Ab initio* rotational parameters calculated at B3LYP-D3/6-311++G(d,p) level of theory for the *cis*-formanilide (*cis*-fa) and *trans*-formanilide (*trans*-fa) complexes with one molecule of water.

Parameter[a]	*Cis*-fa-w-a	*Cis*-fa-w-a'	*Cis*-fa-w-b	*Trans*-fa-w-a	*Trans*-fa-w-b	*Trans*-fa-w-c
A /MHz	2831.32	2839.04	3036.62	1870.86	4122.42	1562.54
B /MHz	663.09	660.98	555.65	866.31	538.12	948.66
C /MHz	550.06	549.98	479.17	593.41	476.03	591.93
P_a /uÅ^2	751.21	752.74	898.90	582.45	939.11	531.53
P_b /uÅ^2	167.56	166.16	155.80	269.21	122.55	322.24
P_c /uÅ^2	10.94	11.85	10.63	0.92	0.05	1.19
Δ_J /kHz	0.038	0.039	0.128	0.160	0.025	0.311
Δ_{JK} /kHz	-0.024	-0.002	-1.602	-0.216	0.483	-1.462
Δ_K /kHz	1.759	1.717	11.108	1.168	2.229	2.901
δ_J /kHz	0.009	0.009	0.028	0.059	0.003	0.141
δ_K /kHz	0.384	0.445	0.656	0.341	0.272	0.078
μ_a /D	2.35	-2.34	-3.36	-2.02	-2.77	2.55
μ_b /D	0.30	0.76	1.01	3.77	1.47	5.80
μ_c /D	-1.11	-0.93	-0.42	0.84	0.39	0.00
^{14}N χ_{aa} /MHz	2.29	2.28	2.14	1.84	1.98	2.18
^{14}N χ_{bb} /MHz	0.93	1.01	1.53	1.99	1.90	1.36
^{14}N χ_{cc} /MHz	-3.21	-3.30	-3.67	-3.82	-3.88	-3.54
ΔE /cm^{-1}	0.0	35.5	1335.8	1299.5	1088.2	983.0
ΔE /kJmol^{-1}	0.0	0.4	16.0	15.5	13.0	11.8

[a] A, B and C are the rotational constants. P_α (α= a, b or c) are the planar moments of inertia, these are derived from the moments of inertia I_α as for example $P_c = (I_a+I_b-I_c)/2$. Δ_J, Δ_{JK}, Δ_K, δ_J and δ_K are the quartic centrifugal distortion constants. μ_α (α = a, b or c) are the electric dipole moment components, 1 D = $3.33 \cdot 10^{-30}$ C·m. χ_{aa}, χ_{bb}, and χ_{cc}, are the quadrupole coupling tensor diagonal elements for ^{14}N atom. ΔE is the energy relative to the most stable conformer.

Table S6.2. *Ab initio* rotational parameters calculated at MP2/6-311++G(2d,p) level of theory for the *cis*-formanilide (*cis*-fa) and *trans*-formanilide (*trans*-fa) complexes with one molecule of water.

Parameter[a]	*Cis*-fa-w-a	*Cis*-fa-w-a'	*Cis*-fa-w-b	*Trans*-fa-w-a	*Trans*-fa-w-b	*Trans*-fa-w-c
A /MHz	2840.71	2851.89	2910.66	1830.28	4125.16	1561.92
B /MHz	664.06	659.95	569.75	889.16	542.43	942.17
C /MHz	554.39	554.93	490.67	602.60	479.62	589.30
P_a /uÅ^2	747.36	749.65	871.68	565.46	931.44	535.22
P_b /uÅ^2	164.23	161.07	158.30	273.20	122.25	322.38
P_c /uÅ^2	13.68	16.14	15.33	2.92	0.26	1.18
Δ_J /kHz	0.038	0.038	0.127	2.231	0.026	0.318
Δ_{JK} /kHz	0.015	0.074	-1.216	-5.732	0.315	3.035
Δ_K /kHz	1.779	1.674	8.640	7.285	1.751	-1.521
δ_J /kHz	0.009	0.007	0.027	0.576	0.003	0.143
δ_K /kHz	0.430	0.531	0.785	1.940	0.228	0.068
μ_a /D	2.26	2.26	3.23	1.51	2.57	-2.74
μ_b /D	0.34	0.86	1.06	3.72	1.55	5.47
μ_c /D	-1.11	0.85	0.46	-0.97	-0.66	0.00
^{14}N χ_{aa} /MHz	2.24	2.23	2.06	1.68	1.90	2.10
^{14}N χ_{bb} /MHz	0.66	0.77	1.34	1.84	1.71	1.21
^{14}N χ_{cc} /MHz	-2.89	-3.00	-3.40	-3.52	-3.60	-3.31
ΔE /cm^{-1}	0.0	38.3	1254.1	1293.3	1038.2	850.4
ΔE /kJmol^{-1}	0.0	0.5	15.0	15.5	12.4	10.2

[a] A, B and C are the rotational constants. P_α (α= a, b or c) are the planar moments of inertia, these are derived from the moments of inertia I_α as for example $P_c = (I_a+I_b-I_c)/2$. Δ_J, Δ_{JK}, Δ_K, δ_J and δ_K are the quartic centrifugal distortion constants. μ_α (α = a, b or c) are the electric dipole moment components, 1 D = $3.33\cdot10^{-30}$ C·m. χ_{aa}, χ_{bb}, and χ_{cc}, are the quadrupole coupling tensor diagonal elements for ^{14}N atom. ΔE is the energy relative to the most stable conformer.

Table S6.3. *Ab initio* rotational parameters calculated at B3LYP-D3/6-311++G(d,p) level of theory for the *cis*-formanilide (*cis*-fa) and *trans*-formanilide (*trans*-fa) complexes with two molecules of water.

Parameter[a]	*Cis*-fa-w_2-a	*Cis*-fa-w_2-a'	*Cis*-fa-w_2-b	*Trans*-fa-w_2-b	*Trans*-fa-w_2-c
A /MHz	2016.92	2040.30	1926.49	2645.14	1012.56
B /MHz	496.28	487.95	486.09	385.61	876.91
C /MHz	406.85	403.62	389.87	336.95	554.24
P_a /uÅ^2	1004.96	1020.06	1036.81	1309.69	494.52
P_b /uÅ^2	237.20	232.04	259.47	190.17	417.32
P_c /uÅ^2	13.37	15.66	2.86	0.89	81.79
Δ_J /kHz	0.049	0.045	0.048	0.011	0.602
Δ_{JK} /kHz	-0.384	-0.375	-0.285	0.091	-1.347
Δ_K /kHz	2.134	2.373	2.232	0.596	0.855
δ_J /kHz	0.015	0.011	0.013	0.001	0.096
δ_K /kHz	0.207	0.253	0.121	0.077	-1.495
μ_a /D	-1.84	-1.98	-1.95	-1.98	0.00
μ_b /D	0.61	0.47	0.00	-1.43	-3.78
μ_c /D	-0.01	0.21	0.37	-0.22	-0.57
^{14}N χ_{aa} /MHz	2.12	2.13	1.86	1.99	2.20
^{14}N χ_{bb} /MHz	0.97	1.03	1.37	1.81	0.75
^{14}N χ_{cc} /MHz	-3.09	-3.16	-3.23	-3.80	-2.95
ΔE /cm^{-1}	0.0	197.3	1634.4	1744.7	1711.6
ΔE /kJmol^{-1}	0.0	2.4	19.6	20.9	20.5

[a] *A*, *B* and *C* are the rotational constants. P_α (α= *a*, *b* or *c*) are the planar moments of inertia, these are derived from the moments of inertia I_α as for example $P_c = (I_a+I_b-I_c)/2$. Δ_J, Δ_{JK}, Δ_K, δ_J and δ_K are the quartic centrifugal distortion constants. μ_α (α = *a*, *b* or *c*) are the electric dipole moment components, 1 D = $3.33\cdot10^{-30}$ C·m. χ_{aa}, χ_{bb}, and χ_{cc}, are the quadrupole coupling tensor diagonal elements for ^{14}N atom. ΔE is the energy relative to the most stable conformer.

Table S6.4. *Ab initio* rotational parameters calculated at MP2/6-311++G(2d,p) level of theory for the *cis*-formanilide (*cis*-fa) and *trans*-formanilide (*trans*-fa) complexes with two molecules of water.

Parameter[a]	*Cis*-fa-w_2-a	*Cis*-fa-w_2-a'	*Cis*-fa-w_2-b	*Trans*-fa-w_2-b	*Trans*-fa-w_2-c
A /MHz	2007.09	2029.38	1885.33	2625.78	1019.09
B /MHz	496.02	486.15	490.98	386.22	894.62
C /MHz	408.56	406.36	391.60	337.32	571.63
P_a /uÅ^2	1002.02	1017.10	1025.91	1307.15	476.55
P_b /uÅ^2	234.94	226.58	264.63	191.08	407.56
P_c /uÅ^2	16.85	22.46	3.43	1.39	88.36
Δ_J /kHz	0.051	0.051	0.056	0.013	0.428
Δ_{JK} /kHz	-0.372	-0.389	2.410	0.114	0.364
Δ_K /kHz	2.175	2.576	-0.315	0.722	-0.640
δ_J /kHz	0.015	0.011	0.015	0.002	0.086
δ_K /kHz	0.221	0.282	0.134	0.103	2.337
μ_a /D	-1.76	-1.92	-1.85	-1.83	-1.06
μ_b /D	0.69	0.58	-0.03	1.38	3.38
μ_c /D	-0.01	0.28	-0.39	0.18	0.75
^{14}N χ_{aa} /MHz	2.07	2.09	1.78	1.92	2.31
^{14}N χ_{bb} /MHz	0.79	0.86	1.30	1.61	0.66
^{14}N χ_{cc} /MHz	-2.86	-2.95	-3.08	-3.53	-2.96
ΔE /cm^{-1}	0.0	197.5	1587.3	1719.3	1320.2
ΔE /kJmol^{-1}	0.0	2.4	19.0	20.6	15.8

[a] *A*, *B* and *C* are the rotational constants. P_α (α= *a*, *b* or *c*) are the planar moments of inertia, these are derived from the moments of inertia I_α as for example $P_c = (I_a+I_b-I_c)/2$. Δ_J, Δ_{JK}, Δ_K, δ_J and δ_K are the quartic centrifugal distortion constants. μ_α (α = *a*, *b* or *c*) are the electric dipole moment components, 1 D = $3.33\cdot10^{-30}$ C·m. χ_{aa}, χ_{bb}, and χ_{cc}, are the quadrupole coupling tensor diagonal elements for ^{14}N atom. ΔE is the energy relative to the most stable conformer.

Table S6.5. Observed rotational parameters obtained for the *cis*-fa-w-a complex for the parent species and the observed isotopologues compared to the *ab initio* (MP2/6-311++G(2d,p)) values.

Fitted Parameters[a]	parent		$^{18}O_w$		*ab initio*	*ab initio* 33.6[d]
	v=0	v=1	v=0	v=1		
A /MHz	2831.4048(56)[b]		2759.106(12)		2840.71	2834.29
B /MHz	662.38699(14)	662.38850(14)	643.35029(13)	643.34919(13)	664.06	666.35
C /MHz	549.51811(11)		533.950622(85)		554.39	552.19
Δ_J /kHz	0.04469(47)		[0.04469][c]		0.038	
δ_J /kHz	0.01078(36)		[0.01078]		0.009	
δ_K /kHz	0.480(27)		[0.480]		0.430	
^{14}N 3/2(χ_{aa}) /MHz	3.2149(93)		[3.2149]		3.36	
^{14}N ¼(χ_{bb}-χ_{cc}) /MHz	0.9885(67)		[0.9885]		0.89	
N	246/41/41		89/15/15			
σ /kHz	2.5/2.9/2.0		3.8/3.8/3.8			
Derived Parameters						
P_a /uÅ^2	752.07627(21)		774.09936(42)		747.36	747.67
P_b /uÅ^2	167.60044(21)		172.39079(42)		164.23	167.55
P_c /uÅ^2	10.89011(21)		11.44316(42)		13.68	10.76
^{14}N χ_{aa} /MHz	2.1433(61)		[2.1433]		2.24	
^{14}N χ_{bb} /MHz	0.905(16)		[0.905]		0.66	
^{14}N χ_{cc} /MHz	-3.049(16)		[-3.049]		-2.89	

[a] A, B and C are the rotational constants. Δ_J, Δ_{JK}, Δ_K, δ_J and δ_K are the quartic centrifugal distortion constants. χ_{aa}, χ_{bb} and χ_{cc} are the quadrupole coupling tensor diagonal elements for ^{14}N atom. N is the number of quadrupole hyperfine components/rotational transitions fitted. σ is the rms deviations of the fit. P_α (α= a, b or c) are the planar moments of inertia, these are derived from the moments of inertia I_α as for example $P_c = (I_a+I_b-I_c)/2$. [b] Standard errors are given in parentheses in units of the last digit. [c] Parameters in square brackets were kept fixed to those given for the parent species in the fit. [d] Rotational constants obtained by setting the C_1–N–C_2–C_3 dihedral angle to its experimental value keeping fixed the rest of the molecular parameters.

Table S6.5. Continued.

Fitted Parameters[a]	parent		$^2H_{w1}$	$^2H_{w2}$	$^2H_1$	*ab initio*	*ab initio* 33.6[d]
	v=0	v=1					
A /MHz	2831.4048(56)[b]		2829.08(10)	2766.81(10)	2817.460(78)	2840.71	2834.29
B /MHz	662.38699(14)	662.38850(14)	651.19251(60)	648.27840(81)	661.20570(57)	664.06	666.35
C /MHz	549.51811(11)		541.78375(55)	537.81920(76)	547.90770(59)	554.39	552.19
Δ_J /kHz	0.04469(47)		[0.04469][c]	[0.04469]	[0.04469]	0.038	
δ_J /kHz	0.01078(36)		[0.01078]	[0.01078]	[0.01078]	0.009	
δ_K /kHz	0.480(27)		[0.480]	[0.480]	[0.480]	0.430	
^{14}N 3/2(χ_{aa}) /MHz	3.2149(93)		[3.2149]	[3.2149]	[3.2149]	3.36	
^{14}N ¼(χ_{bb}-χ_{cc}) /MHz	0.9885(67)		[0.9885]	[0.9885]	[0.9885]	0.89	
N	246/41/41		29/18	27/12	28/13		
σ /kHz	2.5/2.9/2.0		7.6	9.5	6.1		
Derived Parameters							
P_a /uÅ^2	752.07627(21)		765.1254(64)	768.2976(68)	753.6677(26)	747.36	747.67
P_b /uÅ^2	167.60044(21)		167.6803(64)	171.3843(68)	168.7122(26)	164.23	167.55
P_c /uÅ^2	10.89011(21)		10.9569(64)	11.2733(68)	10.6618(26)	13.68	10.76
^{14}N χ_{aa} /MHz	2.1433(61)		[2.1433]	[2.1433]	[2.1433]	2.24	
^{14}N χ_{bb} /MHz	0.905(16)		[0.905]	[0.905]	[0.905]	0.66	
^{14}N χ_{cc} /MHz	-3.049(16)		[-3.049]	[-3.049]	[-3.049]	-2.89	

[a] *A*, *B* and *C* are the rotational constants. Δ_J, Δ_{JK}, Δ_K, δ_J and δ_K are the quartic centrifugal distortion constants. χ_{aa}, χ_{bb} and χ_{cc} are the quadrupole coupling tensor diagonal elements for ^{14}N atom. *N* is the number of quadrupole hyperfine components/rotational transitions fitted. σ is the rms deviations of the fit. P_α (α= *a*, *b* or *c*) are the planar moments of inertia, these are derived from the moments of inertia I_α as for example $P_c = (I_a+I_b-I_c)/2$. [b] Standard errors are given in parentheses in units of the last digit. [c] Parameters in square brackets were kept fixed to those given for the parent species in the fit. [d] Rotational constants obtained by setting the C_1–N–C_2–C_3 dihedral angle to its experimental value keeping fixed the rest of the molecular parameters.

Table S6.6. Observed rotational parameters obtained for the *trans*-fa-w-b complex for the parent species and the observed isotopologues compared to the *ab initio* (MP2/6-311++G(2d,p)) values.

Fitted Parameters[a]	parent	$^{18}O_w$	$^{2}H_{w1}$	*ab initio*	*ab initio* planar[d]
A /MHz	4094.8678(75)[b]	4093.4250(30)	4078.59(36)	4125.16	4014.89
B /MHz	539.02116(10)	513.41306(10)	530.25227(59)	542.43	545.05
C /MHz	476.89366(10)	456.722450(81)	469.82724(55)	479.62	480.59
Δ_J /kHz	0.02959(23)	[0.02959][c]	[0.02959]	0.026	
Δ_{JK} /kHz	0.4586(77)	[0.4586]	[0.4586]	0.315	
Δ_K /kHz	4.44(74)	[4.44]	[4.44]	1.751	
δ_J /kHz	0.00323(27)	[0.00323]	[0.00323]	0.003	
^{14}N 3/2(χ_{aa}) /MHz	2.802(16)	[2.802]	[2.802]	2.85	
^{14}N ¼(χ_{bb}-χ_{cc}) /MHz	1.3153(44)	[1.3153]	[1.3153]	1.33	
N	111/38	33/11	18/11		
σ /kHz	2.5	2.3	7.3		
Derived Parameters					
P_a /uÅ^2	936.94997(36)	983.71235(29)	952.425(11)	931.44	926.47
P_b /uÅ^2	122.78105(36)	122.82184(29)	123.244(11)	122.25	125.12
P_c /uÅ^2	0.63661(36)	0.63932(29)	0.666(11)	0.26	0.76
^{14}N χ_{aa} /MHz	1.868(11)	[1.868]	[1.868]	1.90	
^{14}N χ_{bb} /MHz	1.697(14)	[1.697]	[1.697]	1.71	
^{14}N χ_{cc} /MHz	-3.565(14)	[-3.565]	[-3.565]	-3.60	

[a] A, B and C are the rotational constants. Δ_J, Δ_{JK}, Δ_K, δ_J and δ_K are the quartic centrifugal distortion constants. χ_{aa}, χ_{bb} and χ_{cc} are the quadrupole coupling tensor diagonal elements for ^{14}N atom. N is the number of quadrupole hyperfine components/rotational transitions fitted. σ is the rms deviations of the fit. P_α (α= a, b or c) are the planar moments of inertia, these are derived from the moments of inertia I_α as for example $P_c = (I_a+I_b-I_c)/2$. [b] Standard errors are given in parentheses in units of the last digit. [c] Parameters in square brackets were kept fixed to those given for the parent species in the fit. [d] Rotational constants obtained by constraining the structure in a plane with the exception of the H_{w2} atom.

Table S6.7. Observed rotational parameters obtained for the *trans*-fa-w-c complex for the parent species and the observed isotopologue compared to the *ab initio* (MP2/6-311++G(2d,p)) values.

Fitted Parameters[a]	parent		$^{18}O_w$		*ab initio*
	v=0	v=1	v=0	v=1	
A /MHz	1608.09000(26)[b]	1607.55924(26)	1562.3190(27)	1561.7594(27)	1561.92
B /MHz	907.81842(11)	907.76796(11)	878.7953(10)	878.7719(10)	942.17
C /MHz	581.604742(46)	581.640188(46)	563.67834(14)	563.71477(14)	589.30
Δ_J /kHz	0.4732(12)		[0.4732][c]		0.318
Δ_{JK} /kHz	5.711(18)		[5.711]		3.035
Δ_K /kHz	-2.6208(51)		[-2.6208]		-1.521
δ_J /kHz	0.21434(63)		[0.21434]		0.143
δ_K /kHz	0.1124(65)		[0.1124]		0.068
^{14}N 3/2(χ_{aa}) /MHz	3.0600(42)		[3.0600]		3.244
^{14}N ¼(χ_{bb}-χ_{cc}) /MHz	1.16089(85)		[1.16089]		1.187
N	274/46		48/6/6		
σ /kHz	1.3/1.3/1.3		1.1/1.0/1.2		
Derived Parameters					
P_a /uÅ^2	555.68112(11)	555.61823(11)	574.08748(89)	574.00822(89)	535.22
P_b /uÅ^2	313.25781(11)	313.26775(11)	322.48592(89)	322.50724(89)	322.38
P_c /uÅ^2	1.01502(11)	1.10885(11)	0.99411(89)	1.08870(89)	1.18
^{14}N χ_{aa} /MHz	2.0400(28)		[2.0400]		2.10
^{14}N χ_{bb} /MHz	1.3018(31)		[1.3018]		1.21
^{14}N χ_{cc} /MHz	-3.3418(31)		[-3.3418]		-3.31

[a] *A*, *B* and *C* are the rotational constants. Δ_J, Δ_{JK}, Δ_K, δ_J and δ_K are the quartic centrifugal distortion constants. χ_{aa}, χ_{bb} and χ_{cc} are the quadrupole coupling tensor diagonal elements for ^{14}N atom. *N* is the number of quadrupole hyperfine components/rotational transitions fitted. σ is the rms deviations of the fit. P_α (α= *a*, *b* or *c*) are the planar moments of inertia, these are derived from the moments of inertia I_α as for example $P_c = (I_a+I_b-I_c)/2$. [b] Standard errors are given in parentheses in units of the last digit. [c] Parameters in square brackets were kept fixed to those given for the parent species in the fit.

Table S6.8. Observed rotational parameters obtained for the *cis*-fa-w_2 complex for the parent species and the $^{18}O_w$ observed isotopologues compared to the *ab initio* (MP2/6-311++G(2d,p)) values.

Fitted Parameters[a]	parent	$^{18}O_{w1}$	$^{18}O_{w2}$	*ab initio*	*ab initio* 33.6[b]
A /MHz	1992.9001(14)[c]	1928.1500(92)	1991.1356(48)	2007.09	2004.56
B /MHz	494.434394(34)	489.95744(10)	477.788224(49)	496.02	497.45
C /MHz	405.007349(26)	399.433590(87)	393.704503(37)	408.56	407.53
Δ_J /kHz	0.058560(87)	[0.058560][d]	[0.058560]	0.051	
Δ_{JK} /kHz	-0.4858(11)	[-0.4858]	[-0.4858]	-0.372	
δ_J /kHz	0.016610(57)	[0.016610]	[0.016610]	0.015	
δ_K /kHz	0.1667(46)	[0.1667]	[0.1667]	0.221	
^{14}N 3/2(χ_{aa}) /MHz	3.0130(72)	[3.0130]	[3.0130]	3.10	
^{14}N ¼(χ_{bb}-χ_{cc}) /MHz	0.9797(23)	[0.9797]	[0.9797]	0.91	
N	156/52	33/11	36/12		
σ /kHz	0.8	2.6	1.4		
Derived Parameters					
P_a /uÅ^2	1008.18632(21)	1017.3043(13)	1043.79149(63)	1002.02	1001.96
P_b /uÅ^2	239.64043(21)	247.9347(13)	239.85907(63)	234.94	238.14
P_c /uÅ^2	13.94930(21)	14.1709(13)	13.95539(63)	16.85	13.97
^{14}N χ_{aa} /MHz	2.0087(48)	[2.0087]	[2.0087]	2.07	
^{14}N χ_{bb} /MHz	0.9551(70)	[0.9551]	[0.9551]	0.79	
^{14}N χ_{cc} /MHz	-2.9637(70)	[-2.9637]	[-2.9637]	-2.86	

[a] *A*, *B* and *C* are the rotational constants. Δ_J, Δ_{JK}, Δ_K, δ_J and δ_K are the quartic centrifugal distortion constants. χ_{aa}, χ_{bb} and χ_{cc} are the quadrupole coupling tensor diagonal elements for ^{14}N atom. *N* is the number of quadrupole hyperfine components/rotational transitions fitted. σ is the rms deviations of the fit. P_α (α= *a*, *b* or *c*) are the planar moments of inertia, these are derived from the moments of inertia I_α as for example $P_c = (I_a+I_b-I_c)/2$. [b] Rotational constants obtained by setting the C_1–N–C_2–C_3 dihedral angle to its experimental value keeping fixed the rest of the molecular parameters. [c] Standard errors are given in parentheses in units of the last digit. [d] Parameters in square brackets were kept fixed to those given for the parent species in the fit.

Table S6.9. Comparison of the planar moments of inertia for the observed complexes in this work with the values reported [ref. 23] for the monomers of *cis* and *trans* formanilide.

	Cis-fa	*cis*-fa-w-a	*cis*-fa-w$_2$
P_a /uÅ^2	539.9978(10)	752.07627(21)	1008.18632(21)
P_b /uÅ^2	95.9417(10)	167.60044(21)	239.64043(21)
P_c /uÅ^2	3.9009(10)	10.89011(21)	13.94930(21)

Cis-fa *Cis*-fa-w-a *Cis*-fa-w$_2$

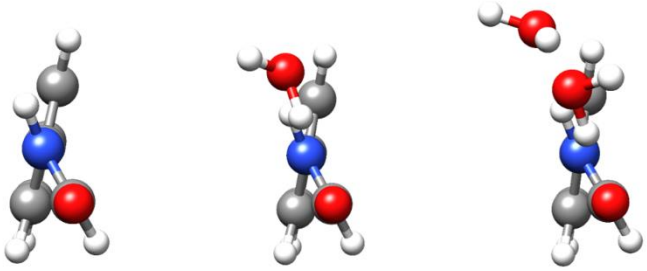

	Trans-fa	*trans*-fa-w-b	*trans*-fa-w-c
P_a /uÅ^2	449.44891(15)	936.94997(36)	555.68112(11)
P_b /uÅ^2	119.61512(15)	122.78105(36)	313.25781(11)
P_c /uÅ^2	0.30034(15)	0.63661(36)	1.01502(11)

Trans-fa *Trans*-fa-w-b *Trans*-fa-w-c

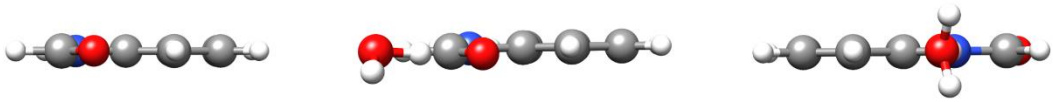

Table S6.10. r_0 structure obtained by the fitting of the rotational constants for all the available isotopologues for the *cis*-fa-w-a complex and comparison with the r_s and r_e (MP2/6-311++G(2d,p)) structures. The geometrical parameters for water were fixed to its r_0 values [Harmony, M. D., Laurie, V. W., Kuczkowski, R. L., Schwendeman, R. H., Ramsay, D. A., Lovas, F. J., Lafferty, W. J., Maki, A. G. *J. Phys. Chem. Ref. Data* 1979, 8, 619–721].

Fitted parameter	r_0	r_e	F-w-a[a]
$r(H_{w1}\cdots O_1)$ /Å	1.931(3)	1.925	1.93(1)
$\angle(H_{w1}\cdots O_1–C_1)$ /°	108.24(4)	107.4	110.3(3)
$\angle(C_1–N–C_2–C_3)$ /°	33.5(1)	[33.6]	
Derived parameter	r_0	r_e	F-w-a
$r(O_w\cdots H_1)$ /Å	2.011(1)	1.976	2.061(4)
$r(O_w\cdots O_1)$ /Å	2.804(2)	2.796	
$r(O_w\cdots N)$ /Å	2.890(1)	2.858	
$\angle(N–H_1\cdots O_w)$ /°	142.56(8)	142.8	139.5(3)
$\angle(H_1\cdots O_w–H_{w1})$ /°	81.46(8)	81.9	78.2(6)
$\angle(N\cdots O_w\cdots O_1)$ /°	47.39(2)	47.75	
$\angle(O_w\cdots O_1\cdots N)$ /°	68.27(3)	67.55	
$\angle(O_1\cdots N\cdots O_w)$ /°	64.35	64.69	
$\angle(H_{w2}–O_w\cdots O_1\cdots N)$ /°	130.7(2)	130.4	
Fixed parameter	r_0	r_e	F-w-a
$\angle(O_w–H_{w1}\cdots O_1)$ /°	[147.20(7)]	147.2	153(1)

[a] r_0 structure for formamide-w-a, [ref. 16]

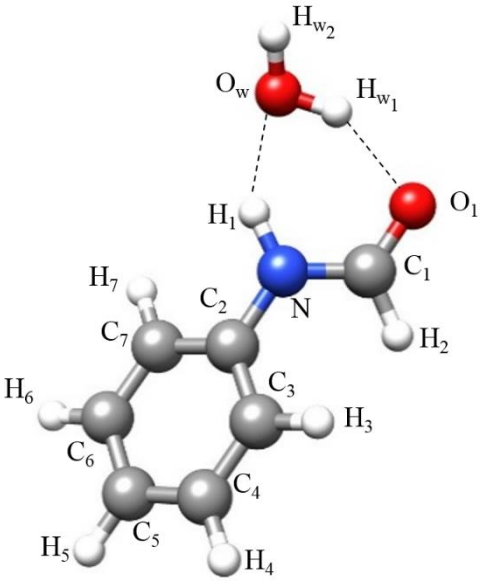

	atom	*a*	*b*	*c*
$\lvert r_s\rvert$		|3.35040(45)|	|1.52958(99)|	|0.3436(44)|
r_0	O_w	-3.3519(9)	-1.54(1)	0.323(2)
r_e		-3.331	-1.526	0.363
$\lvert r_s\rvert$		|3.61365(61)|	|0.2860(78)|	|0.2613(85)|
r_0	H_{w1}	-3.5768(5)	-0.607(1)	0.147(1)
r_e		-3.560	-0.601	0.148
$\lvert r_s\rvert$		|4.01537(56)|	|1.9705(12)|	|0.6337(37)|
r_0	H_{w2}	-3.970(1)	-1.850(2)	0.998(3)
r_e		-3.957	-1.809	1.036
$\lvert r_s\rvert$		|1.26(1)|	|1.06(1)|	|0.48i|
r_0	H_1	-1.4868(3)	-0.795(1)	0.262(1)
r_e		-1.496	-0.786	0.323
$\lvert r_s\rvert$		1.2737(77)		
r_0	$r(O_w\text{-}H_{w1})$	0.979(2)		
r_e		0.971		
$\lvert r_s\rvert$		0.8490(22)		
r_0	$r(O_w\text{-}H_{w2})$	0.965(3)		
r_e		0.959		
$\lvert r_s\rvert$		-		
r_0	$r(O_w\cdots H_1)$	2.011(1)		
r_e		1.976		

Table S6.11. r_0 structure obtained by the fitting of the rotational constants for all the available isotopologues for the *trans*-fa-w-b complex and comparison with the r_s and r_e (MP2/6-311++G(2d,p)) structures. The geometrical parameters for water were fixed to its r_0 values [Harmony, M. D., Laurie, V. W., Kuczkowski, R. L., Schwendeman, R. H., Ramsay, D. A., Lovas, F. J., Lafferty, W. J., Maki, A. G. *J. Phys. Chem. Ref. Data* 1979, 8, 619–721].

Fitted parameter	r_0	r_e	F-w-b[a]
$r(H_{w1}\cdots O_1)$ /Å	1.941(3)	1.929	1.932
$\angle(H_{w1}\cdots O_1–C_1)$ /°	100.8(3)	98.8	110.3(3)
Derived parameter	r_0	r_e	F-w-b
$r(O_w\cdots H_2)$ /Å	2.681(7)	2.603	2.715
$r(O_w\cdots O_1)$ /Å	2.841(3)	2.827	
$\angle(C–H_2\cdots O_w)$ /°	103.5(6)	104.8	104.0
$\angle(H_2\cdots O_w–H_{w1})$ /°	61.6(4)	62.3	59.1
$\angle(H_{w2}–O_w\cdots O_1\cdots N)$ /°	151.0(5)	151.1	
Fixed parameter	r_0	r_e	F-w-b
$\angle(O_w–H_{w1}\cdots O_1)$ /°	[152.3(5)]	152.3	155.4

[a] r_0 structure for formamide-w-b, [ref. 16]

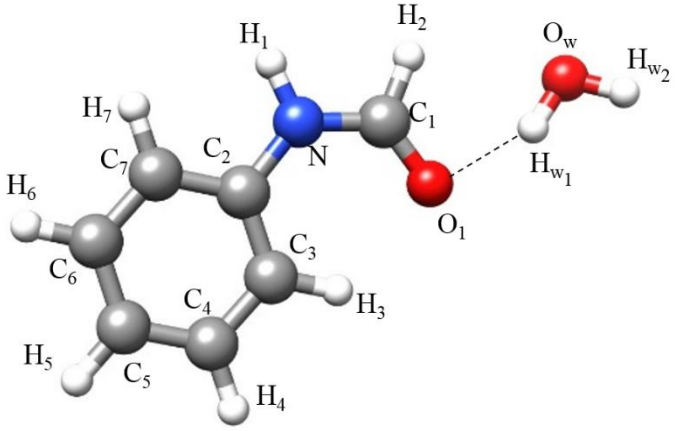

	atom	*a*	*b*	*c*
$\lvert r_s\rvert$		|4.86484(31)|	|0.147(10)|	|0.038(39)|
r_0	O_w	-4.8670(9)	0.164(8)	-0.0513(4)
r_e		-4.837	0.132	-0.053
$\lvert r_s\rvert$		|3.93463(80)|	|0.6872(46)|	|0.172(18)|
r_0	H_{w1}	-3.998(2)	-0.622(3)	0.0067(3)
r_e		-3.978	-0.620	0.006

$\lvert r_s\rvert$		1.0837(78)
r_0	$r(O_w\text{-}H_{w1})$	0.975(5)
r_e		0.969

Table S6.12. r_0 structure obtained by the fitting of the rotational constants for all the available isotopologues for the *trans*-fa-w-c complex and comparison with the r_s and r_e (MP2/6-311++G(2d,p)) structures. The geometrical parameters for water were fixed to its r_0 values [Harmony, M. D., Laurie, V. W., Kuczkowski, R. L., Schwendeman, R. H., Ramsay, D. A., Lovas, F. J., Lafferty, W. J., Maki, A. G. *J. Phys. Chem. Ref. Data* 1979, 8, 619–721].

Fitted parameter	r_0	r_e	F-w-c[a]
$r(O_w\cdots H_1)$ /Å	2.0093(9)	1.992	2.008
$\angle(O_w\cdots H_1–N)$ /°	184.85(3)	177.2	177.6
Derived parameter	r_0	r_e	F-w-c
$r(O_w\cdots N)$ /Å	3.0236(8)	3.008	3.019
Fixed parameter	r_0	r_e	F-w-c
$\angle(H_1\cdots O_w–H_{w1})$ /°	[124.45(7)]	124.45	126.8
$\angle(H_1\cdots O_w–H_{w2})$ /°	[124.45(7)]	124.45	126.8
$\angle(N–H_1\cdots O_w–H_{w1})$ /°	[105.5(1)]	105.5	84.0
$\angle(N–H_1\cdots O_w–H_{w2})$ /°	[-105.5(1)]	-105.5	-84.0

[a] *ab initio* structure for formamide-w-c, [ref. 16]

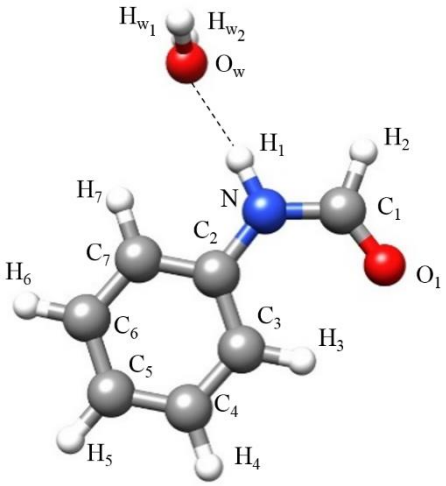

	atom	*a*	*b*	*c*
$\lvert r_s\rvert$		|2.99363(50)|	|2.24178(67)|	|0.105i|
r_0	O_w	-3.0135(9)	-2.2249(6)	[0.000]
r_e		-2.788	-2.373	0.000

Table S6.13. r_0 structure obtained by the fitting of the rotational constants for all the available isotopologues for the *cis*-fa-w_2 complex and comparison with the r_s and r_e (MP2/6-311++G(2d,p)) structures. The geometrical parameters for water were fixed to its r_0 values [Harmony, M. D., Laurie, V. W., Kuczkowski, R. L., Schwendeman, R. H., Ramsay, D. A., Lovas, F. J., Lafferty, W. J., Maki, A. G. *J. Phys. Chem. Ref. Data* 1979, 8, 619–721].

Fitted parameter	r_0	r_e	F-w_2[a]
$r(O_1\cdots H_{w1})$ /Å	1.809(7)	1.788	1.797(8)
$r(H_1\cdots O_{w2})$ /Å	1.874(4)	1.845	1.874(4)
$\angle(H_{w1}\cdots O_1–C_1)$ /°	128.1(3)	127.8	130.2(8)
$\angle(O_{w2}\cdots H_1–N)$ /°	176.5(2)	175.4	178.9(3)
$\angle(C_1–N–C_2–C_3)$ /°	32.73(9)	[33.3]	
Derived parameter	r_0	r_e	F-w_2
$r(O_{w1}\cdots H_{w3})$ /Å	1.777(6)	1.775	1.829(4)
$r(O_{w1}\cdots O_1)$ /Å	2.784(5)	2.761	2.784(5)
$r(O_{w2}\cdots N)$ /Å	2.902(4)	2.872	2.902(4)
$r(O_{w1}\cdots O_{w2})$ /Å	2.727(5)	2.721	2.727(5)
$\angle(H_1\cdots O_{w2}–H_{w3})$ /°	96.2(4)	96.4	97.6(7)
$\angle(O_{w2}–H_{w3}\cdots O_{w1})$ /°	161.0(5)	160.4	160(1)
$\angle(H_{w3}\cdots O_{w1}–H_{w1})$ /°	99.9(2)	100.1	99(1)
$\angle(N\cdots O_{w2}\cdots O_{w1})$ /°	84.5(1)	84.4	
$\angle(O_{w2}\cdots O_{w1}\cdots C_1)$ /°	86.7(1)	86.9	
$\angle(O_{w1}\cdots C_1–N)$ /°	96.0(1)	95.7	
$\angle(C_1–N\cdots O_{w2})$ /°	92.8(1)	93.0	
$\angle(H_{w2}–O_{w1}\cdots O_1\cdots N)$ /°	-130.7(3)	-130.7	
$\angle(H_{w4}–O_{w2}\cdots O_1\cdots N)$ /°	96.8(4)	97.0	
Fixed parameter	r_0	r_e	F-w_2
$\angle(O_{w1}–H_{w1}\cdots O_1)$ /°	[169.9(3)]	169.9	171(2)

[a] r_0 structure for formamide-w_2, [ref. 16]

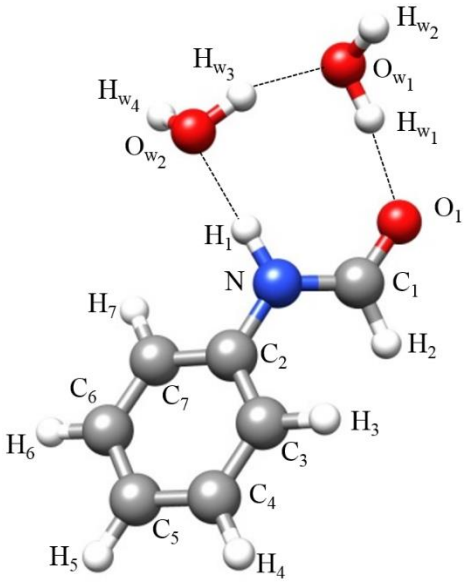

	atom	*a*	*b*	*c*
r_s		|4.24103(35)|	|0.3399(44)|	|0.056(27)|
r_0	O_{w1}	-4.244(1)	-0.356(6)	0.007(2)
r_e		-4.224	-0.357	0.026
$\|r_s\|$		|2.13464(71)|	|2.05833(73)|	|0.3422(44)|
r_0	O_{w2}	-2.140(3)	-2.060(4)	0.353(1)
r_e		-2.121	-2.047	0.376

$\|r_s\|$		2.7327(39)
r_0	$r(O_{w1}\text{-}O_{w2})$	2.727(5)
r_e		2.721

Table S6.14. Observed rotational frequencies and residuals (all the values in MHz) for the parent species of the complex *cis*-fa-w-a in the *v = 0* and *v = 1* vibrational states for $J'K'_{-1}K'_{+1}v'F' \leftarrow J''K''_{-1}K''_{+1}v''F''$ transitions.

$J'K'_{-1}K'_{+}$	$J''K''_{-1}K''_{+}$	v	F'	F''	Obs.	Res.
$5_{1,5}$	$4_{1,4}$	*0*	6	5	5759.5790	0.0023
			4	3	5759.6336	0.0019
			5	4	5759.6540	0.0011
		1	6	5	5759.5790	-0.0012
			4	3	5759.6336	-0.0016
			5	4	5759.6540	-0.0023
$5_{0,5}$	$4_{0,4}$	*0*	6	5	5975.4706	0.0031
			4	3	5975.4968	0.0014
			5	4	5975.5633	0.0023
		1	6	5	5975.4706	-0.0015
			4	3	5975.4968	-0.0032
			5	4	5975.5648	-0.0007
$5_{2,4}$	$4_{2,3}$	*0*	4	3	6049.9068	0.0020
			6	5	6049.9233	0.0008
			5	4	6050.0894	0.0014
		1	4	3	6049.9139	0.0016
			6	5	6049.9292	-0.0007
			5	4	6050.0952	-0.0002
$5_{3,3}$	$4_{3,2}$	*0*	4	3	6073.0434	-0.0002
			6	5	6073.1229	-0.0004
			5	4	6073.4409	0.0004
		1	4	3	6073.0507	-0.0010
			6	5	6073.1314	0.0000
			5	4	6073.4489	0.0003
$5_{3,2}$	$4_{3,1}$	*0*	4	3	6075.1822	0.0001
			6	5	6075.2614	0.0003
			5	4	6075.5748	0.0008
		1	4	3	6075.1927	0.0023
			6	5	6075.2692	0.0000
			5	4	6075.5824	0.0002
$5_{2,3}$	$4_{2,2}$	*0*	4	3	6133.9185	-0.0033
			6	5	6133.9303	-0.0004
			5	4	6134.0129	-0.0010
		1	4	3	6133.9341	0.0022
			6	5	6133.9417	0.0009
			5	4	6134.0240	0.0000
$5_{1,4}$	$4_{1,3}$	*0*	4	3	6321.7700	-0.0004
			6	5	6321.7840	0.0000
			5	4	6321.8438	0.0000
		1	4	3	6321.7792	-0.0020
			6	5	6321.7943	-0.0005
			5	4	6321.8550	0.0005
$6_{1,6}$	$5_{1,5}$	*0*	7	6	6901.2088	0.0007
			5	4	6901.2478	0.0009
			6	5	6901.2672	0.0003
		1	7	6	6901.2124	0.0002
			5	4	6901.2511	0.0001
			6	5	6901.2709	0.0000
$6_{0,6}$	$5_{0,5}$	*0*	7	6	7127.5845	0.0021
			5	4	7127.6017	0.0026
			6	5	7127.6868	0.0026
		1	7	6	7127.5845	-0.0031
			5	4	7127.6017	-0.0025
			6	5	7127.6868	-0.0025
$6_{2,5}$	$5_{2,4}$	*0*	7	6	7252.0734	-0.0007
			5		7252.0734	0.0011
			6	5	7252.1822	0.0009
		1	7	6	7252.0819	-0.0010
			5	4	7252.0819	0.0008
			6	5	7252.1886	-0.0014
$6_{3,4}$	$5_{3,3}$	*0*	5	4	7292.1438	-0.0018
			7	6	7292.1753	0.0001
			6	5	7292.3581	0.0010
		1	5	4	7292.1548	-0.0007
			7	6	7292.1863	0.0013
			6	5	7292.3671	0.0002
$6_{3,3}$	$5_{3,2}$	*0*	5	4	7297.8238	-0.0020
			7	6	7297.8545	0.0002
			6	5	7298.0290	0.0005
		1	5	4	7297.8355	-0.0004
			7	6	7297.8655	0.0011
			6	5	7298.0386	0.0000
$6_{2,4}$	$5_{2,3}$	*0*	7	6	7395.8019	-0.0010
			5	4	7395.8070	-0.0018
			6	5	7395.8157	-0.0008
		1	7	6	7395.8157	-0.0001
			5	4	7395.8227	0.0009
			6	5	7395.8326	0.0031
$6_{1,5}$	$5_{1,4}$	*0*	5	4	7572.7188	-0.0012
			7	6	7572.7268	-0.0007
			6	5	7572.7785	-0.0003
		1	5	4	7572.7326	0.0007
			7	6	7572.7401	0.0007
			6	5	7572.7902	-0.0004

Table S6.14. Continued.

$J'K'_{-1}K'_{+}$	$J''K''_{-1}K''_{+}$	v	F'	F''	Obs.	Res.
$7_{1,7}$	$6_{1,6}$	*0*	8	7	8038.0556	0.0008
			6	5	8038.0834	0.0000
			7	6	8038.1051	0.0004
		1	8	7	8038.0594	0.0000
			6	5	8038.0882	0.0002
			7	6	8038.1093	0.0000
$7_{0,7}$	$6_{0,6}$	*0*	8	7	8260.9484	0.0010
			6	5	8260.9595	0.0010
			7	6	8261.0548	0.0014
		1	8	7	8260.9510	-0.0018
			6	5	8260.9624	-0.0015
			7	6	8261.0572	-0.0015
$7_{2,6}$	$6_{2,5}$	*0*	8	7	8449.9664	0.0011
			6	5	8449.9730	0.0017
			7	6	8450.0431	0.0014
		1	8	7	8449.9730	-0.0021
			6	5	8449.9800	-0.0011
			7	6	8450.0499	-0.0016
$7_{4,4}$	$6_{4,3}$	*0*	6	5	8504.4505	0.0006
			8	7	8504.4831	0.0003
			7	6	8504.6870	-0.0002
		1	6	5	8504.4613	0.0000
			8	7	8504.4928	-0.0013
$7_{4,3}$	$6_{4,2}$	*0*	6	5	8504.6990	0.0083
			8	7	8504.7239	0.0004
			7	6	8504.9284	0.0007
		1	6	5	8504.7074	0.0053
			8	7	8504.7367	0.0018
			7	6	8504.9382	-0.0008
$7_{3,5}$	$6_{3,4}$	*0*	6	5	8512.7523	-0.0003
			8	7	8512.7655	0.0018
			7	6	8512.8778	0.0013
		1	6	5	8512.7655	0.0013
			8	7	8512.7746	-0.0006
			7	6	8512.8877	-0.0003
$7_{3,4}$	$6_{3,3}$	*0*	6	5	8525.4546	-0.0001
			8	7	8525.4653	0.0010
			7	6	8525.5644	0.0000
		1	6	5	8525.4653	-0.0016
			8	7	8525.4761	-0.0002
			7	6	8525.5748	-0.0017
$7_{2,5}$	$6_{2,4}$	*0*	7	6	8672.0269	-0.0002
			8	7	8672.0486	0.0003
			6	5	8672.0562	-0.0011
		1	7	6	8672.0486	0.0053
			8	7	8672.0650	0.0007
			6	5	8672.0756	0.0021
$7_{1,6}$	$6_{1,5}$	*0*	6	5	8815.3977	-0.0007
			8	7	8815.4034	-0.0003
			7	6	8815.4540	-0.0006
		1	6	5	8815.4115	0.0004
			8	7	8815.4175	0.0011
			7	6	8815.4681	0.0008
$8_{1,8}$	$7_{1,7}$	*0*	9	8	9169.9495	-0.0003
			7	6	9169.9718	0.0000
			8	7	9169.9949	0.0002
		1	9	8	9169.9551	0.0003
			7	6	9169.9769	0.0002
			8	7	9170.0004	0.0008
$8_{0,8}$	$7_{0,7}$	*0*	9	8	9377.2898	-0.0002
			7	6	9377.3035	0.0000
			8	7	9377.3979	-0.0003
		1	9	8	9377.2948	-0.0007
			7	6	9377.3090	0.0000
			8	7	9377.4029	-0.0007
$8_{2,7}$	$7_{2,6}$	*0*	9	8	9642.9565	0.0020
			7	6	9642.9565	0.0011
			8	7	9643.0208	0.0014
		1	7	6	9642.9634	-0.0028
			9	8	9642.9634	-0.0019
			8	7	9643.0278	-0.0024
$8_{3,6}$	$7_{3,5}$	*0*	7	6	9734.5101	-0.0123
			9	8	9734.5146	-0.0110
			8	7	9734.5860	-0.0141
		1	7	6	9734.5330	-0.0027
			9	8	9734.5372	-0.0017
			8	7	9734.6119	-0.0015
$8_{3,5}$	$7_{3,4}$	*0*	7	6	9759.6907	0.0015
			9	8	9759.6907	0.0001
			8	7	9759.7472	0.0013
		1	7	6	9759.7019	-0.0016
			9	8	9759.7019	-0.0030
			8	7	9759.7566	-0.0036
$8_{2,6}$	$7_{2,5}$	*0*	8	7	9960.1156	0.0065

Table S6.14. Continued.

$J'K'_{-1}K'_{+1}$	$J''K''_{-1}K''_{+1}$	v	F'	F''	Obs.	Res.
			9	8	9960.1494	0.0042
			7	6	9960.1543	0.0004
		1	8	7	9960.1244	-0.0038
			9	8	9960.1605	-0.0038
			7	6	9960.1691	-0.0039
$8_{1,7}$	$7_{1,6}$	*0*	7	6	10047.6740	-0.0005
			9	8	10047.6794	0.0004
			8	7	10047.7335	-0.0001
		1	7	6	10047.6887	0.0009
			9	8	10047.6940	0.0018
			8	7	10047.7482	0.0013
$9_{1,9}$	$8_{1,8}$	*0*	10	9	10296.9370	0.0000
			8	7	10296.9537	-0.0005
			9	8	10296.9780	-0.0003
		1	10	9	10296.9438	0.0015
			8	7	10296.9612	0.0017
			9	8	10296.9844	0.0008
$9_{0,9}$	$8_{0,8}$	*0*	10	9	10480.1602	-0.0052
			8	7	10480.1641	-0.0036
			9	8	10480.2552	-0.0059
		1	10	9	10480.1710	0.0002
			8	7	10480.1752	0.0021
			9	8	10480.2677	0.0011
$9_{2,8}$	$8_{2,7}$	*0*	10	9	10830.4121	0.0004
			8	7	10830.4176	0.0020
			9	8	10830.4687	0.0023
		1	10	9	10830.4208	-0.0025
			8	7	10830.4248	-0.0025

$J'K'_{-1}K'_{+1}$	$J''K''_{-1}K''_{+1}$	v	F'	F''	Obs.	Res.
			9	8	10830.4761	-0.0019
$9_{3,7}$	$8_{3,6}$	*0*	8	7	10956.8916	0.0078
			10	9	10956.8916	0.0077
			9	8	10956.9430	0.0074
		1	8	7	10956.9041	0.0053
			10	9	10956.9042	0.0054
			9	8	10956.9545	0.0039
$9_{3,6}$	$8_{3,5}$	*0*	10	9	11002.3852	-0.0004
			8	7	11002.3879	0.0000
			9	8	11002.4121	0.0016
		1	10	9	11002.3992	-0.0034
			8	7	11002.4020	-0.0029
			9	8	11002.4270	-0.0004
$9_{2,7}$	$8_{2,6}$	*0*	9	8	11255.6345	-0.0060
			10	9	11255.6745	-0.0046
			8	7	11255.6852	-0.0009
		1	9	8	11255.6648	0.0023
			10	9	11255.7020	0.0008
			8	7	11255.7096	0.0014
$9_{1,8}$	$8_{1,7}$	*0*	8	7	11267.1540	0.0000
			10	9	11267.1592	0.0010
			9	8	11267.2192	0.0001
		1	8	7	11267.1677	0.0000
			10	9	11267.1742	0.0023
			9	8	11267.2327	-0.0001
$10_{1,10}$	$9_{1,9}$	*0*	11	10	11419.2460	-0.0001
			9	8	11419.2610	0.0006
			10	9	11419.2835	-0.0014

$J'K'_{-1}K'_{+1}$	$J''K''_{-1}K''_{+1}$	v	F'	F''	Obs.	Res.
		1	11	10	11419.2532	0.0015
			9	8	11419.2677	0.0018
			10	9	11419.2912	0.0007
$10_{0,10}$	$9_{0,9}$	*0*	11	10	11574.0023	-0.0028
			9	8	11574.0118	0.0000
			10	9	11574.0966	0.0023
		1	11	10	11574.0118	0.0015
			9	8	11574.0157	-0.0011
			10	9	11574.1010	0.0015
$10_{2,9}$	$9_{2,8}$	*0*	11	10	12011.7987	-0.0027
			9	8	12011.8032	-0.0018
			10	9	12011.8537	0.0022
		1	11	10	12011.8103	-0.0036
			9	8	12011.8181	0.0005
			10	9	12011.8675	0.0035
$10_{1,9}$	$9_{1,8}$	*0*	9	8	12471.2857	0.0000
			11	10	12471.2909	0.0011
			10	9	12471.3602	0.0018
		1	9	8	12471.2994	-0.0004
			11	10	12471.3049	0.0010
			10	9	12471.3723	-0.0002

Table S6.15. Observed rotational frequencies and residuals (all the values in MHz) for the $^{18}O_w$ isotopologue of the complex *cis*-fa-w-a in the *v = 0* and *v = 1* vibrational states for $J'K'_{-1}K'_{+1}v'F' \leftarrow J''K''_{-1}K''_{+1}v''F''$ transitions.

$J'K'_{-1}K'_{+1}$	$J''K''_{-1}K''_{+1}$	v	F'	F''	Obs.	Res.	$J'K'_{-1}K'_{+1}$	$J''K''_{-1}K''_{+1}$	v	F'	F''	Obs.	Res.
$5_{1,5}$	$4_{1,4}$	*0*	6	5	5595.8735	0.0017				5	4	6925.1825	0.0008
			4	3	5595.9280	0.0012				6	5	6925.2713	0.0162
			5	4	5595.9496	0.0017	$6_{1,5}$	$5_{1,4}$	*0*	5	4	7356.0649	-0.0088
		1	6	5	5595.8735	-0.0001				7	6	7356.0845	0.0032
			4	3	5595.9280	-0.0007				6	5	7356.1271	-0.0052
			5	4	5595.9496	-0.0001			*1*	5	4	7356.0649	0.0027
$5_{0,5}$	$4_{0,4}$	*0*	6	5	5805.5100	0.0014				7	6	7356.0845	0.0148
			4	3	5805.5382	0.0016				6	5	7356.1271	0.0063
			5	4	5805.6015	0.0000	$7_{1,7}$	$6_{1,6}$	*0*	8	7	7809.7781	0.0055
		1	6	5	5805.5100	0.0023				6	5	7809.8041	0.0029
			4	3	5805.5382	0.0025				7	6	7809.8245	0.0021
			5	4	5805.6015	0.0008			*1*	8	7	7809.7781	0.0012
$5_{1,4}$	$4_{1,3}$	*0*	4	3	6140.8160	0.0020				6	5	7809.8041	-0.0013
			6	5	6140.8289	0.0013				7	6	7809.8245	-0.0021
			5	4	6140.8890	0.0019	$7_{0,7}$	$6_{0,6}$	*0*	8	7	8026.6899	0.0021
		1	4	3	6140.8007	-0.0035				6	5	8026.7043	0.0054
			6	5	6140.8160	-0.0017				7	6	8026.7978	0.0044
			5	4	6140.8753	-0.0019			*1*	8	7	8026.6899	-0.0034
$6_{1,6}$	$5_{1,5}$	*0*	7	6	6705.1332	0.0018				6	5	8026.7043	-0.0001
			5	4	6705.1753	0.0051				7	6	8026.7978	-0.0011
			6	5	6705.1918	0.0018	$7_{1,6}$	$6_{1,5}$	0	6	5	8563.3699	-0.0062
		1	7	6	6705.1332	-0.0011				8	7	8563.3818	0.0003
			5	4	6705.1753	0.0022				7	6	8563.4322	0.0001
			6	5	6705.1918	-0.0011			1	6	5	8563.3616	-0.0017
$6_{0,6}$	$5_{0,5}$	*0*	7	6	6925.1636	0.0006				8	7	8563.3732	0.0045
			5	4	6925.1825	0.0028				7	6	8563.4195	0.0002
			6	5	6925.2713	0.0069	$8_{1,8}$	$7_{1,7}$	0	9	8	8909.6348	0.0043
		1	7	6	6925.1636	-0.0013				7	6	8909.6556	0.0032

Table S6.15. Continued.

$J'K'_{-1}K'_{+1}$	$J''K''_{-1}K''_{+1}$	v	F'	F''	Obs.	Res.
$8_{1,8}$	$7_{1,7}$	0	9	8	8909.6348	0.0043
			7	6	8909.6556	0.0032
			8	7	8909.6766	0.0014
		1	9	8	8909.6348	-0.0015
			7	6	8909.6556	-0.0026
			8	7	8909.6766	-0.0043
$8_{0,8}$	$7_{0,7}$	0	7	6	9111.6823	0.0049
			9	8	9111.7110	0.0044
			8	7	9111.7539	0.0072
		1	7	6	9111.6823	-0.0061
			9	8	9111.7110	-0.0050
			8	7	9111.7539	-0.0083
$8_{1,7}$	$7_{1,6}$	0	7	6	9760.6721	-0.0015
			9	8	9760.6785	0.0004
			8	7	9760.7325	0.0000
		1	7	6	9760.6574	-0.0031
			9	8	9760.6648	-0.0001
			8	7	9760.7184	-0.0008
$9_{1,9}$	$8_{1,8}$	0	10	9	10004.7437	0.0009
			8	7	10004.7589	-0.0010
			9	8	10004.7834	-0.0005
		1	10	9	10004.7509	0.0005
			8	7	10004.7681	0.0004
			9	8	10004.7907	-0.0009
$9_{0,9}$	$8_{0,8}$	0	10	9	10183.6118	-0.0011
			8	7	10183.6567	-0.0012
		1	10	9	10183.6221	-0.0039
			8	7	10183.6698	0.0003
			9	8	10183.7756	-0.0078
$9_{1,8}$	$8_{1,7}$	0	10	9	10945.6670	-0.0019
			8	7	10945.6670	0.0021
			9	8	10945.7322	0.0027
		1	10	9	10945.6515	-0.0051
			8	7	10945.6515	-0.0010
			9	8	10945.7184	0.0012

Table S6.16. Observed rotational frequencies and residuals (all the values in MHz) for the $^{2}H_{w1}$ isotopologue of the complex *cis*-fa-w-a in the ground vibrational state for $J'K'_{-1}K'_{+1}F' \leftarrow J''K''_{-1}K''_{+1}F''$ transitions.

$J'K'_{-1}K'_{+1}$	$J''K''_{-1}K''_{+1}$	F'	F''	Obs.	Res.
$3_{1,3}$	$2_{1,2}$	4	3	3412.2721	0.0075
		2	1	3412.3853	-0.0019
$3_{2,2}$	$2_{2,1}$	3	3	3578.7658	-0.0051
$3_{1,2}$	$2_{1,1}$	2	1	3740.3271	0.0123
		2	1	3740.3271	0.0123
		4	3	3740.4325	-0.0046
$4_{1,4}$	$3_{1,3}$	5	4	4545.2555	-0.0093
$4_{0,4}$	$3_{0,3}$	5	4	4731.9995	0.0078
$4_{2,3}$	$3_{2,2}$	5	4	4768.6959	0.0083
$4_{2,2}$	$3_{2,1}$	5	4	4808.5554	-0.0161
$5_{1,5}$	$4_{1,4}$	6	5	5674.6708	-0.0035
$5_{0,5}$	$4_{0,4}$	6	5	5886.0325	-0.0036
$5_{2,4}$	$4_{2,3}$	6	5	5955.8849	0.0026
$5_{2,3}$	$4_{2,2}$	4	3	6034.6806	0.0099
		6	5	6034.6806	0.0008
$5_{1,4}$	$4_{1,3}$	6	5	6219.7907	0.0073
$6_{1,6}$	$5_{1,5}$	5	4	6799.9847	0.0141
		6	5	6799.9847	-0.0051
$6_{0,6}$	$5_{0,5}$	7	6	7022.7481	0.0025
		5	4	7022.7481	-0.0143
$6_{2,5}$	$5_{2,4}$	7	6	7139.7167	-0.0052
		5	4	7139.7167	-0.0033
$6_{2,4}$	$5_{2,3}$	5	4	7274.7285	-0.0009
		7	6	7274.7285	0.0047
		6	5	7274.7285	-0.0106
$6_{1,5}$	$5_{1,4}$	5	4	7451.2131	-0.0065
		7	6	7451.2131	-0.0139
$7_{1,7}$	$6_{1,6}$	8	7	7920.6782	0.0190
		6	5	7920.6782	-0.0095

Table S6.17. Observed rotational frequencies and residuals (all the values in MHz) for the $^{2}H_{w2}$ isotopologue of the complex *cis*-fa-w-a in the ground vibrational state for $J'K'_{-1}K'_{+1}F' \leftarrow J''K''_{-1}K''_{+1}F''$ transitions.

$J'K'_{-1}K'_{+1}$	$J''K''_{-1}K''_{+1}$	F'	F''	Obs.	Res.
$3_{1,3}$	$2_{1,2}$	4	3	3389.9335	-0.0052
		3	2	3390.1694	0.0057
$3_{1,2}$	$2_{1,1}$	4	3	3721.2498	-0.0052
		3	2	3721.4416	0.0082
$5_{1,5}$	$4_{1,4}$	5	4	5636.9765	-0.0103
		4	3	5636.9765	0.0108
$5_{0,5}$	$4_{0,4}$	6	5	5848.0544	-0.0176
		5	4	5848.1584	-0.0073
$5_{2,4}$	$4_{2,3}$	6	5	5921.0801	0.0093
		5	4	5921.2512	0.0150
$5_{2,3}$	$4_{2,2}$	6	5	6003.4192	-0.0179
		4	3	6003.4192	-0.0090
		5	4	6003.5097	-0.0105
$5_{1,4}$	$4_{1,3}$	6	5	6187.1235	0.0163
$6_{1,6}$	$5_{1,5}$	7	6	6754.2226	0.0106
		6	5	6754.2655	-0.0051
		5	4	6754.2655	0.0148
$6_{0,6}$	$5_{0,5}$	5	4	6975.5716	-0.0043
		7	6	6975.5716	0.0123
		6	5	6975.6493	-0.0119
$6_{2,5}$	$5_{2,4}$	7	6	7097.6049	0.0000
		5	4	7097.6049	0.0019
$6_{2,4}$	$5_{2,3}$	5	4	7238.5179	-0.0010
		7	6	7238.5179	0.0048
		6	5	7238.5179	-0.0087
$6_{1,5}$	$5_{1,4}$	7	6	7411.3690	-0.0041
		5	4	7411.3690	0.0033

Table S6.18. Observed rotational frequencies and residuals (all the values in MHz) for the $^{2}H_{1}$ isotopologue of the complex *cis*-fa-w-a in the ground vibrational state for $J'K'_{-1}K'_{+1}F' \leftarrow J''K''_{-1}K''_{+1}F''$ transitions.

$J'K'_{-1}K'_{+1}$	$J''K''_{-1}K''_{+1}$	F'	F''	Obs.	Res.
$3_{0,3}$	$2_{0,2}$	4	3	3609.9691	0.0223
		3	2	3609.9691	-0.0534
$3_{1,2}$	$2_{1,1}$	4	3	3794.4802	0.0097
		3	2	3794.6517	0.0029
$4_{0,4}$	$3_{0,3}$	3	2	4793.3353	-0.0246
		5	4	4793.3353	0.0276
$5_{1,5}$	$4_{1,4}$	6	5	5744.3229	0.0035
$5_{0,5}$	$4_{0,4}$	6	5	5960.4173	-0.0064
$5_{2,4}$	$4_{2,3}$	4	3	6035.8110	-0.0083
		5	4	6036.0051	0.0024
$5_{2,3}$	$4_{2,2}$	4	3	6120.9097	-0.0116
		5	4	6121.0147	0.0016
$5_{1,4}$	$4_{1,3}$	6	5	6308.6546	0.0318
		5	4	6308.6546	-0.0280
$6_{1,6}$	$5_{1,5}$	6	5	6882.8118	-0.0231
		5	4	6882.8118	-0.0029
		7	6	6882.8118	0.0357

$J'K'_{-1}K'_{+1}$	$J''K''_{-1}K''_{+1}$	F'	F''	Obs.	Res.
$6_{0,6}$	$5_{0,5}$	6	5	7109.0658	-0.0686
		5	4	7109.0658	0.0171
		7	6	7109.0658	0.0337
$6_{2,5}$	$5_{2,4}$	7	6	7235.0719	0.0043
		5	4	7235.0719	0.0062
		6	5	7235.1740	-0.0007
$6_{2,4}$	$5_{2,3}$	7	6	7380.6010	0.0066
		6	5	7380.6010	-0.0064
		5	4	7380.6010	0.0007
$6_{1,5}$	$5_{1,4}$	7	6	7556.7612	0.0215
		6	5	7556.7612	-0.0301

Table S6.19. Observed rotational frequencies and residuals (all the values in MHz) for the parent species of the complex *trans*-fa-w-b in the ground vibrational state for $J'K'_{-1}K'_{+1}F' \leftarrow J''K''_{-1}K''_{+1}F''$ transitions.

$J'K'_{-1}K'_{+}$	$J''K''_{-1}K''_{+}$	F'	F''	Obs.	Res.
$5_{0,5}$	$4_{0,4}$	6	5	5063.4394	0.0000
		4	3	5063.4677	0.0007
		5	4	5063.4885	-0.0006
$5_{2,4}$	$4_{2,3}$	4	3	5077.6948	0.0027
		6	5	5077.7068	0.0001
		5	4	5077.8571	0.0114
$5_{2,3}$	$4_{2,2}$	4	3	5093.8049	-0.0014
		6	5	5093.8185	0.0020
		5	4	5093.9140	-0.0014
$5_{1,4}$	$4_{1,3}$	4	3	5231.2395	-0.0003
		6	5	5231.2659	0.0000
		5	4	5231.3035	0.0006
$6_{1,6}$	$5_{1,5}$	7	6	5902.7788	-0.0002
		6	5	5902.8248	-0.0009
		5	4	5902.8248	0.0008
$6_{0,6}$	$5_{0,5}$	7	6	6067.3474	0.0000
		5	4	6067.3638	-0.0005
		6	5	6067.4024	-0.0002
$6_{2,5}$	$5_{2,4}$	5	4	6091.7820	-0.0004
		7	6	6091.7820	-0.0012
		6	5	6091.8696	-0.0002
$6_{2,4}$	$5_{2,3}$	7	6	6119.8891	-0.0012
		5	4	6119.8947	0.0006
		6	5	6119.9285	-0.0005
$6_{1,5}$	$5_{1,4}$	5	4	6275.1760	-0.0003
		7	6	6275.1916	-0.0001
		6	5	6275.2192	-0.0002
$7_{1,7}$	$6_{1,6}$	8	7	6883.7109	-0.0002
$J'K'_{-1}K'_{+1}$	$J''K''_{-1}K''_{+1}$	F'	F''	Obs.	Res.
		6	5	6883.7434	-0.0006
		7	6	6883.7492	0.0002
$7_{0,7}$	$6_{0,6}$	8	7	7066.5913	-0.0001
		6	5	7066.6023	-0.0002
		7	6	7066.6525	-0.0002
$7_{2,6}$	$6_{2,5}$	8	7	7105.0426	-0.0011
		6	5	7105.0463	-0.0006
		7	6	7105.1022	-0.0017
$7_{2,5}$	$6_{2,4}$	8	7	7149.8078	0.0030
		7	6	7149.8124	0.0033
		6	5	7149.8124	0.0004
$7_{1,6}$	$6_{1,5}$	6	5	7317.7749	0.0000
		8	7	7317.7853	0.0000
		7	6	7317.8094	-0.0003
$8_{1,8}$	$7_{1,7}$	9	8	7863.4030	0.0000
		7	6	7863.4272	-0.0008
		8	7	7863.4363	0.0003
$8_{0,8}$	$7_{0,7}$	9	8	8060.5651	-0.0004
		7	6	8060.5758	0.0025
		8	7	8060.6322	-0.0005
$8_{2,7}$	$7_{2,6}$	9	8	8117.3560	-0.0012
		7	6	8117.3607	-0.0007
		8	7	8117.4019	-0.0010
$8_{2,6}$	$7_{2,5}$	8	7	8184.0128	-0.0009
		9	8	8184.0293	-0.0014
		7	6	8184.0381	-0.0008
$8_{1,7}$	$7_{1,6}$	7	6	8358.7664	-0.0001
		9	8	8358.7745	0.0002
$J'K'_{-1}K'_{+1}$	$J''K''_{-1}K''_{+1}$	F'	F''	Obs.	Res.
		8	7	8358.7978	-0.0002
$9_{1,9}$	$8_{1,8}$	10	9	8841.7397	0.0004
		8	7	8841.7582	-0.0008
		9	8	8841.7696	0.0001
$9_{0,9}$	$8_{0,8}$	10	9	9048.7998	-0.0007
		8	7	9048.8056	-0.0001
		9	8	9048.8727	-0.0003
$9_{2,8}$	$8_{2,7}$	10	9	9128.5917	-0.0006
		8	7	9128.5965	0.0000
		9	8	9128.6286	-0.0010
$9_{2,7}$	$8_{2,6}$	9	8	9222.8681	-0.0007
		10	9	9222.8992	-0.0012
		8	7	9222.9085	0.0001
$9_{1,8}$	$8_{1,7}$	8	7	9397.8554	-0.0004
		10	9	9397.8622	0.0002
		9	8	9397.8865	-0.0002
$10_{1,10}$	$9_{1,9}$	11	10	9818.6272	0.0005
		9	8	9818.6424	0.0000
		10	9	9818.6558	0.0006
$10_{0,10}$	$9_{0,9}$	11	10	10031.0100	-0.0007
		9	8	10031.0149	0.0005
		10	9	10031.0870	-0.0005
$10_{2,9}$	$9_{2,8}$	11	10	10138.6177	-0.0007
		9	8	10138.6227	0.0004
		10	9	10138.6503	-0.0004
$10_{2,8}$	$9_{2,7}$	10	9	10266.5177	0.0000
		11	10	10266.5583	-0.0007
		9	8	10266.5662	-0.0001

Table S6.19. Continued.

$J'K'_{-1}K'_{+}$	$J''K''_{-1}K''_{+}$	F'	F''	Obs.	Res.
$10_{1,9}$	$9_{1,8}$	9	8	10434.7195	-0.0004
		11	10	10434.7257	0.0006
		10	9	10434.7518	0.0000
$11_{1,11}$	$10_{1,10}$	12	11	10793.9948	0.0004
		10	9	10794.0083	0.0009
		11	10	10794.0224	0.0004
$11_{0,11}$	$10_{0,10}$	12	11	11007.1313	-0.0010
		10	9	11007.1354	0.0003
		11	10	11007.2120	-0.0003
$11_{2,10}$	$10_{2,9}$	12	11	11147.3068	0.0000
		10	9	11147.3111	0.0009
		11	10	11147.3365	0.0003
$11_{2,9}$	$10_{2,8}$	11	10	11314.8786	0.0000
		12	11	11314.9267	0.0002
		10	9	11314.9337	0.0007
$11_{1,10}$	$10_{1,9}$	10	9	11469.0064	0.0002
		12	11	11469.0119	0.0014
		11	10	11469.0402	0.0005
$1_{1,1}$	$0_{0,0}$	2	1	4571.7271	0.0070
		1	1	4572.2146	-0.0138
$2_{1,2}$	$1_{0,1}$	3	2	5525.4275	-0.0009
		1	0	5525.6275	-0.0050
		2	1	5526.0275	0.0138
$3_{1,3}$	$2_{0,2}$	4	3	6448.4162	0.0021
		3	2	6449.1461	-0.0014
$4_{1,4}$	$3_{0,3}$	5	4	7341.6784	0.0001
		4	3	7342.4659	-0.0019

Table S6.20. Observed rotational frequencies and residuals (all the values in MHz) for the $^{18}O_w$ isotopologue of the complex *trans*-fa-w-b in the ground vibrational state for $J'K'_{-1}K'_{+1}F' \leftarrow J''K''_{-1}K''_{+1}F''$ transitions.

$J'K'_{-1}K'_{+1}$	$J''K''_{-1}K''_{+1}$	F'	F''	Obs.	Res.
$6_{1,5}$	$5_{1,4}$	5	4	5985.3502	0.0013
		7	6	5985.3652	0.0010
		6	5	5985.3887	-0.0018
$7_{1,7}$	$6_{1,6}$	8	7	6584.0085	-0.0006
		6	5	6584.0386	-0.0036
		7	6	6584.0462	0.0002
$7_{0,7}$	$6_{0,6}$	8	7	6753.7849	0.0002
		6	5	6753.7962	0.0001
		7	6	6753.8410	0.0000
$7_{2,6}$	$6_{2,5}$	6	5	6785.6699	-0.0029
		8	7	6785.6699	0.0003
		7	6	6785.7258	-0.0030
$7_{2,5}$	$6_{1,4}$	8	7	6822.7791	-0.0031
		7	6	6822.7902	-0.0020
		6	5	6822.7902	-0.0006
$7_{1,6}$	$6_{1,5}$	6	5	6980.2196	-0.0006
		8	7	6980.2251	-0.0054
		7	6	6980.2591	0.0055
$8_{1,8}$	$7_{1,7}$	9	8	7521.4961	-0.0001
		7	6	7521.5190	-0.0023
		8	7	7521.5286	0.0006
$8_{0,8}$	$7_{0,7}$	9	8	7705.6600	-0.0001
		7	6	7705.6676	0.0010
		8	7	7705.7220	0.0000
$8_{1,8}$	$7_{0,7}$	7	6	10401.3640	0.0002
		9	8	10401.4481	0.0027
		8	7	10402.2184	0.0002
$9_{1,9}$	$8_{0,8}$	8	7	11153.5542	-0.0034
		10	9	11153.6271	0.0013
		9	8	11154.3696	0.0038
$10_{0,10}$	$9_{1,9}$	10	9	7093.0165	0.0027
		11	10	7093.6167	0.0012
		9	8	7093.6959	0.0013

Table S6.21. Observed rotational frequencies and residuals (all the values in MHz) for the $^{2}H_{w1}$ isotopologue of the complex *trans*-fa-w-b in the ground vibrational state for $J'K'_{-1}K'_{+1}F' \leftarrow J''K''_{-1}K''_{+1}F''$ transitions.

$J'K'_{-1}K'_{+}$	$J''K''_{-1}K''_{+}$	F'	F''	Obs.	Res.
$5_{1,5}$	$4_{1,4}$	6	5	4846.0096	0.0103
$6_{0,6}$	$5_{0,5}$	7	6	5973.7691	-0.0162
$6_{2,5}$	$5_{2,4}$	7	6	5996.9626	0.0029
		5	4	5996.9627	0.0038
		6	5	5997.0500	0.0040
$6_{2,4}$	$5_{2,3}$	7	6	6023.6091	-0.0078
		5	4	6023.6091	-0.0115
$6_{1,5}$	$5_{1,4}$	7	6	6175.4227	0.0014
$7_{1,7}$	$6_{1,6}$	8	7	6779.3499	0.0088
$7_{0,7}$	$6_{0,6}$	8	7	6958.0506	0.0063
		6	5	6958.0507	-0.0046
$7_{2,6}$	$6_{2,5}$	6	5	6994.5276	0.0026
		8	7	6994.5276	0.0058
$7_{2,5}$	$6_{2,4}$	8	7	7036.9874	0.0039
		7	6	7036.9874	-0.0014
		6	5	7036.9876	-0.0029
$7_{1,6}$	$6_{1,5}$	7	6	7201.5874	0.0030
$8_{1,8}$	$7_{1,7}$	9	8	7744.2958	-0.0103

Table S6.22. Observed rotational frequencies and residuals (all the values in MHz) for the parent species of the complex *trans*-fa-w-c in the *v = 0* and *v = 1* vibrational states for $J'K'_{-1}K'_{+1}v'F' \leftarrow J''K''_{-1}K''_{+1}v''F''$ transitions.

$J'K'_{-1}K'_{+}$	$J''K''_{-1}K''_{+}$	v	F'	F''	Obs.	Res.
$4_{1,4}$	$3_{1,3}$	*0*	5	4	5163.4679	0.0002
			4	3	5163.6481	0.0000
		1	5	4	5163.5819	0.0012
			3	2	5163.6596	0.0000
			4	3	5163.7597	-0.0014
$4_{0,4}$	$3_{0,3}$	*0*	5	4	5300.0497	0.0012
			3	2	5300.0942	0.0000
			4	3	5300.3061	0.0010
		1	5	4	5300.0424	-0.0019
			3	2	5300.0887	-0.0014
			4	3	5300.2994	-0.0015
$4_{2,3}$	$3_{2,2}$	*0*	3	2	5886.0755	-0.0004
			5	4	5886.1628	-0.0003
			4	3	5886.5024	0.0008
		1	3	2	5886.0111	0.0005
			5	4	5886.0965	-0.0012
			4	3	5886.4363	0.0000
$4_{2,2}$	$3_{1,2}$	*0*	3	2	6541.1750	0.0031
			5	4	6541.2462	-0.0004
			4	3	6541.3479	0.0000
		1	3	2	6541.0475	-0.0011
			5	4	6541.1237	0.0002
			4	3	6541.2252	0.0005
$4_{1,3}$	$3_{1,2}$	*0*	3	2	6375.8713	0.0007
			5	4	6375.9477	-0.0001
			4	3	6376.1892	0.0009
		1	3	2	6375.6056	0.0004
			5	4	6375.6815	-0.0010

$J'K'_{-1}K'_{+1}$	$J''K''_{-1}K''_{+1}$	v	F'	F''	Obs.	Res.
			4	3	6375.9236	0.0005
$5_{1,5}$	$4_{1,4}$	*0*	6	5	6365.5694	0.0005
			4	3	6365.6241	0.0012
			5	4	6365.7040	-0.0013
		1	6	5	6365.7240	0.0012
			4	3	6365.7794	0.0026
			5	4	6365.8606	0.0012
$5_{0,5}$	$4_{0,4}$	*0*	6	5	6432.0353	-0.0004
			4	3	6432.0777	0.0003
			5	4	6432.2155	0.0007
		1	6	5	6432.1150	0.0011
			4	3	6432.1569	0.0014
			5	4	6432.2931	0.0003
$5_{2,4}$	$4_{2,3}$	*0*	4	3	7248.0508	-0.0011
			6	5	7248.0831	0.0008
			5	4	7248.3203	0.0007
		1	4	3	7247.9648	-0.0005
			6	5	7247.9938	-0.0018
			5	4	7248.2322	-0.0008
$5_{2,3}$	$4_{2,2}$	*0*	4	3	8244.1638	0.0009
			6	5	8244.2032	-0.0002
			5	4	8244.2911	0.0001
		1	4	3	8243.9099	0.0006
			6	5	8243.9497	0.0000
			5	4	8244.0380	0.0006
$5_{3,3}$	$4_{3,2}$	*0*	4	3	7625.5025	0.0054
			6	5	7625.5751	-0.0008
			5	4	7625.8597	-0.0008

$J'K'_{-1}K'_{+1}$	$J''K''_{-1}K''_{+1}$	v	F'	F''	Obs.	Res.
		1	4	3	7625.3997	-0.0007
			6	5	7625.4772	-0.0021
			5	4	7625.7648	0.0008
$5_{3,2}$	$4_{3,1}$	*0*	4	3	7910.1360	0.0004
			6	5	7910.1857	-0.0020
			5	4	7910.3079	0.0003
		1	4	3	7910.1206	0.0003
			6	5	7910.1714	-0.0009
			5	4	7910.2927	0.0005
$5_{1,4}$	$4_{1,3}$	*0*	4	3	7711.4550	-0.0001
			6	5	7711.5068	-0.0009
			5	4	7711.7860	0.0009
		1	4	3	7711.0999	0.0019
			6	5	7711.1503	-0.0002
			5	4	7711.4275	-0.0004
$6_{1,6}$	$5_{1,5}$	*0*	7	6	7547.0179	0.0005
			5	4	7547.0579	0.0005
			6	5	7547.1234	-0.0008
		1	7	6	7547.2242	0.0007
			5	4	7547.2628	-0.0007
			6	5	7547.3308	0.0003
$6_{0,6}$	$5_{0,5}$	*0*	7	6	7574.7954	0.0001
			5	4	7574.8324	0.0009
			6	5	7574.9218	0.0022
		1	7	6	7574.9632	0.0009
			5	4	7574.9975	-0.0009
			6	5	7575.0859	-0.0006
$6_{2,5}$	$5_{2,4}$	*0*	5	4	8550.8346	0.0001

Table S6.22. Continued.

$J'K'_{-1}K'_{+1}$	$J''K''_{-1}K''_{+1}$	v	F'	F''	Obs.	Res.
			7	6	8550.8474	0.0000
			6	5	8551.0433	0.0014
		1	5	4	8550.7312	-0.0010
			7	6	8550.7447	-0.0004
			6	5	8550.9395	-0.0001
$6_{2,4}$	$5_{2,3}$	*0*	5	4	9833.4566	-0.0002
			7	6	9833.4903	-0.0001
			6	5	9833.6193	-0.0008
		1	5	4	9833.0442	0.0011
			7	6	9833.0768	0.0001
			6	5	9833.2069	0.0004
$6_{1,5}$	$5_{1,4}$	*0*	5	4	8896.6194	0.0016
			7	6	8896.6534	0.0002
			6	5	8896.9357	0.0003
		1	5	4	8896.2220	0.0039
			7	6	8896.2516	-0.0018
			6	5	8896.5335	-0.0021
$7_{1,7}$	$6_{1,6}$	*0*	8	7	8717.7449	0.0002
			6	5	8717.7754	-0.0006
			7	6	8717.8260	-0.0034
		1	8	7	8718.0123	0.0004
			6	5	8718.0431	-0.0001
			7	6	8718.0964	-0.0002
$7_{0,7}$	$6_{0,6}$	*0*	8	7	8728.3679	0.0003
			6	5	8728.3978	0.0000
			7	6	8728.4589	0.0003
		1	8	7	8728.6168	-0.0003
			6	5	8728.6477	0.0003
			7	6	8728.7083	0.0002

$J'K'_{-1}K'_{+1}$	$J''K''_{-1}K''_{+1}$	v	F'	F''	Obs.	Res.
$7_{2,6}$	$6_{2,5}$	*0*	6	5	9800.7796	-0.0006
			8	7	9800.7859	0.0003
			7	6	9800.9525	-0.0015
		1	6	5	9800.6749	-0.0018
			8	7	9800.6824	0.0003
			7	6	9800.8520	0.0014
$7_{1,6}$	$6_{1,5}$	*0*	6	5	10005.1477	0.0011
			8	7	10005.1659	0.0004
			7	6	10005.4052	0.0007
		1	6	5	10004.8039	0.0025
			8	7	10004.8215	0.0012
			7	6	10005.0594	0.0001
$8_{1,8}$	$7_{1,7}$	*0*	9	8	9883.6862	0.0003
			7	6	9883.7102	-0.0010
			8	7	9883.7537	-0.0001
		1	9	8	9884.0200	0.0005
			7	6	9884.0447	-0.0001
			8	7	9884.0873	-0.0001
$8_{0,8}$	$7_{0,7}$	*0*	9	8	9887.5264	-0.0002
			7	6	9887.5496	-0.0021
			8	7	9887.5954	-0.0013
		1	9	8	9887.8539	0.0010
			7	6	9887.8779	0.0000
			8	7	9887.9232	0.0002
$8_{2,7}$	$7_{2,6}$	*0*	7	6	11011.1803	0.0010
			9	8	11011.1803	-0.0002
			8	7	11011.3269	0.0000
		1	7	6	11011.0962	0.0013
			9	8	11011.0962	0.0000

$J'K'_{-1}K'_{+1}$	$J''K''_{-1}K''_{+1}$	v	F'	F''	Obs.	Res.
			8	7	11011.2424	-0.0001
$8_{1,7}$	$7_{1,6}$	*0*	7	6	11112.2307	-0.0023
			9	8	11112.2409	0.0005
			8	7	11112.4277	0.0024
		1	7	6	11111.9955	-0.0022
			9	8	11112.0089	0.0038
			8	7	11112.1897	-0.0002
$4_{0,4}$	$3_{1,3}$	*0*	5	4	5052.7499	-0.0003
			3	2	5052.8475	0.0006
			4	3	5052.8614	-0.0002
		1	5	4	5053.0077	0.0000
			3	2	5053.1029	-0.0015
			4	3	5053.1198	0.0004
$5_{0,5}$	$4_{1,4}$	*0*	6	5	6321.3178	-0.0005
			4	3	6321.3783	0.0006
			5	4	6321.4281	-0.0001
		1	6	5	6321.5403	-0.0006
			4	3	6321.6027	0.0023
			5	4	6321.6509	0.0000
$6_{0,6}$	$5_{1,5}$	*0*	7	6	7530.5450	0.0002
			5	4	7530.5863	0.0000
			6	5	7530.6421	-0.0003
		1	7	6	7530.7801	-0.0003
			5	4	7530.8221	0.0000
			6	5	7530.8784	0.0002
$7_{0,7}$	$6_{1,6}$	*0*	8	7	8711.8950	0.0000
			6	5	8711.9230	-0.0038
			7	6	8711.9766	-0.0001
		1	8	7	8712.1746	0.0005

Table S6.22. Continued.

$J'K'_{-1}K'_{+1}$	$J''K''_{-1}K''_{+1}$	v	F'	F''	Obs.	Res.
			6	5	8712.2070	0.0010
			7	6	8712.2558	0.0000
$8_{0,8}$	$7_{1,7}$	*0*	9	8	9881.6776	0.0006
			7	6	9881.7035	0.0009
			8	7	9881.7437	-0.0003
		1	9	8	9882.0153	0.0001
			7	6	9882.0408	0.0001
			8	7	9882.0821	0.0000
$3_{1,3}$	$2_{0,2}$	*0*	4	3	4392.6805	0.0002
			3	2	4393.1389	0.0003
		1	4	3	4392.3725	-0.0011
			2	1	4392.4003	0.0039
			3	2	4392.8306	-0.0013
$4_{1,4}$	$3_{0,3}$	*0*	5	4	5410.7663	0.0004
			3	2	5410.7933	-0.0006
			4	3	5411.0921	0.0006
		1	5	4	5410.6151	-0.0021
			3	2	5410.6414	-0.0038
			4	3	5410.9411	-0.0016
$5_{1,5}$	$4_{0,4}$	*0*	6	5	6476.2859	-0.0004
			4	3	6476.3219	-0.0005
			5	4	6476.4904	-0.0014
		1	6	5	6476.2963	0.0006
			4	3	6476.3322	0.0003
			5	4	6476.5014	0.0002
$6_{1,6}$	$5_{0,5}$	*0*	7	6	7591.2699	0.0020
			5	4	7591.3030	0.0005
			6	5	7591.4018	0.0004
		1	7	6	7591.4068	0.0015
			5	4	7591.4394	-0.0005
			6	5	7591.5376	-0.0011
$7_{1,7}$	$6_{0,6}$	*0*	8	7	8734.2179	0.0006
			6	5	8734.2460	-0.0010
			7	6	8734.3118	0.0005
		1	8	7	8734.4549	0.0000
			6	5	8734.4839	-0.0007
			7	6	8734.5492	0.0003
$8_{1,8}$	$7_{0,7}$	*0*	9	8	9889.5354	0.0000
			7	6	9889.5600	-0.0004
			8	7	9889.6073	0.0007
		1	9	8	9889.8570	-0.0001
			7	6	9889.8833	0.0011
			8	7	9889.9288	0.0005
$5_{1,4}$	$4_{2,3}$	*0*	6	5	6523.2351	-0.0013
			4	3	6523.2484	-0.0034
			5	4	6523.2484	-0.0011
		1	6	5	6523.9816	-0.0013
			4	3	6523.9966	-0.0017
			5	4	6523.9966	0.0004
$6_{1,5}$	$5_{2,4}$	*0*	7	6	8171.8074	0.0000
			5	4	8171.8180	0.0002
			6	5	8171.8656	0.0003
		1	7	6	8172.2400	-0.0007
			5	4	8172.2510	0.0000
			6	5	8172.2987	0.0000
$7_{1,6}$	$6_{2,5}$	*0*	8	7	9626.1252	-0.0004
			6	5	9626.1303	0.0005
			7	6	9626.2282	0.0003
		1	8	7	9626.3157	-0.0002
			6	5	9626.3209	0.0007
			7	6	9626.4184	0.0001
$8_{1,7}$	$7_{2,6}$	*0*	9	8	10937.5780	-0.0023
			7	6	10937.5813	-0.0013
			8	7	10937.6995	0.0003
		1	9	8	10937.6365	-0.0024
			7	6	10937.6411	0.0000
			8	7	10937.7581	0.0004
$3_{2,2}$	$2_{1,1}$	*0*	2	1	6568.7378	-0.0023
			4	3	6568.9768	0.0038
			3	2	6569.3919	0.0006
		1	2	1	6567.2524	-0.0018
			4	3	6567.4837	-0.0033
			3	2	6567.9051	-0.0002
$4_{2,3}$	$3_{1,2}$	*0*	3	2	7564.0725	-0.0012
			5	4	7564.2224	0.0032
			4	3	7564.7259	0.0021
		1	3	2	7562.7040	-0.0008
			5	4	7562.8499	-0.0002
			4	3	7563.3549	0.0000
$5_{2,4}$	$4_{1,3}$	*0*	4	3	8436.2561	0.0009
			6	5	8436.3531	-0.0003
			5	4	8436.8561	0.0010
		1	4	3	8435.0635	-0.0014
			6	5	8435.1614	-0.0018
			5	4	8435.6614	-0.0034
$3_{3,0}$	$2_{2,1}$	*0*	3	2	8851.3200	-0.0012
			2	1	8851.5800	-0.0003

Table S6.22. Continued.

$J'K'_{-1}K'_{+}$	$J''K''_{-1}K''_{+}$	v	F'	F''	Obs.	Res.
			4	3	8851.6116	-0.0015
		1	3	2	8848.6699	0.0015
			2	1	8848.9304	0.0028
			4	3	8848.9619	0.0015
$3_{3,1}$	$2_{2,0}$	*0*	2	1	8745.0144	0.0046
			3	2	8745.1598	-0.0002
			4	3	8745.1837	-0.0007
		1	2	1	8742.3427	-0.0017
			3	2	8742.4951	0.0003
			4	3	8742.5199	0.0006
$4_{3,2}$	$3_{2,1}$	*0*	3	2	10053.4683	-0.0034
			5	4	10053.5535	-0.0014
			4	3	10053.6861	-0.0023
		1	3	2	10050.7926	0.0023
			5	4	10050.8735	0.0000
			4	3	10051.0057	-0.0014

Table S6.23. Observed rotational frequencies and residuals (all the values in MHz) for the $^{18}O_w$ isotopologue of the complex *trans*-fa-w-c in the *v = 0* and *v = 1* vibrational states for $J'K'_{-1}K'_{+1}v'F' \leftarrow J''K''_{-1}K''_{+1}v''F''$ transitions.

$J'K'_{-1}K'_{+}$	$J''K''_{-1}K''_{+}$	v	F'	F''	Obs.	Res.	$J'K'_{-1}K'_{+}$	$J''K''_{-1}K''_{+}$	v	F'	F''	Obs.	Res.
$7_{1,7}$	$6_{1,6}$	*0*	7	6	8449.1341	0.0001	$7_{0,7}$	$6_{1,6}$	*0*	7	6	8443.2265	-0.0012
			6	5	8449.0797	-0.0008				6	5	8443.1763	-0.0016
			8	7	8449.0503	0.0011				8	7	8443.1460	-0.0001
		1	7	6	8449.4326	0.0002			*1*	7	6	8443.5400	-0.0019
			6	5	8449.3771	-0.0017				6	5	8443.4911	-0.0009
			8	7	8449.3478	0.0003				8	7	8443.4604	0.0001
$7_{0,7}$	$6_{0,6}$	*0*	7	6	8459.7625	0.0009	$5_{1,5}$	$4_{0,4}$	*0*	5	4	6278.8699	0.0002
			6	5	8459.6993	-0.0012				6	5	6278.6620	-0.0008
			8	7	8459.6716	0.0012				4	3	6278.6979	-0.0007
		1	7	6	8460.0369	-0.0001			*1*	5	4	6278.8720	-0.0037
			6	5	8459.9757	-0.0002				6	5	6278.6701	0.0011
			8	7	8459.9463	0.0005				4	3	6278.7052	0.0004
$5_{0,5}$	$4_{1,4}$	*0*	5	4	6124.9210	-0.0009	$6_{1,6}$	$5_{0,5}$	*0*	6	5	7358.5009	0.0011
			4	3	6124.8725	0.0001				5	4	7358.4003	0.0002
			6	5	6124.8155	0.0026				7	6	7358.3662	0.0006
		1	5	4	6125.1972	-0.0003			*1*	6	5	7358.6517	0.0023
			4	3	6125.1483	0.0003				5	4	7358.5493	-0.0002
			6	5	6125.0892	0.0007				7	6	7358.5167	0.0015
$6_{0,6}$	$5_{1,5}$	*0*	6	5	7297.8142	-0.0014	$7_{1,7}$	$6_{0,6}$	*0*	7	6	8465.6676	-0.0001
			5	4	7297.7599	0.0000				6	5	8465.6038	0.0006
			7	6	7297.7175	-0.0008				8	7	8465.5744	0.0010
		1	6	5	7298.0915	-0.0006			*1*	7	6	8465.9284	0.0010
			5	4	7298.0373	0.0009				6	5	8465.8627	0.0000
			7	6	7297.9946	-0.0001				8	7	8465.8337	0.0006

Table S6.24. Observed rotational frequencies and residuals (all the values in MHz) for the parent species of the complex *cis*-fa-w_2 in the ground vibrational state for $J'K'_{-1}K'_{+1}F' \leftarrow J''K''_{-1}K''_{+1}F''$ transitions.

$J'K'_{-1}K'_{+}$	$J''K''_{-1}K''_{+}$	F'	F''	Obs.	Res.
$6_{1,6}$	$5_{1,5}$	7	6	5100.0812	0.0001
		5	4	5100.1182	0.0000
		6	5	5100.1399	-0.0003
$6_{0,6}$	$5_{0,5}$	7	6	5268.0416	0.0003
		5	4	5268.0561	0.0001
		6	5	5268.1513	0.0002
$6_{2,5}$	$5_{2,4}$	5	4	5379.1364	0.0002
		7	6	5379.1386	0.0001
		6	5	5379.2427	0.0006
$6_{3,4}$	$5_{3,3}$	5	4	5415.0931	0.0003
		7	6	5415.1210	0.0006
		6	5	5415.2897	0.0005
$6_{3,3}$	$5_{3,2}$	5	4	5420.9569	-0.0005
		7	6	5420.9835	-0.0001
		6	5	5421.1422	-0.0002
$6_{2,4}$	$5_{2,3}$	6	5	5507.6041	-0.0010
		7	6	5507.6041	0.0004
		5	4	5507.6108	0.0011
$6_{1,5}$	$5_{1,4}$	5	4	5630.7534	0.0004
		7	6	5630.7628	0.0008
		6	5	5630.8157	-0.0003
$7_{1,7}$	$6_{1,6}$	8	7	5938.3481	0.0001
		6	5	5938.3743	-0.0010
		7	6	5938.3996	0.0007
$7_{0,7}$	$6_{0,6}$	8	7	6099.0136	-0.0003
		6	5	6099.0237	0.0000
		7	6	6099.1256	-0.0003
$7_{2,6}$	$6_{2,5}$	8	7	6265.9080	-0.0006
$J'K'_{-1}K'_{+1}$	$J''K''_{-1}K''_{+1}$	F'	F''	Obs.	Res.
		6	5	6265.9113	0.0000
		7	6	6265.9849	-0.0006
$7_{3,5}$	$6_{3,4}$	6	5	6322.0057	-0.0006
		8	7	6322.0165	0.0000
		7	6	6322.1213	0.0001
$7_{3,4}$	$6_{3,3}$	6	5	6335.0954	-0.0001
		8	7	6335.1043	0.0003
		7	6	6335.1920	-0.0002
$7_{2,5}$	$6_{2,4}$	7	6	6462.5888	0.0005
		8	7	6462.6165	-0.0002
		6	5	6462.6266	0.0012
$7_{1,6}$	$6_{1,5}$	6	5	6551.2015	-0.0004
		8	7	6551.2095	0.0009
		7	6	6551.2647	0.0005
$8_{1,8}$	$7_{1,7}$	9	8	6772.4113	0.0013
		7	6	6772.4276	-0.0033
		8	7	6772.4569	0.0008
$8_{0,8}$	$7_{0,7}$	9	8	6916.8738	0.0010
		7	6	6916.8820	0.0005
		8	7	6916.9806	-0.0006
$8_{2,7}$	$7_{2,6}$	9	8	7148.2585	-0.0010
		7	6	7148.2635	0.0007
		8	7	7148.3237	0.0006
$8_{3,6}$	$7_{3,5}$	7	6	7229.6881	-0.0005
		9	8	7229.6930	0.0011
		8	7	7229.7603	-0.0006
$8_{3,5}$	$7_{3,4}$	9	8	7255.5449	0.0000
		7	6	7255.5449	0.0008
$J'K'_{-1}K'_{+1}$	$J''K''_{-1}K''_{+1}$	F'	F''	Obs.	Res.
		8	7	7255.5907	0.0010
$8_{2,6}$	$7_{2,5}$	8	7	7425.9782	0.0000
		9	8	7426.0157	-0.0013
		7	6	7426.0251	0.0003
$8_{1,7}$	$7_{1,6}$	7	6	7461.8923	-0.0004
		9	8	7461.8991	0.0006
		8	7	7461.9606	0.0008
$9_{1,9}$	$8_{1,8}$	10	9	7602.3976	0.0000
		8	7	7602.4142	-0.0001
		9	8	7602.4397	-0.0005
$9_{0,9}$	$8_{0,8}$	10	9	7725.3539	0.0000
		8	7	7725.3618	0.0010
		9	8	7725.4529	0.0007
$9_{2,8}$	$8_{2,7}$	10	9	8025.6610	-0.0019
		8	7	8025.6653	-0.0010
		9	8	8025.7184	-0.0006
$9_{3,7}$	$8_{3,6}$	10	9	8137.5319	-0.0004
		8	7	8137.5319	-0.0002
		9	8	8137.5811	0.0001
$9_{1,8}$	$8_{1,7}$	8	7	8360.5691	-0.0015
		10	9	8360.5774	0.0015
		9	8	8360.6452	0.0000
$9_{2,7}$	$8_{2,6}$	9	8	8393.2138	-0.0003
		10	9	8393.2505	-0.0002
		8	7	8393.2560	-0.0005
$10_{1,10}$	$9_{1,9}$	11	10	8428.6025	0.0001
		9	8	8428.6165	0.0006
		10	9	8428.6408	-0.0013

Table S6.24. Continued.

$J'K'_{-1}K'_{+1}$	$J''K''_{-1}K''_{+1}$	F'	F''	Obs.	Res.
$10_{0,10}$	$9_{0,9}$	11	10	8528.4388	-0.0002
		9	8	8528.4477	0.0017
		10	9	8528.5254	0.0000
$10_{2,9}$	$9_{2,8}$	11	10	8897.6672	0.0002
		9	8	8897.6710	0.0008
		10	9	8897.7194	0.0002
$10_{4,7}$	$9_{4,6}$	9	8	9042.2793	-0.0002
		11	10	9042.2827	0.0003
		10	9	9042.3405	-0.0001
$10_{3,8}$	$9_{3,7}$	11	10	9044.7640	0.0000
		9	8	9044.7640	-0.0009
		10	9	9044.8005	-0.0003
$10_{3,7}$	$9_{3,6}$	10	9	9122.4572	0.0001
		11	10	9122.4652	0.0001
		9	8	9122.4707	0.0011
$10_{1,9}$	$9_{1,8}$	9	8	9244.9358	-0.0011
		11	10	9244.9428	0.0007
		10	9	9245.0205	0.0000
$10_{2,8}$	$9_{2,7}$	10	9	9359.3813	-0.0001
		11	10	9359.4077	-0.0012
		9	8	9359.4123	-0.0002
$11_{1,11}$	$10_{1,10}$	12	11	9251.4311	0.0007
		10	9	9251.4413	-0.0003
		11	10	9251.4670	-0.0005
$11_{0,11}$	$10_{0,10}$	12	11	9329.3892	-0.0002
		10	9	9329.3967	0.0004
		11	10	9329.4632	0.0003
$11_{2,10}$	$10_{2,9}$	12	11	9763.9166	-0.0001
		10	9	9763.9200	0.0005
		11	10	9763.9672	0.0004
$11_{3,9}$	$10_{3,8}$	12	11	9950.5021	-0.0003
		10	9	9950.5021	-0.0019
		11	10	9950.5316	-0.0009
$11_{4,8}$	$10_{4,7}$	12	11	9954.9607	-0.0014
		10	9	9954.9607	-0.0006
		11	10	9955.0034	0.0004
$11_{3,8}$	$10_{3,7}$	11	10	10072.1982	0.0005
		12	11	10072.2232	0.0000
		10	9	10072.2288	0.0004
$11_{1,10}$	$10_{1,9}$	10	9	10112.9832	-0.0005
		12	11	10112.9890	0.0001
		11	10	10113.0764	-0.0002
$11_{2,9}$	$10_{2,8}$	11	10	10320.1384	-0.0009
		12	11	10320.1537	-0.0005
		10	9	10320.1558	-0.0002
$12_{1,12}$	$11_{1,11}$	13	12	10071.3519	-0.0005
		11	10	10071.3615	-0.0005
		12	11	10071.3862	-0.0008
$12_{0,12}$	$11_{0,11}$	13	12	10130.3350	-0.0002
		11	10	10130.3426	0.0006
		12	11	10130.3974	0.0005
$12_{2,11}$	$11_{2,10}$	11	10	10624.1796	-0.0015
		13	12	10624.1796	0.0008
		12	11	10624.2285	0.0008
$12_{3,10}$	$11_{3,9}$	13	12	10853.8096	-0.0009
		11	10	10853.8121	0.0001
		12	11	10853.8365	-0.0010
$12_{1,11}$	$11_{1,10}$	11	10	10963.4878	-0.0005
		13	12	10963.4931	0.0001
		12	11	10963.5887	-0.0005
$12_{3,9}$	$11_{3,8}$	12	11	11033.9799	0.0014
		13	12	11034.0171	0.0003
		11	10	11034.0235	0.0012
$13_{1,13}$	$12_{1,12}$	14	13	10888.8559	-0.0002
		12	11	10888.8648	0.0004
		13	12	10888.8882	0.0000
$13_{0,13}$	$12_{0,12}$	14	13	10932.3699	-0.0008
		12	11	10932.3773	0.0001
		13	12	10932.4215	-0.0006
$13_{2,12}$	$12_{2,11}$	14	13	11478.3609	0.0003
		12	11	11478.3638	0.0011
		13	12	11478.4107	0.0018

Table S6.25. Observed rotational frequencies and residuals (all the values in MHz) for the $^{18}O_{w1}$ isotopologue of the complex *cis*-fa-w_2 in the ground vibrational state for $J'K'_{-1}K'_{+1}F' \leftarrow J''K''_{-1}K''_{+1}F''$ transitions.

$J'K'_{-1}K'_{+1}$	$J''K''_{-1}K''_{+1}$	F'	F''	Obs.	Res.
$7_{0,7}$	$6_{0,6}$	8	7	6017.6862	-0.0010
		6	5	6017.6978	0.0011
		7	6	6017.8023	0.0007
$8_{0,8}$	$7_{0,7}$	9	8	6822.3376	-0.0016
		7	6	6822.3471	-0.0013
		8	7	6822.4474	-0.0017
$9_{1,9}$	$8_{1,8}$	10	9	7502.1654	-0.0002
		8	7	7502.1821	-0.0001
		9	8	7502.2031	-0.0059
$9_{0,9}$	$8_{0,8}$	10	9	7618.1270	-0.0016
		8	7	7618.1449	0.0089
		9	8	7618.2280	0.0011
$9_{2,8}$	$8_{2,7}$	8	7	7930.7332	-0.0045
		10	9	7930.7332	-0.0012
		9	8	7930.7908	-0.0011
$9_{3,7}$	$8_{3,6}$	8	7	8048.7923	0.0007
		10	9	8048.7923	0.0004
		9	8	8048.8400	-0.0008
$9_{3,6}$	$8_{3,5}$	8	7	8100.7483	-0.0019
		10	9	8100.7483	0.0010
		9	8	8100.7652	0.0062
$9_{1,8}$	$8_{1,7}$	8	7	8264.7780	-0.0028
		10	9	8264.7855	-0.0009
		9	8	8264.8617	0.0019
$9_{2,7}$	$8_{2,6}$	9	8	8314.7210	-0.0001
		10	9	8314.7580	0.0021
		8	7	8314.7580	-0.0031
$10_{1,10}$	$9_{1,9}$	11	10	8316.5441	-0.0001
		9	8	8316.5593	0.0016
		10	9	8316.5829	-0.0017
$12_{0,12}$	$11_{0,11}$	13	12	9988.6770	-0.0005
		11	10	9988.6853	0.0007
		12	11	9988.7391	0.0017

Table S6.26. Observed rotational frequencies and residuals (all the values in MHz) for the $^{18}O_{w2}$ isotopologue of the complex *cis*-fa-w_2 in the ground vibrational state for $J'K'_{-1}K'_{+1}F' \leftarrow J''K''_{-1}K''_{+1}F''$ transitions.

$J'K'_{-1}K'_{+1}$	$J''K''_{-1}K''_{+1}$	F'	F''	Obs.	Res.	$J'K'_{-1}K'_{+1}$	$J''K''_{-1}K''_{+1}$	F'	F''	Obs.	Res.
$7_{0,7}$	$6_{0,6}$	8	7	5925.5262	-0.0019	$9_{3,6}$	$8_{3,5}$	8	7	7920.2319	-0.0004
		6	5	5925.5381	0.0001			10	9	7920.2319	0.0020
		7	6	5925.6360	-0.0004			9	8	7920.2500	0.0019
$8_{0,8}$	$7_{0,7}$	9	8	6723.1304	-0.0006	$9_{1,8}$	$8_{1,7}$	8	7	8103.1118	-0.0014
		7	6	6723.1406	0.0006			10	9	8103.1193	0.0010
		8	7	6723.2377	0.0000			9	8	8103.1822	-0.0002
$9_{1,9}$	$8_{1,8}$	10	9	7384.8021	-0.0008	$9_{2,7}$	$8_{2,6}$	9	8	8113.1067	0.0004
		8	7	7384.8193	-0.0003			10	9	8113.1440	-0.0008
		9	8	7384.8435	-0.0009			8	7	8113.1525	0.0013
$9_{0,9}$	$8_{0,8}$	10	9	7511.2266	-0.0006	$10_{1,10}$	$9_{1,9}$	11	10	8188.5280	-0.0025
		8	7	7511.2345	0.0011			9	8	8188.5421	-0.0019
		9	8	7511.3261	0.0009			10	9	8188.5659	-0.0035
$9_{2,8}$	$8_{2,7}$	10	9	7782.5339	-0.0001	$12_{0,12}$	$11_{0,11}$	13	12	9851.3609	0.0007
		8	7	7782.5339	-0.0036			11	10	9851.3684	0.0019
		9	8	7782.5877	-0.0005			12	11	9851.4247	0.0007
$9_{3,7}$	$8_{3,6}$	8	7	7881.9117	0.0000	$9_{3,6}$	$8_{3,5}$	14	13	10582.1370	0.0005
		10	9	7881.9117	0.0000			12	11	10582.1475	0.0028
		9	8	7881.9596	-0.0004			13	12	10582.1694	0.0011

Chapter VII

The Effect of Microsolvation over Structure, Nuclear Quadrupole and Internal Rotation: The Methyl Carbamate···(H_2O) and Methyl Carbamate···(H_2O)$_2$ Complexes.

Manuscript in preparation.

Abstract

Mono and dihydrated complexes of methyl carbamate formed in a supersonic jet expansion have been studied by high-resolution microwave spectroscopy, using both chirped-pulse and cavity Fourier transform microwave instruments covering the frequency range 2-18 GHz. From the rotational constants of the parent and ^{18}O–water monosubstituted isotopologues, accurate structures have been derived for the complexes. In both mono and dihydrated species water molecules close sequential cycles with methyl carbamate through N–H···O–H···O=C and N–H···O–H···O–H···O=C hydrogen bond networks respectively. The steady variation observed for the χ_{cc} quadrupole coupling constant or the V_3 methyl torsion barrier with the degree of hydration can be associated to resonance assisted hydrogen bonding effects.

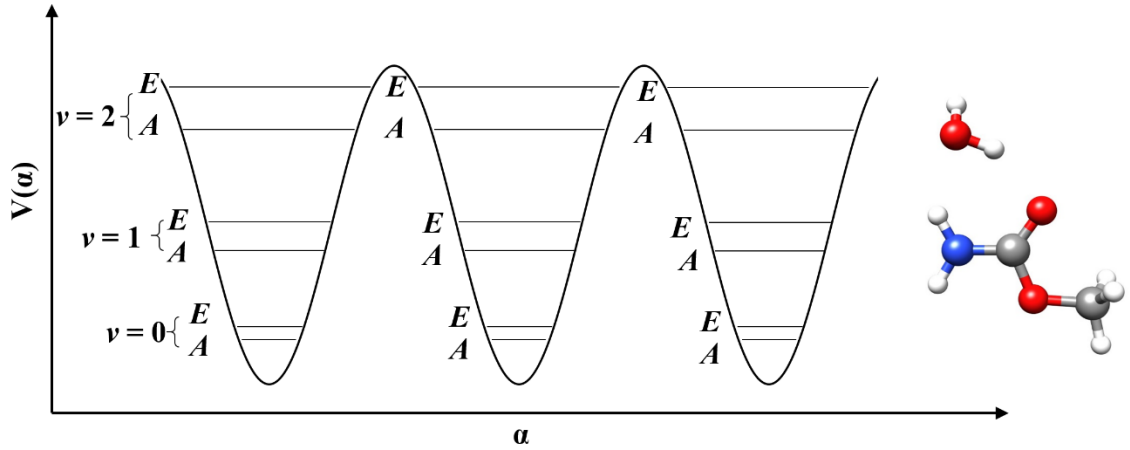

7.1 Introduction

The carbamate group (-NCO_2-) is recurrent in many biologically active molecules with pharmacological[1,2] and industrial[3] applications, especially in polyurethane polymer production.[4] It can be considered as an ester derivative of an amide and therefore it offers part of functionalities of the peptide bond. In consequence, these are used as peptide bond substitutes in medicinal chemistry.[2] One interesting aspect of its functionality is that they can mediate inter- and intramolecular interactions with enzymes or receptors. In fact, carbamate may act as hydrogen bond donor, through the N–H end or as acceptor through the C=O group. This allows carbamates to form sequential cycles with other molecules having the same Lewis acid/base double character. It is thus possible to study the formation of the hydrogen bonding with water molecules, since they also behave as double hydrogen donor/acceptor. It is important to characterize at a molecular level the hydrogen bond interaction of water and their effects on the structure of the peptide bond. Those effects can be exemplified by the study of microsolvation complexes of model molecules at different degrees of hydration.[5-14] Microsolvated complexes with different hydration degrees can be easily formed in a supersonic expansion and further characterized in an isolated environment by high-resolution microwave spectroscopy.

The simplest representative in this family of compounds is methyl carbamate ($C_2H_5NO_2$, mcb), which is also supposed to be present in the interstellar medium as precursor of biological molecules. It has been thoroughly studied in the gas phase by microwave spectroscopy in the ground[15-17] and in vibrational states,[18] and by IR[19] spectroscopy, to provide an extensive basis (supported by rotational constants, quartic distortion constants, quadrupole coupling constants and internal rotation parameters) for its search in the interstellar medium. Methyl carbamate can adopt two configurations regarding the orientation of the methyl group in relation to the carbonyl oxygen atom, *syn* or *anti* (see Scheme 7.1). Experimentally only the *syn* configuration has been reported, being the *anti* disposition much higher in energy according to all previous studies.[15-19]

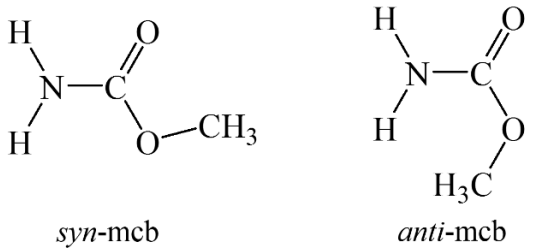

syn-mcb *anti*-mcb

Scheme 7.1. The *syn* and *anti* configurations of methyl carbamate (mcb).

Previous studies on microsolvation of small organic molecules[5-14] of different nature have given a better understanding of the interactions with water, revealing its preferred sites of interaction with different functional groups, or the role of hydrogen bond cooperativity in the solvation process. The carbamate group microsolvation in methyl carbamate can contribute with relevant information about the hydrogen bond interactions on a substituted *cis*-peptide linkage, and how water affects the structure of peptide-like molecules in the first steps of solvation. The microsolvated complexes of methyl carbamate can be considered as an extension of the microsolvation studies on amides such as formamide[5,8,12,13] or formanilide.[14] In this work, we present the complexes of methyl carbamate with one and two molecules of water, generated in a supersonic expansion and characterized by high-resolution microwave spectroscopy. We have continued the investigations of the use of nuclear quadrupole constants as a probe for the

polarization inductive effects reported for formamide[12,13] and formanilide.[14] Furthermore, we have searched for an evidence of a correlation between the nuclear quadrupole constants and internal rotation based on the changes in the values for the internal rotation barrier as the number of water molecules increases.

7.2 Experimental and theoretical methods

Methyl carbamate is a white crystalline solid with melting point of *ca*. 57 ºC. The sample mixture, containing approximately 1-4% methyl carbamate in argon at a stagnation pressure of about 2 bars, was prepared by heating the methyl carbamate to approximately 90ºC in a stainless steel heating pulsed nozzle. A receptacle containing water was placed in the gas line before the nozzle to provide enough water in the gas phase. A supersonic expansion pulse of about 900 μs length through the small diameter nozzle (1 mm) in the high-vacuum chamber, provided the appropriate environment for the generation of complexes and their subsequent study in a collision-free regime. The microwave spectrum of methyl carbamate was initially recorded from 2 to 8 GHz using chirped-pulse Fourier transform spectrometer (CP-FTMW),[20,21] with an accuracy of frequency measurement better than 10 kHz. Measurements in the 5-18 GHz regions were done in two narrow band Fourier transform microwave spectrometers (MB-FTMW), one in Valladolid[22] and the other in the Institute of Physics in Warsaw.[23] The sample was prepared with similar conditions of pressure and temperature as described above. In these instruments, a narrow band of *ca*. 2 MHz can be recorded in a single step; however, the accuracy of the frequency measurement is better than 3 kHz. The superior resolution of these instruments allowed to fully resolve the hyperfine structure due to the nuclear quadrupole coupling and to determine precisely the diagonal elements of the quadrupole coupling tensor.

The intensity of the spectra was not enough for the observation of isotopologues in their natural abundance. The microwave spectra of the complexes monoisotopically substituted with ^{18}O in the water subunits were recorded in the cavity spectrometer of Valladolid using a mixture of isotopically enriched $H_2{}^{18}O$ with water in a proportion of 1:3. Selected transitions were measured to determine the rotational constants for the isotopic species.

Before running the experiments, *ab initio* calculations[24] were performed to study the preferred sites of interaction for both *syn* and *anti* configurations of methyl carbamate with water. Different structures were tested for the 1:1 and 1:2 complexes (see Figures S7.1 and S7.2 in supplementary material) based on the microsolvated complexes previously reported for formamide[10,12,13] and formanilide,[14] with which the carbamate group share structural features. The considered geometries were optimized using the functional B3LYP[25] combined with Pople´s basis set 6-311++G(d,p).[26] Grimme´s empirical dispersion correction (GD3)[27] was implemented to improve the predictions performed by the B3LYP functional, due to its poor results for structures containing long-range forces such as hydrogen bonds.[28] Frequencies were calculated using only vibrational harmonic terms to confirm that the optimized structures are true minima. Additionally, dissociation energies for the complexes using the counterpoise procedure[29] were calculated to compare the strength of the hydrogen bonding to related systems. On the basis of the rotational constants, dipole moment components and nuclear quadrupole coupling constants, the microwave spectra for the different stable complexes were simulated. The predicted internal rotation barrier was considered to reproduce the experimental *A*-*E* splittings in the rotational transitions.

7.3 Results and discussion

7.3.1 *Syn*-methyl carbamate···(H_2O)

The microwave spectrum registered in the CP-FTMW is very dense with few transitions from the methyl carbamate monomer lying in the 2–8 GHz region. Once the lines from the monomer were removed, there were still many very intense lines that were assigned to *syn*-methyl carbamate···(H_2O)-a complex (*syn*-mcb-w-a). As expected, each rotational transition for this complex appeared as a doublet of equal intensity arising from the coupling of methyl group internal rotation and overall rotation. One of the components of the doublet has the non-degenerate *A* symmetry, and the other has the double-degenerate *E* symmetry according to the symmetry of the methyl top (C_3). Each transition further shows the hyperfine structure (hfs) arising from nuclear quadrupole coupling due to the presence of a ^{14}N nucleus (I = 1) in methyl carbamate (see Figure 7.1). No splittings attributable to tunneling motions of the water molecule were observed.

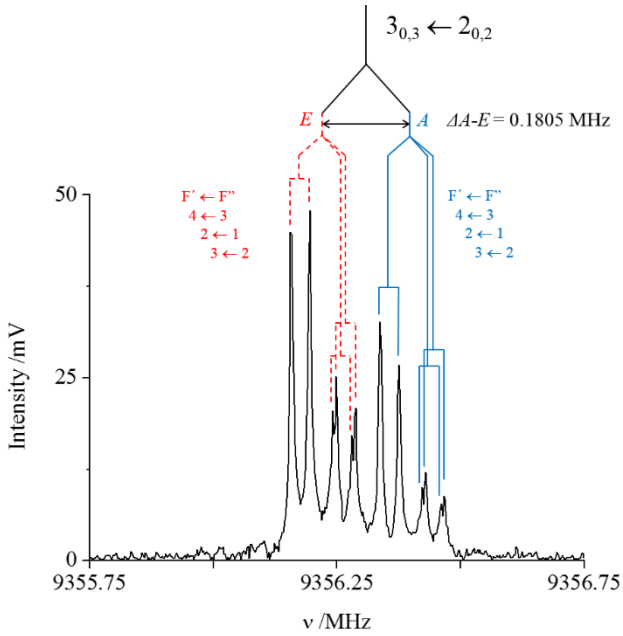

Figure 7.1. MB-FTMW recording of the $3_{0,3} \leftarrow 2_{0,2}$ rotational transition for the *syn*-mcb-w-a complex showing the coupling scheme. The transition is split in two internal rotation components *A* (upper ν, blue) and *E* (lower ν, red). Each component is further split due to the nuclear quadrupole coupling (F´ ← F´´ transitions). All the lines appear as a doublet due to Doppler effect.

Many *a*-type and several *b*-type transitions with *J* up to 5 and K_{-1} up to 2 have been observed for this complex. In a first approximation, the spectrum was fitted using Pickett´s CALPGM package,[30] which requires to analyze the *A* and *E* substates independently. The *A* substate can be fit easily using a Hamiltonian with terms for overall rotation ($\hat{H}_{rot}$), centrifugal distortion ($\hat{H}_{cd}$) using Watson´s *A* reduction[31] in the I^r representation, and nuclear quadrupole coupling ($\hat{H}_{quad}$).[32]

$$\hat{H}_A = \hat{H}_{rot} + \hat{H}_{cd} + \hat{H}_{quad} \qquad (1)$$

The deviation of the transitions in the *E* substate from that predicted by the semirigid-rotor approximation, can be taken into account in CALPGM by a perturbation treatment of the

internal rotation. The Hamiltonian is set up as for the *A* substate (eq. 1) with an additional term for the internal rotation[33,34] ($\widehat{H}_{int}$).

$$\widehat{H}_E = \widehat{H}_{rot} + \widehat{H}_{cd} + \widehat{H}_{quad} + \widehat{H}_{int} \quad (2)$$

$$\widehat{H}_{int} = \hat{P}_a\left(D_a + D_a^J\hat{P}^2 + D_a^K\hat{P}_a^2 + \cdots\right) + \hat{P}_b\left(D_b + D_b^J\hat{P}^2 + D_b^K\hat{P}_a^2 + \cdots\right) + \hat{P}_c\left(D_c + D_c^J\hat{P}^2 + D_c^K\hat{P}_a^2 + \cdots\right) \quad (3)$$

where the D_α, D_α^J, D_α^K parameters, account for the contribution of internal rotation. The final fit reproduces very accurately the microwave spectrum with low rms deviation (see Table S7.3 for the results of the fit using CALPGM), however it is not possible to obtain the main internal rotation parameters, such as the methyl group internal rotation barrier, the inertial moment, or other geometrical parameters of the rotating group. To overcome this, the lines were fitted also using the Xiam program,[35] which is based on the inertial axis method derived by Woods.[36] In this procedure, the Hamiltonian operator term for the internal rotation is defined in its own internal axes system, the so-called rho axes system, in which ρ is a dimensionless vector accounting for the interaction between overall rotation and internal rotation:[35]

$$\widehat{H}_{int} = F(\hat{p}_\alpha - \rho\hat{P}_\rho)^2 + \frac{1}{2}V_3(1-\cos(3\alpha)) \quad (4)$$

where F is the internal rotation constant, $\hat{p}_\alpha$ is the internal rotation top angular momentum operator, $\hat{P}_\rho$ is the total angular momentum along the ρ axis, V_3 is the three-fold hindering barrier, and α is the angle that defines the internal rotation motion. The transformation between the rho axes system and the principal axes system is done through the rotation of two angles, β and γ.[35] Analysis of the split transitions allowed fitting the *A* and *E* substates together and the determination of the methyl top three-fold barrier height (V_3); F_0, the inverse of the rotational top inertia moment (I_α); ρ, as defined above, and β, the angle define between ρ and the *a* axis in the principal axes system (see Table 7.1). The angle γ was not fit, its value was fixed to 0 assuming the planarity of the heavy atom skeleton. See Chapter II for more details on the internal rotation treatment.

From the experimental data set, it was possible to determine the rotational constants, the quartic centrifugal distortion constants except Δ_K and δ_K, the diagonal elements for the nuclear quadrupole coupling, and the parameters for the internal rotation described previously. For the $^{18}O_w$ isotopologue, the rotational constants and the internal rotation parameters were fit by keeping the rest of parameters fixed to the values of the parent species with both CALPGM (see Table S7.4) and Xiam fits (see Table 7.1). The frequencies observed for this complex are collected in Table S7.10 for the parent and in Table S7.11 for the $^{18}O_w$ isotopologue.

The good agreement between the *ab initio* and the determined parameters suggest that the structure for the *syn*-mcb-w-a complex is very close to that given by *ab initio* calculations. This is similar in structure and in the nature of the interactions established as those reported as the most stable for formamide[5,10] and formanilide.[14] The molecule of water closes a cycle with the H–N–C=O group through $C_1{=}O_1\cdots H_{w1}{-}O_w\cdots H_1{-}N$ hydrogen bonds (see Figure 7.2). This demonstrates that water and methyl carbamate act simultaneously as hydrogen donor and hydrogen acceptor. The molecule of water locates in the same plane of the heavy atom skeleton of methyl carbamate, as reflected by the almost non-changing value of P_c from the monomer (1.623677(19) uÅ^2)[16] to the water complex (1.892781(52) uÅ^2). The value of P_c in the ^{18}O water isotopologue (1.89466(38) uÅ^2) can be considered further evidence in favor of the planarity of

the complex. An approach to the molecular structure can be obtained by a least-squares fit of some selected structural parameters (distances and angles) to the rotational constants for all the available isotopologues species.[37] This structure reproduces the rotational constants in the lowest vibrational level of the potential energy function,[38] reason for which it is commonly known as the r_0 structure. The results obtained by this procedure for the *syn*-mcb-w-a complex are shown in Figure 7.2 and are collected in Table S7.7 showing a reasonable agreement with the predicted r_e structure by *ab initio* calculations. For the $^{18}O_w$ monoisotopologue, the r_s coordinates for the substituted atom; *a*, *b* and *c*, can be obtained using Kraitchman equations.[39] Kraitchman equations give absolute values for the coordinates, therefore the sign was assigned by comparison with r_0 and r_e structures coordinates. The uncertainty in the coordinates was quoted according to the Costain rule.[40] The values obtained for the *syn*-mcb-w-a complex are compared with r_0 and r_e structures coordinates in Figure 7.2, which shows a good agreement.

Table 7.1. Rotational parameters obtained from the analysis of the spectrum of the observed *syn*-mcb-w-a complex for the parent and the $^{18}O_w$ isotopologue using the Xiam program, compared with *ab initio* (B3LYP-D3/6-311++G(d,p)).

Fitted Parameters[a]	*syn*-mcb-w-a	*syn*-mcb-w-a $^{18}O_w$	*ab initio*
A /MHz	8056.7753(11)[b]	8030.9743(12)[b]	8068.53
B /MHz	1707.32139(37)	1615.37034(22)	1709.39
C /MHz	1423.80899(33)	1358.56086(23)	1427.33
Δ_J /kHz	0.4861(56)	[0.4861]	0.418
Δ_{JK} /kHz	0.782(46)	[0.782]	0.326
Δ_K /kHz	[0.]	[0.]	21.0
δ_J /kHz	0.1006(55)	[0.1006]	0.0765
δ_K /kHz	[0.]	[0.]	1.49
V_3 /cm^{-1}	373.13(67)	372.71(98)	302.7
F_0 /MHz	158.13(38)	158.04(55)	164.48
I_α / uÅ^2	3.1960(76)	3.198(11)	3.155
ρ	0.036258(48)	0.035766(77)	0.032
β /rad	0.21574(47)	0.20876(55)	0.260
^{14}N 3/2(χ_{aa}) /MHz	2.4363(44)	[2.4363]	2.70
^{14}N ¼(χ_{bb}-χ_{cc}) /MHz	1.602(75)	[1.602]	1.81
N	198/28	54/9	
σ /kHz	6.9	4.0	
Derived Parameters			
P_a /uÅ^2	294.114173(52)	310.96178(38)	293.54
P_b /uÅ^2	60.834425(52)	61.03407(38)	60.53
P_c /uÅ^2	1.892781(52)	1.89466(38)	2.11

[a] A, B and C are the rotational constants. Δ_J, Δ_{JK}, Δ_K, δ_J and δ_K are the quartic centrifugal distortion constants. V_3 is the internal rotation barrier for the methyl top. F_0 is the inverse of the moment of inertia of the methyl top, I_α. ρ is a dimensionless vectorial magnitude describing the coupling beetwen internal and overall rotation. β is the angle between ρ and the a principal inertial axis. χ_{aa}, χ_{bb} and χ_{cc} are the quadrupole coupling tensor diagonal elements for ^{14}N atom. N is the number of quadrupole hyperfine components/rotational transitions fitted. σ is the rms deviation of the fit. P_α (α= *a*, *b* or *c*) are the planar moments of inertia, these are derived from the moments of inertia I_α as for example $P_c = (I_a+I_b-I_c)/2$. [b] Standard errors in parentheses in units of the last digits. [c] Parameters in square brackets were kept fixed to those given for the parent species in the fit.

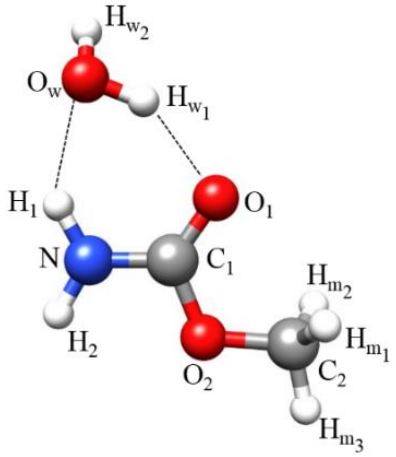

Fitted parameter	r_0	r_e
$r(O_w\cdots H_1)$ /Å	2.0830(4)	2.074
$r(H_{w1}\cdots O_1)$ /Å	1.94(1)	1.920
$\angle(O_w\cdots H_1–N)$ /°	138.25(2)	138.3
$\angle(H_{w1}\cdots O_1–C_1–N)$ /°	1.14(8)	5.2
Derived parameter	r_0	r_e
$r(O_w–H_{w1})$ /Å	0.951(9)	0.975
$\angle(O_1–C_1–N)$ /°	125.302(9)	125.3
$\angle(H_1\cdots O_w–H_{w1})$ /°	81.9(4)	82.0
$\angle(O_w–H_{w1}\cdots O_1)$ /°	148.2(4)	147.9

	atom	*a*	*b*	*c*
$\lvert r_s\rvert$ /Å		|2.9291(5)|	|0.330(4)|	|0.03(5)|
r_0 /Å	O_w	2.9286(5)	-0.3375(3)	0.0365(2)
r_e /Å		2.92	-0.34	0.09

Figure 7.2. The *syn*-mcb-w-a complex showing atom labeling with the r_0 structure derived parameters, the r_s structure coordinates and comparison with r_e structure.

A search for the next monohydrated complexes in order of energy, with similar interactions to those found for formamide,[8] was carried out (see figure S7.1 for the structures). It was expected to observe any *a*-type transition on the basis of the appreciable μ_a component predicted for both *syn*-mcb Ib and *syn*-mcb Ic rotamers. Despite considerable efforts, the spectra of those conformations were not detected. The complexes between one molecule of water and *anti*-methyl carbamate are of much higher energy and are not expected to be present in the supersonic expansion as occurs for the monomer in the *anti* configuration.

7.3.2 *Syn*-methyl carbamate$\cdots(H_2O)_2$

After the assignment of the lines corresponding to the monohydrated complex, groups of lines with intensities of about 5-10 times less than the 1:1 complex, and showing a characteristic R-branch μ_a-type pattern were detected and assigned to the *syn*-methyl carbamate$\cdots(H_2O)_2$ complex (*syn*-mcb-w_2). The lines assigned to the dihydrated complex present a small splitting due to internal rotation of the methyl group together with the hyperfine structure arising from the nuclear quadrupole coupling as occurs for the monomer and the monohydrated complex (see Figure 7.3).

Only *a*-type transitions with J up to 9 and K_{-1} up to 2 have been detected for this complex, which is in correspondence with the dipole moment components predicted (see Table S7.2). As in the 1:1 complex, in a first approximation the spectrum was fitted with CALPGM independently for the *A* and *E* substates as for the *syn*-mcb-w-a complex. For the fitting of the *E* substate only the D_a parameter was included (see Table S7.5 in supplementary material for the determined parameters and rms deviation). From the fit of the experimental frequencies using Xiam, the rotational constants, the quartic centrifugal distortion constants except Δ_K, the diagonal elements for the nuclear quadrupole coupling, and the internal rotation parameters V_3, F_0, I_α and β were accurately determined (see Table 7.2). It was not possible to determine ρ or γ, being fixed to the *ab initio* values. For the observed $^{18}O_w$ species, the rotational constants and the internal rotation parameters were fit by keeping the rest of parameters fixed to those determined for the parent species (see Table 7.2 and Table S7.6). The complete list of the

frequencies observed for this complex is collected in Table S7.12 for the parent and in Tables S7.13 and S7.14 for the $^{18}O_w$ isotopologues in supplementary material.

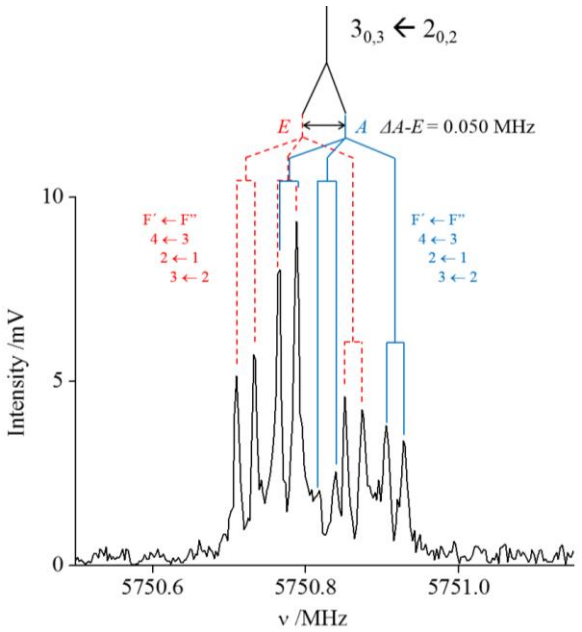

Figure 7.3. MB-FTMW recording of the $3_{0,3} \leftarrow 2_{0,2}$ rotational transition for the *syn*-mcb-w_2 complex showing the coupling scheme. The transition is split in two internal rotation components *A* (upper ν, blue) and *E* (lower ν, red). Each component is further split due to the nuclear quadrupole coupling (F´ ← F´´ transitions). All the lines appear as a doublet due to Doppler effect.

The experimental molecular parameters are quite well reproduced by the *ab initio* predicted structure, therefore it is possible to assume that the molecular structure of *syn*-mcb-w_2 is close to that described by the calculations. The two molecules of water close an 8-membered sequential cycle acting as a bridge between the amino and the carbonyl ends. The three molecules act simultaneously as hydrogen donor and hydrogen acceptor establishing a $C_1{=}O_1\cdots H_{w1}{-}O_{w1}\cdots H_{w3}{-}O_{w2}\cdots H_1{-}N$ hydrogen bond network (see Figure 7.4). The water molecules locate almost in the plane defined by the heavy atom skeleton in methyl carbamate as indicated by P_c (2.65801(40) uÅ^2). The values of P_c for the observed $^{18}O_{w1}$ (2.65273(30) uÅ^2) and $^{18}O_{w2}$ (2.66011(42) uÅ^2) indicate that these atoms are in the *ab* inertial plane. The similar values of Pc from the monomer (1.623677(19) uÅ^2)[16] to the monohydrated complex (1.892781(52) uÅ^2), to the dihydrated complex (2.65801(40) uÅ^2) also points out to this structure. The slightly increase can be attributable to an augmentation on the number of out-of-plane vibrations when we add a water molecule.

The r_0 structure for the hydrogen bonds parameters in this complex was derived by fitting it to the rotational constants from the parent and both $^{18}O_w$ isotopologues. The results obtained are given in Figure 7.4 and are collected in Table S7.8. The r_s structure was also derived from the rotational constant of the $^{18}O_w$ monoisotopologues as described above. In the *syn*-mcb-w_2 complex, the coordinates of the two water oxygen atoms allowed us to derive the distance between them. The r_s structure coordinates for both oxygen atoms together with their distance are collected and compared with r_0 and r_e structures coordinates in Figure 7.4.

Table 7.2. Rotational parameters obtained from the analysis of the spectrum of the observed *syn*-mcb-w_2 complex for the parent and the ^{18}Ow isotopologues using the Xiam program, compared with *ab initio* (B3LYP-D3/6-311++G(d,p)).

Fitted Parameters[a]	*syn*-mcb-w_2	*syn*-mcb-w_2 $^{18}O_{w1}$	*syn*-mcb-w_2 $^{18}O_{w2}$	*ab initio*
A /MHz	3819.180(18)[b]	3681.308(16)	3756.211(23)	3874.89
B /MHz	1083.85347(72)	1059.32764(18)	1047.49457(23)	1092.44
C /MHz	851.82404(55)	829.77940(16)	826.20223(21)	859.90
Δ_J /kHz	0.1874(45)	[0.1874][d]	[0.1874]	0.141
Δ_{JK} /kHz	1.093(19)	[1.093]	[1.093]	0.638
Δ_K /kHz	[0.]	[0.]	[0.]	4.32
δ_J /kHz	0.0459(20)	[0.0459]	[0.0459]	0.0344
δ_K /kHz	0.98(22)	[0.98]	[0.98]	0.762
V_3 /cm^{-1}	415.4(1.2)	404.1(2.1)	420.8(2.5)	318.7
F_0 /MHz	171.74(43)	167.2(1.3)	174.5(1.4)	162.47
I_α / uÅ^2	2.9426(73)	3.022(23)	2.897(23)	3.152
ρ	[0.016][c]	[0.016][c]	[0.016][c]	0.016
β /rad	2.8362(17)	2.8379(47)	2.8618(48)	2.789
^{14}N 3/2(χ_{aa}) /MHz	2.0187(57)	[2.0187]	[2.0187]	2.15
^{14}N ¼(χ_{bb}-χ_{cc}) /MHz	1.55(12)	[1.55]	[1.55]	1.76
N	171/28	69/12	71/12	
σ /kHz	5.4	3.8	5.0	
Derived Parameters				
P_a /uÅ^2	463.62181(40)	474.42252(31)	479.80445(42)	459.95
P_b /uÅ^2	129.66856(40)	134.62972(31)	131.88478(42)	127.76
P_c /uÅ^2	2.65801(40)	2.65273(31)	2.66011(42)	2.66

[a] A, B and C are the rotational constants. Δ_J, Δ_{JK}, Δ_K, δ_J and δ_K are the quartic centrifugal distortion constants. V_3 is the internal rotation barrier for the methyl top. F_0 is the inverse of the moment of inertia of the methyl top, I_α. ρ is a dimensionless vectorial magnitude describing the coupling beetwen internal and overall rotation. β is the angle between ρ and the a principal inertial axis. χ_{aa}, χ_{bb} and χ_{cc} are the quadrupole coupling tensor diagonal elements for ^{14}N atom. N is the number of quadrupole hyperfine components fitted. After the slash is the number of rotational transitions fitted. σ is the rms deviation of the fit. P_α (α= a, b or c) are the planar moments of inertia, these are derived from the moments of inertia I_α as for example $P_c = (I_a+I_b-I_c)/2$. [b] Standard errors in parentheses in units of the last digits. [c] ρ was kept fixed to the *ab initio* value in the fit. [d] Parameters in square brackets were kept fixed to those given for the parent species in the fit.

The second complex explored with two molecules of water, *anti*-mcb-w_2 is predicted to be much higher in energy than the *syn* complex, and as occurs for the monomer and the monohydrated complex it is missing in the microwave spectrum.

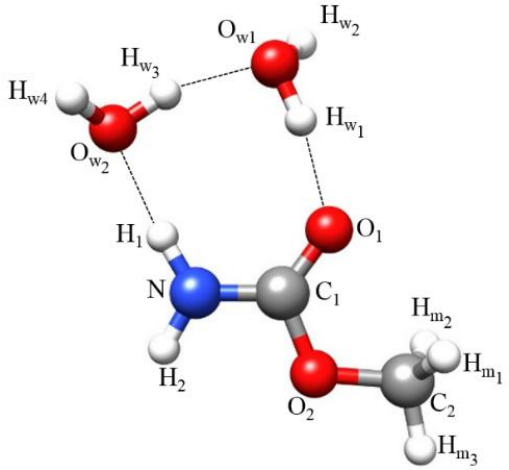

Fitted parameter	r_0	r_e
$r(O_{w2}\cdots H_1)$ /Å	1.9016(17)	1.872
$r(H_{w1}\cdots O_1)$ /Å	1.8055(20)	1.771
$\angle(H_{w1}\cdots O_1–C_1)$ /°	130.0485(39)	129.4
$\angle(H_{w1}\cdots O_1–C_1–O_2)$ /°	177.38(49)	176.6
Derived parameter	r_0	r_e
$r(H_{w3}\cdots O_{w1})$ /Å	1.826(1)	1.776
$r(O_{w2}\cdots O_{w1})$ /Å	2.756(1)	2.723
$\angle(O_{w2}–H_{w3}\cdots O_{w1})$ /°	161.0(2)	160.9
$\angle(H_{w3}\cdots O_{w1}–H_{w1})$ /°	98.44(9)	98.9

	atom	*a*	*b*	*c*
$\lvert r_s\rvert$ /Å		|2.8575(5)|	|1.086(1)|	|0.03(4)|
r_0 /Å	O_{w1}	2.863(2)	1.0831(9)	-0.023(3)
r_e /Å		2.84	1.07	-0.04
$\lvert r_s\rvert$ /Å		|2.3248(6)|	|1.6129(9)|	|0.0534i|
r_0 /Å	O_{w2}	2.329(2)	-1.6206(7)	0.006(5)
r_e /Å		2.32	-1.60	0.01

r_s /Å		2.7516(18)
r_0 /Å	O_{w1}-O_{w2}	2.756(1)
r_e /Å		2.72

Figure 7.4. The *syn*-mcb-w_2 complex showing atom labeling with the r_0 structure derived parameters, the r_s structure coordinates and comparison with r_e structure.

7.3.3 Nuclear quadrupole coupling and π-cooperative effects

Resonance Assisted Hydrogen Bonding (RAHB)[41,42] or π-cooperative bonding was first pointed out to occur in the case of the peptide linkage in crystal studies of small amides.[43] In this work (see chapters IV and V) it has been demonstrated in the gas phase by microwave spectroscopy for the microsolvation system of formamide.[12,13] The main effect of cooperativity on the peptide linkage is the C=O bond enlargement and the C–N bond shortening due to the clustering. Since methyl carbamate presents a substituted amide group, resembling the peptide bond, RAHB inductive effects are expected to occur. No isotopologues for the methyl carbamate molecule have been observed in this work, therefore there is a lack of experimental structural information about the C=O or C–N distances. Instead, the *ab initio* values (B3LYP-D3/6-311++G(d,p)) could be used as an approximation (see Scheme 7.2), based on the good correspondence between predicted and observed rotational parameters.

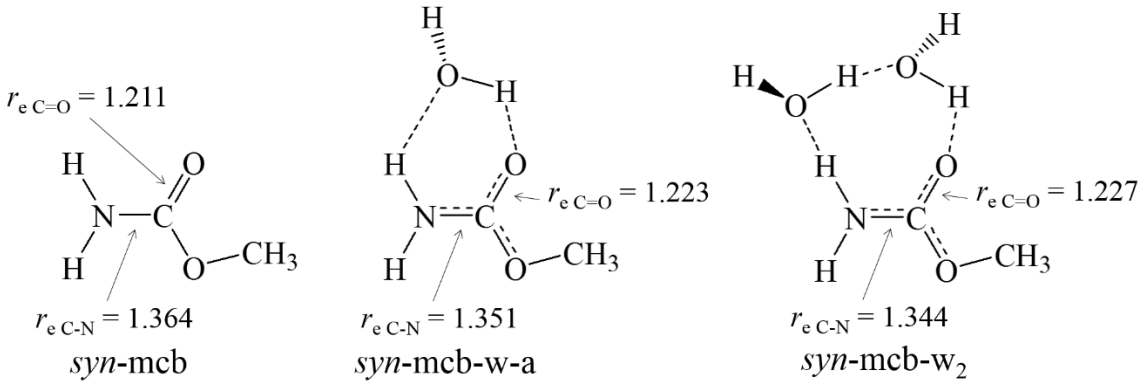

Scheme 7.2. RAHB inductive effects in the microsolvation series of methyl carbamate as evidenced by the C=O bond enlargement and the C–N shortening.

As it was illustrated for the microsolvation of formamide,[12,13] the nuclear quadrupole coupling constants can be used as a probe for the subtle changes occurring in the electronic environment at the ^{14}N nucleus. An exhaustive picture of the electric field gradient can be only obtained from the complete determination of the nuclear quadrupole coupling tensor, however, in general, only the diagonal elements can be determined, as is the case for methyl carbamate. Given the almost planarity of the complexes of methyl carbamate, as reflected by the low values of P_c (see Tables 7.1 and 7.2), the *c* inertial axis is practically perpendicular to the molecular frame plane, and therefore $\chi_{cc} \approx \chi_{zz}$. Table S7.9 evidences a trend in the value of χ_{cc} for the series of monomer – monohydrated – dihydrated complexes of methyl carbamate. The good agreement between the experimental values for χ_{cc} and those predicted by *ab initio* calculations, which are based on a static picture, allows us to discard intermolecular motions as the origin of the change. Thus, the tendency in the experimental value of χ_{cc} indicates that the electronic environment at the ^{14}N nucleus is altered by the complexation.

As explained for formamide-water complexes, the electric field gradient that couples to nuclear quadrupole has been attributed to an unequal filling of the valence shell *p* orbitals from the coupling nucleus.[32] Therefore, the χ_{zz} constant can be related to the unbalanced $2p_z$ electronic charge $-(U_p)_z$, by:

$$\chi_{zz}/eQq_{210} = -(U_p)_z \qquad (5)$$

$$(U_p)_z = \left[\left(n_x - n_y\right)/2 - n_z\right] \qquad (6)$$

where n_α (α = *x*, *y*, and *z*) are the p_α occupation numbers and q_{210} is the electric field gradient associated to an electron in the 2*p* orbital in an isolated atom. For a N nucleus eQq_{210} is estimated to be approximately -10 MHz.[32] Figure 7.5 shows the excellent correlation between the experimental values of χ_{zz}/eQq_{210} and the quantity $-(U_p)_z$ calculated from a natural bond orbital (NBO) analysis.[44]

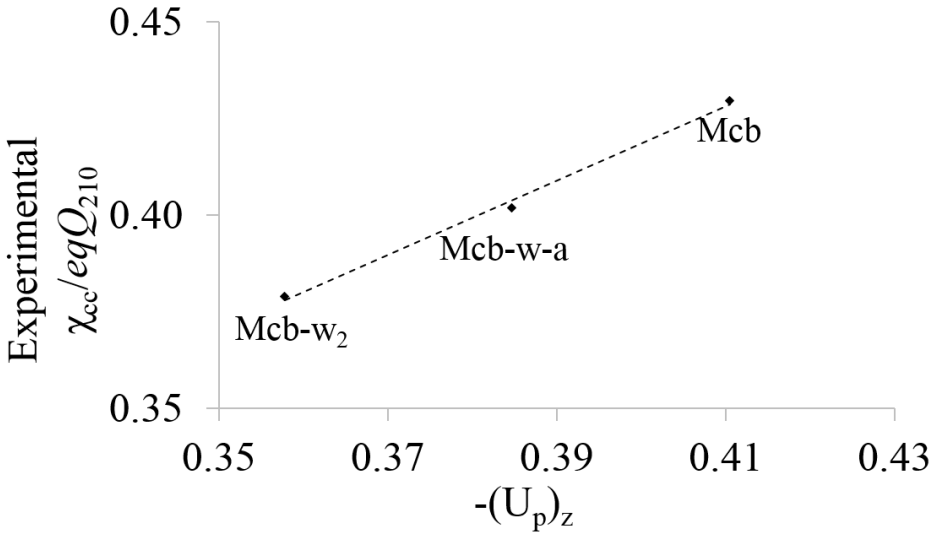

Figure 7.5. Correlation between the experimental values of χ_{zz}/eQq_{210} *vs.* -$(U_p)_z$.

The values of $(U_p)_z$ indicate that the electron density along the *z* axis decreases progressively with the hydration degree. This illustrates the polarization of methyl carbamate due to inductive effects, which are stronger as the number of cooperative hydrogen bond increases. The main effect of the polarization can be seen in the tendencies in the predicted C–N and C=O distances (see Scheme 7.2). Despite these subtle changes can not be confirmed by the direct measurement of the distances, the nuclear quadrupole constant χ_{cc}, associated to the electric field gradient in the N nucleus, can serve as a probe for the inductive polarization effects in the microsolvated complexes.

7.3.4 Effect of microsolvation over the internal rotation barrier

Inspection on the experimental barrier for the internal rotation when passing from the monomer to the monohydrated and dihydrated species reveals a steady increment in the barrier values (see Table 7.3). This increment is larger than that observed for another series of monomer – monohydrated – dihydrated complexes presenting internal rotation as methyl lactate,[45,46] where it was attributed to be as a result of the shortening of the $O_1\cdots H_{m1}$ and $O_1\cdots H_{m2}$ distances (see Figure 7.2 and Figure 7.4 for atom labeling). This shortening is also predicted to occur in the microsolvated series of methyl carbamate (as reflected in Table 7.4) together with other structural changes, such as the opening of the O_1–C_1–O_2 angle. Changes in the electronic structure of methyl carbamate, such as those due to the RAHB effects demonstrated in previous section, could be also at the origin of the internal rotation barrier increase.

Table 7.3. Evolution of the internal rotation barrier for the series of monomer – monohydrated – dihydrated complexes in methyl carbamate, methyl lactate and acetic acid. All the barriers are given in cm^{-1}.

	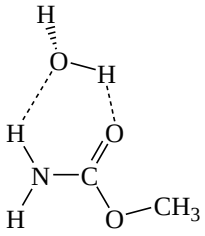	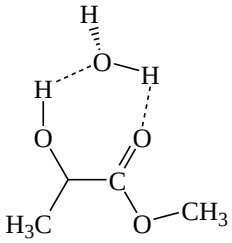	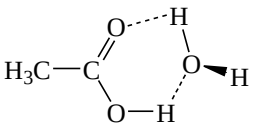
	Methyl carbamate	Methyl lactate	Acetic acid
Monomer	352.18(29)[a]	398.07(25)[c]	170.217(1)[e]
Monohydrated complex	373.13(67)[b]	428(2)[d]	138.396(5)[f]
Dihydrated complex	415.4(1.2)[b]	433.74(66)[d]	118.482(2)[f]

[a] Reference [16]. [b] This work. [c] Reference [45]. [d] Reference [46]. [e] Reference [47]. [f] Reference [48].

The increasing tendency of the internal rotation barrier for the series monomer – monohydrated – dihydrated complex in methyl carbamate is in contrast with the results found for acetic acid, where the barrier was found to decrease along the series (see Table 7.3).[47,48] In this case, the experimental barrier height was correlated to the hydrogen bond strengthening, measured as the dissociation energy (counterpoise corrected) per hydrogen bond predicted by *ab initio* calculations. The hydrogen bond strength in the microsolvated complexes of methyl carbamate, measured in the same way, follows the same tendency found for acetic acid (see Table 7.4). However, it is relevant to remark that in acetic acid, the environment of the methyl top is different. In all the cases it seems that the steady changes of the internal barriers are due to cooperative effects. Thus, the hypothesis that RAHB effects may have any influence on these barriers observed, is reinforced.

Table 7.4. Evolution of some predicted parameters for the series of monomer – monohydrated – dihydrated complexes in methyl carbamate (mcb), methyl lactate (Ml) and acetic acid (Aa). Distances in Å, bond angles in degrees, D_e in cm^{-1}.

	$r(O_1\cdots H_{m1})$	$r(O_1\cdots H_{m2})$	$\angle(O_1–C_1–O_2)$	D_e/HB[d]
[a]Δ Mcb – Mcb-w-a	0.017	0.023	-0.195	1569
[a]Δ Mcb-w-a – Mcb-w_2	0.012	0.008	-0.198	2342
[b]Δ Ml – Ml I	0.016	0.013	-	-
[b]Δ Ml I – Ml II	0.019	0.029	-	-
[c]Δ Aa – Aa I	-	-	-	1590
[c]Δ Aa I – Aa II	-	-	-	2226

[a] At the B3LYP-D3/6-311++G(d,p) level of theory. [b] At the MP2/6-311++G(d,p) level of theory. [c] At the MP2/6-311++G(2df,2pd) level of theory. Since the level of theory employed is different, it is not possible to correlate the values, but the trends observed are similar. [d] Dissociation energy per hydrogen bond performed using the counterpoise procedure at the same level of theory indicated for methyl carbamate and acetic acid.

7.4 Conclusions

One monohydrated and one dihydrated complexes of methyl carbamate have been observed by high-resolution microwave spectroscopy. The rotational, centrifugal distortion and nuclear quadrupole coupling constants have been determined with high accuracy. From the rotational constants of the parent and $^{18}O_w$ monoisotopologues, experimental structures have been derived, allowing to assign the observed complexes to those predicted as the most stable. The complexes present splittings arising from the internal rotation of the methyl top as reported for the monomer. The internal rotation parameters have been determined using two different approaches, arising in comparable results for the reproduction of the experimental frequencies. Two noticeable trends have been observed for the series of monomer – monohydrated – dihydrated complexes: a decrease in the χ_{zz}/eQq_{210} value, and an increase in the energy of the V_3 internal rotation barrier. Both trends seem to be correlated between them and with RAHB inductive effects in methyl carbamate. The use of quadrupole coupling constants as a probe for those effects has already be demonstrated, thus the correlation between them and internal rotation barrier could be also taken as an additional evidence for the polarization inductive effects due to RAHB.

References

[1] Abraham, D. J., Rotella, D. P. *Burger´s medicinal chemistry, drug discovery and development*, 7th edition, Wiley, Hoboken, 2010.

[2] Ghosh, A. K., Brindisi, M. "Organic Carbamates in Drug Design and Medicinal Chemistry" *J. Med. Chem.*, **2015**, 58, 2895–2940.

[3] Fukuto, T. R. "Mechanism of Action of Organophosporus and Carbamate Insecticides" *Environ. Health Perspect.*, **1990**, 87, 245–254.

[4] Heyn, R. H., Jacobs, I. Carr, R. H. "Synthesis of Aromatic Carbamates from CO2: Implications for the Polyurethane Industry" *Adv. Inorg. Chem.*, **2014**, 66, 83–115.

[5] Lovas, F. J., Suenram, R. D., Fraser, G. T., Gillies, C. W., Zozom, J. "The Microwave Spectrum of Formamide-Water and Formamide-Methanol Complexes" *J. Chem. Phys.*, **1988**, 88, 722–729.

[6] Held, A., Pratt, D. W. "Hydrogen Bonding in Water Complexes. Structures of 2-Pyridone-H_2O and 2-Pyrididone-$(H_2O)_2$ in Their S_0 and S_1 Electronic States" *J. Am. Chem. Soc.*, **1993**, 115, 9708–9717.

[7] Lavrich, R. J., Tubergen, M. J. "Conformation and Hydrogen Bonding in the Alaninamide-Water van der Waals Complex" *J. Am. Chem. Soc.*, **2000**, 122, 2938–2943.

[8] Blanco, S., López, J. C., Lesarri, A., Alonso, J. L. "Microsolvation of Formamide: A Rotational Study" *J. Am. Chem. Soc.*, **2006**, 128, 12111–12121.

[9] Canagaratna, M., Phillips, J. A., Ott, M. E. Leopold, K. R. "The Nitric-Acid Complex: Microwave Spectrum, Structure and Tunneling" *J. Phys. Chem. A*, **1998**, 102, 1489–1497.

[10] Caminati, W., López, J. C., Blanco, S., Mata, S., Alonso, J. L. "How Water Links to *Cis* and *Trans* Peptidic Groups: The Rotational Spectrum of N-Methylformamide-Water" *Phys. Chem. Chem. Phys.*, **2010**, 12, 10230–10234.

[11] Thomas, J., Sukhorukov, O., Jäger, W., Xu, Y. "Direct Spectroscopic Detection of the Orientation of Free OH Groups in Methyl Lactate-$(Water)_{1,2}$ Clusters: Hydration of a Chiral Hydroxy Ester" *Angew. Chem. Int. Ed.*, **2014**, 53, 1156–1159.

[12] Blanco, S., Pinacho, P., López, J. C. "Hydrogen-Bond Cooperativity in $Formamide_2$-Water: A Model for Water Mediated Interactions" *Angew. Chem. Int. Ed.*, **2016**, 128, 9477–9481. Chapter IV within this Thesis.

[13] Blanco, S., Pinacho, P., López, J. C. "Structure and Dynamics in Formamide-$(H_2O)_3$: A Water Pentamer Analogue" *J. Phys. Chem. Lett.*, **2017**, 8, 6060–6066. Chapter V within this Thesis.

[14] "Microsolvation of Formanilide Conformers: A Model for Peptide Solvation". Chapter VI within this Thesis.

[15] Marstokk, K. M., Møllendal, H. "Microwave Spectrum, Conformation, Barrier to Internal Rotation, ^{14}N Quadrupole Coupling Constants, Dipole Moment and Quantum Chemical Calculations for Methyl Carbamate" *Acta Chem. Scan.*, **1999**, 53, 79–84.

[16] Bakri, B., Demaison, J., Kleiner, I., Margulès, L., Mollendal, H., Petitprez, D., Wlodarczak, G. "Rotational Spectrum, Hyperfine Structure, and Internal Rotation of Methyl Carbamate" *J. Mol. Spectrosc.*, **2002**, 215, 312–316.

[17] Groner, P., Winnewisser, M., Medvedev, R., De Lucia, F. C., Herbst, E. Sastry, K. V. L. N. "The Millimeter- and Submillimeter-Wave Spectrum of Methyl Carbamate $[CH_3OC(:O)NH_2]$" *ApJS*, **2007**, 169, 28–36.

[18] Ilyushin, V., Alekseev, E., Demaison, J., Kleiner, I. "The Ground and First Excited Torsional States of Methyl Carbamate" *J. Mol. Spectrosc.*, **2006**, 240, 127–132.

[19] Kydd, R. A., Rauk, A. "The Equilibrium Geometry of Methyl Carbamate" *J. Mol. Struct.*, **1981**, 77, 227c238.

[20] Brown, G. G., Dian, B. C., Douglass, K. O., Geyer, S. M., Pate, B. H. "The Rotational Spectrum of Epifluorohydrin Measured by Chirped-Pulse Fourier Transform Microwave Spectroscopy" *J. Mol. Spectrosc.*, **2006**, 238, 200–212.

[21] Brown, G. G., Dian, B. C., Douglass, K. O., Geyer, S. M., Shipman, S. T., Pate, B. H. "A Broadband Fourier Transform Microwave Spectrometer Based on Chirped Pulse Excitation" *Rev. Sci. Instrum.*, **2008**, 79, 053103.

[22] Alonso, J. L., Lorenzo, F. J., López, J. C., Lesarri, A., Mata, S., Dreizler, H. "Construction of a Molecular Beam Fourier Transform Microwave Spectrometer Used to Study the 2,5-Dihydrofuran-Argon Van Der Waals Complex" *Chem. Phys.*, **1997**, 218, 267–275.

[23] Kisiel, Z., Kosarzewski, J., Pszczółkowski, L. "Nuclear Quadrupole Coupling Tensor of CH_2Cl_2: Comparison of Quadrupolar and Structural Angles in Methylene Halides" *Acta Phys. Pol. A*, **1997**, 92, 507–516.

[24] Gaussian 09, Revision D.01, Frisch M. J., Trucks G. W., Schlegel H. B., Scuseria G. E., Robb M. A., Cheeseman J. R., Scalmani G., Barone V., Petersson G. A., Nakatsuji H., Li X., Caricato M., Marenich A., Bloino J., Janesko B. G., Gomperts R., Mennucci B., Hratchian H. P., Ortiz J. V., Izmaylov A. F., Sonnenberg J. L., Williams-Young D., Ding F., Lipparini F., Egidi F., Goings J., Peng B., Petrone A., Henderson T., Ranasinghe D., Zakrzewski V. G., Gao J., Rega N., Zheng G., Liang W., Hada M., Ehara M., Toyota K., Fukuda R., Hasegawa J., Ishida M., Nakajima T., Honda Y., Kitao O., Nakai H., Vreven T., Throssell K., Montgomery, Jr. J. A., Peralta J. E., Ogliaro F., Bearpark M., Heyd J. J., Brothers E., Kudin K. N., Staroverov V. N., Keith T., Kobayashi R., Normand J., Raghavachari K., Rendell A., Burant J. C., Iyengar S. S., Tomasi J., Cossi M., Millam J. M., Klene M., Adamo C., Cammi R., Ochterski J. W., Martin R. L., Morokuma K., Farkas O., Foresman J. B., Fox D. J., *Gaussian, Inc., Wallingford CT*, 2016.

[25] a) Lee, C., Yang, W., Parr, R. G. "Development of the Colle-Salvetti Correlation-Energy Formula into a Functional of the Electron Density" *Phys. Rev. B*, **1988**, 37, 785–789. b) Becke, A. D. "Density-Functional Thermochemistry. III. The Role of Exact Exchange" *J. Chem. Phys.*, **1993**, 98, 5648–5652. c) Vosko, S. H., Wilk, L., Nusair, M. "Accurate Spin-Dependent Electron Liquid Correlation Energies for Local Spin Density Calculations: a Critical Analysis" *Can. J. Phys.*, **1980**, 58, 1200–1211.

[26] Ditchfield, R., Hehre, W. J., Pople, J. A. "Self-Consistent Molecular-Orbital Methods. IX. An Extended Gaussian-Type Basis for Molecular-Orbital Studies of Organic Molecules" *J. Chem. Phys.*, **1971**, 54, 724–728.

[27] Grimme, S., Antony, J., Ehrlich, Krieg, H. "A Consistent and Accurate *Ab Initio* Parametrization of Density Functional Dispersion Correction (DFT-D) for the 94 Elements H-Pu" *J. Chem. Phys.*, **2010**, 132, 154101.

[28] Pinacho, P., López, J. C., Blanco, S. "Prediction of the Rotational Spectra of Microsolvated Complexes with Low Cost DFT Methods" *J. Mol. Spectrosc.*, **2017**, 337, 145–152.

[29] a) Boys, S., Bernardi, F. "The Calculation of Small Molecular Interactions by the Differences of Separate Total Energies. Some Procedures with Reduced Errors" *Mol. Phys.*, **1970**, 19, 553–566. b) Xantheas, S. S. "On the Importance of the Fragment Relaxation Energy Terms in the Estimation of the Basis Set Superposition Error Correction to the Intermolecular Interaction Energy" *J. Chem. Phys.*, **1996**, 21, 8821–8824.

[30] Pickett, H. M. "The Fitting and Prediction of Vibrational-Rotation Spectra with Spin Interaction" *J. Mol. Spectrosc.*, **1991**, 148, 371–377.

[31] Watson, J. K. G. in *Vibrational Spectra and Structure a Series of Advances, Vol 6* ed. J. R. Durig, Elsevier, New York, 1977, pp. 1–89.

[32] Gordy, W., Cook, R. L. *Microwave Molecular Spectra*, Wiley-Interscience, New York, 1984.

[33] Kisiel, Z., Pszczółkowski, L., Białkowska-Jaworska, E., Charnley. S. B. "The Millimeter Wave Rotational Spectrum of Pyruvic Acid" *J. Mol. Spectrosc.*, **2007**, 241, 220–229.

[34] Gerhard, D., Hellweg, A., Merke, I., Stahl, W., Baudelet, M., Petitprez, D., Wlodarczak, G. "Internal Rotation and Chlorine Nuclear Quadrupole Coupling of o-Chlorotoluene Studied by Microwave Spectroscopy and *Ab Initio* Calculations" *J. Mol. Spectrosc.*, **2003**, 220, 234–214.

[35] Hartwig, H., Dreizler, H. "The Microwave Spectrum of *Trans*-2,3-Dimethyloxirane in Torsional Excited States" *Z. Naturforsch*, **1996**, 51a, 923–932.

[36] a) Woods, R. C. "A General Program for the Calculation of Internal Rotation Splittings in Microwave Spectroscopy" *J. Mol. Spectrosc.*, **1966**, 21, 4–24. b) Woods, R. C. "A General Program for the Calculation of Internal Rotation Splittings in Microwave Spectroscopy – Part II. The n-Top Problem" *J. Mol. Spectrosc.*, **1967**, 22, 49–59.

[37] Kisiel, Z. "Least-Squares Mass-Dependence Molecular Structures for Selected Weakly Bound Intermolecular Clusters" *J. Mol. Spectrosc.*, **2003**, 218, 58–67.

[38] Rudolph, H. D. "Contribution to the Systematics of r_0-Derived Molecular Structure Determinations from Rotational Parameters" *Struct. Chem.*, **1991**, 2, 581–588.

[39] Kraitchman, J. "Determination of Molecular Structure from Microwave Spectroscopic Data" *Am. J. Phys.*, **1953**, 21, 17–24.

[40] Costain, C. C. "Further Comments on the Accuracy of r_s Substitution Structures" *Trans. Am. Crystallogr. Assoc.*, **1966**, 2, 157–164.

[41] Jeffrey, G. A. *An Introduction to Hydrogen Bonding*; Topics in Physical Chemistry - Oxford University Press, Oxford University Press, 1997.

[42] Gilli, P., Bertolasi, V., Ferretti, V., Gilli, G. "Evidence for Intramolecular N-H···O Resonance Assisted Hydrogen Bonding in β-Enaminones and Related Heterodienes. A Combined Crystal-Structural, IR, and NMR Spectroscopic, and Quantum-Mechanical Investigation" *J. Am. Chem. Soc.*, **2000**, 122, 10405–10417.

[43] Ottersen, T. “On the structure of the Peptide Linkage. The Structures of Formamide and Acetamide at -165 Degrees C and an *Ab Initio* Study of Formamide, Acetamide and N-methylformamide” *Acta Chemica Scandinavica*., **1975**, 29a, 939–944.
[44] Reed, A. E., Weinstock, R. B., Weinhold, F. “Natural Population Analysis” *J. Chem. Phys.* **1985**, *83*, 735-746.
[45] Borho, N., Xu, Y. “Rotational Spectrum of a Chiral α-Hydroxyester: Conformation Stability and Internal Rotation Barrier Heights of Methyl Lactate” *Phys. Chem. Chem. Phys.*, **2007**, 9, 1324–1328.
[46] Thomas, J., Sukhorukov, O., Jäger, W., Xu, Y. “Direct Spectroscopic Detection of The Orientation of Free OH groups in Methyl Lactate-$(Water)_{1,2}$ Clusters: Hydration of a Chiral Hydroxy Ester” *Angew. Chem. Int. Ed.*, **2014**, 53, 1156–1159.
[47] Ilyushin, V. V., Alekseev, E. A., Dyubko, S. F., Podnos, S. V., Kleiner, I., Margulès, L., Wlodarczak, G., Demaison, J., Cosléou, J., Maté, B., Karyakin, E. N., Golubiatnikov, G. Y., Fraser, G. T., Suenram, R. D., Hougen, J. T. “The Ground and First Excited Torsional States of Acetic Acid” *J. Mol. Spectrosc.*, **2001**, 205, 286–303.
[48] Ouyang, B., Howard. B. J. “The Monohydrate and Dihydrate of Acetic Acid: A High-Resolution Microwave Spectroscopic Study” *Phys. Chem. Chem. Phys.*, **2009**, 11, 366–373.

Supplementary material for Chapter VII

The Effect of Microsolvation over Structure, Nuclear Quadrupole and Internal Rotation: The Methyl Carbamate···(H_2O) and Methyl Carbamate···(H_2O)$_2$ Complexes.

Manuscript in preparation.

Abstract

Mono and dihydrated complexes of methyl carbamate formed in a supersonic jet expansion have been studied by high-resolution microwave spectroscopy, using both chirped-pulse and cavity Fourier transform microwave instruments covering the frequency range 2-18 GHz. From the rotational constants of the parent and ^{18}O–water monosubstituted isotopologues, accurate structures have been derived for the complexes. In both mono and dihydrated species water molecules close sequential cycles with methyl carbamate through N–H···O–H···O=C and N–H···O–H···O–H···O=C hydrogen bond networks respectively. The steady variation observed for the χ_{cc} quadrupole coupling constant or the V_3 methyl torsion barrier with the degree of hydration can be associated to resonance assisted hydrogen bonding effects.

- **Figure S7.1.** Conformers predicted for *syn* and *anti* methyl carbamate complexes with one molecule of water.

- **Figure S7.2.** Conformers predicted for *syn* and *anti* methyl carbamate complexes with two molecules of water.

- **Table S7.1.** *Ab initio* rotational parameters (B3LYP-D3/6-311++G(d,p)) for *syn* and *anti* methyl carbamate complexes with one molecule of water.

- **Table S7.2.** *Ab initio* rotational parameters (B3LYP-D3/6-311++G(d,p)) for *syn* and *anti* methyl carbamate complexes with two molecules of water.

- **Tables S7.3-S7.4.** Observed rotational parameters for the *syn*-mcb-w-a complex for the parent and the observed isotopologue.

- **Tables S7.5-S7.6.** Observed rotational parameters for the *syn*-mcb-w_2 complex for the parent and the observed isotopologues.

- **Table S7.7.** r_0 structure for the *syn*-mcb-w-a complex compared to r_e values.

- **Table S7.8.** r_0 structure for the *syn*-mcb-w_2 complex compared to r_e values.

- **Table S7.9.** Experimental and *ab initio* (B3LYP-D3/6-311++G(d,p) quadrupole coupling for methyl carbamate together with the values of the unbalanced $2p_z$ electronic charge ($(U_p)_z$).

- **Tables S7.10-S7.11.** Observed transition frequencies for the *syn*-mcb-w-a complex for the parent and the observed isotopologue.

- **Tables S7.12-S7.14.** Observed transition frequencies for the *syn*-mcb-w_2 complex for the parent and the observed isotopologue.

Figure S7.1. Conformers predicted for *syn* and *anti* methyl carbamate complexes with one molecule of water. ΔE is the stabilization energy relative to the most stable complex (*syn*-mcb-w-a) calculated at the B3LYP-D3/6-311++G(d,p) level of theory. The corresponding rotational parameters are given in Table S7.1.

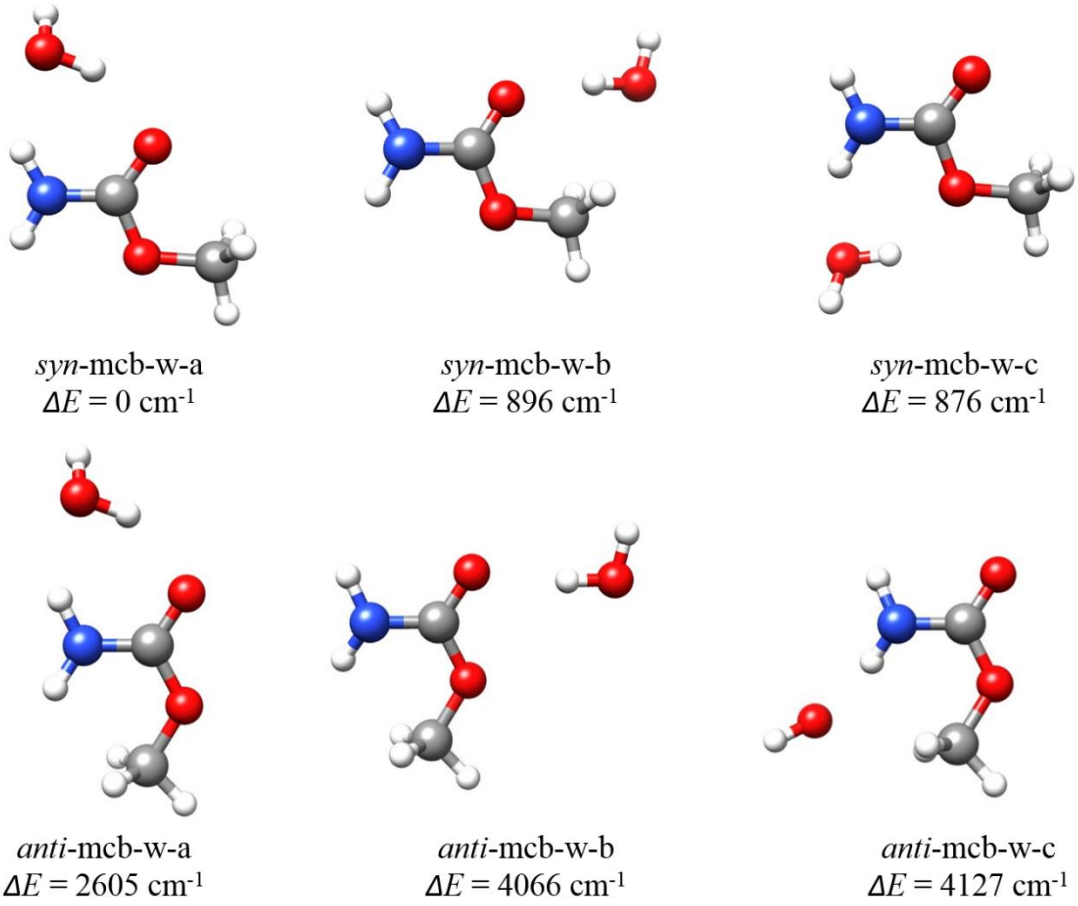

Figure S7.2. Conformers predicted for *syn* and *anti* methyl carbamate complexes with two molecules of water. ΔE is the stabilization energy relative to the most stable complex (*syn*-mcb-w_2) calculated at the B3LYP-D3/6-311++G(d,p) level of theory. The corresponding parameters are given in Table S7.2.

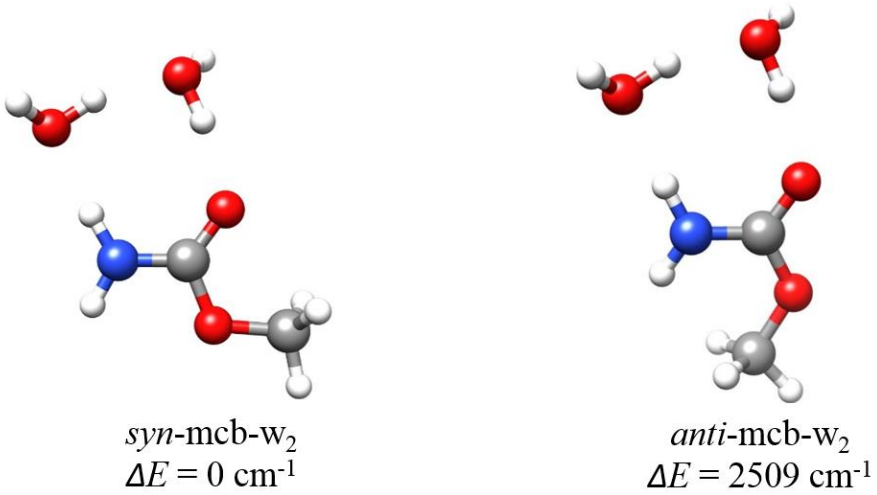

Table S7.1. *Ab initio* rotational parameters calculated at B3LYP-D3/6-311++G(d,p) level of theory for the stable *syn* and *anti* methyl carbamate complexes with one molecule of water.

Parameter[a]	*syn*-mcb-w-a	*syn*-mcb-w-b	*syn*-mcb-w-c	*anti*-mcb-w-a	*anti*-mcb-w-b	*anti*-mcb-w-c
A /MHz	8068.53	5249.44	4371.02	8773.65	4955.83	4766.47
B /MHz	1709.39	1980.44	2357.18	1655.99	1781.75	1826.58
C /MHz	1427.33	1451.26	1552.14	1411.26	1322.72	1382.93
Δ_J /kHz	0.418	0.659	1.09	0.379	5.63	1.29
Δ_{JK} /kHz	0.326	4.35	1.46	-0.517	-19.3	-3.24
Δ_K /kHz	21.0	5.49	0.182	18.1	54.6	26.6
δ_J /kHz	0.0765	0.163	0.380	0.0634	1.96	0.217
δ_K /kHz	1.49	2.89	2.62	1.26	13.9	2.60
P_a /uÅ^2	293.54	253.57	212.19	302.84	281.87	268.05
P_b /uÅ^2	60.53	94.66	113.41	55.26	100.20	97.39
P_c /uÅ^2	2.11	1.61	2.21	2.34	1.77	8.63
μ_a /D	1.28	3.30	2.01	2.16	6.71	7.97
μ_b /D	0.84	0.26	1.61	3.44	1.21	0.13
μ_c /D	0.88	0.27	1.13	0.74	0.35	0.47
χ_{aa} /MHz	1.80	2.73	2.03	1.50	2.46	2.12
χ_{bb} /MHz	2.72	2.16	2.55	2.79	2.20	2.04
χ_{cc} /MHz	-4.53	-4.89	-4.58	-4.29	-4.65	-4.16
ΔE /cm^{-1}	0.00	896.38	875.90	2604.75	4065.72	4127.55
ΔE /kJmol^{-1}	0.00	10.72	10.48	31.16	48.64	49.38

[a] A, B and C are the rotational constants. Δ_J, Δ_{JK}, Δ_K, δ_J and δ_K are the quartic centrifugal distortion constants. P_α (α= a, b or c) are the planar moments of inertia, these are derived from the moments of inertia I_α as for example $P_c = (I_a+I_b-I_c)/2$. μ_α (α = a, b or c) are the electric dipole moment components, 1 D = $3.33\cdot10^{-30}$ C·m. χ_{aa}, χ_{bb}, and χ_{cc}, are the quadrupole coupling tensor diagonal elements for ^{14}N atom. ΔE is the energy relative to the most stable conformer (*syn*-mcb-w-a).

Table S7.2. *Ab initio* rotational parameters calculated at B3LYP-D3/6-311++G(d,p) level of theory for the stable *syn* and *anti* methyl carbamate complexes with two molecules of water.

Parameter[a]	*syn*-mcb-w_2	*anti*-mcb-w_2
A /MHz	3874.89	4017.11
B /MHz	1092.44	1065.03
C /MHz	859.90	850.79
Δ_J /kHz	0.141	0.112
Δ_{JK} /kHz	0.638	3.09
Δ_K /kHz	4.32	1.20
δ_J /kHz	0.0343	0.0195
δ_K /kHz	0.762	0.839
P_a /uÅ^2	459.95	471.36
P_b /uÅ^2	127.76	122.65
P_c /uÅ^2	2.66	3.16
μ_a /D	1.35	2.10
μ_b /D	0.43	3.04
μ_c /D	0.17	0.43
^{14}N χ_{aa} /MHz	1.44	1.24
^{14}N χ_{bb} /MHz	2.79	2.82
^{14}N χ_{cc} /MHz	-4.23	-4.06
ΔE /cm^{-1}	0.00	2508.77
ΔE /kJmol^{-1}	0.00	30.01

[a] *A*, *B* and *C* are the rotational constants. Δ_J, Δ_{JK}, Δ_K, δ_J and δ_K are the quartic centrifugal distortion constants. P_α (α= *a*, *b* or *c*) are the planar moments of inertia, these are derived from the moments of inertia I_α as for example $P_c = (I_a+I_b-I_c)/2$. μ_α (α = *a*, *b* or *c*) are the electric dipole moment components, 1 D = $3.33\cdot10^{-30}$ C·m. χ_{aa}, χ_{bb}, and χ_{cc}, are the quadrupole coupling tensor diagonal elements for ^{14}N atom. ΔE is the energy relative to the most stable conformer (*syn*-mcb-w_2).

Table S7.3. Rotational parameters obtained from the analysis of the spectrum of the observed *syn*-mcb-w-a complex using XIAM and SPFIT programs for the parent species compared to the *ab initio* values at the B3LYP-D3/6-311++G(d,p) level of theory.

	xiam	spfit		*ab initio*
Fitted Parameters[a]	*syn*-mcb-w-a	*syn*-mcb-w-a *A*	*syn*-mcb-w-a *E*	*syn*-mcb-w-a
A /MHz	8056.7753(11)[b]	8057.63799(69)	8056.3430(18)	8068.53
B /MHz	1707.32139(37)	1707.34705(24)	1707.28244(36)	1709.39
C /MHz	1423.80899(33)	1423.82349(21)	1423.82747(40)	1427.33
Δ_J /kHz	0.4861(56)	0.4762(29)	0.4811(40)	0.418
Δ_{JK} /kHz	0.782(46)	0.792(23)	0.738(37)	0.326
Δ_K /kHz	[0.]	[0.]	[0.]	21.0
δ_J /kHz	0.1006(55)	0.0984(28)	0.0969(43)	0.0765
δ_K /kHz	[0.]	[0.]	[0.]	1.49
V_3 /cm^{-1}	373.13(67)	-	-	302.7
F_0 /MHz	158.13(38)	-	-	164.48
I_α / uÅ^2	3.1960(76)	-	-	3.155
ρ	0.036258(48)	-	-	0.032
β /rad	0.21574(47)	-	-	0.260
D_a /MHz	-	-	20.1537(12)	
D_{aJ} /MHz	-	-	-0.00147(11)	
D_b /MHz	-	-	4.53(25)	
^{14}N 3/2(χ_{aa}) /MHz	2.4363(44)	2.4418(38)	2.4326(48)	2.70
^{14}N ¼(χ_{bb}-χ_{cc}) /MHz	1.602(75)	1.6017(12)	1.6026(23)	1.81
N	198/28	99/28	97/28	
σ /kHz	6.9	4.4	4.6	
Derived Parameters				
P_a /uÅ^2	294.114173(52)	294.113499(34)	294.113563(59)	293.54
P_b /uÅ^2	60.834425(52)	60.831484(34)	60.830428(59)	60.53
P_c /uÅ^2	1.892781(52)	1.889006(34)	1.90014(59)	2.11
^{14}N χ_{aa} /MHz	1.6242(29)	1.6279(25)	1.6217(32)	1.80
^{14}N χ_{bb} /MHz	2.393(16)	2.3895(37)	2.3943(62)	2.72
^{14}N χ_{cc} /MHz	-4.017(16)	-4.0173(37)	-4.0161(62)	-4.53

[a] A, B and C are the rotational constants. Δ_J, Δ_{JK}, Δ_K, δ_J and δ_K are the quartic centrifugal distortion constants. V_3 is the internal rotation barrier for the methyl top. F_0 is the inverse of the moment of inertia of the methyl top, I_α. ρ is a dimensionless vectorial magnitude describing the coupling beetwen internal and overall rotation. β is the angle between ρ and the a principal inertial axis. D_a, D_{aJ}, D_b are terms describing the coupling beetwen internal and overall rotation using a perturbation treatment Hamiltonian in SPFIT. χ_{aa}, χ_{bb} and χ_{cc} are the quadrupole coupling tensor diagonal elements for ^{14}N atom. N is the number of quadrupole hyperfine components/rotational transitions fitted. σ is the rms deviation of the fit. P_α (α= a, b or c) are the planar moments of inertia, these are derived from the moments of inertia I_α as for example $P_c = (I_a+I_b-I_c)/2$. [b] Standard errors are given in parentheses in units of the last digit.

Table S7.4. Rotational parameters obtained from the analysis of the spectrum of the observed *syn*-mcb-w-a complex using XIAM and SPFIT programs for the observed $^{18}O_w$ atom isotopologue with *A* and *E* internal rotation substates compared to the *ab initio* values at the B3LYP-D3/6-311++G(d,p) level of theory.

	xiam	spfit		*ab initio*
Fitted Parameters[a]	*syn*-mcb-w-a $^{18}O_w$	*syn*-mcb-w-a $^{18}O_w$ *A*	*syn*-mcb-w-a $^{18}O_w$ *E*	*syn*-mcb-w-a
A /MHz	8030.9743(12)[b]	8031.8161(11)	8030.5514(14)	8068.53
B /MHz	1615.37034(22)	1615.39362(24)	1615.33596(25)	1709.39
C /MHz	1358.56086(23)	1358.57450(28)	1358.57653(30)	1427.33
Δ_J /kHz	[0.4861][c]	[0.4762]	[0.4811]	0.418
Δ_{JK} /kHz	[0.782]	[0.792]	[0.738]	0.326
Δ_K /kHz	[0.]	[0.]	[0.]	21.0
δ_J /kHz	[0.1006]	[0.0984]	[0.0969]	0.0765
δ_K /kHz	[0.]	[0.]	[0.]	1.49
V_3 /cm^{-1}	372.71(98)	-	-	302.7
F_0 /MHz	158.04(55)	-	-	164.48
I_α / uÅ^2	3.198(11)	-	-	3.155
ρ	0.035766(77)	-	-	0.032
β /rad	0.20876(55)	-	-	0.260
D_a /MHz	-	-	19.914(14)	
D_{aJ} /MHz	-	-	[-0.00147]	
D_b /MHz	-	-	[4.53]	
^{14}N 3/2(χ_{aa}) /MHz	[2.4363]	[2.4418]	[2.4326]	2.70
^{14}N ¼(χ_{bb}-χ_{cc}) /MHz	[1.602]	[1.6017]	[1.6026]	1.81
N	54/9	27/9	27/9	
σ /kHz	4.0	3.2	3.3	
Derived Parameters				
P_a /uÅ^2	310.96178(38)	310.960955(45)	310.961306(48)	293.54
P_b /uÅ^2	61.03407(38)	61.031163(45)	61.030256(48)	60.53
P_c /uÅ^2	1.89466(38)	1.890971(45)	1.901787(48)	2.11
^{14}N χ_{aa} /MHz	[1.6242]	[1.6279]	[1.6217]	1.80
^{14}N χ_{bb} /MHz	[2.393]	[2.3895]	[2.3943]	2.72
^{14}N χ_{cc} /MHz	[-4.017]	[-4.0173]	[-4.0161]	-4.53

[a] *A*, *B* and *C* are the rotational constants. Δ_J, Δ_{JK}, Δ_K, δ_J and δ_K are the quartic centrifugal distortion constants. V_3 is the internal rotation barrier for the methyl top. F_0 is the inverse of the moment of inertia of the methyl top, I_α. ρ is a dimensionless vectorial magnitude describing the coupling beetwen internal and overall rotation. β is the angle between ρ and the *a* principal inertial axis. D_a, D_{aJ}, D_b are terms describing the coupling beetwen internal and overall rotation using a perturbation treatment Hamiltonian in SPFIT. χ_{aa}, χ_{bb} and χ_{cc} are the quadrupole coupling tensor diagonal elements for ^{14}N atom. *N* is the number of quadrupole hyperfine components/rotational transitions fitted. σ is the rms deviation of the fit. P_α (α= *a*, *b* or *c*) are the planar moments of inertia, these are derived from the moments of inertia I_α as for example $P_c = (I_a+I_b-I_c)/2$. [b] Standard errors are given in parentheses in units of the last digit. [c] Parameters in square brackets were kept fixed to those given for the parent species in the fit.

Table S7.5. Rotational parameters obtained from the analysis of the spectrum of the observed *syn*-mcb-w_2 complex using XIAM or SPFIT with *A* and *E* internal rotation substates for the parent species compared to the *ab initio* values at the B3LYP-D3/6-311++G(d,p) level of theory.

	xiam	spfit		*ab initio*
Fitted Parameters[a]	*syn*-mcb-w_2	*syn*-mcb-w_2 *A*	*syn*-mcb-w_2 *E*	*syn*-mcb-w_2
A /MHz	3819.180(18)[b]	3819.329(14)	3819.083(13)	3874.89
B /MHz	1083.85347(72)	1083.86475(61)	1083.84281(54)	1092.44
C /MHz	851.82404(55)	851.82579(45)	851.82761(41)	859.90
Δ_J /kHz	0.1874(45)	0.1867(36)	0.1813(33)	0.141
Δ_{JK} /kHz	1.093(19)	1.084(41)	1.050(35)	0.638
Δ_K /kHz	[0.]	[0.]	[0.]	4.32
δ_J /kHz	0.0459(20)	0.0460(17)	0.0460(15)	0.0344
δ_K /kHz	0.98(22)	0.95(17)	0.74(16)	0.762
V_3 /cm^{-1}	415.4(1.2)	-	-	318.7
F_0 /MHz	171.74(43)	-	-	162.47
I_α / uÅ^2	2.9426(73)	-	-	3.152
ρ	[0.016][c]	-	-	0.016
β /rad	2.8362(17)	-	-	2.789
D_a /MHz	-	-	7.4191(21)	
^{14}N 3/2(χ_{aa}) /MHz	2.0187(57)	2.0215(88)	2.0134(87)	2.15
^{14}N ¼(χ_{bb}-χ_{cc}) /MHz	1.554(58)	1.5545(47)	1.5518(51)	1.76
N	171/28	90/28	81/26	
σ /kHz	5.4	3.8	3.1	
Derived Parameters				
P_a /uÅ^2	463.62181(40)	463.62136(46)	463.62118(29)	459.95
P_b /uÅ^2	129.66856(40)	129.66780(46)	129.66671(29)	127.76
P_c /uÅ^2	2.65801(40)	2.65361(46)	2.66323(29)	2.66
^{14}N χ_{aa} /MHz	1.3458(38)	1.3477(59)	1.3423(58)	1.44
^{14}N χ_{bb} /MHz	2.435(28)	2.435(12)	2.432(13)	2.79
^{14}N χ_{cc} /MHz	-3.781(28)	-3.783(12)	-3.775(13)	-4.23

[a] *A*, *B* and *C* are the rotational constants. Δ_J, Δ_{JK}, Δ_K, δ_J and δ_K are the quartic centrifugal distortion constants. V_3 is the internal rotation barrier for the methyl top. F_0 is the inverse of the moment of inertia of the methyl top, I_α. ρ is a dimensionless vectorial magnitude describing the coupling beetwen internal and overall rotation. β is the angle between ρ and the *a* principal inertial axis. D_a, D_{aJ}, D_b are terms describing the coupling beetwen internal and overall rotation using a perturbation treatment Hamiltonian in SPFIT. χ_{aa}, χ_{bb} and χ_{cc} are the quadrupole coupling tensor diagonal elements for ^{14}N atom. *N* is the number of quadrupole hyperfine components/rotational transitions fitted. σ is the rms deviation of the fit. P_α (α= *a*, *b* or *c*) are the planar moments of inertia, these are derived from the moments of inertia I_α as for example $P_c = (I_a+I_b-I_c)/2$. [b] Standard errors are given in parentheses in units of the last digit. [c] ρ was kept fixed to the *ab initio* value in the fit.

Table S7.6. Rotational parameters obtained from the analysis of the spectrum of the observed *syn*-mcb-w_2 complex using XIAM and SPFIT programs for the observed $^{18}O_{w1}$ and $^{18}O_{w2}$ isotopologues compared to the *ab initio* values at the B3LYP-D3/6-311++G(d,p) level of theory.

	Xiam	Spfit		Xiam	Spfit		
Fitted Parameters[a]	*syn*-mcb-w_2 $^{18}O_{w1}$	*syn*-mcb-w_2 $^{18}O_{w1}$ *A*	*syn*-mcb-w_2 $^{18}O_{w1}$ *E*	*syn*-mcb-w_2 $^{18}O_{w2}$	*syn*-mcb-w_2 $^{18}O_{w2}$ *A*	*syn*-mcb-w_2 $^{18}O_{w2}$ *E*	*Ab initio*
A /MHz	3681.308(16)[b]	3681.428(24)	3681.248(12)	3756.211(23)	3756.314(13)	3756.152(19)	3874.89
B /MHz	1059.32764(18)	1059.33842(21)	1059.31726(13)	1047.49457(23)	1047.50451(11)	1047.48447(18)	1092.44
C /MHz	829.77940(16)	829.78154(20)	829.78269(12)	826.20223(21)	826.20405(10)	826.20586(16)	859.90
Δ_J /kHz	[0.1874][c]	[0.1867]	[0.1813]	[0.1874]	[0.1867]	[0.1813]	0.141
Δ_{JK} /kHz	[1.093]	[1.084]	[1.050]	[1.093]	[1.084]	[1.050]	0.638
Δ_K /kHz	[0.]	[0.]	[0.]	[0.]	[0.]	[0.]	4.32
δ_J /kHz	[0.0459]	[0.0460]	[0.0460]	[0.0459]	[0.0460]	[0.0460]	0.0344
δ_K /kHz	[0.98]	[0.95]	[0.74]	[0.98]	[0.95]	[0.74]	0.762
V_3 /cm^{-1}	404.1(2.1)	-	-	420.8(2.5)	-	-	318.7
F_0 /MHz	167.2(1.3)	-	-	174.5(1.4)	-	-	162.47
I_α / uÅ^2	3.022(23)	-	-	2.897(23)	-	-	3.152
ρ	[0.016][d]	-	-	[0.016][d]	-	-	0.016
β /rad	2.8379(47)	-	-	2.8618(48)	-	-	2.789
D_a /MHz	-	-	6.93(10)		-	7.22(12)	
^{14}N 3/2(χ_{aa}) /MHz	[2.0187]	[2.0215]	[2.0134]	[2.0187]	[2.0215]	[2.0134]	2.15
^{14}N ¼(χ_{bb}-χ_{cc}) /MHz	[1.554]	[1.5545]	[1.5518]	[1.554]	[1.5545]	[1.5518]	1.76
N	69/12	35/12	34/12	71/12	36/12	35/12	
σ /kHz	3.8	3.6	2.1	5.0	3.0	2.6	
Derived Parameters							
P_a /uÅ^2	474.42252(31)	474.42155(46)	474.42253(23)	479.80445(42)	479.80333(24)	479.80437(35)	459.95
P_b /uÅ^2	134.62972(31)	134.62913(46)	134.62730(23)	131.88478(42)	131.88455(24)	131.88217(35)	127.76
P_c /uÅ^2	2.65273(31)	2.64886(46)	2.65740(23)	2.66011(42)	2.65665(24)	2.66484(35)	2.66
^{14}N χ_{aa} /MHz	[1.3458]	[1.3477]	[1.3423]	[1.3458]	[1.3477]	[1.3423]	1.44
^{14}N χ_{bb} /MHz	[2.435]	[2.435]	[2.432]	[2.435]	[2.435]	[2.432]	2.79
^{14}N χ_{cc} /MHz	[-3.781]	[-3.783]	[-3.775]	[-3.781]	[-3.783]	[-3.775]	-4.23

[a] *A*, *B* and *C* are the rotational constants. Δ_J, Δ_{JK}, Δ_K, δ_J and δ_K are the quartic centrifugal distortion constants. V_3 is the internal rotation barrier for the methyl top. F_0 is the inverse of the moment of inertia of the methyl top, I_α. ρ is a dimensionless vectorial magnitude describing the coupling beetwen internal and overall rotation. β is the angle between ρ and the *a* principal inertial axis. D_a is a term describing the coupling beetwen internal and overall rotation using a perturbation treatment Hamiltonian in SPFIT. χ_{aa}, χ_{bb} and χ_{cc} are the quadrupole coupling tensor diagonal elements for ^{14}N atom. *N* is the number of quadrupole hyperfine components/rotational transitions fitted. σ is the rms deviation of the fit. P_α (α= *a*, *b* or *c*) are the planar moments of inertia, these are derived from the moments of inertia I_α as for example $P_c = (I_a+I_b-I_c)/2$. [b] Standard errors are given in parentheses in units of the last digit. [c] Parameters in square brackets were kept fixed to those given for the parent species in the fit using the same program. [d] ρ was kept fixed to the *ab initio* value in the fit.

Table S7.7. r_0 structure obtained by the fitting of the rotational constants from the Xiam program for all the available isotopologues for the *syn*-mcb-w-a complex and comparison with the r_e (B3LYP-D3/6-311++G(d,p)) *ab initio* structure. The geometrical parameters for water were fixed to its r_0 values [Harmony, M. D., Laurie, V. W., Kuczkowski, R. L., Schwendeman, R. H., Ramsay, D. A., Lovas, F. J., Lafferty, W. J., Maki, A. G. *J. Phys. Chem. Ref. Data* **1979**, 8, 619–721]. The rest of the parameters were fixed to the r_e values, the uncertainties given in parenthesis were obtained from the coordinates uncertainties resulting from the r_0 fitting.

Fitted parameter	r_0	r_e	Derived parameter	r_0	r_e
$r(O_w\cdots H_1)$ /Å	2.0830(4)	2.074	$r(O_w–H_{w1})$ /Å	0.951(9)	0.975
$r(H_{w1}\cdots O_1)$ /Å	1.94(1)	1.920	$\angle(O_1–C_1–N)$ /°	125.302(9)	125.3
$\angle(O_w\cdots H_1–N)$ /°	138.25(2)	138.3	$\angle(H_1\cdots O_w–H_{w1})$ /°	81.9(4)	82.0
$\angle(H_{w1}\cdots O_1–C_1–N)$ /°	1.14(8)	5.2	$\angle(O_w–H_{w1}\cdots O_1)$ /°	148.2(4)	147.9

Fixed parameter	r_0	r_e	Fixed parameter	r_0	r_e
$r(O_1–C_1)$ /Å	[1.223]	1.223	$\angle(O_1–C_1–O_2–C_2)$ /°	[0.0]	0.1
$r(N–C_1)$ /Å	[1.351]	1.351	$\angle(N–C_1–O_2–C_2)$ /°	[180.0]	179.6
$r(O_2–C_1)$ /Å	[1.352]	1.352	$\angle(H_1–N–C_1–O_2)$ /°	[180.0]	176.0
$r(O_2–C_2)$ /Å	[1.439]	1.439	$\angle(H_2–N–C_1–O_2)$ /°	[0.0]	5.3
$r(N–H_1)$ /Å	[1.013]	1.013	$\angle(C_1–O_2–C_2–H_{m1})$ /°	[60.0]	60.2
$r(N–H_2)$ /Å	[1.005]	1.005	$\angle(C_1–O_2–C_2–H_{m2})$ /°	[-60.0]	-60.8
$r(O_w–H_{w2})$ /Å	[0.965]	0.961	$\angle(C_1–O_2–C_2–H_{m3})$ /°	[180.0]	179.7
$r(C_2–H_{m1})$ /Å	[1.091]	1.091	$\angle(O_w\cdots H_1–N–C_1)$ /°	[-1.3]	-1.3
$r(C_2–H_{m2})$ /Å	[1.091]	1.091			
$r(C_2–H_{m3})$ /Å	[1.088]	1.088			
$\angle(O_1–C_1–O_2)$ /°	[123.2]	123.2			
$\angle(O_2–C_1–N)$ /°	[125.3]	125.3			
$\angle(C_1–O_2–C_2)$ /°	[115.5]	115.5			
$\angle(C_1–N–H_1)$ /°	[117.8]	117.8			
$\angle(C_1–N–H_2)$ /°	[120.2]	120.2			
$\angle(O_2–C_2–H_{m1})$ /°	[110.6]	110.6			
$\angle(O_2–C_2–H_{m2})$ /°	[110.6]	110.6			
$\angle(O_2–C_2–H_{m3})$ /°	[105.3]	105.3			
$\angle(H_{w1}\cdots O_1–C_1)$ /°	[108.4]	108.4			
$\angle(H_{w2}–O_w–H_{w1})$ /°	[104.8]	106.4			

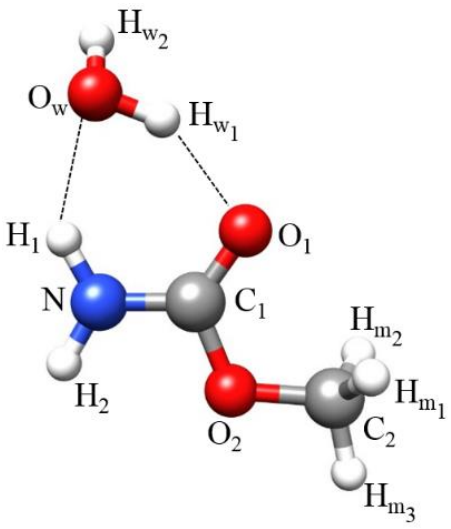

Table S7.8. r_0 structure obtained by the fitting of the rotational constants from the Xiam program for all the available isotopologues for the *syn*-mcb-w_2 complex and comparison with the r_e (B3LYP-D3/6-311++G(d,p)) *ab initio* structure. The geometrical parameters for water were fixed to its r_0 values [Harmony, M. D., Laurie, V. W., Kuczkowski, R. L., Schwendeman, R. H., Ramsay, D. A., Lovas, F. J., Lafferty, W. J., Maki, A. G. *J. Phys. Chem. Ref. Data* **1979**, 8, 619–721]. The rest of the parameters were fixed to the r_e values, the uncertainties given in parenthesis were obtained from the coordinates uncertainties resulting from the r_0 fitting.

Fitted parameter	r_0	r_e	Derived parameter	r_0	r_e
$r(O_{w2}\cdots H_1)$ /Å	1.902(2)	1.872	$r(H_{w3}\cdots O_{w1})$ /Å	1.826(1)	1.776
$r(H_{w1}\cdots O_1)$ /Å	1.805(2)	1.771	$r(O_{w2}\cdots O_{w1})$ /Å	2.756(1)	2.723
$\angle(H_{w1}\cdots O_1–C_1)$ /°	130.05(4)	129.4	$\angle(O_{w2}–H_{w3}\cdots O_{w1})$ /°	161.0(2)	160.9
$\angle(H_{w1}\cdots O_1–C_1– C_2)$ /°	177.4(5)	176.6	$\angle(H_{w3}\cdots O_{w1}–H_{w1})$ /°	98.44(9)	98.9

Fixed parameter	r_0	r_e	Fixed parameter	r_0	r_e
$r(O_1–C_1)$ /Å	[1.227]	1.227	$\angle(O_1–C_1–O_2–C_2)$ /°	[0.0]	0.1
$r(N–C_1)$ /Å	[1.344]	1.344	$\angle(N–C_1–O_2–C_2)$ /°	[-180.0]	-179.6
$r(O_2–C_1)$ /Å	[1.354]	1.354	$\angle(H_1–N–C_1–O_2)$ /°	[-180.0]	-178.2
$r(O_2–C_2)$ /Å	[1.438]	1.438	$\angle(H_2–N–C_1–O_2)$ /°	[0.0]	2.7
$r(N–H_1)$ /Å	[1.022]	1.022	$\angle(C_1–O_2–C_2–H_{m1})$ /°	[60.0]	60.1
$r(N–H_2)$ /Å	[1.006]	1.006	$\angle(C_1–O_2–C_2–H_{m2})$ /°	[-60.0]	-61.0
$r(C_2–H_{m1})$ /Å	[1.091]	1.091	$\angle(C_1–O_2–C_2–H_{m3})$ /°	[180.0]	179.5
$r(C_2–H_{m2})$ /Å	[1.091]	1.091	$\angle(O_{w2}\cdots H_1–N–C_1)$ /°	[15.0]	15.0
$r(C_2–H_{m3})$ /Å	[1.088]	1.088	$\angle(H_{w3}–O_{w2}\cdots H_1–N)$ /°	[-13.3]	-13.3
$r(O_{w2}–H_{w3})$ /Å	[0.965]	0.982	$\angle(H_{w4}–O_{w2}–H_{w3}–N)$ /°	[130.3]	130.3
$r(O_{w2}–H_{w4})$ /Å	[0.965]	0.961	$\angle(O_{w1}–H_{w1}\cdots O_1–C_1)$ /°	[-9.3]	-9.3
$r(O_{w1}–H_{w1})$ /Å	[0.965]	0.982	$\angle(H_{w2}–O_{w1}–H_{w1}\cdots O_1)$ /°	[-118.5]	-118.5
$r(O_{w1}–H_{w2})$ /Å	[0.965]	0.961			
$\angle(O_1–C_1–O_2)$ /°	[122.3]	122.3			
$\angle(O_2–C_1–N)$ /°	[111.6]	111.6			
$\angle(C_1–O_2–C_2)$ /°	[115.7]	115.7			
$\angle(C_1–N–H_1)$ /°	[120.5]	120.5			
$\angle(C_1–N–H_2)$ /°	[119.2]	119.2			
$\angle(O_2–C_2–H_{m1})$ /°	[110.6]	110.6			
$\angle(O_2–C_2–H_{m2})$ /°	[110.6]	110.6			
$\angle(O_2–C_2–H_{m3})$ /°	[105.3]	105.3			
$\angle(O_{w2}\cdots H_1–N)$ /°	[174.0]	174.0			
$\angle(H_{w3}–O_{w2}\cdots H_1)$ /°	[99.5]	99.5			
$\angle(H_{w4}–O_{w2}–H_{w3})$ /°	[104.8]	106.0			
$\angle(O_{w1}–H_{w1}\cdots O_1)$ /°	[170.0]	170.0			
$\angle(H_{w2}–O_{w1}–H_{w1})$ /°	[104.8]	106.2			

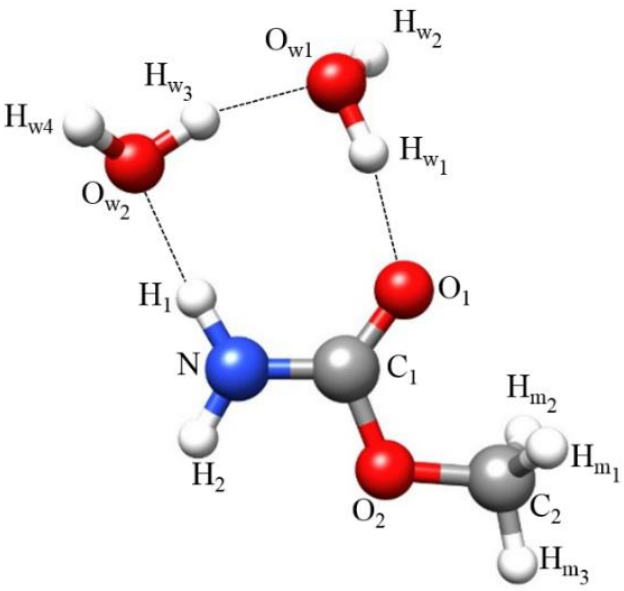

Table S7.9. Experimental and *ab initio* (B3LYP-D3/6-311++G(d,p) quadrupole coupling constants for the ^{14}N atom of the water complexes observed in this work with the values reported for the monomer of *syn*-mcb [reference 7], with the values of the unbalanced $2p_z$ electronic charge ($(U_p)_z$) both calculated from χ_{cc} and from the natural atomic orbital populations obtained by a Natural Bond Orbital Analysis [reference 40]. Representations of the correlations between a) experimental χ_{cc}/eQq_{210} *vs*. $-(U_p)_z$. b) *Ab initio* χ_{cc}/eQq_{210}, *vs*. $-(U_p)_z$. c) *Ab initio* r(C–N) *vs*. experimental χ_{cc}/eQq_{210}. d) *Ab initio* r(C=O) *vs*. experimental χ_{cc}/eQq_{210}.

Experimental	Mcb	Mcb-w-a	Mcb-w_2
χ_{aa} /MHz	2.28325(71)	1.6242(29)	1.3458(38)
χ_{bb} /MHz	2.01283(75)	2.393(16)	2.435(28)
χ_{cc} /MHz	-4.29609(75)	-4.017(16)	-3.781(28)
χ_{cc}/eQq_{210}	0.4296	0.4017	0.3781
Ab initio			
χ_{aa} /MHz	2.55	1.80	1.44
χ_{bb} /MHz	2.33	2.72	2.79
χ_{cc} /MHz	-4.87	-4.53	-4.23
χ_{ab} /MHz	-0.29	0.38	0.36
χ_{ac} /MHz	-0.53	0.13	-0.15
χ_{bc} /MHz	0.39	-0.40	0.39
χ_{xx} /MHz	2.81	2.87	2.90
χ_{yy} /MHz	2.13	1.67	1.36
χ_{zz} /MHz	-4.93	-4.56	-4.26
χ_{zz}/eQq_{210}	0.49	0.46	0.43
$-(U_p)_z$ NBO	0.41	0.38	0.35

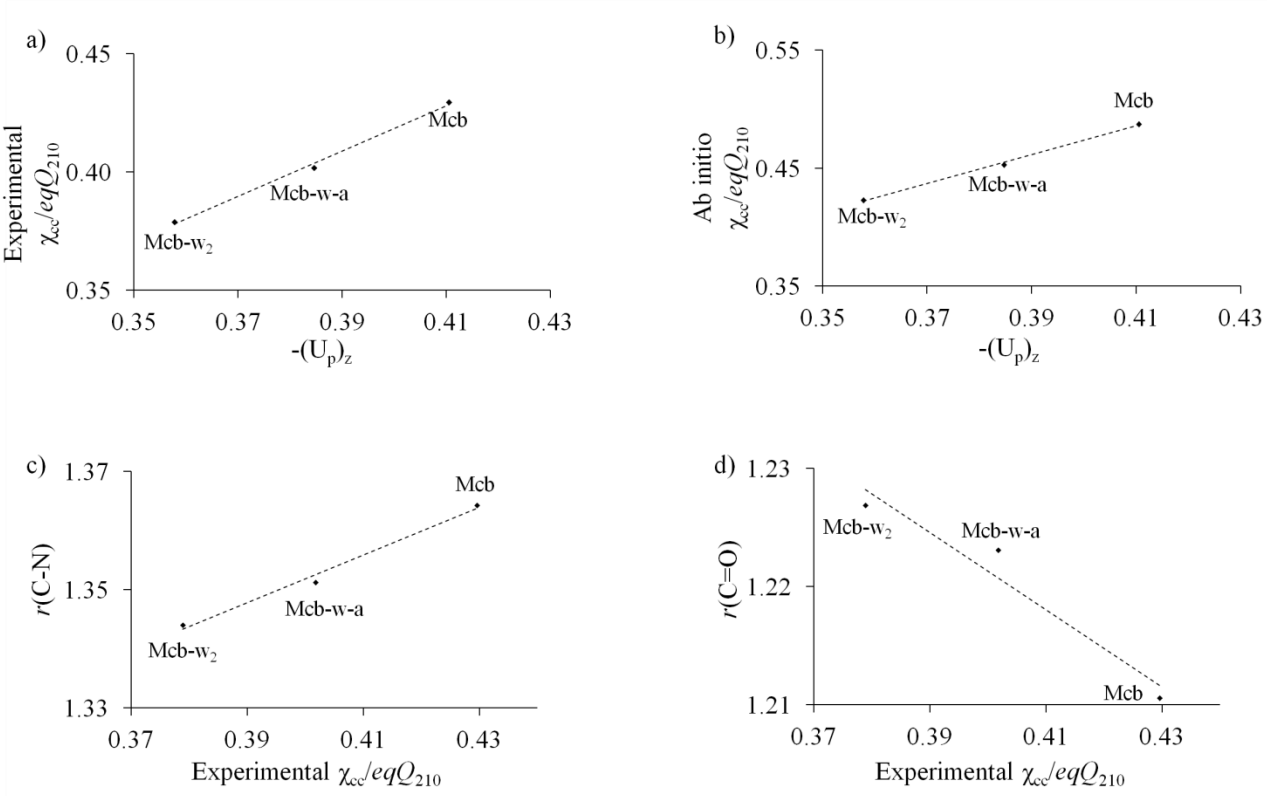

Table S7.10. Observed rotational frequencies and residuals (all the values in MHz) for the parent species of the *syn*-mcb-w-a complex for A and E substates $J'K'_{-1}K'_{+1}F' \leftarrow J''K''_{-1}K''_{+1}F''$ transitions using the Xiam program.

$J'K'_{-1}K'_{+}$	$J''K''_{-1}K$	F'	F''	S	Obs.	Res.
$1_{0,1}$	$0_{0,0}$	0	1	*A*	3130.3535	-0.0044
		2	1	*A*	3131.0881	-0.0007
		1	1	*A*	3131.5700	-0.0060
$1_{0,1}$	$0_{0,0}$	0	1	*E*	3130.2887	-0.0039
		2	1	*E*	3131.0265	0.0030
		1	1	*E*	3131.5087	-0.0021
$2_{1,2}$	$1_{1,1}$	1	1	*A*	5977.2000	-0.0049
		3	2	*A*	5978.6373	-0.0027
		1	0	*A*	5978.9941	-0.0054
		2	1	*A*	5979.2097	-0.0037
		2	2	*A*	5979.9247	-0.0065
$2_{1,2}$	$1_{1,1}$	1	1	*E*	5978.1077	0.0032
		3	2	*E*	5979.5333	0.0039
		1	0	*E*	5979.8787	0.0035
		2	1	*E*	5980.1150	0.0038
		2	2	*E*	5980.8162	-0.0032
$2_{0,2}$	$1_{0,1}$	1	1	*A*	6252.1975	-0.0010
		3	2	*A*	6252.9988	-0.0018
		2	1	*A*	6253.0780	-0.0019
		1	0	*A*	6253.4032	-0.0134
		2	2	*A*	6253.5653	-0.0019
$2_{0,2}$	$1_{0,1}$	1	1	*E*	6252.0691	-0.0017
		3	2	*E*	6252.8742	0.0013
		1	0	*E*	6253.2874	-0.0016
		2	2	*E*	6253.4493	0.0098
$2_{1,1}$	$1_{1,0}$	1	0	*A*	6544.4333	0.0011
		2	2	*A*	6545.0572	0.0138
		3	2	*A*	6545.8164	0.0039
$J'K'_{-1}K'_{+}$	$J''K''_{-1}K$	F'	F''	S	Obs.	Res.
		2	1	*A*	6546.2491	0.0006
		1	1	*A*	6547.4467	0.0018
$2_{1,1}$	$1_{1,0}$	1	0	*E*	6543.3098	-0.0015
		2	2	*E*	6543.9056	-0.0045
		3	2	*E*	6544.6753	-0.0027
		2	1	*E*	6545.1003	-0.0052
		1	1	*E*	6546.3034	0.0033
$3_{1,3}$	$2_{1,2}$	4	3	*A*	8962.3861	-0.0069
		3	2	*A*	8962.5823	-0.0079
		2	1	*A*	8962.5823	-0.0070
$3_{1,3}$	$2_{1,2}$	4	3	*E*	8962.5482	0.0081
		2	1	*E*	8962.7450	0.0091
		3	2	*E*	8962.7450	0.0068
$3_{0,3}$	$2_{0,2}$	2	2	*A*	9355.5560	-0.0075
		4	3	*A*	9356.3566	-0.0034
		2	1	*A*	9356.4412	-0.0038
		3	2	*A*	9356.4481	-0.0019
		3	3	*A*	9357.0095	-0.0071
$3_{0,3}$	$2_{0,2}$	2	2	*E*	9355.3939	0.0149
		4	3	*E*	9356.1761	0.0007
		3	2	*E*	9356.2615	0.0011
		2	1	*E*	9356.2678	0.0024
		3	3	*E*	9356.8447	0.0127
$3_{2,2}$	$2_{2,1}$	2	1	*A*	9393.0320	-0.0050
		4	3	*A*	9393.3273	0.0002
		3	2	*A*	9393.8533	0.0042
$3_{2,2}$	$2_{2,1}$	2	1	*E*	9405.5073	0.0061
		4	3	*E*	9405.7893	-0.0028
$J'K'_{-1}K'_{+}$	$J''K''_{-1}K$	F'	F''	S	Obs.	Res.
		3	2	*E*	9406.3114	0.0065
$3_{2,1}$	$2_{2,0}$	2	1	*A*	9430.1335	-0.0029
		4	3	*A*	9430.4049	-0.0060
		3	2	*A*	9430.8667	0.0044
$3_{2,1}$	$2_{2,0}$	2	1	*E*	9417.2947	-0.0003
		4	3	*E*	9417.5734	0.0048
		3	2	*E*	9418.0219	-0.0073
$3_{1,2}$	$2_{1,1}$	2	1	*A*	9812.6204	0.0014
		4	3	*A*	9812.8214	0.0017
		3	2	*A*	9812.9446	0.0033
$3_{1,2}$	$2_{1,1}$	2	1	*E*	9812.1046	-0.0015
		4	3	*E*	9812.3044	-0.0019
		3	2	*E*	9812.4261	-0.0010
$4_{1,4}$	$3_{1,3}$	5	4	*A*	11939.4715	-0.0072
		4	3	*A*	11939.5822	-0.0063
		3	2	*A*	11939.5822	-0.0070
$4_{1,4}$	$3_{1,3}$	5	4	*E*	11939.4595	0.0056
		3	2	*E*	11939.5698	0.0062
		4	3	*E*	11939.5698	0.0052
$4_{0,4}$	$3_{0,3}$	5	4	*A*	12432.2894	-0.0037
		3	2	*A*	12432.3210	-0.0054
		4	3	*A*	12432.3965	-0.0044
$4_{0,4}$	$3_{0,3}$	5	4	*E*	12432.0642	0.0047
		3	2	*E*	12432.0935	0.0007
		4	3	*E*	12432.1730	0.0057
$4_{2,3}$	$3_{2,2}$	3	2	*A*	12517.1903	-0.0025
		5	4	*A*	12517.2521	-0.0005
		4	3	*A*	12517.4826	-0.0025

Table S7.10. Continuation.

$J'K'_{-1}K'_{.}$	$J''K''_{-1}K$	F'	F''	S	Obs.	Res.
$4_{2,3}$	$3_{2,2}$	3	2	*E*	12529.4097	0.0010
		5	4	*E*	12529.4749	-0.0001
		4	3	*E*	12529.7224	0.0002
$4_{2,2}$	$3_{2,1}$	3	2	*A*	12609.4581	-0.0030
		5	4	*A*	12609.5055	-0.0016
		4	3	*A*	12609.6413	-0.0028
$4_{2,2}$	$3_{2,1}$	3	2	*E*	12596.7416	0.0061
		5	4	*E*	12596.7785	0.0036
		4	3	*E*	12596.9010	0.0037
$4_{1,3}$	$3_{1,2}$	3	2	*A*	13072.3453	0.0034
		5	4	*A*	13072.4192	0.0006
		4	3	*A*	13072.4840	0.0011
$4_{1,3}$	$3_{1,2}$	3	2	*E*	13071.8769	-0.0046
		5	4	*E*	13071.9540	-0.0041
		4	3	*E*	13072.0192	-0.0030
$5_{1,5}$	$4_{1,4}$	6	5	*A*	14908.1476	-0.0084
		4	3	*A*	14908.2099	-0.0154
		5	4	*A*	14908.2254	-0.0103
$5_{1,5}$	$4_{1,4}$	6	5	*E*	14908.0688	0.0116
		4	3	*E*	14908.1313	0.0048
		5	4	*E*	14908.1476	0.0107
$5_{0,5}$	$4_{0,4}$	6	5	*A*	15472.8643	-0.0053
		4	3	*A*	15472.8792	-0.0055
		5	4	*A*	15472.9913	-0.0048
$5_{0,5}$	$4_{0,4}$	6	5	*E*	15472.6053	0.0086
		4	3	*E*	15472.6227	0.0109
		5	4	*E*	15472.7314	0.0082
$5_{2,4}$	$4_{2,3}$	4	3	*A*	15634.9173	0.0142
		5	4	*A*	15634.9173	-0.0006
		6	5	*A*	15635.0543	0.0028
$5_{2,4}$	$4_{2,3}$	4	3	*E*	15640.5007	0.0156
		6	5	*E*	15640.5007	-0.0019
		5	4	*E*	15640.6538	0.0083
$5_{2,3}$	$4_{2,2}$	4	3	*A*	15817.6104	-0.0177
		5	4	*A*	15817.6104	-0.0198
		4	3	*A*	15817.6353	-0.0106
$5_{2,3}$	$4_{2,2}$	6	5	*E*	15811.3957	-0.0022
		4	3	*E*	15811.3957	-0.0029
$5_{1,4}$	$4_{1,3}$	6	5	*A*	16321.6714	0.0044
		5	4	*A*	16321.7144	0.0058
		5	4	*A*	16321.7690	0.0093
$5_{1,4}$	$4_{1,3}$	4	3	*E*	16321.1635	-0.0014
		6	5	*E*	16321.2056	-0.0009
		5	4	*E*	16321.2568	-0.0008
$3_{0,3}$	$2_{1,2}$	3	2	*A*	3279.8312	-0.0006
		4	3	*A*	3280.4718	0.0054
		2	1	*A*	3280.9527	-0.0012
$3_{0,3}$	$2_{1,2}$	3	2	*E*	3281.2913	-0.0030
		4	3	*E*	3281.9260	-0.0017
$4_{0,4}$	$3_{1,3}$	4	3	*A*	6749.6492	0.0067
		5	4	*A*	6750.3724	0.0059
		3	2	*A*	6750.6867	-0.0042
$4_{0,4}$	$3_{1,3}$	4	3	*E*	6750.7248	0.0014
		5	4	*E*	6751.4442	-0.0029
		3	2	*E*	6751.7686	-0.0028
$5_{0,5}$	$4_{1,4}$	5	4	*A*	10283.0539	0.0045
		6	5	*A*	10283.7641	0.0066
		4	3	*A*	10283.9938	0.0067
$5_{0,5}$	$4_{1,4}$	5	4	*E*	10283.8717	-0.0103
		6	5	*E*	10284.5804	-0.0095
		4	3	*E*	10284.8144	-0.0052
$1_{1,1}$	$0_{0,0}$	0	1	*A*	9480.2615	-0.0047
		2	1	*A*	9481.3378	-0.0051
		1	1	*A*	9482.0512	-0.0096
$1_{1,1}$	$0_{0,0}$	0	1	*E*	9477.5548	0.0025
		2	1	*E*	9478.6163	0.0015
		1	1	*E*	9479.3219	-0.0011
$2_{1,2}$	$1_{0,1}$	3	2	*A*	12328.8866	-0.0076
		1	0	*A*	12328.9066	-0.0012
		2	1	*A*	12329.6944	-0.0037
$2_{1,2}$	$1_{0,1}$	3	2	*E*	12327.1273	0.0066
		1	0	*E*	12327.1460	0.0111
		2	1	*E*	12327.9338	0.0104
$3_{1,3}$	$2_{0,2}$	2	1	*A*	15038.0677	-0.0128
		4	3	*A*	15038.2743	-0.0123
		3	2	*A*	15039.1960	-0.0124
$3_{1,3}$	$2_{0,2}$	2	1	*E*	15036.5954	0.0136
		4	3	*E*	15036.7997	0.0119
		3	2	*E*	15037.7265	0.0171
$1_{1,0}$	$1_{0,1}$	1	1	*A*	6632.4084	0.0061
		1	2	*A*	6632.8878	-0.0018
		2	1	*A*	6633.6153	0.0079
		1	0	*A*	6633.6153	-0.0051
		2	2	*A*	6634.0890	-0.0057

Table S7.10. Continuation.

$J'K'_{-1}K'_{.}$	$J''K''_{-1}K$	F'	F''	S	Obs.	Res.
		0	1	*A*	6635.4137	-0.0013
$1_{1,0}$	$1_{0,1}$	1	1	*E*	6632.5448	-0.0069
		1	2	*E*	6633.0377	-0.0013
		2	1	*E*	6633.7360	-0.0111
		2	2	*E*	6634.2146	-0.0198
$2_{1,1}$	$2_{0,2}$	2	2	*A*	6925.5731	0.0022
		2	3	*A*	6926.1393	0.0018
		3	2	*A*	6926.3493	0.0093
		2	1	*A*	6926.4649	0.0126
		1	2	*A*	6926.7780	0.0107
		3	3	*A*	6926.9092	0.0026
		1	1	*A*	6927.6562	0.0075
$2_{1,1}$	$2_{0,2}$	2	2	*E*	6924.7020	-0.0029
		2	3	*E*	6925.2587	-0.0128
		3	2	*E*	6925.4684	-0.0045
		1	2	*E*	6925.8961	-0.0034
		3	3	*E*	6926.0346	-0.0049
		1	1	*E*	6926.7780	-0.0030
$3_{1,2}$	$3_{0,3}$	3	3	*A*	7382.0706	0.0084
		2	3	*A*	7382.9554	0.0191
		3	2	*A*	7382.9554	0.0067
		4	4	*A*	7383.3747	0.0084
		2	2	*A*	7383.8304	0.0077
$3_{1,2}$	$3_{0,3}$	3	3	*E*	7380.8606	-0.0060
		4	3	*E*	7381.5153	0.0016
		3	4	*E*	7381.5153	-0.0079
		2	3	*E*	7381.7271	-0.0131
		3	2	*E*	7381.7535	0.0005
		4	4	*E*	7382.1647	-0.0056
		2	2	*E*	7382.6210	-0.0057

Table S7.11. Observed rotational frequencies and residuals (all the values in MHz) for the $^{18}O_w$ isotopologue species of the *syn*-mcb-w-a complex A and E substates $J'K'_{-1}K'_{+1}F' \leftarrow J''K''_{-1}K''_{+1}F''$ transitions using the Xiam program.

$J'K'_{-1}K'_{+1}$	$J''K''_{-1}K$	F'	F''	S	Obs.	Res.	$J'K'_{-1}K'_{+1}$	$J''K''_{-1}K$	F'	F''	S	Obs.	Res.
$3_{1,3}$	$2_{1,2}$	4	3	*A*	8531.8876	-0.0061	$4_{0,4}$	$3_{0,3}$	5	4	*E*	11820.3437	0.0059
		3	2	*A*	8532.0846	-0.0049			3	2	*E*	11820.3785	0.0061
		2	1	*A*	8532.0846	-0.0059			4	3	*E*	11820.4407	0.0044
$3_{1,3}$	$2_{1,2}$	4	3	*E*	8532.0722	0.0058	$4_{1,3}$	$3_{1,2}$	3	2	*A*	12393.7393	0.0016
		3	2	*E*	8532.2695	0.0063			5	4	*A*	12393.8157	0.0019
		2	1	*E*	8532.2695	0.0070			4	3	*A*	12393.8815	0.0059
$3_{0,3}$	$2_{0,2}$	4	3	*A*	8891.6353	-0.0038	$4_{1,3}$	$3_{1,2}$	3	2	*E*	12393.3070	0.0038
		2	1	*A*	8891.7193	-0.0063			5	4	*E*	12393.3791	-0.0001
		3	2	*A*	8891.7193	-0.0027			4	3	*E*	12393.4444	0.0035
$3_{0,3}$	$2_{0,2}$	4	3	*E*	8891.4718	0.0014	$4_{0,4}$	$3_{1,3}$	4	3	*A*	6012.5613	0.0046
		2	1	*E*	8891.5557	-0.0012			5	4	*A*	6013.2991	-0.0011
		3	2	*E*	8891.5557	0.0024			3	2	*A*	6013.6283	-0.0012
$3_{1,2}$	$2_{1,1}$	2	1	*A*	9302.0588	-0.0043	$4_{0,4}$	$3_{1,3}$	4	3	*E*	6013.6556	-0.0041
		4	3	*A*	9302.2634	0.0001			5	4	*E*	6014.4038	0.0010
		3	2	*A*	9302.3833	-0.0001			3	2	*E*	6014.7254	-0.0065
$3_{1,2}$	$2_{1,1}$	2	1	*E*	9301.5544	-0.0033	$1_{1,1}$	$0_{0,0}$	0	1	*A*	9389.1872	-0.0052
		4	3	*E*	9301.7537	-0.0036			2	1	*A*	9390.2679	-0.0012
		3	2	*E*	9301.8725	-0.0039			1	1	*A*	9390.9802	-0.0069
$4_{1,4}$	$3_{1,3}$	5	4	*A*	11367.3813	0.0028	$1_{1,1}$	$0_{0,0}$	0	1	*E*	9386.4100	-0.0025
		3	2	*A*	11367.4909	0.0021			2	1	*E*	9387.4734	0.0010
		4	3	*A*	11367.4909	0.0038			1	1	*E*	9388.1797	0.0009
$4_{1,4}$	$3_{1,3}$	5	4	*E*	11367.3689	-0.0025	$2_{1,1}$	$2_{0,2}$	2	2	*A*	6936.5768	0.0059
		3	2	*E*	11367.4785	-0.0030			3	3	*A*	6937.9067	0.0045
		4	3	*E*	11367.4785	-0.0015			1	1	*A*	6938.6470	0.0052
$4_{0,4}$	$3_{0,3}$	5	4	*A*	11820.5500	-0.0022	$2_{1,1}$	$2_{0,2}$	2	2	*E*	6935.7770	-0.0015
		3	2	*A*	11820.5850	-0.0019			3	3	*E*	6937.1028	-0.0056
		4	3	*A*	11820.6483	-0.0024			1	1	*E*	6937.8454	-0.0018

Table S7.12. Observed rotational frequencies and residuals (all the values in MHz) for the parent species of the *syn*-mcb-w_2 complex for A and E substates $J'K'_{-1}K'_{+1}F' \leftarrow J''K''_{-1}K''_{+1}F''$ transitions using the Xiam program.

$J'K'_{-1}K'_{+1}$	$J''K''_{-1}K''_{+1}$	F'	F''	S	Obs.	Res.
$2_{1,2}$	$1_{1,1}$	1	1	*A*	3637.7825	-0.0024
		3	2	*A*	3639.1902	-0.0003
		1	0	*A*	3639.6074	-0.0037
		2	1	*A*	3639.6681	-0.0071
		2	2	*A*	3640.4090	0.0033
$2_{1,2}$	$1_{1,1}$	3	2	*E*	3639.3289	0.0010
		1	0	*E*	3639.7424	-0.0034
		2	1	*E*	3639.8169	0.0025
		2	2	*E*	3640.5463	0.0034
$2_{0,2}$	$1_{0,1}$	1	1	*A*	3856.4916	-0.0058
		3	2	*A*	3857.1818	-0.0042
		2	1	*A*	3857.2911	-0.0037
		1	0	*A*	3857.5180	0.0112
		2	2	*A*	3857.7074	0.0089
$2_{0,2}$	$1_{0,1}$	3	2	*E*	3857.1505	0.0059
		2	1	*E*	3857.2503	-0.0031
		1	0	*E*	3857.4655	0.0001
		2	2	*E*	3857.6465	-0.0106
$2_{1,1}$	$1_{1,0}$	3	2	*A*	4103.3898	0.0013
		2	1	*A*	4103.7469	0.0069
$2_{1,1}$	$1_{1,0}$	1	0	*E*	4101.9105	0.0012
		3	2	*E*	4103.1758	0.0026
		2	1	*E*	4103.5210	-0.0020
$3_{1,3}$	$2_{1,2}$	4	3	*A*	5450.3337	-0.0026
		3	2	*A*	5450.5117	-0.0065
		2	1	*A*	5450.5144	-0.0079
$3_{1,3}$	$2_{1,2}$	4	3	*E*	5450.3445	-0.0016
		3	2	*E*	5450.5315	0.0033
		2	1	*E*	5450.5315	-0.0005
$3_{0,3}$	$2_{0,2}$	2	2	*A*	5750.0414	0.0052
		4	3	*A*	5750.7762	-0.0015
		2	1	*A*	5750.8271	-0.0065
		3	2	*A*	5750.9165	-0.0026
$3_{0,3}$	$2_{0,2}$	2	2	*E*	5749.9826	0.0035
		4	3	*E*	5750.7211	0.0005
		2	1	*E*	5750.7762	-0.0002
		3	2	*E*	5750.8627	0.0007
$3_{2,2}$	$2_{2,1}$	2	1	*A*	5806.6817	-0.0076
		4	3	*A*	5806.9283	-0.0014
		3	2	*A*	5807.3621	-0.0001
$3_{2,1}$	$2_{2,0}$	2	1	*A*	5862.9845	0.0094
		4	3	*A*	5863.1877	-0.0003
		3	2	*A*	5863.4946	-0.0006
		2	2	*A*	5863.7688	-0.0037
$3_{1,2}$	$2_{1,1}$	2	1	*A*	6145.7655	0.0036
		4	3	*A*	6145.9687	0.0073
		3	2	*A*	6146.0740	0.0022
$3_{1,2}$	$2_{1,1}$	2	1	*E*	6145.6361	0.0002
		4	3	*E*	6145.8353	0.0000
		3	2	*E*	6145.9350	-0.0105
$4_{1,4}$	$3_{1,3}$	5	4	*A*	7251.8614	-0.0033
		4	3	*A*	7251.9606	-0.0045
		3	2	*A*	7251.9772	-0.0018
$4_{1,4}$	$3_{1,3}$	5	4	*E*	7251.8455	0.0029
		4	3	*E*	7251.9456	0.0027
		3	2	*E*	7251.9608	0.0039
$4_{0,4}$	$3_{0,3}$	5	4	*A*	7604.2893	-0.0025
		3	2	*A*	7604.3048	-0.0021
		4	3	*A*	7604.4632	-0.0029
$4_{0,4}$	$3_{0,3}$	5	4	*E*	7604.2248	0.0013
		3	2	*E*	7604.2412	0.0019
		4	3	*E*	7604.3989	0.0007
$4_{2,3}$	$3_{2,2}$	3	2	*A*	7731.5774	0.0109
		5	4	*A*	7731.6186	-0.0002
		4	3	*A*	7731.8225	0.0003
$4_{2,3}$	$3_{2,2}$	3	2	*E*	7733.4356	-0.0017
		5	4	*E*	7733.4902	-0.0017
		4	3	*E*	7733.7011	-0.0004
$4_{2,2}$	$3_{2,1}$	3	2	*A*	7869.9806	-0.0055
		5	4	*A*	7870.0128	-0.0024
		4	3	*A*	7870.0536	-0.0006
$4_{2,2}$	$3_{2,1}$	3	2	*E*	7867.9455	-0.0006
		5	4	*E*	7867.9729	0.0000
		4	3	*E*	7868.0049	-0.0007
$4_{1,3}$	$3_{1,2}$	3	2	*A*	8176.7082	0.0001
		5	4	*A*	8176.7947	0.0048
		4	3	*A*	8176.8684	0.0036
$4_{1,3}$	$3_{1,2}$	3	2	*E*	8176.5748	-0.0018
		5	4	*E*	8176.6561	-0.0022
		4	3	*E*	8176.7284	-0.0048
$5_{1,5}$	$4_{1,4}$	6	5	*A*	9041.7821	-0.0047
		4	3	*A*	9041.8472	-0.0018
		5	4	*A*	9041.8734	-0.0047
$5_{1,5}$	$4_{1,4}$	6	5	*E*	9041.7536	0.0038

Table S7.12. Continued.

$J'K'_{-1}K'_{.}$	$J''K''_{-1}K$	F'	F''	S	Obs.	Res.
		4	3	*E*	9041.8461	0.0041
		5	4	*E*	9041.8443	0.0032
$5_{0,5}$	$4_{0,4}$	4	3	*A*	9410.0584	-0.0014
		6	5	*A*	9410.0584	0.0025
		5	4	*A*	9410.2549	0.0007
$5_{0,5}$	$4_{0,4}$	4	3	*E*	9409.9905	0.0042
		6	5	*E*	9409.9905	0.0081
		5	4	*E*	9410.1832	0.0025
$5_{2,4}$	$4_{2,3}$	4	3	*A*	9646.8493	-0.0049
		6	5	*A*	9646.8739	0.0045
		5	4	*A*	9646.9961	-0.0012
$5_{2,4}$	$4_{2,3}$	4	3	*E*	9647.3424	-0.0029
		6	5	*E*	9647.3615	0.0007
		5	4	*E*	9647.4900	0.0000
$5_{2,3}$	$4_{2,2}$	5	4	*A*	9914.9664	-0.0005
		6	5	*A*	9915.0281	-0.0019
		4	3	*A*	9915.0427	0.0087
$5_{2,3}$	$4_{2,2}$	5	4	*E*	9914.2555	-0.0016
		6	5	*E*	9914.3197	-0.0018
		4	3	*E*	9914.3197	-0.0061
$5_{1,4}$	$4_{1,3}$	4	3	*A*	10190.6460	0.0093
		6	5	*A*	10190.6836	-0.0004
		5	4	*A*	10190.7598	0.0000
$5_{1,4}$	$4_{1,3}$	4	3	*E*	10190.4826	-0.0024
		6	5	*E*	10190.5299	-0.0024
		5	4	*E*	10190.6056	-0.0025
$6_{1,6}$	$5_{1,5}$	7	6	*A*	10818.9601	-0.0073
		5	4	*A*	10819.0064	-0.0032
		6	5	*A*	10819.0437	-0.0052
$6_{1,6}$	$5_{1,5}$	7	6	*E*	10818.9264	0.0049
		5	4	*E*	10818.9719	0.0083
		6	5	*E*	10819.0064	0.0034
$6_{0,6}$	$5_{0,5}$	5	4	*A*	11168.0467	-0.0052
		7	6	*A*	11168.0467	-0.0041
		6	5	*A*	11168.2520	-0.0045
$6_{0,6}$	$5_{0,5}$	5	4	*E*	11167.9795	0.0024
		7	6	*E*	11167.9795	0.0035
		6	5	*E*	11168.1840	0.0023
$6_{2,5}$	$5_{2,4}$	5	4	*A*	11550.4401	0.0023
		7	6	*A*	11550.4401	-0.0027
		6	5	*A*	11550.5383	-0.0028
$6_{2,5}$	$5_{2,4}$	7	6	*E*	11550.5525	0.0060
		5	4	*E*	11550.5525	0.0009
		6	5	*E*	11550.6513	0.0010
$6_{2,4}$	$5_{2,3}$	6	5	*A*	11995.6552	-0.0002
		7	6	*A*	11995.7571	0.0005
		5	4	*A*	11995.7735	0.0078
$6_{2,4}$	$5_{2,3}$	6	5	*E*	11995.2782	-0.0010
		7	6	*E*	11995.3786	-0.0022
		5	4	*E*	11995.3936	0.0037
$6_{1,5}$	$5_{1,4}$	5	4	*A*	12181.3388	-0.0014
		7	6	*A*	12181.3726	-0.0007
		6	5	*A*	12181.4635	0.0015
$6_{1,5}$	$5_{1,4}$	5	4	*E*	12181.1621	-0.0042
		7	6	*E*	12181.1949	-0.0046
		6	5	*E*	12181.2854	-0.0027
$7_{1,7}$	$6_{1,6}$	8	7	*A*	12583.1773	-0.0011
		6	5	*A*	12583.2023	-0.0066
		7	6	*A*	12583.2492	-0.0052
$7_{1,7}$	$6_{1,6}$	8	7	*E*	12583.1297	0.0032
		6	5	*E*	12583.1697	0.0127
		7	6	*E*	12583.2178	0.0153
$7_{0,7}$	$6_{0,6}$	6	5	*A*	12886.8372	-0.0055
		8	7	*A*	12886.8372	-0.0033
		7	6	*A*	12887.0319	-0.0040
$7_{0,7}$	$6_{0,6}$	6	5	*E*	12886.7734	0.0041
		8	7	*E*	12886.7734	0.0063
		7	6	*E*	12886.9672	0.0047
$7_{1,6}$	$6_{1,5}$	6	5	*A*	14141.4077	0.0049
		8	7	*A*	14141.4286	-0.0004
		7	6	*A*	14141.5369	0.0004
$7_{1,6}$	$6_{1,5}$	6	5	*E*	14141.2103	0.0011
		8	7	*E*	14141.2317	-0.0037
		7	6	*E*	14141.3411	-0.0018
$8_{1,8}$	$7_{1,7}$	8	7	*A*	14335.0789	-0.0127
$8_{0,8}$	$7_{0,7}$	9	8	*A*	14580.3192	-0.0038
		7	6	*A*	14580.3192	-0.0082
		8	7	*A*	14580.4900	-0.0054
$8_{0,8}$	$7_{0,7}$	9	8	*E*	14580.2603	0.0082
		7	6	*E*	14580.2603	0.0038
		8	7	*E*	14580.4305	0.0061
$9_{0,9}$	$8_{0,8}$	8	7	*A*	16262.1838	-0.0050
		10	9	*A*	16262.1838	-0.0116
		9	8	*A*	16262.3249	-0.0083
$9_{0,9}$	$8_{0,8}$	10	9	*E*	16262.1301	0.0098
		8	7	*E*	16262.1301	0.0033
		9	8	*E*	16262.2752	0.0105

Table S7.13. Observed rotational frequencies and residuals (all the values in MHz) for the $^{18}O_{w1}$ isotopologue species of the *syn*-mcb-w_2 complex for A and E substates $J'K'_{-1}K'_{+1}F' \leftarrow J''K''_{-1}K''_{+1}F''$ transitions using the Xiam program.

$J'K'_{-1}K'_{+1}$	$J''K''_{-1}K$	F'	F''	S	Obs.	Res.
$3_{1,3}$	$2_{1,2}$	4	3	*A*	5314.1813	-0.0035
		2	1	*A*	5314.3626	-0.0049
		3	2	*A*	5314.3626	-0.0080
$3_{1,3}$	$2_{1,2}$	4	3	*E*	5314.1923	-0.0020
		3	2	*E*	5314.3759	-0.0013
		2	1	*E*	5314.3759	-0.0041
$3_{0,3}$	$2_{0,2}$	4	3	*A*	5609.9800	-0.0024
		2	1	*A*	5610.0274	-0.0101
		3	2	*A*	5610.1248	-0.0027
$3_{0,3}$	$2_{0,2}$	4	3	*E*	5609.9265	-0.0006
		2	1	*E*	5609.9800	-0.0022
		3	2	*E*	5610.0719	-0.0003
$3_{1,2}$	$2_{1,1}$	2	1	*A*	6002.1301	-0.0077
		4	3	*A*	6002.3376	0.0000
		3	2	*A*	6002.4481	-0.0008
$3_{1,2}$	$2_{1,1}$	2	1	*E*	6002.0133	-0.0025
		4	3	*E*	6002.2135	-0.0020
		3	2	*E*	6002.3231	-0.0034
$4_{1,4}$	$3_{1,3}$	5	4	*A*	7070.0633	-0.0025
		4	3	*A*	7070.1759	-0.0052
$4_{1,4}$	$3_{1,3}$	5	4	*E*	7070.0463	0.0019
		4	3	*E*	7070.1595	-0.0002
$4_{0,4}$	$3_{0,3}$	5	4	*A*	7415.4752	-0.0029
		3	2	*A*	7415.4912	-0.0022
		4	3	*A*	7415.6539	-0.0033
$4_{0,4}$	$3_{0,3}$	5	4	*E*	7415.4119	-0.0005
		4	3	*E*	7415.5912	-0.0003
$4_{1,3}$	$3_{1,2}$	3	2	*A*	7984.8171	-0.0011
		5	4	*A*	7984.9003	0.0001
		4	3	*A*	7984.9762	-0.0004
$4_{1,3}$	$3_{1,2}$	3	2	*E*	7984.6881	-0.0026
		5	4	*E*	7984.7703	-0.0024
		4	3	*E*	7984.8466	-0.0025
$5_{1,5}$	$4_{1,4}$	6	5	*A*	8814.1886	0.0001
		4	3	*A*	8814.2540	0.0035
		5	4	*A*	8814.2801	-0.0008
$5_{1,5}$	$4_{1,4}$	6	5	*E*	8814.1524	-0.0003
		4	3	*E*	8814.2155	0.0008
		5	4	*E*	8814.2478	0.0027
$5_{0,5}$	$4_{0,4}$	4	3	*A*	9172.7794	-0.0033
		6	5	*A*	9172.7794	-0.0069
		5	4	*A*	9172.9812	-0.0039
$5_{0,5}$	$4_{0,4}$	6	5	*E*	9172.7144	0.0029
		4	3	*E*	9172.7144	-0.0008
		5	4	*E*	9172.9155	0.0015
$5_{1,4}$	$4_{1,3}$	4	3	*A*	9950.0646	0.0032
		6	5	*A*	9950.1119	0.0028
		5	4	*A*	9950.1895	0.0025
$5_{1,4}$	$4_{1,3}$	4	3	*E*	9949.9125	-0.0018
		6	5	*E*	9949.9617	-0.0003
		5	4	*E*	9950.0385	-0.0014
$6_{1,6}$	$5_{1,5}$	7	6	*A*	10545.4591	0.0006
		5	4	*A*	10545.4999	-0.0007
		6	5	*A*	10545.5422	0.0011
$6_{1,6}$	$5_{1,5}$	7	6	*E*	10545.4175	0.0034
		5	4	*E*	10545.4656	0.0095
		6	5	*E*	10545.5065	0.0099
$6_{0,6}$	$5_{0,5}$	7	6	*A*	10882.4847	-0.0048
		5	4	*A*	10882.4847	-0.0060
		6	5	*A*	10882.6941	-0.0039
$6_{0,6}$	$5_{0,5}$	7	6	*E*	10882.4221	0.0050
		5	4	*E*	10882.4221	0.0039
		6	5	*E*	10882.6302	0.0046
$6_{1,5}$	$5_{1,4}$	5	4	*A*	11891.4647	0.0072
		7	6	*A*	11891.4975	0.0065
		6	5	*A*	11891.5884	0.0058
$6_{1,5}$	$5_{1,4}$	5	4	*E*	11891.2899	0.0009
		7	6	*E*	11891.3217	-0.0008
		6	5	*E*	11891.4166	0.0025

Table S7.14. Observed rotational frequencies and residuals (all the values in MHz) for the $^{18}O_{w2}$ isotopologue species of the *syn*-mcb-w_2 complex for A and E substates $J'K'_{-1}K'_{+1}F' \leftarrow J''K''_{-1}K''_{+1}F''$ transitions using the Xiam program.

$J'K'_{-1}K'_{+1}$	$J''K''_{-1}K$	F'	F''	S	Obs.	Res.
$3_{1,3}$	$2_{1,2}$	4	3	*A*	5281.1727	-0.0037
		3	2	*A*	5281.3559	-0.0017
		2	1	*A*	5281.3559	-0.0069
$3_{1,3}$	$2_{1,2}$	4	3	*E*	5281.1951	0.0000
		3	2	*E*	5281.3782	0.0018
		2	1	*E*	5281.3782	-0.0031
$3_{0,3}$	$2_{0,2}$	4	3	*A*	5569.3065	-0.0027
		2	1	*A*	5569.3618	-0.0042
		3	2	*A*	5569.4429	-0.0035
$3_{0,3}$	$2_{0,2}$	4	3	*E*	5569.2571	-0.0016
		2	1	*E*	5569.3168	0.0013
		3	2	*E*	5569.3962	0.0003
$3_{1,2}$	$2_{1,1}$	2	1	*A*	5944.4488	0.0015
		4	3	*A*	5944.6474	0.0009
		3	2	*A*	5944.7569	0.0010
$3_{1,2}$	$2_{1,1}$	2	1	*E*	5944.3282	0.0006
		4	3	*E*	5944.5259	-0.0007
		3	2	*E*	5944.6343	-0.0015
$4_{1,4}$	$3_{1,3}$	5	4	*A*	7027.5024	-0.0013
		3	2	*A*	7027.5919	-0.0124
		4	3	*A*	7027.6157	-0.0011
$4_{1,4}$	$3_{1,3}$	5	4	*E*	7027.4902	0.0019
		4	3	*E*	7027.6036	0.0022
$4_{0,4}$	$3_{0,3}$	5	4	*A*	7367.2451	-0.0023
		3	2	*A*	7367.2645	0.0006
		4	3	*A*	7367.4140	-0.0030
$4_{0,4}$	$3_{0,3}$	5	4	*E*	7367.1884	0.0019
		3	2	*E*	7367.2007	-0.0022
		4	3	*E*	7367.3537	-0.0023
$4_{1,3}$	$3_{1,2}$	3	2	*A*	7909.7592	0.0023
		5	4	*A*	7909.8396	0.0014
		4	3	*A*	7909.9135	0.0020
$4_{1,3}$	$3_{1,2}$	3	2	*E*	7909.6369	-0.0013
		5	4	*E*	7909.7175	-0.0020
		4	3	*E*	7909.7900	-0.0027
$5_{1,5}$	$4_{1,4}$	6	5	*A*	8763.0705	-0.0022
		4	3	*A*	8763.1340	-0.0010
		5	4	*A*	8763.1601	-0.0025
$5_{1,5}$	$4_{1,4}$	6	5	*E*	8763.0456	0.0037
		4	3	*E*	8763.1100	0.0058
		5	4	*E*	8763.1340	0.0022
$5_{0,5}$	$4_{0,4}$	6	5	*A*	9120.7514	0.0010
		4	3	*A*	9120.7514	-0.0032
		5	4	*A*	9120.9405	-0.0033
$5_{0,5}$	$4_{0,4}$	6	5	*E*	9120.6875	0.0043
		4	3	*E*	9120.6875	0.0001
		5	4	*E*	9120.8770	0.0004
$5_{1,4}$	$4_{1,3}$	4	3	*A*	9859.4930	-0.0003
		6	5	*A*	9859.5426	0.0023
		5	4	*A*	9859.6162	0.0026
$5_{1,4}$	$4_{1,3}$	4	3	*E*	9859.3534	-0.0052
		6	5	*E*	9859.4046	-0.0010
		5	4	*E*	9859.4770	-0.0018
$6_{1,6}$	$5_{1,5}$	7	6	*A*	10486.7703	-0.0026
		5	4	*A*	10486.8105	-0.0046
		6	5	*A*	10486.8513	-0.0017
$6_{1,6}$	$5_{1,5}$	7	6	*E*	10486.7392	0.0062
		5	4	*E*	10486.7826	0.0074
		6	5	*E*	10486.8232	0.0101
$6_{0,6}$	$5_{0,5}$	7	6	*A*	10829.1403	-0.0127
		5	4	*A*	10829.1403	-0.0138
		6	5	*A*	10829.3447	-0.0104
$6_{0,6}$	$5_{0,5}$	7	6	*E*	10829.0971	0.0139
		5	4	*E*	10829.0971	0.0128
		6	5	*E*	10829.2945	0.0092
$6_{1,5}$	$5_{1,4}$	5	4	*A*	11788.0434	0.0085
		7	6	*A*	11788.0736	0.0059
		6	5	*A*	11788.1569	0.0040
$6_{1,5}$	$5_{1,4}$	5	4	*E*	11787.8778	-0.0030
		7	6	*E*	11787.9103	-0.0033
		6	5	*E*	11787.9947	-0.0041

Chapter VIII

Microsolvation of Ethyl Carbamate Conformers: Effect of Carrier Gas on the Formation of Complexes.

Manuscript in preparation.

Abstract

Microsolvated complexes of ethyl carbamate with up to three water molecules formed in a supersonic expansion have been characterized by high-resolution microwave spectroscopy. Both chirped-pulse and cavity Fourier transform microwave spectrometers covering the 2-13 GHz frequency range have been used. Ethyl carbamate presents in the gas an equilibrium between the two most stable conformers. The observation of these structures and their microsolvated complexes depends on the carrier gas used in the supersonic expansion due to collisional relaxation. Using argon, only the most stable conformer and its complexes with water are observed, while with neon, both forms and their corresponding water complexes are observed. The structures of the complexes have been characterized and show water molecules closing sequential cycles through hydrogen bonding with the amide group. Complexation of ethyl carbamate with water molecules seems apparently not to alter substantially the potential energy function for the interconversion between the two conformations of ethyl carbamate.

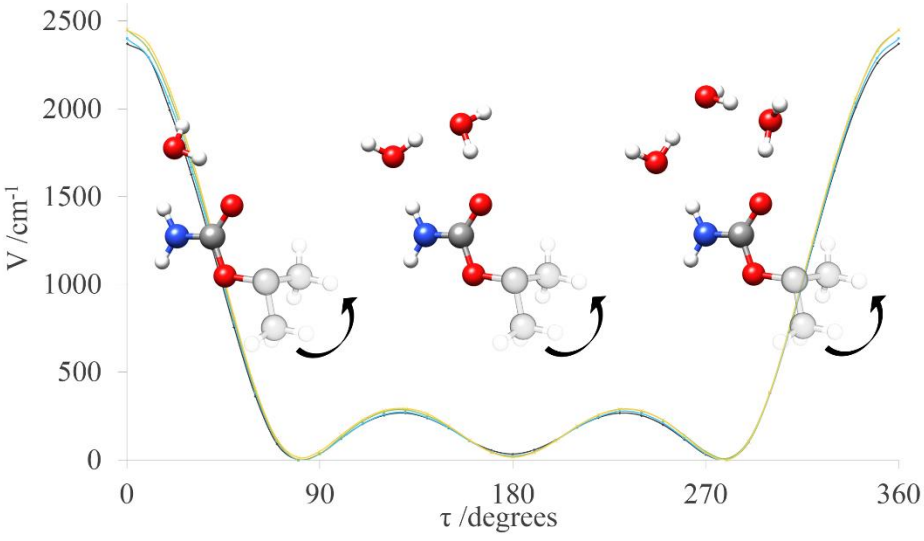

8.1 Introduction

The carbamate group (-NCO_2-) is recurrent in many biologically active molecules with pharmacological applications.[1,2] The carbamate group can be considered as an ester-derivative of an amide, and therefore it offers some of the functionalities of the peptide bond. In consequence, the molecules presenting this group are used as peptide bond substitutes in medicinal chemistry.[2] One of the roles in which this functionality becomes important is in the possible modulation of inter- and intra-molecular interactions with enzymes or molecular receptors. Carbamates may act as hydrogen bond donor or as hydrogen bond acceptor through the N-H or the C=O groups, respectively. This double character, allows carbamates to form sequential cycles with other molecules having the same donor/acceptor character, as for example water molecules. The carbamate group has also wide applications in industry,[3] for example ethyl carbamate or urethane, has special importance for industry in the polyurethane polymer synthesis.[4]

The structure of the ethyl carbamate monomer has been already studied by different experimental techniques as X-ray crystallography,[5] IR spectroscopy in solid state and in solution,[6] or microwave spectroscopy in the gas phase both at room temperature[7] and in supersonic expansion.[8] The studies in gas phase confirmed the existence of two stable conformations very close in energy, in good agreement with the computational predictions. In one of them the heavy atom backbone is planar, in the second one, the carbamate and the ethyl groups form an angle of approximately 80 degrees (see Figure 8.1). However, it was challenging to determine unambiguously which of the two forms is the most stable. Experimental investigations have concluded that the planar rotamer (ethyl carbamate I), is the most stable, based on different experimental evidences, such as the missing of the II form in the crystalline state and in supersonic expansion using Ar as carrier gas.[5,7,8] The effect of carrier gas on relaxation in supersonic jets has been widely studied.[9,10] The heavier carrier gasses are more efficient in relaxation processes through low barriers, as in this case; using Ne both conformations can be observed, while using Ar the conformer II relaxes into the form I.

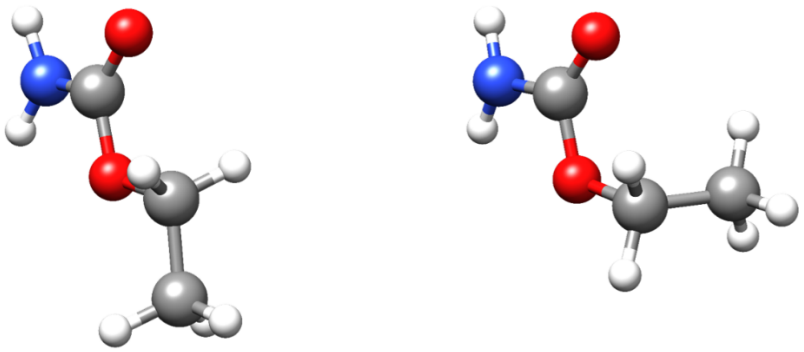

Figure 8.1. Experimentally observed conformations I and II for ethyl carbamate monomer.

In this work, we aimed to characterize at a molecular level the interaction of water with the peptide bond through the formation of hydrogen bonds as shown in precedent chapters. Other examples of the study of microsolvation complexes of model molecules at different degrees of hydration can be found in the literature.[11-17] High-resolution microwave spectroscopy combined with supersonic expansion is the most appropriate experimental technique to generate and characterize with high accuracy the structure and properties of those complexes.

Microsolvation of methyl carbamate, has already been studied using this techniques,[18] giving relevant information about the interactions established between the carbamate group with water molecules, and their effects on the structure. Microsolvated complexes of ethyl carbamate can be considered as an extension of the work on methyl carbamate and on amide-type molecules such as formamide[11,13,15,16] and formanilide,[17] contributing with relevant information about the interactions of water with a substituted *cis*-peptide linkage, and how water affects their structure in the first steps of solvation.

In this work, we have studied the complexes of both forms of ethyl carbamate trying to analyze the possible influence of solvation on the equilibrium conformations of this molecule. We have studied the relaxation processes in the supersonic expansion of the species observed and their possible relation not only with the monomer dynamics, but also with the hydration degree.

8.2 Experimental and theoretical methods

The initial study of the microsolvated complexes of ethyl carbamate was carried out in the chirped-pulse Fourier transform spectrometer (CP-FTMW)[19,20] from the University of Valladolid. Ethyl carbamate is a white crystalline solid, commercially available, with melting point of *ca*. 57 ºC that was held in a stainless steel heatable pulsed nozzle and heated to about 80 ºC. Either Ar or Ne were used as carrier gas with backing pressures close to 2 bar. Temperature and pressure were optimized to ensure maximum signal. The vapor from the sample was mixed with the carrier gas, previously seeded with water. The supersonic jet was generated by the expansion of the gas mixture through a small diameter (0.8 mm) nozzle into the high-vacuum chamber. The spectrum of ethyl carbamate was recorded from 2 to 8 GHz, using a chirped pulse of *ca*. 5 μs for the polarization of the sample. Since the sample injection is perpendicular to the molecular polarization and emission axis, the transitions do not present splittings due to Doppler effect. The frequency measurement accuracy is better than 10 kHz.

Measurements in the 5-12 GHz frequency region were done in the narrow band molecular beam Fourier transform microwave spectrometer (MB-FTMW) in Valladolid.[21] Ethyl carbamate was supported in a small diameter (0.9 mm) stainless steel heating pulsed nozzle,[22] and heated to *ca*. 90 ºC, using Ar as carrier gas at backing pressures of about 2 bars. A short microwave pulse of *ca*. 2 μs at a discrete frequency is emitted, inducing the polarization of the sample in a narrow band of *ca*. 2 MHz. The sample injection is coaxial to the radiation emission-detection, therefore, the observed transitions present Doppler splitting. The transition frequency was calculated as the arithmetic mean of both signals resulting in an accuracy of frequency measurement better than 3 kHz. The higher resolution power of this instrument allowed to fully resolve the hyperfine structure due to the nuclear quadrupole coupling and to determine precisely the diagonal elements of the quadrupole coupling tensor.

No isotopologues in natural abundance were observed for any of the complexes. The microwave spectra of some complexes monoisotopically substituted with ^{18}O in the water subunits were registered in the cavity spectrometer using a mixture of isotopically enriched $H_2{}^{18}O$ (99%) with water in different proportions. Selected transitions were measured to determine the rotational constants for the isotopic species.

Ab initio calculations[23] were performed to study the preferred sites of interaction for both ethyl carbamate I and II conformations with water. Different structures were tested for the 1:1, 1:2 and 1:3 complexes (see Figures S8.1 and S8.2 in supplementary material) based on the

complexes previously reported for the microsolvation system of formamide,[11,13,15,16] formanilide,[17] or methyl carbamate,[18] similar in structure to ethyl carbamate. The geometries for the complexes were optimized using the functional B3LYP[24] combined with Grimme´s empirical dispersion correction (GD3)[25] and Pople´s basis set 6-311++G(d,p).[26] Frequencies using vibrational harmonic terms were also calculated to confirm that the geometries optimized are true minima. The energy values were improved by using the zero point energy (ZPE) correction.[8] Additionally, calculations for the dissociation energies of the complexes were carried out using the Basis Set Superposition Error approximation.[27] On the basis of the rotational constants, dipole moment components and nuclear quadrupole coupling constants, the microwave spectra for the different stable complexes were simulated. All the predicted parameters are collected in Tables S8.1 and S8.2. Calculations for the potential energy function for the interconversion between the rotamers I and II through ethyl carbamate or water movements were also done to help to understand the effect of the carrier gas on the relaxation and complexation.

8.3 Results and discussion

8.3.1 Ethyl carbamate I···$(H_2O)_n$ n = 1, 2 and 3 complexes

The microsolvated complexes of the ethyl carbamate I conformer with up to three water molecules were easily observed in the chirped-pulse spectrum using Ar as carrier gas. The rotational constants were initially derived from this spectrum. Refined measurements in the MB-FTMW cavity allowed accurate determination of the rotational, quartic centrifugal distortion and nuclear quadrupole coupling constants. A search for the next monohydrated complexes of ethyl carbamate I form (see Figure S8.1), was carried out, however those complexes were not detected in these conditions.

8.3.1.1 Ethyl carbamate I···(H_2O)

The lines corresponding to the ethyl carbamate I···(H_2O) (ecb-I-w-a) complex are very intense and show the hyperfine structure (hfs) arising from nuclear quadrupole coupling due to ^{14}N (I=1). No splittings attributable to water motions or large amplitude motions from ethyl carbamate, as internal rotation or inversion, were observed. In the MB-FTMW spectrometer μ_a-type R-branch, together with μ_b-type R-branch and Q-branch transitions with J up to 8 and K_{-1} up to 2 were measured. A semirigid rotor Hamiltonian in the asymmetric reduction and in the I^r representation,[28,29] including a term for the nuclear quadrupole coupling was used to analyze of the spectrum of this complex.[30] From the experimental frequencies it was possible to determine the rotational constants, the quartic centrifugal distortion constants Δ_J, Δ_{JK}, and δ_J, and the diagonal elements of the nuclear quadrupole coupling tensor (see Table 8.1). For the $H_2{}^{18}O$ isotopologue, the rotational constants were fitted by keeping the quartic centrifugal distortion and the nuclear quadrupole coupling constants fixed to the parent species values. The rotational parameters obtained reproduce accurately the observed spectrum with a low rms deviation for both the parent and the $^{18}O_w$ isotopologue (see Table 8.1). The complete list of transitions observed is collected in Tables S8.13-S8.14.

Table 8.1. Observed rotational parameters obtained for the ecb-I-w-a complex for the parent and the $^{18}O_w$ isotopologue compared to *ab initio* (B3LYP-D3/6-311++G(d,p)) values.

Fitted Parameters[a]	ecb-I-w-a	ecb-I-w-a $^{18}O_w$	*ab initio*
A /MHz	7659.94791(44)[b]	7632.97(37)	7689.84
B /MHz	1034.10646(11)	986.93854(11)	1031.44
C /MHz	923.276293(93)	885.14275(12)	921.95
Δ_J /kHz	0.1124(13)	[0.1124][c]	0.098
Δ_{JK} /kHz	0.088(13)	[0.088]	-0.193
Δ_K /kHz	[0.]	[0.]	22.061
δ_J /kHz	0.01594(58)	[0.01594]	0.011
δ_K /kHz	[0.]	[0.]	0.321
^{14}N 3/2(χ_{aa}) /MHz	2.4588(18)	[2.4588]	2.72
^{14}N ¼(χ_{bb}-χ_{cc}) /MHz	1.60147(59)	[1.60147]	1.81
N	138/37	25/9	
σ /kHz	2.4	1.6	
Derived Parameters			
P_a /uÅ^2	485.05484(52)	508.4074(32)	486.21
P_b /uÅ^2	62.32085(52)	62.5501(32)	61.96
P_c /uÅ^2	3.65596(52)	3.6598(32)	3.76

[a] A, B and C are the rotational constants. Δ_J, Δ_{JK}, Δ_K, δ_J and δ_K are the quartic centrifugal distortion constants. χ_{aa}, χ_{bb} and χ_{cc} are the quadrupole coupling tensor diagonal elements for ^{14}N atom. N is the number of quadrupole hyperfine components/rotational transitions fitted. σ is the rms deviation of the fit. P_α (α = a, b or c) are the planar moments of inertia; these are derived from the moments of inertia I_α as for example $P_c = (I_a+I_b-I_c)/2$. [b] Standard errors are given in parentheses in units of the last digits. [c] Parameters in square brackets were kept fixed to those given for the parent species in the fit.

As indicated by the close values between predicted and determined rotational parameters, the *ab initio* geometry can be considered, to a good extent, as a reliable description of the structure of the ecb-I-w-a complex. The interactions established in this complex seems to be of the same nature as those reported before for monohydrated complexes of related molecules such as formamide,[11,13] N-methylformamide,[14] formanilide[17] or methyl carbamate.[18] The water molecule interacts with the amide group of ethyl carbamate and closes a cycle through ecb–C_1=O_1···H_{w1}–O_w···H_1–N–ecb hydrogen bond network, acting both molecules as hydrogen donor and hydrogen acceptor simultaneously (see Figure 8.2). There is a slightly increment in the experimental value of P_c from the monomer (3.3321093 uÅ^2)[8] to the ecb-I-w-a complex (3.65596(52) uÅ^2), indicating an almost planarity of the complex skeleton. The water oxygen atom is in the *ab* plane, as indicated by the almost non-changing P_c value obtained for $^{18}O_w$ isotopologue (3.6598(32) uÅ^2). The value of P_c in the monohydrated complex may include contributions from the out-of-plane hydrogen atoms of the ethyl group, from the hydrogen atom in the water molecule not involved in hydrogen bonding (see Table 8.1), and from vibrational contributions.

An approach to the molecular structure of the ecb-I-w-a complex can be obtained by a least-squares fit of some bond distances and angles to the observed rotational constants for all the available isotopologues species.[31] This effective structure, r_0, reproduces the rotational constants in the ground state.[32] The results obtained by this method are shown in Figure 8.2, where they are compared with the r_e predicted structure. With the experimental values of the rotational constants obtained from the $^{18}O_w$ isotopologue, the *a*, *b* and *c* coordinates in the principal axis system of the parent molecule could be derived using Kraitchman equations.[33] The Kraitchman method gives absolute values for the coordinates, and therefore, the sign must be assigned based on the r_e or the r_0 structure values. The values obtained for the r_s coordinates are resumed in Figure 8.2 together with the r_e or the r_0 coordinates in which it is possible to see the good agreement between them, corroborating the determined structure. The uncertainties in the coordinates were quoted by the Costain rule.[34]

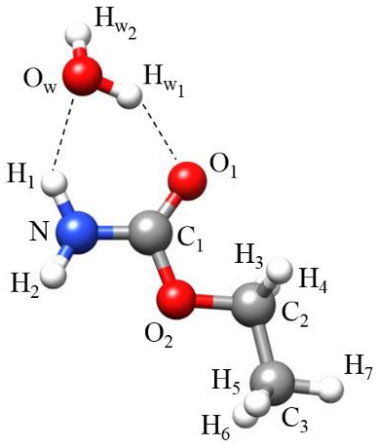

Fitted parameter	r_0	r_e
$r(O_w\cdots H_1)$ /Å	2.0958(6)	2.079
$r(H_{w1}\cdots O_1)$ /Å	1.83(1)	1.913
$\angle(O_w\cdots H_1–N)$ /°	137.66(3)	138.2
$\angle(H_{w1}\cdots O_1–C_1–N)$ /°	-181.5(1)	-175.2
Derived parameter	r_0	r_e
$r(O_w–H_{w1})$ /Å	1.02(1)	0.975
$\angle(O_1–C_1–N)$ /°	125.100(8)	125.1
$\angle(H_1\cdots O_w–H_{w1})$ /°	80.3(4)	81.5
$\angle(O_w–H_{w1}\cdots O_1)$ /°	148.4(4)	148.5

	atom	*a*	*b*	*c*
$\lvert r_s\rvert$ /Å		|3.44428(45)|	|0.3507(44)|	|0.046(34) |
r_0 /Å	O_w	3.4436(9)	-0.3657(7)	-0.0315(3)
r_e /Å		3.44	-0.35	-0.11

Figure 8.2. The ecb-I-w-a complex showing atom labeling with the r_0 structure derived parameters, the r_s structure coordinates and comparison with r_e structure.

8.3.1.2 Ethyl carbamate I···$(H_2O)_2$

Once the lines assigned to the monohydrated complex with the I form of ethyl carbamate were removed from the spectrum, transitions showing the characteristic R-branch μ_a-type pattern were detected and assigned to the ethyl carbamate I···$(H_2O)_2$ complex (ecb-I-w_2). Transitions with *J* up to 10 and K_{-1} up to 3 were measured. As in the monohydrated complex, the lines show the hfs arising from nuclear quadrupole coupling due to the ^{14}N nucleus. A semirigid rotor Hamiltonian similar to that used for the ecb-I-w-a complex was employed to fit the lines observed for ecb-I-w_2. From the experimental dataset, it was possible to determine the rotational constants, the quartic centrifugal distortion constants Δ_J, Δ_{JK}, δ_J and δ_K, and the diagonal elements of the nuclear quadrupole coupling tensor. Both isotopologues with ^{18}O substitution in the water subunits were observed, as shown in Table 8.2. The fitting of their rotational constants were achieved by keeping the quartic centrifugal and the nuclear quadrupole coupling constants fixed to the parent species (see Table 8.2). The complete list of transitions observed is collected in Tables S8.15-S8.17.

Table 8.2. Observed rotational parameters obtained for the ecb-I-w_2 complex for the parent, the $^{18}O_{w1}$ and the $^{18}O_{w2}$ isotopologues compared to *ab initio* (B3LYP-D3/6-311++G(d,p)) values.

Fitted Parameters[a]	ecb-I-w_2	ecb-I-w_2 $^{18}O_{w1}$	ecb-I-w_2 $^{18}O_{w2}$	*ab initio*
A /MHz	3734.1586(72)[b]	3599.386(31)	3675.093(47)	3793.57
B /MHz	701.90967(10)	686.889435(79)	680.60559(11)	704.09
C /MHz	597.04077(10)	582.706572(84)	580.11263(11)	599.88
Δ_J /kHz	0.05569(31)	[0.05569]c	[0.05569]	0.042
Δ_{JK} /kHz	0.2351(29)	[0.2351]	[0.2351]	0.161
Δ_K /kHz	[0.]	[0.]	[0.]	4.566
δ_J /kHz	0.01043(24)	[0.01043]	[0.01043]	0.007
δ_K /kHz	0.291(33)	[0.291]	[0.291]	0.264
^{14}N 3/2(χ_{aa}) /MHz	2.0278(58)	[2.0278]	[2.0278]	2.18
^{14}N ¼(χ_{bb}-χ_{cc}) /MHz	1.5582(57)	[1.5582]	[1.5582]	1.76
N	153/53	25/9	25/9	
σ /kHz	1.4	1.5	2.1	
Derived Parameters				
P_a /uÅ^2	715.56974(31)	731.3195(23)	738.1010(18)	713.51
P_b /uÅ^2	130.90344(31)	135.9763(23)	133.0728(18)	128.96
P_c /uÅ^2	4.43601(31)	4.4306(23)	4.4417(18)	4.26

[a] A, B and C are the rotational constants. Δ_J, Δ_{JK}, Δ_K, δ_J and δ_K are the quartic centrifugal distortion constants. χ_{aa}, χ_{bb} and χ_{cc} are the quadrupole coupling tensor diagonal elements for ^{14}N atom. N is the number of quadrupole hyperfine components/rotational transitions fitted. σ is the rms deviation of the fit. P_α (α = a, b or c) are the planar moments of inertia; these are derived from the moments of inertia I_α as for example P_c = (I_a+I_b-I_c)/2. [b] Standard errors are given in parentheses in units of the last digits. [c] Parameters in square brackets were kept fixed to those given for the parent species in the fit.

As for the monohydrated complex, the reasonable good agreement between experimental and *ab initio* parameters, suggests that the predicted geometry can be considered as a good description of the ecb-I-w_2 structure. In this complex, the two molecules of water close a sequential cycle with the amide group of ethyl carbamate through ecb–C_1=O_1···H_{w1}–O_{w1}···H_{w3}–O_{w2}···H_1–N–ecb hydrogen bond network (see Figure 8.3), acting the three molecules simultaneously as hydrogen donor and hydrogen acceptor. The increment in the P_c value from the monomer (3.3321093 uÅ^2)8 to the ecb-I-w-a (3.65596(52) uÅ^2) to the ecb-I-w_2 complex (4.43601(31) uÅ^2) can be mainly attributable to the out-of-plane contribution from the hydrogen atoms in the water molecules not involved in hydrogen bonding and vibrational contribution. The experimental P_c values for both observed isotopologues, (4.4306(23) uÅ^2 and 4.4417(18) uÅ^2 for $^{18}O_{w1}$ and $^{18}O_{w2}$ respectively) very similar to the parent species value, indicate that each oxygen nuclei from both water molecules is located in the plane defined by the heavy atoms of ethyl carbamate, being the complex skeleton almost planar.

From the fitting of the experimental rotational constants for the three observed species, a partial r_0 structure was derived to characterize the hydrogen bond network. The r_0 structure parameters are shown in Figure 8.3 showing a good agreement with the *ab initio* r_e values. The r_s coordinates of the water oxygen nuclei were obtained by the application of Kraitchman equations for both monoisotopologues. The coordinates obtained from this method are compared with the r_0 and r_e values in Figure 8.3, where it is possible to see the good agreement between them, which confirms the proposed structure.

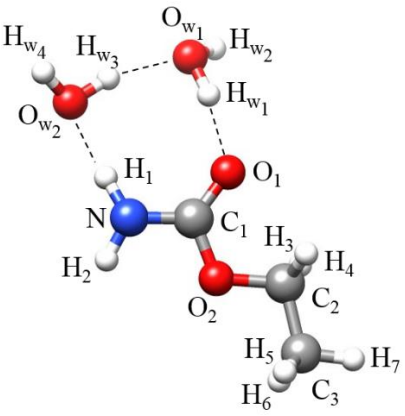

Fitted parameter	r_0	r_e
$r(O_{w2}\cdots H_1)$ /Å	1.887(7)	1.876
$r(H_{w1}\cdots O_1)$ /Å	1.793(1)	1.767
$\angle(O_{w2}\cdots H_1\text{–}N)$ /°	175.0(6)	174.1
$\angle(H_{w1}\cdots O_1\text{–}C_1)$ /°	129.5(3)	129.4
$\angle(H_{w1}\cdots O_1\text{–}C_1\text{–}O_2)$ /°	175.2(2)	176.5
Derived parameter	r_0	r_e
$r(H_{w3}\cdots O_{w1})$ /Å	1.836(5)	1.775
$r(O_{w2}\cdots O_{w1})$ /Å	2.763(5)	2.722
$\angle(O_{w2}\text{–}H_{w3}\cdots O_{w1})$ /°	160.3(5)	161.0
$\angle(H_{w3}\cdots O_{w1}\text{–}H_{w1})$ /°	98.6(2)	98.9

	atom	*a*	*b*	*c*
$\lvert r_s\rvert$ /Å		|2.81334(54)|	|-1.62512(94)|	|0.05381i|
r_0 /Å	O_{w1}	2.813(1)	-1.6316(3)	0.024(2)
r_e /Å		2.82	-1.61	0.00
$\lvert r_s\rvert$ /Å		|3.37335(45)|	|1.0686(14)|	|-0.056(27)|
r_0 /Å	O_{w2}	3.374(1)	1.076(5)	0.016(1)
r_e /Å		3.36	1.06	0.05

r_s /Å		2.7519(18)
r_0 /Å	O_{w1}-O_{w2}	2.763(5)
r_e /Å		2.722

Figure 8.3. The ecb-I-w$_2$ complex showing atom labeling with the r_0 structure derived parameters, the r_s structure coordinates and comparison with r_e structure.

8.3.1.3 Ethyl carbamate I···(H$_2$O)$_3$

Once removed the lines already assigned to other species, there were some weak transitions showing the characteristic R-branch μ_a-type pattern. Those lines were assigned to the ethyl carbamate I···(H$_2$O)$_3$ complex (ecb-I-w$_3$). Transitions with J up to 11 and K_{-1} up to 2 were measured. As in the monohydrated and dihydrated complexes, the lines show the hfs arising from nuclear quadrupole coupling due to the ^{14}N nucleus. In addition the lines corresponding to the ecb-I-w$_3$ show doublets separated about 0.18 - 0.2 MHz (see Figure 8.4), attributable to rotational transitions in two close vibrational states. Similar doublets were observed for the formamide···(H$_2$O)$_3$ complex.[16] As in that case the doublets may arise from a motion in the water subunits connecting two equivalent forms. It can be assumed that a path similar to that described for the formamide···(H$_2$O)$_3$ complex could be at the origin of the doublets observed in

ecb-I-w_3. The path proposed involves a coordinate water movement in which the consecutive flipping motions of one water molecule at a time pass through reasonable low hindering barriers.[16]

The lines were fitted using a semirigid rotor Hamiltonian in the asymmetric reduction and in the I^r representation. From the experimental set of transitions available, the rotational constants could be determined for each torsional state. The quartic centrifugal distortion constants Δ_J, Δ_{JK}, and δ_J, and the diagonal elements of the nuclear quadrupole coupling tensor were determined simultaneously for both states (see Table 8.3). No isotopologues were detected for the complex ecb-I-w_3, therefore the molecular structure could not be further investigated. The complete list of transitions observed is collected in Table S8.18.

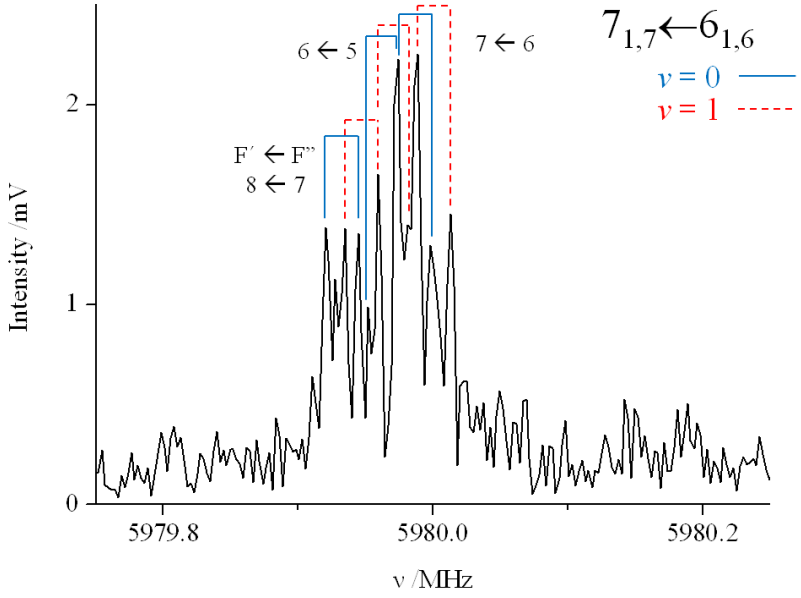

Figure 8.4. The $7_{1,7}\leftarrow 6_{1,6}$ rotational transition for the ecb-I-w_3 complex with the hyperfine structure arising from the quadrupole coupling interaction (F´←F´´ transitions). The small splittings of *ca*. 0.2 MHz correspond to the rotational transitions in the v = 0 (lower ν, blue) and v = 1 (higher ν, red) torsional states due to tunneling between two equivalent configurations. Each transition appears as a doublet due to Doppler effect.

The good agreement between observed and predicted values for the rotational parameters indicate that the structure of the complex is well reproduced by *ab initio* calculations. The hydrogen bond network established in ecb-w_3 is similar to that found in the f-w_3 complex,[16] being the disposition of water molecules almost identical for the lowest conformation (see Figure 8.5). The water molecules act as a bridge between the amine and the carbonyl ends of ethyl carbamate and close a sequential cycle through ecb–C_1=O_1···H_{w1}–O_{w1}···H_{w3}–O_{w2}···H_{w5}–O_{w3}···H_1–N–ecb hydrogen bonds (see Figure 8.5). The four molecules act simultaneously as hydrogen donor and hydrogen acceptor. The experimental P_c value (14.84648(69) uÅ^2 for the v = 0) (see Table 8.3) indicates that the molecules of water are slightly out of the plane defined by ethyl carbamate I, as shown in Figure 8.5.

No more lines were detected in the spectrum, which evidences the non-presence of other complexes.

Table 8.3. Observed rotational parameters obtained for the ecb-I-w_3 complex compared to *ab initio* (B3LYP-D3/6-311++G(d,p)) values.

Fitted Parameters[a]	ecb-I-w_3		*ab initio*
	$v = 0$	$v = 1$	
A /MHz	2254.4370(61)[b]	2254.4248(61)	2260.09
B /MHz	486.842445(98)	486.843300(98)	493.14
C /MHz	410.026213(87)	410.027428(87)	413.03
Δ_J /kHz	0.08650(18)		0.062
Δ_{JK} /kHz	-1.104(10)		-0.595
Δ_K /kHz	[0.]		6.594
δ_J /kHz	0.01445(21)		0.010
δ_K /kHz	[0.]		0.217
^{14}N 3/2(χ_{aa}) /MHz	1.734(36)		1.79
^{14}N ¼(χ_{bb}-χ_{cc}) /MHz	1.4378(63)		1.38
N	180/30/30		
σ /kHz	2.0		
Derived Parameters	$v = 0$	$v = 1$	
P_a /uÅ^2	1023.22858(69)	1023.22523(69)	1012.40
P_b /uÅ^2	209.32433(69)	209.32402(69)	211.19
P_c /uÅ^2	14.84648(69)	14.84801(69)	12.42

[a] A, B and C are the rotational constants. Δ_J, Δ_{JK}, Δ_K, δ_J and δ_K are the quartic centrifugal distortion constants. χ_{aa}, χ_{bb} and χ_{cc} are the quadrupole coupling tensor diagonal elements for ^{14}N atom. N is the number of quadrupole hyperfine components/rotational transitions fitted for the 0 and 1 states. σ is the rms deviation of the fit. P_α ($\alpha = a$, b or c) are the planar moments of inertia; these are derived from the moments of inertia I_α as for example $P_c = (I_a+I_b-I_c)/2$. [b] Standard errors are given in parentheses in units of the last digits.

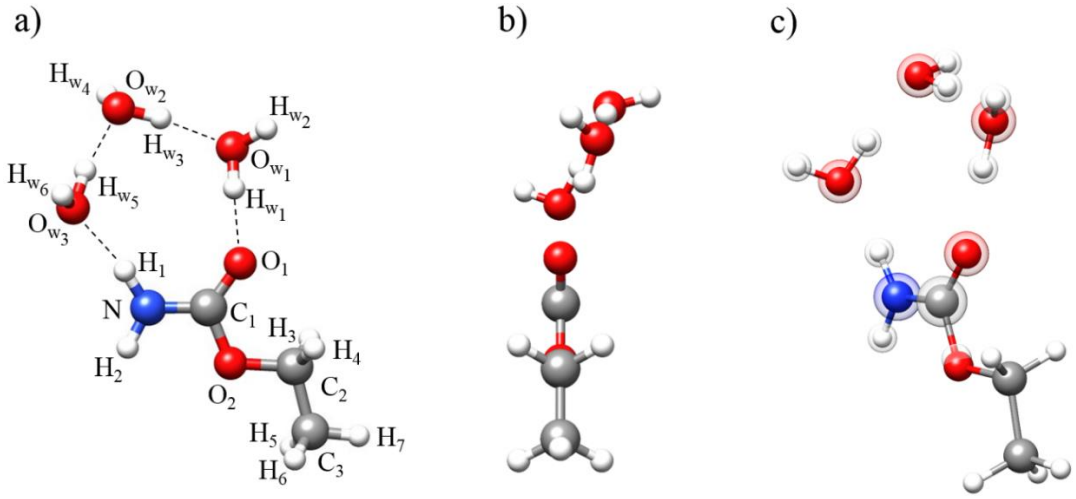

Figure 8.5. The ecb-I-w_3 complex a) with atom labeling b) in a side view showing the out of plane disposition for the water molecules c) The outer semi-transparent spheres depict the positions for the f-w_3 atoms.

8.3.2 Ethyl carbamate II···$(H_2O)_n$ n = 1, 2 and 3 complexes

In the CP-FTMW spectrum registered using Ne as carrier gas the microsolvated complexes with up to three water molecules of both I and II forms of ethyl carbamate could be observed. It is possible to compare qualitatively the intensity for the same rotational transition for the complexes with one, two or three molecules of water with both forms of ethyl carbamate (see Figure 8.6). As shown in Figure 8.6, the intensities are slightly lower for the complexes in ethyl carbamate II, but are of the same order of magnitude. It is possible to estimate populations in the supersonic jet from the intensities in the chirped-pulse spectrometer, assuming those intensities are proportional to $N_i \cdot \mu_{i,\alpha}^2$, being N_i the number density of the species I in the supersonic jet and $\mu_{i,\alpha}$ the electric dipole moment component allowing for the transition. Since the dipole moment component in the case of the transitions shown in Figure 8.6 (μ_a) is predicted to be slightly larger for the complexes with the I form (see Tables S8.1 and S8.2), the population of the complexes of both forms can be estimated to be almost equal, in good agreement with previous studies[7,8] and with the energies predicted.

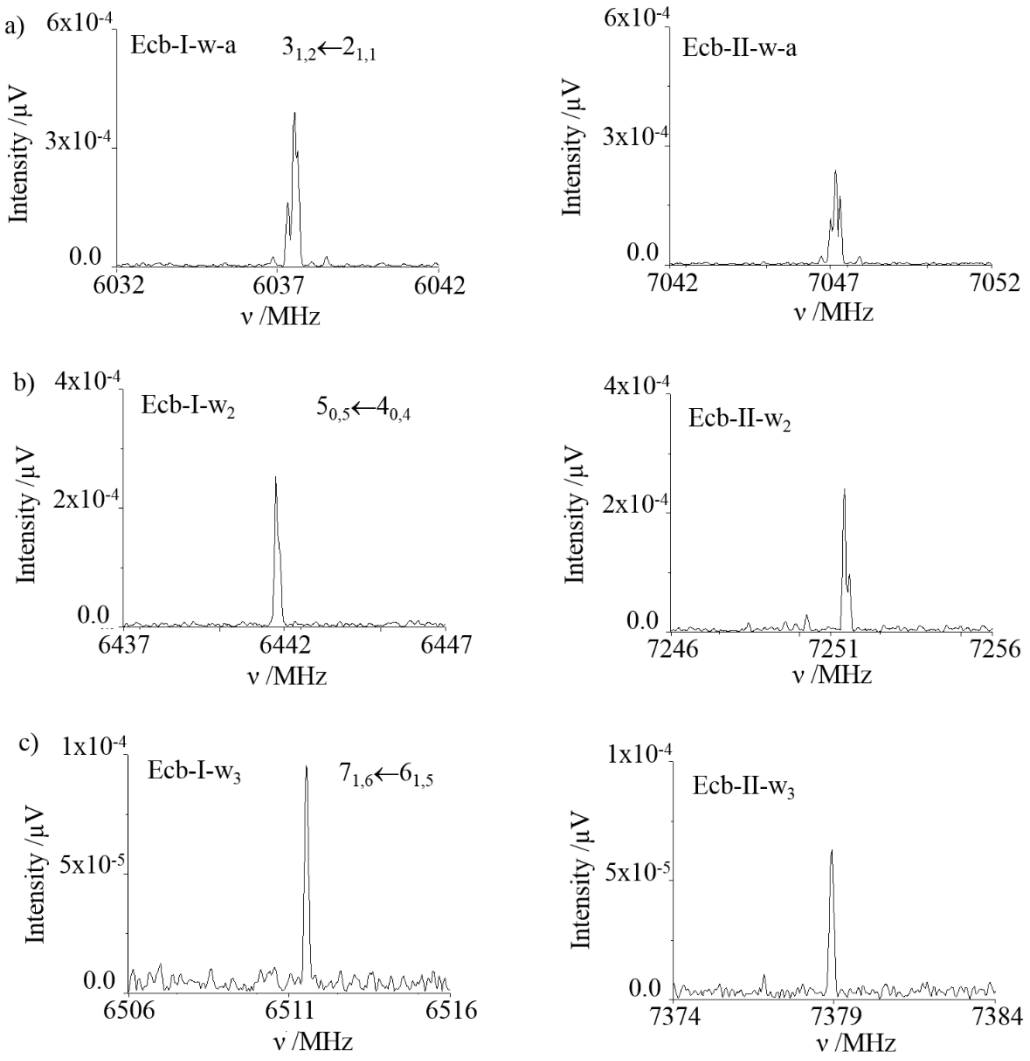

Figure 8.6. a) The $3_{1,2}\leftarrow2_{1,1}$ rotational transition for the ecb-I-w-a and ecb-II-w-a complexes. b) The $5_{0,5}\leftarrow4_{0,4}$ rotational transition for the ecb-I-w$_2$ and ecb-II-w$_2$ complexes. c) The $7_{1,6}\leftarrow6_{1,5}$ rotational transition for the ecb-I-w$_3$ and ecb-II-w$_3$ complexes. All the transitions compared were measured using the chirped pulse spectrometer in the same conditions of pressure (Ne at 3.2 bar) and heating temperature (75ºC).

The observed complexes with the conformation II of ethyl carbamate are predicted to be identical in the nature of the interactions established with the water molecules to the corresponding complexes with the I form, being the only difference the disposition of the ethyl group (see Figure 8.7).

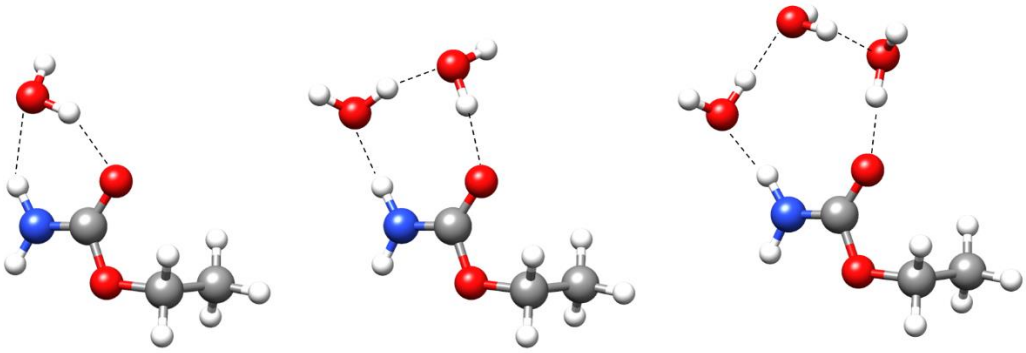

Ecb-II-w-a Ecb-II-w_2 Ecb-II-w_3

Figure 8.7. The complexes with one, two and three molecules of water with II ethyl carbamate.

For the ecb-II-w-a complex, μ_a-type R-branch, together with μ_b-type R-branch and Q-branch transitions with J up to 5 and K_{-1} up to 2 were measured. For the ecb-II-w_2 and ecb-II-w_3 complexes only μ_a-type R-branch transitions were observed, with J up to 5 and K_{-1} up to 3 for ecb-II-w_2 and J up to 8 and K_{-1} up to 3 for ecb-II-w_3. A semirigid rotor Hamiltonian in the asymmetric reduction and in the I^r representation was employed in the fittings of the three complexes. From the experimental frequencies the rotational constants, the quartic centrifugal distortion constants Δ_J, Δ_{JK}, and δ_J, and the diagonal elements of the nuclear quadrupole coupling tensor were determined for the three complexes (see Table 8.4). The corresponding *ab initio* rotational parameters are compared with the experimentally derived in Tables S8.6-S8.8. The complete list of transitions observed is collected in Tables S8.19-S8.21.

No doublets due to tunneling attributable to water motions were observed for any of the complexes, not even for the complex with three molecules of water as occur in the ecb-I-w_3 complex. Furthermore, from the two possible conformations for the complexes arising with the rotamer II of ethyl carbamate (see Section 8.3.3), only one seems to appear in the microwave spectrum for each of the microsolvated complexes.

Table 8.4. Observed rotational parameters obtained for the ecb-II-w-a, ecb-II-w_2 and ecb-II-w_3 complexes.

Fitted Parameters[a]	ecb-II-w-a	ecb-II-w_2	ecb-II-w_3
A /MHz	5196.3808(28)[b]	3023.593(94)	1885.263(24)
B /MHz	1212.1730(10)	797.6169(12)	557.96382(68)
C /MHz	1063.34957(89)	672.6464(11)	458.15647(59)
Δ_J /kHz	0.471(34)	0.168(11)	0.2207(32)
Δ_{JK} /kHz	-2.35(14)	-0.942(62)	-1.619(33)
Δ_K /kHz	[0.]	[0.]	[0.]
δ_J /kHz	0.076(13)	0.064(16)	0.0392(37)
δ_K /kHz	[0.]	[0.]	[0.]
^{14}N 3/2(χ_{aa}) /MHz	2.3891(81)	2.001(12)	1.900(50)
^{14}N ¼(χ_{bb}-χ_{cc}) /MHz	1.2977(28)	1.503(13)	1.281(22)
N	54/16	51/18	76/27
σ /kHz	6.6	5.5	6.0
Derived Parameters			
P_a /uÅ^2	397.46735(26)	608.8977(27)	870.3792(19)
P_b /uÅ^2	77.80345(26)	142.4317(27)	232.6915(19)
P_c /uÅ^2	19.45251(26)	24.7135(27)	35.3766(19)

[a] A, B and C are the rotational constants. Δ_J, Δ_{JK}, Δ_K, δ_J and δ_K are the quartic centrifugal distortion constants. χ_{aa}, χ_{bb} and χ_{cc} are the quadrupole coupling tensor diagonal elements for ^{14}N atom. N is the number of quadrupole hyperfine components/rotational transitions fitted. σ is the rms deviation of the fit. P_α (α = a, b or c) are the planar moments of inertia; these are derived from the moments of inertia I_α as for example $P_c = (I_a+I_b-I_c)/2$. [b] Standard errors are given in parentheses in units of the last digits.

8.3.3 Potential energy function and relaxation

In the supersonic expansion using Ar, only rotamer I is observed, and therefore only complexes with the conformer I are formed. In the supersonic expansion using Ne, both monomers and their complexes appear. Thus, the relaxation analysis can be reduced to the relaxation of ethyl carbamate monomer. The potential energy function for the interconversion of ethyl carbamate conformers can be defined by the rotation of the C_1–O_2–C_2–C_3 τ dihedral angle. The global minimum corresponds to the rotamer I, in which τ takes a value of 180 degrees. For the monomer of ethyl carbamate, as a result of the almost planarity of the heavy atom skeleton, a rotation of +100 or -100 degrees from the global minimum leads to the two equivalent conformations of the II form. The periodic potential energy function has been calculated at the B3LYP-D3/6-311++G(d,p) level of theory predict a low-energy barrier for the interconversion of about 290 cm^{-1}. This barrier is lower than the cutoff of 350-400cm^{-1} given in literature for conformer relaxation[9] in a molecular beam jet in the same conditions as we have used.

For the complexes with ethyl carbamate II, two different conformations may exist almost isoenergetic between them. In ecb-II mono and dihydrated complexes this is due to the non-bonded water hydrogen atoms which lie out of the carbamate plane. For the ecb-II trihydrated complexes, the arrangement of water molecules is not planar. As shown in Figure 8.8 for ecb-II-w_3, the two possible ecb-II forms which are equivalent for the monomer turns out to be non-equivalent for the complexes. Experimentally only one of those conformations has been observed with ethyl carbamate II for the monohydrated, dihydrated or trihydrated complexes. The total inversion of the complex in order to obtain the equivalent structure would require coordinated motions of both water and the ethyl group. The potential energy function for the dihedral angle seems not to change very much with complexation (see Figure 8.8).

Although computational calculations may miscalculate the energy order of the complexes due to the close values between them, the observation of only the complexes with ethyl carbamate I in the supersonic expansion using Ar indicates that those are most stable, and the complexes with ethyl carbamate II relax into them. In the supersonic expansion with Ne complexes with both I and II forms can be observed with comparable intensities, making another confirmation of their similar stability, as discussed above.

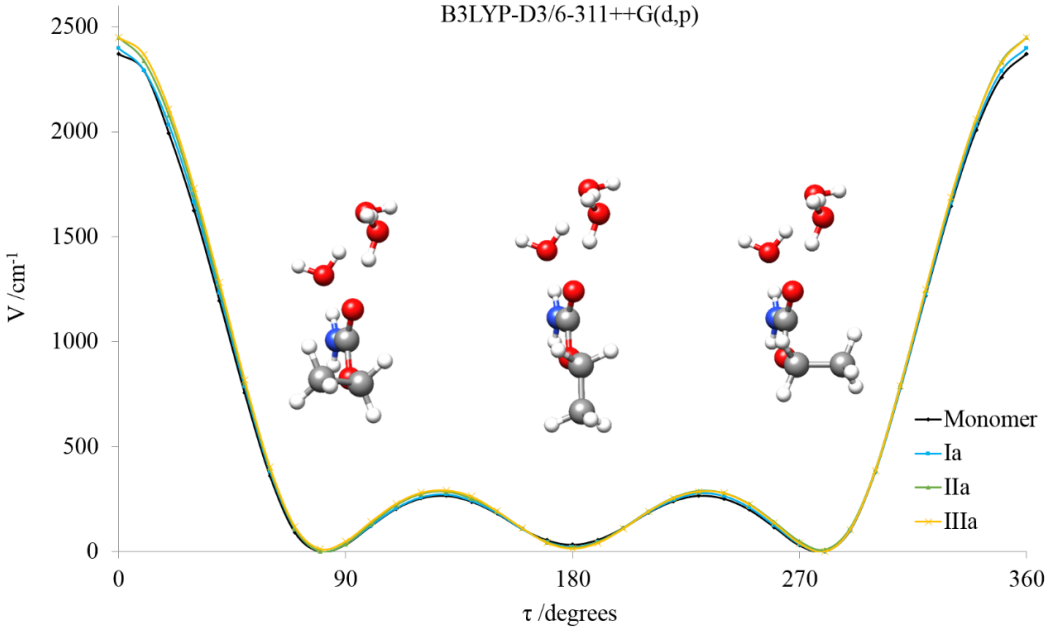

Figure 8.8. Potential energy function of ethyl carbamate performed at the B3LYP-D3/6-311++G(d,p) level of theory for the rotation of the C_1–O_2–C_2–C_3 τ dihedral angle for the monomer (black) and the complexes with one (blue) two (green) or three (yellow) molecules of water. The corresponding structures for the minima points are represented for the complex with three molecules of water in side view.

Nuclear quadrupole coupling and π-cooperative effects

σ-cooperativity[35,36] is associated with complexes in which there are groups capable of acting simultaneously as hydrogen donor and hydrogen acceptor, closing cycles or forming chains, as the –OH group in water. When water establishes hydrogen bonds, it polarizes incrementing the strength of the interactions reflected by a shortening in the hydrogen bond distance. In addition to σ-cooperativity, another kind of effect resulting in the polarization of the molecule can be

expected for amides, as ethyl carbamate, Resonance Assisted Hydrogen Bonding (RAHB)[37,38] or π-cooperative bonding. Both σ- and π-cooperative effects are stronger as the number of water molecules increases. RAHB effects have been demonstrated to occur in the gas phase by microwave spectroscopy for the microsolvation of formamide.[15,16] The main effects of RAHB on the peptide bond is the polarization of the linkage resulting in the enlargement of the C=O distance and the shortening of the C–N bond. No isotopologues in the ethyl carbamate molecule have been observed in this work. However, based on the good agreement between predicted and observed rotational parameters, the lack of experimental information can be supplied by *ab initio* values as an approximation (see Scheme 8.1).

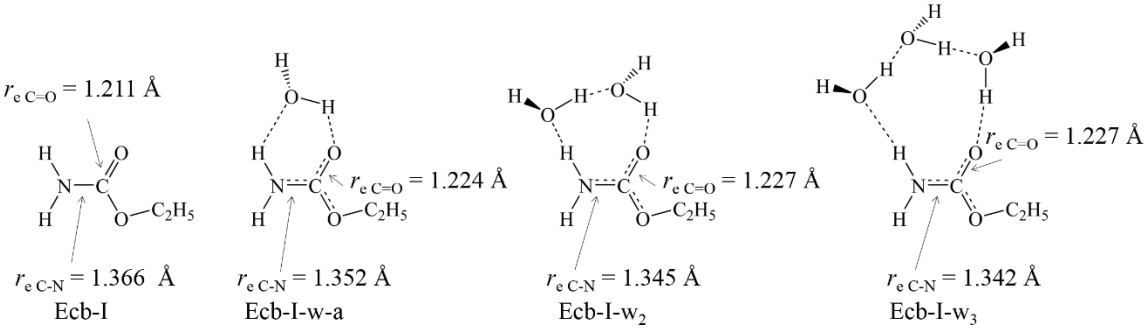

Scheme 8.1. RAHB inductive effects in the microsolvation series of ethyl carbamate evidenced by the C=O bond enlargement and the C–N shortening.

As already demonstrated in the microsolvation system of formamide,[15,16] the nuclear quadrupole coupling constants can be used to probe the changes in the electronic environment at the ^{14}N nucleus. In general, only the diagonal elements from the nuclear quadrupole coupling tensor can be determined and therefore an exhaustive picture of the electric field gradient can not be obtained. In planar molecules, its *c* inertial axis is parallel to the principal ^{14}N quadrupole coupling *z* axis. For almost planar complexes, as those observed with the rotamer I of ethyl carbamate it is possible to reasonable correlate $\chi_{cc} \approx \chi_{zz}$. However, the complexes with the form II of ethyl carbamate are far from planarity, and therefore this correlation is not valid. Table 8.5 shows a clear tendency in the experimental values of χ_{cc} for the microsolvation series of ethyl carbamate I, almost identical to those found for formamide-water complexes.[15,16]

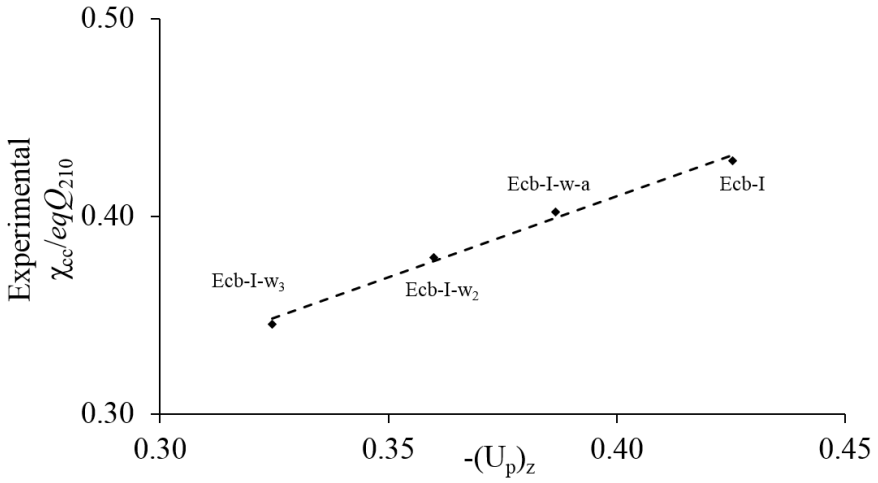

Figure 8.9. Correlation between the experimental values of χ_{cc}/eQq_{210} and $-(U_p)_z$ for the monomer and observed complexes with up to three water molecules of ethyl carbamate I.

Table 8.5. Experimental and *ab initio* (B3LYP-D3/6-311++G(d,p) quadrupole coupling constants for ethyl carbamate I and II monomers[8] and complexes, together with the $-((U_p)_z)$ values both calculated from χ_{cc} and from the natural atomic orbital populations obtained by a Natural Bond Orbital Analysis.[39]

Experimental	ecb-I	ecb-I-w-a	ecb-I-w_2	ecb-I-w_3
χ_{aa} /MHz	2.1151(14)	1.6392(12)	1.3519(39)	1.156(24)
χ_{bb} /MHz	2.1667(15)	2.3833(18)	2.440(13)	2.298(25)
χ_{cc} /MHz	-4.2818(15)	-4.0225(18)	-3.792(13)	-3.454(25)
χ_{cc}/eQq_{210}	0.42818	0.40225	0.3792	0.3454

Ab initio	ecb-I	eb-I-w-a	ecb-I-w_2	ecb-I-w_3
χ_{aa} /MHz	2.39	1.81	1.45	1.25
χ_{bb} /MHz	2.47	2.72	2.79	2.53
χ_{cc} /MHz	-4.86	-4.53	-4.24	-3.78
χ_{xx} /MHz	2.80	2.87	2.90	2.88
χ_{yy} /MHz	2.13	1.69	1.37	1.29
χ_{zz} /MHz	-4.93	-4.56	-4.27	-4.17
χ_{zz}/eQq_{210}	0.49	0.46	0.43	0.42
$-(U_p)_z$ NBO	0.43	0.39	0.36	0.32

Experimental	ecb-II	ecb-II-w-a	ecb-II-w_2	ecb-II-w_3
χ_{aa} /MHz	1.8923(11)	1.5927(54)	1.3340(80)	1.267(33)
χ_{bb} /MHz	1.8918(11)	1.799(16)	2.339(30)	1.929(61)
χ_{cc} /MHz	-3.7841(11)	-3.392(16)	-3.673(30)	-3.195(61)
χ_{cc}/eQq_{210}	0.37841	0.3392	0.3673	0.3195

Ab initio	ecb-II	ecb-II-w-a	ecb-II-w_2	ecb-II-w_3
χ_{aa} /MHz	2.37	1.75	1.49	1.37
χ_{bb} /MHz	2.26	2.36	2.43	1.99
χ_{cc} /MHz	-4.62	-4.11	-3.92	-3.36
χ_{xx} /MHz	2.78	2.86	2.88	2.87
χ_{yy} /MHz	2.12	1.67	1.36	1.27
χ_{zz} /MHz	-4.89	-4.53	-4.25	-4.15
χ_{zz}/eQq_{210}	0.49	0.45	0.42	0.41
$-(U_p)_z$ NBO	0.40	0.34	0.30	0.28

The trend in ethyl carbamate I indicates that the electronic environment at the ^{14}N nucleus is altered by microsolvation. As explained in formamide–water complexes,[15,16] the electric field gradient coupling to nuclear quadrupole can be related to the unequal filling of the valence shell *p* orbitals from the coupling nucleus.[28] The χ_{zz} constant can be correlated then to the unbalanced $2p_z$ electronic charge $(U_p)_z$. Figure 8.9 shows the correlation between the experimental χ_{cc}/eQq_{210} and $-(U_p)_z$ calculated from a Natural Bond Orbital analysis.[39] The $-(U_p)_z$ values indicate that the electron density along the *z* axis decreases with the hydration degree, showing that the polarization of ethyl carbamate due to RAHB inductive effects is stronger when the number of cooperative hydrogen bond increases. When considering the *ab initio* diagonal quadrupole coupling tensor elements (see Table 8.5) the values of χ_{zz} are practically the same in both series of complexes for ecb-I and ecb-II. This indicates that practically the same RAHB effects can be expected in the amide group, independently of the ethyl carbamate conformation.

8.4 Conclusions

Microsolvated complexes of ethyl carbamate with up to three molecules of water have been observed for the first time in the gas phase by high-resolution microwave spectroscopy. The rotational, quartic centrifugal distortion and nuclear quadrupole coupling constants have been obtained with high accuracy. Since no doublets due to methyl internal rotation are present in any system of ethyl carbamate, either monomer or complexes, it is no possible to assert the presence or the absence of water effects influencing the hindering methyl rotation. The observation of $H_2{}^{18}O$ species has allowed to precisely locate the water molecules in the molecular frame. The hydrogen bond distances obtained using the r_0 methodology indicate that the dominant interaction is, as already observed in related systems, the C=O···H_w–O_w. In the gas phase ethyl carbamate presents an equilibrium between two close energy conformations with a low interconversion barrier. The detection of these structures and their microsolvated complexes depends strongly on the carrier gas used in the supersonic expansion due to relaxation processes. Using Ar, only the most stable form of ethyl carbamate and its complexes are observable, while using Ne, both forms and their complexes could be detected with comparable line intensities. It is noticeable that the inclusion of water molecules seems not to alter the potential energy function for the interconversion between the two forms of ethyl carbamate. As in previous studies of microsolvation of amides and amide-type molecules, a decreasing trend in the experimental value of χ_{cc}/eQq_{210} has been found as the number of water molecules in the complex increase. RAHB inductive effect seems to be at the origin of this trend in ethyl carbamate, that causes the enlargement of the C=O bond distance while shortens the C–N bond distance. This has been shown to occur also for the microsolvation series of ethyl carbamate I.

References

[1] Abraham, D. J., Rotella, D. P. *Burger´s medicinal chemistry, drug discovery and development*, 7th edition, Wiley, Hoboken, 2010.

[2] Ghosh, A. K., Brindisi, M. "Organic Carbamates in Drug Design and Medicinal Chemistry" *J. Med. Chem.*, **2015**, 58, 2895–2940.

[3] Fukuto, T. R. "Mechanism of Action of Organophosporus and Carbamate Insecticides" *Environ. Health Perspect.*, **1990**, 87, 245–254.

[4] Heyn, R. H., Jacobs, I. Carr, R. H. "Synthesis of Aromatic Carbamates from CO_2: Implications for the Polyurethane Industry" *Adv. Inorg. Chem.*, **2014**, 66, 83–115.

[5] Bracher, B. H., Small, R. W. H. "The Crystal Structure of Ethyl Carbamate" *Acta Crystallogr.*, **1967**, 23, 410–418.

[6] Furer, V. L. "Hydrogen Bonding in Ethyl Carbamate Studied by IR Spectroscopy" *J. Mol. Struct.*, **1998**, 449, 53–59.

[7] Marstokk, K. M., Møllendal, H. "Microwave Spectrum, Conformational Equilibrium and Quantum Chemical Calculations of Urethane (Ethyl Carbamate)" *Acta Chem. Scan.*, **1999**, 53, 329–334.

[8] Goubet, M., Motiyenko, R. A., Réal, F., Margulès, L., Huet, T. R., Asselin, P., Soulard, P., Krasnicki, A., Kisiel, Z., Alekseev, E. A. "Influence of the Geometry of a Hydrogen Bond on Conformational Stability: A Theoretical and Experimental Study of Ethyl Carbamate" *Phys. Chem. Chem. Phys.*, **2009**, 11, 1719–1728.

[9] Ruoff, R. S., Klots, T. D., Emilsson, T., Gutowsky, H. S. "Relaxation of Conformers and Isomers in Seeded Supersonic Jets of Inert Gases" *J. Chem. Phys.*, **1990**, 93, 3142–3150.

[10] Godfrey, P. D., Brown, R. D., Rodgers, F. M. "The Missing Conformers of Glycine and Alanine: Relaxation in seeded Supersonic Jets" *J. Mol. Struct.*, **1996**, 376, 65–81.

[11] Lovas, F. J., Suenram, R. D., Fraser, G. T., Gillies, C. W., Zozom, J. "The microwave Spectrum of Formamide-Water and Formamide-Methanol Complexes" *J. Chem. Phys.*, **1988**, 88, 722–729.

[12] Held, A., Pratt, D. W. "Hydrogen Bonding in Water Complexes. Structures of 2-Pyridone-H_2O and 2-Pyrididone-$(H_2O)_2$ in Their S_0 and S_1 Electronic States" *J. Am. Chem. Soc.*, **1993**, 115, 9708–9717.

[13] Blanco, S., López, J. C., Lesarri, A., Alonso, J. L. "Microsolvation of Formamide: A Rotational Study" *J. Am. Chem. Soc.*, **2006**, 128, 12111–12121.

[14] Caminati, W., López, J. C., Blanco, S., Mata, S., Alonso, J. L. "How Water Links to *Cis* and *Trans* Peptidic Groups: The rotational Spectrum of N-Methylformamide-Water" *Phys. Chem. Chem. Phys.*, **2010**, 12, 10230–10234.

[15] Blanco, S., Pinacho, P., López, J. C. "Hydrogen-Bond Cooperativity in Formamide$_2$-Water: A Model for Water Mediated Interactions" *Angew. Chem. Int. Ed.*, **2016**, 128, 9477–9481. Chapter IV within this Thesis.

[16] Blanco, S., Pinacho, P., López, J. C. "Structure and Dynamics in Formamide-$(H_2O)_3$: A Water Pentamer Analogue" *J Phys. Chem. Lett.*, **2017**, 8, 6060–6066. Chapter V within this Thesis.

[17] "Microsolvation of Formanilide Conformers: A Model for Peptide Solvation". Chapter VI within this Thesis.

[18] "The Effect of Microsolvation over Structure, Nuclear Quadrupole and Internal Rotation: The Methyl Carbamate$\cdots(H_2O)$ and Methyl Carbamate$\cdots(H_2O)_2$ Complexes.". Chapter VII within this Thesis.

[19] Brown, G. G., Dian, B. C., Douglass, K. O., Geyer, S. M., Pate, B. H. "The Rotational Spectrum of Epifluorohydrin Measured by Chirped-Pulse Fourier Transform Microwave Spectroscopy" *J. Mol. Spectrosc.*, **2006**, 238, 200–212.

[20] Brown, G. G., Dian, B. C., Douglass, K. O., Geyer, S. M., Shipman, S. T., Pate, B. H. "A Broadband Fourier Transform Microwave Spectrometer Based on Chirped Pulse Excitation" *Rev. Sci. Instrum.*, **2008**, 79, 053103.

[21] Alonso, J. L., Lorenzo, F. J., López, J. C., Lesarri, A., Mata, S., Dreizler, H. "Construction of a Molecular Beam Fourier Transform Microwave Spectrometer Used to Study the 2,5-Dihydrofuran-Argon Van Der Waals Complex" *Chem. Phys.*, **1997**, 218, 267–275.

[22] Blanco, S., López, J. C., Alonso, J. L., Ottaviani, P., Caminati, W. "Pure Rotational Spectrum and Model Calculations of Indole-Water" *J. Chem. Phys.*, **2003**, 119, 880–886.

[23] Gaussian 09, Revision D.01, Frisch M. J., Trucks G. W., Schlegel H. B., Scuseria G. E., Robb M. A., Cheeseman J. R., Scalmani G., Barone V., Petersson G. A., Nakatsuji H., Li X., Caricato M., Marenich A., Bloino J., Janesko B. G., Gomperts R., Mennucci B., Hratchian H. P., Ortiz J. V., Izmaylov A. F., Sonnenberg J. L., Williams-Young D., Ding F., Lipparini F., Egidi F., Goings J., Peng B., Petrone A., Henderson T., Ranasinghe D., Zakrzewski V. G., Gao J., Rega N., Zheng G., Liang W., Hada M., Ehara

M., Toyota K., Fukuda R., Hasegawa J., Ishida M., Nakajima T., Honda Y., Kitao O., Nakai H., Vreven T., Throssell K., Montgomery, Jr. J. A., Peralta J. E., Ogliaro F., Bearpark M., Heyd J. J., Brothers E., Kudin K. N., Staroverov V. N., Keith T., Kobayashi R., Normand J., Raghavachari K., Rendell A., Burant J. C., Iyengar S. S., Tomasi J., Cossi M., Millam J. M., Klene M., Adamo C., Cammi R., Ochterski J. W., Martin R. L., Morokuma K., Farkas O., Foresman J. B., Fox D. J., *Gaussian, Inc., Wallingford CT*, 2016.

[24] a) Lee, C., Yang, W., Parr, R. G. "Development of the Colle-Salvetti Correlation-Energy Formula into a Functional of the Electron Density" *Phys. Rev. B*, **1988**, 37, 785–789. b) Becke, A. D. "Density-Functional Thermochemistry. III. The Role of Exact Exchange" *J. Chem. Phys.*, **1993**, 98, 5648–5652. c) Vosko, S. H., Wilk, L., Nusair, M. "Accurate Spin-Dependent Electron Liquid Correlation Energies for Local Spin Density Calculations: a Critical Analysis" *Can. J. Phys.*, **1980**, 58, 1200–1211.

[25] Grimme, S., Antony, J., Ehrlich, Krieg, H. "A Consistent and Accurate *Ab Initio* Parametrization of Density Functional Dispersion Correction (DFT-D) for the 94 Elements H-Pu" *J. Chem. Phys.*, **2010**, 132, 154101.

[26] Ditchfield, R., Hehre, W. J., Pople, J. A. "Self-Consistent Molecular-Orbital Methods. IX. An Extended Gaussian-Type Basis for Molecular-Orbital Studies of Organic Molecules" *J. Chem. Phys.*, **1971**, 54, 724–728.

[27] a) Boys, S., Bernardi, F. "The Calculation of Small Molecular Interactions by the Differences of Spearate Total Energies. Some Procedures with Reduced Errors" *Mol. Phys.*, 1970, **19**, 553–566. b) Xantheas, S. S. "On the Importance of the Fragment Relaxation Energy Terms in the Estimation of the Basis Set Superposition Error Correction to the Intermolecular Interaction Energy" *J. Chem. Phys.*, 1996, **21**, 8821–8824.

[28] Gordy, W., Cook, R. L. *Microwave Molecular Spectra*, Wiley-Interscience, New York, 1984.

[29] Watson, J. K. G. in *Vibrational Spectra and Structure a Series of Advances, Vol 6* ed. J. R. Durig, Elsevier, New York, 1977, pp. 1–89.

[30] Pickett, H. M. "The Fitting and Prediction of Vibrational-Rotation Spectra with Spin Interaction" *J. Mol. Spectrosc.*, **1991**, 148, 371–377.

[31] Kisiel, Z. "Least-Squares Mass-Dependence Molecular Structures for Selected Weakly Bound Intermolecular Clusters" *J. Mol. Spectrosc.*, **2003**, 218, 58–67.

[32] Rudolph, H. D. "Contribution to the Systematics of r_0-Derived Molecular Structure Determinations from Rotational Parameters" *Struct. Chem.*, **1991**, **2**, 581–588.

[33] Kraitchman, J. "Determination of Molecular Structure from Microwave Spectroscopic Data" *Am. J. Phys.*, **1953**, 21, 17–24.

[34] Costain, C. C. "Further Comments on the Accuracy of r_s Substitution Structures" *Trans. Am. Crystallogr. Assoc.*, **1966**, 2, 157–164.

[35] Saenger, W., Jeffrey, G. A. *Hydrogen Bonding in Biological Structures*, Springer-Verlag, Berlin, 1991.

[36] Jeffrey, G. A. *Introduction to Hydrogen Bonding*, Oxford University Press, Oxford, 1997.

[37] Jeffrey, G. A. *An Introduction to Hydrogen Bonding*; Topics in Physical Chemistry - Oxford University Press, Oxford University Press, 1997.

[38] Gilli, P., Bertolasi, V., Ferretti, V., Gilli, G. "Evidence for Intramolecular N-H···O Resonance Assisted Hydrogen Bonding in *β*-Enaminones and Related Heterodienes. A Combined Crystal-Structural, IR, and NMR Spectroscopic, and Quantum-Mechanical Investigation" *J. Am. Chem. Soc.*, **2000**, 122, 10405–10417.

[39] Reed, A. E., Weinstock, R. B., Weinhold, F. "Natural Population Analysis" *J. Chem. Phys.* **1985**, *83*, 735-746.

Supplementary material for Chapter VIII

Microsolvation of Ethyl Carbamate Conformers: Effect of Carrier Gas on the Formation of Complexes.

Abstract

Microsolvated complexes of ethyl carbamate with up to three water molecules formed in a supersonic expansion have been characterized by high-resolution microwave spectroscopy. Both chirped-pulse and cavity Fourier transform microwave spectrometers covering the 2-13 GHz frequency range have been used. Ethyl carbamate presents in the gas an equilibrium between the two most stable conformers. The observation of these structures and their microsolvated complexes depends on the carrier gas used in the supersonic expansion due to collisional relaxation. Using argon, only the most stable conformer and its complexes with water are observed, while with neon, both forms and their corresponding water complexes are observed. The structures of the complexes have been characterized and show water molecules closing sequential cycles through hydrogen bonding with the amide group. Complexation of ethyl carbamate with water molecules seems apparently not to alter substantially the potential energy function for the interconversion between the two conformations of ethyl carbamate.

- Figure S8.1. Conformers predicted for ethyl carbamate I and II complexes with one molecule of water.

- Figure S8.2. Conformers predicted for ethyl carbamate I and II complexes with two and three molecules of water.

- Table S8.1. *Ab initio* rotational parameters (B3LYP-D3/6-311++G(d,p)) for ethyl carbamate I and II complexes with one molecule of water.

- Table S8.2. *Ab initio* rotational parameters (B3LYP-D3/6-311++G(d,p)) for ethyl carbamate I and II with two and three molecules of water.

- Table S8.3. Observed rotational parameters for the ecb-I-w-a complex for the parent and the observed isotopologue.

- Table S8.4. Observed rotational parameters for the ecb-I-w_2 complex for the parent and the observed isotopologues.

- Table S8.5. Observed rotational parameters for the ecb-I-w_3 complex.

- Table S8.6. Observed rotational parameters for the ecb-II-w-a complex.

- Table S8.7. Observed rotational parameters for the ecb-II-w_2 complex.

- Table S8.8. Observed rotational parameters for the ecb-II-w_3 complex.

- Table S8.9. r_0 structure for the ecb-I-w-a complex compared to r_e values.

- Table S8.10. r_0 structure for the ecb-I-w_2 complex compared to r_e values.

- Table S8.11. Experimental and *ab initio* (B3LYP-D3/6-311++G(d,p) quadrupole coupling for ethyl carbamate I together with the values of the unbalanced $2p_z$ electronic charge ($(U_p)_z$).

- Table S8.12. Experimental and *ab initio* (B3LYP-D3/6-311++G(d,p) quadrupole coupling for ethyl carbamate II together with the values of the unbalanced $2p_z$ electronic charge ($(U_p)_z$).

- Tables S8.13-S8.14. Observed transition frequencies for the ecb-I-w-a complex for the parent and the observed isotopologue.

- Tables S8.15-S8.17. Observed transition frequencies for the ecb-I-w_2 complex for the parent and the observed isotopologue.

- Table S8.18. Observed transition frequencies for the ecb-I-w_3 complex.

- Table S8.19. Observed transition frequencies for the ecb-II-w-a complex.

- Table S8.20. Observed transition frequencies for the ecb-II-w_2 complex.

- Table S8.21. Observed transition frequencies for the ecb-II-w_3 complex.

Figure S8.1. Conformers predicted for ethyl carbamate I (ecb-I) and ethyl carbamate II (ecb-II) complexes with one molecule of water. ΔE is the stabilization energy relative to the most stable complex (ecb-I-w-a) calculated at the B3LYP-D3/6-311++G(d,p) level of theory including ZPE correction. The corresponding parameters are given in Table S8.1.

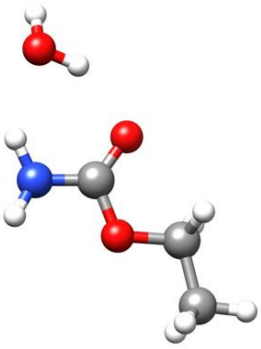

Ecb-I-w-a
ΔE = 0 cm^{-1}

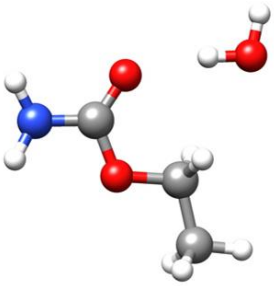

Ecb-I-w-b
ΔE = 723 cm^{-1}

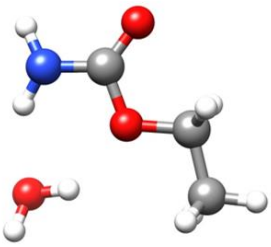

Ecb-I-w-c
ΔE = 741 cm^{-1}

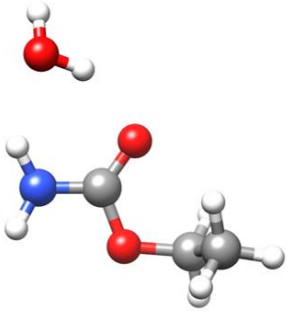

Ecb-II-w-a
ΔE = 23 cm^{-1}

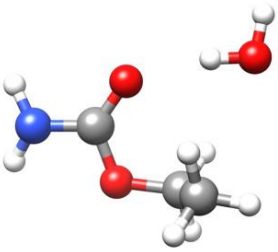

Ecb-II-w-b
ΔE = 728 cm^{-1}

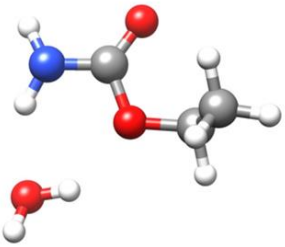

Ecb-II-w-c
ΔE = 825 cm^{-1}

Figure S8.2. Conformers predicted for ethyl carbamate I (ecb-I) and ethyl carbamate II (ecb-II) complexes with two and three molecules of water. ΔE is the stabilization energy relative to the most stable complex (ecb-I-w_2 and ecb-I-w_3) calculated at the B3LYP-D3/6-311++G(d,p) level of theory including ZPE correction. The corresponding parameters are given in Table S8.2.

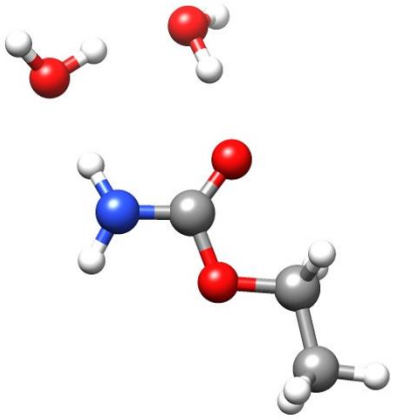

Ecb-I-w_2
ΔE = 0 cm^{-1}

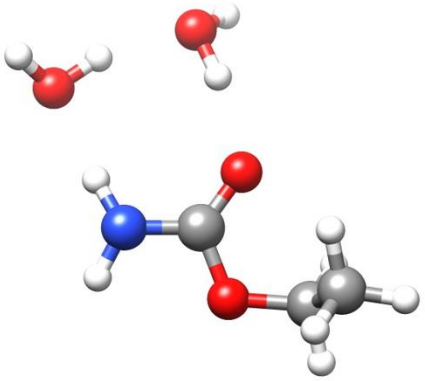

Ecb-II-w_2
ΔE = 10 cm^{-1}

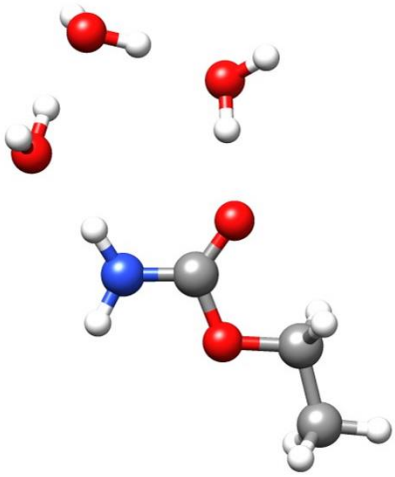

Ecb-I-w_3
ΔE = 0 cm^{-1}

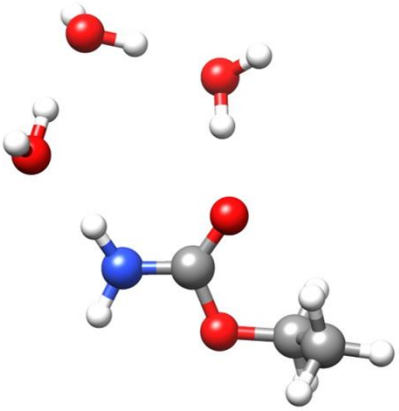

Ecb-II-w_3
ΔE = 26 cm^{-1}

Table S8.1. *Ab initio* rotational parameters calculated at B3LYP-D3/6-311++G(d,p) level of theory for the ethyl carbamate I (ecb-I) and ethyl carbamate II (ecb-II) complexes with one molecule of water.

Parameter[a]	Ecb-I-w-a	Ecb-I-w-b	Ecb-I-w-c	Ecb-II-w-a	Ecb-II-w-b	Ecb-II-w-c
A /MHz	7689.84	2257.73	2338.56	5109.80	3052.59	2874.51
B /MHz	1031.44	1922.35	2091.43	1220.31	1722.13	1752.29
C /MHz	921.95	1052.07	1123.12	1067.74	1210.17	1184.88
P_a /uÅ^2	486.21	259.71	237.76	394.28	272.76	269.56
P_b /uÅ^2	61.96	220.66	212.22	79.04	144.85	156.96
P_c /uÅ^2	3.76	3.19	3.89	19.86	20.70	18.85
μ_a /D	1.56	3.05	1.59	1.16	3.13	0.62
μ_b /D	0.89	1.04	2.22	1.15	0.28	2.53
μ_c /D	0.89	0.31	1.07	0.65	0.29	1.01
^{14}N χ_{aa} /MHz	1.81	2.77	2.68	1.80	2.76	2.29
^{14}N χ_{bb} /MHz	2.72	2.10	1.91	1.87	1.70	1.94
^{14}N χ_{cc} /MHz	-4.53	-4.88	-4.59	-3.67	-4.45	-4.24
ΔE /cm^{-1}	23	863	818	0	814	842
ΔE_{ZPE} /cm^{-1}	0	723	741	23	728	825
ΔE /kJmol^{-1}	0.3	10.3	9.8	0.0	9.7	10.1
ΔE_{ZPE} /kJmol^{-1}	0.0	8.7	8.9	0.3	8.7	9.9

[a] A, B and C are the rotational constants. P_α (α= a, b or c) are the planar moments of inertia, these are derived from the moments of inertia I_α as for example $P_c = (I_a+I_b-I_c)/2$. μ_α (α = a, b or c) are the electric dipole moment components, 1 D = $3.33\cdot10^{-30}$ C·m. χ_{aa}, χ_{bb}, and χ_{cc}, are the quadrupole coupling tensor diagonal elements for ^{14}N atom. ΔE is the energy relative to the most stable conformer. ΔE_{ZPE} is the energy relative to the most stable conformer including zero point energy correction.

Table S8.2. *Ab initio* rotational parameters calculated at B3LYP-D3/6-311++G(d,p) level of theory for the ethyl carbamate I (ecb-I) and ethyl carbamate II (ecb-II) complexes with two and three molecules of water.

Parameter[a]	Ecb-I-w_2	Ecb-II-w_2	Ecb-I-w_3	Ecb-II-w_3
A /MHz	3793.57	3060.95	2260.09	2017.15
B /MHz	704.09	802.41	493.14	543.22
C /MHz	599.88	676.37	413.03	452.44
P_a /uÅ^2	713.51	605.96	1012.40	898.40
P_b /uÅ^2	128.96	141.24	211.19	218.60
P_c /uÅ^2	4.26	23.87	12.42	31.94
μ_a /D	1.62	1.42	1.68	1.60
μ_b /D	0.47	0.50	0.08	0.11
μ_c /D	0.16	0.09	0.47	0.49
^{14}N χ_{aa} /MHz	1.45	1.42	1.25	1.09
^{14}N χ_{bb} /MHz	2.79	2.68	2.53	2.62
^{14}N χ_{cc} /MHz	-4.24	-4.10	-3.78	-3.71
ΔE /cm^{-1}	20	0	3	0
ΔE_{ZPE} /cm^{-1}	0	10	0	26
ΔE /kJmol^{-1}	0.2	0.0	0.0	0.0
ΔE_{ZPE} /kJmol^{-1}	0.0	0.1	0	26

[a] A, B and C are the rotational constants. P_α (α= a, b or c) are the planar moments of inertia, these are derived from the moments of inertia I_α as for example $P_c = (I_a+I_b-I_c)/2$. μ_α (α = a, b or c) are the electric dipole moment components, 1 D = $3.33\cdot10^{-30}$ C·m. χ_{aa}, χ_{bb}, and χ_{cc}, are the quadrupole coupling tensor diagonal elements for ^{14}N atom. ΔE is the energy relative to the most stable conformer. ΔE_{ZPE} is the energy relative to the most stable conformer including zero point energy correction.

Table S8.3. Observed rotational parameters obtained for the ecb-I-w-a complex for the parent and the $^{18}O_w$ isotopologue compared to *ab initio* (B3LYP-D3/6-311++G(d,p)) values.

Fitted Parameters[a]	ecb-I-w-a	ecb-I-w-a $^{18}O_w$	*ab initio*
A /MHz	7659.94791(44)[b]	7632.97(37)	7689.84
B /MHz	1034.10646(11)	986.93854(11)	1031.44
C /MHz	923.276293(93)	885.14275(12)	921.95
Δ_J /kHz	0.1124(13)	[0.1124][c]	0.098
Δ_{JK} /kHz	0.088(13)	[0.088]	-0.193
Δ_K /kHz	[0.]	[0.]	22.061
δ_J /kHz	0.01594(58)	[0.01594]	0.011
δ_K /kHz	[0.]	[0.]	0.321
^{14}N 3/2(χ_{aa}) /MHz	2.4588(18)	[2.4588]	2.72
^{14}N ¼(χ_{bb}-χ_{cc}) /MHz	1.60147(59)	[1.60147]	1.81
N	138/37	25/9	
σ /kHz	2.4	1.6	
Derived Parameters			
P_a /uÅ^2	485.05484(52)	508.4074(32)	486.21
P_b /uÅ^2	62.32085(52)	62.5501(32)	61.96
P_c /uÅ^2	3.65596(52)	3.6598(32)	3.76
^{14}N χ_{aa}/MHz	1.6392(12)	[1.6392]	1.81
^{14}N χ_{bb}/MHz	2.3833(18)	[2.3833]	2.72
^{14}N χ_{cc}/MHz	-4.0225(18)	[-4.0225]	-4.53

[a] A, B and C are the rotational constants. Δ_J, Δ_{JK}, Δ_K, δ_J and δ_K are the quartic centrifugal distortion constants. χ_{aa}, χ_{bb} and χ_{cc} are the quadrupole coupling tensor diagonal elements for ^{14}N atom. N is the number of quadrupole hyperfine components/rotational transitions fitted. σ is the rms deviation of the fit. P_α ($\alpha = a$, b or c) are the planar moments of inertia, these are derived from the moments of inertia I_α as for example $P_c = (I_a+I_b-I_c)/2$. [b] Standard errors are given in parentheses in units of the last digits. [c] Parameters in square brackets were kept fixed to those given for the parent species in the fit.

Table S8.4. Observed rotational parameters obtained for the ecb-I-w_2 complex for the parent the $^{18}O_{w1}$ and the $^{18}O_{w2}$ isotopologues compared to *ab initio* (B3LYP-D3/6-311++G(d,p)) values.

Fitted Parameters[a]	ecb-I-w_2	ecb-I-w_2 $^{18}O_{w7}$	ecb-I-w_2 $^{18}O_{w8}$	*ab initio*
A /MHz	3734.1586(72)[b]	3599.386(31)	3675.093(47)	3793.57
B /MHz	701.90967(10)	686.889435(79)	680.60559(11)	704.09
C /MHz	597.04077(10)	582.706572(84)	580.11263(11)	599.88
Δ_J /kHz	0.05569(31)	[0.05569]c	[0.05569]	0.042
Δ_{JK} /kHz	0.2351(29)	[0.2351]	[0.2351]	0.161
Δ_K /kHz	[0.]	[0.]	[0.]	4.566
δ_J /kHz	0.01043(24)	[0.01043]	[0.01043]	0.007
δ_K /kHz	0.291(33)	[0.291]	[0.291]	0.264
^{14}N 3/2(χ_{aa}) /MHz	2.0278(58)	[2.0278]	[2.0278]	2.18
^{14}N ¼(χ_{bb}-χ_{cc}) /MHz	1.5582(57)	[1.5582]	[1.5582]	1.76
N	153/53	25/9	25/9	
σ /kHz	1.4	1.5	2.1	
Derived Parameters				
P_a /uÅ^2	715.56974(31)	731.3195(23)	738.1010(18)	713.51
P_b /uÅ^2	130.90344(31)	135.9763(23)	133.0728(18)	128.96
P_c /uÅ^2	4.43601(31)	4.4306(23)	4.4417(18)	4.26
^{14}N χ_{aa}/MHz	1.3519(39)	[1.3519]	[1.3519]	1.45
^{14}N χ_{bb}/MHz	2.440(13)	[2.440]	[2.440]	2.79
^{14}N χ_{cc}/MHz	-3.792(13)	[-3.792]	[-3.792]	-4.24

[a] A, B and C are the rotational constants. Δ_J, Δ_{JK}, Δ_K, δ_J and δ_K are the quartic centrifugal distortion constants. χ_{aa}, χ_{bb} and χ_{cc} are the quadrupole coupling tensor diagonal elements for ^{14}N atom. N is the number of quadrupole hyperfine components/rotational transitions fitted. σ is the rms deviation of the fit. P_α ($\alpha = a$, b or c) are the planar moments of inertia, these are derived from the moments of inertia I_α as for example $P_c = (I_a+I_b-I_c)/2$. [b] Standard errors are given in parentheses in units of the last digits. [c] Parameters in square brackets were kept fixed to those given for the parent species in the fit.

Table S8.5. Observed rotational parameters obtained for the ecb-I-w_3 complex compared to *ab initio* (B3LYP-D3/6-311++G(d,p)) values.

Fitted Parameters[a]	ecb-I-w_3	*ab initio*
A_0 /MHz	2254.4370(61)	2260.09
B_0 /MHz	486.842445(98)	493.14
C_0 /MHz	410.026213(87)	413.03
A_1 /MHz	2254.4248(61)	
B_1 /MHz	486.843300(98)	
C_1 /MHz	410.027428(87)	
Δ_J /kHz	0.08650(18)	0.062
Δ_{JK} /kHz	-1.104(10)	-0.595
Δ_K /kHz	[0.]	6.594
δ_J /kHz	0.01445(21)	0.010
δ_K /kHz	[0.]	0.217
^{14}N 3/2(χ_{aa}) /MHz	1.734(36)	1.79
^{14}N ¼(χ_{bb}-χ_{cc}) /MHz	1.4378(63)	1.38
N	180/30/30	
σ /kHz	2.0/1.7/2.2	
Derived Parameters		
P_{a0} /uÅ^2	1023.22858(69)	1012.40
P_{b0} /uÅ^2	209.32433(69)	211.19
P_{c0} /uÅ^2	14.84648(69)	12.42
P_{a1} /uÅ^2	1023.22523(69)	
P_{b1} /uÅ^2	209.32402(69)	
P_{c1} /uÅ^2	14.84801(69)	
^{14}N χ_{aa}/MHz	1.156(24)	1.19
^{14}N χ_{bb}/MHz	2.298(25)	2.17
^{14}N χ_{cc}/MHz	-3.454(25)	-3.36

[a] A, B and C are the rotational constants. Δ_J, Δ_{JK}, Δ_K, δ_J and δ_K are the quartic centrifugal distortion constants. χ_{aa}, χ_{bb} and χ_{cc} are the quadrupole coupling tensor diagonal elements for ^{14}N atom. N is the number of quadrupole hyperfine components/rotational transitions fitted. σ is the rms deviation of the fit. P_α ($\alpha = a$, b or c) are the planar moments of inertia, these are derived from the moments of inertia I_α as for example $P_c = (I_a+I_b-I_c)/2$. [b] Standard errors are given in parentheses in units of the last digits. [c] Parameters in square brackets were kept fixed to those given for the parent species in the fit.

Table S8.6. Observed rotational parameters obtained for the ecb-II-w-a complex compared to *ab initio* (B3LYP-D3/6-311++G(d,p)) values.

Fitted Parameters[a]	ecb-II-w-a	*ab initio*
A /MHz	5196.3808(28)	5109.79
B /MHz	1212.1730(10)	1220.31
C /MHz	1063.34957(89)	1067.74
Δ_J /kHz	0.471(34)	0.392
Δ_{JK} /kHz	-2.35(14)	-3.545
Δ_K /kHz	[0.]	33.579
δ_J /kHz	0.076(13)	0.082
δ_K /kHz	[0.]	0.149
^{14}N 3/2(χ_{aa}) /MHz	2.3891(81)	2.70
^{14}N ¼(χ_{bb}-χ_{cc}) /MHz	1.2977(28)	1.38
N	54/16	
σ /kHz	6.6	
Derived Parameters		
P_a /uÅ^2	397.46735(26)	394.28
P_b /uÅ^2	77.80345(26)	79.04
P_c /uÅ^2	19.45251(26)	19.86
^{14}N χ_{aa}/MHz	1.5927(54)	1.80
^{14}N χ_{bb}/MHz	1.799(16)	1.87
^{14}N χ_{cc}/MHz	-3.392(16)	-3.67

[a] A, B and C are the rotational constants. Δ_J, Δ_{JK}, Δ_K, δ_J and δ_K are the quartic centrifugal distortion constants. χ_{aa}, χ_{bb} and χ_{cc} are the quadrupole coupling tensor diagonal elements for ^{14}N atom. N is the number of quadrupole hyperfine components/rotational transitions fitted. σ is the rms deviation of the fit. P_α ($\alpha = a$, b or c) are the planar moments of inertia, these are derived from the moments of inertia I_α as for example $P_c = (I_a+I_b-I_c)/2$. [b] Standard errors are given in parentheses in units of the last digits. [c] Parameters in square brackets were kept fixed to those given for the parent species in the fit.

Table S8.7. Observed rotational parameters obtained for the ecb-II-w_2 complex compared to *ab initio* (B3LYP-D3/6-311++G(d,p)) values.

Fitted Parameters[a]	ecb-II-w_2	*ab initio*
A /MHz	3023.593(94)	3060.94
B /MHz	797.6169(12)	802.41
C /MHz	672.6464(11)	676.36
Δ_J /kHz	0.168(11)	0.132
Δ_{JK} /kHz	-0.942(62)	-0.561
Δ_K /kHz	[0.]	6.122
δ_J /kHz	0.064(16)	0.028
δ_K /kHz	[0.]	0.219
^{14}N 3/2(χ_{aa}) /MHz	2.001(12)	2.13
^{14}N ¼(χ_{bb}-χ_{cc}) /MHz	1.503(13)	1.69
N	51/18	
σ /kHz	5.5	
Derived Parameters		
P_a /uÅ^2	608.8977(27)	605.96
P_b /uÅ^2	142.4317(27)	141.24
P_c /uÅ^2	24.7135(27)	23.86
^{14}N χ_{aa}/MHz	1.3340(80)	1.42
^{14}N χ_{bb}/MHz	2.339(30)	2.68
^{14}N χ_{cc}/MHz	-3.673(30)	-4.10

[a] A, B and C are the rotational constants. Δ_J, Δ_{JK}, Δ_K, δ_J and δ_K are the quartic centrifugal distortion constants. χ_{aa}, χ_{bb} and χ_{cc} are the quadrupole coupling tensor diagonal elements for ^{14}N atom. N is the number of quadrupole hyperfine components/rotational transitions fitted. σ is the rms deviation of the fit. P_α ($\alpha = a$, b or c) are the planar moments of inertia, these are derived from the moments of inertia I_α as for example $P_c = (I_a+I_b-I_c)/2$. [b] Standard errors are given in parentheses in units of the last digits. [c] Parameters in square brackets were kept fixed to those given for the parent species in the fit.

Table S8.8. Observed rotational parameters obtained for the ecb-II-w_3 complex compared to *ab initio* (B3LYP-D3/6-311++G(d,p)) values.

Fitted Parameters[a]	ecb-II-w_3	*ab initio*
A /MHz	1885.263(24)	2017.14
B /MHz	557.96382(68)	543.21
C /MHz	458.15647(59)	452.44
Δ_J /kHz	0.2207(32)	0.080
Δ_{JK} /kHz	-1.619(33)	-0.342
Δ_K /kHz	[0.]	3.816
δ_J /kHz	0.0392(37)	0.016
δ_K /kHz	[0.]	0.180
^{14}N 3/2(χ_{aa}) /MHz	1.900(50)	1.64
^{14}N ¼(χ_{bb}-χ_{cc}) /MHz	1.281(22)	1.58
N	76/27	
σ /kHz	6.0	
Derived Parameters		
P_a /uÅ^2	870.3792(19)	898.41
P_b /uÅ^2	232.6915(19)	218.60
P_c /uÅ^2	35.3766(19)	31.95
^{14}N χ_{aa}/MHz	1.267(33)	1.09
^{14}N χ_{bb}/MHz	1.929(61)	2.62
^{14}N χ_{cc}/MHz	-3.195(61)	-3.71

[a] A, B and C are the rotational constants. Δ_J, Δ_{JK}, Δ_K, δ_J and δ_K are the quartic centrifugal distortion constants. χ_{aa}, χ_{bb} and χ_{cc} are the quadrupole coupling tensor diagonal elements for ^{14}N atom. N is the number of quadrupole hyperfine components/rotational transitions fitted. σ is the rms deviation of the fit. P_α ($\alpha = a$, b or c) are the planar moments of inertia, these are derived from the moments of inertia I_α as for example $P_c = (I_a+I_b-I_c)/2$. [b] Standard errors are given in parentheses in units of the last digits. [c] Parameters in square brackets were kept fixed to those given for the parent species in the fit.

Table S8.9. r_0 structure obtained by the fitting of the rotational constants for all the available isotopologues for the ecb-I-w-a complex and comparison with the r_e (B3LYP-D3/6-311++G(d,p)) *ab initio* structure. The geometrical parameters for water were fixed to its r_0 values [Harmony, M. D., Laurie, V. W., Kuczkowski, R. L., Schwendeman, R. H., Ramsay, D. A., Lovas, F. J., Lafferty, W. J., Maki, A. G. *J. Phys. Chem. Ref. Data* **1979**, 8, 619–721]. The rest of the parameters were fixed to the r_e values, the uncertainties given in parenthesis were obtained from the coordinates uncertainties resulting from the r_0 fitting.

Fitted parameter	r_0	r_e	Derived parameter	r_0	r_e
$r(O_w\cdots H_1)$ /Å	2.0958(6)	2.079	$r(O_w–H_{w1})$ /Å	1.02(1)	0.975
$r(H_{w1}\cdots O_1)$ /Å	1.83(1)	1.913	$\angle(O_1–C_1–N)$ /°	125.100(8)	125.1
$\angle(O_w\cdots H_1–N)$ /°	137.66(3)	138.2	$\angle(H_1\cdots O_w–H_{w1})$ /°	80.3(4)	81.5
$\angle(H_{w1}\cdots O_1–C_1–N)$ /°	-181.5(1)	-175.2	$\angle(O_w–H_{w1}\cdots O_1)$ /°	148.4(4)	148.5

Fixed parameter	r_0	r_e	Fixed parameter	r_0	r_e
$r(O_1–C_1)$ /Å	[1.224]	1.224	$\angle(O_1–C_1–O_2–C_2)$ /°	[0.0]	0.0
$r(N–C_1)$ /Å	[1.352]	1.352	$\angle(C_1–O_2–C_2–C_3)$ /°	[180.0]	179.8
$r(O_2–C_1)$ /Å	[1.351]	1.351	$\angle(N–C_1–O_2–C_2)$ /°	[180.0]	179.4
$r(O_2–C_2)$ /Å	[1.448]	1.448	$\angle(H_1–N–C_1–O_2)$ /°	[180.0]	175.7
$r(C_2–C_3)$ /Å	[1.515]	1.515	$\angle(H_2–N–C_1–O_2)$ /°	[0.0]	5.7
$r(N–H_1)$ /Å	[1.013]	1.013	$\angle(C_1–O_2–C_2–H_3)$ /°	[60.0]	58.4
$r(N–H_2)$ /Å	[1.005]	1.005	$\angle(C_1–O_2–C_2–H_4)$ /°	[-60.0]	-58.8
$r(O_w–H_{w2})$ /Å	[0.965]	0.965	$\angle(O_2–C_2–C_3–H_5)$ /°	[60.0]	60.3
$r(C_2–H_3)$ /Å	[1.092]	1.092	$\angle(O_2–C_2–C_3–H_6)$ /°	[-60.0]	-60.3
$r(C_2–H_4)$ /Å	[1.092]	1.092	$\angle(O_2–C_2–C_3–H_7)$ /°	[180.0]	180.0
$r(C_3–H_5)$ /Å	[1.092]	1.092	$\angle(O_w\cdots H_1–N–C_1)$ /°	[0.0]	-0.8
$r(C_3–H_6)$ /Å	[1.092]	1.092			
$r(C_3–H_7)$ /Å	[1.093]	1.093			
$\angle(O_1–C_1–O_2)$ /°	[123.4]	123.4			
$\angle(O_2–C_1–N)$ /°	[111.5]	111.5			
$\angle(C_1–O_2–C_2)$ /°	[116.1]	116.1			
$\angle(C_1–N–H_1)$ /°	[117.8]	117.8			
$\angle(C_1–N–H_2)$ /°	[120.1]	120.1			
$\angle(O_2–C_2–C_3)$ /°	[107.1]	107.1			
$\angle(O_2–C_2–H_3)$ /°	[108.8]	108.8			
$\angle(O_2–C_2–H_4)$ /°	[108.8]	108.8			
$\angle(C_2–C_3–H_5)$ /°	[110.9]	110.9			
$\angle(C_2–C_3–H_6)$ /°	[110.9]	110.9			
$\angle(C_2–C_3–H_7)$ /°	[109.7]	109.7			
$\angle(H_{w2}–O_w–H_{w1})$ /°	[104.8]	106.4			
$\angle(H_{w1}\cdots O_1–C_1)$ /°	[108.5]	108.5			

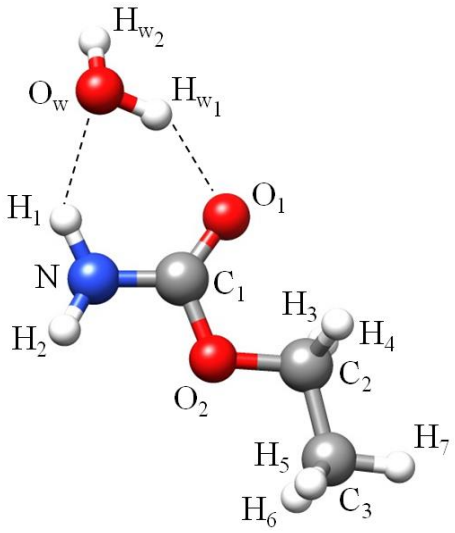

Table S8.10. r_0 structure obtained by the fitting of the rotational constants for all the available isotopologues for the ecb-I-w_2 complex and comparison with the r_e (B3LYP-D3/6-311++G(d,p)) *ab initio* structure. The geometrical parameters for water were fixed to its r_0 values [Harmony, M. D., Laurie, V. W., Kuczkowski, R. L., Schwendeman, R. H., Ramsay, D. A., Lovas, F. J., Lafferty, W. J., Maki, A. G. *J. Phys. Chem. Ref. Data* **1979**, 8, 619–721]. The rest of the parameters were fixed to the r_e values, the uncertainties given in parenthesis were obtained from the coordinates uncertainties resulting from the r_0 fitting.

Fitted parameter	r_0	r_e	Derived parameter	r_0	r_e
$r(O_{w2}\cdots H_1)$ /Å	1.887(7)	1.876	$r(H_{w3}\cdots O_{w1})$ /Å	1.836(5)	1.775
$r(H_{w1}\cdots O_1)$ /Å	1.793(1)	1.767	$r(O_{w2}\cdots O_{w1})$ /Å	2.763(5)	2.722
$\angle(O_{w2}\cdots H_1–N)$ /°	175.0(6)	174.1	$\angle(O_{w2}–H_{w3}\cdots O_{w1})$ /°	160.3(5)	161.0
$\angle(H_{w1}\cdots O_1–C_1)$ /°	129.5(3)	129.4	$\angle(H_{w3}\cdots O_{w1}–H_{w1})$ /°	98.6(2)	98.9
$\angle(H_{w1}\cdots O_1–C_1–O_2)$ /°	175.2(2)	176.5			

Fixed parameter	r_0	r_e	Fixed parameter	r_0	r_e
$r(O_1–C_1)$ /Å	[1.227]	1.227	$\angle(O_1–C_1–O_2–C_2)$ /°	[0.0]	0.2
$r(N–C_1)$ /Å	[1.345]	1.345	$\angle(N–C_1–O_2–C_2)$ /°	[-180.0]	-179.6
$r(O_2–C_1)$ /Å	[1.352]	1.352	$\angle(C_1–O_2–C_2–C_3)$ /°	[180.0]	179.5
$r(O_2–C_2)$ /Å	[1.447]	1.447	$\angle(H_1–N–C_1–O_2)$ /°	[-180.0]	-178.0
$r(C_2–C_3)$ /Å	[1.515]	1.515	$\angle(H_2–N–C_1–O_2)$ /°	[0.0]	-2.8
$r(N–H_1)$ /Å	[1.021]	1.021	$\angle(C_1–O_2–C_2–H_3)$ /°	[60.0]	58.2
$r(N–H_2)$ /Å	[1.006]	1.006	$\angle(C_1–O_2–C_2–H_4)$ /°	[-60.0]	-59.1
$r(C_2–H_3)$ /Å	[1.092]	1.092	$\angle(O_2–C_2–C_3–H_5)$ /°	[-60.0]	-60.4
$r(C_2–H_4)$ /Å	[1.092]	1.092	$\angle(O_2–C_2–C_3–H_6)$ /°	[60.0]	60.2
$r(C_2–H_{m5})$ /Å	[1.092]	1.092	$\angle(O_2–C_2–C_3–H_7)$ /°	[180.0]	179.9
$r(C_2–H_{m6})$ /Å	[1.092]	1.092	$\angle(O_{w2}\cdots H_1–N–C_1)$ /°	[16.0]	16.0
$r(C_2–H_{m7})$ /Å	[1.093]	1.093	$\angle(H_{w3}–O_{w2}\cdots H_1–N)$ /°	[[-14.5]	-14.5
$r(O_{w2}–H_{w3})$ /Å	[0.965]	0.982	$\angle(H_{w4}–O_{w2}–H_{w3}\cdots N)$ /°	[130.0]	130.0
$r(O_{w2}–H_{w4})$ /Å	[0.965]	0.961	$\angle(O_{w1}–H_{w1}\cdots O_1–C_1)$ /°	[-10.2]	-10.2
$r(O_{w1}–H_{w1})$ /Å	[0.965]	0.982	$\angle(H_{w2}–O_{w1}–H_{w1}\cdots O_1)$ /°	[-117.7]	-117.7
$r(O_{w1}–H_{w2})$ /Å	[0.965]	0.961			
$\angle(O_1–C_1–O_2)$ /°	[122.5]	122.5			
$\angle(O_2–C_1–N)$ /°	[111.6]	111.6			
$\angle(C_1–O_2–C_2)$ /°	[116.3]	116.3			
$\angle(O_2–C_2–C_3)$ /°	[107.1]	107.1			
$\angle(C_1–N–H_1)$ /°	[120.5]	120.5			
$\angle(C_1–N–H_2)$ /°	[119.1]	119.1			
$\angle(O_2–C_2–H_3)$ /°	[108.5]	108.5			
$\angle(O_2–C_2–H_4)$ /°	[108.5]	108.5			
$\angle(C_2–C_3–H_5)$ /°	[110.8]	110.8			
$\angle(C_2–C_3–H_6)$ /°	[110.8]	110.8			
$\angle(C_2–C_3–H_7)$ /°	[109.7]	109.7			
$\angle(H_{w3}–O_{w2}\cdots H_1)$ /°	[99.2]	99.2			
$\angle(H_{w4}–O_{w2}–H_{w3})$ /°	[104.8]	105.9			
$\angle(O_{w1}–H_{w1}\cdots O_1)$ /°	[170.3]	170.3			
$\angle(H_{w2}–O_{w1}–H_{w1})$ /°	[104.8]	106.2			

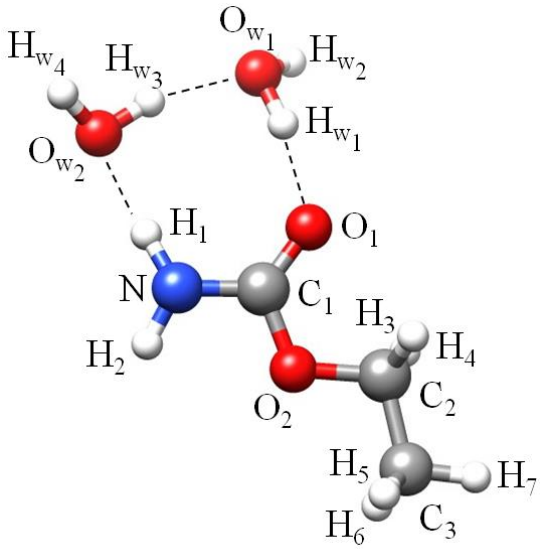

Table S8.11. Experimental and *ab initio* (B3LYP-D3/6-311++G(d,p) quadrupole coupling constants for the ^{14}N atom of the observed complexes with up to three water molecules for the rotamer ecb-I and values reported [reference 8] for the monomer, together with the values of the unbalanced $2p_z$ electronic charge ($(U_p)_z$) both calculated from χ_{cc} and from the natural atomic orbital populations obtained by a Natural Bond Orbital Analysis [reference 35]. The plots represent the correlations between a) experimental values of χ_{cc}/eQq_{210} *vs.* $-(U_p)_z$. b) *Ab initio* values of χ_{cc}/eQq_{210} *vs.* $-(U_p)_z$. c) *Ab initio r*(C–N) *vs.* experimental χ_{cc}/eQq_{210}. d) *Ab initio r*(C=O) *vs.* experimental χ_{cc}/eQq_{210}.

Experimental	Ecb-I	Ecb-I-w-a	Ecb-I-w$_2$	Ecb-I-w$_3$
χ_{aa} /MHz	2.1151(14)	1.6392(12)	1.3519(39)	1.156(24)
χ_{bb} /MHz	2.1667(15)	2.3833(18)	2.440(13)	2.298(25)
χ_{cc} /MHz	-4.2818(15)	-4.0225(18)	-3.792(13)	-3.454(25)
χ_{cc}/eQq_{210}	0.42818	0.40225	0.3792	0.3454

Ab initio	Ecb-I	Ecb-I-w-a	Ecb-I-w$_2$	Ecb-I-w$_3$
χ_{aa} /MHz	2.39	1.81	1.45	1.25
χ_{bb} /MHz	2.47	2.72	2.79	2.53
χ_{cc} /MHz	-4.86	-4.53	-4.24	-3.78
χ_{ab} /MHz	0.30	0.37	0.36	0.43
χ_{ac} /MHz	0.44	-0.07	0.12	0.62
χ_{bc} /MHz	0.56	0.43	-0.40	-1.41
χ_{xx} /MHz	2.80	2.87	2.90	2.88
χ_{yy} /MHz	2.13	1.69	1.37	1.29
χ_{zz} /MHz	-4.93	-4.56	-4.27	-4.17
χ_{zz}/eQq_{210}	0.49	0.46	0.43	0.42
$-(U_p)_z$ NBO	0.43	0.39	0.36	0.32

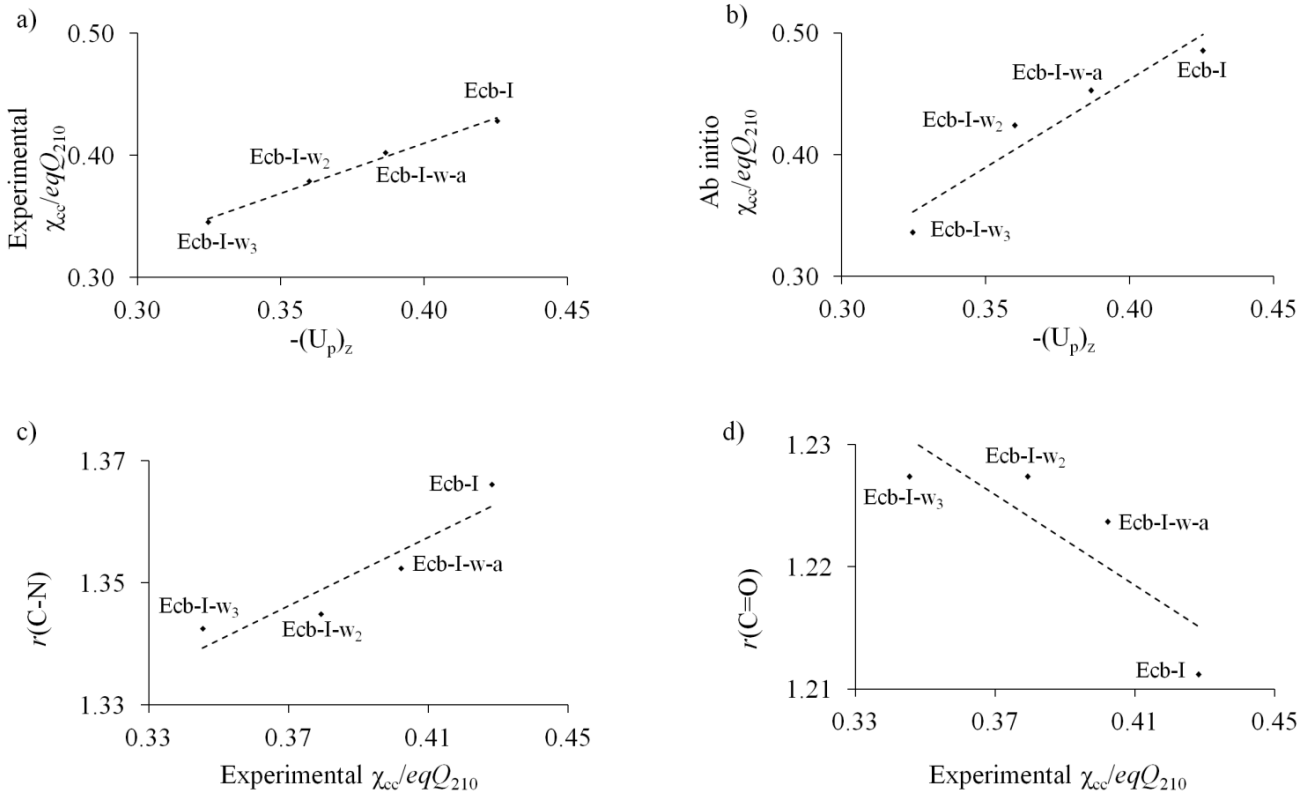

Table S8.12. Experimental and *ab initio* (B3LYP-D3/6-311++G(d,p) quadrupole coupling constants for the ^{14}N atom of the observed complexes with up to three water molecules for the rotamer ecb-II and values reported [reference 8] for the monomer, together with the values of the unbalanced $2p_z$ electronic charge ($(U_p)_z$) both calculated from χ_{cc} and from the natural atomic orbital populations obtained by a Natural Bond Orbital Analysis [reference 35]. The plots represent the correlations between a) experimental values of χ_{cc}/eQq_{210} *vs.* $-(U_p)_z$. b) *Ab initio* values of χ_{cc}/eQq_{210} *vs.* $-(U_p)_z$. c) *Ab initio r*(C–N) *vs*. experimental χ_{cc}/eQq_{210}. d) *Ab initio r*(C=O) *vs*. experimental χ_{cc}/eQq_{210}.

Experimental	Ecb-II	Ecb-II-w-a	Ecb-II-w_2	Ecb-II-w_3
χ_{aa} /MHz	1.8923(11)	1.5927(54)	1.3340(80)	1.267(33)
χ_{bb} /MHz	1.8918(11)	1.799(16)	2.339(30)	1.929(61)
χ_{cc} /MHz	-3.7841(11)	-3.392(16)	-3.673(30)	-3.195(61)
χ_{cc}/eQq_{210}	0.37841	0.3392	0.3673	0.3195

Ab initio	Ecb-II	Ecb-II-w-a	Ecb-II-w_2	Ecb-II-w_3
χ_{aa} /MHz	2.37	1.75	1.49	1.37
χ_{bb} /MHz	2.26	2.36	2.43	1.99
χ_{cc} /MHz	-4.62	-4.11	-3.92	-3.36
χ_{ab} /MHz	-0.21	-0.28	-0.37	-0.48
χ_{ac} /MHz	-1.35	1.10	0.61	-0.14
χ_{bc} /MHz	0.41	-1.31	-1.36	-2.17
χ_{xx} /MHz	2.78	2.86	2.88	2.87
χ_{yy} /MHz	2.12	1.67	1.36	1.27
χ_{zz} /MHz	-4.89	-4.53	-4.25	-4.15
χ_{zz}/eQq_{210}	0.49	0.45	0.42	0.41
$-(U_p)_z$ NBO	0.40	0.34	0.30	0.28

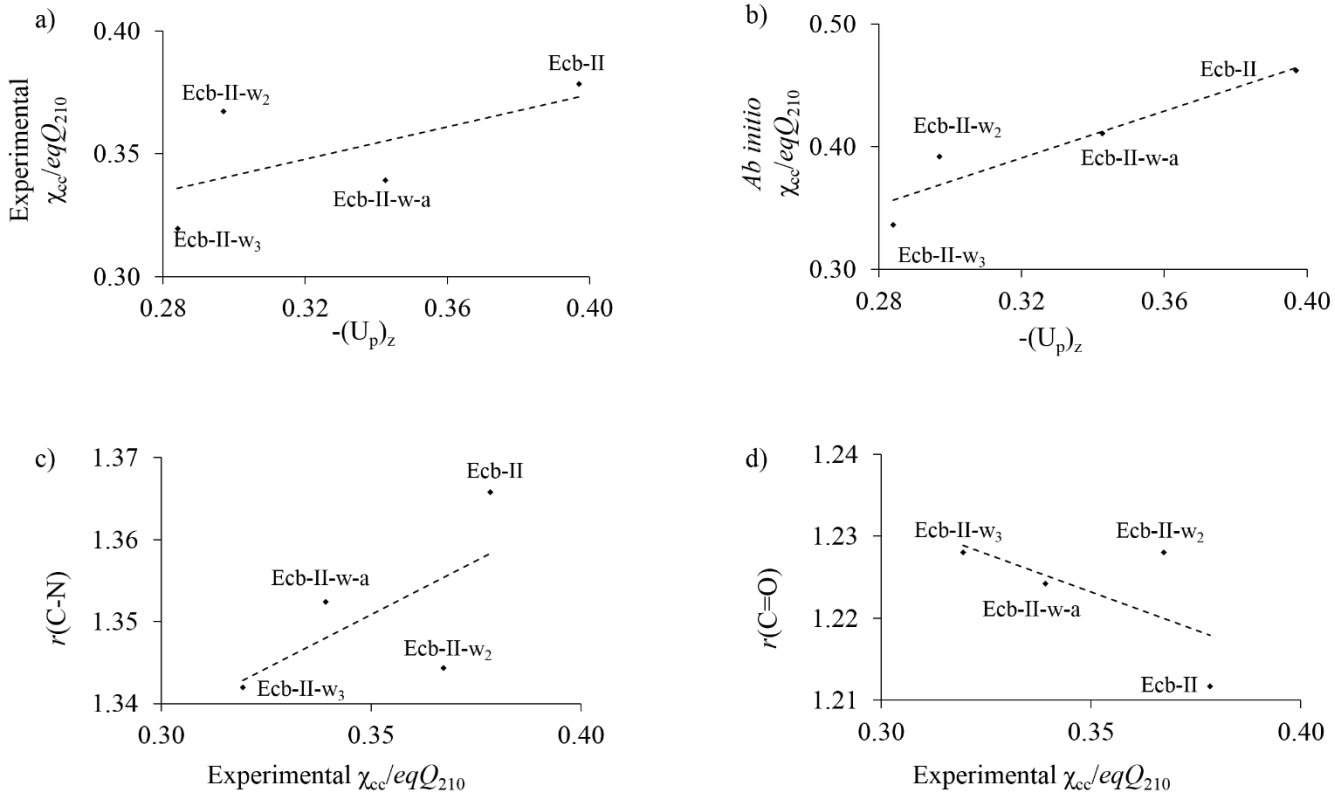

Table S8.13. Observed rotational frequencies and residuals (all the values in MHz) for the parent species of the ecb-I-w-a complex for $J'K'_{-1}K'_{+1}F' \leftarrow J''K''_{-1}K''_{+1}F''$ transitions.

$J'K'_{-1}K'_{+1}$	$J''K''_{-1}K''_{+1}$	F'	F''	Obs.	Res.
$2_{1,2}$	$1_{1,1}$	1	1	3802.3333	0.0023
		3	2	3803.7650	0.0012
		3	2	3803.7679	0.0041
		1	0	3804.1166	-0.0013
		2	1	3804.3415	-0.0005
		2	2	3805.0564	-0.0002
$2_{0,2}$	$1_{0,1}$	1	1	3912.5532	0.0028
		3	2	3913.3455	0.0012
		1	0	3913.7768	-0.0029
		2	2	3913.8908	0.0026
$2_{1,1}$	$1_{1,0}$	1	0	4024.1759	-0.0003
		2	2	4024.7951	0.0006
		3	2	4025.5631	0.0027
		2	1	4025.9963	-0.0047
$3_{1,3}$	$2_{1,2}$	2	2	5703.1407	0.0002
		4	3	5704.9527	0.0004
		3	2	5705.1417	-0.0005
		3	3	5706.4341	-0.0010
$3_{0,3}$	$2_{0,2}$	2	2	5865.8462	0.0009
		4	3	5866.5970	0.0012
		3	2	5866.6425	0.0001
		2	1	5866.6896	-0.0015
		3	3	5867.1804	-0.0058
$3_{2,2}$	$2_{2,1}$	2	1	5871.7186	-0.0056
		4	3	5872.0251	0.0080
		3	2	5872.5435	-0.0004
$3_{2,1}$	$2_{2,0}$	2	1	5877.2441	-0.0069
		4	3	5877.5437	0.0058
$3_{1,2}$	$2_{1,1}$	3	3	6036.8519	-0.0007
		2	1	6037.3084	0.0011
		4	3	6037.5042	-0.0005
		3	2	6037.6177	-0.0008
		2	2	6038.5035	0.0040
$4_{1,4}$	$3_{1,3}$	3	3	7603.1792	-0.0003
		5	4	7605.0696	0.0007
		4	3	7605.1672	0.0002
		3	2	7605.1837	0.0023
$4_{0,4}$	$3_{0,3}$	3	3	7814.9492	-0.0004
		5	4	7815.7057	0.0010
		3	2	7815.7452	-0.0015
		4	3	7815.7545	0.0004
		4	4	7816.3482	0.0036
$4_{2,3}$	$3_{2,2}$	3	2	7828.3103	0.0025
		5	4	7828.3684	0.0020
		4	3	7828.5951	0.0010
$4_{2,2}$	$3_{2,1}$	3	2	7842.0987	0.0004
		5	4	7842.1520	0.0005
		4	3	7842.3427	0.0004
$4_{1,3}$	$3_{1,2}$	4	4	8047.7605	-0.0026
		3	2	8048.2898	-0.0022
		5	4	8048.3646	-0.0008
		4	3	8048.4152	0.0000
		3	3	8049.1730	0.0002
$5_{1,5}$	$4_{1,4}$	4	4	9501.9174	-0.0005
		6	5	9503.8341	0.0003
$5_{0,5}$	$4_{0,4}$	4	4	9758.5413	-0.0022
		6	5	9759.3250	0.0000
		4	3	9759.3491	0.0011
		5	4	9759.3802	-0.0002
		5	5	9760.0151	-0.0052
$5_{2,4}$	$4_{2,3}$	4	3	9783.7370	-0.0033
		6	5	9783.7546	0.0011
		5	4	9783.8771	0.0000
$5_{2,3}$	$4_{2,2}$	4	3	9811.2663	-0.0026
		6	5	9811.2780	0.0011
		5	4	9811.3535	-0.0002
$5_{1,4}$	$4_{1,3}$	4	3	10057.7367	-0.0017
		6	5	10057.7772	0.0002
		5	4	10057.8047	-0.0029
$6_{1,6}$	$5_{1,5}$	7	6	11400.9629	0.0003
		5	4	11401.0115	-0.0003
		6	5	11401.0115	0.0012
$6_{0,6}$	$5_{0,5}$	7	6	11696.1573	0.0011
		5	4	11696.1704	0.0005
		6	5	11696.2198	0.0010
$6_{2,5}$	$5_{2,4}$	5	4	11737.9656	-0.0001
		7	6	11737.9656	-0.0010
		6	5	11738.0467	0.0018
$6_{2,4}$	$5_{2,3}$	7	6	11786.0006	-0.0003
		5	4	11786.0070	0.0018

Table S8.13. Continued.

$J'K'_{-1}K'_{+1}$	$J''K''_{-1}K''_{+1}$	F'	F''	Obs.	Res.
		6	5	11786.0217	-0.0013
$6_{1,5}$	$5_{1,4}$	5	4	12065.3149	-0.0011
		7	6	12065.3397	-0.0005
		6	5	12065.3648	0.0000
$5_{0,5}$	$4_{1,4}$	6	5	3615.3815	0.0007
		5	4	3614.4999	0.0048
		4	3	3615.6521	0.0065
$6_{0,6}$	$5_{1,5}$	6	5	5806.8166	0.0001
		7	6	5807.7022	-0.0008
		5	4	5807.9098	-0.0002
$7_{0,7}$	$6_{1,6}$	7	6	8030.8655	0.0027
		8	7	8031.7255	-0.0016
		6	5	8031.8938	0.0005
$1_{1,1}$	$0_{0,0}$	0	1	8582.0311	-0.0010
		2	1	8583.1034	-0.0010
		1	1	8583.8154	-0.0037
$2_{1,2}$	$1_{0,1}$	1	1	10428.3625	0.0045
		3	2	10429.5686	0.0006
		2	1	10430.3705	0.0014
		2	2	10430.8616	0.0008
$3_{1,3}$	$2_{0,2}$	2	1	12220.9587	-0.0003
		4	3	12221.1769	0.0009
		3	2	12222.1135	-0.0013
$1_{1,0}$	$1_{0,1}$	1	1	6735.2560	0.0000
		1	2	6735.7494	0.0015
		2	1	6736.4614	-0.0012
		1	0	6736.4872	0.0018
		2	2	6736.9621	0.0076
		0	1	6738.2750	0.0020

$J'K'_{-1}K'_{+1}$	$J''K''_{-1}K''_{+1}$	F'	F''	Obs.	Res.
$2_{1,1}$	$2_{0,2}$	2	2	6847.8602	0.0005
		3	2	6848.6264	0.0002
		2	1	6848.7075	0.0008
		1	2	6849.0505	0.0023
		3	3	6849.1659	0.0046
$3_{1,2}$	$3_{0,3}$	3	3	7018.8366	0.0003
		3	2	7019.6376	0.0035
		2	3	7019.7153	0.0025
		4	4	7020.0793	0.0003
		2	2	7020.5131	0.0017
$4_{1,3}$	$4_{0,4}$	4	4	7251.4967	0.0014
		5	5	7252.7394	0.0011
		3	3	7253.0624	0.0022
$5_{1,4}$	$5_{0,5}$	5	5	7549.9246	0.0007
		6	6	7551.1927	0.0003
		4	4	7551.4503	0.0003
$6_{1,5}$	$6_{0,6}$	6	6	7919.0695	0.0019
		7	7	7920.3780	0.0014
		5	5	7920.5957	0.0013
$7_{1,6}$	$7_{0,7}$	7	7	8364.6679	0.0032
		8	8	8366.0198	0.0031
		6	6	8366.2107	0.0011
$8_{1,7}$	$8_{0,8}$	8	8	8893.0279	0.0047
		9	9	8894.4365	0.0015
		7	7	8894.6194	0.0043

Table S8.14. Observed rotational frequencies and residuals (all the values in MHz) for the $^{18}O_w$ species of the ecb-I-w-a complex for $J'K'_{-1}K'_{+1}F' \leftarrow J''K''_{-1}K''_{+1}F''$ transitions.

$J'K'_{-1}K'_{+1}$	$J''K''_{-1}K''_{+1}$	F'	F''	Obs.	Res.
$3_{1,3}$	$2_{1,2}$	4	3	5462.7346	-0.0002
		3	2	5462.9225	-0.0018
$3_{0,3}$	$2_{0,2}$	4	3	5611.5641	-0.0007
		3	2	5611.6109	0.0016
$3_{1,2}$	$2_{1,1}$	4	3	5768.1891	0.0023
		3	2	5768.2966	-0.0033
		2	1	5767.9907	0.0014
$4_{1,4}$	$3_{1,3}$	5	4	7282.3609	-0.0004
		4	3	7282.4586	0.0000
		3	2	7282.4774	0.0034
$4_{0,4}$	$3_{0,3}$	5	4	7476.6779	-0.0012
		4	3	7476.7259	0.0003
		3	2	7476.7259	0.0041
$4_{1,3}$	$3_{1,2}$	3	2	7689.4615	-0.0003
		5	4	7689.5353	0.0001
		4	3	7689.5844	0.0002
$5_{1,5}$	$4_{1,4}$	6	5	9100.8424	0.0000
		5	4	9100.9014	-0.0035
		4	3	9100.9159	0.0019
$5_{0,5}$	$4_{0,4}$	6	5	9337.1655	-0.0010
		4	3	9337.1898	-0.0001
		5	4	9337.2189	0.0008
$5_{1,4}$	$4_{1,3}$	4	3	9609.6272	0.0003
		6	5	9609.6653	0.0001
		5	4	9609.6937	-0.0011

Table S8.15. Observed rotational frequencies and residuals (all the values in MHz) for the parent species of the ecb-I-w$_2$ complex for $J'K'_{-1}K'_{+1}F' \leftarrow J''K''_{-1}K''_{+1}F''$ transitions.

$J'K'_{-1}K'_{+1}$	$J''K''_{-1}K''_{+1}$	F'	F''	Obs.	Res.	$J'K'_{-1}K'_{+1}$	$J''K''_{-1}K''_{+1}$	F'	F''	Obs.	Res.	$J'K'_{-1}K'_{+1}$	$J''K''_{-1}K''_{+1}$	F'	F''	Obs.	Res.
$2_{1,2}$	$1_{1,1}$	3	2	2492.8792	-0.0027			5	4	6221.3337	-0.0013			6	5	7781.6729	0.0000
		2	1	2493.3695	0.0004			4	3	6221.3337	0.0001	$6_{3,4}$	$5_{3,3}$	5	4	7807.1168	0.0026
$2_{0,2}$	$1_{0,1}$	3	2	2595.1920	0.0025	$5_{0,5}$	$4_{0,4}$	6	5	6441.7459	-0.0003			7	6	7807.1314	-0.0009
$2_{1,1}$	$1_{1,0}$	3	2	2702.7495	-0.0007			4	3	6441.7585	-0.0007			6	5	7807.2413	0.0006
$3_{1,3}$	$2_{1,2}$	4	3	3737.8195	0.0019			5	4	6441.8434	-0.0010	$6_{3,3}$	$5_{3,2}$	5	4	7809.4936	-0.0018
		3	2	3737.9842	-0.0020	$5_{2,4}$	$4_{2,3}$	4	3	6488.7288	-0.0024			7	6	7809.5118	-0.0010
$3_{0,3}$	$2_{0,2}$	4	3	3886.1355	0.0017			6	5	6488.7433	0.0000			6	5	7809.6151	-0.0002
		3	2	3886.2050	0.0014			5	4	6488.8538	0.0005	$6_{2,4}$	$5_{2,3}$	6	5	7873.2717	-0.0013
		2	1	3886.2050	-0.0004	$5_{3,3}$	$4_{3,2}$	4	3	6503.3554	0.0046			7	6	7873.3039	-0.0014
$3_{1,2}$	$2_{1,1}$	2	1	4052.2538	-0.0014			6	5	6503.4025	0.0022			5	4	7873.3133	0.0007
		4	3	4052.4502	0.0001			5	4	6503.5973	0.0033	$6_{1,5}$	$5_{1,4}$	5	4	8085.6172	0.0001
		3	2	4052.5465	0.0017	$5_{3,2}$	$4_{3,2}$	4	3	6504.2457	0.0001			7	6	8085.6435	-0.0009
$4_{1,4}$	$3_{1,3}$	5	4	4980.7878	0.0035			6	5	6504.2927	-0.0019			6	5	8085.6814	0.0000
		4	3	4980.8800	0.0017			5	4	6504.4836	-0.0017	$7_{1,7}$	$6_{1,6}$	8	7	8693.0521	0.0007
		3	2	4980.8800	-0.0089	$5_{2,3}$	$4_{2,2}$	6	5	6541.7089	-0.0009			6	5	8693.0831	-0.0005
$4_{0,4}$	$3_{0,3}$	5	4	5169.1287	-0.0003			4	3	6541.7089	0.0012			7	6	8693.1008	-0.0004
		3	2	5169.1587	0.0011			5	4	6541.7293	0.0006	$7_{0,7}$	$6_{0,6}$	8	7	8948.2324	0.0013
		4	3	5169.2117	-0.0006	$5_{1,4}$	$4_{1,3}$	4	3	6744.6914	-0.0011			6	5	8948.2324	-0.0011
$4_{2,3}$	$3_{2,2}$	3	2	5193.6018	0.0019			6	5	6744.7336	-0.0009			7	6	8948.3550	0.0000
		5	4	5193.6486	-0.0008			5	4	6744.7721	0.0001	$7_{2,6}$	$6_{2,5}$	6	5	9071.7807	-0.0011
		4	3	5193.8436	0.0013	$6_{1,6}$	$5_{1,5}$	7	6	7458.8127	0.0000			8	7	9071.7807	-0.0002
$4_{2,2}$	$3_{2,1}$	3	2	5220.2625	0.0043			5	4	7458.8539	-0.0033			7	6	9071.8391	0.0000
		5	4	5220.2965	-0.0004			6	5	7458.8685	0.0004	$7_{3,5}$	$6_{3,4}$	6	5	9112.1299	-0.0024
		4	3	5220.4180	0.0012	$6_{0,6}$	$5_{0,5}$	7	6	7701.9213	-0.0005			8	7	9112.1394	0.0005
$4_{1,3}$	$3_{1,2}$	3	2	5399.9646	0.0000			5	4	7701.9294	0.0012			7	6	9112.2030	-0.0001
		5	4	5400.0405	-0.0006			6	5	7702.0339	-0.0002	$7_{3,4}$	$6_{3,3}$	6	5	9117.4715	-0.0026
		4	3	5400.0886	-0.0007	$6_{2,5}$	$5_{2,4}$	7	6	7781.5970	-0.0011			8	7	9117.4797	0.0000
$5_{1,5}$	$4_{1,4}$	6	5	6221.2680	0.0000			5	4	7781.5970	0.0009			7	6	9117.5337	-0.0009

Table S8.15. Continued.

$J'K'_{-1}K'_{+1}$	$J''K''_{-1}K''_{+1}$	F'	F''	Obs.	Res.
$7_{2,5}$	$6_{2,4}$	7	6	9215.9928	-0.0005
		8	7	9216.0547	-0.0002
		6	5	9216.0660	0.0017
$7_{1,6}$	$6_{1,5}$	6	5	9421.7534	-0.0006
		8	7	9421.7740	0.0000
		7	6	9421.8134	-0.0014
$8_{1,8}$	$7_{1,7}$	9	8	9923.7200	-0.0007
		7	6	9923.7458	0.0006
		8	7	9923.7682	0.0002
$8_{0,8}$	$7_{0,7}$	7	6	10180.1704	0.0000
		9	8	10180.1704	0.0008
		8	7	10180.3011	0.0000
$8_{2,7}$	$7_{2,6}$	7	6	10358.8643	-0.0009
		9	8	10358.8643	0.0006
		8	7	10358.9186	0.0047
$8_{3,6}$	$7_{3,5}$	7	6	10418.3499	-0.0005
		9	8	10418.3499	-0.0023
		8	7	10418.3936	0.0016
$8_{3,5}$	$7_{3,4}$	7	6	10428.9876	-0.0010
		9	8	10428.9876	-0.0012
		8	7	10429.0138	-0.0006
$8_{2,6}$	$7_{2,5}$	8	7	10569.9180	0.0010
		9	8	10569.9947	-0.0002
		7	6	10570.0056	0.0016
$8_{1,7}$	$7_{1,6}$	7	6	10751.9801	-0.0005
		9	8	10751.9971	0.0008
		8	7	10752.0441	0.0010
$9_{1,9}$	$8_{1,8}$	10	9	11150.6694	0.0013
		8	7	11150.6857	-0.0013
		9	8	11150.7153	0.0015
$9_{0,9}$	$8_{0,8}$	10	9	11398.3373	0.0003
		8	7	11398.3373	0.0001
		9	8	11398.4710	-0.0002
$9_{2,8}$	$8_{2,7}$	10	9	11642.4313	0.0006
		8	7	11642.4313	-0.0005
		9	8	11642.4776	0.0005
$9_{3,7}$	$8_{3,6}$	10	9	11725.5909	-0.0006
		8	7	11725.5909	-0.0009
		9	8	11725.6165	-0.0002
$9_{3,6}$	$8_{3,5}$	10	9	11744.9736	0.0000
		8	7	11744.9736	-0.0020
		9	8	11744.9796	0.0011
$9_{2,7}$	$8_{2,6}$	9	8	11933.9528	-0.0003
		10	9	11934.0363	-0.0016
		8	7	11934.0469	0.0011
$9_{1,8}$	$8_{1,7}$	8	7	12075.0301	0.0013
		10	9	12075.0432	0.0015
		9	8	12075.0953	-0.0006
$10_{1,10}$	$9_{1,9}$	11	10	12373.8510	0.0005
		9	8	12373.8644	-0.0013
		10	9	12373.8953	0.0000
$10_{0,10}$	$9_{0,9}$	9	8	12604.4093	0.0003
		11	10	12604.4093	0.0001
		10	9	12604.5408	0.0000
$10_{2,9}$	$9_{2,8}$	11	10	12922.0819	0.0006
		9	8	12922.0819	-0.0023
		10	9	12922.1243	-0.0012
$10_{3,8}$	$9_{3,7}$	9	8	13033.5654	0.0001
		11	10	13033.5654	0.0013
		10	9	13033.5805	0.0000
$10_{3,7}$	$9_{3,6}$	10	9	13066.4950	-0.0007
		11	10	13066.5102	0.0031
		9	8	13066.5102	-0.0001
$10_{2,8}$	$9_{2,7}$	10	9	13305.9092	0.0001
		11	10	13305.9915	-0.0016
		9	8	13306.0004	0.0011
$10_{1,9}$	$9_{1,8}$	9	8	13389.4862	-0.0006
		11	10	13389.4971	-0.0006
		10	9	13389.5607	0.0002

Table S8.16. Observed rotational frequencies and residuals (all the values in MHz) for the $^{18}O_{w1}$ species of the ecb-I-w$_2$ complex for $J'K'_{-1}K'_{+1}F' \leftarrow J''K''_{-1}K''_{+1}F''$ transitions.

$J'K'_{-1}K'_{+1}$	$J''K''_{-1}K''_{+1}$	F'	F''	Obs.	Res.
$5_{1,5}$	$4_{1,4}$	6	5	6075.9230	0.0003
		5	4	6075.9885	-0.0018
		4	3	6075.9885	0.0004
$5_{0,5}$	$4_{0,4}$	6	5	6293.5834	-0.0001
		4	3	6293.5951	-0.0012
		5	4	6293.6845	-0.0001
$5_{1,4}$	$4_{1,3}$	4	3	6595.8623	0.0003
		6	5	6595.9021	-0.0019
		5	4	6595.9412	-0.0010
$6_{1,6}$	$5_{1,5}$	7	6	7284.2396	0.0006
		5	4	7284.2826	-0.0009
		6	5	7284.2940	-0.0011
$6_{0,6}$	$5_{0,5}$	7	6	7523.4512	-0.0008
		5	4	7523.4512	-0.0068
$6_{1,5}$	$5_{1,4}$	5	4	7906.7799	-0.0011
		7	6	7906.8082	-0.0003
		6	5	7906.8473	0.0005
$7_{1,7}$	$6_{1,6}$	8	7	8489.1857	0.0018
		7	6	8489.2354	0.0008
$7_{0,7}$	$6_{0,6}$	8	7	8739.2213	0.0016
		6	5	8739.2213	-0.0007
		7	6	8739.3483	0.0015
$7_{1,6}$	$6_{1,5}$	6	5	9212.7619	0.0042
		8	7	9212.7777	0.0000
		7	6	9212.8197	-0.0002

Table S8.17. Observed rotational frequencies and residuals (all the values in MHz) for the $^{18}O_{w2}$ species of the ecb-I-w$_2$ complex for $J'K'_{-1}K'_{+1}F' \leftarrow J''K''_{-1}K''_{+1}F''$ transitions.

$J'K'_{-1}K'_{+1}$	$J''K''_{-1}K''_{+1}$	F'	F''	Obs.	Res.
$5_{1.5}$	$4_{1.4}$	5	4	6041.8857	0.0000
		4	3	6041.8857	0.0009
$5_{0.5}$	$4_{0.4}$	6	5	6254.2467	0.0002
		4	3	6254.2593	-0.0005
		5	4	6254.3413	-0.0008
$5_{1.4}$	$4_{1.3}$	4	3	6543.4492	-0.0015
		6	5	6543.4898	-0.0027
		5	4	6543.5274	-0.0018
$6_{1.6}$	$5_{1.5}$	7	6	7243.9250	0.0002
		5	4	7243.9679	-0.0015
		6	5	7243.9796	0.0001
$6_{0.6}$	$5_{0.5}$	7	6	7478.8206	0.0005
		5	4	7478.8206	-0.0059
		6	5	7478.9293	-0.0003
$6_{1.5}$	$5_{1.4}$	7	6	7844.7338	0.0028
		6	5	7844.7743	0.0072
$7_{1.7}$	$6_{1.6}$	8	7	8442.9348	-0.0008
		6	5	8442.9688	0.0008
		7	6	8442.9861	0.0012
$7_{0.7}$	$6_{0.6}$	8	7	8690.3887	0.0026
		6	5	8690.3887	0.0000
		7	6	8690.5080	0.0008
$7_{1.6}$	$6_{1.5}$	6	5	9141.5214	-0.0009
		8	7	9141.5405	-0.0016
		7	6	9141.5806	-0.0011

Table S8.18. Observed rotational frequencies and residuals (all the values in MHz) for the parent species of the ecb-I-w$_3$ complex in the $v = 0$ and $v = 1$ vibrational states for $J'K'_{-1}K'_{+1}v'F' \leftarrow J''K''_{-1}K''_{+1}v''F''$ transitions.

$J'K'_{-1}K'_{+1}$	$J''K''_{-1}K''_{+1}$	v	F'	F''	Obs.	Res.
$6_{1,6}$	$5_{1,5}$	*0*	7	6	5132.4223	0.0008
		0	5	4	5132.4673	0.0058
		0	6	5	5132.4761	-0.0003
		1	7	6	5132.4350	0.0000
		1	5	4	5132.4761	0.0011
		1	6	5	5132.4917	0.0017
$6_{0,6}$	$5_{0,5}$	*0*	7	6	5297.9925	-0.0008
		0	5	4	5297.9925	-0.0037
		0	6	5	5298.1181	0.0005
		1	7	6	5298.0066	0.0006
		1	5	4	5298.0066	-0.0022
		1	6	5	5298.1304	0.0002
$6_{2,5}$	$5_{2,4}$	*0*	5	4	5370.1514	-0.0001
		0	7	6	5370.1514	-0.0027
		0	6	5	5370.2223	-0.0010
		1	5	4	5370.1645	0.0004
		1	7	6	5370.1645	-0.0020
		1	6	5	5370.2352	-0.0005
$6_{2,4}$	$5_{2,3}$	*0*	6	5	5453.2147	0.0008
		0	7	6	5453.2607	-0.0037
		0	5	4	5453.2729	0.0007
		1	6	5	5453.2323	0.0061
		1	7	6	5453.2813	0.0046
		1	5	4	5453.2874	0.0030
$6_{1,5}$	$5_{1,4}$	*0*	5	4	5590.5654	0.0017
		0	7	6	5590.5918	0.0011
		0	6	5	5590.6293	-0.0022
		1	5	4	5590.5773	0.0022
		1	7	6	5590.6039	0.0019
		1	6	5	5590.6424	-0.0005
$7_{1,7}$	$6_{1,6}$	*0*	8	7	5979.9326	0.0000
		0	6	5	5979.9615	0.0002
		0	7	6	5979.9861	0.0030
		1	8	7	5979.9470	-0.0013
		1	6	5	5979.9705	-0.0065
		1	7	6	5980.0002	0.0013
$7_{0,7}$	$6_{0,6}$	*0*	8	7	6148.2422	-0.0008
		0	6	5	6148.2422	-0.0013
		0	7	6	6148.3776	0.0002
		1	8	7	6148.2574	-0.0004
		1	6	5	6148.2574	-0.0009
		1	7	6	6148.3912	-0.0009
$7_{2,6}$	$6_{2,5}$	*0*	6	5	6258.9883	-0.0008
		0	8	7	6258.9883	-0.0010
		0	7	6	6259.0437	-0.0018
		1	6	5	6259.0031	-0.0006
		1	8	7	6259.0031	-0.0008
		1	7	6	6259.0590	-0.0011
$7_{2,5}$	$6_{2,4}$	*0*	7	6	6388.5315	-0.0016
		0	8	7	6388.6058	-0.0019
		0	6	5	6388.6168	0.0001
		1	7	6	6388.5456	-0.0017
		1	8	7	6388.6191	-0.0028
		1	6	5	6388.6311	0.0001
$7_{1,6}$	$6_{1,5}$	*0*	6	5	6511.4976	-0.0004
		0	8	7	6511.5190	0.0010
		1	6	5	6511.5623	-0.0026
		1	7	6	6511.5190	0.0076
		1	8	7	6511.5324	0.0011
		1	7	6	6511.5772	-0.0010
$8_{1,8}$	$7_{1,7}$	*0*	9	8	6824.4004	0.0015
		0	7	6	6824.4184	-0.0021
		0	8	7	6824.4487	0.0014
		1	9	8	6824.4184	0.0014
		1	7	6	6824.4372	-0.0014
		1	8	7	6824.4666	0.0012
$8_{0,8}$	$7_{0,7}$	*0*	9	8	6987.0686	-0.0014
		0	7	6	6987.0686	-0.0009
		0	8	7	6987.2067	-0.0014
		1	9	8	6987.0856	-0.0015
		1	7	6	6987.0856	-0.0009
		1	8	7	6987.2268	0.0016
$8_{2,7}$	$7_{2,6}$	*0*	9	8	7144.9923	0.0014
		0	7	6	7144.9923	-0.0014
		0	8	7	7145.0406	0.0005
		1	9	8	7145.0073	-0.0001
		1	7	6	7145.0073	-0.0030
		1	8	7	7145.0553	-0.0014
$8_{2,6}$	$7_{2,5}$	*0*	8	7	7332.3411	-0.0005
		0	9	8	7332.4272	0.0006
		0	7	6	7332.4373	0.0027
		1	8	7	7332.3552	-0.0026
		1	9	8	7332.4455	0.0027
		1	7	6	7332.4507	0.0000

Table S8.18. Continued.

$J'K'_{-1}K'_{+1}$	$J''K''_{-1}K''_{+1}$	v	F'	F''	Obs.	Res.
$8_{1,7}$	$7_{1,6}$	*0*	7	6	7426.7362	0.0000
		0	9	8	7426.7515	-0.0003
		0	8	7	7426.8072	0.0001
		1	7	6	7426.7515	0.0000
		1	9	8	7426.7671	0.0000
		1	8	7	7426.8216	-0.0006
$9_{1,9}$	$8_{1,8}$	*0*	10	9	7665.7711	0.0011
		0	8	7	7665.7848	-0.0020
		0	9	8	7665.8185	0.0015
		1	10	9	7665.7923	0.0019
		1	8	7	7665.8052	-0.0020
		1	9	8	7665.8395	0.0021
$9_{0,9}$	$8_{0,8}$	*0*	10	9	7815.8974	-0.0010
		0	8	7	7815.8974	-0.0041
		0	9	8	7816.0356	-0.0007
		1	10	9	7815.9161	-0.0016
		1	8	7	7815.9161	-0.0047
		1	9	8	7816.0551	-0.0005
$9_{2,8}$	$8_{2,7}$	*0*	10	9	8027.8006	0.0010
		0	8	7	8027.8006	0.0013
		0	9	8	8027.8499	0.0020
		1	10	9	8027.8180	-0.0002
		1	8	7	8027.8180	0.0000
		1	9	8	8027.8669	0.0003
$9_{2,7}$	$8_{2,6}$	*0*	9	8	8282.7422	-0.0009
		0	10	9	8282.8250	-0.0028
		0	8	7	8282.8331	-0.0008
		1	9	8	8282.7565	-0.0046

$J'K'_{-1}K'_{+1}$	$J''K''_{-1}K''_{+1}$	v	F'	F''	Obs.	Res.
		1	10	9	8282.8414	-0.0044
		1	8	7	8282.8511	-0.0008
$9_{1,8}$	$8_{1,7}$	*0*	8	7	8334.9995	-0.0003
		0	10	9	8335.0154	0.0020
		0	9	8	8335.0799	0.0016
		1	8	7	8335.0154	-0.0016
		1	10	9	8335.0284	-0.0021
		1	9	8	8335.0952	-0.0001
$10_{1,10}$	$9_{1,9}$	*0*	11	10	8504.1014	-0.0007
		0	9	8	8504.1164	0.0004
		0	10	9	8504.1508	0.0028
		1	11	10	8504.1285	0.0036
		1	9	8	8504.1361	-0.0025
		1	10	9	8504.1716	0.0009
$10_{0,10}$	$9_{0,9}$	*0*	11	10	8636.9773	-0.0016
		0	9	8	8636.9773	-0.0009
		0	10	9	8637.1052	-0.0002
		1	11	10	8636.9996	-0.0010
		1	9	8	8636.9996	-0.0002
		1	10	9	8637.1264	-0.0007
$10_{2,9}$	$9_{2,8}$	*0*	11	10	8907.0669	0.0019
		0	9	8	8907.0669	0.0013
		0	10	9	8907.1136	0.0012
		1	11	10	8907.0876	0.0018
		1	9	8	8907.0876	0.0012
		1	10	9	8907.1344	0.0012
$10_{2,8}$	$9_{2,7}$	*0*	10	9	9236.9771	0.0004
		0	11	10	9237.0517	-0.0013

$J'K'_{-1}K'_{+1}$	$J''K''_{-1}K''_{+1}$	v	F'	F''	Obs.	Res.
		0	9	8	9237.0562	-0.0009
		1	10	9	9236.9988	0.0022
		1	11	10	9237.0719	-0.0010
		1	9	8	9237.0778	0.0008
$10_{1,9}$	$9_{1,8}$	*0*	9	8	9234.8897	0.0029
		0	11	10	9234.8973	-0.0012
		0	10	9	9234.9760	0.0017
		1	9	8	9234.9089	0.0030
		1	11	10	9234.9159	-0.0017
		1	10	9	9234.9943	0.0009
$11_{1,11}$	$10_{1,10}$	*0*	12	11	9339.5438	-0.0010
		0	10	9	9339.5571	0.0012
		0	11	10	9339.5904	0.0010
		1	12	11	9339.5701	0.0002
		1	10	9	9339.5831	0.0022
		1	11	10	9339.6165	0.0021
$11_{0,11}$	$10_{0,10}$	*0*	12	11	9452.8708	-0.0028
		0	10	9	9452.8708	-0.0045
		0	11	10	9452.9855	-0.0037
		1	12	11	9452.8965	-0.0012
		1	10	9	9452.8965	-0.0028
		1	11	10	9453.0127	-0.0005
$11_{2,10}$	$10_{2,9}$	*0*	12	11	9782.4917	0.0038
		0	10	9	9782.4917	0.0033
		0	11	10	9782.5347	-0.0011
		1	12	11	9782.5139	0.0030
		1	10	9	9782.5139	0.0025
		1	11	10	9782.5556	-0.0031

Table S8.18. Continued.

$J'K'_{-1}K'_{+1}$	$J''K''_{-1}K''_{+1}$	v	F'	F''	Obs.	Res.
$11_{2,9}$	$10_{2,8}$	*0*	11	10	10191.9160	-0.0005
		0	12	11	10191.9798	0.0006
		0	10	9	10191.9798	-0.0014
		1	11	10	10191.9399	0.0017
		1	12	11	10191.9988	-0.0020
		1	10	9	10191.9988	-0.0041
$11_{1,10}$	$10_{1,9}$	*0*	10	9	10124.9342	0.0013
		0	12	11	10124.9442	0.0007
		0	11	10	10125.0316	0.0007
		1	10	9	10124.9556	0.0017
		1	12	11	10124.9639	-0.0006
		1	11	10	10125.0516	-0.0002

Table S8.19. Observed rotational frequencies and residuals (all the values in MHz) for the parent species of the ecb-II-w-a complex for $J'K'_{-1}K'_{+1}F' \leftarrow J''K''_{-1}K''_{+1}F''$ transitions.

$J'K'_{-1}K'_{+1}$	$J''K''_{-1}K''_{+1}$	F'	F''	Obs.	Res.
$1_{0,1}$	$0_{0,0}$	0	1	2274.7162	-0.0081
		2	1	2275.4418	0.0007
		1	1	2275.9202	0.0013
$2_{1,2}$	$1_{1,1}$	3	2	4402.0643	-0.0018
		1	0	4402.2719	0.0018
		2	1	4402.6252	0.0083
		2	2	4403.1645	0.0082
$2_{0,2}$	$1_{0,1}$	1	1	4546.1221	0.0036
		3	2	4546.8944	-0.0031
		2	1	4546.9538	-0.0080
		1	0	4547.3124	-0.0005
		2	2	4547.4337	-0.0060
$2_{1,1}$	$1_{1,0}$	1	0	4698.6173	0.0026
		3	2	4699.8205	0.0012
		2	1	4700.2554	-0.0032
		1	1	4701.1592	0.0007
$3_{1,3}$	$2_{1,2}$	4	3	6600.7096	0.0044
		2	1	6600.8481	-0.0170
		3	2	6600.9004	0.0125
$3_{0,3}$	$2_{0,2}$	4	3	6810.1419	0.0025
		3	2	6810.2021	-0.0042
$3_{2,2}$	$2_{2,1}$	2	1	6826.1683	-0.0067
		4	3	6826.4673	0.0078
		3	2	6826.9866	0.0151
$3_{2,1}$	$2_{2,0}$	2	1	6842.5486	0.0044
		4	3	6842.7994	-0.0185
		3	2	6843.2785	-0.0034
$3_{1,2}$	$2_{1,1}$	2	1	7046.9842	-0.0044
		4	3	7047.1497	-0.0004
		3	2	7047.2693	-0.0021
$3_{0,3}$	$2_{1,2}$	2	2	2969.4752	0.0105
		3	2	2970.2884	0.0011
		4	3	2970.7689	0.0008
		2	1	2971.1647	0.0043
		3	3	2971.3706	-0.0068
$4_{0,4}$	$3_{1,3}$	4	3	5430.6961	0.0086
		5	4	5431.2809	0.0071
		3	2	5431.5264	-0.0161
$1_{1,0}$	$1_{0,1}$	1	2	4132.2702	0.0027
		1	0	4132.9751	-0.0090
		2	2	4133.2929	0.0080
		0	1	4134.3325	-0.0009
$2_{1,1}$	$2_{0,2}$	2	2	4285.0857	-0.0006
		3	3	4286.2095	0.0027
		1	1	4286.8369	0.0073
$4_{1,3}$	$4_{0,4}$	4	4	4852.1304	-0.0026
		5	5	4853.2172	0.0004
		3	3	4853.4934	-0.0022
$3_{1,2}$	$3_{0,3}$	3	3	4522.1508	-0.0006
		4	4	4523.2179	0.0002
		2	2	4523.5927	0.0017
$5_{1,4}$	$5_{0,5}$	5	5	5286.4076	0.0002
		6	6	5287.5396	0.0018
		4	4	5287.7685	0.0003

Table S8.20. Observed rotational frequencies and residuals (all the values in MHz) for the parent species of the ecb-II-w_2 complex for $J'K'_{-1}K'_{+1}F' \leftarrow J''K''_{-1}K''_{+1}F''$ transitions.

$J'K'_{-1}K'_{+1}$	$J''K''_{-1}K''_{+1}$	F'	F''	Obs.	Res.
$2_{1,2}$	$1_{1,1}$	3	2	2815.4147	0.0035
		1	0	2815.8066	-0.0014
		2	1	2815.8873	-0.0030
$2_{0,2}$	$1_{0,1}$	3	2	2935.3681	0.0024
		2	1	2935.4486	0.0021
		1	0	2935.6898	-0.0088
$2_{1,1}$	$1_{1,0}$	3	2	3065.4751	-0.0017
		2	1	3065.8301	0.0031
$3_{1,3}$	$2_{1,2}$	4	3	4220.1222	0.0033
		3	2	4220.2974	0.0071
		2	1	4220.2974	-0.0041
$3_{0,3}$	$2_{0,2}$	4	3	4390.3320	0.0023
		3	2	4390.4276	-0.0006
$3_{2,2}$	$2_{2,1}$	2	1	4410.4490	-0.0118
		4	3	4410.6933	-0.0057
		3	2	4411.1322	0.0043
$3_{2,1}$	$2_{2,0}$	2	1	4430.9087	0.0036
		4	3	4431.1210	-0.0041
		3	2	4431.4684	-0.0029
$3_{1,2}$	$2_{1,1}$	2	1	4594.7673	0.0006
		4	3	4594.9567	-0.0001
		3	2	4595.0571	-0.0004
$4_{1,4}$	$3_{1,3}$	5	4	5621.1989	0.0034
		3	2	5621.2964	0.0014
		4	3	5621.2964	0.0001
$4_{0,4}$	$3_{0,3}$	5	4	5830.3222	-0.0054
		3	2	5830.3623	0.0119
		4	3	5830.4501	0.0015
$4_{2,3}$	$3_{2,2}$	3	2	5876.9458	-0.0122
		5	4	5877.0026	-0.0057
		4	3	5877.1982	-0.0050
$4_{3,2}$	$3_{3,1}$	3	2	5890.6978	0.0099
		5	4	5890.8419	0.0052
		4	3	5891.2132	0.0050
$4_{2,2}$	$3_{2,1}$	5	4	5927.6798	0.0019
		4	3	5927.7573	-0.0045
$4_{1,3}$	$3_{1,2}$	3	2	6120.2303	0.0017
		5	4	6120.3095	0.0052
		4	3	6120.3670	0.0040
$5_{1,5}$	$4_{1,4}$	6	5	7017.7618	-0.0058
		4	3	7017.8462	0.0164
		5	4	7017.8462	0.0022
$5_{0,5}$	$4_{0,4}$	6	5	7251.3879	0.0000
		4	3	7251.3879	-0.0084
		5	4	7251.5342	0.0044
$5_{2,4}$	$4_{2,3}$	6	5	7339.8609	-0.0105
		4	3	7339.8609	0.0030
		5	4	7339.9759	-0.0116
$5_{2,3}$	$4_{2,2}$	6	5	7439.6854	-0.0009
		5	4	7439.6854	0.0179
		4	3	7439.6854	-0.0020

Table S8.21. Observed rotational frequencies and residuals (all the values in MHz) for the parent species of the ecb-II-w$_3$ complex for $J'K'_{-1}K'_{+1}F' \leftarrow J''K''_{-1}K''_{+1}F''$ transitions.

$J'K'_{-1}K'_{+1}$	$J''K''_{-1}K''_{+1}$	F'	F''	Obs.	Res.
$3_{1,3}$	$2_{1,2}$	4	3	2895.2719	0.0005
		3	2	2895.4329	-0.0003
		2	1	2895.4329	0.0072
$3_{0,3}$	$2_{0,2}$	4	3	3026.7290	0.0030
		3	2	3026.8270	-0.0064
$3_{1,2}$	$2_{1,1}$	2	1	3194.3978	0.0000
		4	3	3194.5675	0.0062
		3	2	3194.6643	0.0007
$4_{1,4}$	$3_{1,3}$	5	4	3854.4749	-0.0059
		3	2	3854.5731	0.0068
		4	3	3854.5731	-0.0051
$4_{0,4}$	$3_{0,3}$	3	2	4011.1289	-0.0180
		5	4	4011.1289	0.0012
		4	3	4011.2535	-0.0058
$4_{2,3}$	$3_{2,2}$	3	2	4060.1557	-0.0047
		5	4	4060.2139	0.0050
$4_{1,3}$	$3_{1,2}$	3	2	4252.5545	-0.0054
		5	4	4252.6289	0.0044
		4	3	4252.6931	0.0050
$5_{1,5}$	$4_{1,4}$	6	5	4809.1184	-0.0041
		4	3	4809.2011	0.0252
		5	4	4809.2011	0.0034
$5_{0,5}$	$4_{0,4}$	4	3	4976.5887	-0.0042
		6	5	4976.5887	0.0023
		5	4	4976.7378	0.0004
$5_{2,4}$	$4_{2,3}$	6	5	5068.4788	-0.0039
		4	3	5068.4788	0.0083
		5	4	5068.5976	0.0017
$5_{2,3}$	$4_{2,2}$	5	4	5172.2936	-0.0159
		4	3	5172.3452	0.0034
		6	5	5172.3452	0.0050
$5_{1,4}$	$4_{1,3}$	4	3	5304.2547	-0.0071
		6	5	5304.3040	0.0057
		5	4	5304.3602	0.0025
$6_{1,6}$	$5_{1,5}$	7	6	5758.6793	0.0029
		6	5	5758.7482	0.0062
$6_{0,6}$	$5_{0,5}$	7	6	5922.2588	0.0011
		5	4	5922.2588	-0.0031
		6	5	5922.4146	-0.0041
$6_{2,5}$	$5_{2,4}$	7	6	6072.2460	-0.0048
		5	4	6072.2460	-0.0006
		6	5	6072.3368	0.0016
$6_{3,4}$	$5_{3,3}$	5	4	6121.5727	0.0185
		7	6	6121.5727	0.0015
		6	5	6121.6624	-0.0040
$6_{3,3}$	$5_{3,2}$	5	4	6131.7295	-0.0111
		7	6	6131.7623	0.0075
		6	5	6131.8277	-0.0019
$6_{2,4}$	$5_{2,3}$	6	5	6246.2693	0.0076
		7	6	6246.3340	0.0015
		5	4	6246.3340	-0.0063
$6_{1,5}$	$5_{1,4}$	5	4	6347.2507	-0.0117
		7	6	6347.2964	0.0089
		6	5	6347.3562	0.0023
$7_{1,7}$	$6_{1,6}$	8	7	6702.9396	-0.0088
		7	6	6703.0117	0.0026
$7_{0,7}$	$6_{0,6}$	8	7	6850.4824	0.0044
		6	5	6850.4824	0.0028
		7	6	6850.6327	-0.0018
$7_{2,6}$	$6_{2,5}$	6	5	7070.6842	0.0032
		8	7	7070.6842	0.0023
		7	6	7070.7539	0.0009
$7_{3,5}$	$6_{3,4}$	8	7	7146.9228	-0.0090
		6	5	7146.9228	-0.0025
$7_{3,4}$	$6_{3,3}$	6	5	7169.5455	-0.0080
		6	7	7169.5455	-0.0026
		7	6	7169.5899	0.0094
$7_{2,5}$	$6_{2,4}$	7	6	7332.0412	0.0016
		6	5	7332.1190	-0.0082
		8	7	7332.1190	-0.0012
$7_{1,6}$	$6_{1,5}$	8	7	7378.8746	-0.0011
		6	5	7378.8746	0.0183
		7	6	7378.9481	-0.0063
$8_{0,8}$	$7_{0,7}$	9	8	7766.0969	0.0082
		7	6	7766.0969	0.0048
		8	7	7766.2247	-0.0070

Chapter IX

Microsolvated complexes of ibuprofen as revealed by high-resolution rotational spectroscopy.

Direct transcription from the manuscript accepted for publication in *Phys. Chem. Chem. Phys.*

P. Pinacho, A. Krin, C. Pérez, S. Zinn, J. C. López, S. Blanco, M. Schnell

Abstract

Hydrogen-bonded complexes between ibuprofen and water generated in a supersonic expansion were characterized by chirped-pulse Fourier transform microwave spectroscopy in the 2-8 GHz frequency range. Four spectra were observed allowing to determine their rotational parameters. Comparison with quantum-chemical calculations led to their identification as the lowest energy 1:1 ibuprofen – water complexes. These correspond to the complexes between water and the four different conformers of ibuprofen previously detected in the gas phase, owing to their similar stabilization energies and abundances. Water seems to not change the conformational distribution of ibuprofen.

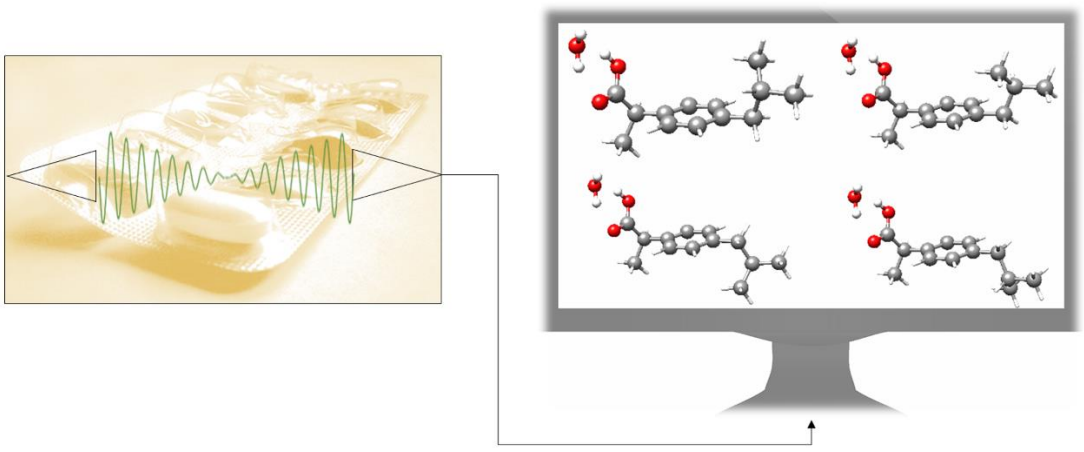

9.1 Introduction

(*RS*)-2-(4-(2-Methylpropyl)phenyl)propanoic acid, best known as ibuprofen (Scheme 9.1), is one of the most used non-steroidal anti-inflammatory medicines.[1,2] Ibuprofen has a polar end, the carboxylic acid group, which can act both as hydrogen donor and hydrogen acceptor establishing moderate to strong interactions with other polar molecules. The other part of ibuprofen is non-polar. Ibuprofen has a high solubility in organic solvents, such as acetone or propanol, but exhibits a low solubility in water.[3] It should be noted that ibuprofen has a chiral center (marked atom in Scheme 9.1), the α–carbon atom, connecting the carboxylic acid and the phenyl ring. It is reported that the *S*-enantiomer of ibuprofen has a higher pharmacological activity than the *R*-enantiomer.[4] In mammals, an enzyme of the alpha-methylacyl-CoA racemase family transforms *in vivo* the less-active *R* to the active *S* form. This conversion is of importance because it allows ibuprofen to be distributed as a racemate.[4,5]

The anti-inflammatory properties of ibuprofen arise from inhibiting the formation of prostaglandins, the molecules responsible for several pathological processes such as cellular inflammation or pain sensitization, by blocking the catalytic active site of cyclooxygenase (COX) enzymes[6] that convert arachidonic acid into prostaglandin PGH_2,[7] the precursor of various other prostaglandins. This blocking occurs through the interaction of the carboxyl group of ibuprofen with the amino acid residues inside the enzymatic channel.

It is well known that water molecules form part of the structures of biological macromolecules,[8] playing a decisive role in many biological processes such as protein folding,[9] conformational[10] or tautomeric[11] equilibria among others. Water molecules are also present inside the cyclooxygenase channels and seem to play an important structural role through water-mediated interactions between different amino acid residues.[7] However, the extent to which water molecules contribute to the inhibition on COX enzymes has not been shown. Furthermore, addition of water might influence the structures of the respective solute molecules.[12] This makes it interesting to study the interactions between ibuprofen and water.

A better knowledge of the solute-solvent interactions can be achieved by studying the microsolvated solute complex in the isolated environment of a supersonic jet, where other interactions occurring in condensed phases are not present. Those complexes can be considered as the first steps of the solvation process. Microsolvated complexes with different degrees of hydration formed in a supersonic expansion can be characterized by high-resolution rotational spectroscopy.

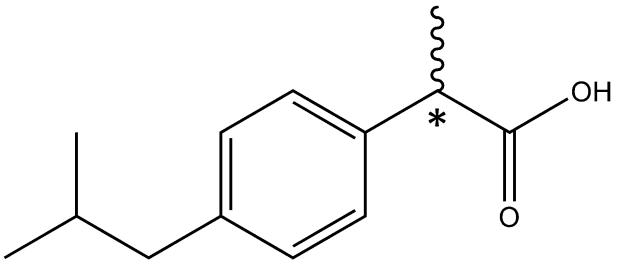

Scheme 9.1. Ibuprofen (IUPAC: (*RS*)-2-(4-(2-Methylpropyl)phenyl)propanoic acid). The asterisk denotes the stereogenic center.

Complexes of different kinds of biologically important molecules with water have been already studied, contributing relevant information about solute-solvent interactions in those systems.[13] For example, it has been recently shown that microsolvation may not only affect the structure of the solute,[12] but also its conformational preferences as observed for the 12C4 crown ether.[13d]

The ibuprofen monomer has already been studied in the gas phase by high-resolution chirped-pulse Fourier transform microwave (CP-FTMW) spectroscopy[14] to elucidate its structure.[15] Four conformers were found which differ in the arrangement of the flexible isobutyl group. Their structures are closely related and share the same kind of stabilization forces, which explains why the spectra of the four conformers showed similar intensities, pointing to comparable populations in the molecular beam.

In the present work, we studied the microwave spectrum of ibuprofen in order to characterize the microsolvated complexes generated in the supersonic expansion and analyze the stabilization forces involved in their formation. Different possibilities for the interaction between ibuprofen and water have been explored, which may serve as a model for the hydrogen bond interactions taking place inside the COX enzymes. An important aspect in this case is the possible influence of water on the conformational landscape of ibuprofen.

9.2 Experimental and theoretical methods

Broadband Fourier transform microwave spectroscopy.

The study of the microsolvated complexes of ibuprofen was carried out using the Hamburg broadband chirped-pulse Fourier transform microwave (CP-FTMW) spectrometer COMPACT.[16] Ibuprofen was purchased (Sigma-Aldrich 98%, melting point 76°C) and used without further purification. Ibuprofen was held in a reservoir and heated to 115°C. Its vapour was mixed with the carrier gas (Ne, 3 bar stagnation pressure) before the supersonic expansion into the vacuum chamber. No water was added to the experiment, which lets us assume that the ibuprofen-water complexes were formed from water molecules remaining in the carrier gas and the gas tubes. Another source might be crystallization water present in the commercial sample. The complexes were excited using a 4 μs long linear frequency chirp covering the range from 2 to 8 GHz (300000 acquisitions). The chirp was amplified by a TWT amplifier (300 W power) and broadcast into the vacuum chamber using a horn antenna. The free induction decay (FID) emission signal was recorded for 40 μs and Fourier transformed to the frequency domain, resulting in a frequency resolution of 25 kHz. The fast-frame option was applied.[17]

Quantum-chemical calculations.

Prior to the analysis of the microwave spectrum, the Potential Energy Surface (PES) for the microsolvation of ibuprofen was explored using quantum-chemical calculations[18] at the B3LYP-D3/aug-cc-pVDZ level of theory.[19,20] Grimme´s empirical dispersion correction (GD3)[21] has been used to obtain more accurate predictions. Based on the resulting structures, further optimizations were performed at the MP2/6-311++G(d,p) level of theory.[22,23] From the PES study, optimized geometries for several ibuprofen – water

complexes were obtained and used to predict their spectra on the basis of the calculated rotational constants and electric dipole moment components.

9.3 Results and discussion

Ibuprofen – water complexes potential energy surface.

As mentioned previously, the carboxyl group is the only polar group present in ibuprofen. It can present stabilizing hydrogen bond interactions with the water molecule. For each of the observed conformers of ibuprofen (C1, C2, C3 and C4)[15] different possibilities for the interactions with one water molecule have been explored (Figure 9.1 and Figures S9.2-S9.4). Table 9.1 summarizes the rotational parameters obtained at the B3LYP-D3/aug-cc-pVDZ level of theory. Additional calculated rotational parameters are presented in Table S9.2 (supplementary material). The results of the MP2/6-311++G(d,p) calculations are given in Table S9.3. Both levels of theory led to comparable results with respect to the relative stability of the complexes and their structures. The results from the B3LYP-D3/aug-cc-pVDZ level of theory are given here since this level requires less computational resources and seems to match slightly better with the experimental rotational parameters than the MP2/6-311++G(d,p).

In the complexes labeled as 1a the water molecule closes a sequential cycle with the carboxyl group acting both simultaneously as hydrogen donors and acceptors and thus forming two O–H···O hydrogen bonds. This is the most stable arrangement for the interaction between an acid group and one water molecule, as reported before in detail.[24] The calculated relative energies for the four complexes are predicted to be in a narrow range (within 32 $cm^{-1} \approx 0.4$ kJ/mol), similar to the monomer conformers.[15] However, the calculated stability ordering of the complexes is not the same as that calculated for the corresponding monomer forms. Altogether, this makes it impossible to discriminate whether one of the complexes is more stable than the others (see discussion on conformer population below). In the complexes labeled as 1b, the water molecule establishes an O–H···O hydrogen bond to the carbonyl oxygen, which acts as hydrogen acceptor, an O···H–C secondary weak interaction with the hydrogen atom in the methyl group in β-position, and an O···H–C secondary weak interaction with the closest hydrogen atom in the phenyl ring (Figure 9.1). The calculated energy difference between the four 1b complexes is within 30 cm^{-1} or 0.35 kJ/mol. The energy difference between 1a and 1b conformers is approximately 1150 cm^{-1} or 14 kJ/mol (Table 9.1).

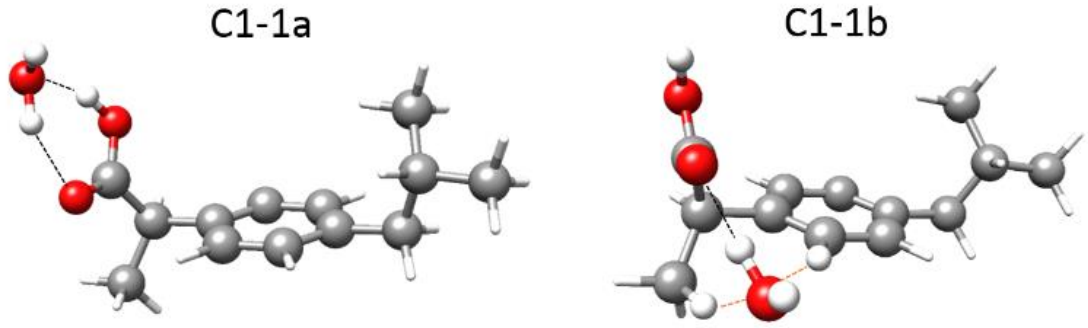

Figure 9.1. Lower energy complexes predicted at the B3LYP-D3/aug-cc-pVDZ level of theory for 1:1 ibuprofen – water complexes in the C1 conformation of the ibuprofen molecule showing the hydrogen bonds (black dashed lines) and the secondary weak interactions (orange dashed lines). The hydrogen atoms from the water molecule and those involved in long-range interactions are displayed as balls. The other hydrogen atoms are displayed as sticks. The corresponding parameters are given in Table 9.1 and Table S9.2 in the supplementary material.

Microwave spectrum.

The recorded broadband microwave spectrum is very dense and dominated by the rotational transitions of the four monomer conformers,[15] which show the characteristic patterns of R-branch μ_a-type transitions (Figure 9.2a). Once we excluded the monomer lines, new sets of R-branch μ_a-type transitions could be identified (Figure 9.2b). Detailed analysis allowed the assignment[25] of four different species (labeled I, II, III and IV). No μ_b- or μ_c-type lines associated with these species were observed. The spectra were fit using a semirigid rotor Hamiltonian in the asymmetric reduction and in the I^r representation.[26] The obtained rotational parameters are given in Table 9.2. The complete list of measured frequencies for those complexes is collected in Tables S9.6-S9.9 in the supplementary material. In accordance with the previous work,[15] the lines do not present splittings attributable to the internal rotation of the methyl groups of ibuprofen, or to tunneling associated to water motions.

A plausible identification of the complexes giving rise to each observed rotational spectrum can be achieved by analyzing the experimental rotational parameters and comparing them with those predicted for the different conformers based on quantum-chemical calculations. The observation of only μ_a-type spectra allowed excluding the 1b complexes since they are predicted to have high μ_b values (Table 9.1) and thus should have sizable *b*-type transitions. This is also plausible because of their high energy difference of 14 kJ/mol.

Table 9.1. Quantum-chemical rotational parameters calculated at the B3LYP-D3/aug-cc-pVDZ level of theory for the 1:1 ibuprofen – water complexes.

Parameter[a]	C1-1a	C2-1a	C3-1a	C4-1a	C1-1b	C2-1b	C3-1b	C4-1b
A /MHz	851.9	865.2	1148.3	1135.2	860.9	880.0	966.4	954.5
B /MHz	223.4	225.0	195.1	196.6	232.3	229.5	224.4	223.2
C /MHz	200.0	198.6	188.1	186.8	219.2	219.0	204.4	205.7
κ	-0.93	-0.92	-0.98	-0.98	-0.96	-0.97	-0.95	-0.95
μ_a /D	-1.88	-1.92	-1.88	-1.84	0.51	0.59	0.09	0.07
μ_b /D	-0.25	-0.19	0.51	0.57	1.67	1.62	-1.94	-1.63
μ_c /D	0.16	-0.03	0.09	0.05	1.06	1.40	-0.52	-0.87
ΔE /cm^{-1}	0	27	32	9	1165	1175	1146	1167
D_e /cm^{-1}	-4016	-4020	-4018	-4017	-2722	-2708	-2706	-2721
D_e /kJmol^{-1}	-48	-48	-48	-48	-33	-32	-32	-33

[a] *A*, *B* and *C* are the rotational constants. κ is the asymmetry parameter derived from the rotational constants; $\kappa = (2B\text{-}A\text{-}C)/(A\text{-}C)$. μ_α (α = *a*, *b* or *c*) are the electric dipole moment components, 1 D $\approx 3.33 \cdot 10^{-30}$ C·m. ΔE is the energy relative to the most stable complex. D_e is the dissociation energy calculated using BSSE corrections.[27]

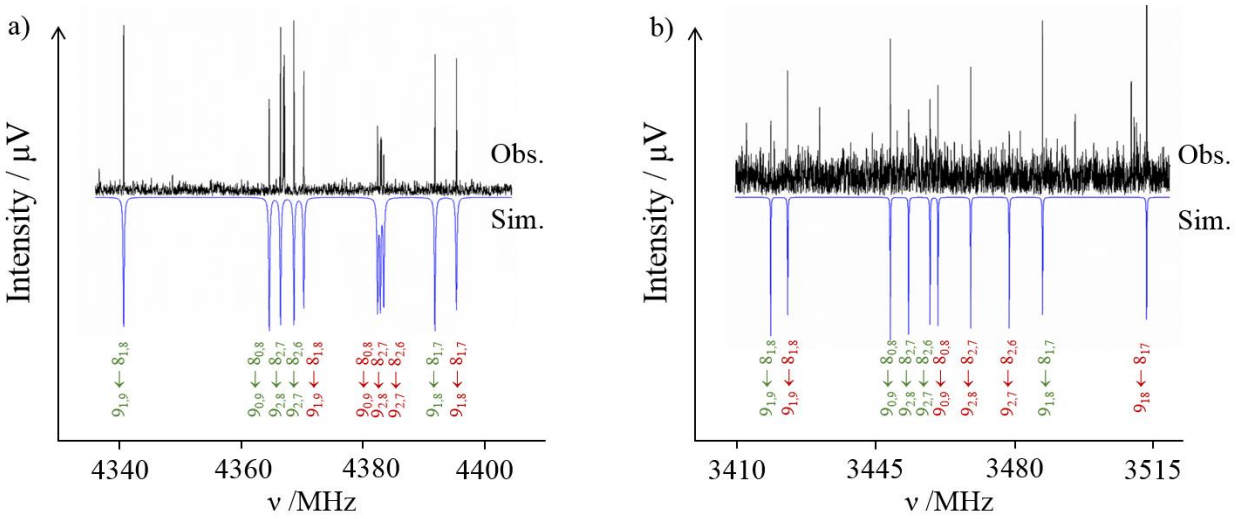

Figure 9.2. Excerpt of the ibuprofen microwave spectrum. a) Observed (upwards) and simulated (downwards) spectra showing the rotational transitions $9_{1,9} \leftarrow 8_{1,8}$; $9_{0,9} \leftarrow 8_{0,8}$; $9_{2,8} \leftarrow 8_{2,7}$; $9_{2,7} \leftarrow 8_{2,6}$ and $9_{1,8} \leftarrow 8_{1,7}$ for the ibuprofen monomer conformers C3 (green) and C4 (red). b) Observed (upwards) and calculated (downwards) spectra showing the rotational transitions $9_{1,9} \leftarrow 8_{1,8}$; $9_{0,9} \leftarrow 8_{0,8}$; $9_{2,8} \leftarrow 8_{2,7}$; $9_{2,7} \leftarrow 8_{2,6}$ and $9_{1,8} \leftarrow 8_{1,7}$ for ibuprofen – water complexes C3-1a (green) and C4-1a (red). The relative intensity between the monomer and the complex spectra is more than 20:1.

A first look at the rotational parameters in Table 9.2 allows classifying the complexes into two families corresponding to the different values of the *A* rotational constant for the complexes. The first family comprises species I and II with *A* values around 850-870 MHz and very similar values of *B* and *C* rotational constants. This family can be correlated with the predicted conformers C1-1a and C2-1a in which the isobutyl group of ibuprofen is on the same side of the phenyl ring as the carboxyl group (see Figure 9.3), i.e., in a *cis* arrangement. The values of the *A* rotational constant for rotamers I and II are sufficiently distinct to assign species I to C1-1a and species II to C2-1a, respectively. The second family comprises species III and IV with *A* values between 1120 and 1160 MHz and again with very similar values of *B* and *C* rotational constants. They can be related to the forms C3-1a and C4-1a, having the isobutyl and the carboxyl groups on opposite sides of the phenyl ring (see Figure 9.3), i.e., in a *trans* arrangement. Again, the difference in *A* rotational constant seems to correlate rotamers III and IV to forms C3-1a and C4-1a, respectively. The differences in orientation of the isobutyl group from conformer C1-1a to C2-1a and from C3-1a to C4-1a cause small shifts in the values of the rotational constants, which can be used to further identify the rotamers.

Another corroboration of the assignment can be obtained attending to the planar moments of inertia, derived from the inertial moments [$P_{\alpha\alpha} = (I_{\beta\beta}+I_{\gamma\gamma}-I_{\alpha\alpha})/2$ (α, β, γ = *a*, *b* or *c*)]. These provide information about the mass extension out of a given inertial plane. For example, P_{cc} reflects the mass extension out of the *ab* inertial plane. Table 9.3 compares the experimental and calculated values of the planar moments of inertia. This comparison corroborates the identification done based on the rotational constants. The trends in the variation of the experimental planar moment values for species I and II or for species III and IV are well reproduced by the theoretical values.

Table 9.2. Experimental rotational parameters for the 1:1 ibuprofen – water complexes observed.

Fitted Parameters[a]	I (C1-1a)	II (C2-1a)	III (C3-1a)	IV (C4-1a)
A /MHz	851.363(28)[b]	872.598(39)	1156.72(18)	1129.39(11)
B /MHz	225.08507(24)	225.15642(29)	195.75673(18)	197.90286(19)
C /MHz	200.49914(23)	198.35992(35)	188.10105(17)	187.77533(22)
Δ_J /kHz	0.01832(73)	0.02003(98)	0.00732(48)	0.00661(57)
Δ_{JK} /kHz	-0.115(18)	-0.096(14)	-0.0650(66)	-0.0696(67)
N	47	39	50	55
σ/kHz	6.5	6.7	4.4	5.2

[a] *A*, *B* and *C* are the rotational constants. Δ_J, and Δ_{JK} are quartic centrifugal distortion constants. *N* is the number of rotational transitions fitted. σ is the rms deviation of the fit. [b] Standard errors are given in parentheses in units of the last digits.

No isotopic information on the ibuprofen – water complexes has been obtained, since the signal to noise (S/N) level for the complexes was approximately 4:1. Thus, it was not possible to acquire further information on their structures. However, given the agreement between the observed and the theoretical rotational constants, the predicted structures can be taken as a reasonable description of the geometries of the observed species.

Table 9.3. Planar moments of inertia for the experimentally observed 1:1 ibuprofen – water complexes (I-IV) compared with the predicted values calculated at the B3LYP-D3/aug-cc-pVDZ level of theory.

Experimental	I	II	III	IV
P_{aa} /uÅ^2	2086.136(20)	2106.595(26)	2415.751(68)	2398.797(44)
P_{bb} /uÅ^2	434.468(20)	441.192(26)	270.990(68)	292.605(44)
P_{cc} /uÅ^2	159.143(20)	137.973(26)	165.916(68)	154.874(44)

B3LYP-D3	C1-1a	C2-1a	C3-1a	C4-1a
P_{aa} /uÅ^2	2101.17	2103.35	2418.50	2415.43
P_{bb} /uÅ^2	428.19	441.34	268.25	290.02
P_{cc} /uÅ^2	164.25	142.76	171.85	155.16

The main difference between the detected forms of ibuprofen – water complexes is the orientation of the isobutyl group of the ibuprofen molecule with respect to the phenyl ring, similar to the corresponding monomers, and not in the arrangement of the water molecule. As mentioned before, the interaction occurs through the two hydrogen bonds between the carboxyl group of ibuprofen and the water molecule (Figure 9.2). The calculated distances and angles for the hydrogen bonds are very similar for the four complexes and are of the same order as those reported for other complexes between an acid group with one water molecule (Table S9.4 in supplementary material).[24] The interaction between water and the acid group can thus be interpreted to be nearly identical for the four conformers.

Theoretical calculations predict that in the case of the four observed conformers, the formation of the complex does not drive any significant conformational or structural change. In fact, the rotational constants of the monomer and those calculated assigning zero mass to water in the complex are almost identical (Table S9.5 in supplementary material).

Conformer line intensities.

The intensities of the observed spectra of the ibuprofen – water complexes are approximately equal. Those intensities are assumed to be proportional to $N_i \cdot \mu_{i,\alpha}^2$, with N_i being the number density of species i in the supersonic jet, and $\mu_{i,\alpha}$ the corresponding electric dipole moment component, in this case μ_a. Since this dipole moment component is predicted to have similar values ($\mu_a \approx$ -1.9 D, Table 9.1) for the four complexes, their population in the supersonic jet can be deduced to be similar. Complex formation takes place in the expansion region close to the nozzle orifice where the rate of three-body collisions is high enough. Once formed, the complexes are cooled down to their ground vibrational state as the supersonic expansion progresses. It can be reasonably assumed that all the ibuprofen molecules existing in the jet have the same probability to form the corresponding 1a complexes with water. As observed previously,[15] all four monomer conformers are present in the jet with similar populations. Thus, our observation that the four 1a complexes have similar relative populations and thus almost equal intensities is a

consistent result. Furthermore, given that in all the complexes the interaction with water is the same, it is possible to assume the same relative energy for them as for the monomer conformers. This result is not in contrast with the different energy order predicted by theoretical calculations. The predicted energy differences are smaller than the accuracy limits of common theoretical methods.

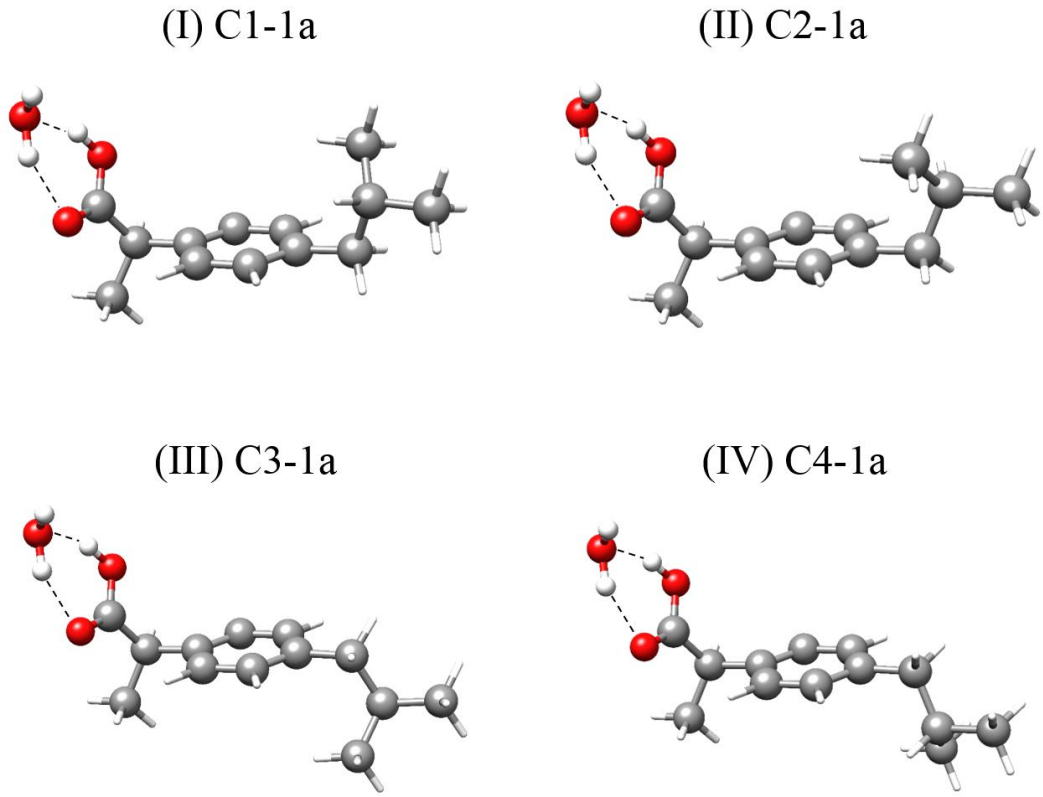

Figure 9.3. Observed 1:1 ibuprofen – water complexes showing the different orientations of the isobutyl that arise from the four different monomer conformers.

Dissociation energies.

Table 9.1 gives the dissociation energies of the complexes calculated using the Basis Set Superposition Error (BSSE) correction.[27] There is practically no difference between the dissociation energies obtained for the four 1a complexes, which is another confirmation that the hydrogen bonds established between water and ibuprofen have the same energies for the four complexes. The same behavior can be seen for the four 1b complexes with almost equal dissociation energies. There is a difference in the dissociation energy between the 1a and the 1b complexes of *ca*. 15.5 kJ mol^{-1}, however, implying that the 1a complexes are more tightly bound. If the dissociation energy of a complex is related to its survival probability in the first stages of the supersonic expansion, this difference could explain why only the 1a complexes have been detected.

9.4 Conclusions

The microwave spectra of four different complexes between ibuprofen and water formed in a supersonic jet were observed using CP-FTMW spectroscopy. The good agreement between quantum-chemically predicted and experimentally determined rotational parameters led to the identification of the observed species as the four lower energy forms of the complex between ibuprofen and water. In the four cases, the water molecule closes a sequential cycle with the carboxyl group establishing two hydrogen bonds. The main structural difference between the observed forms lies in the conformation of ibuprofen that corresponds to those structures reported before.[15] Water does not drive any conformational change in the ibuprofen molecule and essentially does not modify energetically the distribution of conformers from the monomer. In other words, the interaction of the carboxyl group with water does not alter the conformational landscape of ibuprofen, which solely arises from the different orientations of the isobutyl group. This result might be important with respect to transporting the molecule to the COX enzyme and its molecular recognition. The conservation of the ibuprofen flexibility when the carboxyl group of ibuprofen interacts with other polar groups resulting in a cyclic interaction structure might be essential in the recognition process.

References

[1] Rainsford, K. D. "Ibuprofen: From Invention to an OTC Therapeutic Mainstay" *Int. J. Clin. Pract.*, **2013**, 67, 9–20.

[2] World Health Organization model list of essential medicines: http://www.who.int/medicines/publications/essentialmedicines/en/.

[3] Filippa, M. A., Gasull, E. I. "Ibuprofen Solubility in Pure Organic Solvent and Aqueous Mixtures of Cosolvents: Interactions and Thermodynamic Parameters Relating to the Solvation Process" *Fluid Phase Equilib.*, **2013**, 354, 185–190.

[4] Woodman, T. J., Wood, P. J., Thompson, A. S., Hutchings, T. J., Steel, G. R., Jiao, P., Threadgill M. D., Lloyd, M. D. "Chiral Inversion of 2-Arylpropionyl-CoA Esters by Human α–Methylacyl-CoA racemase 1A (P504S) – A Potential Mechanism for the Anti-cancer effects of Ibuprofen" *Chem. Commun.*, **2011**, 47, 7332–7334.

[5] a) Rainsford, K. D. "Ibuprofen: Pharmacology, Efficacy and Safety" *Inflammopharmacology*, **2009**, 17, 275–342. b) G. Q. Lin, Q. D. You and J. F. Cheng, *Chiral drugs: Chemistry and Biological Action*, John Wiley & Sons, Hoboken, New Jersey, 2011.

[6] a) Dannhardt, G., Kiefer, W. "Cyclooxygenase Inhibitors – Current Status and Future Prospects" *Eur. J. Med. Chem.*, **2001**, 36, 109–126. b) Limongelli, V., Bonomi, M., Marinelli, L., Gervasio, F. L., Cavalli, A., Novellino, E., Parrinello, M. "Molecular Basis of Cyclooxygenase Enzymes (COXs) Selective Inhibition" *Proc. Natl. Acad. Sci.*, **2010**, 107, 5411–5416.

[7] a) Selinsky, B. S., Gupta, K., Sharkey, C. T., Loll, P. J. "Structural Analysis of NSAID by Prostaglandin H_2 Synthase: Time-Dependent and Time-Independent Inhibitors Elicit Identical Enzyme Conformations" *Biochemistry*, **2001**, 40, 5172–5180. b) Blobaum, A. L., Marnett, L. J. "Structural and Functional Basis of Cyclooxygenase Inhibition" *J. Med. Chem.*, **2007**, 50, 1425–1441.

[8] a) Baker, E. N., Hubbard, R. E. "Hydrogen bonding in globular proteins" *Prog. Biophys. Mol. Biol.*, **1984**, 44, 97–179. b) Saenger, W. "Structure and Dynamics of Water Surrounding Biomolecules" *Ann. Rev. Biophys. Chem.*, **1987**, 16, 93–114. c) Ball, P. "Water as an Active Constituent in Cell Biology" *Chem. Rev.*, **2008**, 108, 74–108.

[9] a) Saenger, W., Jeffrey, G. A. "*Hydrogen Bonding in Biological Structures"*, Springer-Verlag, Berlin, 1991. b) Jeffrey, G. A. "*Introduction to Hydrogen Bonding"*, Oxford University Press, Oxford, 1997. c) M. Jarrold, F. "Unfolding, Refolding, and Hydration of Proteins in the Gas Phase" *Acc. Chem. Res.*, **1999**, 32, 360-367.

[10] a) Schmitt, M., Böhm, M., Ratzer, C., Vu, C., Kalkman, I., Meerts, W. L. "Structural Selection by Microsolvation: Conformational Locking of Tryptamine" *J. Am. Chem. Soc.*, **2005**, 127, 10356–10364. b) Caminati, W., López, J. C., Blanco, S., Mata, S., Alonso, J. L. "How Water Links to *Cis* and *Trans* Peptidic Groups: The rotational Spectrum of N-Methylformamide-Water" *Phys. Chem. Chem. Phys.*, **2010**, 12, 10230–10234.

[11] a) Maris, A., Ottaviani P., Caminati, W. "Pure Rotational Spectrum of 2-Pyridone···Water and Quantum Chemical Calculations on the Tautomeric Equilibrium 2-Pyridone···Water/2-Hydroxypyridine···Water" *Chem. Phys. Lett.*, **2002**, 360, 155–160. b) Mata, S., Cortijo, V., Caminati, W., Alonso, J. L., Sanz, M. E., López, J. L., Blanco, S. "Tautomerism and Microsolvation in 2-Hydroxypyridine/2-Pyridone" *J. Phys. Chem. A*, **2010**, 114, 11393–11398.

[12] a) Blanco, S., Pinacho, P., López, J. C. "Hydrogen-Bond Cooperativity in Formamide$_2$-Water: A Model for Water Mediated Interactions" *Angew. Chem. - Int. Ed.*, 2016, **55**, 9331–9335. b) Blanco, S., Pinacho, P., López, J. C. "Structure and Dynamics in Formamide-$(H_2O)_3$: A Water Pentamer Analogue" *J Phys. Chem. Lett.*, **2017**, 8, 6060–6066.

[13] a) Pérez, C., Neill, J. L., Muckle, M. T., Zaleski, D. P., Peña, I., López, J. C., Alonso, J. L., Pate, B. H. "Water-Water and Water-Solute Interactions in Microsolvated Organic Complexes" *Angew. Chem. Int. Ed.* **2014**, 54, 979–982. b) Blanco, S., López, J. C., Lesarri, A., Alonso, J. L. "Microsolvation of Formamide: A Rotational Study" *J. Am. Chem. Soc.*, **2006**, 128, 12111–12121. c) Pérez, C., Krin, A., Steber, A. L., López, J. C., Kisiel, Z., Schnell, M. "Wetting Camphor: Multi-Isotopic Substitution Identifies the Complementary Roles of Hydrogen Bonding and Dispersive Forces" *J. Phys. Chem. Lett.* **2016**, *7*, 154–160. d) Pérez, C., López, J. C., Blanco, S., Schnell, M. "Water-Induced Structural Changes in Crown Ethers from Broadband Rotational Spectroscopy" *J. Phys. Chem. Lett.* **2016**, *7*, 4053–4058.

[14] Brown, G. G., Dian, B. C., Douglass, K. O., Geyer, S. M., Shipman, S. T., Pate, B. H. "A Broadband Fourier Transform Microwave Spectrometer Based on Chirped Pulse Excitation" *Rev. Sci. Instrum.*, **2008**, 79, 053103.

[15] Betz, T., Zinn S., Schnell, M. "The Shape of Ibuprofen in the Gas Phase" *Phys. Chem. Chem. Phys.*, **2015**, 17, 4538–4541.
[16] Schmitz, D., Shubert, V. A., Betz, T., Schnell, M. "Multi-Resonance Effects within a Single Chirp in Broadband Rotational Spectroscopy: The Rapid Adiabatic Passage Regime for Benzonitrile" *J. Mol. Spectrosc.*, **2012**, 280, 77–84.
[17] Pérez, C., Lobsiger, S., Seifert, N. A., Zaleski, D. P., Temelso, B., Shields, G. C., Kisiel, Z., Pate, B. H. "Broadband Fourier Transform Rotational Spectroscopy for structure Determination: The Water Heptamer" *Chem. Phys. Lett.* **2013**, 571, 1–15.
[18] Gaussian 09, Revision D.01, Frisch M. J., Trucks G. W., Schlegel H. B., Scuseria G. E., Robb M. A., Cheeseman J. R., Scalmani G., Barone V., Petersson G. A., Nakatsuji H., Li X., Caricato M., Marenich A., Bloino J., Janesko B. G., Gomperts R., Mennucci B., Hratchian H. P., Ortiz J. V., Izmaylov A. F., Sonnenberg J. L., Williams-Young D., Ding F., Lipparini F., Egidi F., Goings J., Peng B., Petrone A., Henderson T., Ranasinghe D., Zakrzewski V. G., Gao J., Rega N., Zheng G., Liang W., Hada M., Ehara M., Toyota K., Fukuda R., Hasegawa J., Ishida M., Nakajima T., Honda Y., Kitao O., Nakai H., Vreven T., Throssell K., Montgomery, Jr. J. A., Peralta J. E., Ogliaro F., Bearpark M., Heyd J. J., Brothers E., Kudin K. N., Staroverov V. N., Keith T., Kobayashi R., Normand J., Raghavachari K., Rendell A., Burant J. C., Iyengar S. S., Tomasi J., Cossi M., Millam J. M., Klene M., Adamo C., Cammi R., Ochterski J. W., Martin R. L., Morokuma K., Farkas O., Foresman J. B., Fox D. J., *Gaussian, Inc., Wallingford CT*, 2016.
[19] a) a) Lee, C., Yang, W., Parr, R. G. "Development of the Colle-Salvetti Correlation-Energy Formula into a Functional of the Electron Density" *Phys. Rev. B*, **1988**, 37, 785–789. b) Becke, A. D. "Density-Functional Thermochemistry. III. The Role of Exact Exchange" *J. Chem. Phys.*, **1993**, 98, 5648–5652. c) Vosko, S. H., Wilk, L., Nusair, M. "Accurate Spin-Dependent Electron Liquid Correlation Energies for Local Spin Density Calculations: a Critical Analysis" *Can. J. Phys.*, **1980**, 58, 1200–1211.
[20] a) a) Dunning, T. H. "Gaussian Basis Sets for Use in Correlated Molecular Calculations. I. The Atoms Boron Through Neon and Hydrogen" *J. Chem. Phys.*, **1989**, 90, 1007–1023. b) Kendall, R. A., Dunning, T. H., Harrison, R. J. "Electron Affinities of the First-Row Atoms Revisited. Systematic Basis Sets and Wave Functions" *J. Chem. Phys.*, **1992**, 96, 6796–6806.
[21] Grimme, S., Antony, J., Ehrlich, Krieg, H. "A Consistent and Accurate *Ab Initio* Parametrization of Density Functional Dispersion Correction (DFT-D) for the 94 Elements H-Pu" *J. Chem. Phys.*, **2010**, 132, 154101.
[22] Møller, C., Plesset, M. S. "Note on an Approximation Treatment for Many-Electron Systems" *Phys. Rev.*, **1934**, 46, 618–622.
[23] Ditchfield, R., Hehre, W. J., Pople, J. A. "Self-Consistent Molecular-Orbital Methods. IX. An Extended Gaussian-Type Basis for Molecular-Orbital Studies of Organic Molecules" *J. Chem. Phys.*, **1971**, 54, 724–728.
[24] a) Canagaratna, M., Phillips, J. A., Ott, M. E. Leopold, K. R. "The Nitric-Acid Complex: Microwave Spectrum, Structure and Tunneling" *J. Phys. Chem. A*, **1998**, 102, 1489–1497. b) Priem, D., Ha, T.-K., Bauder, A. "Rotational Spectra and Structures of Three Hydrogen-Bonded Complexes between Formic Acid and Water" *J. Chem. Phys.*, **2000**, 113, 169–175. c) Alonso, J. L., Cocinero, E. J., Lesarri, A., Sanz, M. E., López, J. C. "The Glycine-Water Complex" *Angew. Chem. Int. Ed.*, **2006**, 45, 3471–3474. d) Schnitzler, E. G., Jäger, W. "The Benzoic Acid-Water Complex: A Potential Atmospheric Nucleation Precursor Studied Using Microwave Spectroscopy and *Ab Initio* Calculations" *Phys. Chem. Chem. Phys.*, **2014**, 16, 2305–2314.
[25] Pickett, H. M. "The Fitting and Prediction of Vibrational-Rotation Spectra with Spin Interaction" *J. Mol. Spectrosc.*, **1991**, 148, 371–377.
[26] Watson, J. K. G. in *Vibrational Spectra and Structure a Series of Advances*, ed. J. R. Durig, Elsevier, Amsterdam, 1977, vol. 6, pp. 1-89.
[27] a) Boys, S., Bernardi, F. "The Calculation of Small Molecular Interactions by the Differences of Spearate Total Energies. Some Procedures with Reduced Errors" *Mol. Phys.*, 1970, **19**, 553–566. b) Xantheas, S. S. "On the Importance of the Fragment Relaxation Energy Terms in the Estimation of the Basis Set Superposition Error Correction to the Intermolecular Interaction Energy" *J. Chem. Phys.*, 1996, **21**, 8821–8824.

Supplementary material for chapter IX

Microsolvated complexes of ibuprofen as revealed by high-resolution rotational spectroscopy.

Direct transcription from the manuscript accepted for publication in *Phys. Chem. Chem. Phys.*

P. Pinacho, A. Krin, C. Pérez, S. Zinn, J. C. López, S. Blanco, M. Schnell

Abstract

Hydrogen-bonded complexes between ibuprofen and water generated in a supersonic expansion were characterized by chirped-pulse Fourier transform microwave spectroscopy in the 2-8 GHz frequency range. Four spectra were observed allowing to determine their rotational parameters. Comparison with quantum-chemical calculations led to their identification as the lowest energy 1:1 ibuprofen – water complexes. These correspond to the complexes between water and the four different conformers of ibuprofen previously detected in the gas phase, owing to their similar stabilization energies and abundances. Water seems to not change the conformational distribution of ibuprofen.

- **Figure S9.1.** Detected conformers of ibuprofen showing the inertial axis.

- **Figure S9.2.** Most stable conformers predicted at the B3LYP-D3/aug-cc-pVDZ level of theory for 1:1 ibuprofen – water complexes.

- **Figure S9.3.** Ibuprofen – water complex C1-1a predicted at the B3LYP-D3/aug-cc-pVDZ level of theory showing the atom labeling.

- **Figure S9.4.** Additional stable conformers predicted at the B3LYP-D3/aug-cc-pVDZ level of theory for 1:1 ibuprofen – water complexes.

- **Figure S9.5.** 3D model for the predicted structures for 1:1 ibuprofen – water complexes.

- **Table S9.1.** Experimental rotational parameters for the ibuprofen monomers previously reported.

- **Table S9.2.** Quantum-chemical rotational parameters calculated at the B3LYP-D3/aug-cc-pVDZ level of theory for the 1:1 ibuprofen – water complexes.

- **Table S9.3.** Quantum-chemical rotational parameters calculated at the MP2/6-311++G(d,p) level of theory for the 1:1 ibuprofen – water complexes.

- **Table S9.4.** Comparison between the hydrogen bond parameters predicted in this work for the 1:1 ibuprofen – water complexes and different acid molecules – water complexes reported.

- **Table S9.5.** Calculated rotational constants, moments of inertia and planar moments of inertia for the monomer, and those corresponding to the 1a complex assigning zero mass to the water molecule.

- **Table S9.6.** Observed rotational transitions and residuals for the 1:1 ibuprofen – water complex C1-1a in the ground vibrational state.

- **Table S9.7.** Observed rotational transitions and residuals for the 1:1 ibuprofen – water complex C2-1a in the ground vibrational state.

- **Table S9.8.** Observed rotational transitions and residuals for the 1:1 ibuprofen – water complex C3-1a in the ground vibrational state.

- **Table S9.9.** Observed rotational transitions and residuals for the 1:1 ibuprofen – water complex C4-1a in the ground vibrational state.

Figure S9.1. Detected conformers of ibuprofen [ref. 15] showing the inertial axis. The experimentally determined parameters are given in Table S1.

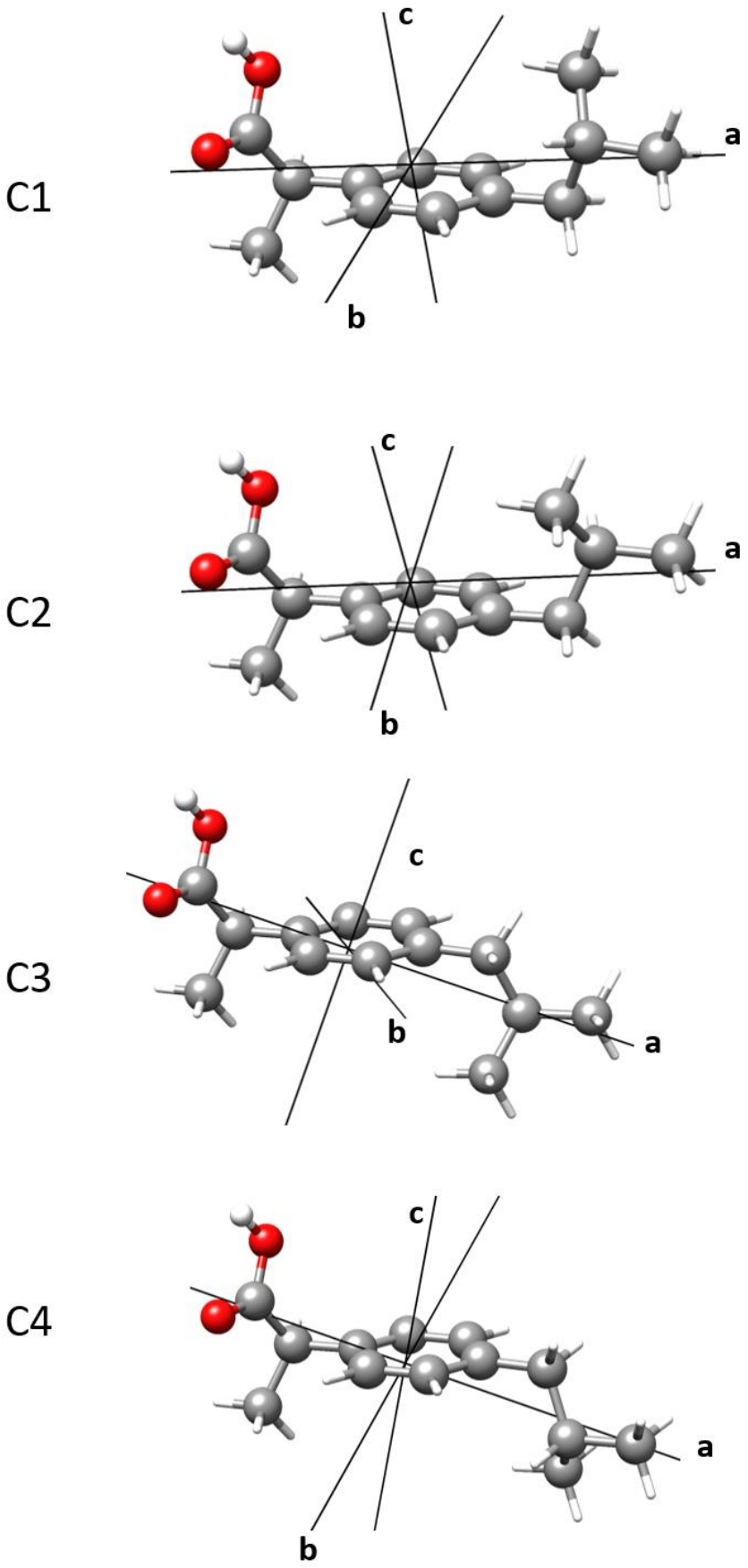

Figure S9.2. Most stable conformers predicted at the B3LYP-D3/aug-cc-pVDZ level of theory for 1:1 ibuprofen – water complexes showing the inertial axis. The corresponding parameters are given in Table S2.

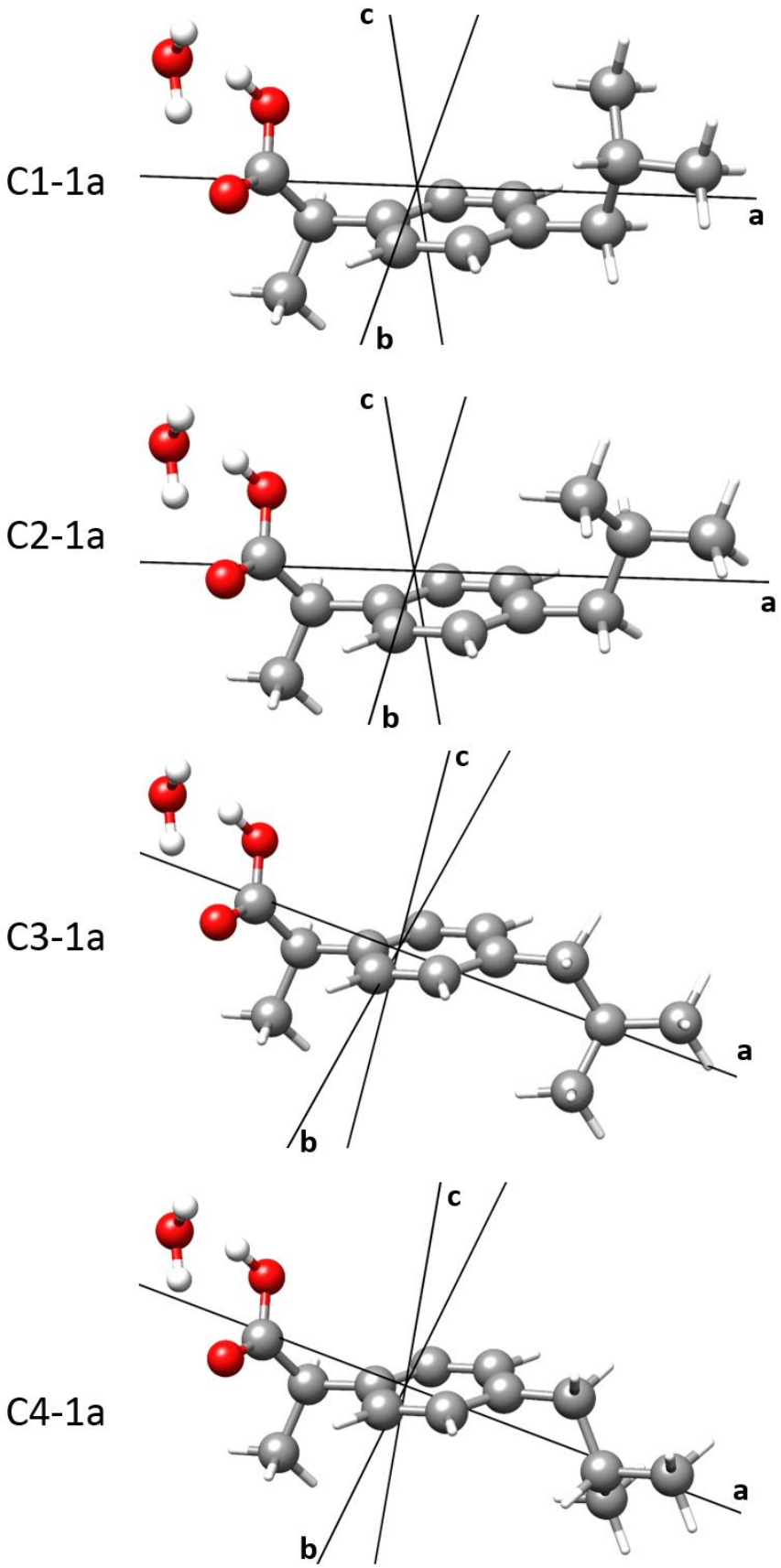

Figure S9.3. Ibuprofen – water complex C1-1a predicted at the B3LYP-D3/aug-cc-pVDZ level of theory showing the atom labeling.

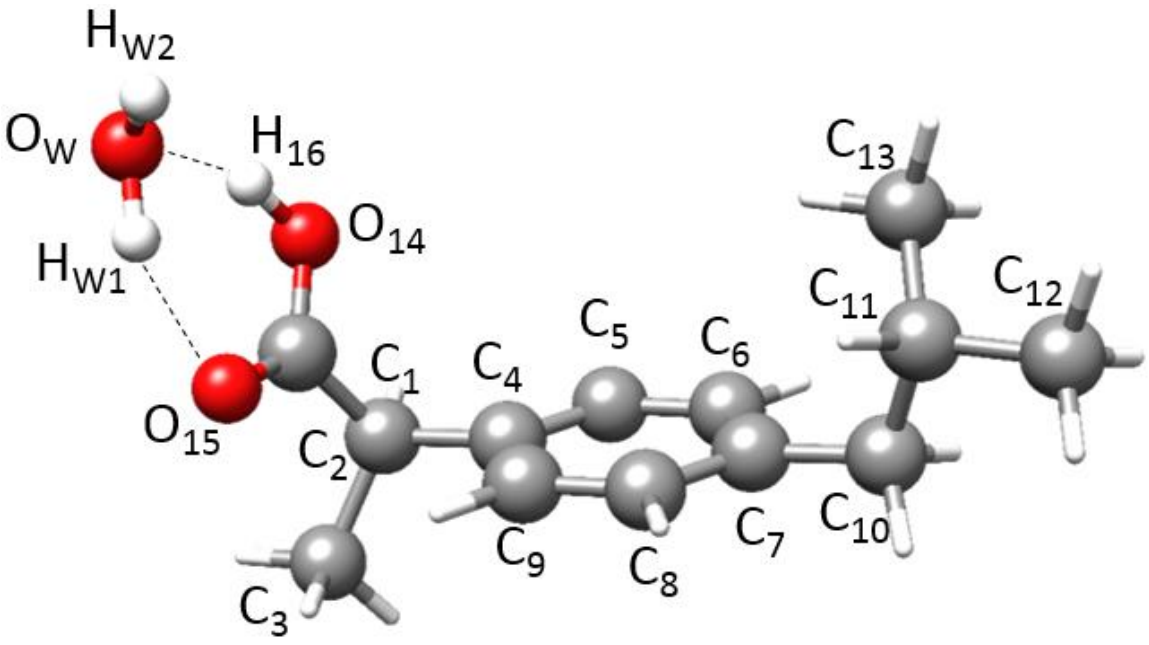

Figure S9.4. Additional stable conformers predicted at the B3LYP-D3/aug-cc-pVDZ level of theory for 1:1 ibuprofen – water complexes showing the inertial axis. The corresponding parameters are given in Table S2.

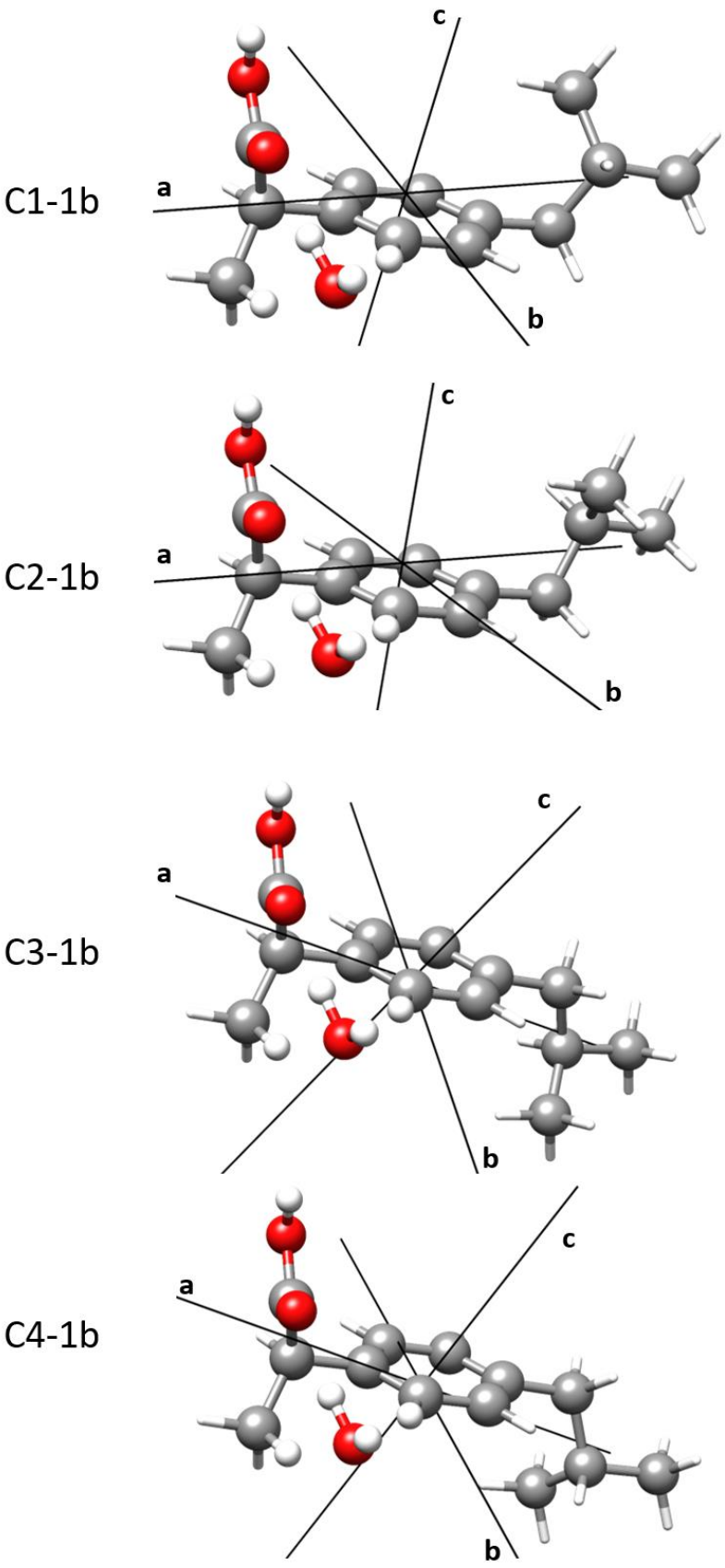

Figure S9.5. 3D model for the predicted structures for 1:1 ibuprofen – water complexes.

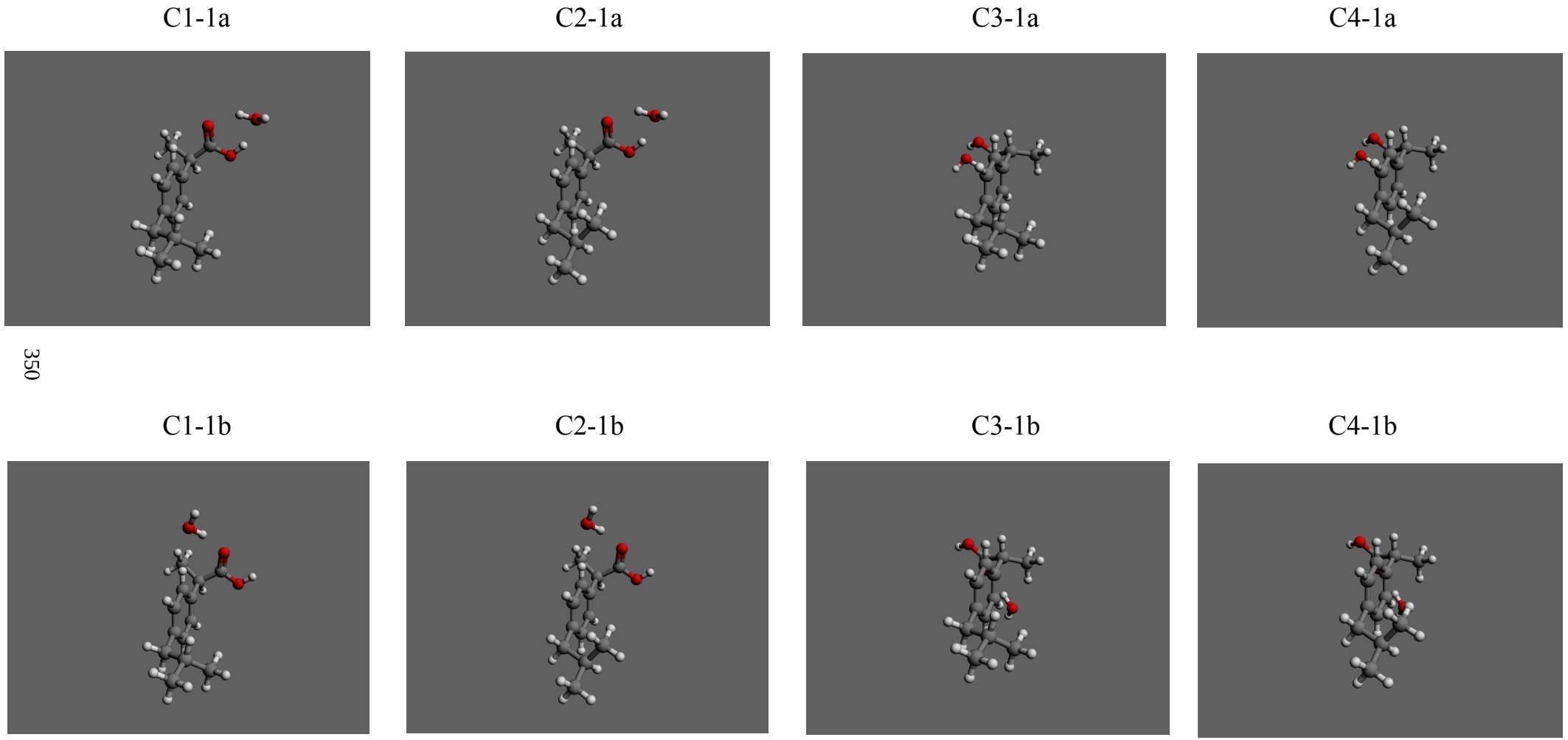

Table S9.1. Experimental rotational parameters for the ibuprofen monomers previously reported [ref. 15].

Fitted Parameters[a]	C1	C2	C3	C4
A /MHz	1325.656(3)[b]	1357.716(3)	1570.534(4)	1534.787(5)
B /MHz	260.7159(5)	261.4567(4)	245.4447(4)	244.8941(6)
C /MHz	251.1813(5)	248.3119(4)	239.7532(5)	242.1034(6)
Δ_J /kHz	0.89(21)	0.50(20)	0.69(48)	0.85(55)
Δ_{JK} /kHz	-0.049(14)	-0.068(12)	0.014(22)	0.013(22)
Δ_K /kHz	0.012(15)	0.012(13)	0.063(13)	0.067(15)
N	139	151	113	109
σ /kHz	33	31	29	38
Derived Parameters				
P_{aa} /uÅ^2	1784.604(5)	1797.984(4)	1922.580(6)	1910.916(7)
P_{bb} /uÅ^2	227.405(5)	237.275(4)	185.334(6)	176.535(7)
P_{cc} /uÅ^2	153.824(5)	134.952(4)	136.454(6)	152.748(7)

[a] A, B and C are the rotational constants. Δ_J, Δ_{JK} and Δ_K, are quartic centrifugal distortion constants. N is the number of rotational transitions fitted. σ is the rms deviation of the fit. $P_{\alpha\alpha}$ (α = a, b or c) are the planar moments of inertia; these are derived from the moments of inertia I_α as for example $P_{cc}=(I_a+I_b-I_c)/2$. [b] Standard errors are given in parentheses in units of the last digit.

Table S9.2. Quantum-chemical rotational parameters calculated at the B3LYP-D3/aug-cc-pVDZ level of theory for the 1:1 ibuprofen – water complexes.

Parameter[a]	C1-1a	C2-1a	C3-1a	C4-1a	C1-1b	C2-1b	C3-1b	C4-1b
A /MHz	851.9	865.2	1148.3	1135.2	860.9	880.0	966.4	954.5
B /MHz	223.4	225.0	195.1	196.6	232.3	229.5	224.4	223.2
C /MHz	200.0	198.6	188.1	186.8	219.2	219.0	204.4	205.7
Δ_J /kHz	0.017	0.016	0.006	0.006	0.009	0.010	0.010	0.010
Δ_{JK} /kHz	-0.070	-0.070	-0.060	-0.071	0.013	0.024	0.016	0.009
Δ_K /kHz	0.441	0.458	0.936	0.956	0.160	0.150	0.202	0.202
δ_J /kHz	0.004	0.004	0.001	0.001	0.000	0.000	0.001	0.000
δ_K /kHz	0.053	0.048	0.006	0.012	0.004	-0.002	0.036	-0.004
κ	-0.93	-0.92	-0.98	-0.98	-0.96	-0.97	-0.95	-0.95
P_{aa} /uÅ^2	2101.2	2103.3	2418.5	2415.4	1947.0	1967.7	2100.8	2095.8
P_{bb} /uÅ^2	428.2	441.3	268.2	290.0	358.5	339.9	371.6	361.0
P_{cc} /uÅ^2	164.2	142.8	171.8	155.2	228.5	234.3	151.3	168.4
μ_a /D	-1.9	-1.9	-1.9	-1.8	0.5	0.6	0.1	0.1
μ_b /D	-0.2	-0.2	0.5	0.6	1.7	1.6	-1.9	-1.6
μ_c /D	0.2	0.0	0.1	0.0	1.1	1.4	-0.5	-0.9
ΔE /cm^{-1}	0	27	32	9	1165	1175	1146	1167
ΔE /kJmol^{-1}	0	0	0	0	14	14	14	14
D_e/cm^{-1}	-4016	-4020	-4018	-4017	-2722	-2708	-2706	-2721
D_e/kJmol^{-1}	-48	-48	-48	-48	-33	-32	-32	-32

[a] A, B and C are the rotational constants. Δ_J, Δ_{JK}, Δ_K, δ_J and δ_K are the quartic centrifugal distortion constants. κ is the asymmetry parameter derived from the rotational constants; $\kappa = (2B\text{-}A\text{-}C)/(A\text{-}C)$. $P_{\alpha\alpha}$ ($\alpha = a$, b or c) are the planar moments of inertia; these are derived from the moments of inertia I_α as for example $P_{cc}=(I_a+I_b-I_c)/2$. μ_α ($\alpha = a$, b or c) are the electric dipole moment components, 1 D ≈ $3.33\cdot10^{-30}$ C·m. ΔE is the energy relative to the most stable complex. D_e is the dissociation energy calculated using BSSE corrections [27].

Table S9.3. Quantum-chemical rotational parameters calculated at the MP2/6-311++G(d,p) level of theory for the 1:1 ibuprofen – water complexes.

Parameter[a]	C1-1a	C2-1a	C3-1a	C4-1a	C1-1b	C2-1b	C3-1b	C4-1b
A /MHz	840.8	864.5	1168.3	1135.9	850.2	874.4	964.7	941.7
B /MHz	229.5	228.4	197.0	199.3	237.8	234.4	227.7	228.7
C /MHz	203.6	201.2	189.5	189.7	224.4	223.7	207.8	209.7
Δ_J /kHz	0.022	0.022	0.007	0.007	0.010	0.010	0.005	0.005
Δ_{JK} /kHz	-0.088	-0.111	-0.081	-0.081	0.024	0.009	0.038	0.039
Δ_K /kHz	0.502	0.634	1.150	1.090	0.150	0.202	0.127	0.132
δ_J /kHz	0.005	0.005	0.001	0.001	0.000	0.000	0.000	0.000
δ_K /kHz	0.065	0.063	0.014	0.010	-0.002	-0.004	0.026	0.005
κ	-0.92	-0.92	-0.98	-0.98	-0.96	-0.97	-0.95	-0.95
P_{aa} /uÅ^2	2041.6	2070.0	2399.8	2377.5	1891.5	1918.6	2063.8	2041.6
P_{bb} /uÅ^2	440.6	441.9	267.0	286.6	360.7	340.5	368.2	368.4
P_{cc} /uÅ^2	160.5	142.7	165.5	158.3	233.8	237.4	155.7	168.2
μ_a /D	-1.4	-1.4	-1.3	-1.3	0.0	0.1	-0.3	-0.4
μ_b /D	-0.7	-0.7	0.8	1.0	1.2	1.3	-1.5	-1.2
μ_c /D	0.5	0.3	-0.3	-0.3	1.4	1.5	-0.7	-0.9
ΔE /cm^{-1}	48	0	8	41	1135	1104	1110	1099
ΔE /kJmol^{-1}	1	0	0	0	14	13	13	13
D_e/cm^{-1}	-2967	-2971	-2971	-2969	-1910	-1906	-1914	-1919
D_e/kJmol^{-1}	-35	-35	-35	-35	-23	-23	-23	-23

[a] A, B and C are the rotational constants. Δ_J, Δ_{JK}, Δ_K, δ_J and δ_K are the quartic centrifugal distortion constants. κ is the asymmetry parameter derived from the rotational constants; $\kappa = (2B\text{-}A\text{-}C)/(A\text{-}C)$. $P_{\alpha\alpha}$ ($\alpha = a$, b or c) are the planar moments of inertia; these are derived from the moments of inertia I_α as for example $P_{cc}=(I_a+I_b-I_c)/2$. μ_α ($\alpha = a$, b or c) are the electric dipole moment components, 1 D ≈ $3.33\cdot10^{-30}$ C·m. ΔE is the energy relative to the most stable complex. D_e is the dissociation energy calculated using BSSE corrections [27].

Table S9.4. Comparison between the hydrogen bond parameters predicted in this work for the 1:1 ibuprofen – water complexes and different acid molecules – water complexes reported.

B3LYP-D3[a]	C1-1a	C2-1a	C3-1a	C4-1a
$r(O_W\cdots H_{16})$ /Å[b]	1.791	1.790	1.791	1.791
$r(O_{15}\cdots H_{W1})$ /Å	1.929	1.930	1.930	1.931
$\angle(O_W{-}H_{W1}\cdots O_{15})$ /°	141.0	140.9	141.0	140.9
$\angle(O_{14}{-}H_{16}\cdots O_W)$ /°	156.4	156.5	156.5	156.5
$\angle(H_{W1}\cdots O_{15}{=}C)$ /°	107.5	107.5	107.5	107.5
$\angle(H_{16}\cdots O_W{-}H_{W1})$ /°	82.9	82.9	82.9	82.9
$\tau(H_{W2}{-}O_W{-}H_{W1}\cdots O_{15})$ /°	125.5	125.4	125.3	125.1

MP2[a]	C1-1a	C2-1a	C3-1a	C4-1a
$r(O_W\cdots H_{16})$ /Å	1.802	1.803	1.801	1.802
$r(O_{15}\cdots H_{W1})$ /Å	2.036	2.035	2.035	2.035
$\angle(O_W{-}H_{W1}\cdots O_{15})$ /°	133.3	133.3	133.4	133.4
$\angle(O_{14}{-}H_{16}\cdots O_W)$ /°	158.3	158.2	158.3	158.3
$\angle(H_{W1}\cdots O_{15}{=}C)$ /°	108.6	108.6	108.6	108.6
$\angle(H_{16}\cdots O_W{-}H_{W1})$ /°	87.8	87.8	87.8	87.8
$\tau(H_{W2}{-}O_W{-}H_{W1}\cdots O_{15})$ /°	136.6	136.8	136.5	136.4

Reported[c]	Nitric – water[d]	Form – water[e]	Gly – water[f]	Benz – water[g]
$r(O_W\cdots H_{16})$ /Å	1.779(33)	1.810	1.806(1)	1.80
$r(O_{15}\cdots H_{W1})$ /Å	2.3	2.2210	2.073(2)	1.95
$\angle(O_W{-}H_{W1}\cdots O_{15})$ /°	-	120.3	126.4(5)	139.5
$\angle(O_{14}{-}H_{16}\cdots O_W)$ /°	174.5(41)	157.7	161.8(1)	157.4
$\angle(H_{W1}\cdots O_{15}{=}C)$ /°	-	110.6	112.4(1)	-
$\angle(H_{16}\cdots O_W{-}H_{W1})$ /°	92(8)	97.2	91.4(7)	-
$\tau(H_{W2}{-}O_W{-}H_{W1}\cdots O_{15})$ /°	-	-	140.0	-

[a] Optimized geometries at the B3LYP-D3/aug-cc-pVDZ or at the MP2/6-311++G(d,p) level of theory. [b] See Figure S3 for atom labeling. [c] Notation represents the similar atoms of the ibuprofen – water complexes. The use of the same notation scheme denote that we are giving the same hydrogen bond parameters. [d] Values from reference [24a] for the nitric acid – water complex. [e] Values from reference [24b] for the formic acid – water complex. [f] Values from reference [24c] for the glycine – water complex. [g] Values from reference [24d] for the benzoic acid – water complex.

Table S9.5. a) Calculated rotational constants, moments of inertia and planar moments of inertia for the monomer, and b) those corresponding to the 1a complex assigning zero mass to the water molecule.

a)	B3LYP-D3[a]	C1	C2	C3	C4
	A /MHz	1314.5	1339.5	1559.9	1531.3
	B /MHz	257.8	259.2	243.6	242.7
	C /MHz	249.2	246.5	238.2	240.2
	I_a /uÅ^2	384.5	377.3	324.0	330.0
	I_b /uÅ^2	1959.9	1949.6	2074.4	2082.4
	I_c /uÅ^2	2027.6	2050.0	2121.7	2103.6
	P_{aa} /uÅ^2	1801.5	1811.2	1936.1	1928.0
	P_{bb} /uÅ^2	226.1	238.9	185.6	175.6
	P_{cc} /uÅ^2	158.4	138.4	138.3	154.4

b)	B3LYP-D3[a]	C1	C2	C3	C4
	A /MHz	1311.4	1331.6	1558.2	1538.6
	B /MHz	258.7	260.4	244.1	242.2
	C /MHz	250.0	248.2	238.0	239.9
	I_a /uÅ^2	385.4	379.5	324.3	328.4
	I_b /uÅ^2	1953.7	1940.9	2070.6	2086.5
	I_c /uÅ^2	2021.2	2036.5	2123.4	2106.3
	P_{aa} /uÅ^2	1794.7	1798.9	1934.8	1932.2
	P_{bb} /uÅ^2	226.4	237.5	188.6	174.1
	P_{cc} /uÅ^2	158.9	142.0	135.8	154.3

[a] Optimized geometries at the B3LYP-D3/aug-cc-pVDZ level of theory.

Table S9.6. Observed rotational transitions and residuals (all the values in MHz) for the 1:1 ibuprofen – water complex C1-1a in the ground vibrational state for transitions of the type $J'K'_{-1}K'_{+1} \leftarrow J''K''_{-1}K''_{+1}$.

J'	K'_{-1}	K'_{+1}	J''	K''_{-1}	K''_{+1}	Obs.	Res.
5	1	5	4	1	4	2063.4583	-0.0165
5	0	5	4	0	4	2113.8883	-0.0044
5	1	4	4	1	3	2186.1456	0.0096
6	1	6	5	1	5	2474.3987	-0.0059
6	0	6	5	0	5	2529.2721	-0.0051
6	2	5	5	2	4	2550.3104	0.0073
6	2	4	5	2	3	2574.5085	0.0002
6	1	5	5	1	4	2621.2157	0.0101
7	1	7	6	1	6	2884.4736	-0.0064
7	0	7	6	0	6	2941.1301	0.0060
7	3	5	6	3	4	2984.2012	0.0043
7	3	4	6	3	3	2985.8025	0.0028
7	2	5	6	2	4	3011.4814	0.0056
7	1	6	6	1	5	3054.9841	0.0054
8	1	8	7	1	7	3293.6370	-0.0055
8	0	8	7	0	7	3349.4223	0.0041
8	2	7	7	2	6	3395.9790	-0.0139
8	2	6	7	2	5	3451.1528	0.0050
8	1	7	7	1	6	3487.1427	0.0019
9	1	9	8	1	8	3701.8600	-0.0054
9	0	9	8	0	8	3754.4646	0.0047
9	2	8	8	2	7	3817.4963	-0.0010
9	3	7	8	3	6	3839.2729	-0.0005
9	3	6	8	3	5	3845.0694	-0.0050
9	2	7	8	2	6	3893.0883	-0.0026
9	1	8	8	1	7	3917.3409	0.0048
10	1	10	9	1	9	4109.1528	0.0003
10	0	10	9	0	9	4156.8220	0.0021
10	2	9	9	2	8	4237.9689	-0.0006
10	4	6	9	4	5	4265.0680	0.0037
10	3	8	9	3	7	4267.0502	-0.0017
10	3	7	9	3	6	4276.8850	-0.0026
10	2	8	9	2	7	4336.5940	0.0017
10	1	9	9	1	8	4345.1664	-0.0044
11	1	11	10	1	10	4515.5408	0.0061
11	0	11	10	0	10	4557.2159	-0.0055
11	2	10	10	2	9	4657.3000	-0.0158
11	3	9	10	3	8	4694.8442	0.0057
11	1	10	10	1	9	4770.2215	-0.0034
11	2	9	10	2	8	4780.7760	0.0025
12	1	12	11	1	11	4921.0709	0.0040
12	0	12	11	0	11	4956.4039	0.0086
12	2	11	11	2	10	5075.4607	0.0064
12	2	10	11	2	9	5224.7295	-0.0020
13	0	13	12	0	12	5354.9725	0.0105
13	2	12	12	2	11	5492.3116	-0.0059
13	1	12	12	1	11	5610.3340	-0.0102

Table S9.7. Observed rotational transitions and residuals (all the values in MHz) for the 1:1 ibuprofen – water complex C2-1a in the ground vibrational state for transitions of the type $J'K'_{-1}K'_{+1} \leftarrow J''K''_{-1}K''_{+1}$.

J'	K'_{-1}	K'_{+1}	J''	K''_{-1}	K''_{+1}	Obs.	Res.
5	1	5	4	1	4	2047.1666	-0.0096
5	0	5	4	0	4	2101.5026	0.0011
5	1	4	4	1	3	2180.8406	0.0064
6	0	6	5	0	5	2513.3599	-0.0042
6	2	5	5	2	4	2537.4238	0.0021
6	4	2	5	4	1	2543.8694	-0.0055
6	4	3	5	4	2	2543.8694	0.0032
6	3	4	5	3	3	2545.1424	-0.0064
6	3	3	5	3	2	2546.0067	-0.0059
6	2	4	5	2	3	2565.1438	0.0143
6	1	5	5	1	4	2614.5161	0.0038
7	0	7	6	0	6	2921.2395	-0.0061
7	2	6	6	2	5	2958.2705	0.0044
7	2	5	6	2	4	3001.5911	0.0131
7	1	6	6	1	5	3046.6887	0.0003
8	1	8	7	1	7	3266.4673	-0.0046
8	0	8	7	0	7	3325.1828	-0.0073
8	2	7	7	2	6	3378.1681	-0.0011
8	2	6	7	2	5	3440.9921	0.0035
8	1	7	7	1	6	3476.9920	-0.0014
9	1	9	8	1	8	3670.8455	0.0040
9	0	9	8	0	8	3725.6074	-0.0022
9	2	8	8	2	7	3797.0132	0.0054
9	4	6	8	4	5	3819.3601	0.0026
9	4	5	8	4	4	3819.5543	0.0045
9	3	7	8	3	6	3821.8420	0.0071
9	3	6	8	3	5	3828.8253	-0.0067
9	2	7	8	2	6	3882.7941	-0.0004
9	1	8	8	1	7	3905.0030	-0.0073
10	0	10	9	0	9	4123.2106	-0.0005
10	2	8	9	2	7	4326.1237	0.0007
10	1	9	9	1	8	4330.2788	0.0000
11	1	11	10	1	10	4476.4893	-0.0102
11	2	9	10	2	8	4769.9351	-0.0102
12	0	12	11	0	11	4913.3333	0.0198
12	4	9	11	4	8	5098.7178	-0.0027
12	3	10	11	3	9	5099.3684	-0.0079
12	4	8	11	4	7	5100.2572	-0.0018
12	3	9	11	3	8	5128.1649	0.0061

Table S9.8. Observed rotational transitions and residuals (all the values in MHz) for the 1:1 ibuprofen – water complex C3-1a in the ground vibrational state for transitions of the type $J'K'_{-1}K'_{+1} \leftarrow J''K''_{-1}K''_{+1}$.

J'	K'_{-1}	K'_{+1}	J''	K''_{-1}	K''_{+1}	Obs.	Res.
6	1	6	5	1	5	2279.8126	-0.0017
6	0	6	5	0	5	2301.5446	-0.0029
6	2	5	5	2	4	2302.9345	-0.0039
6	2	4	5	2	3	2304.5321	0.0008
6	1	5	5	1	4	2325.7476	0.0086
7	0	7	6	0	6	2684.4447	-0.0036
7	2	6	6	2	5	2686.6404	-0.0032
7	2	5	6	2	4	2689.1888	-0.0009
7	1	6	6	1	5	2713.1844	0.0028
8	1	8	7	1	7	3039.3336	-0.0019
8	0	8	7	0	7	3067.0367	0.0029
8	2	7	7	2	6	3070.2934	-0.0011
8	4	5	7	4	4	3071.1775	-0.0062
8	4	4	7	4	3	3071.1775	-0.0064
8	3	6	7	3	5	3071.4006	0.0185
8	3	5	7	3	4	3071.4006	-0.0241
8	2	6	7	2	5	3074.1067	-0.0013
8	1	7	7	1	6	3100.5367	-0.0016
9	1	9	8	1	8	3418.9753	0.0027
9	0	9	8	0	8	3449.2551	-0.0071
9	2	8	8	2	7	3453.8778	-0.0056
9	4	5	8	4	4	3455.1519	-0.0031
9	4	6	8	4	5	3455.1519	-0.0027
9	2	7	8	2	6	3459.3208	0.0013
9	1	8	8	1	7	3487.7962	0.0008
10	1	10	9	1	9	3798.5222	0.0069
10	0	10	9	0	9	3831.0923	-0.0029
10	5	6	9	5	5	3838.9739	0.0005
10	5	5	9	5	4	3838.9739	0.0005
10	4	7	9	4	6	3839.1591	0.0080
10	4	6	9	4	5	3839.1591	0.0071
10	3	8	9	3	7	3839.5194	0.0004
10	3	7	9	3	6	3839.6642	0.0112
10	2	8	9	2	7	3844.8566	0.0018
10	1	9	9	1	8	3874.9434	0.0053
11	1	11	10	1	10	4177.9564	0.0002
11	0	11	10	0	10	4212.5018	0.0040
11	2	10	10	2	9	4220.8446	0.0007
11	4	7	10	4	6	4223.1753	-0.0025
11	4	8	10	4	7	4223.1754	-0.0006
11	3	9	10	3	8	4223.6491	0.0002
11	3	8	10	3	7	4223.8710	0.0044
11	2	9	10	2	8	4230.7371	-0.0037
11	1	10	10	1	9	4261.9548	0.0039
12	1	12	11	1	11	4557.2955	0.0078
12	2	11	11	2	10	4604.1925	-0.0076
12	2	10	11	2	9	4616.9928	-0.0070
13	0	13	12	0	12	4973.8898	-0.0071
14	0	14	13	0	13	5353.8536	0.0011
14	1	13	13	1	12	5422.0416	0.0000

Table S9.9. Observed rotational transitions and residuals (all the values in MHz) for the 1:1 ibuprofen – water complex C4-1a in the ground vibrational state for transitions of the type $J'K'_{-1}K'_{+1} \leftarrow J''K''_{-1}K''_{+1}$.

J'	K'_{-1}	K'_{+1}	J''	K''_{-1}	K''_{+1}	Obs.	Res.
6	1	6	5	1	5	2283.0417	0.0054
6	0	6	5	0	5	2311.1938	-0.0009
6	2	5	5	2	4	2313.7019	0.0047
6	3	3	5	3	2	2314.5258	-0.0086
6	3	4	5	3	3	2314.5258	0.0146
6	1	5	5	1	4	2343.7784	0.0003
7	0	7	6	0	6	2695.1580	0.0015
7	2	6	6	2	5	2699.0983	-0.0051
7	4	3	6	4	2	2700.1613	-0.0016
7	4	4	6	4	3	2700.1613	-0.0013
7	3	4	6	3	3	2700.4590	0.0028
7	2	5	6	2	4	2703.6873	0.0021
7	1	6	6	1	5	2734.0811	0.0000
8	1	8	7	1	7	3043.3115	-0.0007
8	0	8	7	0	7	3078.5553	-0.0024
8	2	7	7	2	6	3084.4111	-0.0018
8	5	3	7	5	2	3085.8439	0.0024
8	5	4	7	5	3	3085.8439	0.0024
8	4	5	7	4	4	3086.0089	0.0024
8	4	4	7	4	3	3086.0089	0.0019
8	3	6	7	3	5	3086.3545	-0.0012
8	3	5	7	3	4	3086.4629	0.0023
8	2	6	7	2	5	3091.2667	0.0000
8	1	7	7	1	6	3124.2274	-0.0002
9	1	9	8	1	8	3423.2337	-0.0013
9	0	9	8	0	8	3461.3285	-0.0021
9	2	8	8	2	7	3469.6092	-0.0025
9	3	7	8	3	6	3472.3606	-0.0108
9	3	6	8	3	5	3472.5675	0.0039
9	2	7	8	2	6	3479.3644	0.0003
9	1	8	8	1	7	3514.1878	-0.0030
10	1	10	9	1	9	3803.0003	0.0042
10	0	10	9	0	9	3843.4117	-0.0040
10	2	9	9	2	8	3854.6869	0.0006
10	5	5	9	5	4	3857.5023	0.0046
10	5	6	9	5	5	3857.5026	0.0049
10	4	6	9	4	5	3857.8272	-0.0018
10	4	7	9	4	6	3857.8272	0.0011
10	3	8	9	3	7	3858.4405	-0.0134
10	3	7	9	3	6	3858.7782	-0.0047
10	2	8	9	2	7	3868.0193	-0.0036
10	1	9	9	1	8	3903.9628	0.0204
11	1	11	10	1	10	4182.5871	0.0041
11	0	11	10	0	10	4224.7603	-0.0048
11	4	7	10	4	6	4243.8159	-0.0023
11	4	8	10	4	7	4243.8159	0.0036
11	3	9	10	3	8	4244.5902	-0.0142
11	3	8	10	3	7	4245.1370	-0.0013
11	2	9	10	2	8	4257.2767	0.0000
11	1	10	10	1	9	4293.4522	0.0003
12	1	12	11	1	11	4561.9874	0.0013
12	0	12	11	0	11	4605.3524	0.0071
13	1	13	12	1	12	4941.2016	0.0049
13	2	11	12	2	10	5037.6302	0.0028
14	0	14	13	0	13	5364.1469	-0.0042

Conclusions

Conclusions for each molecular system are presented in the corresponding chapter from this work. Besides this, some general conclusions can be extracted by a global comparison of molecular parameters between the observed complexes. The most important parameters analyzed throughout this Thesis: hydrogen bond, C–N and C=O distances, dissociation energies and the quadrupole coupling constant χ_{cc}, are collected in Table C.1

- Diverse microsolvated complexes with up to three molecules of water have been generated in a supersonic expansion and characterized by microwave spectroscopy. The influence of water on structural parameters such us bond distances, internal rotation or conformational flexibility has been studied.

- The most stable complexes model the interactions of water with the *cis*-peptide bond, in which the water interacts simultaneously with the N–H and the C=O ends. Higher energy microsolvated complexes have been found which can model the interaction with the *trans*-peptide linkage, with higher presence in the biological environment, in which the water interacts solely with either the C=O or the H–N group.

- Based on the determined hydrogen bond parameters, the preferred interaction sites between water and amides have been clearly identified. In all the studied cases, the shorter distances of the hydrogen bond C=O···H_w–O_w interaction indicate that this is dominant in relation to the N–H···O_w hydrogen bond.

- The interactions established between water and carbamates are slightly stronger, due to the distortion of the amide group. This is reflected by shorter hydrogen bond distances in complexes with carbamates.

- The analysis of the structure in the f-w_3 allowed to demonstrate a similitude between its structure and dynamics and those of the water pentamer, and in general for formamide-water complexes and those of pure water. The similitude can be extended to other amides presented here resembling the *cis*-peptide bond, which could be seen as a water-dimer substitute.

- σ–bond cooperative effects have been identified in the studied complexes by a shortening in the hydrogen bond distances with higher hydration degree. The dissociation energies corresponding to the same type complexes are very similar, indicating that interactions of the same nature take place. The dissociation energy per hydrogen bond indicates the strengthening as the number of water molecules increases, corroborating σ–cooperativity.

- Polarization inductive effects attributable to π–cooperativity have been pointed out to occur in the gas phase for the complexes studied in this Thesis. The results of both effects are hydrogen bonds of enhanced strength and a major contribution of the charged resonant forms, revealed by the shortening of the C–N bond and the enlargement of the C=O bond.

- Polarization inductive effects are very difficult to identify experimentally. However, they can be evidenced indirectly by other properties measurable from the microwave spectrum. It has been extensively demonstrated the use of the nuclear quadrupole constant χ_{cc} as a probe for the subtle changes in the electronic environment at the N nucleus arising from polarization inductive effects. It has been suggested also the use of the internal rotation barrier as a probe of π–cooperativity since it has been observed a correlation between this barrier, the nuclear quadrupole coupling and polarization inductive effects.

Table C.1 r_0 structure hydrogen bond, C–N and C=O distances (in Å), dissociation energy per hydrogen bond (in kJ/mol) and nuclear quadrupole constant χ_{cc} for the ^{14}N nuclei (in MHz) for the complexes observed in this work complemented with data previously reported.

	$r(O\cdots H_{w1})$	$r(O_{w1}\cdots H_{w3})$	$r(O_{w2}\cdots H_{w5})$	$r(O_{w3}\cdots H_1)$	D_E /HB	r(C–N)	r(C=O)	^{14}N χ_{cc}
formamide[a]	-	-	-	-	-	1.363(3)	1.217(3)	-3.8538(51)
f-w-a[a]	1.9304(98)	-	-	2.0607(45)	22.6	[1.345][j]	[1.230]	-3.3693(96)
f-w_2[a]	1.7969(83)	1.829(4)	-	1.9363(60)	33.0	[1.343]	[1.231]	-3.0802(45)
f_2-w N_1[b]	1.788(9)	-	-	1.808(8)	36.4	1.328(7)	1.267(8)	-2.9757(86)
f_2-w N_2[b]								-2.9952(83)
f-w_3[c]	1.7777(64)	1.7380(49)	1.7810(52)	1.8748(44)	35.3	1.343	1.232(11)	-2.8204(14)
f-w-b[a]	1.932	-	-	-	31.1	[1.356]	[1.224]	-3.6018(39)
f-w-c[a]	-	-	-	2.045	25.2	[1.358]	[1.221]	-[3.62]
Formanilide								
cis-fa[d]	-	-	-	-	-	[1.370]	[1.219]	-2.767(87)
cis-fa-w-a[e]	1.931(3)	-	-	2.011(3)	23.2	[1.357]	[1.230]	-3.049(16)
cis-fa-w_2[e]	1.809(7)	1.777(6)	-	1.874(4)	33.2	[1.350]	[1.233]	-2.9637(70)
trans-fa[d]	-	-	-	-	-	[1.376]	[1.230]	-3.6713(60)
trans-fa-w-b[e]	1.905(13)	-	-	-	30.3	[1.361]	[1.227]	-3.565(14)
trans-fa-w-c[e]	-	-	-	2.0093(3)	28.8	[1.365]	[1.222]	-3.3418(31)
Methyl carbamate								
syn-mcb[f]	-	-	-	-	-	[1.364]	[1.211]	-4.29609(75)
syn-mcb-w-a[g]	1.94(1)	-	-	2.0830(4)	22.2	[1.351]	[1.223]	-4.017(16)
syn-mcb-w_2[g]	1.8055(20)	1.826(1)	-	1.9016(17)	32.3	[1.344]	[1.227]	-3.781(28)
Ethyl carbamate								
Ecb-I[h]	-	-	-	-	-	[1.366]	[1.211]	-4.2818(15)
Ecb-I-w-a[i]	1.83(1)	-	-	2.0958(6)	22.4	[1.352]	[1.224]	-4.0225(18)
Ecb-I-w_2[i]	1.793(1)	1.836(5)	-	1.887(7)	32.4	[1.345]	[1.227]	-3.792(13)
Ecb-I-w_3[i]	[1.745]	[1.731]	[1.750]	[1.845]	34.7	[1.342]	[1.227]	-3.454(25)
Ecb-II[h]	-	-	-	-	-	[1.374]	[1.213]	-3.7841(11)
Ecb-II-w-a[i]	[1.914]	-	-	[2.077]	22.2	[1.352]	[1.224]	-3.392(16)
Ecb-II-w_2[i]	[1.766]	[1.776]	-	[1.876]	32.3	[1.344]	[1.228]	-3.673(30)
Ecb-II-w_3[i]	[1.742]	[1.732]	[1.751]	[1.843]	34.7	[1.342]	[1.228]	-3.195(61)

[a] Reference [1]. [b] Reference [2]. [c] Reference [3]. [d] Reference [4]. [e] Reference [5]. [f] References [6,7]. [g] Reference [8]. [h] References [9,10]. [i] Reference [11]. [j] *Ab initio* values in square brackets where no experimental information is available.

References

[1] Blanco, S., López, J. C., Lesarri, A., Alonso, J. L. "Microsolvation of Formamide: A Rotational Study" *J. Am. Chem. Soc.*, **2006**, 128, 12111–12121.

[2] Blanco, S., Pinacho, P., López, J. C. "Hydrogen-Bond Cooperativity in Formamide$_2$-Water: A Model for Water Mediated Interactions" *Angew. Chem. Int. Ed.*, **2016**, 128, 9477–9481. Chapter IV within this Thesis.

[3] Blanco, S., Pinacho, P., López, J. C. "Structure and Dynamics in Formamide-$(H_2O)_3$: A Water Pentamer Analogue" *J Phys. Chem. Lett.*, **2017**, 8, 6060–6066. Chapter V within this Thesis.

[4] Blanco, S., López, J. C., Lesarri, A., Caminati, W., Alonso, J. L. "Conformational Equilibrium of Formanilide: Detection of the Pure Rotational Spectrum of the Tunnelling *cis* conformer" *Mol. Phys.*, **2005**, 103, 1473-1479.

[5] "Microsolvation of Formanilide Conformers: A Model for Peptide Solvation". Chapter VI within this Thesis.

[6] Marstokk, K. M., Møllendal, H. "Microwave Spectrum, Conformation, Barrier to Internal Rotation, ^{14}N Quadrupole Coupling Constants, Dipole Moment and Quantum Chemical Calculations for Methyl Carbamate" *Acta Chem. Scan.*, **1999**, 53, 79–84.

[7] Bakri, B., Demaison, J., Kleiner, I., Margulès, L., Mollendal, H., Petitprez, D., Wlodarczak, G. "Rotational Spectrum, Hyperfine Structure, and Internal Rotation of Methyl Carbamate" *J. Mol. Spectrosc.*, **2002**, 215, 312–316.

[8] "The Effect of Microsolvation over Structure, Nuclear Quadrupole and Internal Rotation: The Methyl Carbamate$\cdots(H_2O)$ and Methyl Carbamate$\cdots(H_2O)_2$ Complexes". Chapter VII within this Thesis.

[9] Marstokk, K. M., Møllendal, H. "Microwave Spectrum, Conformational Equilibrium and Quantum Chemical Calculations of Urethane (Ethyl Carbamate)" *Acta Chem. Scan.*, **1999**, 53, 329–334.

[10] Goubet, M., Motiyenko, R. A., Réal, F., Margulès, L., Huet, T. R., Asselin, P., Soulard, P., Krasnicki, A., Kisiel, Z., Alekseev, E. A. "Influence of the Geometry of a Hydrogen Bond on Conformational Stability: A Theoretical and Experimental Study of Ethyl Carbamate" *Phys. Chem. Chem. Phys.*, **2009**, 11, 1719–1728.

[11] "Microsolvation of Ethyl Carbamate I and II Conformations: Effect of the Carrier Gas on the Formation of Complexes". Chapter VIII within this Thesis.

Appendix I

Resumen en Español

La actividad de las biomoléculas depende de su estructura, la cual queda determinada por interacciones inter e intramoleculares,[1,2] siendo dominante el enlace de hidrógeno.[3-5] La presencia de agua en el medio biológico tiene una importancia especial, no solo como disolvente, sino como un componente activo. Por ejemplo, los cristales de proteínas se pueden considerar como una disolución altamente concentrada con ≈ 20-50% del volumen total ocupado por agua.[6] El pequeño tamaño de la molécula de agua junto con su doble capacidad de aceptor/dador de protones le confiere una flexibilidad particular para formar enlaces de hidrógeno, que tienen un papel central en los procesos de solvatación. Estas fuerzas no covalentes pueden controlar diversos tipos de fenómenos como equilibrios conformacionales[7,8] o tautoméricos,[9,10] procesos de estabilización de carga,[11,12] reconocimiento molecular,[13,14] y pueden influir sobre la estructura, dinámica y funcionalidad de las biomoléculas.[15,16]

En las hélices α de las proteínas, se ha observado como el agua encaja entre los grupos funcionales carbonilo y amino, y está involucrada en los procesos de plegamiento de las proteínas.[17-20] Para ello, la proteína minimiza la interacción con el agua al situar las cadenas hidrofóbicas en el interior, donde la interacción principal es el enlace de hidrógeno peptídico N–H···O=C. Por otra parte, las cadenas laterales polares se localizan en la superficie quedando expuestas a interacciones con el agua. Se ha descrito que el agua desempeña una función determinante en el mecanismo de nucleación en el plegamiento de la proteína como un intermediario en la formación del enlace de hidrógeno peptídico.

El efecto de la interacción con agua sobre diferentes tipos de moléculas se ha estudiado con detalle en las fases condensadas por diversas técnicas experimentales como ^{1}H-NMR,[21-23] espectroscopía de rayos X,[24,25] o espectroscopía de IR.[26-29] Sin embargo, el conocimiento a nivel molecular del papel de las fuerzas de interacción no covalentes responsables de la solvatación requiere aislar las moléculas de las fases condensadas, y estudiarlas en la fase gaseosa con un grado de hidratación controlado. Este entorno, en el cual un número limitado de moléculas de agua interacciona con otra molécula (el soluto) aislada, se denomina microsolvatación. La microsolvatación es un campo de investigación consolidado, como se demuestra por la cantidad de trabajos dedicados a él.[30-33] En la fase gaseosa, los estudios pioneros de moléculas con interés biológico microsolvatadas se hicieron por espectroscopía electrónica acoplada con expansión supersónica.[34-37] En espectroscopía de microondas, diversos estudios pormenorizados de moléculas y complejos de diversa naturaleza han sentado las bases de la investigación sobre los complejos con enlaces de hidrógeno,[38-42] abriendo la posibilidad del estudio de los complejos de microsolvatación.

La espectroscopía de rotación a la que se le ha implementado la técnica de expansión supersónica ha demostrado ser una herramienta experimental adecuada para caracterizar complejos microsolvatados.[43] Estos, pueden formarse fácilmente en la expansión supersónica y estudiarse posteriormente en un ambiente aislado,[34,44-47] pudiéndose determinar sus propiedades intrínsecas. El espectro puede registrarse en un espectrómetro de microondas con transformación de Fourier y expansión supersónica en modo pulsado (molecular beam Fourier transform microwave spectrometer, MB-FTMW). La muestra diluida en un gas portador a alta presión (valores típicos entre 1 y 15 bares de presión), se introduce a través de una tobera o nozzle de pequeño diámetro (del orden de 1 mm) en una cámara de alto vacío, generándose un jet supersónico por efecto de la relación entre la presión en el interior de la cámara y la presión de la mezcla. En las proximidades del nozzle tienen lugar colisiones de varios cuerpos que generan los complejos de interés pudiéndose controlar el número de moléculas de agua en los complejos microsolvatados mediante las condiciones de expansión. Según avanza la expansión se entra en un régimen libre de colisiones por lo que los complejos pueden ser estudiados en un entorno aislado. En este momento se procede a emitir un pulso de radiación electromagnética en el rango de las microondas que provoca la polarización macroscópica de la muestra que altera la población de los distintos niveles de rotación de los complejos. La energía entre los niveles de rotación está estrechamente relacionada con la distribución de masa en la molécula o complejo. Por tanto, las estructuras moleculares proporcionadas por la espectroscopía de rotación se caracterizan por una altísima precisión. Cuando cesa el pulso, los complejos retornan al estado inicial, produciéndose una desexcitación o relajación molecular y emitiéndose radiación electromagnética de una frecuencia correspondiente a la separación energética de los niveles de rotación implicados en la polarización. Se recoge esta señal de emisión molecular a través de unas antenas situadas en el centro de los espejos reflectores de la cavidad resonante Fabry-Perot. La señal se registra en el dominio del tiempo y mediante el empleo de la transformada de Fourier se obtiene la señal en el dominio de la frecuencia. También se puede registrar el espectro usando un espectrómetro de microondas con transformación de Fourier de banda ancha con expansión supersónica en modo pulsado (chirped-pulse Fourier transform microwave spectrometer, CP-FTMW), que consta de una cámara a alto vacío y que dispone de unas antenas en forma de bocina a través de las cuales se emite y se recoge la radiación electromagnética. La radiación que polariza a los sistemas moleculares consiste en un barrido lineal de toda la banda de frecuencias (de 2-8 GHz) que se realiza en un intervalo de tiempo del orden de los microsegundos. Esto permite registrar todo el espectro de rotación entre (2 y 8 GHz en el espectrómetro usado en esta Tesis) en un único ciclo de operación muy rápidamente.

Normalmente, antes de registrar el espectro se realiza un estudio de la Superficie de Energía Potencial molecular usando diferentes métodos basados en la Teoría del Funcional de la Densidad o *ab initio* y con diferentes bases de funciones. Se plantean varias estructuras posibles y se realiza una optimización de sus geometrías. Las conformaciones de menor energía se analizan en mayor profundidad, haciéndose una predicción del espectro de microondas con los valores obtenidos de las constates de rotación, de las constantes de acoplamiento de cuadrupolo nuclear y del momento dipolar eléctrico. La comparación entre el espectro experimental y las predicciones para las distintas conformaciones obtenidas teóricamente permiten el ajuste de los espectros detectados e identificarlos con los correspondientes confórmeros. En algunos casos, los confórmeros tienen una estructura suficientemente semejante, de tal forman que sus constantes de rotación son muy similares, y resulta difícil obtener una asignación inequívoca de los espectros. Para solucionar este hecho, se puede recurrir al patrón de acoplamiento de cuadrupolo nuclear, que es muy sensible a la disposición espacial del complejo dando lugar a

una estructura hiperfina completamente diferente, y que ocurre cuando en el sistema de estudio hay presente al menos un átomo con momento de cuadrupolo nuclear igual o mayor a 1.[48,49]

Un aspecto muy importante de los estudios de espectroscopía de rotación es la posibilidad de determinar las constantes de rotación para los isotopólogos, permitiendo obtener estructuras moleculares muy precisas a través de diferentes metodologías.[50,51] Las coordenadas, distancias y ángulos para las moléculas de agua en los complejos pueden determinarse directamente, por lo que es posible obtener información sobre la evolución de dichas distancias y ángulos al pasar de la molécula aislada a las primeras etapas de la solvatación. Además de estructuras muy precisas las técnicas de espectroscopía de microondas proporcionan otros parámetros moleculares relevantes. Gracias a su alto poder de resolución se pueden determinar con precisión los valores de las constantes de acoplamiento de cuadrupolo nuclear. Dichas constantes están relacionadas con el gradiente del campo eléctrico generado en el núcleo de N por el resto de cargas moleculares, y por tanto al entorno electrónico. Por esto, pueden servir para demostrar los pequeños cambios debidos a la microsolvatación. La información obtenida del espectro de rotación no está limitada a propiedades estructurales estáticas. En muchos casos, es posible obtener información sobre movimientos asociados con efecto túnel. Un ejemplo de dichos movimientos que puede medirse en los espectros de microondas es la rotación interna en aquellos sistemas que presenten un rotor interno como el grupo metilo,[52,53] para los cuales se puede determinar la barrera que impide la rotación interna. Esta, depende en un alto grado del entorno del rotor,[54] y por tanto es posible correlacionar los valores de la barrera de rotación interna con los cambios estructurales que tienen lugar en las moléculas al pasar de aislamiento a microsolvatación.

Diversos trabajos de espectroscopía de rotación sobre la microsolvatación de moléculas orgánicas de pequeño tamaño[8-10,55-69] han proporcionado un amplio conocimiento sobre las interacciones del disolvente en moléculas mayores.[70] La mayoría de dichos estudios se han realizado para complejos monohidratados, proporcionando información sobre la dinámica del agua y sirviendo para caracterizar los sitios de interacción preferentes. Al aumentar el número de moléculas de agua es posible obtener información adicional, como el papel de la cooperatividad de los enlaces de hidrógeno en el proceso de solvatación,[4] la contribución de las interacciones débiles a la estabilidad,[67,69] la manera en la que la solvatación induce cambios estructurales,[68] o la competitividad existente entre auto-asociación y solvatación.

En la mayoría de los casos, la auto-asociación del agua domina las interacciones, ya que las moléculas de agua tienden a enlazarse con otras moléculas de agua formando cadenas o ciclos, como ocurre en aquellos complejos donde únicamente existe un grupo aceptor de enlace de hidrógeno.[66,67,69] Sin embargo, en moléculas que presentan dos posiciones dador/aceptor como pueden ser amidas,[55-59] ácidos carboxílicos,[60-63] o esteres,[64,65] las moléculas de agua tienden a cerrar ciclos secuenciales dador-aceptor-dador. La detección por espectroscopía de microondas de complejos microsolvatados de más de dos moléculas de agua en moléculas orgánicas es complicada, y solo se han reportado unos pocos ejemplos.[61,62,67,69] Esto contrasta con la investigación en los complejos formados únicamente por agua,[71-80] que ha progresado de manera significativa desde el desarrollo de las técnicas de espectroscopía de microondas con jets supersónicos.[45,46]

La cooperatividad del enlace de hidrógeno presenta una especial relevancia en la estabilización de los complejos hidratados de biomoléculas, y ha sido ampliamente descrita en la literatura.[81-83] La cooperatividad de tipo σ se asocia con complejos formados por cadenas o moléculas conteniendo el grupo –OH o cualquier otro grupo capaz de actuar simultáneamente como dador y aceptor de hidrógeno.[3,4] Las moléculas de agua al establecer enlaces de hidrógeno se polarizan, incrementando su capacidad de dador y aceptor de protones y haciendo más fuertes las interacciones que presentan. La cooperatividad σ se ha descrito con detalle en la literatura,[3,4] siendo sus principales efectos el acortamiento de las distancias de los enlaces de hidrógeno y un incremento en la energía de estabilización del enlace de hidrógeno. Estos efectos son más fuertes según el número de moléculas implicadas en la cooperatividad aumenta.

En el enlace peptídico se encuentra el grupo funcional amida, cuando este grupo participa de enlaces de hidrógeno puede ocurrir otro tipo de efecto que provoca la polarización de la molécula.[3,4] Esto se representa por una mayor contribución de las formas resonantes con cargas parciales (véase Esquema 1), incrementando sus capacidades de dador y aceptor. El principal efecto de dicha polarización es el acortamiento del enlace C–N debido a un mayor carácter de enlace doble, y el alargamiento del enlace C=O debido a una cesión electrónica en la forma resonante. Además, si el enlace peptídico presenta sustitución, los grupos sustituyentes pueden también participar en la resonancia, extendiendo los efectos de la polarización a un mayor número de grupos dentro de la molécula, tal y como ocurre en los carbamatos, que son ésteres derivados de las amidas (véase Esquema 2).

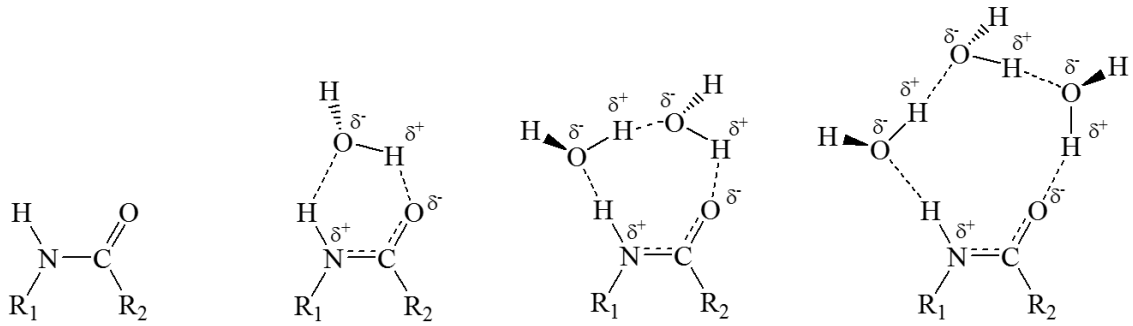

Esquema 1. Formas resonantes para complejos entre agua y grupos peptídicos. Formamida: $R_{1,2}$ = H. Formanilida: R_1 = fenilo, R_2 = H. Metil carbamato: R_1 = H, R_2 = O–CH_3. Etil carbamato: R_1 = H, R_2 = O–C_2H_5.

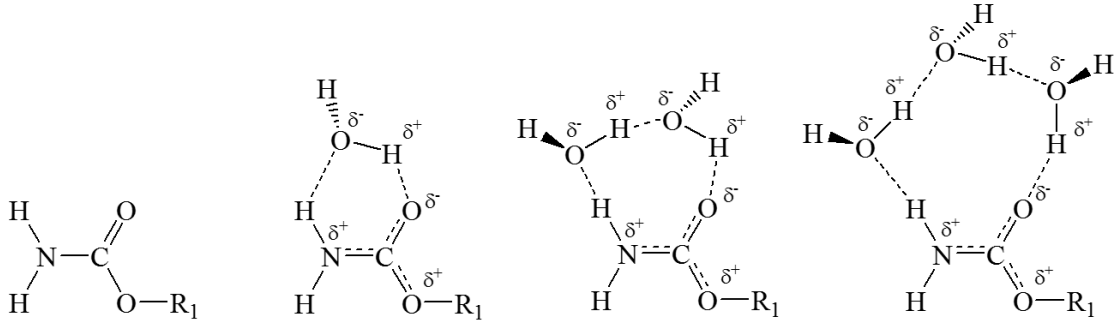

Esquema 2. Formas resonantes adicionales para los complejos entre agua y carbamatos. Metil carbamato: R_1 = O–CH_3. Etil carbamato: R_1 = O–C_2H_5.

Por lo tanto, las interacciones de enlace de hidrógeno son potenciadas por la resonancia con la deslocalización de tipo π, lo que se ha llamado Enlace de Hidrógeno Asistido por Resonancia "Resonance Assisted Hydrogen Bonding (RAHB)" o también cooperatividad de tipo π.[84-86] Éste, es un mecanismo sinérgico que provoca el refuerzo tanto del enlace de hidrógeno como de la deslocalización de tipo π, siendo los efectos más fuertes según aumenta el número de enlaces de hidrógeno cooperativos.[84,85] En el caso del enlace peptídico, se señaló la existencia de dicho efecto en estudios cristalográficos por espectroscopía de rayos X de amidas de pequeño tamaño.[86,87] Los efectos cooperativos del RAHB se han descrito también para cadenas formadas por varias amidas que pueden servir para explicar la estabilización de la estructura secundaria de las proteínas.[88] Sin embargo, los efectos de polarización debidos a RAHB apenas se han observado en la fase gas.[55]

Debido a los efectos de vibraciones, los pequeños cambios en las distancias C–N y C=O asociados a la cooperatividad de tipo π se encuentran normalmente en el límite de detección por los métodos experimental habituales, y por tanto resulta complicado determinar de manera directa si dichos cambios ocurren o no. La falta de información experimental directa se puede compensar sin embargo por otras propiedades que sí se pueden determinar de manera directa en el espectro de rotación. Una de dichas propiedades es el acoplamiento de cuadrupolo nuclear del ^{14}N presente en el grupo amida. Como ya se ha explicado anteriormente, es posible resolver la estructura hiperfina presente en el espectro de rotación y determinar las constantes de acoplamiento de cuadrupolo nuclear asociadas, las cuales están relacionadas con el gradiente del campo eléctrico y el entorno electrónico del núcleo de ^{14}N.[48,49] Estas constantes son muy sensibles a los pequeños cambios debidos a los efectos inductivos asociados a la cooperatividad de tipo π. Por otra parte, se ha relacionado el gradiente de campo eléctrico con el llenado desigual de los orbitales *p* de la capa de valencia en el núcleo que se acopla,[49] y por tanto es posible esperar una posible correlación entre las constantes de acoplamiento de cuadrupolo nuclear y la carga electrónica 2*p* obtenida a partir de un análisis de los orbitales naturales de enlace (Natural Bond Orbital, NBO).[89] Los efectos cooperativos de tipo π se pueden detectar analizando las tendencias en los valores de las constantes de acoplamiento de cuadrupolo nuclear al pasar de la molécula aislada a complejos con distintos grados de hidratación, y consecuentemente las constantes de acoplamiento de cuadrupolo se pueden utilizar como una sonda de los efectos debidos a la cooperatividad de tipo π. Una segunda sonda para los efectos de RAHB podrían ser los valores de los parámetros de rotación interna del grupo metilo unido directamente a alguno de los átomos del grupo amida.

Las investigaciones de complejos mono y dihidratados de diferentes amidas realizados por espectroscopía de microondas[55-58] han aportado información relevante, como la preferencia por el agua de interaccionar con el grupo carbonilo. En esta Tesis se presentan los estudios de microsolvatación de amidas con diferentes grupos sustituyentes (véase Figura 1) con el objetivo de describir las interacciones locales entre el agua y el enlace peptídico en diferentes situaciones. Otros objetivos de este trabajo son i) extender los estudios previos a complejos de microsolvatación con un número mayor de moléculas de agua o moléculas de soluto, ii) caracterizar los cambios estructurales debidos a los efectos cooperativos del enlace de hidrógeno; mientras que aquellos asociados a cooperatividad de tipo σ se encuentran bien descritos, hay poca información disponible sobre los efectos de polarización inductivos asociados con la cooperatividad de tipo π, iii) determinar la relación entre las constantes de acoplamiento de cuadrupolo nuclear y los efectos de distorsión en la estructura provocados por la polarización, iv) explorar las interacciones de enlace de hidrógeno que ocurren entre grupos peptídicos, las cuales apenas han sido estudiadas en la fase gas.

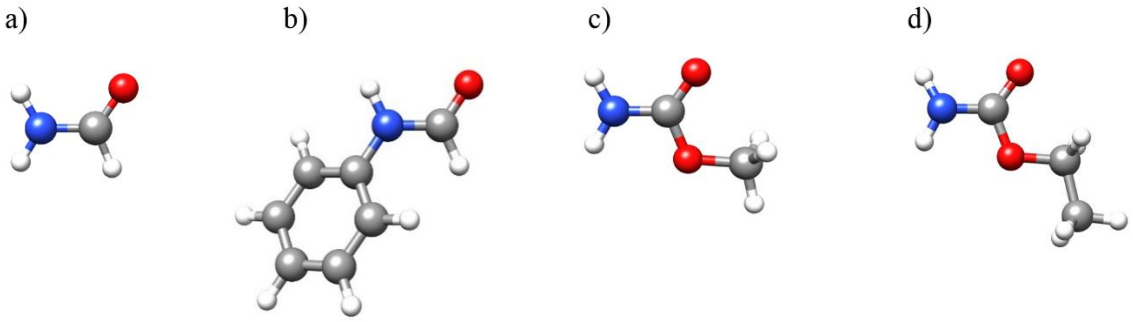

Figura 1. Moléculas para las cuales se han estudiado sus complejos microsolvatados en este trabajo. a) Formamida. b) Formanilida. c) Metil carbamato. d) Etil carbamato.

Los estudios experimentales llevados a cabo se detallan en los correspondientes capítulos en esta tesis. A continuación se dará una breve descripción de ellos y de las conclusiones generales que se han podido extraer.

Formamida$_2$···(H$_2$O)[90]

Hydrogen-Bond Cooperativity in Formamide$_2$-Water: A Model for Water Mediated Interactions.
Susana Blanco, Pablo Pinacho, Juan Carlos López.
Angewandte Chemie International Edition, 2016, **55**, 9331–9335.

La formamida es la amida más sencilla, y por tanto puede ser tomada como un sistema de referencia. Sus complejos microsolvatados con una y dos moléculas de agua se han descrito con alto nivel de detalle.[55,58] La molécula de formamida presenta múltiples sitios de interacción y sus complejos con agua pueden servir de modelo de la interacción entre el agua y el enlace peptídico en configuración *cis* o *trans*.

Nuestra intención al estudiar esta molécula era ampliar el conocimiento de la microsolvatación a complejos con más moléculas de formamida. Centramos la búsqueda en un complejo en el cual el agua actúa como ligando entre dos moléculas de formamida, formándose en total tres enlaces de hidrógeno (véase Figura 2). El interés de este complejo radica en que presenta una conectividad de enlaces de hidrógeno muy particular, que puede servir como modelo de las interacciones amida-agua, amida-amida y de las interacciones amida-amida intermediadas por agua. El estudio de dicho complejo podría proporcionar un mejor conocimiento de la competitividad entre microsolvatación o auto-asociación.

Pusimos especial cuidado a la hora de determinar de manera muy precisa la estructura del complejo y las constantes de acoplamiento de cuadrupolo nuclear para probar su posible uso como una sonda de los efectos inductivos asociados a la cooperatividad de tipo π, combinando los resultados con aquellos disponibles previamente.[58]

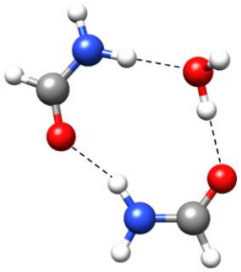

Figura 2. El complejo formamida$_2$···(H_2O).

Formamida···$(H_2O)_3$[91]
Structure and Dynamics in Formamide-$(H_2O)_3$: A Water Pentamer Analogue.
Susana Blanco, Pablo Pinacho, Juan Carlos López.
The Journal of Physical Chemistry Letters, **2017**, 8, 6060–6066.

Después de la observación del complejo formamida$_2$···(H_2O), buscamos el complejo más estable entre formamida y tres moléculas de agua, ya que hasta la fecha no se ha detectado ningún complejo de este tipo para amidas. En este complejo, se supone que las moléculas de agua interaccionan con la amida cerrando un ciclo secuencial de 10 miembros (véase Figura 3), y podría ser considerado como una continuación de los complejos monohidratado y dihidratado de formamida, presentando interacciones similares con una conectividad de enlaces de hidrógeno extendida. Por tanto, el estudio del complejo formamida···$(H_2O)_3$ podría servir como un modelo de las interacciones entre agua y el enlace *cis*-peptídico.

Una de las propiedades más interesantes que buscamos en este complejo era su posible planaridad o no planaridad, y las similitudes entre su estructura y movimientos dinámicos con aquellos que presentan los agregados de agua, $(H_2O)_n$ n = 2–5.[71-76] También tratamos de continuar las investigaciones sobre los efectos cooperativos de tipo π y el uso de las constantes de acoplamiento de cuadrupolo nuclear como una sonda de los efectos asociados a la polarización en complejos planos y angulares.

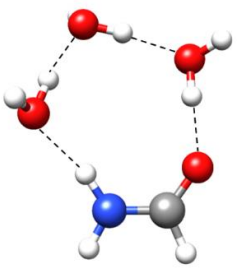

Figura 3. La configuración más estable del complejo formamida···$(H_2O)_3$.

Formanilida···$(H_2O)_n$ n = 1,2
Artículo en preparación.

La unión entre diferentes péptidos tiene lugar a través de enlaces amida que pueden adoptar disposiciones *cis* o *trans*, dependiendo de las posiciones relativas de los grupos amino y carbonilo, siendo el enlace peptídico de tipo *trans* el más abundante en la naturaleza.

La formanilida, o N-fenilformamida (véase Figura 4) también puede adoptar dos conformaciones en la fase gas, con el grupo peptídico en disposiciones *cis* o *trans*, que se asemejan a las configuraciones del enlace peptídico en sistemas más grandes. Nos hemos propuesto investigar los complejos con agua de formanilida en fase gas mediante espectroscopía de microondas para describir las interacciones locales del agua con ambas conformaciones del enlace peptídico y encontrar las principales diferencias entre ellos.

Otra conclusión interesante que se puede estudiar con este sistema es la posible alteración de las estructuras de la formanilida según aumenta el número de moléculas de agua en el complejo. La configuración *cis* no es plana, y se espera que en los complejos con agua el ángulo entre los grupos fenilo y amida no se altere de manera significativa. Por otra parte, la configuración *trans* es plana y el anillo bencénico ejerce un impedimento estérico que bloquea la posibilidad de formar ciclos secuenciales con la amida, tal y como se han visto para la formamida.

También quisimos continuar con la investigación de la cooperatividad de tipo π en complejos de amidas y el uso de las constantes de acoplamiento de cuadrupolo nuclear como una sonda de los efectos asociados a la polarización en complejos planos y no planos.

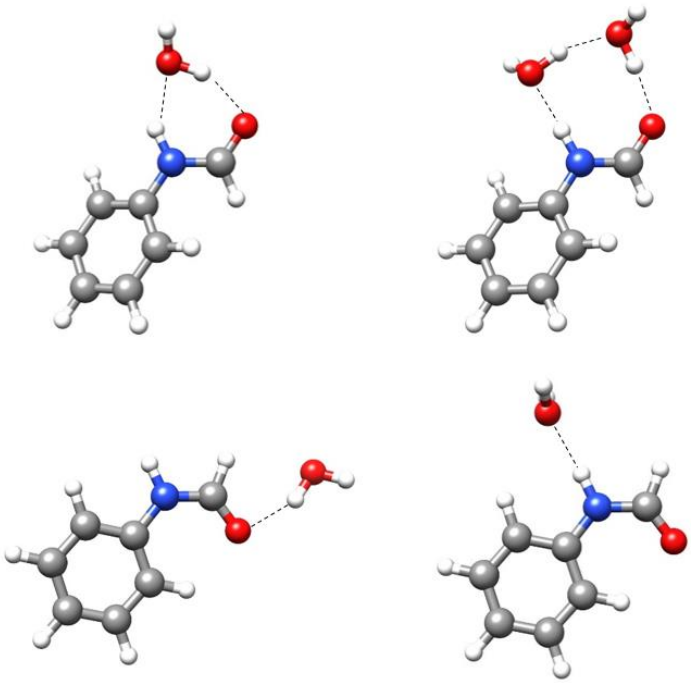

Figura 4. Los complejos monohidratados y dihidratados más estables de formanilida para las configuraciones *cis* (arriba) y *trans* (abajo).

Metil carbamato···$(H_2O)_n$ n = 1,2
Artículo en preparación.

El metil carbamato es un éster derivado de una amida (véase Figura 5). El objetivo al estudiar sus complejos microsolvatados es describir las interacciones de enlace de hidrógeno que tienen lugar con un enlace *cis*-peptídico sustituido. El punto de partida para este trabajo fueron complejos con interacciones similares a aquellos vistos para formamida y formanilida.

El metil carbamato presenta un esqueleto plano, y se espera que las moléculas de agua en los complejos se dispongan en el plano formado por el metil carbamato. Por tanto, estos complejos podrían servir como una continuación de las investigaciones del uso del acoplamiento de cuadrupolo para explorar los efectos cooperativos de tipo π iniciados en estudios anteriores.

Otro objetivo principal de este estudio es intentar encontrar una evidencia experimental que demuestre que la rotación interna puede servir también para poner de manifiesto los efectos de polarización debido a RAHB. Se ha buscado por tanto una correlación entre las constantes de acoplamiento de cuadrupolo y la barrera de rotación interna del grupo metilo.

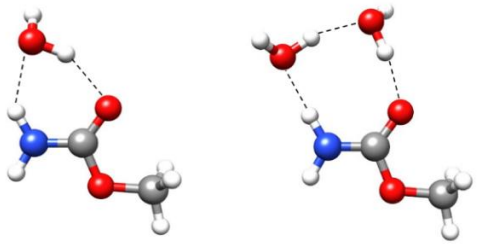

Figura 5. Los complejos entre metil carbamato - agua.

Etil carbamato···$(H_2O)_n$ n = 1,2,3
Artículo en preparación.

El etil carbamato (véase Figura 6) presenta dos configuraciones, plana y angular, que se interconvierten a través de una función de potencial periódica caracterizada por una baja barrera de energía potencial. En una expansión supersónica la observación de ambas conformaciones depende del gas portador usado debido a la relajación conformacional en el seno del jet supersónico.

El objetivo al estudiar sus complejos microsolvatados es, además de servir como modelo de las interacciones del agua con el grupo carbamato, estudiar la posible influencia de la microsolvatación en el correspondiente equilibrio conformacional.

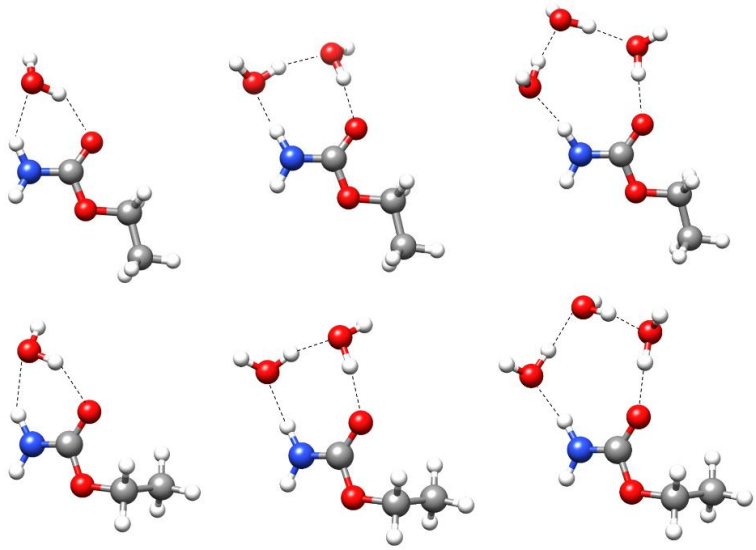

Figura 6. Complejos entre etil carbamato I (arriba) y II (abajo) con hasta tres moléculas de agua.

Ibuprofeno···(H_2O)
Artículo en preparación.

El ibuprofeno es uno de los medicamentos más populares. La molécula de ibuprofeno presenta un ácido carboxílico además de un grupo isobutilo con una flexibilidad particular. Se ha llevado a cabo el estudio de sus complejos microsolvatados con la intención de describir las interacciones locales entre el agua y grupos ácido en moléculas de mayor tamaño.

El punto de partida del trabajo fueron los complejos monohidratados formados con los cuatro monómeros de ibuprofeno descritos previamente en fase gaseosa. El objetivo era observar los complejos con las cuatro configuraciones, caracterizarlos, y analizar la posible influencia del agua en el equilibrio conformacional. Es de esperar que la molécula de agua cierre un ciclo secuencial con el grupo carboxílico, tal y como se representa en la Figura 7.

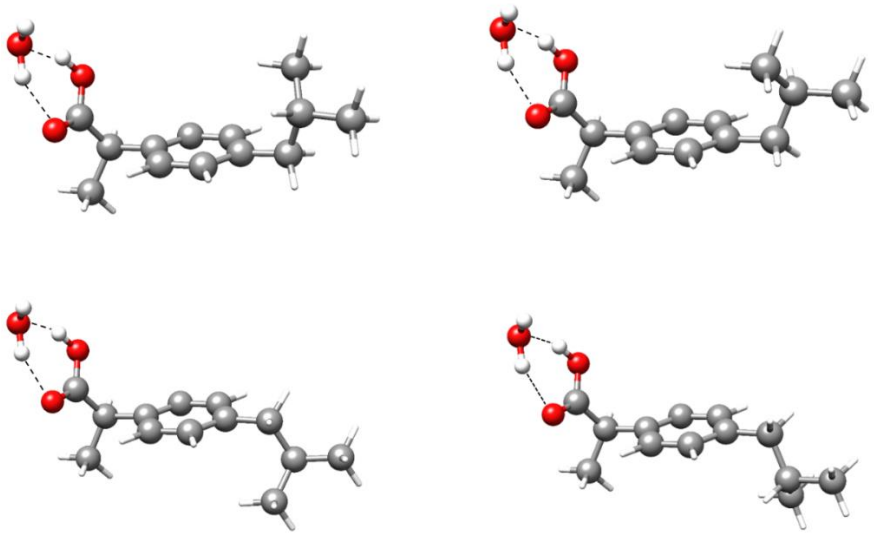

Figura 7. Los complejos más estables predichos de agua con las cuatro configuraciones observadas del ibuprofeno.

Conclusiones

Aparte de las conclusiones que se presentan para cada sistema molecular en los correspondientes capítulos de esta tesis, se pueden extraer ciertas conclusiones generales a partir de una comparación global de los parámetros moleculares entre los complejos observados. Los parámetros más importantes analizados a lo largo de esta Tesis incluyen las distancias de enlace de hidrógeno y de los enlaces C–N y C=O, las energías de disociación y la constante de acoplamiento de cuadrupolo χ_{cc}.

- Se han generado varios sistemas microsolvatados con hasta tres moléculas de agua en una expansión supersónica y se han caracterizado mediante espectroscopía de microondas. Se ha estudiado la influencia de la interacción con las moléculas de agua en parámetros estructurales tales como las distancias de enlace, las constantes de rotación interna o la flexibilidad conformacional.

- Los complejos más estables observados describen las interacciones del agua con el enlace peptídico en configuración *cis*, en los cuales el agua interacciona de manera simultánea con los grupos N–H y C=O. Se han observado también complejos microsolvatados de mayor energía, que pueden describir interacciones con el enlace *trans*-peptídico, en estos, el agua interacciona únicamente con el grupo C=O, o con el N–H.

- En base a los parámetros de enlace de hidrógeno determinados, los sitios de interacción preferentes entre el agua y las amidas han sido identificados de manera inequívoca. En todos los casos estudiados, las distancias de enlace de hidrógeno C=O···H_w–O_w son más cortas que las N–H···O_w, indicando que la primera interacción podría ser dominante respecto a la segunda.

- En base a las distancias de enlace de hidrógeno más cortas observadas en los complejos con carbamatos, se puede concluir que las interacciones formadas entre agua y el grupo carbamato son ligeramente más fuertes, en principio debido a la distorsión del esqueleto de la amida.

- El análisis de la estructura en el complejo f-w_3 ha permitido demostrar la existencia de una similitud entre su estructura y movimientos y los correspondientes al pentámero de agua, y en general entre los complejos entre formamida-agua y los agregados de agua. La similitud se puede extender a otras moléculas que presenten el grupo amida estudiadas en este trabajo, que desde el punto de vista estructural, podría considerarse equivalente a un dímero de agua.

- Los efectos de la cooperatividad de tipo σ se han identificado en los complejos observados debido a un acortamiento en las distancias de los enlaces de hidrógeno según aumenta el grado de hidratación. Las energías de disociación correspondientes a complejos del mismo tipo son muy similares, indicando que las interacciones que tienen lugar son de la misma naturaleza. La energía de disociación por enlace de hidrógeno sugiere que el enlace de hidrógeno se hace más fuerte según aumenta el número de moléculas de agua en el complejo, confirmando la cooperatividad de tipo σ.

- Se ha demostrado la existencia de efectos de polarización inductivos debidos a cooperatividad de tipo π en fase gas para los complejos estudiados en esta Tesis. Los resultados de los efectos cooperativos son enlaces de hidrógeno más fuertes y con una mayor contribución de las formas resonantes con cargas parciales, tal y como lo prueba el acortamiento de la distancia C–N y el alargamiento del enlace C=O.

- Los efectos de polarización inductivos son muy difíciles de observar de manera directa experimentalmente. Sin embargo, se pueden evidenciar a través de otras propiedades que sí son determinables a partir del espectro de microondas. Ha sido ampliamente demostrado en esta Tesis el uso de las constantes de acoplamiento de cuadrupolo nuclear como una sonda de los cambios que ocurren en el entorno electrónico del núcleo de N debido a los efectos inductivos. Se ha demostrado también que el uso del valor de la barrera de rotación interna puede servir como una sonda adicional de la cooperatividad de tipo π ya que se ha podido observar una correlación entre dicha barrera, las constantes de cuadrupolo nuclear y los efectos de polarización.

Referencias

[1] Hofacker G.L. "Intra- and Intermolecular Interactions" in *Biophysics*, eds. Hoppe W., Lohmann W., Markl H., Ziegler H. Springer, Berlin, 1982.
[2] Baker, E. N., Hubbard, R. E. "Hydrogen bonding in globular proteins" *Prog. Biophys. Mol. Biol.*, **1984**, 44, 97–179.
[3] Saenger, W., Jeffrey, G. A. *Hydrogen Bonding in Biological Structures*, Springer-Verlag, Berlin, 1991.
[4] Jeffrey, G. A. *An Introduction to Hydrogen Bonding*, Oxford University Press, Oxford, 1997.
[5] McNaught, A. D., Wilkinson, A. *IUPAC, Compendium of Chemical Terminology (The "Gold Book")*, 2nd ed., Blackwell Scientific Publications, Oxford, 1997.
[6] Saenger, W. "Structure and Dynamics of Water Surrounding Biomolecules" *Ann. Rev. Biophys. Chem.*, **1987**, 16, 93–114.
[7] Schmitt, M., Böhm, M., Ratzer, C., Vu, C., Kalkman, I., Meerts, W. L. "Structural Selection by Microsolvation: Conformational Locking of Tryptamine" *J. Am. Chem. Soc.*, **2005**, 127, 10356–10364.
[8] Caminati, W., López, J. C., Blanco, S., Mata, S., Alonso, J. L. "How Water Links to *Cis* and *Trans* Peptidic Groups: The rotational Spectrum of N-Methylformamide-Water" *Phys. Chem. Chem. Phys.*, **2010**, 12, 10230–10234.
[9] Maris, A., Ottaviani P., Caminati, W. "Pure Rotational Spectrum of 2-Pyridone···Water and Quantum Chemical Calculations on the Tautomeric Equilibrium 2-Pyridone···Water/2-Hydroxypyridine···Water" *Chem. Phys. Lett.*, **2002**, 360, 155–160.
[10] Mata, S., Cortijo, V., Caminati, W., Alonso, J. L., Sanz, M. E., López, J. L., Blanco, S. "Tautomerism and Microsolvation in 2-Hydroxypyridine/2-Pyridone" *J. Phys. Chem. A*, **2010**, 114, 11393–11398.
[11] Wyttenbach, T., Paizs, B., Barran, P., Breci, L., Liu, D., Suhai, S., Wysocki, V. H., Bowers, M. T. "The Effect of the Initial Water of Hydration on the Energetics, Structures, and H/D Exchange Mechanism of a Family of Pentapeptides: An Experimental and Theoretical Study" *J. Am. Chem. Soc.*, **2003**, 125, 13768–13775.
[12] Xu, S. J., Nilles, M., Bowen, K. H., "Zwitterion Formation in Hydrated Amino Acid, Dipole Bound Anions: How Many Water Molecules Are Required?" *J. Chem. Phys.*, **2003**, 119, 10696–10701.
[13] Robinson, C. R., Sligar, S. G. "Molecular Recognition Mediated by Bound Water: A Mechanism for Star Activity of the Restriction Endonuclease *Eco*RI" *J. Mol. Biol.*, **1993**, 234, 302–306.
[14] Jayaram, B., Jain, T. A. "The Role of Water in Protein-DNA Recognition" *Annu. Rev. Biophys. Biomol. Struct.*, **2004**, 33, 343–361.
[15] Levy, Y., Onuchic, J. N. "Water Mediation in Protein Folding and Molecular Recognition" *Annu. Rev. Biophys. Biomol. Struct.*, **2006**, 35, 389–415.
[16] Biedermannová, L., Schneider, B. "Hydration of Proteins and Nucleic Acids: Advances in Experiment and Theory. A Review" *Biochimica et Biophysica Acta*, **2016**, 1860, 1821–1835.
[17] Groot, B. L., Grubmüller, H. "Water Permeation across Biological Membranes: Mechanism and Dynamics of Aquaporin-1 and GlpF" *Science*, **2001**, 294, 2353–2357.
[18] Ball, P. "Water as an Active Constituent in Cell Biology" *Chem. Rev.*, **2008**, 108, 74–108.
[19] Venkatachalam, C. M. "Stereochemical criteria for Polypeptides and Proteins. V. Conformation of a System of Three Linked Peptide Units" *Biopolymers*, **1968**, 6, 1425–1436.
[20] Chaplin, M. "Do We Underestimate the Importance of Water in Cell Biology?" *Nat. Rev. Mol. Cell Biol.*, **2006**, 7, 861–866.
[21] Modig, K., Liepinsh, E., Otting, G., Halle, B. "Dynamics of Protein and Peptide Hydration" *J. Am. Chem. Soc.*, **2004**, 126, 102–114.
[22] Nucci, N. V., Pometun, M. S., Wand, A. J. "Site-Resolved Measurement of Water-Protein Interactions by Solution NMR" *Nat. Struct. Mol. Biol.*, **2011**, 18, 245–249.
[23] Hilser, V. J. "Structural Biology: Finding the Wet Spots" *Nature*, **2011**, 469, 166–167.
[24] Egli, M., Portmann, S., Usman, N. "RNA Hydration: A Detailed Look" *Biochemistry*, **1996**, 35, 8489–8494.
[25] Schotte, F., Lim, M., Jackson, T. A., Smirnov, A. V., Soman, J., Olson, J. S., Phillips Jr, G. N., Wulff, M., Anfinrud, P. A. "Watching a Protein as it Functions with 150-ps Time-Resolved X-Ray Crystallography" *Science*, **2003**, 300, 1944–1947.
[26] Nibbering, E. T. J., Elsaesser, T. "Ultrafast Vibrational Dynamics of Hydrogen Bonds in the Condensed Phase" *Chem. Rev.*, **2004**, 104, 1887–1914.
[27] Bakker, H. J., Skinner, J. L. "Vibrational Spectroscopy as a Probe of Structure and Dynamics in Liquid Water" *Chem. Rev.*, **2010**, 110, 1498–1517.

[28] Tielrooij, K. J., García-Araez, N., Bonn, M., Bakker, H. J. "Cooperativity in Ion Hydration" *Science*, **2010**, 328, 1006–1009.
[29] Perera, A. S., Thomas, J., Poopari, M. R., Xu, Y. "The Clusters-in-a-Liquid Approach for Solvation: New Insights from the Conformer Specific Gas Phase Spectroscopy and Vibrational Optical Activity Spectroscopy" *Front. Chem.*, **2016**, 4, 1–17.
[30] *Chem. Rev.*, **2016**, 116, Issue 9 "Noncovalent interactions", 4911–5688.
[31] *Chem. Rev.*, **2016**, 116, Issue 13 "Water – The most anomalous liquid", 7459–7726.
[32] Bagchi, B. *Water in Biological and Chemical Processes: From structure and Dynamics to Function*, Cambridge University Press, Cambridge, 2013.
[33] Gerhards, M. "Spectroscopy of Neutral Peptides in the Gas Phase: Structure, reactivity, Microsolvation, Molecular Recognition*"* in *Principles of Mass Spectrometry Applied to Biomolecules*, eds. Laskin, J., Lifshitz, C., 2006.
[34] Levy, D. H. "Laser Spectroscopy of Cold Gas-Phase Molecules" *Annu. Rev. Phys. Chem.*, **1980**, 31, 197–225.
[35] Rizzo, T. R., Park, Y. D., Petenau, L., Levy, D. H. "Electronic Spectrum of the Amino Acid Tryptophan Cooled in a Supersonic Molecular Beam" *J. Chem. Phys.*, **1985**, 83, 4819–4820.
[36] Philips, L. A., Levy, D. H. "The Rotationally Resolved Electronic Spectrum of Indole in the Gas Phase" *J. Chem. Phys.*, **1986**, 85, 1327–1332.
[37] Philips, L. A., Levy, D. H. "Rotationally Resolved Electronic Spectroscopy of Tryptamine Conformers in a Supersonic Jet" *J. Chem. Phys.*, **1988**, 89, 85–90.
[38] Legon, A. C., Soper, P. D., Flygare, W. H. "The Rotational Spectrum, H, ^{19}F Nuclear Spin-Nuclear Spin Coupling, D Nuclear Quadrupole Coupling, and Molecular Geometry of a Weakly Bound Dimer of Carbon Monoxide and Hydrogen Fluoride" *J. Chem. Phys.*, **1981**, 74, 4944–4950.
[39] Legon, A. C., Aldrich, P. D., Flygare, W. H. "The Rotational Spectrum, Chlorine Nuclear Quadrupole Coupling Constants, and Molecular Geometry of a Hydrogen-Bonded Dimer of Cyclopropane and Hydrogen Chloride" *J. Am. Chem. Soc.*, **1982**, 104, 1486–1490.
[40] Legon, A. C., Millen, D. J. "Gas-Phase Spectroscopy and the Properties of Hydrogen-Bonded Dimers: HCN···HF as the Spectroscopic Prototype" *Chem. Rev.*, **1986**, 86, 635–657.
[41] Kisiel, Z., Fowler, P. W., Legon, A. C. "Investigation of the Rotational Spectrum of the Hydrogen-Bonded Dimer Formed between Methylenecyclopropane and HCl" *J. Chem. Phys.*, **1994**, 101, 4635–4643.
[42] Legon, A. C. "Prereactive Complexes of Dihalogens XY with Lewis Bases B in the Gas Phase: A Systematic Case for the Halogen Analogue B···XY of the Hydrogen Bond B···HX" *Angew. Chem. Int. Ed.*, **1999**, 38, 2686–2714.
[43] Becucci, M., Melandri, S. "High-Resolution Spectroscopic Studies of Complexes Formed by Medium-Size Organic Molecules" *Chem. Rev.* **2016**, *116*, 5014–5037.
[44] Levy, D. H. "The Spectroscopy of Very Cold Gases" *Science*, **1981**, 214, 263–269.
[45] Miller, D. R. "Free Jet Sources" in *Atomic and Molecular Beam Methods* ed. Scoles, G. Oxford University press, Oxford, 1988, Volume 1, pp. 14–53.
[46] Montero, S., Maté, B., Tejeda, G., Fernández, J. M., Ramos, A. "Raman Studies of Free Jet Expansion" in *Atomic and Molecular Beams. The state of Art 2000* ed. Campargue, R. Springer-Verlag, Berlin, 2001, pp. 295–306.
[47] Maté, B., Graur, I. A., Elizarova, T., Chirokov, I., Tejeda, G., Fernández, J. M., Montero, S. "Experimental and Numerical Investigation of an Axisymmetric Supersonic Jet" *J. Fluid Mech.*, **2001**, 426, 177–197.
[48] Braag, J. K. "The Interaction of Nuclear Electric Quadrupole Moments with Molecular Rotation in Asymmetric-Top Molecules. I" *Phys. Rev.*, **1948**, 74, 533–538.
[49] Gordy, W., Cook, R. L. *Microwave Molecular Spectra*, Wiley-Interscience, New York, 1984.
[50] Domenicano, A., Hargittai, I. *Accurate Molecular Structures: Their Determination and Importance* Oxford University Press, New York, 1992.
[51] Demaison, J. "Accurate Structures of Non-Rigid Molecules by Microwave Spectroscopy" in *Structures and Conformations of Non-Rigid Molecules* eds. Laane, J., Dakkouri, M., van der Veken, B., Oberhammer, H. Springer, Dordrecht, 1993, Volume 410, pp. 239–256.
[52] Lin, C. C., Swalen, J. D. "Internal Rotation and Microwave Spectroscopy" *Rev. Mod. Phys.*, **1959**, 31, 841–892.
[53] Lister, D. G., Macdonald, J. N., Owen, N. L. "Internal Rotation and Inversion. An Introduction to Large Amplitude Motions in Molecules" Academic Press, London, 1978.

[54] Herschbach, D. R. "Calculation of Energy Levels for Internal Torsion and Over-All Rotation. III" *J. Chem. Phys.*, **1959**, 31, 91–108.
[55] Lovas, F. J., Suenram, R. D., Fraser, G. T., Gillies, C. W., Zozom, J. "The Microwave Spectrum of Formamide-Water and Formamide-Methanol Complexes" *J. Chem. Phys.*, **1988**, 88, 722–729.
[56] Held, A., Pratt, D. W. "Hydrogen Bonding in Water Complexes. Structures of 2-Pyridone-H_2O and 2-Pyrididone-$(H_2O)_2$ in Their S_0 and S_1 Electronic States" *J. Am. Chem. Soc.*, **1993**, 115, 9708–9717.
[57] Lavrich, R. J., Tubergen, M. J. "Conformation and Hydrogen Bonding in the Alaninamide-Water van der Waals Complex" *J. Am. Chem. Soc.* **2000**, 122, 2938–2943.
[58] Blanco, S., López, J. C., Lesarri, A., Alonso, J. L. "Microsolvation of Formamide: A Rotational Study" *J. Am. Chem. Soc.*, **2006**, 128, 12111–12121.
[59] López, J. C., Sanchez, R., Blanco, S., Alonso, J. L. "Microsolvation of 2-Azetidinone: A Model for the Peptide Group-Water Interactions" *Phys. Chem. Chem. Phys.* **2015**, 17, 2054–2066.
[60] Canagaratna, M., Phillips, J. A., Ott, M. E. Leopold, K. R. "The Nitric-Acid Complex: Microwave Spectrum, Structure and Tunneling" *J. Phys. Chem. A*, **1998**, 102, 1489–1497.
[61] Ouyang, B., Starkey, T. G., Howard, B. J. "High-Resolution Microwave Studies of Ring-Structured Complexes between Trifluoroacetic Acid and Water" *J. Phys. Chem. A* **2007**, 111, 6165–6175.
[62] Ouyang, B., Howard, B. J. "Hydrates of *trans*- and *gauche*-Difluoroacetic Acids: A High-Resolution Microwave Spectroscopic Study" *J. Phys. Chem. A* **2010**, 114, 4109–4117.
[63] Schnitzler, E. G., Jäger, W. "The Benzoic Acid-Water Complex: A Potential Atmospheric Nucleation Precursor Studied Using Microwave Spectroscopy and *Ab Initio* Calculations" *Phys. Chem. Chem. Phys.*, **2014**, 16, 2305–2314.
[64] Thomas, J., Sukhorukov, O., Jäger, W., Xu, Y. "Direct Spectroscopic Detection of the Orientation of Free OH Groups in Methyl Lactate-$(Water)_{1,2}$ Clusters: Hydration of a Chiral Hydroxy Ester" *Angew. Chem. Int. Ed.* **2014**, 53, 1156–1159.
[65] Gall, J. T. A., Thomas, J., Xie, F., Wang, Z., Jäger, W., Xu, Y. "Rotational Spectroscopy of the Methyl-Glycidate-Water Complex: Conformation and Water and Methyl Rotor Tunneling Motions" *Phys. Chem. Chem. Phys.* **2017**, 19, 29508–29515.
[66] Su, Z., Xu, Y. "Hydration of a Chiral Molecule: The Propylene Oxide$\cdots(Water)_2$ Cluster in the Gas Phase" *Angew. Chem. Int. Ed.* **2007**, *119*, 6275–6278.
[67] Pérez, C., Neill, J. L., Muckle, M. T., Zaleski, D. P., Peña, I., López, J. C., Alonso, J. L., Pate, B. H. "Water-Water and Water-Solute Interactions in Microsolvated Organic Complexes" *Angew. Chem. Int. Ed.* **2014**, 54, 979–982.
[68] Pérez, C., López, J. C., Blanco, S., Schnell, M. "Water-Induced Structural Changes in Crown Ethers from Broadband Rotational Spectroscopy" *J. Phys. Chem. Lett.* **2016**, *7*, 4053–4058.
[69] Pérez, C., Krin, A., Steber, A. L., López, J. C., Kisiel, Z., Schnell, M. "Wetting Camphor: Multi-Isotopic Substitution Identifies the Complementary Roles of Hydrogen Bonding and Dispersive Forces" *J. Phys. Chem. Lett.* **2016**, *7*, 154–160.
[70] Bellissent-Funel, M.-C.; Hassanali, A.; Havenith, M.; Henchman, R.; Pohl, P.; Sterpone, F.; van der Spoel, D.; Xu, Y.; Garcia, A. E. "Water Determines the Structure and Dynamics of Proteins" *Chem. Rev.* **2016**, 116, 7673–7697.
[71] Dyke, T. R.; Mack, K. M.; Muenter, J. S. "The Structure of Water Dimer from Molecular Beam Electric Resonance Spectroscopy" *J. Chem. Phys.* **1977**, 66, 498-510.
[72] Keutsch, F. N.; Cruzan, J. D.; Saykally, R. J. "The Water Trimer" *Chem. Rev.* **2003**, 103, 2533–2577.
[73] Cruzan, J. D.; Braly, L. B.; Liu, K.; Brown, M. G.; Loeser, J. G.; Saykally, R. J. "Quantifying Hydrogen Bond Cooperativity in Water: VRT Spectroscopy of the Water Tetramer" *Science* **1996**, 271, 59–62.
[74] Liu, K.; Brown, M. G.; Cruzan, J. D.; Saykally, R. J. "Vibration-Rotation Tunneling Spectra of the Water Pentamer: Structure and Dynamics" *Science* **1996**, 271, 62–64.
[75] Ramírez, F.; Hadad, C. Z.; Guerra, D.; David, J.; Restrepo, A. "Structural Studies of the Water Pentamer" *Chem. Phys. Lett.* **2011**, 507, 229–233.
[76] Cole, W. T. S.; Fellers, R. S.; Viant, M. R.; Saykally, R. J. "Hydrogen Bond breaking Dynamics in the Water Pentamer: Terahertz VRT Spectroscopy of a 20 μm Libration" *J. Chem. Phys.* **2017**, 146, 14306.
[77] Pérez, C., Muckle, M. T., Zaleski, D. P., Seifert, N. A., Temelso, B., Shields, G. C., Kisiel, Z., Pate, B. H. "Structures of Cage, Prism, and Book Isomers of Water Hexamer from Broadband Rotational Spectroscopy" *Science* **2012**, 336, 897–901.
[78] Richardson, J. O., Pérez, C., Lobsiger, S., Reid, A. A., Temelso, B., Shields, G. C., Kisiel, Z., Wales, D. J., Pate, B. H., Althorpe, S. C. "Concerted Hydrogen-Bond Breaking by Quantum Tunneling in the Water Hexamer Prism" *Science* **2016**, 351, 1310–1313.

[79] Pérez, C., Lobsiger, S., Seifert, N. A., Zaleski, D. P., Temelso, B., Shields, G. C., Kisiel, Z., Pate, B. H. "Broadband Fourier Transform Rotational Spectroscopy for structure Determination: The Water Heptamer" *Chem. Phys. Lett.* **2013**, 571, 1–15.
[80] Pérez, C., Zaleski, D. P., Seifert, N. A., Temelso, B., Shields, G. C., Kisiel, Z., Pate, B. H. "Hydrogen Bond Cooperativity and the Three-Dimensional Structures of Water Nonamers and Decamers" *Angew. Chem. Int. Ed.* **2014**, 53, 14368–14372.
[81] Del Bene, J. E. "Molecular Orbital Theory of the Hydrogen Bond. 18. Methyl Substituent Effects on Amide Hydrogen Bonding" *J. Am. Chem. Soc.*, **1978**, 100, 1387–1394
[82] Liang, W., Li, H., Hu, X., Han, S. "Proton Transfer of Formamide + *n*H2O (*n* = 0-3): Protective and Assistant Effect of the Water Molecule" *J. Phys. Chem. A*, **2004**, 108, 10219–10224.
[83] Venkataramanan, N. S. "Cooperativity of Intermolecular Hydrogen Bonds in Microsolvated DMSO and DMF Clusters: A DFT, AIM, and NCI Analysis" *J. Mol. Model*, **2016**, 22, 151–162.
[84] Gilli, G., Bellucci, F., Ferretti, V., Bertolasi, V. "Evidence for Resonance-Assisted Hydrogen Bonding from Crystal-Structure Correlations on the Enol Form of the *β*–Diketone Fragment" *J. Am. Chem. Soc.*, **1989**, 111, 1023–1028.
[85] Bertolasi, V., Gilli, P., Ferretti, V., Gilli, G. "Evidence for Resonance-Assisted Hydrogen Bonding. 2. Intercorrelation between Crystal Structure and Spectroscopic Parameters in Eight Intramolecularly Hydrogen Bonded 1,3.Diaryl-1,3-propanedione Enols" *J. Am. Chem. Soc.*, **1991**, 113, 4917–4925.
[86] Gilli, P., Bertolasi, V., Ferretti, V., Gilli, G. "Evidence for Intramolecular N-H···O Resonance Assisted Hydrogen Bonding in *β*-Enaminones and Related Heterodienes. A Combined Crystal-Structural, IR, and NMR Spectroscopic, and Quantum-Mechanical Investigation" *J. Am. Chem. Soc.*, **2000**, 122, 10405–10417.
[87] Ottersen, T. "On the structure of the Peptide Linkage. The Structures of Formamide and Acetamide at -165 Degrees C and an *Ab Initio* Study of Formamide, Acetamied and N-methylformamide" *Acta Chemica Scandinavica*. **1975**, 29a, 939–944.
[88] Kobko, N., Dannenberg, J. J. "Cooperativity in Amide Hydrogen Bonding Chains. Relation between Energy, Position, and H-Bond Chain in Peptide and Protein Folding Models" *J. Phys. Chem. A*, **2003**, 107, 10389–10395.
[89] Reed, A. E., Weinstock, R. B., Weinhold, F. "Natural Population Analysis" *J. Chem. Phys.* **1985**, *83*, 735-746.
[90] Blanco, S., Pinacho, P., López, J. C. "Hydrogen-Bond Cooperativity in Formamide$_2$-Water: A Model for Water Mediated Interactions" *Angew. Chem. - Int. Ed.*, 2016, **55**, 9331–9335.
[91] Blanco, S., Pinacho, P., López, J. C. "Structure and Dynamics in Formamide-$(H_2O)_3$: A Water Pentamer Analogue" *J Phys. Chem. Lett.*, **2017**, 8, 6060–6066.

Appendix II

Flexibility Unleashed in Acyclic Monoterpenes: Conformational Space of Citronellal Revealed by Broadband Rotational Spectroscopy

PCCP

PAPER

View Article Online
View Journal | View Issue

Cite this: *Phys. Chem. Chem. Phys.*, 2016, **18**, 16682

Flexibility unleashed in acyclic monoterpenes: conformational space of citronellal revealed by broadband rotational spectroscopy†

Sérgio R. Domingos,[abc] Cristóbal Pérez,[abc] Chris Medcraft,‡[a] Pablo Pinacho[ad] and Melanie Schnell*[abc]

Received 29th April 2016,
Accepted 7th June 2016

DOI: 10.1039/c6cp02876d

www.rsc.org/pccp

Conformational flexibility is intrinsically related to the functionality of biomolecules. Elucidation of the potential energy surface is thus a necessary step towards understanding the mechanisms for molecular recognition such as docking of small organic molecules to larger macromolecular systems. In this work, we use broadband rotational spectroscopy in a molecular jet experiment to unravel the complex conformational space of citronellal. We observe fifteen conformations in the experimental conditions of the molecular jet, the highest number of conformers reported to date for a chiral molecule of this size using microwave spectroscopy. Studies of relative stability using different carrier gases in the supersonic expansion reveal conformational relaxation pathways that strongly favour ground-state structures with globular conformations. This study provides a blueprint of the complex conformational space of an important biosynthetic precursor and gives insights on the relation between its structure and biological functionality.

1 Introduction

Understanding the interplay between the three-dimensional structure of a biomolecule and its functionality is critical for rationalising ligand–receptor mechanisms in biochemistry.[1,2] Aspects such as conformational flexibility and chirality come into play if one is to understand these ligand–receptor interactions. Exploration and mapping of the potential energy surface of such key biomolecular systems is thus of utmost importance in revealing the underpinning mechanisms. Citronellal is a prominent acyclic monoterpene, predominantly formed by the secondary metabolism of plants, and a versatile precursor in many key biochemical reactions.[3–5] A known example in acid catalysis is the Prins reaction of citronellal where the protonation of the carbonyl group results in the synthesis of several isopulegol isomers as a consequence of the many conformations that citronellal can adopt.[6] The conformational flexibility of citronellal, arising from five C–C single bonds along the backbone (Fig. 1), results in many stable energy minima and thus plays a pivotal role in biosynthesis of monoterpenes.

Citronellal is a known insect repellent[7,8] and the main component found in citronella oil giving it its distinctive lemon scent, a property that is regularly exploited in the cosmetics industry. Citronellal is chiral and as such exists as one of two stereoisomers. As an odourant molecule (−)-citronellal has been subject of multiple studies that aim at the elucidation of its binding interactions with olfactory receptors.[9] The biological selectivity of the olfactory system is well known,[10] for example the olfactory discrimination between the stereoisomers of carvone: while the *R* enantiomer smells like spearmint, the *S* enantiomer smells like caraway seeds. Studies suggest that selective docking to olfactory receptors is governed by the handedness and conformation of the ligand.[10,11] In particular, recent investigations addressing binding efficiencies of citronellal to olfactory receptors indicate that the orientation of the reactive carbonyl group is crucial and governs the docking efficiency to the receptors.[9,11]

Rotational spectroscopy is a powerful spectroscopic method to obtain information on the structure of molecules in the gas phase with high precision and resolution.[12,13] Recent advances such as the implementation of short and intense microwave chirps in broadband excitation spectroscopic schemes revolutionised the field of rotational spectroscopy.[14] Using chirped-pulse Fourier-transform microwave (CP-FTMW) spectroscopy, it is possible to record rotational spectra of complex, flexible

[a] *Max Planck Institute for the Structure and Dynamics of Matter, Luruper Chaussee 149, 22761 Hamburg, Germany. E-mail: melanie.schnell@mpsd.mpg.de*
[b] *Center for Free-Electron Laser Science, Luruper Chaussee 149, 22761 Hamburg, Germany*
[c] *The Hamburg Centre for Ultrafast Imaging, Universität Hamburg, Luruper Chaussee 149, 22761 Hamburg, Germany*
[d] *Department of Physical Chemistry and Inorganic Chemistry, Universidad de Valladolid, Valladolid, Spain*

† Electronic supplementary information (ESI) available: Fi. See DOI: 10.1039/c6cp02876d

‡ Current address: School of Chemistry, Newcastle University, Newcastle upon Tyne, NE1 7RU, UK.

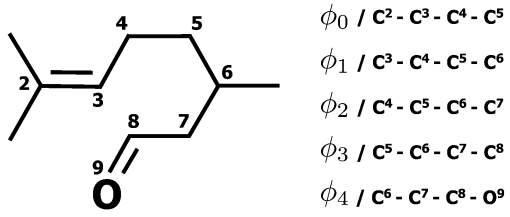

Fig. 1 Schematic drawing of the chemical structure of citronellal, also known as rhodinal or 3,7-dimethyloct-6-en-1-al ($C_{10}H_{18}O$).

molecules spanning several GHz with a single acquisition. Complemented by substantial improvements in quantum–chemical calculations and the aid of automated spectral assignment programs,[15,16] an unprecedented amount of structural information and internal dynamics of isolated molecules and clusters can now be extracted from a broadband rotational spectrum. We refer to some recent work on terpenes,[15,17–20] pharmaceutical compounds,[21,22] amino acids,[23,24] sugars,[25,26] water clusters[27,28] and micro-solvated organic compounds.[29–32] In addition, broadband rotational spectroscopy can now also be exploited to investigate chiral molecules and determine the absolute configuration of molecular species within chiral mixtures with high precision.[33,34]

In this work, we use CP-FTMW spectroscopy to investigate the conformational flexibility of citronellal under the conditions of a cold molecular beam. Citronellal, with its acyclic and extremely flexible structure, is a good candidate to benchmark both the quality of quantum–chemical calculations for the prediction of gas-phase conformations and the sensitivity of the spectroscopic technique to unambiguously identify molecular species with complex conformational spaces. In the following, we discuss the observed conformations, their structural similarities, stabilisation mechanisms and how they are energetically ordered. Additionally, we investigate how the relative population of each conformer is influenced by the carrier gas used for the expansion and tentatively devise conformational relaxation trajectories to interpret our observations. We find that citronellal has a preference for certain types of conformations and we discuss its implications regarding flexibility and functionality.

2 Methods

2.1 Experimental methods

The sample was purchased from Sigma-Aldrich (99% purity) and used without further purification. All the broadband rotational spectra used in this study were obtained with the Hamburg COMPACT spectrometer,[35] which has been described elsewhere and thus only a brief description is given here. A supersonic expansion brings the sample into the vacuum chamber where a 4 μs chirp spanning 2 → 8 GHz polarises the ensemble of molecules. The seeding of molecules into a supersonic expansion is done using a pulsed nozzle (Parker General Valve Series 9) operating at 3 Hz with a constant flow of carrier gas (neon or argon) at stagnation pressures of 3 bar to generate a cold molecular jet. To create sufficient vapour pressure the sample was heated to 80 °C directly at the nozzle. The chirp is generated with an arbitrary waveform generator (AWG) and amplified in a 300 W traveling wave tube (TWT) amplifier before being broadcast into the vacuum chamber using a horn antenna. The horn antennas used here have higher gain and improved directionality compared with those used previously. The reader is referred to ref. 28 for further details on the horn antennas. Upon chirped microwave excitation we record the free induction decay (FID) of the macroscopic dipole moment of the ensemble of molecules. For this experiment, we utilised a new data acquisition scheme using the 'fast frame' option of the digital oscilloscope.[28] In short, eight back-to-back excitation chirps are performed on each pulse of sample and the subsequent eight FID acquisitions are co-added and averaged. This scheme decreases the measurement time and sample consumption, resulting in an effective repetition rate of 24 Hz for the experiment. We record 40 μs of the FIDs which, after a Fourier transformation (FT), gives us a resolution of 25 kHz in our microwave spectrum. 1.5 million FIDs (equivalent to 14 hours of measurement time) were co-added to obtain the final spectrum.

2.2 Computational methods

The conformational space of citronellal was explored in two stages. Initially, a semi-empirical search was performed using the Austin Model 1 (AM1) that is implemented in Spartan.[36] More than one hundred conformations were obtained and further re-optimised at higher levels of theory using Gaussian09.[37] Fifteen conformations were found within an energy cut-off of 6 kJ mol^{-1} using the B3LYP-D3 (Becke, three-parameter, Lee–Yang–Parr) exchange–correlation functional, including Grimme's empirical dispersion correction, and the aug-cc-pVTZ basis set. Additionally, those fifteen structures were also optimised using second-order Moller–Plesset perturbation theory (MP2) with the 6-311++G** basis set. Frequency calculations were performed to ascertain the valid energy minima and obtain the zero-point corrected energies (see ESI†).

Secondly, a more localised and systematic search of the conformational space was performed at the B3LYP/3-21G level of theory by scanning combinations of two dihedral angles in steps of 10 degrees and allowing the remaining coordinates to relax during the optimisation at each step. The potential energy surface obtained from one of these scans is shown in Fig. 2 (top panel). Cross sections of the maps were performed at the B3LYP-D3/aug-cc-pVTZ level of theory (see Fig. 2, lower panels). This methodology revealed two additional conformations, XI and XII, that were not identified semi-empirically and have energies within the 6 kJ mol^{-1} energy cut off.

3 Results and discussion

3.1 Conformational space and assignment

In Fig. 3 we show a portion of the measured rotational spectrum (Ne-seeded, upper trace, in black) plotted against the fitted rotational lines of fifteen conformations of citronellal (lower traces, in colours). The assignment of observed experimental

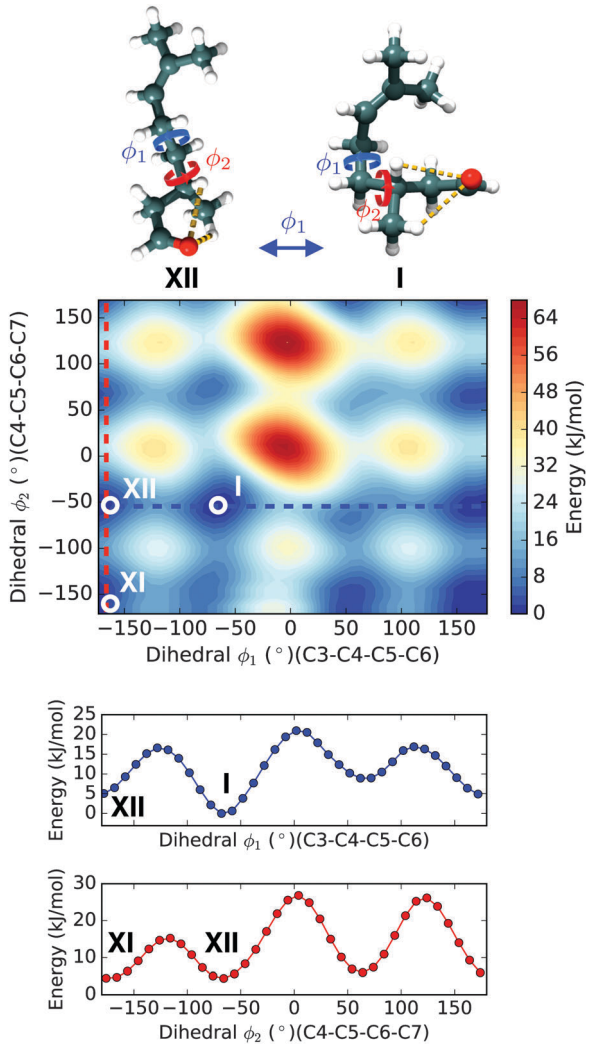

Fig. 2 Top panel: Potential energy landscape of citronellal obtained at the B3LYP/3-21G level of theory by scanning the dihedral coordinates ϕ_1 and ϕ_2 (indicated in blue and red in the molecular structure, respectively) in steps of 10°. Lower panels: Linear transit scans of ϕ_1 (in blue) and ϕ_2 (in red) obtained at the B3LYP-D3/6-311++G** level of theory.

lines to rotational transitions of a certain conformer was performed through a recurrent fit based on Watson's A-reduced rigid rotor Hamiltonian as implemented in PGOPHER[38] and JB95.[39] As a result, rotational constants (A, B, C) and quartic centrifugal distortion constants (D_J, D_K, D_{JK}, δ_J, δ_K) were well determined for most of the conformers. The experimentally determined parameters are shown in Table 1. We note that line splittings due to methyl group internal rotation are present for a number of conformers. However, further analysis concerning internal dynamics is out of the scope of this paper.

A complete assignment of the fifteen reported conformers was facilitated using the automated spectral fitting program AUTOFIT[16] that uses estimated rotational constants and dipole moments as a starting point and delivers refined candidates based on a least-squares fitting algorithm. We note that within the set of fifteen assigned conformers, in addition to their distinct rotational constants, unique signatures differentiate them solely based on the type of spectrum observed (see Table 1). As an example, conformers I, II and III have distinct spectral types: whilst conformer I shows both b- and c-type rotational transitions, conformer II reveals only b-type and conformer III shows a- and b-type transitions. This is a consequence of the extreme flexibility of the molecule itself expressed by the changing orientation of the dipole moment. The large number of flexible coordinates, that are dependent on each other, results in a rich and complex conformational landscape. Therefore, the distinct types of rotational transitions observed for different conformers of citronellal facilitate the reliable assignment of multiple conformations in very dense and congested spectra as the one investigated here.

3.2 Theoretical predictions and structural similarities

Our theoretical predictions using quantum–chemical calculations anticipate a total of seventeen conformations within an energetic window of 6 kJ mol^{-1}. In Fig. 4 we show the calculated structures, depicting also the relative energies and strongest intramolecular interactions (dashed lines) present for each conformer. We find that the predicted conformations can be grouped based on their backbone structural similarities,

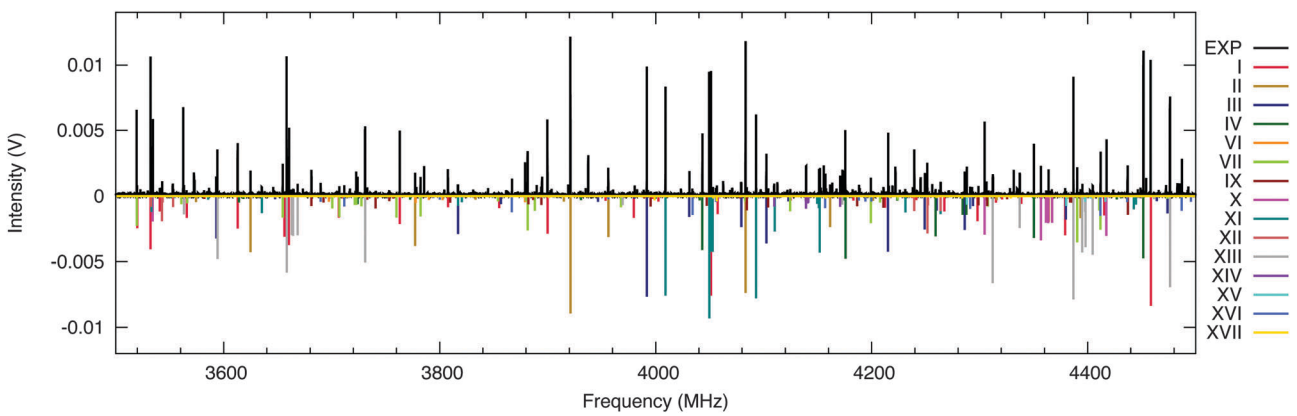

Fig. 3 Portion of the 2–8 GHz spectrum of citronellal (1.5 M acquisitions, 14 h of measurement time). The upper trace (in black) shows the experimental spectrum obtained using neon as a carrier gas. The lower traces (in colour) represent simulations employing the fitted parameters of citronellal as given in Table 1. Intensities are based on calculated dipole moment components and estimated relative populations.

Table 1 Experimentally determined parameters for the 15 conformations of citronellal identified in the microwave spectrum: rotational constants (*A*, *B*, *C* in MHz) and quartic centrifugal distortion constants (in kHz); type of spectrum observed (a-type, b-type, c-type) with y being observed and n being not observed; predicted dipole moments † (see Table S2, ESI); number of lines used in the fit; standard error of the fit (kHz); asymmetry parameter $\kappa = (2B - A - C)/(A - C)$. The dash (—) indicates that the parameter was fixed to zero in the fit. The experimental frequency accuracy is 25 kHz

	I	II	III	IV	VI
A (MHz)	1317.4649(13)	1580.7079(14)	1546.5213(18)	1362.2074(34)	1660.9330(646)
B (MHz)	692.52126(73)	522.02024(65)	567.18188(53)	584.81168(50)	496.59102(68)
C (MHz)	558.53524(84)	472.84994(84)	495.88040(54)	481.86671(44)	451.12094(65)
D_J (kHz)	0.209(16)	0.2442(65)	0.3316(42)	0.2551(36)	0.5479(97)
D_{JK} (kHz)	−0.188(71)	−1.185(23)	−1.706(33)	−0.595(27)	−6.84(11)
D_K (kHz)	0.454(69)	3.635(70)	5.19(17)	2.33(71)	−0.3979(650)
δ_J (kHz)	—	0.0487(29)	0.0831(30)	0.0822(23)	−0.1214(36)
δ_K (kHz)	—	—	—	0.371(71)	0.0211(50)
a/b/c	n/y/y	n/y/n	y/y/n	y/y/n	y/y/y
$\mu_a/\mu_b/\mu_c$†	−0.13/1.37/−1.81	0.12/−2.20/−0.64	−0.79/−2.30/−0.55	2.91/1.37/−0.03	−2.61/1.78/−1.25
N	53	50	51	49	31
σ (kHz)	12.3	14.5	9.1	6.3	8.9
κ	−0.647	−0.911	−0.864	−0.766	−0.925

	VII	IX	X	XI	XII
A (MHz)	1605.4178(12)	1893.5114(11)	1820.05(40)	3118.2631(31)	2574(10)
B (MHz)	509.32052(60)	432.31046(42)	447.53527(86)	344.60535(30)	356.34111(43)
C (MHz)	418.49286(46)	375.05049(40)	424.92546(89)	330.63279(31)	352.28168(41)
D_J (kHz)	0.2299(45)	0.0765(32)	0.0957(49)	0.0453(17)	0.0315(16)
D_{JK} (kHz)	−0.366(27)	−0.549(12)	—	−0.578(51)	—
D_K (kHz)	—	2.94(11)	—	—	—
δ_J (kHz)	0.0754(29)	—	—	—	—
δ_K (kHz)	—	—	—	—	—
a/b/c	y/y/y	n/y/y	y/n/n	y/n/n	y/n/n
$\mu_a/\mu_b/\mu_c$†	−1.35/−1.33/1.22	−0.22/2.10/−1.66	−3.10/−0.85/−0.73	−1.67/−0.76/1.99	−1.70/0.01/1.85
N	77	64	28	43	26
σ (kHz)	13.0	9.7	14.9	9.3	8.8
κ	−0.847	−0.925	−0.968	−0.990	−0.996

	XIII	XIV	XV	XVI	XVII
A (MHz)	2423.0569(23)	2623.4(49)	1679.6748(77)	1513.7868(22)	1434.95789(53)
B (MHz)	380.05537(50)	350.1327(11)	576.72284(69)	589.84641(60)	634.32380(91)
C (MHz)	352.68703(46)	339.9565(10)	523.05132(69)	452.20259(66)	533.68888(54)
D_J (kHz)	0.0597(30)	0.0698(34)	0.1399(73)	0.0358(66)	0.183(14)
D_{JK} (kHz)	—	−1.22(15)	—	0.589(64)	—
D_K (kHz)	—	—	—	—	—
δ_J (kHz)	—	0.0125(36)	—	—	0.0280(81)
δ_K (kHz)	—	—	—	—	—
a/b/c	y/y/y	y/n/n	y/n/y	y/y/y	n/y/y
$\mu_a/\mu_b/\mu_c$†	−2.24/−0.87/1.55	−1.39/−0.43/−2.05	2.03/0.06/−1.81	1.74/1.82/−0.73	0.04/−2.26/−1.41
N	54	20	21	41	21
σ (kHz)	16.1	8.4	8.7	12.8	5.8
κ	−0.974	−0.991	−0.907	−0.741	−0.777

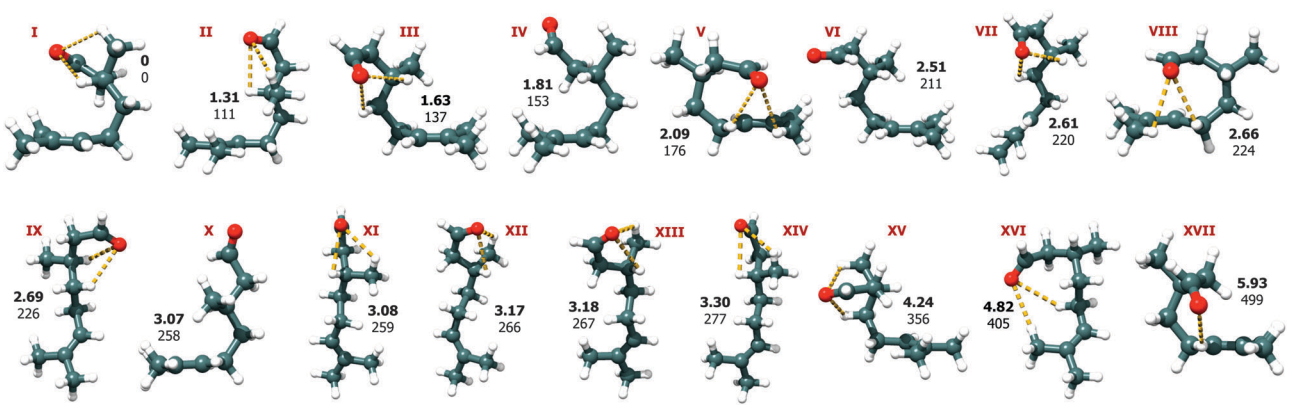

Fig. 4 Molecular structures of seventeen conformations of citronellal obtained from B3LYP-D3/aug-cc-pVTZ calculations. The structures are ordered based on their predicted relative zero-point corrected energies (in kJ mol^{-1} and cm^{-1}, respectively). Results of MP2 calculations are summarised in Table S2 of the ESI.† The dashed coloured lines depict the predominant intramolecular interactions.

i.e., dihedral angles with similar values. We thus define families of conformers based on their similarity for the first two dihedral angles (ϕ_0, ϕ_1). These dihedrals define the general folding of the molecule into a more prolate or globular shape while the precise conformation is determined by structural changes localised on the aldehyde terminus. With this condition we find a total of seven families grouped as follows: (I, IV, V, XVII), (II, III, VI, X), (VII), (VIII), (IX, XI, XII, XVI), (XIII, XIV) and (XV). Table S1 in the ESI† contains all the dihedral angles considered here. It is interesting to note that within their respective families, the following pairs of conformers (I, IV), (II, X) and (III, VI) can be interconverted between one another by a single rotation along ϕ_4 (C^6–C^7–C^8–O^9), and allowing a relaxation of all other dihedral coordinates to take place (see Table S1 and Fig. S3 of the ESI†). This rotation effectively controls the relative orientation of the carbonyl functional group with respect to the backbone. Conformers I, II and III, where the oxygen lone pairs are pointing inwards in a folded-like conformation, result in an overall globular structure. The rotated equivalents IV, X and VI, respectively, have the carbonyl group pointing outwards assuming an exposed prolate-like structure, as indicated by the asymmetry parameters (κ) of these conformers (see Table 1).

Both quantum–chemical methods (B3LYP-D3 and MP2, see Table S2 in the ESI†) predict the global minimum to be conformer I, which is the conformation with the lowest absolute value for κ, reflecting its pronounced globular shape (see Fig. 4). The strong b- and c-type transitions observed (see Table 1 and ESI† for the full broadband spectrum) also support the preliminary assignment of conformer I as the global minimum.

3.3 Conformational relaxation

All fifteen fitted spectra can be assigned to calculated structures as the numbering in Table 1 and Fig. 4 indicate. Two predicted low-energy conformations (conformers V and VIII) could not be identified in the experimental spectrum. A tentative explanation for this has been devised by evaluating potential cooling pathways that could allow the interconversion between conformers V and VIII to other lower-lying conformations. To plot such cooling pathways we performed systematic scans of candidate dihedral coordinates that could facilitate interconversion between conformers. In Fig. 5 we show the results of a suggested cooling trajectory that allows conformational relaxation of conformer V into conformer I, and conformer VIII into conformer II. Interestingly, we find that for both cases, a two-step cooling pathway through sequential rotation of dihedral coordinates is possible. Panels A and C of Fig. 5 show that (1) concerted relaxation by simultaneous rotation of two dihedrals is not energetically favourable compared with that of sequential relaxation steps, and (2) multiple trajectories require attention. We find that for each conformation, the depicted relaxation trajectories are energetically favoured. In Fig. 5 (panel B) we show that conformer V may transit from its initial conformation to an intermediate state through rotation of ϕ_3.

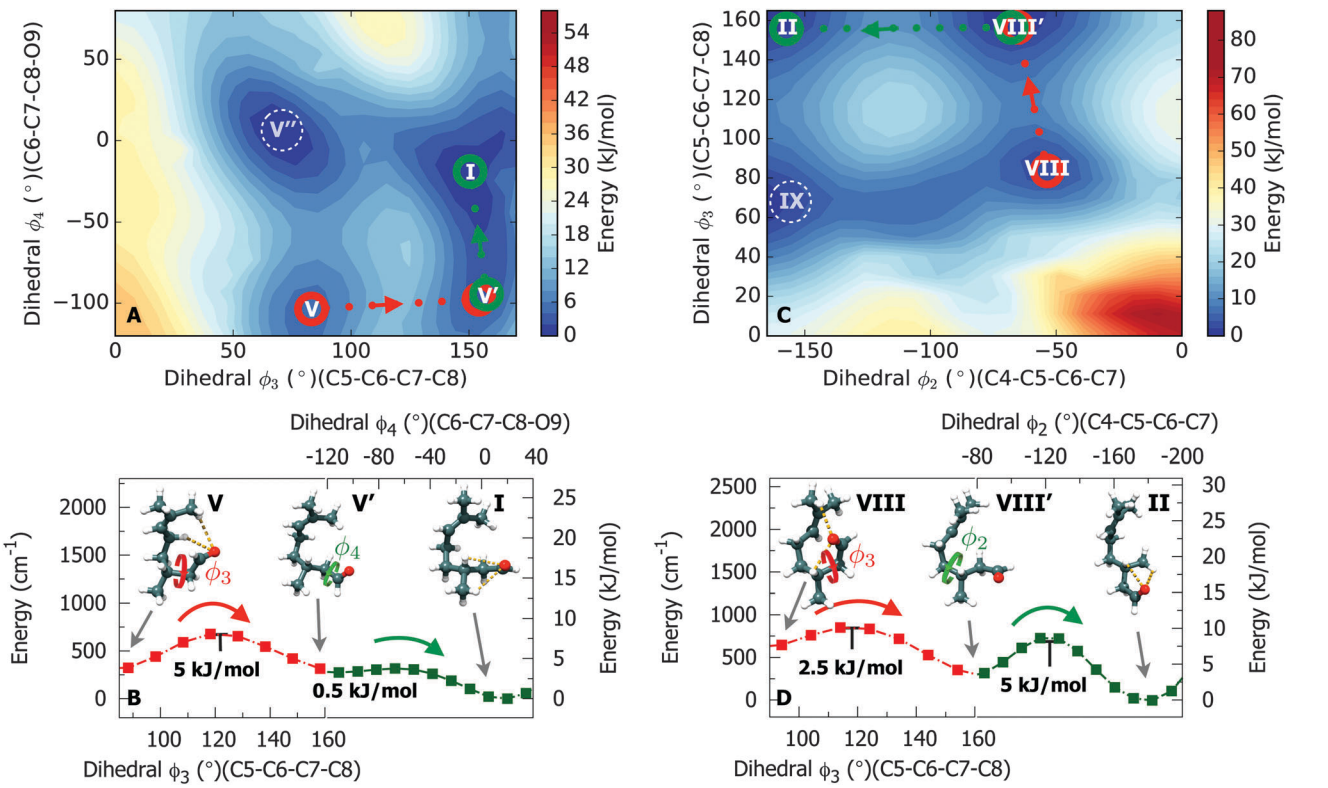

Fig. 5 Conformational relaxation pathways for conformer V (panels A and B) and conformer VIII (panels C and D). The potential energy surfaces (panels A and C) were predicted at the B3LYP/3-21G level of theory. Panels B and D show the relevant cross sections of the surfaces obtained at the B3LYP-D3/6-311++G** level of theory. Relaxation pathways involving two sequential steps were plotted for conformers V → I and VIII → II, respectively, using rotations of dihedral coordinates in a sequential manner.

Consequently, this intermediate state V′ relaxes to the final state as conformation I by rotation of ϕ_4. In a similar way, conformation VIII initially relaxes to an intermediate state VIII′ through rotation of ϕ_3, following rotation of ϕ_2 leading to a new lower local minimum as conformation II (see panel D). The magnitude of the predicted interconversion energy barriers reported here are in line with previously reported studies.[40–42] Moreover, we note that from a purely energetic point of view, our tentative cooling trajectories (V → I and VIII → II) are in agreement with the energy ordering for conformers obtained from the B3LYP-D3 calculation.

3.4 Relative stability of the energy minima

As Fig. 2 illustrates, the potential-energy landscape of citronellal is shaped by deep pockets, where conformers are confined by energy barriers that in most cases are higher than 10 kJ mol^{-1}. Furthermore, nine low-energy minima are predicted by theory within an energy window of less than 3 kJ mol^{-1}, an indication that a correlation between the predicted energy ordering and a confident assignment of a global minimum is not trivial. Therefore, to gain insight into the relative stabilities of the energy minima, we performed the same experiment but using argon as the seeding gas for the supersonic expansion.

Previous studies have shown that heavier inert gases have an enhanced cooling efficiency in supersonic expansions due to the larger collision energies they provide.[43,44] Consequently, an argon-seeded expansion is expected to favour conversion of higher energy conformers to lower ones, facilitating an assignment of the ground-state structure(s) and assisting in quantitatively evaluate our quantum–chemical predictions. In Fig. 6 we show four sections (panels A → D) of the broadband spectrum of citronellal using neon (in red) and argon (in blue) as carrier gases and relevant rotational transitions of conformers I, II, III, IV, VI and X. These six conformations can undergo interconversion by means of rotation of a single dihedral coordinate (ϕ_4). Interconversion barriers for IV → I, VI → III and X → II can be found in Fig. S3 of the ESI.† Panel A displays two rotational transitions of conformer III ($J_{K_aK_c} \leftarrow J_{K_aK_c}'$: $3_{21} \leftarrow 2_{12}$ and $6_{25} \leftarrow 5_{24}$) and one transition of conformer IV ($6_{25} \leftarrow 5_{24}$). Whilst the rotational transitions from conformer III can be observed in both neon- and argon-seeded spectra, the transition from conformer IV is only observed in the neon spectrum thus indicating that IV has relaxed to a lower energy conformation. Similar conclusions can be drawn for the remaining conformers by evaluating the panels B → D. Based on these observations, we conclude that improved cooling is achieved through collisions with argon during the supersonic expansion and thus conformational relaxation of conformers IV, VI and X (in addition to V and VIII) is facilitated, strongly suggesting that conformers I, II and III are the lower-lying energy conformations.

Comparison of the rotational spectra with Ne and Ar provides additional information: whilst in the Ne spectrum we observe fifteen conformations, only eight of those fifteen conformers (I, II, III, VII, XI, XIII, XV and XVI) are observed in the Ar spectrum. Interestingly, we find that in general only one conformer is observed in the Ar spectrum for each of the families. Particular cases are those of conformers II and III, and of conformers XI and XVI, belonging to the same families, which are observed in both Ne and Ar spectra (see Table S1 of the ESI†). Regardless of their similarities, conformers II and III are separated by an energy barrier of 10 kJ mol^{-1} (see Fig. S2, panel D in the ESI†) and thus conformational relaxation is not achieved through higher energy collisions with Ar compared with that of Ne. The same stands for conformations XI and XVI, where dihedrals ϕ_2, ϕ_3 and ϕ_4 assume very distinct values, resulting in higher energy barriers not favouring conformational relaxation. These observations are nevertheless consistent with energetically-favoured relaxation trajectories that allow interconversion between conformers of the same family due to their intrinsic structural similarities. Moreover, it becomes more evident that the relative orientation of the terminus containing the aldehyde functional group – reflected mostly in the dihedral coordinates ϕ_3 and ϕ_4 – is responsible for most of the conformational richness of citronellal.

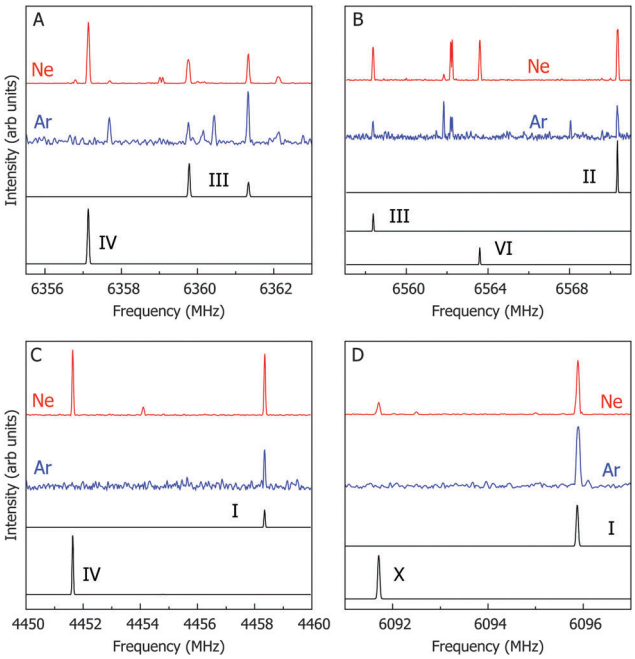

Fig. 6 Coloured traces show portions of the CP-FTMW spectra of 1.5 million co-added FIDs using neon (red trace) and argon (blue trace) as backing gas in the supersonic expansion. The black traces show simulations based on the experimental molecular parameters (Table 1) for the numbered conformers.

4 Conclusions and outlook

We have successfully used broadband rotational spectroscopy and quantum–chemical calculations to probe the complex conformational space of citronellal and assigned fifteen stable conformations in the cold conditions of a molecular jet. To date, structural studies on acyclic terpenes were limited due to the many degrees of freedom allowed by their backbone configuration. This study demonstrates the outstanding performance of the technique to resolve the structure of flexible molecules. We have evaluated the relative stability of energy minima by comparing rotational spectra of citronellal using different seeding gases. Evidence is found for enhanced cooling efficiency in an Ar-seeded expansion

compared with that of Ne, which facilitates the assignment of the global minimum structure of citronellal, and aids in the prediction of conformational relaxation trajectories. Globular structures, instead of linear ones, are found to be more stable due to intramolecular stabilisation of the aldehyde functional group.

Putative bindings of citronellal to olfactory receptors have been previously investigated and assume a docking with different hydrogen bond connections to the aldehyde group.[9] The relative orientation of the aldehyde moiety with respect to the rest of the molecule is critical in establishing a relation between conformation and functionality.[11] Our findings reveal that citronellal has strong preference for conformations that have the aldehyde moiety pointing inwards, assuming a stable chair-like folded conformation, in prejudice to linear prolate-like forms with the aldehyde group pointing outwards. We also note that regardless if the preferred conformations are of the folded or unfolded type, the great majority of observed species utilises the aldehyde functional group to stabilise the overall structure, resulting in less electronic density available for intermolecular interactions to take place. However, we show that rotation of the aldehyde terminus can be achieved with significant ease for many conformers, resulting in a rich and rather complex conformational space. This appears to be in contrast with a recent microwave study on another acyclic monoterpene, linalool, that has revealed a single conformer under similar experimental conditions.[45] Our observations are also consistent with previous reports that show that the origin of isopulegol isomer formation is strongly dependent on the energetically most-favoured chair-like conformations of (*S*)-citronellal.[6]

The role of conformational flexibility and molecular handedness in the selectivity of olfactory receptors upon docking of ligands such as citronellal is yet not fully understood. This case study should not be considered exceptionally unusual due to its large conformational flexibility, but an example of how maneuverable and complex potential-energy landscapes can be even for molecules of this size. Moreover, this study provides particular structural insights that may aid in assessing the roles of conformational flexibility and docking efficiency of systems with bio-selectivity.

Acknowledgements

We acknowledge financial support by the Deutsche Forschungsgemeinschaft in the context of the priority program SPP1807 (SCHN1280/4-1). Furthermore, this work has been supported by the excellence cluster "The Hamburg Centre for Ultrafast Imaging – Structure, Dynamics and Control of Matter at the Atomic Scale" of the Deutsche Forschungsgemeinschaft. S. R. D. and C. P. acknowledge a Postdoctoral Research Fellowship from the Alexander von Humboldt Foundation. We acknowledge the use of the GWDG computer cluster.

References

1 B. Malnic, J. Hirono, T. Sato and L. B. Buck, *Cell*, 1999, **96**, 713–723.
2 W. B. Floriano, N. Vaidehi, W. A. Goddard, M. S. Singer and G. M. Shepherd, *Proc. Natl. Acad. Sci. U. S. A.*, 2000, **97**, 10712–10716.
3 G. Siedenburg, M. Breuer and D. Jendrossek, *Appl. Microbiol. Biotechnol.*, 2012, **97**, 1571–1580.
4 G. Siedenburg, D. Jendrossek, M. Breuer, B. Juhl, J. Pleiss, M. Seitz, J. Klebensberger and B. Hauer, *Appl. Environ. Microbiol.*, 2012, **78**, 1055–1062.
5 P. Mäki-Arvela, N. Kumar, V. Nieminen, R. Sjöholm, T. Salmi and D. Y. Murzin, *J. Catal.*, 2004, **225**, 155–169.
6 S. C. Hammer, A. Marjanovic, J. M. Dominicus, B. M. Nestl and B. Hauer, *Nat. Chem. Biol.*, 2015, **11**, 121–126.
7 U. Sakulku, O. Nuchuchua, N. Uawongyart, S. Puttipipatkhachorn, A. Soottitantawat and U. Ruktanonchai, *Int. J. Pharm.*, 2009, **372**, 105–111.
8 W. S. Leal, Y.-M. Choo, P. Xu, C. S. B. da Silva and C. Ueira-Vieira, *Proc. Natl. Acad. Sci. U. S. A.*, 2013, **110**, 18704–18709.
9 A. Stary, C. Suwattanasophon, P. Wolschann and G. Buchbauer, *Biochem. Biophys. Res. Commun.*, 2007, **361**, 941–945.
10 J. C. Brookes, A. Horsfield and A. Stoneham, *J. R. Soc., Interface*, 2009, **6**, 75–86.
11 R. C. Araneda, A. D. Kini and S. Firestein, *Nat. Neurosci.*, 2000, **3**, 1248–1255.
12 C. H. Townes and A. L. Schawlow, *Microwave Spectroscopy*, Dover, New York, 1975.
13 W. Gordy and R. L. Cook, *Microwave Molecular Spectra*, Wiley, New York, 1984.
14 G. G. Brown, B. C. Dian, K. O. Douglass, S. M. Geyer, S. T. Shipman and B. H. Pate, *Rev. Sci. Instrum.*, 2008, **79**, 053103.
15 D. Schmitz, V. A. Shubert, T. Betz and M. Schnell, *Front. Chem.*, 2015, **3**, 15.
16 N. A. Seifert, I. A. Finneran, C. Pérez, D. P. Zaleski, J. L. Neill, A. L. Steber, R. D. Suenram, A. Lesarri, S. T. Shipman and B. H. Pate, *J. Mol. Spectrosc.*, 2015, **312**, 13–21.
17 J. R. A. Moreno, T. R. Huet and J. J. L. Gonzalez, *Struct. Chem.*, 2012, **24**, 1163–1170.
18 D. Schmitz, V. A. Shubert, B. M. Giuliano and M. Schnell, *J. Chem. Phys.*, 2014, **141**, 034304.
19 C. Medcraft and M. Schnell, *Z. Phys. Chem.*, 2015, **230**, 1.
20 V. A. Shubert, D. Schmitz, C. Medcraft, A. Krin, D. Patterson, J. M. Doyle and M. Schnell, *J. Chem. Phys.*, 2015, **142**, 214201.
21 M. Varela, C. Cabezas, J. C. Lopez and J. L. Alonso, *J. Phys. Chem. A*, 2013, **117**, 13275–13278.
22 T. Betz, S. Zinn and M. Schnell, *Phys. Chem. Chem. Phys.*, 2015, **17**, 4538–4541.
23 C. Pérez, S. Mata, C. Cabezas, J. C. Lopez and J. L. Alonso, *J. Phys. Chem. A*, 2015, **119**, 3731–3735.
24 C. Pérez, S. Mata, S. Blanco, J. C. Lopez and J. L. Alonso, *J. Phys. Chem. A*, 2011, **115**, 9653–9657.
25 E. J. Cocinero, A. Lesarri, P. Écija, F. J. Basterretxea, J.-U. Grabow, J. A. Fernandez and F. Castaño, *Angew. Chem., Int. Ed.*, 2012, **51**, 3119–3124.
26 E. J. Cocinero, A. Lesarri, P. Écija, A. Cimas, B. G. Davis, F. J. Basterretxea, J. A. Fernandez and F. Castaño, *J. Am. Chem. Soc.*, 2013, **135**, 2845–2852.
27 C. Pérez, M. T. Muckle, D. P. Zaleski, N. A. Seifert, B. Temelso, G. C. Shields, Z. Kisiel and B. H. Pate, *Science*, 2012, **336**, 897–901.

28 C. Pérez, S. Lobsiger, N. A. Seifert, D. P. Zaleski, B. Temelso, G. C. Shields, Z. Kisiel and B. H. Pate, *Chem. Phys. Lett.*, 2013, **571**, 1–15.
29 J. Thomas, O. Sukhorukov, W. Jäger and Y. Xu, *Angew. Chem., Int. Ed.*, 2014, **53**, 1156–1159.
30 S. Ghosh, J. Thomas, W. Huang, Y. Xu and W. Jäger, *J. Phys. Chem. Lett.*, 2015, **6**, 3126–3131.
31 C. Pérez, J. L. Neill, M. T. Muckle, D. P. Zaleski, I. Peña, J. C. Lopez, J. L. Alonso and B. H. Pate, *Angew. Chem., Int. Ed.*, 2015, **54**, 979–982.
32 C. Pérez, A. Krin, A. L. Steber, J. C. Lopez, Z. Kisiel and M. Schnell, *J. Phys. Chem. Lett.*, 2016, **7**, 154–160.
33 D. Patterson, M. Schnell and J. M. Doyle, *Nature*, 2013, **497**, 475–477.
34 V. A. Shubert, D. Schmitz, C. Pérez, C. Medcraft, A. Krin, S. R. Domingos, D. Patterson and M. Schnell, *J. Phys. Chem. Lett.*, 2016, **7**, 341–350.
35 D. Schmitz, V. Alvin Shubert, T. Betz and M. Schnell, *J. Mol. Spectrosc.*, 2012, **280**, 77–84.
36 *Spartan 10*, www.wavefun.com.
37 M. Frisch, G. Trucks, H. Schlegel, G. Scuseria, M. Robb, J. Cheeseman, G. Scalmani, V. Barone, B. Mennucci, G. Petersson, H. Nakatsuji, M. Caricato, X. Li, H. Hratchian, A. Izmaylov, J. Bloino, G. Zheng, J. Sonnenberg, M. Hada, M. Ehara, K. Toyota, R. Fukuda, J. Hasegawa, M. Ishida, T. Nakajima, Y. Honda, O. Kitao, H. Nakai, T. Vreven, J. Montgomery, J. Peralta, F. Ogliaro, M. Bearpark, J. Heyd, E. Brothers, K. Kudin, V. Staroverov, R. Kobayashi, J. Normand, K. Raghavachari, A. Rendell, J. Burant, S. Iyengar, J. Tomasi, M. Cossi, N. Rega, J. Millam, M. Klene, J. Knox, J. Cross, V. Bakken, C. Adamo, J. Jaramillo, R. Gomperts, R. Stratmann, O. Yazyev, A. Austin, R. Cammi, C. Pomelli, J. Ochterski, R. Martin, K. Morokuma, V. Zakrzewski, G. Voth, P. Salvador, J. Dannenberg, S. Dapprich, A. Daniels, O. Farkas, J. Foresman, J. Ortiz, J. Cioslowski and D. Fox, *Gaussian 09*, 2009.
38 C. M. Western, *PGOPHER, a Program for Simulating Rotational, Vibrational and Electronic Structure*, http://pgopher.chm.bris.ac.uk.
39 D. Plusquellic, JB95 Spectral fitting program, 2001.
40 P. D. Godfrey and R. D. Brown, *J. Am. Chem. Soc.*, 1998, **120**, 10724–10732.
41 G. M. Florio, R. A. Christie, K. D. Jordan and T. S. Zwier, *J. Am. Chem. Soc.*, 2002, **124**, 10236–10247.
42 J. L. Alonso, C. Pérez, M. Eugenia Sanz, J. C. Lopez and S. Blanco, *Phys. Chem. Chem. Phys.*, 2009, **11**, 617–627.
43 R. S. Ruoff, T. D. Klots, T. Emilsson and H. S. Gutowsky, *J. Chem. Phys.*, 1990, **93**, 3142–3150.
44 U. Erlekam, M. Frankowski, G. von Helden and G. Meijer, *Phys. Chem. Chem. Phys.*, 2007, **9**, 3786–3789.
45 H. V. L. Nguyen, H. Mouhib, S. Klahm, W. Stahl and I. Kleiner, *Phys. Chem. Chem. Phys.*, 2013, **15**, 10012–10018.

Appendix III

Prediction of the Rotational Spectra of Microsolvated Complexes with Low Cost DFT Methods

Journal of Molecular Spectroscopy 337 (2017) 145–152

Contents lists available at ScienceDirect

Journal of Molecular Spectroscopy

journal homepage: www.elsevier.com/locate/jms

Prediction of the rotational spectra of microsolvated complexes with low cost DFT methods

Pablo Pinacho, Juan Carlos López, Susana Blanco *

Physical Chemistry Department, University of Valladolid, Paseo Belén 7, 47011 Valladolid, Spain

ARTICLE INFO

Article history:
Received 17 January 2017
In revised form 23 February 2017
Accepted 28 February 2017
Available online 9 March 2017

Keywords:
Hydrogen bond
Microwave Spectroscopy
Microsolvation clusters
Structure
Density Functional Theory

ABSTRACT

Some of the most used DFT methods together with MP2 have been tested using 6-311++G(d,p) and TZVP basis sets to probe their usefulness in prediction of the rotational spectra of several microsolvated complexes of formamide, *t*-*N*-methylformamide, glycine and β-propiolactone. Results obtained for the rotational parameters and the prediction of the spectra have been compared to experimental data previously measured by Fourier Transform Microwave Spectroscopy. Analysis of the standard deviation of the predicted rotational spectra for all the levels tested indicates that the methods which better approach to the MP2 results are mPW91LYP and B3LYP-D3.

1. Introduction

The changes in the molecular structure in going to solution environment is a main subject to chemistry since solvation can affect the properties and reactivity of chemical species. Many phenomena associated to solvation can be found in the field of biomolecules. Molecular shape, protein folding [1] or conformational equilibria [2] are only some examples. The evolution of the spectroscopic techniques in combination with supersonic jets, has allowed the isolation of microsolvated molecules with different hydration degrees making possible to understand the role of the solvation forces present in solution at a molecular level. Microwave Spectroscopy has contributed heavily in this field with many studies of microsolvated organic molecules [3]. The inherent flexibility of these complexes, yielding many possible conformers, make the prediction of the rotational spectra a difficult task. Besides, the spectra of the monomers and all possible complexes are present simultaneously, so reasonable good simulations of the spectra are needed in order to assign the different species. *Ab initio* computations are of great help to predict the structures and energies of the possible complexes and their most stable conformers. One of the most used levels of theory is MP2/6-311++G(d,p) which for systems of a reasonable size can be used to have rather good starting predictions of the spectra. This is based on the rotational constants, quadrupole coupling constants and dipole moments obtained from geometry optimization of the different possible conformers. There are methods giving very accurate predictions of the rotational parameters [4] but those are based in a composite scheme of different methods and levels that account for basis sets and correlation effects with a higher computational effort. When the size of the system [5] and the number of water molecules increase [6,7], the calculations with those levels of theory are time-consuming and increase the requirements of the computer properties. An alternative has been using Density Functional Theory (DFT) [8] methods which requires much less computational resources. So that it could be useful to test those methods to see which one gives best overall results for the prediction of the spectra taking into account the balance between computation cost and the accuracy of the results, which is the aim of this work.

In this context, geometry optimization for several water complexes previously studied by rotational spectroscopy have been done with different DFT methods and compared to MP2 and the experiment. Selected complexes cover several of the most important possible interactions in microsolvation processes. As a reference we have chosen the microsolvation complexes of formamide (FMA) with one and two water molecules. This system serves as a model of interaction between water and peptide bond in proteins. The experimentally observed geometries [9] are depicted in Fig. 1.

Microsolvated complexes of *N*-methylformamide (NMF) are also a good model for the study of interaction between water and the peptide linkage. NMF has *cis* and *trans* conformations, but only *t*-NMF complexes have been observed. The experimentally observed geometries [10] are depicted in Fig. 2.

* Corresponding author.
E-mail address: sblanco@qf.uva.es (S. Blanco).

http://dx.doi.org/10.1016/j.jms.2017.02.018
0022-2852/

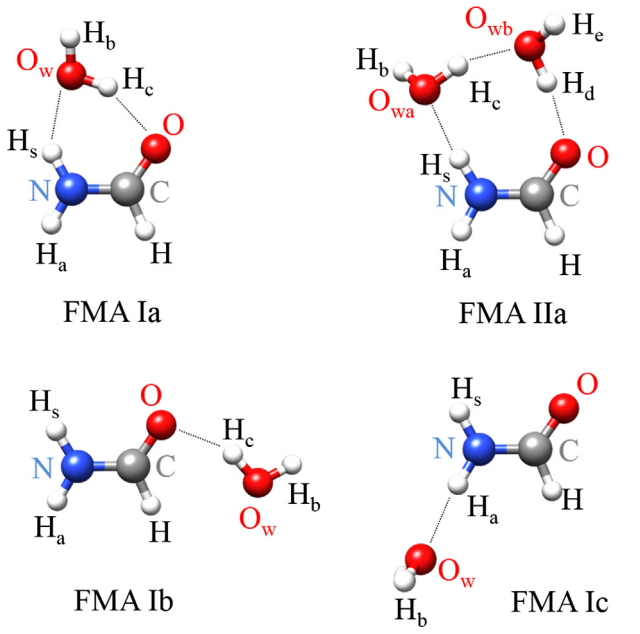

Fig. 1. Observed complexes of formamide with one and two molecules of water [9].

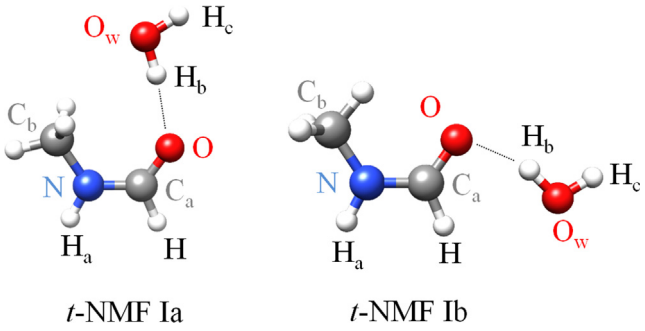

Fig. 2. Observed complexes of *t*-*N*-methyl formamide with one molecule of water [10].

We have also considered the gas phase complexes of glycine (GLY), the simplest amino acid, with one and two molecules of water. In gas phase conditions glycine adopts several conformations, but microsolvated complexes have been observed experimentally only with the lowest energy configuration of glycine [11], as shown in Fig. 3.

β-propiolactone (BPL) is a four-membered plane ring molecule which has been studied microsolvated with up to five water molecules [7] and shows interesting features as n → π* interactions. In this work we have analyzed the results of theoretical calculations for the microsolvated complexes with one and two molecules of water depicted in Fig. 4.

2. Computational methods

All the calculations have been done using Gaussian G09 [12]. A total of 13 DFT functionals described below have been used together with MP2 method [13] combined with two basis sets to optimize the geometry of the different molecular complexes. This allows to calculate the different spectroscopic parameters needed to have initial predictions of the rotational spectra. In this case we have to remark that all the calculations correspond to equilibrium geometries while vibrational contributions have not been taken into account.

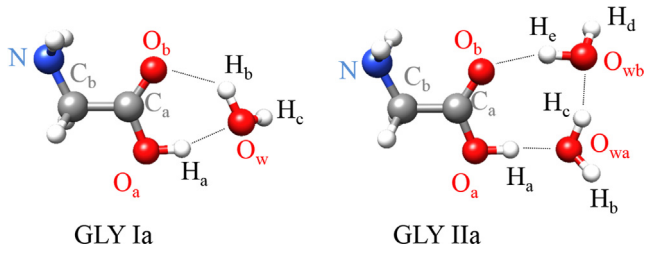

Fig. 3. Observed complexes of glycine with one and two molecules of water [11].

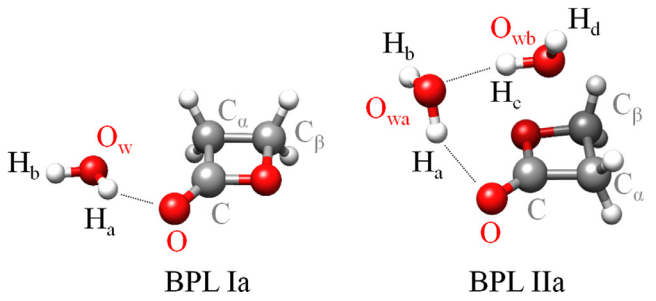

Fig. 4. Observed complexes of β-propiolactone with one and two water molecules [7].

The unique *ab initio* method used in this work has been MP2. In this method, the Møller-Plesset perturbation theory allows implementing corrections for the electronic correlation in several orders. We have selected second order correction in the frozen core approximation as a reference for several reasons: It gives rather good results in the prediction of the geometry and spectroscopic parameters in a variety of systems including hydrogen bonded ones and for its affordable computational cost compared to other higher level *ab initio* methods. It is well known that MP2 usually overestimates the barriers involved in large amplitude motions associated to the existence of equivalent conformers but in general it gives reasonable results [14].

DFT is an alternative to obtain the molecular geometry and energy [8]. Many different functionals have been developed accounting for exchange and correlation expressions. From their combination many different DFT methods arise, each one useful to predict different properties of molecular systems. We have evaluated the performance of the functionals: BLYP, B3LYP, B3LYP-D3, X3LYP, mPW91LYP, PBE1PBE, mPW91PBE, PW91PBE, B3PW91, M06, M06-L, M06-2X and TPSSh. DFT functionals performance has been widely studied in biological environment and for organic hydrates [15]. Those used in this work have been selected because they have proved to perform reasonably well for hydrogen bonds, for their popularity in calculations or because they are designed for long-range interactions.

BLYP is a popular functional arising from the combination of Becke's exchange functional [16] together with Lee, Yang and Parr correlation functional [17]. B3LYP is a hybrid functional using 3 experimental parameters fitted by Becke to combine the HF exchange expression along with the Lee-Yang-Parr correlation functional [17, 18]. We have included this functional because is the most popular despite it has been reported that has difficulties in predicting accurate structures involving hydrogen bond interactions [19] due to a poor description of dispersion forces. To minimize this problem we included the empirical dispersion correction (GD3) by Grimme (B3LYP-D3) [20]. X3LYP is a hybrid functional developed by Xu to describe non-bonded interactions [17, 21].

Perdew, Burke and Ernzerhof's PBE1PBE, most known as PBE0, is a pure functional converted into a hybrid one [22]. Performance

of this functional for hydrogen bonded systems has been widely studied with good results [19,23]. Modified and unmodified PW91 exchange functional [24] combined with Perdew, Burke and Ernzerhof (PBE) gradient corrected correlation functional result in mPW91PBE and PW91PBE. The same mPW91 exchange functional together with Lee, Yang and Parr correlation functional gives rise to mPW91LYP [17,24].

The B3PW91 functional combines the Becke parameters [18] with Perdew and Wang correlation functional [24]. The TPSSh is a hybrid version of Tao, Perdew, Staroverov and Scuseria gradient corrected functional [25].

The hybrid functionals M06 and M06-2X [26] and the pure functional M06-L [27] come from the Minnesota 06 suites of functionals.

Basis set selection is critical to adequately describe the orbitals involved in the hydrogen bonds. In a first step, we tested the basis sets [12]: 6-311++G(d,p), 6-311++G(3df,3dp), cc-pVDZ, aug-cc-pVDZ and TZVP on the complexes of formamide and water combined with PBE0, B3LYP and MP2 methods. The cc-pVDZ basis set does not describe satisfactorily the systems and its results are far from being acceptable. On the contrary, 6-311++G(3df,3dp) guaranties a good description and requires higher computational resources but the results do not constitute a big improvement in comparison with 6-311++G(d,p) basis set. Similar behavior is observed when comparing the results for aug-cc-pVDZ and TZVP basis sets. According to this, we have finally selected Pople's 6-311++G(d,p) [28], which implements polarization and diffuse functions to improve description of the non-covalent interactions, and Ahlrichs's triple-ζ TZVP [29], which includes polarization functions. These basis sets are adequate for geometry optimization of the studied complexes since both describe correctly the atoms of the two first rows of periodic table and are not too big to require excessive computational resources.

3. Results and discussion

3.1. Conformers of the formamide···$(H_2O)_n$ complexes

The experimentally observed 1:1 and 1:2 complexes of formamide-water are shown in Fig. 1. In the most stable 1:1 complex, Ia, two hydrogen bonds are established. Both molecules act simultaneously as hydrogen donors and acceptors and close a cyclic structure. The calculated hydrogen bond parameters for a representative selection of all the methods with the 6-311++G(d,p) basis set are compared to the experimental r_0 geometry in Table 1. The corresponding rotational constants are compared in Table 2. Tables S1–S4 in supplementary material collect the complete set of the calculated data.

The experimental results [9b] show that the complex is almost planar as indicated by the value of the planar moment P_{cc} (0.054 uÅ^2) which give the mass extension out of the *ab* plane. The calculated values range from 0.149 uÅ^2 for M06-2X/6-311++G(d,p) to 0.481 uÅ^2 for PW91PBE/TZVP (Tables S3–S4). The complex is predicted to have two equivalent conformers with the non-bonded hydrogen atom of water lying out of the *ab* plane at equilibrium with formamide slightly non-planar. Out of plane P_{cc} contributions come mainly from the out of plane hydrogen atom. This is shown from the correlation between the calculated values of P_{cc} and the dihedral angle τ given in Table 1. However, it should be noted that if ground state is above the barrier at the planar configuration, the experimental value would reflect an almost planar structure.

The geometrical parameters other than this dihedral angle could show discrepancies with the experimental data, but since the effective structure is obtained from a fit of the rotational constants, it is perhaps better to directly compare the experimental and theoretical values of the rotational parameters in order to test

Table 1
Experimental (r_0) and theoretical (r_e) values of the hydrogen bond interaction for conformer Ia of the complex formamide···(H_2O) for a selection of methods using 6-311++G(d,p) basis set.

Parameter[a]	Exp.[b]	BLYP	B3LYP-D3	mPW91LYP	M06-2X	MP2
$r(H_s\cdots O_w)$/Å	2.061(4)[c]	2.07	2.06	2.05	2.01	2.05
$r(H_c\cdots O)$/Å	1.93(1)	1.93	1.92	1.92	1.91	1.95
∠(N—$H_s\cdots O_w$)/deg	139.5(3)	137.3	137.2	137.0	137.0	138.2
∠($H_s\cdots O_w$—H_c)/deg	78.2(6)	82.2	83.1	83.3	85.4	83.1
∠(O_w—$H_c\cdots O$)/deg	153(1)	148.2	147.0	146.9	144.8	146.5
∠($H_c\cdots$O=C)/deg	110.3(3)	108.0	108.4	108.4	108.4	107.6
τ(H_b—O_w—H_c—H_s)/deg	165(1)	139.9	141.0	145.9	152.7	143.0

[a] Atom labeling as in Fig. 1.
[b] Values reported in Ref. [9b].
[c] Standard error in units of the last digit.

Table 2
Experimental and theoretical values of the rotational parameters for conformer Ia of the complex formamide···(H_2O) for a selection of methods using 6-311++G(d,p) basis set.

	Exp.[e]	BLYP	B3LYP-D3	mPW91LYP	M06-2X	MP2
A[a]/MHz	11227.9330(23)[f]	10950.5	11154.6	11199.8	11250.8	11067.5
B/MHz	4586.9623(16)	4587.1	4659.3	4679.2	4774.1	4628.0
C/MHz	3258.8277(12)	3245.8	3299.0	3310.1	3358.4	3279.4
P_{cc}[b]/uÅ^2	0.054070(52)	0.311	0.291	0.227	0.149	0.377
χ_{aa}[c]/MHz	1.3321(37)	1.48	1.50	1.51	1.45	1.37
χ_{bb}/MHz	2.0371(20)	2.30	2.31	2.31	2.21	2.18
χ_{cc}/MHz	−3.3693(96)	−3.78	−3.81	−3.82	−3.66	−3.56
σ[d]/MHz	–	14.4	60.7	77.5	156.8	34.1

[a] *A*, *B*, *C* are the rotational constants.
[b] Planar moment $P_{cc} = (I_a + I_b - I_c)/2 = \sum_i m_i c_i^2$.
[c] χ_{xy} ($x.y$ = *a*, *b* or *c*) are the ^{14}N nuclear quadrupole coupling constants.
[d] Standard deviation of the prediction considering the R-branch *a*-type transitions.
[e] Values reported in Ref. [9b].
[f] Standard error in units of the last digit.

the methods. This comparison can be seen in Table 2 and in Tables S3–S4 in supplementary material. The *B* rotational constant is systematically predicted to be higher than the experimental value, while *A* and *C* have values lower or higher. The most typical case for large deviations of theory and experiment are shown by the *A* rotational constant. In general, all levels of theory give a value of this constant much worse than of *B* and *C*, introducing a source of error in the prediction of the spectrum. However, in many cases the complexes behave as near-prolate rotors with a μ_a dipole moment component of reasonable magnitude. The R-branch *a*-type spectrum is dominant and strongly dependent on the value of *B* + *C*, being less dependent on the *A* value. Attending to this fact, simple comparison of the values for molecular parameters might not be good enough to discriminate whether a level of theory performs better to predict the spectrum. Instead we have used the standard deviation of the prediction, σ, calculated from the differences between observed and predicted R-branch *a*-type frequencies.

Table 3 and Figs. 5 and 6, summarize the values for σ obtained for all the complexes studied in this work. For formamide···(H_2O) Ia it shows slight differences between the two basis sets, been the results of 6-311++G(d,p) basis set better in general. Apart from MP2, the best performance is observed for those DFT methods including LYP correlational functional, being BLYP the method which gives the best agreement. The results obtained with PBE and M06 families are worst because they give a specially deviated value for rotational constant *B*, yielding bad predictions of the spectrum, although rotational constant *A* is reasonably well determined as shown in Tables S3-S4 in supplementary material. The quadrupole coupling constants needed to predict hyperfine structure give in all cases reasonable values.

The IIa conformer (shown in Fig. 1) presents three hydrogen bonds closing a sequential cycle between formamide and two molecules of water and could be considered as an extension of formamide···(H_2O) Ia conformer, and in fact, presents a similar behavior. Table 4 presents a selection of results while the whole set of rotational parameters are presented in Tables S7-S8 in supplementary material.

All the atoms except the non-bonded water hydrogens lie in the formamide plane [9b]. These non-bonded hydrogen atoms adopt an up-down configuration. This is reflected in the P_{cc} experimental value of 0.654 uÅ^2. As in conformer Ia the calculations predict a higher value of P_{cc}. This complex presents larger deviation for hydrogen bond parameters when compared to the experimentally derived effective structure even for the levels of theory that better predict the transitions frequencies.

Considering the rotational constants and the value of the standard deviation for the predictions of the spectrum (Table 3 and Figs. 5 and 6), there are not big differences between the two basis sets, although in general 6-311++G(d,p) is slightly more accurate than TZVP. BLYP followed by MP2 are the best methods according to the values of σ. The LYP family gives better results, with the exception of X3LYP functional, than M06 and PBE families. As in conformer Ia, the quadrupole coupling constants give reasonable results.

In conformer Ib (see Fig. 1), the main interaction is the hydrogen bond O—H···O=C stabilized by a weak C—H···O hydrogen bond. This complex shows a small splitting in the rotational spectrum arising from two close vibrational states [9b]. Because the values for rotational parameters are similar in the two states, only the observed values for v = 0 have been compared to theoretical constants (Tables S11-S12). Experimentally the complex appears to be planar and this is well predicted in all cases on the basis of the P_{cc} value.

Considering the standard deviation (see Table 3 and Figs. 5 and 6), MP2 gives the best results, being the TZVP basis set better than

Table 3
Standard deviation (σ/MHz) corresponding to the comparison of the observed R-branch *a*-type spectra prediction for all microsolvated complexes considered in this work with those calculated with the different levels of theory. The general trends are shown in Figs. 5 and 6.

	FMA[b] Ia	FMA Ib	FMA Ic	FMA IIa	*t*-NMF Ia	*t*-NMF Ib	GLY Ia	GLY IIa	BPL Ia	BPL IIa	Average[c]
BLYP/1[a]	14.4	466.1	173.6	3.9	74.5	245.1	54.5	36.2	271.1	288.6	155.9
BLYP/2	10.7	272.2	102.5	18.9	92.3	188.0	40.0	28.2	190.0	195.3	106.8
B3LYP/1	61.1	251.6	57.7	35.3	36.8	143.1	5.1	11.4	104.6	156.2	87.5
B3LYP/2	74.8	141.3	6.6	57.6	36.5	103.1	18.8	13.3	72.5	116.9	68.8
B3LYP-D3/1	60.7	61.1	91.2	57.2	187.7	28.9	11.0	12.3	74.9	107.3	43.7
B3LYP-D3/2	71.3	59.4	135.8	78.0	189.4	33.6	22.9	19.9	80.7	367.7	52.3
X3LYP/1	93.3	113.1	6.7	388.0	54.4	98.6	20.0	11.5	46.1	120.2	110.1
X3LYP/2	108.2	44.6	41.7	73.6	93.3	67.8	34.3	18.0	18.8	81.3	52.2
mPW91LYP/1	77.5	67.6	22.8	39.7	70.3	83.6	12.0	10.1	29.0	121.8	45.6
mPW91LYP/2	94.8	21.3	66.1	63.9	64.8	58.2	27.8	14.8	10.9	71.8	41.7
B3PW91/1	100.5	354.7	50.9	71.6	11.4	192.8	45.6	23.2	180.6	167.5	138.4
B3PW91/2	114.4	211.8	25.6	92.7	10.8	122.4	60.3	30.4	152.1	142.9	112.0
mPW91PBE/1	139.0	182.2	4.6	91.1	25.2	116.8	68.9	34.0	78.2	103.2	101.5
mPW91PBE/2	158.0	92.3	37.2	115.2	25.1	68.3	82.5	42.4	70.6	80.8	89.9
PW91PBE/1	202.6	81.8	4.6	119.3	110.0	79.4	66.4	33.8	53.9	90.5	91.0
PW91PBE/2	215.5	46.2	90.3	145.8	92.7	55.2	81.5	44.0	29.7	38.4	88.3
PBE0/1	156.4	28.6	57.2	97.3	71.2	45.5	74.5	35.6	24.2	74.9	66.0
PBE0/2	180.3	47.6	94.3	123.1	110.5	26.0	89.8	44.7	28.0	54.0	77.1
M06/1	187.2	179.0	483.5	73.4	178.4	80.9	69.2	19.7	126.6	193.5	105.2
M06/2	178.9	153.9	441.1	81.9	175.9	51.8	74.7	21.1	117.4	208.7	97.1
M06-L/1	168.7	12.8	517.0	62.2	177.1	44.8	60.5	15.8	155.5	189.2	74.3
M06-L/2	188.1	71.2	233.7	77.4	164.3	24.3	78.3	22.4	117.9	267.5	82.8
M06-2X/1	156.8	368.6	469.1	65.1	211.3	164.4	49.1	30.3	216.7	386.8	150.1
M06-2X/2	194.9	335.7	383.6	94.5	219.2	171.2	70.3	39.4	233.8	354.5	162.8
TPSSh/1	147.7	77.2	28.6	83.7	37.5	155.9	52.5	22.8	118.0	106.2	94.0
TPSSh/2	160.4	162.6	4.4	105.1	51.8	105.8	64.2	30.0	98.3	74.5	103.8
MP2/1	34.1	11.1	24.6	17.3	101.0	15.2	1.2	1.4	48.1	84.1	18.3
MP2/2	77.0	11.6	72.2	54.2	87.0	16.8	20.9	14.2	37.0	104.7	33.1

[a] 1 refers to 6-311++G(d,p) basis set, 2 refers to TZVP basis set.
[b] FMA refers to formamide···$(H_2O)_n$ complexes, *t*-NMF refers to *t*-*N*-methylformamide···(H_2O) complexes, GLY refers to glycine···$(H_2O)_n$ complexes and BPL refers to β-propiolactone···$(H_2O)_n$ complexes.
[c] Average of the standard deviation for each method excluding FMA Ic, *t*-NMF Ia and BPL IIa complexes (see conclusions for details).

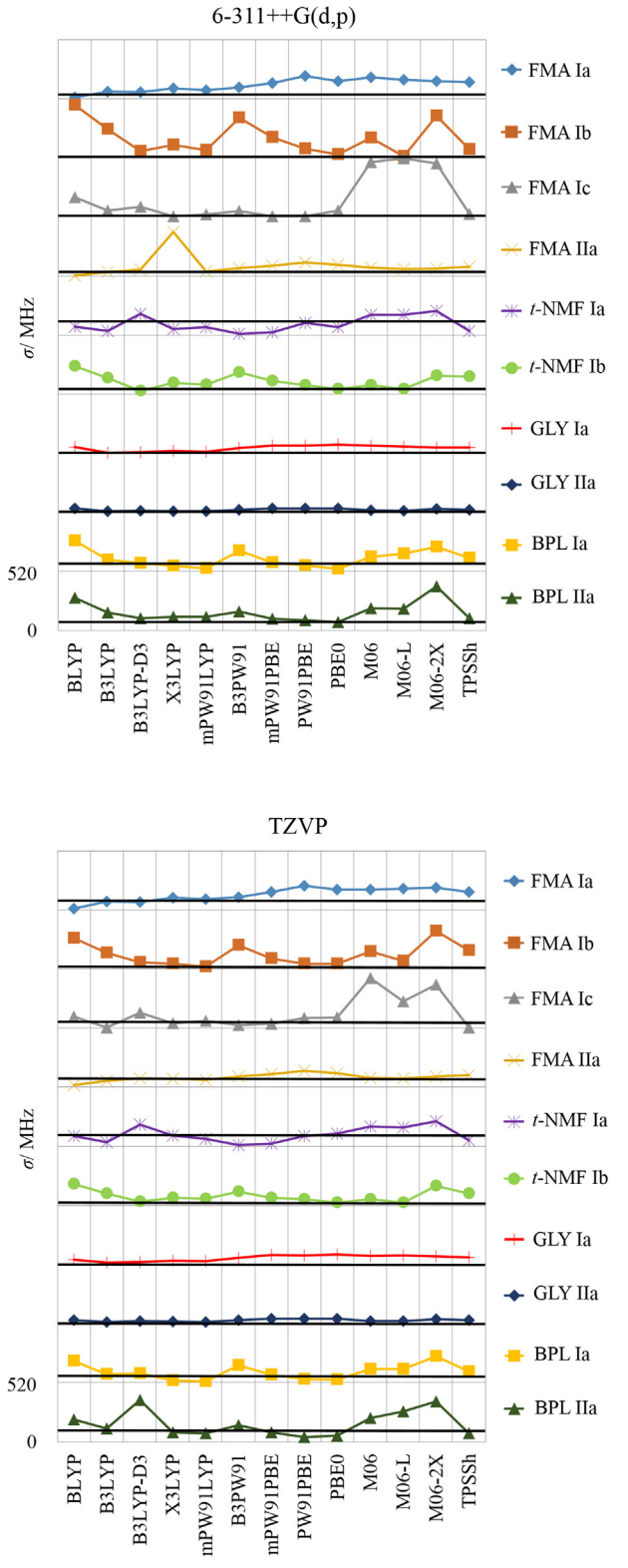

Fig. 5. Stacked plot representations showing the variation of the values of the standard deviation (σ/MHz) collected in Table 3 with the different DFT functionals for each studied complex. The scale for each molecular system is the same showed for BPL IIa (bottom plot). The horizontal straight black lines represent the value of σ obtained for MP2 method taken as a reference. The upper representation corresponds to 6-311++G(d,p) and the lower to TZVP basis sets.

6-311++G(d,p) in practically all cases. LYP methods give results which are very different to those found in Ia and IIa conformers. BLYP provides bad results in this case. B3LYP presents acceptable

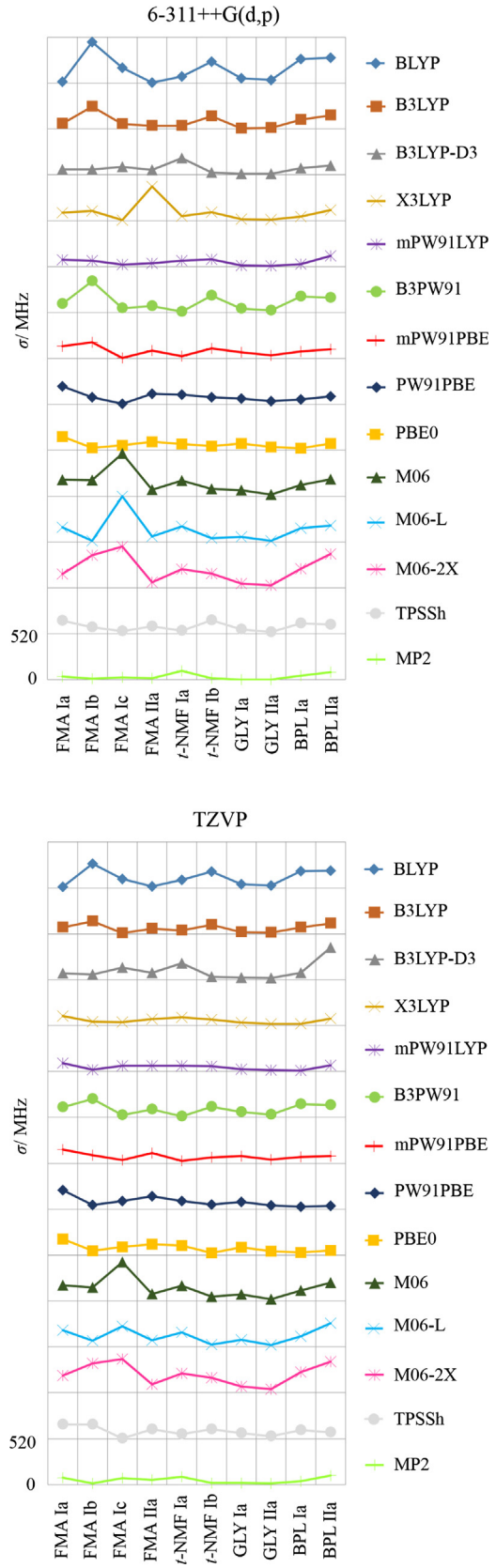

Fig. 6. Stacked plot representations showing the variation of the values of the standard deviation (σ/MHz) collected in Table 3 with the different complex for each studied DFT functionals. The scale for each molecular system is the same showed for MP2 (bottom plot). The upper representation corresponds to 6-311++G(d,p) and the lower to TZVP basis sets.

Table 4
Experimental and theoretical values of the rotational parameters for conformer IIa of the complex formamide···$(H_2O)_2$ for a selection of methods using 6-311++G(d,p) basis set.

	Exp.[e]	BLYP	B3LYP-D3	mPW91LYP	M06-2X	MP2
A[a]/MHz	4384.3559(50)[f]	4364.1	4446.1	4433.2	4458.7	4398.4
B/MHz	2630.4957(16)	2627.2	2684.8	2665.7	2678.1	2642.6
C/MHz	1651.1140(13)	1650.3	1685.2	1674.4	1689.3	1661.6
P_{cc}[b]/uÅ^2	0.65408(24)	0.967	1.004	0.879	1.447	0.993
χ_{aa}[c]/MHz	1.0739(34)	1.12	1.12	1.17	1.11	1.08
χ_{bb}/MHz	2.0063(45)	2.32	2.31	2.31	2.15	2.18
χ_{cc}/MHz	−3.0802(45)	−3.44	−3.44	−3.48	−3.26	−3.25
σ[d]/MHz	–	3.9	57.2	39.7	65.1	17.3

[a] A, B, C are the rotational constants.
[b] Planar moment $P_{cc} = (I_a + I_b - I_c)/2 = \sum_i m_i c_i^2$.
[c] χ_{xy} ($x.y = a$, b or c) are the ^{14}N nuclear quadrupole coupling constants.
[d] Standard deviation of the prediction considering the R-branch a-type transitions.
[e] Values reported in Ref. [9b].
[f] Standard error in units of the last digit.

values only with the empirical dispersion GD3 correction. X3LYP and mPW91LYP yields rather good values. PBE0 and M06-L functionals behave well with the 6-311++G(d,p) basis set. The main difference between conformer Ib and the previous ones comes from the weak secondary hydrogen bond in conformer Ib, which has significant contributions from dispersive forces. The methods which better describe these forces are expected to give better results as occur when comparing B3LYP and B3LYP-D3 methods.

Conformer Ic of the formamide···(H_2O) complex (see Fig. 1) is formed from a different hydrogen bond interaction N—H···O established between the amino group to water oxygen. Water acts in this case only as hydrogen acceptor. The lack of another linkage allows water molecule to rotate along the axis of hydrogen bond. Experimentally, this effect was detected as an appreciable splitting in the spectrum [9b]. The intensity of the transitions was weaker than expected due to the splitting making difficult the observation. From the limited transitions observed, only $B + C$ was determined without any ambiguity. In addition, the fitting of the spectrum did not provide information enough of the vibrational motion and possible vibration-rotation interactions. For this reason, it is difficult to establish any conclusion from the comparison of the experimental and theoretical values of the data. In any case, the results obtained are collected in Table 3 and Tables S13-S14 in supplementary material.

3.2. Conformers of the t-N-methylformamide···(H_2O) complexes

In NMF one of the amino hydrogen atoms of formamide is substituted by a CH_3 group. Thus NMF adopts two possible *cis* and *trans* conformers. Only *t*-NMF complexes with water have been observed (see Fig. 2) [10]. The position of the methyl group on the same side of the carbonyl group prevents the formation of N—H···O hydrogen bond as occurs in conformers Ia and IIa of formamide. Nevertheless, the most abundant conformer of *t*-NMF···(H_2O) formed by a O—H···O=C bond and weak secondary C—H···O interactions involving the methyl group is labeled Ia for analogy. The second conformer labeled Ib presents the same interactions as conformer Ib of formamide. The results of the calculations are given in Table 3 and Tables S15-S18 in supplementary material.

The weak secondary interaction established between the methyl group and water in conformer Ia is the key factor to define the final conformation predicted by the different methods. A bifurcated interaction with two C—H···O weak hydrogen bonds is predicted but the degree of symmetry of this interaction varies with the method. In some cases, it is almost symmetrical while in other cases one of the two interactions is dominant. This corresponds to different equilibrium arrangements of the CH_3 group which affects to the position of the water molecule with respect to the symmetry plane of NMF. Thus there is an evident interaction with the internal rotation of the methyl group. The predictions of the P_{cc} planar moment reflect this behavior. The experimental value of P_{cc} is 1.876 uÅ^2 while the predictions oscillate around this value which range from 1.56 uÅ^2 for B3LYP-D3 to 3.4 uÅ^2 for MP2/6-311++G(d,p). Considering the standard deviation of the prediction of the spectra (Table 3 and Figs. 5 and 6), the LYP family seems to work well with the exception of B3LYP-D3. B3PW91 seems to be optimal with any of the two basis sets as well as mPW91PBE and TPSSh. MP2 and B3LYP-D3, which work fine in other cases, do not give good results here.

Conformer Ib is expected to have a low V_3 barrier similar to that of bare *t*-NMF and this affects to the effective values of the rotational constants as pointed out by Caminati *et al.* [10]. As an example, we can cite the effective value of P_{cc} = 0.793 uÅ^2 which, corrected from the contributions of the methyl group internal rotation, is estimated to be 1.59 uÅ^2. This value is closer to the theoretical values than the effective one and corresponds to an essentially planar skeleton with two out of plane hydrogen atoms, as predicted. Taking into account this fact, some corrections should be made in the predicted rotational constants if internal rotation data were *a priori* known, not being the case. In any case, the behavior of the different methods with respect to standard deviation seem to be correlated with that observed for conformer Ib of formamide water complex, although the result seems to be apparently better (see Tables 3, S17-S18 and Figs. 5 and 6). This can be associated to the fact that hydrogen bond interactions are the same in both complexes.

3.3. Conformers of the glycine···(H_2O)$_n$ complexes

The complexes of glycine with water are very important systems since they had provided the first model for the interactions of amino acids with water [11]. In glycine···(H_2O) and glycine···(H_2O)$_2$ both the water molecules and the carboxyl group act simultaneously as hydrogen donors or acceptors. By this reason, glycine carboxyl group and water molecules close sequential cycles similar to those found for formamide water complexes as shown in Fig. 3. The configuration of the non-bonded hydrogen atoms of water molecules in glycine···(H_2O)$_2$ is also up-down in this case. For these reasons, we have labeled the observed complexes of glycine···(H_2O) as Ia and glycine···(H_2O)$_2$ as IIa by analogy with formamide water complexes. The results are collected in Table 3 and in Tables S21-S24 in supplementary material.

Both complexes have a planar skeleton as reflected by the value of P_{cc} which has out of plane contributions from the hydrogen atoms of methylene and amino groups as well as from the non-bonded water hydrogen atoms. The experimental values of P_{cc} = 3.199 uÅ^2 for conformer Ia and P_{cc} = 3.699 uÅ^2 for conformer IIa are reasonable

well reproduced taking into account that the experimental value corresponds to a ground vibrational state average and the predictions to equilibrium conformers. The same can be seen for the structural parameters of the hydrogen bond in glycine···(H_2O) as shown in Tables S19-S20 in supplementary material.

Considering the prediction of the spectra (see Table 3 and Figs. 5 and 6), the best results in this case are obtained for MP2/6-311++G (d,p). All functionals work reasonably well, being the LYP family that showing the best performances. There are not big differences between B3LYP and B3LYP-D3 indicating that electrostatic forces dominate the interactions.

3.4. Conformers of the β-propiolactone···$(H_2O)_n$ complexes

As we have already mentioned, the microsolvation of BPL has been experimentally studied for complexes up to five water molecules [7]. For the purpose of this work which compares systems with one and two water molecules we have considered only the complexes labeled Ia and IIa for BPL in Fig. 4.

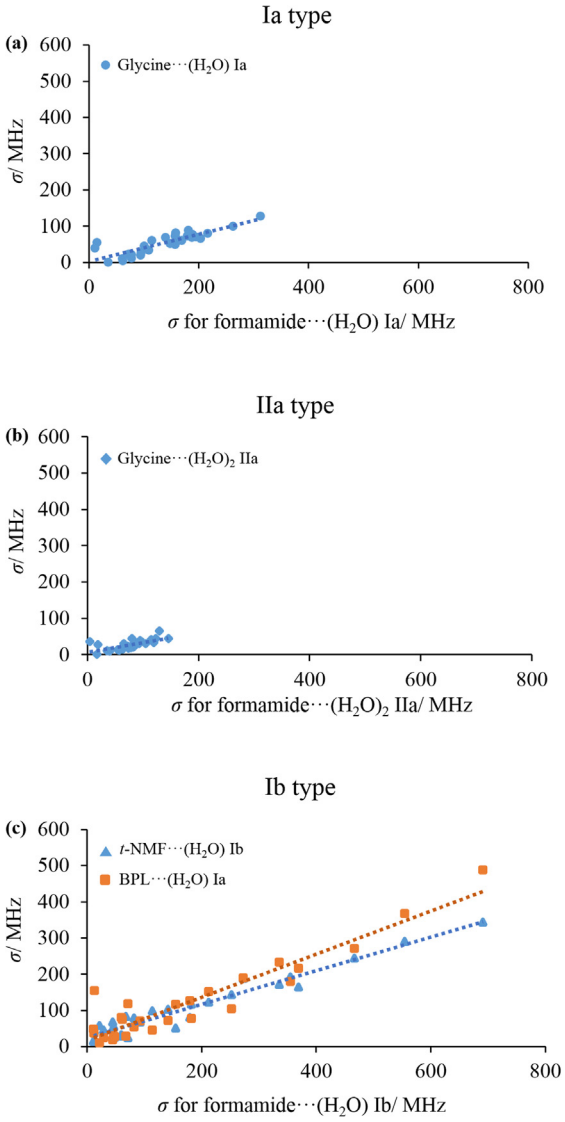

Fig. 7. Plot of the correlation between the standard deviation of (a) glycine···(H_2O) Ia and formamide···(H_2O) Ia. (b) glycine···$(H_2O)_2$ IIa and formamide···$(H_2O)_2$ IIa. (c) *t*-NMF···(H_2O) Ib (blue triangles) or BPL···(H_2O) Ia (orange squares) and formamide···(H_2O) Ib. (For interpretation of the references to colour in this figure legend, the reader is referred to the web version of this article.)

In complex Ia, water interacts through an hydrogen bond with the oxygen in the carbonyl group and a weak secondary bifurcated C_α—H···O_w hydrogen bond with the methylene group in α position. The skeleton of the complex presents a planar configuration. The planar moment P_{cc} = 3.470 uÅ^2 collects the contributions of the methylene groups hydrogen atoms and compared to the value of bare BPL (P_{cc} = 3.242 uÅ^2) [7] shows contributions from the non-bonded hydrogen atom of water molecule or out of plane intermolecular vibrational effects. All DFT functionals predict water molecule being in the symmetry plane of BPL while MP2 locates the non-bonded hydrogen atom of water out of this plane as seen in P_{cc} values collected in Tables S25-S26 in supplementary material. Considering the prediction of the spectrum, TZVP basis set gives better results than 6-311++G(d,p). The best results are obtained with mPW91LYP functional while X3LYP, PW91PBE and PBE0 give also reasonable values of the standard deviation (see Table 3 and Figs. 5 and 6).

In complex IIa, the two water molecules close a sequential cycle with BPL through O_{wa}—H_a···O=C, O_{wb}—H_c···O_{wa} and simultaneous weak C_α—H···O_{wb} and C_β—H···O_{wb} hydrogen bonds. A $n \rightarrow \pi^*$ interaction from the one non-bonded electron pair of O_{wb} to the non-bonding π^* orbital of the carbonyl group may also contribute to stabilize this complex. The two water molecules lie out of the ring plane in a *quasi*-perpendicular arrangement which is reflected by the P_{cc} value of 51.077 uÅ^2 which is well predicted by M06 and MP2 methods (see Tables S27-S28). In general, the prediction of the spectrum (see Table 3 and Figs. 5 and 6) is not very good except for the PW91PBE/TZVP. Probably the description of the weak interactions of H_2O_{wb} with BPL and the possible contribution of intermolecular vibrations are the cause of the deviations. Chemical computations have difficulties in determine precisely the position of the water molecules and there are variations with the level of theory. Even small differences in the disposition of the oxygen atom led to big differences in the rotational constants and large deviations in the prediction of the spectrum.

4. Conclusions

In order to establish some conclusions, we can analyze the results summarized in Table 3 for the standard deviation of the predictions of the R-branch *a*-type spectra, as we have explained in previous sections. Figs. 5 and 6, which represent the values given in Table 3, show a noticeable dispersion of the values of σ arising by the different nature of the intermolecular interactions in each system, the presence of large amplitude intramolecular vibrations and the different kind of functionals used. Despite this apparent dispersion, it is possible to find some interesting correlations between systems with similar interactions as shown in Fig. 7.

In these plots we represent the values of σ obtained with the same method of different systems *vs* those of formamide water complexes which represent all possible kind of interactions. For example formamide···(H_2O) Ia is formed by two moderate hydrogen bonds as occurs for glycine···(H_2O) Ia (see Figs. 1 and 3). Fig. 7a shows the linear correlation existing between the results of both systems for the different calculations. Formamide···$(H_2O)_2$ IIa and glycine···$(H_2O)_2$ IIa can be compared in the same way as is shown in Fig. 7b. Formamide···(H_2O) Ib presents a moderate O—H···O=C hydrogen bond and a weak C—H···O interaction. Similar configurations occur for *t*-NMF···(H_2O) Ib and BPL···(H_2O) Ia and in fact a linear correlation exists between the results for these systems as can be seen in Fig. 7c. An interesting feature can be also observed in Fig. 7 concerning the dispersion of the values and the relative stability of the complexes. The highest dispersion corresponds to formamide···(H_2O) Ib type interactions which are the less stable systems [9b]. Formamide···(H_2O) Ia interactions

correspond to the most stable 1:1 complexes and show a noticeable smaller dispersion compared to Ib type conformers. This trend is more pronounced in the 1:2 complexes which are further stabilized by hydrogen bond cooperativity [30].

The rest of systems cannot be considered within those correlations since they present different interactions. For example, formamide···(H_2O) Ic has only one hydrogen bond and shows an almost free rotation of the water molecule. *t*-NMF···(H_2O) Ia is affected by the internal rotation of the methyl group interacting with water. In BPL···(H_2O)$_2$ IIa one of water molecules interacts with BPL molecule through a hydrogen bond and the other through weak secondary n → π^* interactions.

Not all levels of theory perform equally. Considering the average results for σ (see Table 3), the best performance is, as could be expected, that of MP2 with both basis sets. For the DFT functionals the best results corresponds to mPW91LYP and B3LYP-D3 being the dispersion of the values narrower for B3LYP-D3. This behavior is clearly reflected in Figs. 5 and 6. The use of these methods could be suggested in large systems as an alternative to MP2 since they have a lower computational cost.

Funding

This work was supported by the Junta de Castilla y León (UNVA-13-3E-2103).

Acknowledgments

SB and JCL would like to express their deep gratitude to Professor W. Caminati. We have learned so much from him while cooperating in many interesting problems. We also have had the privilege of enjoying his friendship, hospitality and kindness everywhere.

Appendix A. Supplementary material

Supplementary data associated with this article can be found, in the online version, at http://dx.doi.org/10.1016/j.jms.2017.02.018.

References

[1] (a) D. Liu, T. Wyttenbach, C.J. Carpenter, M.T. Bowers, J. Am. Chem. Soc. 126 (2004) 3261–3270;
(b) A.R. Bizzarri, S. Cannistraro, J. Phys. Chem. B 106 (2002) 6617–6633;
(c) W. Blokzijl, J.B.F.N. Engberts, Angew. Chem. Int. Ed. 32 (1993) 1545–1579.
[2] M. Schmitt, M. Böhm, C. Ratzer, C. Vu, I. Kalkman, W.L. Meerts, J. Am. Chem. Soc. 127 (2005) 10356–10364.
[3] W. Caminati, J.U. Grabow, in: J. Laane (Ed.), Frontiers of Molecular Spectroscopy, Elsevier, Amsterdam, 2009, pp. 383–454.
[4] (a) C. Puzzarini, Int. J. Quantum Chem. 116 (2016) 1513–1519;
(b) C. Puzzarini, V. Barone, Phys. Chem. Chem. Phys. 13 (2011) 7158–7166.
[5] C. Pérez, J.C. López, S. Blanco, M. Schnell, J. Phys. Chem. Lett. 7 (2016) 4053–4058.
[6] C. Pérez, A. Krin, A.L. Steber, J.C. López, Z. Kisiel, M. Schnell, J. Phys. Chem. Lett. 7 (2016) 154–160.
[7] C. Pérez, J.L. Neill, M.T. Muckle, D.P. Zaleski, I. Peña, J.C. López, J.L. Alonso, B.H. Pate, Angew. Chem. Int. Ed. 54 (2015) 979–982.
[8] (a) P. Hohenberg, W. Kohn, Phys. Rev. 136 (1964) B864–B871;
(b) W. Kohn, L.J. Sham, Phys. Rev. 140 (1965) A1133–A1138.
[9] (a) F.J. Lovas, R.D. Suenram, G.T. Fraser, C.W. Gillies, J. Zozom, J. Chem. Phys. 88 (1988) 722;
(b) S. Blanco, J.C. López, A. Lesarri, J.L. Alonso, J. Am. Chem. Soc. 128 (2006) 12111–12121;
(c) S. Blanco, P. Pinacho, J.C. López, Angew. Chem. Int. Ed. 55 (2016) 9331–9335.
[10] W. Caminati, J.C. López, S. Blanco, S. Mata, J.L. Alonso, Phys. Chem. Chem. Phys. 12 (2010) 10230–10234.
[11] (a) J.L. Alonso, E.J. Cocinero, A. Lesarri, M.E. Sanz, J.C. López, Angew. Chem. Int. Ed. 45 (2006) 3471–3474;
(b) J.L. Alonso, I. Peña, M.E. Sanz, V. Vaquero, S. Mata, C. Cabezas, J.C. López, Chem. Commun. 49 (2013) 3443–3445.
[12] Gaussian 09, Revision D.01, M.J. Frisch, G.W. Trucks, H.B. Schlegel, G.E. Scuseria, M.A. Robb, J.R. Cheeseman, G. Scalmani, V. Barone, B. Mennucci, G.A. Petersson, H. Nakatsuji, M. Caricato, X. Li, H.P. Hratchian, A.F. Izmaylov, J. Bloino, G. Zheng, J.L. Sonnenberg, M. Hada, M. Ehara, K. Toyota, R. Fukuda, J. Hasegawa, M. Ishida, T. Nakajima, Y. Honda, O. Kitao, H. Nakai, T. Vreven, J.A. Montgomery, Jr., J.E. Peralta, F. Ogliaro, M. Bearpark, J.J. Heyd, E. Brothers, K.N. Kudin, V.N. Staroverov, R. Kobayashi, J. Normand, K. Raghavachari, A. Rendell, J. C. Burant, S.S. Iyengar, J. Tomasi, M. Cossi, N. Rega, J.M. Millam, M. Klene, J.E. Knox, J.B. Cross, V. Bakken, C. Adamo, J. Jaramillo, R. Gomperts, R.E. Stratmann, O. Yazyev, A. J. Austin, R. Cammi, C. Pomelli, J.W. Ochterski, R.L. Martin, K. Morokuma, V.G. Zakrzewski, G.A. Voth, P. Salvador, J.J. Dannenberg, S. Dapprich, A.D. Daniels, Ö. Farkas, J.B. Foresman, J.V. Ortiz, J. Cioslowski, D.J. Fox, Gaussian Inc, Wallingford CT, 2009.
[13] C. Møller, M.S. Plesset, Phys. Rev. 46 (1934) 618–622.
[14] J.C. López et al. Submitted to J. Mol. Spec. (Volume dedicated to Professor W. Caminati).
[15] (a) T. Wijst, C.F. Guerra, M. Swart, F.M. Bickelhaupt, Chem. Phys. Lett. 426 (2006) 415–421;
(b) Y. Liu, J. Zhao, F. Li, Z. Chen, J. Comp. Chem. 34 (2013) 121–131.
[16] A.D. Becke, Phys. Rev. A 38 (1988) 3098–3100.
[17] C. Lee, W. Yang, R.G. Parr, Phys. Rev. B 37 (1988) 785–789.
[18] (a) A.D. Becke, J. Chem. Phys. 98 (1993) 5648–5652;
(b) S.H. Vosko, L. Wilk, M. Nusair, Can. J. Phys. 58 (1980) 1200–1211.
[19] (a) Y. Zhao, D.G. Trulhar, J. Chem. Theory Comput. 3 (2007) 289–300;
(b) Y. Zhao, D.G. Trulhar, J. Chem. Theory Comput. 1 (2005) 415–432.
[20] S. Grimme, J. Antony, S. Ehrlich, H. Krieg, J. Chem. Phys. 132 (154104) (2010) 1–19.
[21] X. Xu, W.A. Goddard III, Proc. Natl. Acad. Sci. U.S.A. 101 (2004) 2673–2677.
[22] (a) J.P. Perdew, K. Burke, M. Ernzerhof, Phys. Rev. Lett. 77 (1996) 3865–3868;
(b) C. Adamo, V. Barone, J. Chem. Phys. 110 (1999) 6158–6169.
[23] (a) S.M. Bachrach, J. Phys. Chem. A 112 (2008) 3722–3730;
(b) J. Ireta, J. Neugebauer, M. Scheffler, J. Phys. Chem. A 108 (2004) 5692–5698.
[24] J.P. Perdew, P. Ziesche, H. Eschrig, Electronic Structure of Solids '91, Akademie Verlag, Berlin, 1991.
[25] J.M. Tao, J.P. Perdew, V.N. Staroverov, G.E. Scuseria, Phys. Rev. Lett. 91 (146401) (2003) 1–4.
[26] Y. Zhao, D.G. Truhlar, Theor. Chem. Acc. 120 (2008) 215–241.
[27] Y. Zhao, D.G. Truhlar, J. Chem. Phys. 125 (194101) (2006) 1–18.
[28] R. Ditchfield, W.J. Hehre, J.A. Pople, J. Chem. Phys. 54 (1971) 724–728.
[29] A. Schaefer, C. Huber, R. Ahlrichs, J. Chem. Phys. 100 (1994) 5829–5835.
[30] (a) G.A. Jeffrey, W. Saenger, Hydrogen Bonding in Biological Structures, Springer-Verlag, New York, 1991;
(b) G.A. Jeffrey, Introduction to Hydrogen Bonding, Oxford University Press, Oxford, 1997.

Appendix IV

Structure Determination, Conformational Flexibility, Internal Dynamics, and Chiral Analysis of Pulegone and Its Complex with Water

ChemPubSoc Europe

DOI: 10.1002/chem.201704644

CHEMISTRY A European Journal Full Paper

Microwave Spectroscopy

Structure Determination, Conformational Flexibility, Internal Dynamics, and Chiral Analysis of Pulegone and Its Complex with Water

Anna Krin,[a, b, c] Cristóbal Pérez,*[a, b, c] Pablo Pinacho,[f] María Mar Quesada-Moreno,[d] Juan Jesús López-González,[d] Juan Ramón Avilés-Moreno,[e] Susana Blanco,[f] Juan Carlos López,[f] and Melanie Schnell*[a, b, c]

Abstract: In the current work we present a detailed analysis of the chiral molecule pulegone, which is a constituent of essential oils, using broadband rotational spectroscopy. Two conformers are observed under the cold conditions of a molecular jet. We report an accurate experimentally determined structure for the lowest energy conformer. For both conformers, a characteristic splitting pattern is observed in the spectrum, resulting from the internal rotation of the two non-equivalent methyl groups situated in the isopropylidene side chain. The determined energy barriers are 1.961911(46) kJ mol^{-1} and 6.3617(12) kJ mol^{-1} for one conformer, and 1.96094(74) kJ mol^{-1} and 6.705(44) kJ mol^{-1} for the other one. Moreover, a cluster of the lowest energy conformer with one water molecule is reported. The water molecule locks one of the methyl groups by means of a hydrogen bond and some secondary interactions, so that we only observe internal rotation splittings from the other methyl group with an internal rotation barrier of 2.01013(38) kJ mol^{-1}. Additionally, the chirality-sensitive microwave three-wave mixing technique is applied for the differentiation between the enantiomers, which can become of further use for the analysis of essential oils.

Introduction

Essential oils are widely used in medicine, pharmacology, and cosmetics. Some of the major constituents of these oils are terpenes, which are responsible for the anxiolytic,[1] anticonvulsive,[2] or anti-inflammatory[3] properties that essential oils are known for. Furthermore, many terpenes are chiral and thus may exhibit different biological functionality with respect to their enantiomers. For example, the enantiomers of the monoterpene carvone are known to be different in odor and taste. While (*R*)-(−)-carvone smells like spearmint, its enantiomer (*S*)-(+)-carvone smells like caraway, indicating that our olfactory system interacts with the enantiomers of carvone in an enantioselective way. A good knowledge of the structure, intramolecular dynamics, and conformational flexibility of the respective components facilitates a better understanding of the mechanisms behind these biological effects.[4] Such information can be obtained in the gas phase with high-resolution rotational spectroscopy.

A number of monoterpenes have been studied previously by using different techniques to elucidate their molecular structure and to understand their interaction with the environment through hydrogen bonding and dispersive forces. Microwave,[5–11] infrared (IR),[12] Raman,[13] and vibrational circular dichroism (VCD)[14–16] spectroscopy represent just a few examples. Due to the recent developments in microwave spectroscopy, broadband spectra with superb signal-to-noise ratios, maintaining the high resolution of rotational spectroscopy, can be recorded in just a few hours. The high sensitivity of the technique makes it possible to observe isotopically substituted species in natural abundance and thus the changes in the molecular moments of inertia can be determined. This information can be used to determine accurate atomic positions in the molecule by solving the Kraitchman equations.[17]

[a] *A. Krin, Dr. C. Pérez, Prof. Dr. M. Schnell*
Deutsches Elektronen-Synchrotron
Notkestrasse 85, 22607 Hamburg (Germany)
E-mail: cristobal.perez@desy.de
melanie.schnell@desy.de

[b] *A. Krin, Dr. C. Pérez, Prof. Dr. M. Schnell*
Max-Planck Institut für Struktur und Dynamik der Materie
Luruper Chaussee 149, 22761 Hamburg (Germany)

[c] *A. Krin, Dr. C. Pérez, Prof. Dr. M. Schnell*
Christian-Albrechts-Universität zu Kiel, Institute of Physical Chemistry
Max-Eyth-Str. 1, 24118 Kiel (Germany)

[d] *Dr. M. M. Quesada-Moreno, Prof. Dr. J. J. López-González*
Departamento de Química Física y Analítica
Universidad de Jaén, Campus Las Lagunillas, E-23071 Jaen (Spain)

[e] *Dr. J. R. Avilés-Moreno*
Departamento de Sistemas Físicos, Químicos y Naturales
Universidad Pablo de Olavide Sevilla
Carretera de Utrera Km 1, E-41013 Seville (Spain)

[f] *P. Pinacho, Prof. Dr. S. Blanco, Prof. Dr. J. C. López*
Departamento de Química Física y Química Inorgánica
Universidad de Valladolid, Paseo Belen 7, 47011 Valladolid (Spain)

Supporting information and the ORCID identification number(s) for the author(s) of this article can be found under: https://doi.org/10.1002/chem.201704644.

Intramolecular dynamics, such as the internal rotation of a methyl group with respect to the remainder of the molecule, can lead to line splittings in the rotational spectra. Their analysis gives us information on the barrier height and tunneling pathways. It is also assumed that intramolecular dynamics play an important role in molecular recognition.[18] In addition, rotational spectroscopy allows us to characterize intra- and intermolecular interactions, as we showed recently for camphor–water[6] and formamide–water clusters.[19] Relevant questions are what are the preferred binding positions of water to the molecule of interest and the responsible interactions, as well as how the structure of the solutes can be affected by (micro)-solvation?[20]

An unambiguous differentiation of the enantiomers of chiral molecules in the gas phase is possible with the newly developed microwave three-wave mixing (M3WM) technique.[21,22] M3WM has been applied to a number of terpenes and alcohols, including those with several stereogenic centers,[23] as well as for the analysis of chiral mixtures. Very recently, it was demonstrated that this technique can also be extended to achieve enantiomer-selective population transfer.[24,25]

Here, we report our results of a high-resolution broadband rotational spectroscopy study on the monoterpene pulegone (2-isopropylidene-5-methylcyclohexanone, see Figure 1 below) in the gas phase, which provides information on the isolated species free of solvent effects. Pulegone can be found in many plants. It is a constituent of peppermint (*Mentha piperita L.*) and pennyroyal (*Mentha pulegium*) essential oils. It has a wide range of applications in food, fragrance, and pharmaceutical industry.[26] However, it is also known for its hepatotoxicity.[27] Human intoxication with pennyroyal oil can lead to gastritis, hepatic and renal failure, and in severe cases even to death.[28] It is notable that (*S*)-(−)-pulegone is rarely found in essential oils.[29] This enantiomer has also been reported to have much lower toxicity in humans.[30]

In a recent IR–Raman–VCD study on pulegone, two conformers were determined based on quantum-chemical calculations, but only the lowest energy confomer could be observed experimentally in the liquid phase.[31] In the present study we extend the conformational landscape and provide a detailed characterization of pulegone both experimentally and theoretically.

Experimental Section and Computational Methods

Pulegone was purchased as enantioenriched (*R*)-(+)- and (*S*)-(−)-pulegone (97% chemical purity and high enantiopurity, specified optical activity $\alpha_{20}^{D} = +23.5^{\circ}$) from Sigma–Aldrich and used without further purification. Pulegone is a liquid at room temperature and has a boiling point around 224 °C. The sample was heated to 80 °C in a reservoir close to the valve orifice to increase the vapor pressure and then supersonically expanded into a vacuum chamber, using neon as a carrier gas (2 bar neon backing pressure, 1.5 million acquisitions averaged). For the pulegone–water cluster an additional external reservoir for water was used (2 bar neon backing pressure, 2 million acquisitions averaged).

The spectra were recorded with the Hamburg broadband chirped-pulse Fourier transform microwave (CP-FTMW) spectrometer COMPACT in the frequency range from 2–8 GHz.[32] The procedure can be described briefly as follows: a chirped pulse was generated with an arbitrary waveform generator (AWG), amplified with a traveling wave tube amplifier, and broadcasted into the vacuum chamber. The molecular signal was recorded as a free induction decay (FID). After the Fourier transformation of the signal from the time domain into the frequency domain, the spectrum was obtained. The detailed experimental setup is described in reference [32]. A sequence of eight 4 μs long excitation chirps was performed per gas pulse to decrease the measurement time and sample consumption, followed by the recording of the FID for 40 μs. For that, the fast frame option of our digital oscilloscope was employed. More details of such fast frame measurements can be found in reference [33].

The measured rotational transitions were initially fitted to an asymmetric rigid rotor Hamiltonian, using JB95[34] and PGOPHER program packages.[35] Refined fits were obtained using Watson's A-reduced rigid rotor Hamiltonian in the I^r representation with the SPFIT program.[36] The internal dynamics of pulegone were analysed with the program XIAM.[37] XIAM uses the extended internal axis method proposed by Woods[38] to treat internal rotation in an asymmetric top molecule. It can handle up to three symmetric internal rotors, such as methyl groups.

The M3WM approach is described in references [10,21,39,40]. In our experiment, a single-polarization horn was used for excitation, while a dual-polarization horn was employed for detection. M3WM relies on the fact that although the rotational constants and magnitudes of the dipole moment components $|\mu_a|$, $|\mu_b|$ and $|\mu_c|$ of a chiral molecule are the same for an enantiomeric pair, the scalar product $(\vec{\mu}_a \cdot \vec{\mu}_b \times \vec{\mu}_c)$ differs in sign between the enantiomers.[21] By using closed cycles of three rotational transitions, in which each transition depends on one dipole-moment component, the so called *a*-, *b*- and *c*-type transitions, it is possible to distinguish between the enantiomers by a characteristic phase change of π radians in the FID. The experiment was performed with two linearly polarized, single-frequency excitation pulses (drive and twist), which were orthogonal to each other and resonant to two different rotational transitions. In the setup used here, the drive excitation pulse was in the microwave (MW) and the twist pulse in the radio-frequency (RF) range (up to 550 MHz). Both excitation pulses were generated on the same AWG to ensure phase stability. The chiral molecular signal was probed on the listen transition and was recorded in a phase-dependent manner as an FID in the third mutually orthogonal direction. The recorded signal will differ by π radians for the enantiomers due to the above-mentioned difference in sign for the product of the dipole moment components.

Quantum chemical calculations at the M06-2X/6-311++G(d,p) level of theory as implemented in Gaussian 09[41] were performed to predict the structure, the relative energies and the dipole moment components for the most stable conformations of pulegone. Those structures were reoptimized at the MP2/6-311++G(d,p) level of theory, for which we previously obtained reliable predictions of the rotational parameters for molecular systems similar to pulegone, such as menthone.[9] All conformers were tested to be real minima of the potential energy surface by checking for imaginary vibrational frequencies. In addition, several structures for pulegone–water clusters were optimized at the M06-2X/6-311++G(d,p) and B3LYP-D3BJ/6-311++G(d,p) levels of theory.

Results and Discussion

The pulegone monomer

Conformational flexibility

Pulegone is a chiral molecule with the chiral center marked with an asterisk in Figure 1. The chiral center is at C1, for which we adopted the labeling scheme from an earlier IR–Raman–VCD study on pulegone.[31] [Note that our labeling scheme differs from the IUPAC nomenclature, which would label the carbonyl C-atom of the cyclohexanone ring as C1 (our C5)]. The cyclohexanone ring restricts the number of possible conformations. Using quantum chemical calculations, four conformers were identified. They are depicted in Figure 1 together with their energies relative to the lowest-energy conformer. The conformers differ in two structural features: a) the arrangement of the cyclohexanone ring, which can take on either a chair or a twist-boat configuration, and b) the orientation of the methyl group substituted to C1 with respect to the cyclohexanone ring (equatorial or axial). Note that in Figure 1, both *R* and *S* enantiomers of the chair and the *R* enantiomers of the twist-boat conformers are displayed.

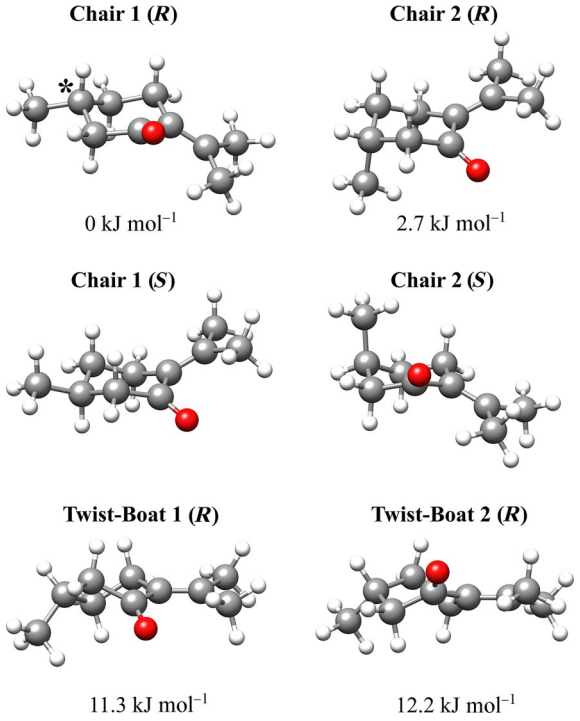

Figure 1. Structures of the four pulegone conformers, optimized at the MP2/6-311++G(d,p) level of theory, as well as their calculated relative energies. The stereogenic center is marked with an asterisk. For Chairs 1 and 2, both enantiomers are shown, while for the Twist-Boats 1 and 2 only the *R* enantiomers are given.

The chair configuration with the methyl group in equatorial position (Chair 1) is the global minimum, followed by the chair configuration with the methyl group arranged axially (Chair 2). The difference between these two conformers can be better visualized by comparing the *S* enantiomer of Chair 1 to the *R* form of Chair 2 (Figure 1).

The calculated energy difference between the two conformers Chair 1 and Chair 2 is about 2.7 kJ mol^{-1}. A large barrier height for the interconversion of these conformers into each other is expected. This assumption is based on the fact that the energy required for ring flipping of an unsubstituted cyclohexane is on the order of 40 kJ mol^{-1}. Although this process can occur at room temperature, it will not take place under the cold conditions of the molecular jet used for our experiment. This means that both conformers should be present in the broadband rotational spectrum. The two conformers with the twist-boat configuration (Twist-Boat 1 and Twist-Boat 2) are higher in energy (11.3 and 12.2 kJ mol^{-1}, respectively) and thus should not be significantly populated.

The experimental rotational spectrum of pulegone is moderately rich, and we can clearly assign and fit the rotational spectra of two asymmetric tops. Both assigned conformers show characteristic internal rotation line splitting. The respective experimental rotational constants are given in Table 1. From a comparison with the calculated rotational values, we can identify our experimentally observed species as Chair 1 and Chair 2, which are the energetically preferred ones.

It is noticeable that Chair 1 and Chair 2 differ clearly in their calculated rotational constants, while for Twist-Boat 1 and Twist-Boat 2 the difference is only approximately 18 MHz. Ray's asymmetry parameter κ is a useful measure of the asymmetry of a molecule. Its value ranges between $\kappa=-1$ for a prolate and $\kappa=1$ for an oblate symmetric top. With $\kappa=-0.76$, pulegone is a near prolate top, with similar κ values for all four conformers. These values are also well represented by the calculations.

An additional criterium for conformer identification are the molecular dipole-moment components μ_a, μ_b, and μ_c in the principal axis system. Their magnitudes determine the strengths of the different types of rotational transitions (*a*-, *b*-, and *c*-type) present in an experimental spectrum. For all conformers, μ_b is predicted to be the largest component. Indeed, the most intense lines correspond to b-type transitions. The values of μ_a and μ_c are significantly smaller. Some *a*- and *c*-type transitions could be assigned, but with significantly lower intensity than the *b*-type transitions.

The conformational assignment is further supported by analysis of the structural parameters like molecular angles, determined from the fit of the torsional transitions arising from methyl group internal rotation, as described in more detail below.

Assuming that the expansion cools down the population of every conformer to its ground vibrational energy state, the relative populations in the supersonic jet can be obtained from the Gibbs energies calculated at the conditions of the pre-expansion mixture (80 °C, 2 bar). Using the results from ab initio calculations (MP2/6-311++G(d,p) level of theory), relative populations of Chair 1/Chair 2/Twist-Boat 1/Twist-Boat 2 are estimated to be 1/0.25/0.02/0.01. This assumption is in agreement with our experimental observation, since only Chair 1 and Chair 2 conformers were observed in the spectrum, and

Table 1. Comparison of experimental and calculated molecular parameters for pulegone (see Figure 1 for the labeling of the conformers). The experimental parameters of Chair 1 and 2 were determined by fitting the internal rotation of methyl tops 1 and 2 (containing C10 and C9, respectively; Figure 2) with XIAM. The observed rotational transitions are given using the following nomenclature: P branch $\Delta J=-1$, Q branch $\Delta J=0$, R branch $\Delta J=+1$; a, b, and c correspond to the respective type of the rotational transitions. *A*, *B*, and *C* are the rotational constants; Δ_J, Δ_{JK}, Δ_K, δ_J, and δ_K are quartic centrifugal distortion constants; $\angle\delta(1)$ and $\angle\delta(2)$ are the angles formed by the internal rotation axes of methyl top 1 and 2, respectively, with the a principal inertial axis.

	Experimental		MP2/6-311++G(d,p)			
Parameter	Chair 1	Chair 2	Chair 1	Chair 2	Twist-Boat 1	Twist-Boat 2
A [MHz]	1908.49282 (69)	1819.9074 (12)	1885.42	1817.17	1974.04	1966.07
B [MHz]	738.85952 (24)	816.68532 (59)	734.76	822.31	764.90	746.45
C [MHz]	578.14126 (23)	635.94683 (29)	584.11	640.85	606.24	588.09
Δ_J [kHz]	0.0330 (25)	0.0414 (23)	0.04	0.03	0.05	0.02
Δ_{JK} [kHz]	−0.281 (11)	0.0786 (58)	−0.32	0.12	−0.22	−0.05
Δ_K [kHz]	1.231 (57)	−0.033 (25)	1.25	−0.02	0.86	0.48
δ_J [kHz]	0.00195 (72)		−0.001	0.005	0.01	0.001
δ_K [kHz]		−0.0067(12)	0.06	0.003	0.01	0.03
κ	−0.76	−0.69	−0.75	−0.69	−0.77	−0.77
$V_3(1)$ [kJ mol^{-1}]	1.961911 (46)	1.96094 (74)	2.2[d]	2.2[d]	–	–
$V_3(2)$[kJ mol^{-1}]	6.3617 (12)	6.705 (44)	5.7[d]	5.7[d]	–	–
$\measuredangle\delta(1)$ [rad]	2.141735 (43)	2.17298 (73)	2.1	2.17	–	–
$\measuredangle\delta(2)$ [rad]	[2.13][e]	0.970 (25)	2.13	0.99	–	–
$\measuredangle\varepsilon(1)$ [rad]	3.15223(54)	3.01264 (19)	3.12	2.95	–	–
$\measuredangle\varepsilon(2)$ [rad]	0.507 (26)	2.880 (24)	0.56	2.78	–	–
$D_{\pi 2J}$[a](1) [MHz]	-0.02207 (35)	−0.0521 (62)	–	–	–	–
$D_{\pi 2K}$[a](1) [MHz]	0.2705 (12)	–	–	–	–	–
$D_{\pi 2K}$[a](2) [MHz]	0.167 (86)	–	–	–	–	–
$D_{\pi 2-}$[a] (1) [MHz]	−0.02643 (20)	−0.0545 (90)	–	–	–	–
μ_a [D]	[a]R	[a]R	0.7	0.4	−0.1	0.5
μ_b [D]	[b]R,[b]Q	[b]R, [b]Q	−2.7	−2.7	−2.8	−2.7
μ_c [D]	[c]R,[c]Q	[c]R, [c]Q	−1.0	−1.1	0.9	0.8
ΔE [kJ mol^{-1}]			0	2.7	11.3	12.2
σ[b] [kHz]	9.09	6.94				
N[c]	234	50				

[a] Empirical internal rotation (overall rotation distortion operator). [b] RMS deviation of the fit. [c] Number of fitted transitions. [d] B3LYP/6-311G level of theory. [e] Fixed to the calculated value.

with the theoretical conformational analysis by Avilés-Moreno et al.[31] There they estimated the expected population for the conformer Ax-1 (corresponds to Twist-Boat 1) to be 1.5% at room temperature (B3LYP/cc-pVDZ level of theory). Note that in reference [31] only the conformers Chair 1 and Twist-Boat 1 were discussed (labeled EQ-1 and AX-1), while the conformers Chair 2 and Twist-Boat 2 were not treated.

Substitution structure

A signal-to-noise (S/N) ratio of 800:1 for the stronger transitions of Chair 1 allowed us to observe and assign the rotational spectra of all singly substituted ^{13}C isotopologues and the ^{18}O isotopologue of the Chair 1 conformer in natural abundance. For each of the ten ^{13}C isotopologues more than 20 transitions were assigned, so that we could reliably determine the heavy-atom backbone structure. The intensity of the transitions for the ^{18}O isotopologue is in accordance with its natural abundance (0.27%), and despite being quite weak in the spectrum, five transitions could be assigned to the ^{18}O isotopologue. Table S2 in the Supporting Information summarizes the rotational parameters for all the detected isotopologues and their comparison with the parent species for the Chair 1 conformer of pulegone. Using the KRA program package,[17,42,43] we could then determine the Kraitchman substitution structure (r_s structure) of Chair 1, which is displayed in Figure 2 (blue spheres).

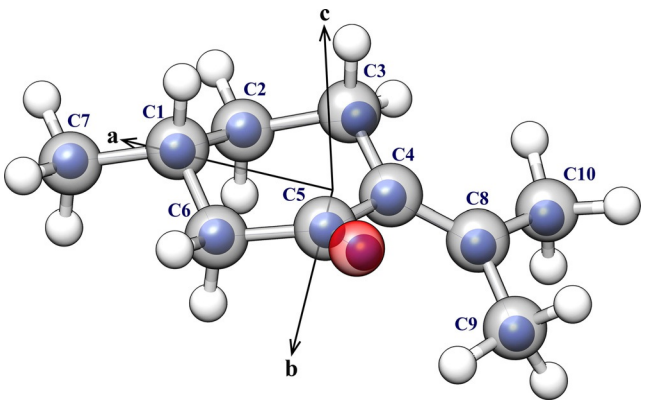

Figure 2. Experimental structures for Chair 1: r_0- (underlying structure, grey for carbon and red for oxygen) and r_s-substitution structure (blue spheres). Table S4 in the Supporting Information summarizes results for bond lengths and angles from r_0- and r_s-treatments, and from ab initio calculations. The principal axis system is also indicated.

Structure determination based on the Kraichman equations is considered a direct way to determine the atomic positions from the changes in the moments of inertia due to isotopic substitution. However, the obtained results can be poor for atoms located close to or in plane of the principal axes. In addition, only the absolute values for the respective atomic coordinates can be determined. The sign is usually taken from ab initio calculations or from chemical intuition. In the case of pulegone, C2 lies in the *ab* plane, and C3 and C5 are located close to the principal axes. The calculated (MP2/6-311++G(d,p)) and the experimental (r_s) positions for the C3 atom differ clearly, while there is good agreement for C2 and C5 (Table S3, Supporting Information).

Improved structural information can be obtained by fitting of the effective ground state structure r_0. The largest difference to the Kraitchman analysis is that it allows to exploit multi- instead of only single-isotopic-substituted species. Such a r_0-fit was successfully applied in our previous studies on camphor–water clusters,[6] producing more accurate results than the r_s-fit. A comparison between the r_0- and the r_s-fit is given in Figure 2. Here, the underlying structure (grey for carbons, red for oxygen) represents the results from the r_0-fit, while the determined r_s atom positions are depicted as blue spheres. As can be seen, there is a good agreement. The results (bond lengths and angles) are summarized in Table S4 in the Supporting Information.

The signal-to-noise ratio was not sufficient (ca. 30:1 for the strongest transitions) to determine any isotopologues for the Chair 2 conformer.

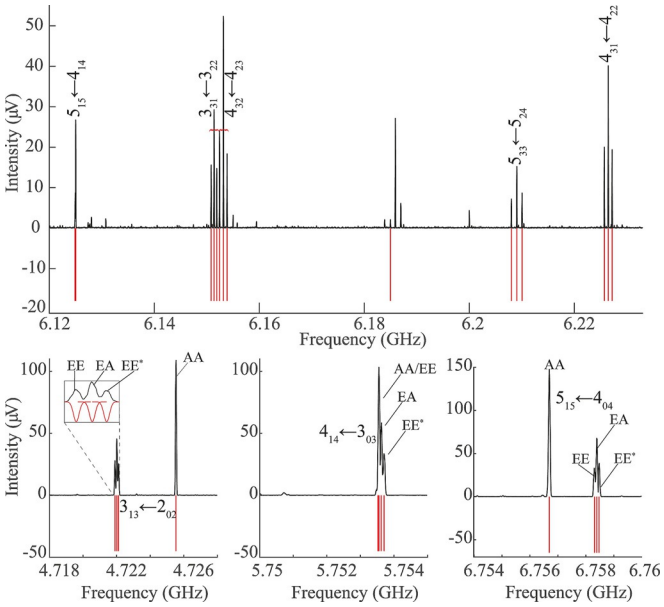

Figure 3. Part of the broadband rotational spectrum (1.5 million acquisitions and using neon as carrier gas) of the pulegone monomer. The upper part gives an overview, while the lower three sections are zoom-ins to individual rotational transitions to illustrate the characteristic multiplet structure due to internal dynamics. In all parts, the upper traces (black) are the experimentally obtained spectra. The lower (red) traces are stick spectra (not taking into account specific intensity distributions) based on simulations using the fitted molecular constants for Chair 1. The labeling of the rotational transitions follows the $J_{K_aK_c}$ scheme.

Internal rotation

The rotational spectrum of pulegone shows clear substructure due to intramolecular dynamics. We identify multiplets with components spaced over several MHz (Figure 3).

Pulegone has three methyl tops (Figure 2), labeled top 1 (containing C10), top 2 (containing C9), and top 3 (containing C7 and being attached to the chiral center of the molecule, C1). Methyl tops 1 and 2 are substituted to the same sp^2 hybridized carbon atom C8, so that a rather low barrier to internal rotation can be expected. Indeed, the calculated barriers are 2.2 and 5.7 kJ mol^{-1} for tops 1 and 2, respectively (B3LYP/6–311G level of theory). For top 3, the calculated barrier is about 12 kJ mol^{-1} (B3LYP/6–311G level of theory), which is too high to give rise to detectable line splittings for the frequency resolution of approximately 25 kHz of the COMPACT spectrometer.[9,44]

The internal rotation of the methyl tops 1 and 2 gives rise to the fine structure illustrated in Figure 3. Multiplets with components spanning several MHz were identified. The multiplets were analyzed and fitted using the program XIAM. First, a subset containing 97 lines was fitted separately to a rigid-rotor Hamiltonian with standard deviation of 7.53 kHz (Table S1, Supporting Information). This fit was then used to predict the splittings for the strongest b-type transitions of the other internal rotation components of Chair 1 using the calculated internal rotation barriers. The coupling scheme is depicted in Figure S2 in the Supporting Information. Within the local mode picture, the multiplets are labeled as AA, AE, EA, EE and EE*. In a step-by-step procedure, a total of 234 lines were assigned and fit with a standard deviation of 9.09 kHz (Table 1).

For Chair 2, the assignment of the torsional transitions was more challenging due to the lower intensity. The values for the experimentally determined internal rotation barriers of Chair 1 were used as a starting point. Overall, 50 lines could be assigned and fitted for Chair 2 with a standard deviation of 6.94 kHz (Table 1). The complete line lists of all assigned transitions for Chair 1 and 2 is provided in the Supporting Information. The multiplet structure due to the internal dynamics of Chair 2 is presented in Figure S3 (Supporting Information).

The internal rotations of the methyl groups of Chair 1 are hindered by only low barriers of 1.961911(46) kJ mol^{-1} for top 1, which is pointing away from the carbonyl group, and 6.3617(12) kJ mol^{-1} for top 2, which interacts with the carbonyl group, thus resulting in the higher barrier. For Chair 2, extremely similar barrier heights were determined (1.96094(74) kJ mol^{-1} for top 1 and 6.705(44) kJ mol^{-1} for top 2). Note that for both Chairs 1 and 2 the internal rotation barrier was determined with higher accuracy for methyl top 1 than for top 2. This is mainly due to the fact that AA and AE splittings could not be resolved in our experiment (with a predicted frequency difference of less than 20 kHz). For an accurate determination of the internal rotation barrier for methyl top 2 these splittings need to be taken into account. The internal rotation barrier for methyl top 1 depends more strongly on

the EA, EE, and EE* splitttings, which are well resolved in the spectrum (Figure 3).

It is interesting to compare the internal rotation of pulegone to that of acetone. Since both molecules have two methyl groups attached to an sp^2-hybridized carbon atom, the patterns for the internal rotation splittings are expected to be similar. The two methyl groups of acetone are equivalent, and their internal motion gives rise to quartets.[45] In pulegone, the two methyl tops are non-equivalent due to their different chemical environment, resulting in a more complex splitting pattern (Figure 3). The experimental three-fold internal rotation barrier V_3 for acetone is 3.18327(59) kJ mol^{-1},[45] which is an intermediate value between the two non-equivalent methyl tops of pulegone. As it could be expected, the barrier for acetone is closer to the barrier of top 1 in pulegone, which is not affected by any interaction with neighboring groups.

An additional aspect in this context is the structural information gained from the internal rotation fits. As mentioned previously, the information about the angles between the internal rotation axis and the respective principal axes can be helpful for identifying molecular conformers. Here, the angle $\varepsilon(2)$, which is defined as the angle between the principal axis *b* and the projection of the internal rotation axis in the principal axis system,[46] is significantly different for Chairs 1 and 2 (0.507(26) rad Chair 1, 2.880(24) rad Chair 2, Table 1). By comparing the values for $\varepsilon(2)$ from the XIAM fit to the ab initio calculations (0.56 rad Chair 1 and 2.78 rad Chair 2, Table 1), the previous identification of the two conformers is further supported.

Enantiomer differentiation using M3WM

M3WM experiments were carried out with enantioenriched samples of pulegone. This allows an unambiguous distinction between the enantiomers, which can then be used for chiral analysis of complex chiral mixtures involving pulegone, such as essential oils. For M3WM, closed cycles consisting of *a*-, *b*-, and *c*-type rotational transitions have to be identified and optimized first, as described in more detail in reference [10]. For pulegone, two M3WM cycles were optimized and successfully applied for conformer Chair 1 (Figure 4). The transitions in these cycles only involve states of AA symmetry with respect to internal dynamics. Cycle 1 solely consists of Q-branch transitions that obey the selection rule $\Delta J = 0$, which is an interesting aspect to note.

The M3WM cycles were optimized with respect to the durations of the two excitation pulses, the drive, and the twist. It has been worked out before that an optimal M3WM signal is obtained for drive pulse durations fulfilling $\pi/2$ Rabi conditions, thus inducing maximum coherence between the two states involved. The twist pulse durations should fulfill π pulse conditions.[47] The π twist pulse transfers coherence from the $5_{24} \leftarrow 5_{14}$ (induced by the $\pi/2$ drive pulse) to the $5_{14} \leftarrow 5_{23}$, which is then recorded (Figure 4, cycle 1).

For optimizing the duration of the drive pulses, the transitions (cycle 1: *c*-type transition $5_{24} \leftarrow 5_{14}$ at 2620.09 MHz; cycle 2: *b*-type transition $5_{05} \leftarrow 4_{14}$ at 5680.25 MHz) were directly excited with increasing duration, and their signal amplitudes

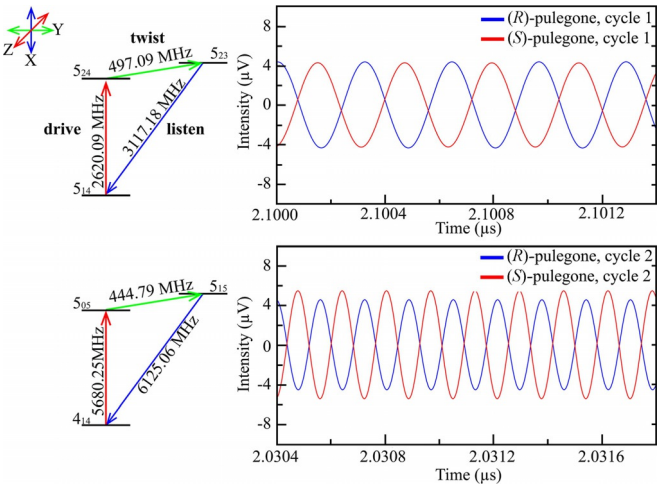

Figure 4. Two M3WM cycles for the pulegone conformer Chair 1. The nomenclature for labeling the respective rotational states is J_{K_a,K_c}. The linearly polarized MW pulse (drive, defined to be along the *Z* axis in the laboratory space) and radio frequency (RF) pulse (twist, defined along the *Y* axis) are the two orthogonal excitation pulses. The molecular M3WM response (listen) in form of an FID is recorded in the *X* direction.

were monitored. For both transitions, the optimal pulse duration was 50 ns to achieve maximum signal and thus $\pi/2$ pulse conditions (Figure S1, Supporting Information).

In our current setup, the twist transitions are in the radio frequency (RF) range between 50–550 MHz and cannot be directly monitored. For optimizing their pulse durations to fulfill π conditions, a double-resonance approach was employed.[48] The amplitude of the respective listen transition was monitored as a function of the twist pulse duration. The optimal twist pulse duration was 1600 ns for $5_{23} \leftarrow 5_{24}$ at 497.09 MHz (*a*-type transition) for cycle 1, and 300 ns for $5_{15} \leftarrow 5_{05}$ (*c*-type transition) at 444.79 MHz for cycle 2. This clear difference in optimal pulse duration mainly arises from the properties of the capacitor plates that we use to broadcast the RF twist excitation pulses. Some frequencies are more strongly supported due to resonances than others.

Using M3WM, enantiomer differentiation is achieved by a characteristic, unambiguous phase difference observed in the time domain (FID) for the listen transition of the M3WM cycle. It arises from the sign difference in the overall product of the dipole-moment components. The results for pulegone are depicted in Figure 4. The phase shift of π rad is clearly visible for both cycles. The M3WM cycles worked out in this study will be used in subsequent experiments on pulegone in essential oils. Comparison of the FID phases for the enantioenriched sample to the ones in the oil will allow us to determine the excess enantiomer of pulegone in the oil. Since it is known that essential oils contain (*R*)-pulegone almost in an enantiopure form, this will give us an opportunity to benchmark our technique for the analysis of complex chiral structures.

The pulegone–water complex

It is reported that pulegone is largely insoluble in water,[49] which is regarded as a major drawback in some applications.

To overcome this, several strategies have been developed, such as supramolecular encapsulation.[50]

We are interested in understanding the interactions of a hydrophobic, insoluble molecule like pulegone with water at the molecular level. There are limited possibilities for water to interact with pulegone. The carbonyl group is the only polar group and can act as a hydrogen bond acceptor. To further explore this, geometry optimizations for different structures of the pulegone–water clusters (for the Chair 1 conformer) were performed at the M06-2X/6-311++G(d,p) and B3LYP-D3BJ/6-311++G(d,p) levels of theory. The two energetically most stable clusters, Chair 1–water a and Chair 1–water b, are represented in Figure 5. The hydrogen-bond interaction between the carbonyl group and water is present in both clusters. In addition, a secondary long-range (dispersion) interaction between the oxygen of the water molecule and the hydrogens of the methyl top 2 can be expected.

One pulegone–water cluster was assigned in our experimental spectrum. The results for the calculated and experimentally determined molecular parameters for the Chair 1–water clusters a and b are presented in Table 2. Direct comparison between the calculated and experimental parameters allows us to assign the experimentally observed species to the energetically most stable Chair 1–water a cluster. Note that the B3LYP calculations with dispersion correction reproduce the experimentally determined values better than the M06-2X. The energy difference between the two clusters is small so that in principle we expect both clusters to be present in the spectrum. However, only Chair 1–water a was experimentally identified. This points to a low interconversion barrier between the two clusters.

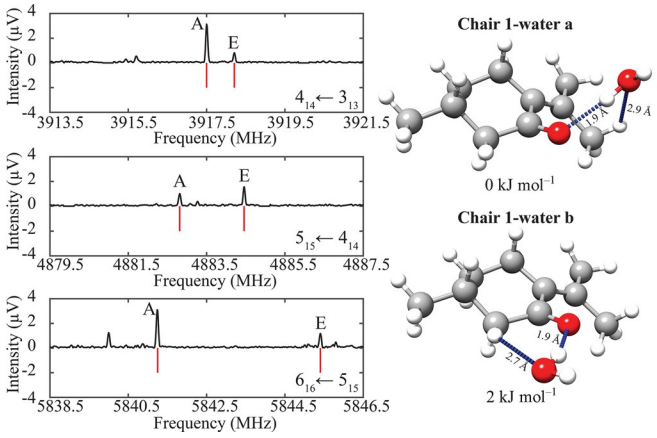

Figure 5. Parts of the broadband rotational spectrum (2 million acquisitions and using neon as carrier gas) of pulegone with water. The three sections are zoom-ins of individual rotational transitions to illustrate the doublet structure due to internal dynamics. In all parts, the upper traces (black) are the experimentally obtained spectrum. The lower (red) traces are stick spectra based on simulations using the fitted molecular constants for Chair 1–water a. The labeling of the rotational transitions follows the $J_{K_aK_c}$ scheme. On the right, two pulegone-water clusters calculated at the B3LYP-D3BJ/6-311++G(d,p) level of theory for the energetically lowest conformer of pulegone, Chair 1, are shown. The calculated hydrogen-bond distances are indicated.

Table 2. Experimental and calculated molecular parameters for pulegone clusters with one water molecule. (The experimental parameters of the Chair 1-water a cluster were determined by fitting the internal rotation of methyl top 1 with XIAM). The observed rotational transitions are given using the following nomenclature: P branch $\Delta J=-1$, Q branch $\Delta J=0$, R branch $\Delta J=+1$; a, b, and c correspond to the respective type of the rotational transitions. *A*, *B*, and *C* are the rotational constants; Δ_J, Δ_{JK}, Δ_K, δ_J, and δ_K are quartic centrifugal distortion constants; $\angle\delta(1)$ and $\angle\delta(2)$ are the angles formed by the internal rotation axes of methyl top 1 and 2, respectively, with the a principal inertial axis.

Parameter	Experimental	M06-2X/6-311++G(d,p)		B3LYP-D3BJ/6-311++G(d,p)	
		Chair 1–water a	Chair 1–water b	Chair 1–water a	Chair 1–water b
A [MHz]	1289.8161 (16)	1356.52	966.72	1295.96	940.30
B [MHz]	565.42463 (59)	568.05	674.96	566.34	677.32
C [MHz]	467.25183 (44)	471.16	416.76	459.45	412.01
Δ_J [kHz]	0.0501 (40)	0.05	0.08	0.05	0.40
Δ_{JK} [kHz]	0.519 (23)	0.41	0.14	0.38	−0.77
Δ_K [kHz]	−1.354 (89)	0.1	0.47	0.15	0.45
δ_J [kHz]	0.0238 (27)	−0.01	0.02	-0.13	0.11
V_3 [kJ mol^{-1}]	2.01013 (38)	1.93[d]	–	–	–
$\measuredangle\delta$ [rad]	1.96917 (37)	1.89	–	–	–
$\measuredangle\varepsilon$ [rad]	2.86344 (21)	2.48	–	–	–
$D_{\pi 2J}$[a] [MHz]	-0.03842 (72)	–	–	–	–
$D_{\pi 2K}$[a] [MHz]	0.280 (18)	–	–	–	–
μ_a [D]	[a]R	2.6	2.5	−2.6	2.9
μ_b [D]	[b]R, [b]Q	1.7	−2.6	1.8	−2.9
μ_c [D]	[c]R	0.3	−0.2	−0.5	−0.3
ΔE [kJ mol^{-1}]		0	2.0	0	2.3
σ[b] [kHz]	9.83				
N[c]	84				

[a] Empirical internal rotation (overall rotation distortion operator). [b] RMS deviation of the fit. [c] Number of fitted transitions. [d] B3LYP/6-311G level of theory.

The secondary interaction of water with the methyl top 2 hinders its internal rotation, while internal rotation of methyl top 1 is still feasible. The calculated barrier for this internal rotation is 1.93 kJ mol^{-1} and consequently low enough to give rise to internal rotation splitting of a single methyl group, resulting in doublets. This is in agreement with our experimental observations. An excerpt from the broadband spectrum of pulegone with water is presented in Figure 5, in which the respective splittings due to the internal rotation of Chair 1 interacting with one water molecule are shown. The results for the internal rotation are summarized in Table 2. The experimentally determined barrier height for the internal rotation is 2.01013(38) kJ mol^{-1}, and thus de facto identical to the value for the pulegone monomer. This shows that methyl top 1 is indeed unaffected by the addition of water.

Conclusions

The internal dynamics of a molecule with two non-equivalent methyl tops was studied on the example of pulegone. Using ab initio calculations (MP2/6-311++G(d,p) level of theory), we analyzed its four stable conformers. The broadband rotational spectrum reveals two conformers, including the previously reported lowest energy structure, and their rich internal dynamics due to the methyl tops attached to an sp^2-hybridized carbon atom. The ^{13}C-monosubstituted isotopologues in natural abundance were assigned, from which we obtained accurate structural information.

No spectroscopic data on the interaction of pulegone with water has been reported before. In the present work, we studied the interaction of the lowest energy conformer of pulegone with one water molecule to improve our knowledge of molecule–water interactions. Water locks the internal rotation of one of the methyl groups due to a secondary interaction, while the other methyl top remains unhindered in its internal rotation.

Finally, M3WM was used to differentiate the enantiomers of pulegone. The main advantages of using the rotational spectroscopy based technique are its fingerprint character regarding different molecular species like isomers, conformers, and isotopologues and its high resolution. M3WM is a nonlinear, coherent and resonant technique, which renders it a powerful method for enantiomeric differentiation in complex mixtures in the gas phase. An interesting next step is thus the chiral analysis in complex mixtures such as essential oils.

Acknowledgements

A.K. acknowledges the financial support of the IMPRS-UFAST and the use of the GWDG computing cluster. C.P. acknowledges a postdoctoral fellowship by the Alexander von Humboldt Stiftung. M.M.Q.M. thanks the Universidad de Jaén for a predoctoral fellowship and the Max Planck Society and the Prince of Asturias Foundation for a Max Planck-Prince of Asturias Award Mobility Grant. The authors are also thankful to the Centro de Servicios de Informática y Redes de Comunicaciones (CSIRC), University of Granada (UGR), for computational time and facilities. J.C.L., S.B., and P.P. acknowledge the Ministerio de Economía y Competitividad (Grant CTQ 2016–75253-P) for financial support. P.P. acknowledges the University of Valladolid for a mobility grant.

Conflict of interest

The authors declare no conflict of interest.

Keywords: chirality · internal rotation · microwave spectroscopy · microwave three-wave mixing · terpenes

[1] T. G. Vale, F. J. A. Matos, T. C. M. de Lima, G. S. B. Viana, *J. Ethnopharmacol.* **1999**, *67*, 127–133.
[2] G. S. B. Viana, T. G. Vale, C. M. Silva, F. J. A. Matos, *Biol. Pharm. Bull.* **2000**, *23*, 1314–1317.
[3] J. Silva, W. Abebe, S. M. Sousa, V. G. Duarte, M. I. L. Machado, F. J. A. Matos, *J. Ethnopharmacol.* **2003**, *89*, 277–283.
[4] J. C. Brookes, A. P. Horsfield, A. M. Stoneham, *J. R. Soc. Interface* **2009**, *6*, 75–86.
[5] D. Schmitz, V. A. Shubert, B. M. Giuliano, M. Schnell, *J. Chem. Phys.* **2014**, *141*, 034304.
[6] C. Pérez, A. Krin, A. L. Steber, J. C. López, Z. Kisiel, M. Schnell, *J. Phys. Chem. Lett.* **2016**, *7*, 154–160.
[7] Z. Kisiel, O. Desyatnyk, E. Białkowska-Jaworska, L. Pszczółkowski, *Phys. Chem. Chem. Phys.* **2003**, *5*, 820–826.
[8] J. R. A. Moreno, T. R. Huet, J. J. L. González, *Struct. Chem.* **2013**, *24*, 1163–1170.
[9] D. Schmitz, V. A. Shubert, T. Betz, M. Schnell, *Front. Chem.* **2015**, *3*, 15.
[10] V. A. Shubert, D. Schmitz, C. Medcraft, A. Krin, D. Patterson, J. M. Doyle, M. Schnell, *J. Chem. Phys.* **2015**, *142*, 214201.
[11] S. R. Domingos, C. Pérez, C. Medcraft, P. Pinacho, M. Schnell, *Phys. Chem. Chem. Phys.* **2016**, *18*, 16682–16689.
[12] B. M. Mitzner, E. T. Theimer, S. K. Freeman, *Appl. Spectrosc.* **1965**, *19*, 169–185.
[13] K. R. Strehle, P. Rösch, D. Berg, H. Schulz, J. Popp, *J. Agric. Food Chem.* **2006**, *54*, 7020–7026.
[14] C. Guo, R. D. Shah, R. Dukor, T. B. Freedman, X. Cao, L. Nafie, *Vib. Spectrosc.* **2006**, *42*, 254–272.
[15] G. Longhi, S. Abbate, R. Gangemi, E. Giorgio, C. Rosini, *J. Phys. Chem. A* **2006**, *110*, 4958–4968.
[16] F. Ureña, J. R. A. Moreno, J. J. L. González, *Tetrahedron: Asymmetry* **2009**, *20*, 89–97.
[17] J. Kraitchman, *Am. J. Phys.* **1953**, *21*, 17–24.
[18] T. Mizutani, T. Ema, H. Ogoshi, *Tetrahedron* **1995**, *51*, 473–484.
[19] S. Blanco, P. Pinacho, J. C. López, *Angew. Chem. Int. Ed.* **2016**, *55*, 9331–9335; *Angew. Chem.* **2016**, *128*, 9477–9481.
[20] C. Pérez, J. C. López, S. Blanco, M. Schnell, *J. Phys. Chem. Lett.* **2016**, *7*, 4053–4058.
[21] D. Patterson, M. Schnell, J. M. Doyle, *Nature* **2013**, *497*, 475–478.
[22] D. Patterson, J. M. Doyle, *Phys. Rev. Lett.* **2013**, *111*, 023008.
[23] V. A. Shubert, D. Schmitz, M. Schnell, *J. Mol. Spectrosc.* **2014**, *300*, 31–36.
[24] S. Eibenberger, J. Doyle, D. Patterson, *Phys. Rev. Lett.* **2017**, *118*, 123002.
[25] C. Pérez, A. L. Steber, S. R. Domingos, A. Krin, D. Schmitz, M. Schnell, *Angew. Chem. Int. Ed.* **2017**, *56*, 12512–12517; *Angew. Chem.* **2017**, *129*, 12686–12691.
[26] *Handbook of Essential Oils, Science Technology and Applications* (Eds.: K. H. Can Baser, G. Buchbauer), CRC, Boca Raton, **2010**.
[27] R. H. McClanahan, D. Thomassen, J. T. Slattery, S. D. Nelson, *Chem. Res. Toxicol.* **1989**, *2*, 349–355.
[28] J. A. Bakerink, S. M. Gospe, R. J. Dimand, M. W. Eldridge, *Pediatrics* **1996**, *98*, 944–947.
[29] W. Engel, *J. Agric. Food Chem.* **2003**, *51*, 6589–6597.
[30] W. P. Gordon, A. C. Huitric, C. L. Seth, R. H. McClanahan, S. D. Nelson, *Drug Metab. Dispos.* **1987**, *15*, 589–594.

[31] J. R. Avilés-Moreno, E. U. Horno, F. P. Urena, J. J. L. González, *Spectrochim. Acta Part A* **2011**, *79*, 767 – 776.
[32] D. Schmitz, V. A. Shubert, T. Betz, M. Schnell, *J. Mol. Spectrosc.* **2012**, *280*, 77 – 84.
[33] C. Pérez, S. Lobsiger, N. A. Seifert, D. P. Zaleski, B. Temelso, G. C. Shields, Z. Kisiel, B. H. Pate, *Chem. Phys. Lett.* **2013**, *571*, 1 – 15.
[34] D. Plusquellic, JB95, available at http://www.nist.gov/pml/electromagnetics/grp05/jb95.cfm.
[35] C. M. Western, *J. Quant. Spectrosc. Radiat. Transfer* **2017**, *186*, 221 – 242.
[36] H. M. Pickett, *J. Mol. Spectrosc.* **1991**, *148*, 371 – 377.
[37] H. Hartwig, H. Dreizler, *Z. Naturforsch. A* **1996**, *51*, 923 – 932.
[38] R. C. Woods, *J. Mol. Spectrosc.* **1966**, *21*, 4 – 24.
[39] V. A. Shubert, D. Schmitz, D. Patterson, J. M. Doyle, M. Schnell, *Angew. Chem. Int. Ed.* **2014**, *53*, 1152 – 1155; *Angew. Chem.* **2014**, *126*, 1171 – 1174.
[40] V. A. Shubert, D. Schmitz, C. Pérez, C. Medcraft, A. Krin, S. R. Domingos, M. Schnell, *J. Phys. Chem. Lett.* **2016**, *7*, 341 – 350.
[41] Gaussian 09 (Revision E.01), M. J. Frisch, G. W. Trucks, H. B. Schlegel, G. E. Scuseria, M. A. Robb, J. R. Cheeseman, G. Scalmani, V. Barone, B. Mennucci, G. A. Petersson, H. Nakatsuji, M. Caricato, X. Li, H. P. Hratchian, A. F. Izmaylov, J. Bloino, G. Zheng, J. L. Sonnenberg, M. Hada, M. Ehara, K. Toyota, R. Fukuda, J. Hasegawa, M. Ishida, T. Nakajima, Y. Honda, O. Kitao, H. Nakai, T. Vreven, J. A. Montgomery, Jr., J. E. Peralta, F. Ogliaro, M. Bearpark, J. J. Heyd, E. Brothers, K. N. Kudin, V. N. Staroverov, R. Kobayashi, J. Normand, K. Raghavachari, A. Rendell, J. C. Burant, S. S. Iyengar, J. Tomasi, M. Cossi, N. Rega, J. M. Millam, M. Klene, J. E. Knox, J. B. Cross, V. Bakken, C. Adamo, J. Jaramillo, R. Gomperts, R. E. Stratmann, O. Yazyev, A. J. Austin, R. Cammi, C. Pomelli, J. W. Ochterski, R. L. Martin, K. Morokuma, V. G. Zakrzewski, G. A. Voth, P. Salvador, J. J. Dannenberg, S. Dapprich, A. D. Daniels, O. Farkas, J. B. Foresman, J. V. Ortiz, J. Cioslowski, D. J. Fox, Gaussian Inc. Wallingford CT **2009**.
[42] Z. Kisiel, PROSPE Programs for ROtational SPEctroscopy, available at http://www.ifpan.edu.pl/~kisiel/prospe.htm; accessed on Sept. 27, 2017.
[43] C. C. Costain, *Trans. Am. Crystallogr. Assoc.* **1966**, *2*, 157 – 164.
[44] C. Medcraft, M. Schnell, *Z. Phys. Chem.* **2016**, *230*, 1 – 14.
[45] J. M. Vacherand, B. P. Van Eijck, J. Burie, J. Demaison, *J. Mol. Spectrosc.* **1986**, *118*, 355 – 362.
[46] H. Hartwig, XIAM Manual, 1996, available at http://www.ifpan.edu.pl/~kisiel/introt/xiam/xiam-v25.txt; accessed on Sept. 27, 2017.
[47] S. Lobsiger, C. Pérez, L. Evangelisti, K. K. Lehmann, B. H. Pate, *J. Phys. Chem. Lett.* **2015**, *6*, 196 – 200.
[48] D. Schmitz, V. A. Shubert, D. Patterson, A. Krin, M. Schnell, *J. Phys. Chem. Lett.* **2015**, *6*, 1493 – 1498.
[49] *The Merck Index—An Encyclopedia of Chemicals, Drugs, and Biologicals* (Ed.: M. O'Neil), RSC, Cambridge, **2013**, p. 1470.
[50] T.-W. Moon, J. W. Lee, K.-H. Jhee, K.-W. Khang, H.-S. Jeong, S.-A. Yang, H.-J. Kim, *Bull. Korean Chem. Soc.* **2008**, *29*, 1579 – 1582.

Manuscript received: September 30, 2017
Accepted manuscript online: October 11, 2017
Version of record online: December 6, 2017